

## Review

# Theory and experiments for disordered elastic manifolds, depinning, avalanches, and sandpiles

Kay Jörg Wiese\* 

Laboratoire de physique, Département de physique de l'ENS, École normale supérieure, UPMC Univ. Paris 06, CNRS, PSL Research University, 75005 Paris, France

E-mail: [wiese@lpt.ens.fr](mailto:wiese@lpt.ens.fr)

Received 22 February 2021, revised 15 November 2021

Accepted for publication 23 December 2021

Published 9 August 2022



CrossMark

### Abstract

Domain walls in magnets, vortex lattices in superconductors, contact lines at depinning, and many other systems can be modeled as an elastic system subject to quenched disorder. The ensuing field theory possesses a well-controlled perturbative expansion around its upper critical dimension. Contrary to standard field theory, the renormalization group (RG) flow involves a function, the disorder correlator  $\Delta(w)$ , and is therefore termed the functional RG.  $\Delta(w)$  is a physical observable, the auto-correlation function of the center of mass of the elastic manifold. In this review, we give a pedagogical introduction into its phenomenology and techniques. This allows us to treat both equilibrium (statics), and depinning (dynamics). Building on these techniques, avalanche observables are accessible: distributions of size, duration, and velocity, as well as the spatial and temporal shape. Various equivalences between disordered elastic manifolds, and sandpile models exist: an elastic string driven at a point and the Oslo model; disordered elastic manifolds and Manna sandpiles; charge density waves and Abelian sandpiles or loop-erased random walks. Each of the mappings between these systems requires specific techniques, which we develop, including modeling of discrete stochastic systems via coarse-grained stochastic equations of motion, super-symmetry techniques, and cellular automata. Stronger than quadratic nearest-neighbor interactions lead to directed percolation, and non-linear surface growth with additional Kardar–Parisi–Zhang (KPZ) terms. On the other hand, KPZ without disorder can be mapped back to disordered elastic manifolds, either on the directed polymer for its steady state, or a single particle for its decay. Other topics covered are the relation between functional RG and replica symmetry breaking, and random-field magnets. Emphasis is given to numerical and experimental tests of the theory.

Keywords: disordered elastic systems, sandpiles, functional renormalization, avalanches

(Some figures may appear in colour only in the online journal)

---

\* Author to whom any correspondence should be addressed.  
'Corresponding Editor Dr Erwin Frey'.

## Contents

1. Disordered elastic manifolds: phenomenology	4	3.2. Field theory of the depinning transition, response function	39
1.1. Introduction	4	3.3. Middleton theorem	39
1.2. Physical realizations, model and observables	5	3.4. Loop expansion	40
1.3. Long-range elasticity (contact line of a fluid, fracture, earthquakes, magnets with dipolar interactions)	6	3.5. Depinning beyond leading order	42
1.4. Flory estimates and bounds	8	3.6. Stability of the depinning fixed points	43
1.5. Replica trick and basic perturbation theory	8	3.7. Non-perturbative FRG	43
1.6. Dimensional reduction	9	3.8. Behavior at the upper critical dimension	44
1.7. Larkin-length, and the role of temperature	10	3.9. Extreme-value statistics: the discretized particle model (DPM)	44
2. Equilibrium (statics)	10	3.10. Mean-field theories	46
2.1. General remarks about renormalization	11	3.11. Effective disorder, and rounding of the cusp by a finite driving velocity	47
2.2. Derivation of the functional RG equations	11	3.12. Simulation strategies	48
2.3. Statistical tilt symmetry	13	3.13. Characterization of the one-dimensional string	49
2.4. Solution of the FRG equation, and cusp	13	3.14. Theory and numerics for long-range elasticity: contact-line depinning and fracture	50
2.5. Fixed points of the FRG equation	14	3.15. Experiments on contact-line depinning	50
2.6. Random-field (RF) fixed point	14	3.16. Fracture	50
2.7. Random-bond (RB) and tricritical fixed points	15	3.17. Experiments for peeling and unzipping	53
2.8. Generic long-ranged fixed point	15	3.18. Creep, depinning and flow regime	54
2.9. Charge-density wave (CDW) fixed point	15	3.19. Quench	55
2.10. The cusp and shocks: a toy model	16	3.20. Barkhausen noise in magnets ( $d = 2$ )	56
2.11. The effective disorder correlator in the field-theory	17	3.21. Experiments on thin magnetic films ( $d = 1$ )	56
2.12. $\Delta(u)$ and the cusp in simulations	18	3.22. Hysteresis	57
2.13. Beyond one-loop order	19	3.23. Inertia, and a large-deviation function	58
2.14. Stability of the fixed point	20	3.24. Plasticity	59
2.15. Thermal rounding of the cusp	21	3.25. Depinning of vortex lines or charge-density waves, columnar defects, and non-potentiality	59
2.16. Disorder chaos	23	3.26. Other universal distributions	60
2.17. Finite $N$	23	4. Shocks and avalanches	60
2.18. Large $N$	24	4.1. Observables and scaling relations	60
2.19. Corrections at order $1/N$	25	4.2. A theory for the velocity	63
2.20. Relation to replica symmetry breaking (RSB)	25	4.3. ABBM model	63
2.21. Droplet picture	26	4.4. End of an avalanche, and an efficient simulation algorithm	63
2.22. Kida model	27	4.5. Brownian force model (BFM)	64
2.23. Sinai model	28	4.6. Short-ranged rough disorder	64
2.24. Random-energy model (REM)	29	4.7. Field theory	64
2.25. Complex disorder and localization	30	4.8. FRG and scaling	64
2.26. Bragg glass and vortex glass	32	4.9. Instanton equation	65
2.27. Bosons and fermions in $d = 2$ , bosonization	32	4.10. Avalanche-size distribution	65
2.28. Sine-Gordon model, Kosterlitz–Thouless transition	33	4.11. Watson–Galton process, and first-return probability	65
2.29. Random-phase sine-Gordon model	34	4.12. Velocity distribution	66
2.30. Multifractality	36	4.13. Duration distribution	66
2.31. Simulations in equilibrium: polynomial versus NP-hard	37	4.14. Temporal shape of an avalanche	66
2.32. Experiments in equilibrium	38	4.15. Local avalanche-size distribution	67
3. Dynamics, and the depinning transition	38	4.16. Spatial shape of avalanches	67
3.1. Phenomenology	38	4.17. Some theorems	69
		4.18. Loop corrections	69

4.19. Simulation results and experiments	71	7.11. An upper critical dimension for KPZ?	96
4.20. Correlations between avalanches	72	7.11.1. Quenched KPZ	96
4.21. Avalanches with retardation	73	7.12. The KPZ equation in dimension $d = 1$	96
4.22. Power-law correlated random forces, relation to fractional Brownian motion	73	7.13. KPZ, polynuclear growth, Tracy–Widom and Baik–Rains distributions	97
4.23. Higher-dimensional shocks	74	7.14. Models in the KPZ universality class, and experimental realizations	98
4.24. Clusters of avalanches in systems with long-range elasticity	75	7.15. From Burgers’ turbulence to Navier–Stokes turbulence?	98
4.25. Earthquakes	75	8. Links between loop-erased random walks, CDWs, sandpiles, and scalar field theories	98
4.26. Avalanches in the SK model	76	8.1. Supermathematics	98
5. Sandpile models, and anisotropic depinning	76	8.2. Basic rules for Grassmann variables	98
5.1. From charge-density waves to sandpiles	76	8.3. Disorder averages with bosons and fermions	99
5.2. Bak–Tang–Wiesenfeld, or Abelian sandpile model	77	8.4. Renormalization of the disorder	100
5.3. Oslo model	77	8.5. Supersymmetry and dimensional reduction	100
5.4. Single-file diffusion, and $\zeta_{d=1}^{\text{dep}} = 5/4$	78	8.6. CDWs and their mapping onto $\phi^4$ -theory with two fermions and one boson	102
5.5. Manna model	78	8.7. Supermathematics: a critical discussion	102
5.6. Hyperuniformity	79	8.8. Mapping loop-erased random walks onto $\phi^4$ -theory with two fermions and one boson	102
5.7. A cellular automaton for fluid invasion, and related models	79	8.9. Other models equivalent to loop-erased random walks, and CDWs	105
5.8. Brief summary of directed percolation	80	8.10. Conformal field theory for critical curves	105
5.9. Fluid invasion fronts from directed percolation	81	9. Further developments and ideas	106
5.10. Anharmonic depinning and FRG	82	9.1. Non-perturbative RG (NPRG)	106
5.11. Other models in the same universality class	82	9.2. Random-field magnets	106
5.12. Quenched KPZ with a reversed sign for the non-linearity	82	9.3. Dynamical selection of critical exponents	109
5.13. Experiments for directed percolation and quenched KPZ	83	9.4. Conclusion and perspectives	110
6. Modeling discrete stochastic systems	84	Acknowledgments	110
6.1. Introduction	84	Appendix A. Basic tools	
6.2. Coherent-state path integral, imaginary noise and its interpretation	84	A.1. Markov chains, Langevin equation, inertia	110
6.3. Stochastic noise as a consequence of the discreteness of the state space	85	A.2. Itô calculus	111
6.4. Reaction-annihilation process	85	A.3. Fokker–Planck equation	111
6.5. Field theory for directed percolation	86	A.4. Martin–Siggia–Rose (MSR) formalism	112
6.6. State variables of the Manna model	87	A.5. Gaussian theory with spatial degrees of freedom	113
6.7. Mean-field solution of the Manna model	88	A.6. The inverse of the Laplace operator	114
6.8. Effective equations of motion for the Manna model: CDP theory	89	A.7. Extreme-value statistics: Gumbel, Weibull and Fréchet distributions	114
6.9. Mapping of the Manna model to disordered elastic manifolds	90	A.8. Gel’fand Yaglom method	116
7. KPZ, Burgers, and the directed polymer	91	References	117
7.1. Non-linear surface growth: KPZ equation	91		
7.2. Burgers equation	92		
7.3. Cole–Hopf transformation	92		
7.4. KPZ as a directed polymer	92		
7.5. Galilean invariance, and scaling relations	93		
7.6. A field theory for the Cole–Hopf transform of KPZ	93		
7.7. Decaying KPZ, and shocks	93		
7.8. All-order $\beta$ -function for KPZ	94		
7.9. Anisotropic KPZ	95		
7.10. KPZ with spatially correlated noise	95		

## Foreword

This review grew out of lectures the author gave in the ICTP master program at ENS Paris. While the beginning of each section is elementary, later parts are more specialized and can be skipped at first reading. Beginners wishing to enter the subject are encouraged to start reading section 1 (introduction), sections 2.1–2.13 (equilibrium/statics), and sections 3.1–3.4 (depinning/dynamics). An introduction to avalanches is given in sections 4.1–4.3, 4.5–4.10. The remaining sections are more specialized: sandpile models and anisotropic depinning are treated in sections 5 and 6. An introduction to the Kardar–Parisi–Zhang (KPZ) equation and its relation to disordered elastic systems is given in section 7. Section 8 discusses links between a class of theories encompassing loop-erased random walks (LERWs), charge density waves (CDWs), Abelian sandpiles, and  $n$ -component  $\phi^4$  theory with  $n = -2$ , linked by supermathematics. Further developments and ideas are collected in section 9. The appendix A contains useful basic tools.

## 1. Disordered elastic manifolds: phenomenology

### 1.1. Introduction

Statistical mechanics is by now a rather mature branch of physics. For pure systems like a ferromagnet, it allows one to calculate with precision details as the behavior of the specific heat on approaching the Curie point. We know that it diverges as a function of the distance in temperature to the Curie temperature, we know that this divergence has the form of a power-law, we can calculate the exponent, and we can do this with at least 3 digits of accuracy using the perturbative RG [1–8], and even more precisely with the newly developed conformal bootstrap [9–11]. Best of all, these findings are in excellent agreement with the most precise simulations [12–14], and experiments [15]. This is a true success story of statistical physics. On the other hand, in nature no system is really pure, i.e. without at least some disorder (‘dirt’). As experiments (and theory) suggest, a little bit of disorder does not change much. Otherwise experiments on the specific heat of helium<sup>1</sup> would not so extraordinarily well confirm theoretical predictions. But what happens for strong disorder? By this we mean that disorder dominates over entropy, so effectively the system is at zero temperature. Then already the question: ‘what is the ground state?’ is no longer simple. This goes hand in hand with the appearance of *metastable states*. States, which in energy are close to the ground-state, but which in configuration-space may be far apart. Any relaxational dynamics will take an enormous time to find the correct ground state, and may fail altogether, as can be seen in computer simulations as well as in experiments, particularly in glasses [17]. This means that our way of thinking, taught in the treatment of pure systems, has to be adapted to account for disorder. We will see that in contrast

to pure systems, whose universal large-scale properties can be ‘modeled by few parameters’, disordered systems demand to model the whole disorder-correlation function (in contrast to its first few moments). We show how universality nevertheless emerges.

Experimental realizations of strongly disordered systems are glasses, or more specifically spin-glasses, vortex-glasses, electron-glasses and structural glasses [17–25]. Furthermore random-field (RF) magnets [26–39], and last not least elastic systems subject to disorder, sometimes termed *disordered elastic systems* or *disordered elastic manifolds* [40–54], on which we focus below.

What is our current understanding of disordered systems? There are a few exact solutions, mostly for idealized or toy systems [55], there are phenomenological approaches (like the droplet-model [56], section 2.21), and there is a mean-field (MF) approximation, involving a method called replica-symmetry breaking (RSB) [57]. This method predicts the properties of infinitely connected systems, as e.g. the Sherrington–Kirkpatrick (SK) model [58, 59]. The solution proposed in 1979 by Parisi [60] is parameterized by a function  $q(x)$ , where  $x$  ‘lives between replica indices 0 and 1’. Today we have a much better understanding of this solution [61–63], and many features can be proven rigorously [64–67]. The most notable feature is the presence of an extensive number of ground states arranged in a hierarchic way (ultrametricity). On the other hand, this solution is inappropriate for systems in which each degree of freedom is coupled only to its neighbors, as is e.g. the case in short-ranged magnetic systems.

While the RSB method mentioned above is intellectually challenging and rewarding, its complexity makes intuition difficult, and performing a field theoretic expansion around this MF solution has proven too challenging a task. RF models, which can be recast in a  $\phi^4$ -type theory are seemingly more tractable, but still the non-linearity of the  $\phi^4$ -interaction makes progress difficult. What one would like to have is a field theory which in absence of disorder is as simple as possible. The simplest such system certainly is a non-interacting, Gaussian, i.e. free theory, to which one could then add disorder. Actually, experimental systems of this type are abundant: magnetic domain walls in presence of disorder a.k.a. Barkhausen noise [68–70], a contact line wetting a disordered substrate [71], fracture in brittle heterogeneous systems [72–74], or earthquakes [75] are good examples for elastic systems subject to quenched disorder. They have a quite different phenomenology from MF models, with notably a single ground state. Asking questions about this ground state, or more generally the probability measure at a given temperature, is termed *equilibrium*. It supposes that if external parameters change, they change so slowly that the system has enough time to explore the full phase space (ergodicity), and find the ground state.

In the opposite limit, notably if there are no thermal fluctuations at all, is *depinning*: increasing an external applied field yields jumps in the center-of-mass of the system (the total magnetization in a magnet). These jumps are termed shocks or avalanches. While one can show that the sequence of avalanches is deterministic given a specific disorder (see

<sup>1</sup> Even though there is some tension between values obtained in a space-shuttle experiment [15] on one side, and simulations [16] and the conformal bootstrap [11] on the other hand.

below), we are more interested in typical behavior, i.e. an average over disorder. The latter average can often be obtained by watching the system for an extended time; one says that the system is *self-averaging*<sup>2</sup>.

In these lectures combined with a review, I aim at explaining the field theory behind these phenomena. All key ingredients are in addition derived analytically in well-chosen toy models. Theoretically most exciting are the connections between seemingly unrelated models. Finally, all main theoretical concepts are checked in experiments. While the field theory has been developed for more than thirty years, no comprehensive and pedagogical introduction is yet available. It is my aim to close this gap. Despite the more than 700 references included in this review, I am aware of omissions. My apologies to all colleagues whose work is not covered in depth. Luckily, some of them have written reviews or lectures themselves, and we refer the reader to [19, 77–83] for complementary presentations.

## 1.2. Physical realizations, model and observables

Before developing the theory to treat elastic systems in a disordered environment, let us give some physical realizations. The simplest one is an Ising magnet. Imposing boundary conditions with all spins up at the upper and all spins down at the lower boundary (see figure 1), at low temperatures, a domain wall separates a region with spins up from a region with spins down. In a pure system at temperature  $T = 0$ , this domain wall is flat. Disorder can deform the domain wall, making it eventually rough. Figure 1 shows, how the domain wall is described by a displacement field  $u(\vec{x})$ . Two types of disorder are common:

- (a) RB disorder, where the bonds between neighboring sites are random. On a course-grained level this also represents missing spins. The correlations of the random potential are short-ranged.
- (b) RF disorder, i.e. coupling of the spins to an external random magnetic field. This disorder is ‘long-ranged’, as the random potential is the sum over the RFs below the domain wall, i.e. effectively has the statistics of a random walk (RW). Taking a derivative of the potential, one obtains short-ranged correlated random forces.

Another example is the contact line of a liquid (water, isobutanol, or liquid helium), wetting a rough (ideally scale-free) substrate, see figure 2. Here, elasticity becomes *long-ranged*, see equation (15) below.

A realization with a two-parameter displacement field  $\vec{u}(x, y, z)$  is the deformation of a vortex lattice, see figure 3: the position of each vortex is deformed from the three-dimensional vector  $\vec{x} = (x, y, z)$  to  $\vec{x} + \vec{u}(\vec{x})$ , with  $\vec{u} \in \mathbb{R}^2$  (its  $z$ -component is 0). Irradiating the sample produces line defects. They allow experimentalists to realize [44]

<sup>2</sup>In contrast to disordered elastic manifolds, some disordered systems such as long-range spin glasses are not self-averaging, which leads to replica-symmetry breaking and a hierarchic organization of states, see [76] for a review, and section 2.20 for a discussion in our context. The presence of a finite correlation length as given in equations (34), (307) and (312) insures self-averaging.

(c) generic *long-range* (LR) correlated disorder. The most extreme example are

(d) *random forces with the statistics of a RW*. This model, the Brownian force model (BFM) of section 4.5, plays an important role as its center-of-mass motion advances as a single degree of freedom, known as the Alessandro, Beatrice, Bertotti and Montorsi (ABBM) or MF model (section 4.3), often used to describe avalanches.

Another example are CDWs, first predicted by Peierls [86]: they can spontaneously form in certain semiconductor devices, where a uniform charge density is unstable toward a superlattice in which the underlying lattice is periodically deformed, and the charge density of the globally neutral device becomes [87–90]

$$\rho(\vec{x}) = \rho_0 \cos(\vec{k}\vec{x}). \quad (1)$$

Adding disorder, the latter locally deforms the phase, modifying the charge density to

$$\rho(\vec{x}, u(\vec{x})) = \rho_0 \cos(\vec{k}\vec{x} + 2\pi u(\vec{x})). \quad (2)$$

As the charge density is invariant under  $u(\vec{x}) \rightarrow u(\vec{x}) + 1$ , we find another disorder class,

(e) *random periodic* (RP) disorder.

All these models have in common that they can be described by a displacement field

$$\vec{x} \in \mathbb{R}^d \rightarrow \vec{u}(\vec{x}) \in \mathbb{R}^N. \quad (3)$$

For simplicity, we suppress the vector notation wherever possible, and mostly consider  $N = 1$ . After some initial coarse-graining, the energy  $\mathcal{H} = \mathcal{H}_{\text{el}} + \mathcal{H}_{\text{conf}} + \mathcal{H}_{\text{dis}}$  consists of three parts: the elastic energy

$$\mathcal{H}_{\text{el}}[u] = \int d^d x \frac{1}{2} [\nabla u(x)]^2, \quad (4)$$

the confining potential

$$\mathcal{H}_{\text{conf}}[u] = \int d^d x \frac{m^2}{2} [u(x) - w]^2, \quad (5)$$

and the disorder

$$\mathcal{H}_{\text{dis}}[u] = \int d^d x V(x, u(x)). \quad (6)$$

In order to proceed, we need to specify the correlations of disorder. Suppose that fluctuations of  $u$  scale as

$$\overline{[u(x) - u(y)]^2} \sim |x - y|^{2\zeta}. \quad (7)$$

Notations are such that  $\langle \dots \rangle$  denotes thermal averages, i.e. averages of an observable using the weight  $e^{-\beta H}$ , properly normalized by the partition function  $\mathcal{Z} = \langle e^{-\beta H} \rangle$ . At zero temperature, this reduces to the contribution of a single state, the ground state. Overbars denote the average over disorder. This defines a *roughness-exponent*  $\zeta$ . Starting from a disorder correlator

$$\overline{V(x, u)V(x', u')} = R(u - u')f(x - x') \quad (8)$$

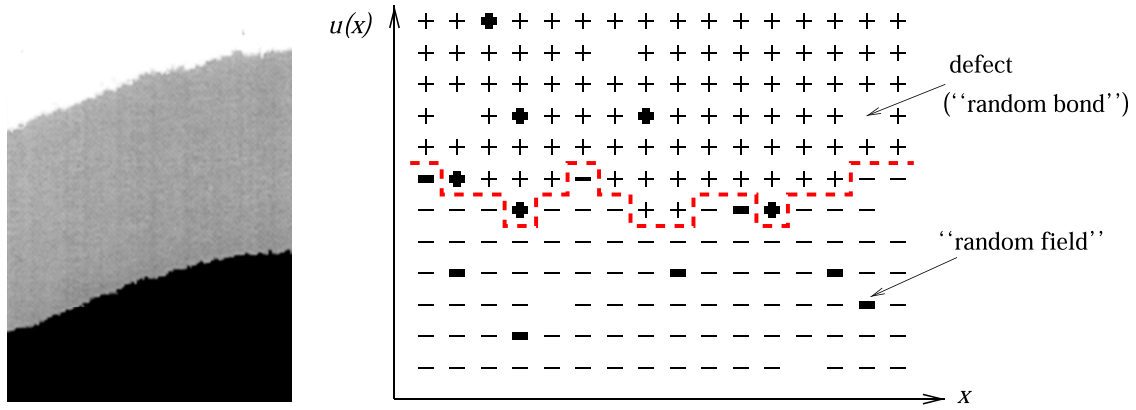


**Figure 1.** An Ising magnet with up (+) and down (-) spins at low temperatures forms a domain wall described by a function  $u(x)$  (right). Reproduced with permission from [42]. Two types of disorder are observed: missing spins, weakening the effective nearest-neighbor interactions (‘random-bond (RB) disorder’), and frozen in magnetic moments aligning its immediate neighbor (‘RF disorder’), indicated by thick  $\pm$  signs. An experiment on a thin cobalt film (left). Reprinted figure with permission from [84], Copyright (1998) by the American Physical Society; with kind permission of the authors.

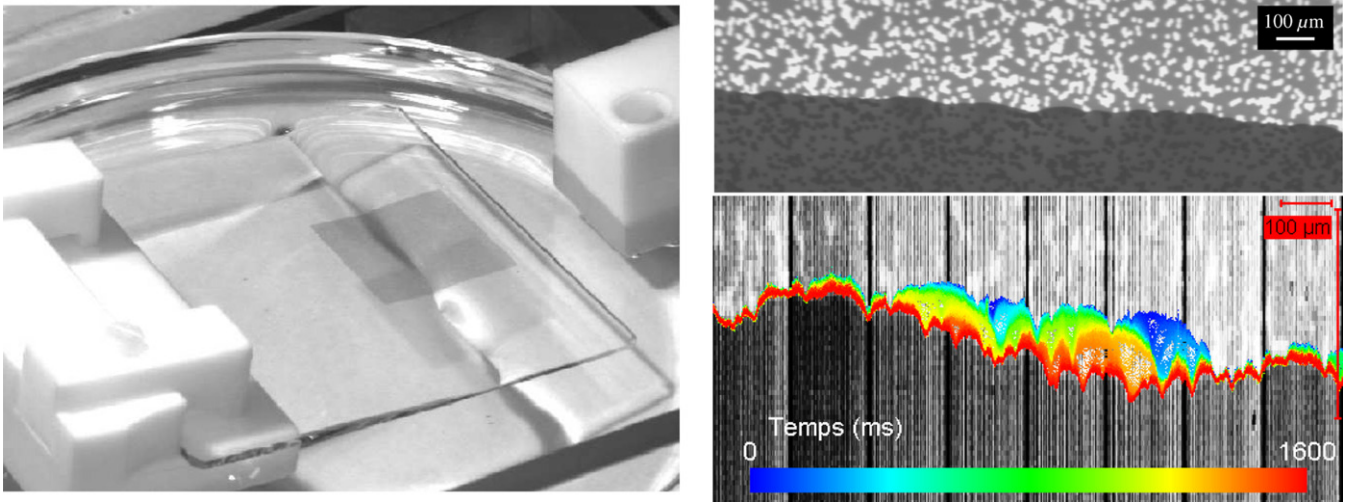


**Figure 2.** A contact line for the wetting of a disordered substrate by glycerine [85]. Experimental setup (left). The disorder consists of randomly deposited islands of chromium, appearing as bright spots (top right), with a correlation length of about  $10 \mu\text{m}$ . Temporal evolution of the retreating contact-line (bottom right). Note the different scales parallel and perpendicular to the contact-line. Credit: Etienne Rolley with permission.

with both  $R(u)$  and  $f(x)$  vanishing at large distances, for each rescaling in the RG-procedure by  $\lambda$  in the  $x$ -direction one rescales by  $\lambda^\zeta$  in the  $u$ -direction. As long as  $\zeta < 1$ , this eventually reduces  $f(x)$  to a  $\delta$ -distribution, whereas the structure of  $R(u)$  may remain visible. We therefore choose as our starting correlations for the disorder

$$\overline{V(x, u)V(x', u')} := R(u - u')\delta^d(x - x'). \quad (9)$$

As we do not consider higher cumulants of the disorder, this implicitly assumes that the distribution of the disorder is Gaussian<sup>3</sup>.

There are a couple of useful observables. We already mentioned the roughness-exponent  $\zeta$ . The second is the renormalized (effective) disorder  $R(u)$ .

<sup>3</sup> For the concept of cumulants see e.g. [91].

Noting by  $F(x, u) := -\partial_u V(x, u)$  the disorder forces, the corresponding force-force correlator can be written as

$$\overline{\langle F(x, u)F(x', u') \rangle} = \Delta(u - u')\delta^d(x - x'). \quad (10)$$

Since  $\overline{\langle F(x, u)F(x', u') \rangle} = \partial_u \partial_{u'} \overline{V(x, u)V(x', u')} = -R''(u - u')\delta^d(x - x')$ , we identify

$$\Delta(u) = -R''(u). \quad (11)$$

### 1.3. Long-range elasticity (contact line of a fluid, fracture, earthquakes, magnets with dipolar interactions)

There are several relevant experimental systems for which the elasticity is different from equation (4). This mostly happens when the elasticity of a lower-dimensional subsystem is mediated by the surrounding bulk. The simplest such example is a

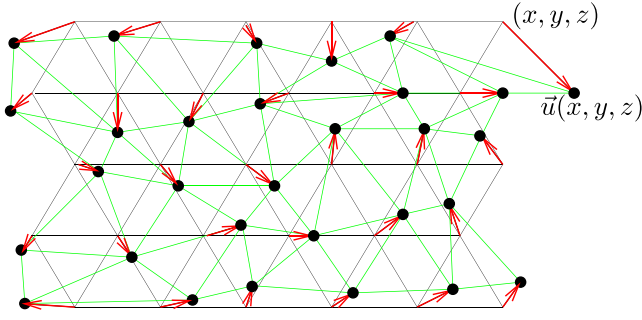


**Figure 3.** A vortex lattice is described by a deformation of a lattice point  $(x, y, z)$  to  $(x, y, z) + \vec{u}(x, y, z)$ . Shown is a cartoon of a single layer, i.e. fixed  $z$ . The vortex lines continue perpendicular to the drawing (figure from [42]).

contact line [92] in a coffee mug or water bottle, i.e. the line where coffee, cup and air meet. A laboratory example is shown in figure 2. For fracture this was introduced in [93].

Consider a liquid with height  $h(x, y)$ , defined in the half-space  $x \geq 0$  (see figure 4). Its elastic energy is surface-tension times surface-area, i.e.

$$\begin{aligned} \mathcal{H}_{\text{el}}^{\text{liquid}}[h] &= \gamma \int_{y, x \geq 0} \sqrt{1 + [\nabla h(x, y)]^2} \\ &\simeq \text{const.} + \int_{y, x \geq 0} \frac{\gamma}{2} [\nabla h(x, y)]^2. \end{aligned} \quad (12)$$

We wish to express this as a function of the height  $u(y) := h(0, y)$  on the boundary at  $x = 0$ . A minimum energy configuration satisfies

$$0 = \frac{\delta \mathcal{H}_{\text{el}}^{\text{liquid}}[h]}{\delta h(x, y)} = -\gamma \nabla^2 h(x, y). \quad (13)$$

This is achieved by the ansatz

$$h(x, y) = \int \frac{dk}{2\pi} \tilde{u}(k) e^{iky - |k|x}, \quad (14)$$

which decays to zero at large  $x$ . On the boundary at  $x = 0$  this is the standard Fourier transform of the height  $u(y)$ . Integrating by parts, the elastic energy as a function of  $\tilde{u}(k)$  becomes with the help of equation (13)

$$\begin{aligned} \mathcal{H}_{\text{el}}^{\text{liquid}}[u] &= \int_{y, x \geq 0} \frac{\gamma}{2} [\nabla h(x, y)]^2 \\ &= \frac{\gamma}{2} \left[ \int_{y, x \geq 0} \nabla \left( h(x, y) \nabla h(x, y) \right) - h(x, y) \nabla^2 h(x, y) \right] \\ &= -\frac{\gamma}{2} \int_y h(x, y) \partial_x h(x, y) \Big|_{x=0} \\ &= \frac{\gamma}{2} \int \frac{dk}{2\pi} |k| \tilde{u}(k) \tilde{u}(-k). \end{aligned} \quad (15)$$

In generalization of equation (15) one can write

$$\mathcal{H}_{\text{el}}^\alpha[u] = \frac{1}{2} \int \frac{d^d k}{(2\pi)^d} |k|^\alpha \tilde{u}(k) \tilde{u}(-k). \quad (16)$$

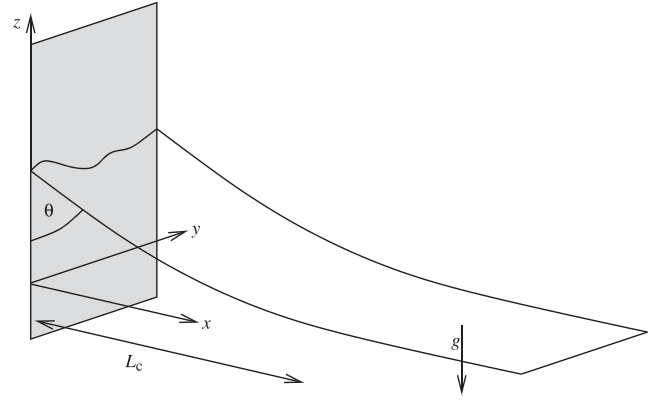


**Figure 4.** The coordinate system for a vertical wall. The air/liquid interface becomes flat for large  $x$ . The height  $h(x, y)$  is along the  $z$ -direction.

For  $\alpha = 2$ , this is equivalent to the local interaction of equation (4). For  $\alpha < 2$ , the interaction is non-local in position space,

$$\mathcal{H}_{\text{el}}^\alpha[u] = \frac{\mathcal{A}_d^\alpha}{2} \int d^d \vec{x} \int d^d \vec{y} \frac{[u(\vec{x}) - u(\vec{y})]^2}{|\vec{x} - \vec{y}|^{d+\alpha}}, \quad (17a)$$

$$\mathcal{A}_d^\alpha = -\frac{2^{\alpha-1} \Gamma(\frac{d+\alpha}{2})}{\pi^{\frac{d}{2}} \Gamma(-\frac{\alpha}{2})}. \quad (17b)$$

For  $d = \alpha = 1$  this yields

$$\mathcal{H}_{\text{el}}^{\alpha=1}[h] = \frac{1}{4\pi} \int dx \int dy \frac{[u(x) - u(y)]^2}{|x - y|^2}. \quad (18)$$

Note that for  $\alpha \rightarrow 2$ ,  $\mathcal{A}_d \sim (2 - \alpha)$ , reducing the LR kernel to the short-range one.

Equation (12) is an approximation, as higher-order terms are neglected. The latter can be generated efficiently [94], and may change the physics of the system [95]. When the contact angle is different from the inclination of the wall, the elastic energy is further modified [96].

The theory we develop below works for arbitrary (positive)  $\alpha$ , with  $\alpha = 2$  for standard *short-ranged* elasticity, and  $\alpha = 1$  for (standard) *long-ranged* elasticity. Apart from contact lines, long-ranged elasticity with  $\alpha = 1$  appears for a  $d$ -dimensional elastic object (a surface), where the elastic interactions are mediated by a bulk material of higher dimension  $D > d$ . Important examples are the displacement of tectonic plates relevant to describe earthquakes ( $d = 2, D = 3$ ) [75, 80, 97] and fracture ( $d = 1, D = 2$  or  $D = 3$ ) [73, 74].

For magnetic domain walls ( $d = 2$ ) with dipolar interactions, the interactions are also long-ranged. The elastic kernel is given by [98] (page 6357)

$$\begin{aligned} \mathcal{H}_{\text{el}}[u] &= \gamma \int d^2 \vec{r}_1 \int d^2 \vec{r}_2 \frac{\partial_{x_1} u(\vec{r}_1) \partial_{x_2} u(\vec{r}_2)}{|\vec{r}_1 - \vec{r}_2|}, \\ \vec{r}_1 &= (x_1, y_1), \quad \vec{r}_2 = (x_2, y_2). \end{aligned} \quad (19)$$

In Fourier space, this reads

$$\mathcal{H}_{\text{el}}[u] = \frac{\gamma}{2\pi} \int d^2\vec{k} \tilde{u}(\vec{k}) \tilde{u}(-\vec{k}) \frac{k_x^2}{|\vec{k}|}. \quad (20)$$

#### 1.4. Flory estimates and bounds

Above, we distinguished four types of disorder, resulting in four different universality classes:

- (a) RB disorder: short-range correlated potential–potential correlations, i.e. a short-range correlated  $R(u)$ .
- (b) RF disorder: a short-range correlated force–force correlator  $\Delta(u) := -R''(u)$ . As the name says, this disorder is relevant for RF systems where the disorder potential is the sum over all magnetic fields below a domain wall.
- (c) Generic LR correlated disorder:  $R(u) \sim |u|^{-\gamma}$ .
- (d) RP disorder: relevant when the disorder couples to a phase, as e.g. in CDWs.  $R(u) = R(u + 1)$ , supposing that  $u$  is periodic with period 1.

To get an idea how large the roughness  $\zeta$  becomes in these situations, one compares the contributions of elastic energy and disorder, and demands that they scale in the same way. This estimate has first been used by Flory [99] for self-avoiding polymers, and is therefore called the Flory estimate<sup>4</sup>. Despite the fact that Flory estimates are conceptually crude, they often give a decent approximation. For RB disorder, this gives for an  $N$ -component field  $u$ :  $\int_x u |\nabla|^\alpha u \sim \int_x \sqrt{V}$ , or  $L^{d-\alpha} u^2 \sim L^d \sqrt{L^{-d} u^{-N}}$ , i.e.  $u \sim L^\zeta$  with

$$\zeta_{\text{Flory}}^{\text{RB}} = \frac{2\alpha - d}{4 + N} \stackrel{\alpha \rightarrow 2}{=} \frac{4 - d}{4 + N}. \quad (21)$$

For RF disorder  $\Delta(u) = -R''(u)$  is short-ranged, and

$$\zeta_{\text{Flory}}^{\text{RF}} = \frac{2\alpha - d}{2 + N} \stackrel{\alpha \rightarrow 2}{=} \frac{4 - d}{2 + N}. \quad (22)$$

For generic LR correlated disorder

$$\zeta_{\text{Flory}}^{\text{LR}} = \frac{2\alpha - d}{4 + \gamma} \stackrel{\alpha \rightarrow 2}{=} \frac{4 - d}{4 + \gamma}. \quad (23)$$

For RP disorder the field  $u$  cannot be rescaled or one would break periodicity, and thus

$$\zeta^{\text{RP}} = 0 \quad (24)$$

exactly. We will see below in section 2.5 that these estimates are a decent approximation, and even exact for RF at  $N = 1$ , or for LR disorder.

#### 1.5. Replica trick and basic perturbation theory

In disordered systems, a particular configuration strongly depends on the disorder, and therefore statements about a specific configuration are in general meaningless. What one needs to calculate are averages, of the form ('gs' denotes the ground state)

<sup>4</sup> For disordered systems this type of argument was employed by Harris [100] and Imry and Ma [101], and the reader will find reference to them as well.

$$\overline{\mathcal{O}[u]} := \frac{\langle \mathcal{O}[u] e^{-\mathcal{H}[u]/T} \rangle}{\langle e^{-\mathcal{H}[u]/T} \rangle}$$

$$\xrightarrow{T \rightarrow 0} \frac{\overline{\mathcal{O}[u_{\text{gs}}]} e^{-\mathcal{H}[u_{\text{gs}}]/T}}{e^{-\mathcal{H}[u_{\text{gs}}]/T}} \equiv \overline{\mathcal{O}[u_{\text{gs}}]}. \quad (25)$$

Note that division by the partition function  $\mathcal{Z} = \langle e^{-\mathcal{H}[u]/T} \rangle$  is crucial. This is particularly pronounced in the limit of  $T \rightarrow 0$ , where  $\mathcal{Z} \rightarrow e^{-\mathcal{H}[u_{\text{gs}}]/T}$  diverges or vanishes when  $T \rightarrow 0$ , except if by chance  $\mathcal{H}[u_{\text{gs}}] = 0$ . Thus the denominator cannot be replaced by its mean. This is a difficult situation: while integer powers  $\mathcal{Z}^n$ , with  $n \in \mathbb{N}$  can be obtained by using  $n$  copies or replicas of the system,  $1/\mathcal{Z}$  cannot. On the other hand, we observe that, independent of  $n$ ,

$$\overline{\mathcal{O}[u]} = \frac{\langle \mathcal{O}[u] e^{-\mathcal{H}[u]/T} \rangle \mathcal{Z}^{n-1}}{\mathcal{Z}^n}. \quad (26)$$

The replica-trick [102, 103]<sup>5</sup> consists in doing the calculations for arbitrary  $n$ . This is possible in perturbation theory, as results there are polynomials in  $n$ . It may become troublesome for exact solutions (notably leading to RSB [57]). Knowing the dependence on  $n$ , the idea is to set  $n \rightarrow 0$  at the end of the calculation, thus eliminating the denominator,

$$\overline{\mathcal{O}[u]} = \lim_{n \rightarrow 0} \overline{\langle \mathcal{O}[u] e^{-\mathcal{H}[u]/T} \rangle \mathcal{Z}^{n-1}}. \quad (27)$$

Since thermal averages over distinct replicas factorize, we write their joint measure as

$$\overline{\langle \mathcal{O}[u] e^{-\mathcal{H}[u]/T} \rangle \mathcal{Z}^{n-1}} = \overline{\left\langle \mathcal{O}[u_1] \prod_{a=1}^n e^{-\mathcal{H}[u_a]/T} \right\rangle}$$

$$= \overline{\left\langle \mathcal{O}[u_1] e^{-\sum_{a=1}^n \mathcal{H}[u_a]/T} \right\rangle}$$

$$= \overline{\left\langle \mathcal{O}[u_1] e^{-\frac{1}{T} \sum_{a=1}^n \mathcal{H}_{\text{el}}[u_a] + \mathcal{H}_{\text{conf}}[u_a] + \mathcal{H}_{\text{dis}}[u_a]} \right\rangle}. \quad (28)$$

Note that in the second equality we have exchanged thermal and disorder averages. We also allowed for different positions  $w$  of the parabola for the different replicas, denoted  $w_a$ .<sup>6</sup> Finally, we assume for simplicity of presentation that  $\mathcal{O}[u]$  does not explicitly depend on the disorder. Since only the last term in the exponential depends on  $V(x, u)$ , and since  $V(x, u)$  is Gauss distributed,

<sup>5</sup> It is not quite clear who 'invented' the replica trick. In [102] Brout stresses that  $\ln \mathcal{Z}$  has to be averaged over disorder, not  $\mathcal{Z}$ . Brout considers a cluster expansion for a quenched disordered system, organizing his expansion in powers of  $n$ , equivalent to a cumulant expansion, or sums over independent replicas, concepts we use below.

<sup>6</sup> The partition function for each of these replicas may be different. The formalism takes this into account.

$$\begin{aligned}
e^{-\frac{1}{T} \sum_{a=1}^n \mathcal{H}_{\text{dis}}[u_a]} &= \exp\left(-\frac{1}{T} \int_x \sum_a V(x, u_a(x))\right) \\
&= \exp\left(\frac{1}{2T^2} \int_x \int_{y, a, b=1}^n \overline{V(x, u_a(x))V(y, u_b(y))}\right) \\
&= \exp\left(\frac{1}{2T^2} \int_x \sum_{a, b=1}^n R(u_a(x) - u_b(x))\right). \tag{29}
\end{aligned}$$

In the second step we used that  $V$  is Gaussian; in the last step we used the correlator (9).

To summarize: to evaluate the expectation of an observable, we take averages with measure  $e^{-S_{\text{rep}}[u]}$  and *replica Hamiltonian* or *action*

$$\begin{aligned}
\mathcal{S}_{\text{rep}}[u] &:= \frac{1}{T} \sum_{a=1}^n \int_x \left\{ \frac{1}{2} [\nabla u_a(x)]^2 + \frac{m^2}{2} [u_a(x) - w_a]^2 \right\} \\
&\quad - \frac{1}{2T^2} \int_x \sum_{a, b=1}^n R(u_a(x) - u_b(x)). \tag{30}
\end{aligned}$$

Note that each replica sum comes with a factor of  $1/T$ . If the disorder had a third cumulant, this would appear as a triple replica sum, and a factor<sup>3,5</sup> of  $1/T^3$ .

Let us now turn to perturbation theory. The free propagator, constructed from the first line of equation (30), and indicated by the index ‘0’, is (first in Fourier, than in real space)

$$\langle \tilde{u}_a(-k) \tilde{u}_b(k) \rangle_0 = T \delta_{ab} \tilde{C}(k), \tag{31}$$

$$\langle u_a(x) u_b(y) \rangle_0 = T \delta_{ab} C(x - y). \tag{32}$$

Noting  $C(x - y)$  the Fourier transform of  $\tilde{C}(k)$ , and  $S_d = 2\pi^{d/2}/\Gamma(d/2)$  the area of the  $d$ -sphere, we have

$$\tilde{C}(k) = \frac{1}{k^2 + m^2}, \tag{33a}$$

$$\begin{aligned}
C(x) &= \int \frac{d^d k}{(2\pi)^d} \frac{e^{ikx}}{k^2 + m^2} \\
&\simeq \frac{1}{(d-2)S_d} |x|^{2-d} \quad \text{for } x \rightarrow 0. \tag{33b}
\end{aligned}$$

On the other hand, for large  $x$ , the correlation function decays exponentially  $\sim e^{-m|x|}$ , which we associate with a correlation length

$$\xi = \frac{1}{m}. \tag{34}$$

Equation (33a) allows us to calculate expectation values in the full theory. As an example consider

$$\begin{aligned}
&\overline{\langle [u(x) - w_1] \rangle_{w_1} \langle [u(z) - w_2] \rangle_{w_2}} \\
&\equiv \langle [u_1(x) - w_1][u_2(z) - w_2] \rangle_{\mathcal{S}_{\text{rep}}} \\
&= - \int_y C(x - y) C(z - y) R''(w_1 - w_2) + \dots \tag{35}
\end{aligned}$$

Let us clarify the notations: firstly,  $\langle [u(x) - w_1] \rangle_{w_1}$  is the thermal average of  $u(x) - w_1$ , obtained by evaluating the path integral for a fixed disorder configuration  $V$ , at a position of the parabola given by  $w_1$ . This procedure is repeated for  $\langle [u(z) - w_2] \rangle_{w_2}$ , with the same  $V$ , and parabola position  $w_2$ . Finally the average over the disorder potential  $V$  is taken. According to the calculations above, this can be evaluated with the help of the replica action  $\mathcal{S}_{\text{rep}}[u]$ , represented by  $\langle [u_1(x) - w_1][u_2(z) - w_2] \rangle_{\mathcal{S}_{\text{rep}}}$ . The latter is already averaged over disorder. The last line shows the leading order in perturbation theory, dropping terms of order  $T$  and higher.

Finally, let us integrate this expression over  $x$  and  $z$ , and multiply by  $m^4/L^d$ . This leads to

$$\begin{aligned}
\frac{m^4}{L^d} \int_{x,z} \overline{\langle [u(x) - w_1] \rangle_{w_1} \langle [u(z) - w_2] \rangle_{w_2}} \\
= -R''(w_1 - w_2) + \dots \tag{36}
\end{aligned}$$

Let us understand the prefactor on the lhs: the combination  $m^2[u(x) - w_1]$  is the force acting on point  $x$  (a density), its integral over  $x$  the total force acting on the interface. Force correlations are short ranged in  $x$ , leading to the factor of  $1/L^d$ . Note that the thermal two-point function (32) is absent, as we consider two distinct copies of the system.

## 1.6. Dimensional reduction

It is an interesting exercise to show that for  $w_1 = w_2$  no perturbative corrections to equation (36) exist in the limit of  $T \rightarrow 0$ , as long as one supposes that  $R(w)$  is an analytic function. Similarly, one shows that in the same limit  $\langle uuuu \rangle^c = 0$ , and the same holds true for higher connected expectations. Thus  $u$  is a Gaussian field with correlations

$$\begin{aligned}
\overline{\langle \tilde{u}(k) \rangle \langle \tilde{u}(-k) \rangle} &= \overline{\langle \tilde{u}(k) \tilde{u}(-k) \rangle} \\
&= \overline{\tilde{u}(k) \tilde{u}(-k)} = -\frac{R''(0)}{(k^2 + m^2)^2}. \tag{37}
\end{aligned}$$

In the third expression we suppressed the thermal expectation values since at  $T = 0$  only a single ground state survives<sup>7</sup>. Fourier-transforming back to position space yields (with some amplitude  $\mathcal{A}$ , and in the limit of  $mx \rightarrow 0$ )

$$\frac{1}{2} \overline{[u(x) - u(y)]^2} = -R''(0) \mathcal{A} |x - y|^{4-d}. \tag{38}$$

This looks very much like the thermal expectation (32), except that the dimension of space has been shifted by 2. Further, both theories are seemingly Gaussian, i.e. higher cumulants vanish.

We have just given a simple version of a beautiful and rather mind-boggling theorem relating disordered systems to pure ones (i.e. without disorder). The theorem applies to a large class of systems, even when non-linearities are present

<sup>7</sup> For disordered elastic manifolds with continuous disorder, the ground state is almost surely unique. This is in strong contrast to mean-field spin glasses, where it is highly degenerate, see e.g. [57].

in the absence of disorder. It is called dimensional reduction [104–106]. We formulate it as follows:

**‘Theorem’.** *A  $d$ -dimensional disordered system at zero temperature is equivalent to all orders in perturbation theory to a pure system in  $d - 2$  dimensions at finite temperature.*

We give in section 8.1 a proof of this theorem using a supersymmetric field theory introduced in [32]. The proof *implicitly assumes that  $R(u)$  is analytic*, thus all derivatives can be taken. The equivalence is rather powerful, since the supersymmetric theory knows about different replicas, and allows one to calculate even away from the critical point.

However, evidence from experiments, simulations, and analytic solutions show that the above ‘theorem’ is actually *wrong*. A prominent counter-example is the three-dimensional RF Ising model at zero temperature [30]; according to the theorem it should be equivalent to the pure one-dimensional Ising-model at finite temperature. While it was shown rigorously [30] that the former has an ordered phase, the latter is disordered at finite temperature [107]. So what went wrong? Let us stress that there are no missing diagrams or any such thing, but that the problem is more fundamental: as we will see later, the proof makes the assumption that  $R(u)$  is analytic. While this assumption is correct in the microscopic model, it is not valid at large scales.

Nevertheless, the above ‘theorem’ remains important since it has a devastating consequence for all perturbative calculations in the disorder: however clever a procedure we invent, as long as we perform a perturbative expansion, expanding the disorder in its moments, all our efforts are futile: dimensional reduction tells us that we get a trivial and unphysical result. Before we try to understand why this is so and how to overcome it, let us give one more counter-example. Dimensional reduction allowed us in equation (38) to calculate the roughness-exponent  $\zeta$  defined in equation (7), as

$$\zeta_{\text{DR}} = \frac{4-d}{2}. \quad (39)$$

On the other hand, the directed polymer in dimension  $d = 1$  does not have a roughness exponent of  $\zeta_{\text{DR}} = 3/2$ , but [108]

$$\zeta_{d=1}^{\text{RB}} = \frac{2}{3}. \quad (40)$$

Experiments and simulations for disordered elastic manifolds discussed below in sections 2.31, 2.32, 3.12, 3.13, 3.15–3.17, and 3.21 all violate dimensional reduction.

### 1.7. Larkin-length, and the role of temperature

To understand the failure of dimensional reduction, let us turn to crucial arguments given by Larkin [109]. He considers a piece of an elastic manifold of size  $L$ . If the disorder has correlation length  $r$ , and characteristic potential energy  $\bar{\mathcal{E}}$ , there are  $(L/r)^d$  independent degrees of freedom, and according to the central-limit theorem this piece of size  $L$  will typically see a potential energy of amplitude

$$\mathcal{E}_{\text{dis}} = \bar{\mathcal{E}} \left( \frac{L}{r} \right)^{\frac{d}{2}}. \quad (41)$$

On the other hand, the elastic energy scales as

$$\mathcal{E}_{\text{el}} = cL^{d-2}. \quad (42)$$

These energies are balanced at the Larkin-length  $L = L_c$  with

$$L_c = \left( \frac{c^2}{\bar{\mathcal{E}}^2} r^d \right)^{\frac{1}{4-d}}. \quad (43)$$

More important than this value is the observation that in all physically interesting dimensions  $d < d_c = 4$ , and at scales  $L > L_c$ , the disorder energy (41) wins; as a consequence the manifold is pinned by disorder, whereas on small scales the elastic energy dominates. For long-ranged elasticity, the same argument implies

$$d_c = 2\alpha, \text{ and disorder relevant for } d < d_c. \quad (44)$$

Since the disorder has many minima which are far apart in configurational space but close in energy (metastability), the manifold can be in either of these minima, and local minimum does not imply global minimum. However, the existence of exactly one minimum is assumed in e.g. the proof of dimensional reduction, even though formally, the field theory sums over all saddle points.

Another important question is the role of temperature. In equation (7) we had supposed that  $u$  scales with the system size as  $u \sim L^\zeta$ . Demanding that the action (30) be dimensionless, the first term in equation (30) scales as  $L^{d-2+2\zeta}/T$ . This implies that

$$T \sim a^\theta, \quad \theta = d - 2 + 2\zeta, \quad (45)$$

where  $a$  is a microscopic cutoff with the dimension of  $L$ , to compensate the factor of  $L^{d-2+2\zeta}$ . For completeness, we also give the result for generic LR-elasticity,

$$\theta_\alpha = d - \alpha + 2\zeta. \quad (46)$$

The thermodynamic limit is obtained by taking  $L \rightarrow \infty$ . Temperature is thus irrelevant when  $\theta > 0$ , which is the case for  $d > 2$ , and when  $\zeta > 0$  even below. As a consequence, the RG fixed point we are looking for is at zero temperature [110]. The same argument applies to the free energy

$$\mathcal{F}[u] = -\frac{1}{T} \ln(\mathcal{Z}[u]) \sim \left( \frac{L}{a} \right)^\theta. \quad (47)$$

We added  $u$  as an argument to  $\mathcal{F}[u]$ , as e.g. in the directed polymer the partition function is the weight of all trajectories arriving at  $u$ . This is important in section 7.1 when considering the KPZ equation.

From the second term in equation (30) we conclude that the (microscopic) disorder scales as

$$R \sim a^{2\theta-d} = a^{d-4+4\zeta}. \quad (48)$$

For  $\zeta = 0$ , this again implies that  $d = 4$  is the upper critical dimension. More thorough arguments are presented in the next section, where we will construct an  $\epsilon = 4 - d$  expansion for the RG flow of  $R(u)$ .

## 2. Equilibrium (statics)

### 2.1. General remarks about renormalization

In the next section 2.2 we derive the central RG equations for disordered elastic manifolds. These equations are obtained in a controlled  $\epsilon = 4 - d$  expansion [111] around the upper critical dimension. Retaining in this expansion only the leading divergences which show up as poles in  $1/\epsilon$ , by using *minimal subtraction*, this expansion is unique. This is a deep result, ensured by the *renormalizability* of the theory (see e.g. [112–116]). We consider it a *gift*: however we set up our RG scheme, we always get the same result. This allows us to choose one scheme, and switch to a different one whenever its particular features help us in our reasoning. The schemes in question are

- Wilson's momentum-shell scheme. This scheme goes back to Wilson, who suggested to integrate over the *fast* modes, i.e. modes  $k$  contained in a momentum shell between  $\Lambda(1 - \delta)$  and  $\Lambda$ , with  $\delta \ll 1$ . Doing this incrementally is interpreted as a flow equation for the effective parameters of the theory. The process stops when one reaches the scale one is interested in, which is zero for correlations of the center of mass. While intuitive, this technique is cumbersome to implement, especially at sub-leading order. We refer to the classical text [117] for an introduction.
- Field theory as used in high-energy physics. This is the standard technique to treat critical phenomena, and is explained in many classical texts [1, 2, 4–7]. A well-oiled machinery, especially for higher-order calculations.
- The operator product expansion as explained in [3], or section 3.4 of [118]. Realizing that the dominant contributions in schemes (a) and (b) come from large momenta implies that they must come from short distances in position space. It is not only very efficient at leading order<sup>8</sup>, it also explains why counter-terms are local (see below).
- Non-perturbative (NP) functional RG: a rather heavy machinery, which we believe should be restricted to cases where other schemes fail (see section 9.2 on RF magnets).
- The experimentalist's point of view: if all RG procedures are equivalent, then we can *choose* to study the flow equations by reducing an experimentally relevant parameter, here the strength  $m^2$  of the confining potential. As we show below in sections 2.10 and 2.11, the theory can be defined at any  $m^2$ , e.g. by doing an experiment or simulation at this scale. This definition does not make reference to any perturbative calculation. The latter can then be viewed as an efficient analytical *tool* to predict in an experiment or a simulation the consequences of a change of the parameter  $m^2$ .

If we think about standard perturbative RG for  $\phi^4$  theory, we remark that the parameter  $\epsilon$  controls the order of perturbation theory necessary<sup>9</sup>, and that at leading order  $\mathcal{O}(\epsilon)$  the

<sup>8</sup> In  $\phi^4$ -theory it gives the two-loop correction to  $\eta$  from a single integral, see section 3.4 of [118].

<sup>9</sup> As a rule of thumb: order  $n$  in  $\epsilon$  necessitate order  $n$  in the interaction  $\int_x \phi^4(x)$ .

differences boil down to a choice of how to evaluate the elementary integral (58). For disordered systems, there is an additional quirk: the *interaction* termed  $R(u)$  in equation (30) is a function of the field differences, and we have no a-priori knowledge of its form. It will turn out in the next section 2.2 that we can write down a flow equation for the function  $R(u)$  itself. We would already like to stress that similar to  $\phi^4$ -theory, the fixed point for  $R(u)$  is of order  $\epsilon$ , thus the calculation remains perturbatively controlled.

### 2.2. Derivation of the functional RG equations

In section 1.7, we had seen that 4 is the upper critical dimension for SR elasticity, which we treat now. As for standard critical phenomena [1–7], we construct an  $\epsilon = (4 - d)$ -expansion. Taking the dimensional-reduction result (39) in  $d = 4$  dimensions tells us that the field  $u$  is dimensionless there. Thus, the width  $\sigma = -R''(0)$  of the disorder is not the only relevant coupling at small  $\epsilon$ , but any function of  $u$  has the same scaling dimension in the limit of  $\epsilon = 0$ , and might equivalently contribute. The natural conclusion is to follow the full function  $R(u)$  under renormalization, instead of just its second derivative  $R''(0)$ .

Such an RG-treatment is most easily implemented in the replica approach: the  $n$  times replicated partition function led after averaging over disorder to a path integral with weight  $e^{-S_{\text{rep}}[u]}$ , with action (30). Perturbation theory is constructed as follows: the bare correlation function for replicas  $a$  and  $b$ , graphically depicted as a solid line, is with momentum  $k$  flowing through, see equations (31)–(33a),

$$\langle \tilde{u}_a(k) \tilde{u}_b(k) \rangle_0 = T \times a \text{ ————— } b = T \delta_{ab} \tilde{C}(k). \quad (49)$$

Note that the factor of  $T$  is explicit in our graphical notation, and not included in the line. The disorder vertex is (we added an index  $R_0$  to  $R$  to indicate that this is the microscopic (bare) disorder)

$$\frac{1}{T^2} \times \begin{array}{c} a \bullet \\ | \\ b \bullet \\ | \\ x \end{array} = \frac{1}{T^2} \times R_0(u_a(x) - u_b(x)). \quad (50)$$

The rules of the game are to find all contributions which correct  $R$ , and which survive in the limit of  $T \rightarrow 0$ . At leading order, i.e. order  $R_0^2$ , counting of factors  $T$  shows that we can use at most two correlators, as each contributes a factor of  $T$ . On the other hand,  $\sum_{a,b} R_0(u_a - u_b)$  has two independent sums over replicas<sup>10</sup>. Thus at order  $R_0^2$  four independent sums over replicas appear, and in order to reduce them to two, one needs at least two correlators (each contributing a  $\delta_{ab}$ ). Thus, at leading order, only diagrams with two propagators survive.

Before writing down these diagrams, we need to see what Wick-contractions do on functions of the field. To see this, remind that a single Wick contraction (indicated by  $\overline{\text{————}}$  sitting on top of the fields to be contracted)

$$\overline{u_a(x)^n u_b(y)^m} = n u_a(x)^{n-1} \times m u_b(y)^{m-1} \times T \delta_{ab} C(x - y). \quad (51)$$

<sup>10</sup> The concept of *sums over independent replicas* already appears in the work by Brout [102], see footnote 5.

Realizing that  $nu^{n-1} = \partial_u u^n$ , we can write the Wick contraction for an arbitrary function  $V(u)$  as

$$\begin{aligned} & \overline{V(u_a(x))V(u_b(y))} \\ &= V'(u_a(x)) \times V'(u_b(y)) \times T\delta_{ab}C(x-y). \end{aligned} \quad (52)$$

Graphically we have at second order for the correction of disorder

$$\frac{1}{2T^2}\delta R = \frac{1}{2!} \left[ \begin{array}{c} 1 \\ \frac{1}{2T^2} \\ b \\ \bullet \\ x \end{array} \right] \begin{array}{c} a \\ \bullet \\ \hline \\ \bullet \\ y \end{array} \begin{array}{c} e \\ \xrightarrow{T} \\ e \end{array} \left[ \begin{array}{c} 1 \\ \frac{1}{2T^2} \\ d \\ \bullet \\ y \end{array} \right] \begin{array}{c} c \\ \bullet \\ \hline \\ \bullet \\ x \end{array} \quad (53)$$

We have explicitly written all factors: a  $1/2!$  from the expansion of the exponential function  $\exp(-\mathcal{S}_{\text{rep}}[u])$ , a factor of  $1/(2T^2)$  per disorder vertex, and a factor of  $T$  per propagator. Using these rules, we obtain two distinct contributions

$$\begin{aligned} \delta R^{(1)} &= \frac{1}{2} \begin{array}{c} a \bullet \text{---} \bullet a \\ | \quad | \\ b \bullet \text{---} \bullet b \\ | \quad | \\ x \quad y \end{array} \\ &= \frac{1}{2} \int_x R_0''(u_a(x)-u_b(x)) R_0''(u_a(y)-u_b(y)) C(x-y)^2, \end{aligned} \quad (54)$$

$$\begin{aligned} \delta R^{(2)} &= \begin{array}{c} a \bullet \text{---} \bullet a \\ | \quad | \\ a \bullet \text{---} \bullet b \\ | \quad | \\ x \quad y \end{array} \\ &= - \int_x R_0''(u_a(x)-u_a(x)) R_0''(u_a(y)-u_b(y)) C(x-y)^2. \end{aligned} \quad (55)$$

Note that all factors of  $T$  have disappeared, and only two replica sums (not written explicitly) remain. Each  $R_0(u_a - u_b)$  has been contracted twice, giving rise to two derivatives. In the first diagram, since once  $u_a$  and once  $u_b$  has been contracted, each  $R_0''$  comes with an additional minus sign; these cancel. In the second diagram, there is a minus sign from the first  $R_0''$ , but not from the second; thus the overall sign is negative.

Note that the following diagram also contains two correlators (correct counting in powers of temperature), but is not a two-replica but a three-replica sum,

$$\begin{array}{c} a \bullet \text{---} \bullet a \\ | \quad | \\ b \bullet \text{---} \bullet c \\ | \quad | \\ x \quad y \end{array} \quad (56)$$

In a renormalization program, we are looking for divergences of these diagrams. These divergences are localized at  $x = y$ : indeed the integral over the difference  $z := y - x$ , is in radial coordinates with  $r = |z|$ ,  $\epsilon = 4 - d$ , and for  $m \rightarrow 0$  (up to a geometrical prefactor)

$$\begin{aligned} \int_z C(z)^2 &\sim \int_a^L \frac{dr}{r} r^d r^{2(2-d)} = \int_a^L \frac{dr}{r} r^{4-d} \\ &= \frac{1}{\epsilon} (L^\epsilon - a^\epsilon). \end{aligned} \quad (57)$$

Note that for  $\epsilon \rightarrow 0$  each scale contributes the same: from  $r = 1/2$  to  $r = 1$  the same as from  $r = 1/4$  to  $r = 1/2$ , and again the same for  $r = 1/8$  to  $r = 1/4$ . Thus the divergence comes from small scales, which allows us to approximate  $R_0''(u_a(y) - u_b(y)) \approx R_0''(u_a(x) - u_b(x))$ . This is formally an analysis of the

theory via an operator product expansion. For an introduction and applications see [3, 118].

Equation (57) is regularized with cutoffs  $a$  and  $L$ . It is convenient to use  $\epsilon > 0$  (what we need anyway), which allows us to take  $a \rightarrow 0$  and  $L \rightarrow \infty$  while keeping  $m$  finite, as the latter appears as the harmonic well introduced in section 2.11. The integral in that limit becomes

$$\begin{aligned} I_1 &:= \begin{array}{c} \bullet \text{---} \bullet \\ \text{---} \\ \bullet \end{array} = \int_{x-y} C(x-y)^2 = \int_k \frac{1}{(k^2 + m^2)^2} \\ &= \frac{m^{-\epsilon}}{\epsilon} \frac{2\Gamma(1 + \frac{\epsilon}{2})}{(4\pi)^{d/2}}. \end{aligned} \quad (58)$$

It is the standard one-loop diagram of massive  $\phi^4$ -theory<sup>11</sup>.

Setting  $u = u_a(x) - u_b(x)$ , we obtain for the effective disorder correlator  $R(u)$  at one-loop order with all combinatorial factors as given above,

$$R(u) = R_0(u) + \left[ \frac{1}{2} R_0''(u)^2 - R_0''(u) R_0''(0) \right] I_1 + \dots \quad (60)$$

We can now study its flow, by taking a derivative w.r.t.  $m$ , and replacing on the rhs  $R_0$  with  $R$ , as given by the above equation. This leads to

$$-m \frac{\partial}{\partial m} R(u) = \left[ \frac{1}{2} R''(u)^2 - R''(u) R''(0) \right] \epsilon I_1. \quad (61)$$

This equation still contains the factor of  $\epsilon I_1$ , which has both a scale  $m^{-\epsilon}$ , as a finite amplitude. There are two convenient ways out of this: we can parameterize the flow by the integral  $I_1$  itself, defining

$$\partial_\ell R(u) := - \frac{\partial}{\partial I_1} R(u) = \frac{1}{2} R''(u)^2 - R''(u) R''(0). \quad (62)$$

This is convenient to study the flow numerically.

To arrive at a fixed point one needs to rescale both  $R$  and  $u$ , in order to make them dimensionless. The field  $u$  has dimension  $u \sim L^\zeta \sim m^{-\zeta}$ , whereas the dimension of  $R$  can be read off from equation (54), namely  $R(u) \sim R''(u)^2 m^{-\epsilon}$ , equivalent to  $R \sim m^{\epsilon-4\zeta}$ . The dimensionless effective disorder  $\tilde{R}$ , as function of the dimensionless field  $\mathbf{u}$  is then defined as

$$\tilde{R}(\mathbf{u}) := \epsilon I_1 m^{4\zeta} R(u = \mathbf{u} m^{-\zeta}). \quad (63)$$

Inserting this into equation (62), we arrive at<sup>12</sup>

$$\begin{aligned} \partial_\ell \tilde{R}(\mathbf{u}) &:= -m \frac{\partial}{\partial m} \tilde{R}(\mathbf{u}) \\ &= (\epsilon - 4\zeta) \tilde{R}(\mathbf{u}) + \zeta \mathbf{u} \tilde{R}'(\mathbf{u}) + \frac{1}{2} \tilde{R}''(\mathbf{u})^2 - \tilde{R}''(\mathbf{u}) \tilde{R}''(0). \end{aligned} \quad (64)$$

<sup>11</sup> The trick to calculate integrals of this type is to write

$$\frac{1}{(k^2 + m^2)^2} = \int_0^\infty ds s e^{-s(k^2 + m^2)}. \quad (59)$$

The integral over  $k$  is then the one-dimensional integral to the power of  $d$ . Finally one integrates over  $s$ .

<sup>12</sup>  $\ell$  in equations (62) and (64) is different.

This is the functional RG flow equation for the renormalized dimensionless disorder  $\tilde{R}(u)$ , first derived in [119] within the Wilson scheme<sup>13</sup>. We will in general set  $\mathbf{u} \rightarrow u$  in the above equation, to simplify notations, and suppress the tilde as long as this does not lead to confusion.

We would like to stress what we already said in section 2.1, namely that the flow equations we derived as functions of  $m$  have a very intuitive interpretation: since the strength  $m^2$  of the confining potential (5) is a parameter of the experimental system which does not renormalise (see the next section 2.3), the RG equation can be taken quite literally: what happens if in an experiment or a simulation the confining potential is weakened? In a peeling or unzipping experiment (sections 2.32 and 3.17) this even happens during the experiment. The answer is that for  $m \rightarrow \infty$ , one sees the microscopic disorder, while for smaller  $m$  an effective scale-dependent disorder is measured. This is explained in detail in section 2.11. Before doing this, let us first ensure that  $m$  does not renormalize (next section 2.3), and then study what happens if  $m$  is lowered (section 2.4).

### 2.3. Statistical tilt symmetry

We claim that there are no renormalizations of the quadratic parts of the action which are replicated copies of

$$\mathcal{H}_0[u] := \mathcal{H}_{\text{el}}[u] + \mathcal{H}_{\text{conf}}[u] \quad (65)$$

given in equations (4) and (5). This is due to the statistical tilt symmetry (STS)

$$u_a(x) \rightarrow u_a(x) + \alpha x. \quad (66)$$

As the interaction is proportional to  $R(u_a(x) - u_b(x))$ , the latter is invariant under the transformation (66). The change in  $\mathcal{H}_0[u]$  becomes

$$\begin{aligned} \delta \mathcal{H}_0[u] = & c \int d^d x \left[ \nabla u(x) \alpha + \frac{1}{2} \alpha^2 \right] \\ & + m^2 \int d^d x \left[ u(x) \alpha x + \frac{1}{2} \alpha^2 x^2 \right]. \end{aligned} \quad (67)$$

To render the presentation clearer, the elastic constant  $c$  set to  $c = 1$  in equation (30) has been introduced. The important observation is that all fields  $u$  involved are *large-scale* variables, which are also present in the renormalized action, where they change according to  $\mathcal{H}^{\text{ren}}[u] \rightarrow \mathcal{H}^{\text{ren}}[u] + \delta \mathcal{H}^{\text{ren}}[u]$ . Since one can either first renormalize and then tilt, or first tilt and then renormalize, we obtain  $\delta \mathcal{H}_0^{\text{ren}}[u] = \delta \mathcal{H}_0^{\text{bare}}[u]$ . This means that neither the elastic constant  $c$ , nor  $m$  change under renormalization.

### 2.4. Solution of the FRG equation, and cusp

We now analyze the FRG flow equations (62) and (64). To simplify our arguments, we first derive them twice w.r.t.  $u$ , to

obtain flow equations for  $\Delta(u) \equiv -R''(u)$ . This yields

$$\text{No rescaling: } \partial_\ell \Delta(u) = -\partial_u^2 \frac{1}{2} \left[ \Delta(u) - \Delta(0) \right]^2, \quad (68)$$

$$\text{With rescaling: } \partial_\ell \tilde{\Delta}(u) = (\epsilon - 2\zeta) \tilde{\Delta}(u) + \zeta u \tilde{\Delta}'(u)$$

$$- \partial_u^2 \frac{1}{2} \left[ \tilde{\Delta}(u) - \tilde{\Delta}(0) \right]^2. \quad (69)$$

For concreteness, consider equation (68), and start with an analytic function,

$$\Delta_{\ell=0}(u) = e^{-u^2/2}. \quad (70)$$

According to our classification, this is microscopically RF disorder. Since  $\Delta(u) - \Delta(0)$  grows quadratically in  $u$  at small  $u$ , the rhs of equation (68) also grows  $\sim u^2$  at  $u = 0$ , and both  $\Delta(0)$  as well as  $\Delta'(0^+)$  do not flow in the beginning. This can be seen on the plots of figure 5.

Integrating further, a cusp forms, i.e.  $\Delta''(0) \rightarrow \infty$ , and as a consequence  $\Delta'(0^+)$  becomes non-zero. This is best seen by taking two more derivatives of equation (68), and then taking the limit of  $u \rightarrow 0$ ,

$$\partial_\ell \Delta''(0^+) = -3\Delta''(0^+)^2 - 4\Delta'(0^+)\Delta'''(0^+). \quad (71)$$

Since in the beginning  $\Delta'(0^+) = 0$ , only the first term survives. Its behavior crucially depends on the sign of  $\Delta''(0)$ . In the example (70),  $\Delta''_{\ell=0}(0) < 0$ . This is true in general, as can be seen by rewriting equation (10) for the unrescaled microscopic disorder correlator at  $x = x'$ , as

$$\Delta(0) - \Delta(u - u') = \frac{1}{2} \langle [F(x, u) - F(x, u')]^2 \rangle \geq 0. \quad (72)$$

Developing the lhs for small  $u - u'$  with a vanishing first derivative implies that  $\Delta''(0) < 0$ , valid also for the rescaled  $\Delta''(0)$ .

Integrating equation (71) with this sign yields

$$\Delta''_\ell(0) = \frac{\Delta''_0(0)}{1 + 3\Delta''_0(0)\ell} = -\frac{1}{3} \frac{1}{\ell_c - \ell}, \quad (73)$$

$$\ell_c = -\frac{1}{3\Delta''_0(0)} \xrightarrow{\Delta''_0(0) \rightarrow -1} \frac{1}{3}.$$

In the last equality we used the initial condition (70). With this,  $\Delta''_\ell(0)$  diverges at  $\ell = \frac{1}{3}$ , thus  $\Delta_\ell(u)$  acquires a cusp, i.e.  $\Delta'_\ell(0^+) \neq 0$  for all  $\ell > 1/3$ . Physically, this is the scale where multiple minima appear. In terms of the Larkin-scale  $L_c$  defined in section 1.7

$$\ell_c = \ln(L_c/a). \quad (74)$$

Our numerical solution shows the appearance of the cusp only approximately, see the inset in the top right plot of figure 5. This discrepancy comes from discretization errors. It is indeed not simple to numerically integrate equation (68) for large times, as  $\Delta''_\ell(0)$  diverges at  $\ell = \ell_c$ , and all further derivatives at  $u = 0^+$  were extracted from numerical *extrapolations* of the obtained functions, in the limit of  $u \rightarrow 0$ .

<sup>13</sup> The RG flow equation (64) is at this order *independent* of the RG scheme. Universal quantities are scheme-independent to all orders [2, 112–114, 118].

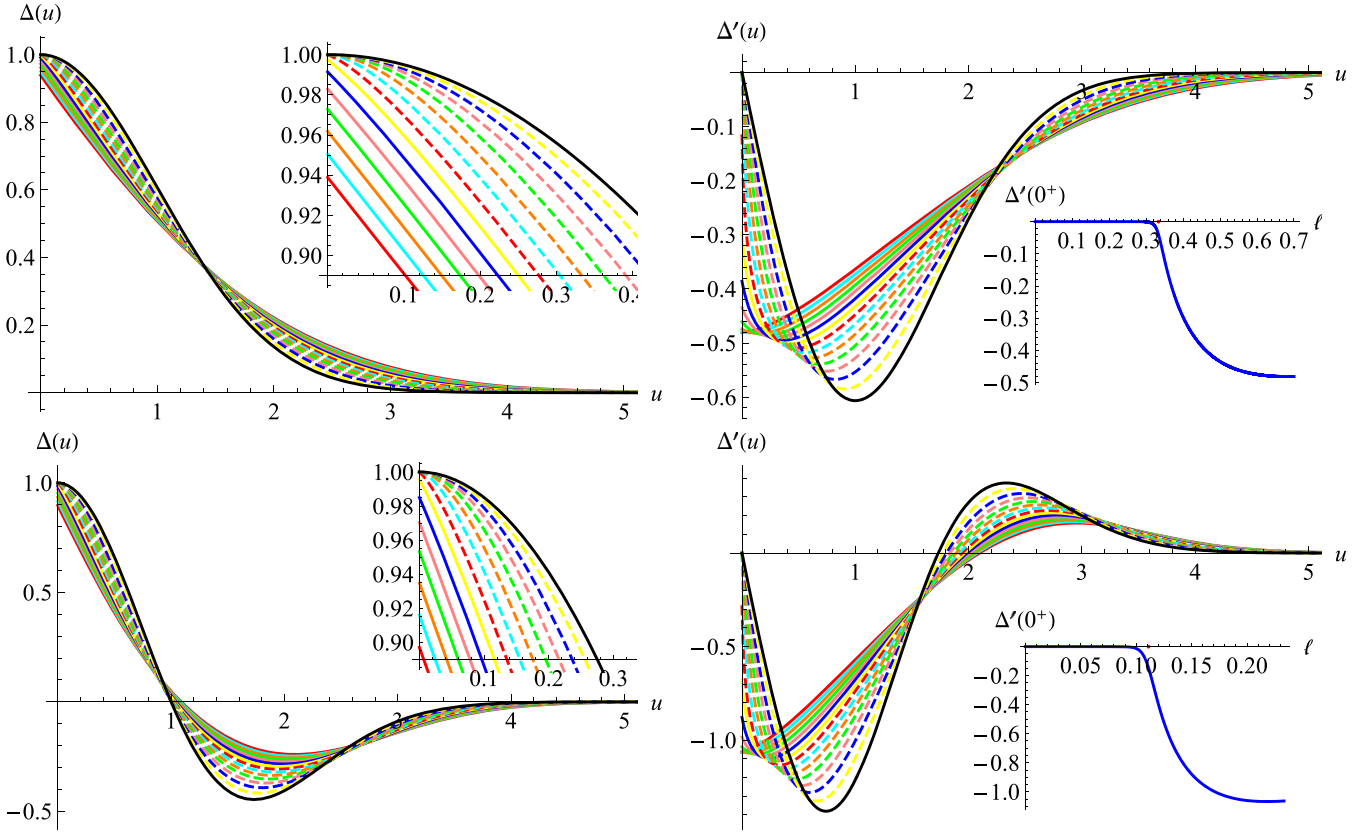


**Figure 5.** (Top) Change of  $\Delta(u) := -R''(u)$  under renormalization and formation of the cusp. (Left) Explicit numerical integration of equation (62), starting from  $\Delta(u) = e^{-u^2/2}$  (in solid black, top curve for  $u \rightarrow 0$ ). The function at scale  $\ell$  is shown in steps of  $\delta\ell = 1/20$ . (Inset) Blow-up. (Right) plots of  $\Delta'(u)$ . (Inset)  $\Delta'(0^+)$  as a function of  $\ell$ . The cusp appears for  $\ell = 1/3$  (red dot); dashed lines are before appearance of the cusp, and solid lines after. (Bottom) The same as the top line for RB disorder, starting from  $R(u) = e^{-u^2/2}$ ; the cusp appears for  $\ell = 1/9$ ;  $\delta\ell = 1/60$ .

Interpreting derivatives in this sense is an *assumption*, to be justified, without which one cannot continue to integrate the flow equations. In this spirit, let us again look at the flow equation for  $\Delta(0)$ , now including the rescaling terms,

$$\partial_\ell \tilde{\Delta}(0) = (\epsilon - 2\zeta)\tilde{\Delta}(0) - \tilde{\Delta}'(0^+)^2. \quad (75)$$

This equation tells us that as long as  $\Delta'(0^+) = 0$ ,

$$\zeta_{\ell < \ell_c} \simeq \zeta_{\text{DR}} = \frac{\epsilon}{2} = \frac{4-d}{2}, \quad (76)$$

the dimensional-reduction result. Beyond that scale, we have (as long as we are at least close to a fixed point)

$$\zeta_{\ell > \ell_c} = \frac{\epsilon}{2} - \frac{\Delta'(0^+)^2}{\Delta(0)} < \frac{\epsilon}{2}, \quad (77)$$

since both  $\Delta'(0^+)^2$  and  $\Delta(0)$  are positive.

Let us repeat our analysis for RB disorder, starting from the microscopic disorder

$$R_0(u) = e^{-u^2/2} \iff \Delta(u) = e^{-u^2/2}(1-u^2). \quad (78)$$

This is shown on the bottom of figure 5. Phenomenologically, the scenario is rather similar, with a critical scale  $\ell_c = 1/9$  instead of  $1/3$ .

## 2.5. Fixed points of the FRG equation

We had seen in the last section that integrating the flow-equation explicitly is rather cumbersome; moreover, an estimation of the critical exponent  $\zeta$  will be rather imprecise. For this purpose, it is better to directly search for a solution of the fixed-point equation (69), i.e.  $\partial_\ell \tilde{\Delta}(u) = 0$ ,

$$0 = (\epsilon - 2\zeta)\tilde{\Delta}(u) + \zeta u \tilde{\Delta}'(u) - \partial_u^2 \frac{1}{2} [\tilde{\Delta}(u) - \tilde{\Delta}(0)]^2. \quad (79)$$

We start our analysis with situations where  $u$  is unbounded, as for the position of an interface. Then the fixed point is not unique; indeed, if  $\tilde{\Delta}(u)$  is solution of equation (79), so is

$$\tilde{\Delta}_\kappa(u) := \kappa^{-2} \tilde{\Delta}(\kappa u). \quad (80)$$

## 2.6. Random-field (RF) fixed point

There is one solution we can find analytically: to this purpose integrate equation (79) from 0 to  $\infty$ , assuming that  $\tilde{\Delta}(u)$  has a cusp at  $u = 0$ , but no stronger singularity,

$$0 = \int_0^\infty (\epsilon - 2\zeta)\tilde{\Delta}(u) + \zeta u \tilde{\Delta}'(u) - \partial_u^2 \frac{1}{2} [\tilde{\Delta}(u) - \tilde{\Delta}(0)]^2 du. \quad (81)$$

Integrating the second term by part, and using that the last term is a total derivative which vanishes both at 0 and at  $\infty$  yields

$$0 = (\epsilon - 3\zeta) \int_0^\infty \tilde{\Delta}(u) du. \quad (82)$$

This equation has two solutions: either the integral vanishes, which is the case for RB disorder<sup>14</sup>, or

$$\zeta_{\text{RF}} = \frac{\epsilon}{3}. \quad (83)$$

This is the exponent (22) (at  $N = 1$ ) predicted by a Flory argument. Let us remark that equation (81) remains valid to all orders in  $\epsilon$ , as long as  $\Delta(u)$  is the second derivative of  $R(u)$ , s.t. the additional terms at two- and higher-loop order are all total derivatives, as is the last term in equation (79).

Let us pursue our analysis with the solution (83). Inserting equation (83) into equation (79), and setting

$$\tilde{\Delta}(u) = \frac{\epsilon}{3} y(u) \quad (84)$$

yields

$$\partial_u \left[ u y(u) - \frac{1}{2} \partial_u (y(u) - y(0))^2 \right] = 0. \quad (85)$$

This implies that the expression in the square bracket is a constant, fixed to 0 by considering either the limit of  $u \rightarrow 0$  or  $u \rightarrow \infty$ . Simplifying yields

$$u y(u) + [y(0) - y(u)] y'(u) = 0. \quad (86)$$

Dividing by  $y(u)$  and integrating once again gives

$$\frac{u^2}{2} - y(u) + y(0) \ln(y(u)) = \text{const}. \quad (87)$$

Let us now use equation (80) to set  $y(0) \rightarrow 1$ . This fixes the constant to  $-1$ . Dropping the argument of  $y$ , we obtain

$$y - \ln(y) = 1 + \frac{u^2}{2}. \quad (88)$$

This is plotted on figure 6.

## 2.7. Random-bond (RB) and tricritical fixed points

The other option for a fixed point is to have the integral in equation (82) vanish,

$$\int_0^\infty \tilde{\Delta}_{\text{RB}}(u) = 0. \quad (89)$$

A numerical analysis of the fixed-point equation (79) proceeds as follows: choose  $\tilde{\Delta}(0) = 1$ ; choose  $\zeta$ ; solve the differential equation (79) for  $\tilde{\Delta}''(u)$ . Integrate the latter from  $u = 0$  to  $u = \infty$ . In practice, to avoid numerical problems for  $u \approx 0$ , one first solves the differential equation in a Taylor-expansion around 0; as the latter does not converge for large  $u$  one then

solves, with the information from the Taylor series evaluated at  $u = 0.1$ , the differential equation numerically up to  $u_\infty \approx 30$ . One then reports, as a function of  $\zeta$ , the value of  $\tilde{\Delta}(u_\infty)$ . As in quantum mechanics, one finds that there are several discrete values of  $\zeta$  with  $\tilde{\Delta}(u_\infty) = 0$ . The largest value of  $\zeta$  is the one given in equation (83), where  $\tilde{\Delta}(u)$  has no zero crossing. The next smaller value of  $\zeta$  is

$$\zeta_{\text{RB}} = 0.208\,298\epsilon. \quad (90)$$

The corresponding function is plotted on figure 6 (right). It has one zero-crossing. Consistent with equation (82), it integrates to zero. This is the RB fixed point. It is surprisingly close, but distinct, from the Flory estimate (21),  $\zeta = \epsilon/5$ .

For  $\epsilon = 3$  we have the directed polymer ( $d = 1$ ) in dimension  $N = 1$ , which has roughness  $\zeta_{d=1}^{\text{RB}} = \frac{2}{3}$ . Our result (90) yields  $\zeta(d = 1) = 0.624\,894 + \mathcal{O}(\epsilon^2)$ . This is quite good, knowing that  $\epsilon = 3$  is rather large. This value gets improved at two-loop order (see section 2.13), with  $\zeta(d = 1) = 0.686\,616 + \mathcal{O}(\epsilon^3)$ . Despite the ‘strange cusp’, it seems the method works!

The next solution is at

$$\zeta_{\text{crit}} = 0.143\,66\epsilon. \quad (91)$$

It has two zero-crossings, and corresponds to a tricritical point. We do not know of any physical realization.

## 2.8. Generic long-ranged fixed point

If  $\zeta$  is not one of these special values, then the solution of the fixed-point equation (79) decays algebraically: suppose that  $\Delta(u) \sim u^\alpha$ . Then the first two terms of equation (79) are dominant over the last one, as long as  $\alpha < 2$ . Solving equation (79) in this limit one finds

$$\Delta_\zeta(u) \sim u^{2-\frac{\epsilon}{\zeta}} \quad \text{for } u \rightarrow \infty. \quad (92)$$

An important application are the ABBM and BFM models discussed in sections 4.3 and 4.5, for which

$$\zeta_{\text{ABBM}} = \epsilon, \quad \Delta_{\text{ABBM}}(0) - \Delta_{\text{ABBM}}(u) = \sigma|u|, \quad (93)$$

such that the correlations of the random forces have the statistics of a RW. One easily checks that the flow equation (62) vanishes for all  $u > 0$ . In this case  $\Delta(0)$  is formally infinite, s.t. the bound (77) does not apply. Generically, however, equation (77) applies, implying that the exponent in equation (92) is negative, and  $\Delta_\zeta(u)$  decays algebraically. This is what we mostly see in numerical solutions of the fixed-point equation (79).

## 2.9. Charge-density wave (CDW) fixed point

In the above considerations, we had supposed that  $u$  can take any real value. There are important applications where the disorder is periodic, or  $u$  is a phase between 0 and  $2\pi$ . This is the case for the CDWs introduced above. To be consistent with the standard conventions employed in the literature [120–125], we take the period of the disorder to be 1. One checks that the

<sup>14</sup> For RB disorder

$$\int_0^\infty du \tilde{\Delta}(u) = - \int_0^\infty du \tilde{R}''(u) = \tilde{R}'(0) - \tilde{R}'(\infty) = 0.$$

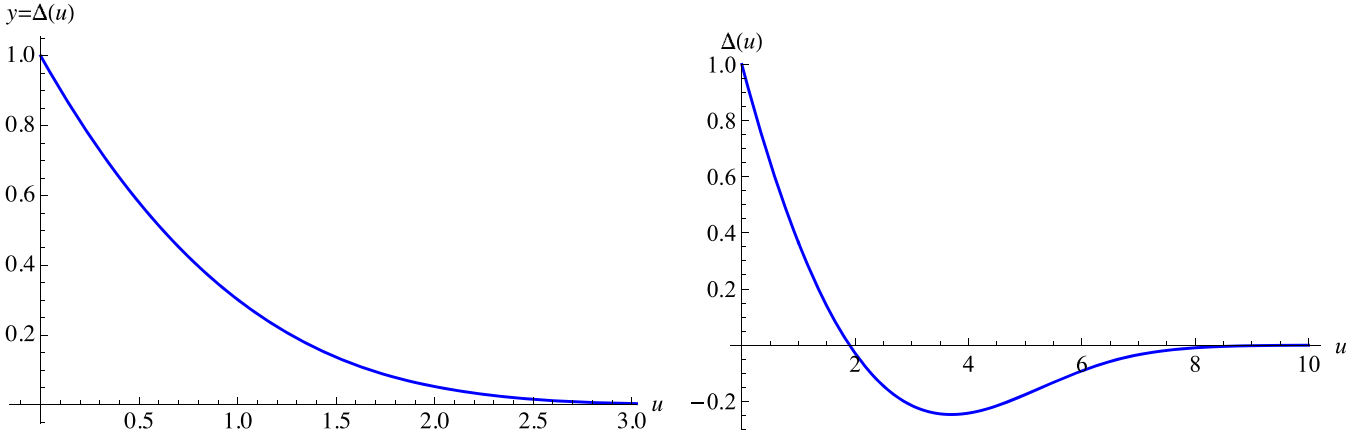


**Figure 6.** (Left) The RF fixed point (88) with  $\zeta_{\text{RP}} = \frac{\epsilon}{3}$ . (Right) The RB fixed point (90), with  $\zeta_{\text{RB}} = 0.208\,298\epsilon$ .

following ansatz is a fixed point of the FRG equation (79)

$$\begin{aligned}\zeta_{\text{RP}} &= 0, \\ \Delta_{\text{RP}}(u) &= \frac{g}{12} - \frac{g}{2}u(1-u), \\ 0 &\leq u \leq 1.\end{aligned}\quad (94)$$

This ansatz is unique, due to the following three constraints: (i)  $\zeta = 0$ , as the period is fixed and cannot change under renormalization. (ii)  $\Delta(u) = \Delta(-u) = \Delta(1-u)$  due to the symmetry  $u \rightarrow -u$ , and periodicity. Thus  $\Delta(u)$  is a polynomial in  $u(1-u)$ . (iii) A polynomial of degree 2 in  $u$  closes under RG. (iv) The integral  $\int_0^1 du \Delta(u) = 0$ , since  $\Delta(u) = -R''(u)$ , and  $R(u)$  itself is periodic. The fixed point has

$$g = \frac{\epsilon}{3} + \dots \quad (95)$$

Instead of a universal scaling exponent  $\zeta$ , the latter vanishes,  $\zeta = 0$ . As a consequence, the two-point function is logarithmic in all dimensions, with a universal amplitude given in equations (119)–(120b). Apart from geometric prefactors, this amplitude is simply the fixed-point value  $g$ .

### 2.10. The cusp and shocks: a toy model

Let us give a simple argument why a cusp is a physical necessity, and not an artifact. The argument is quite old and appeared probably first in the treatment of correlation-functions by shocks in Burgers turbulence. It became popular in [126]. We want to solve the problem for a single degree of freedom which sees both disorder and a parabolic trap centered at  $w$ , which we can view as a spring attached to the point  $w$ . This is graphically represented on figure 7 (upper left), with the quenched disorder realization having roughly a sinusoidal shape. For a given disorder realization  $V(u)$ , the minimum of the potential as a function of  $w$  is

$$\hat{V}(w) := \min_u \left[ V(u) + \frac{m^2}{2}(u-w)^2 \right]. \quad (96)$$

This is reported on figure 7 (upper right). Note that it has non-analytic points, which mark the transition from one minimum

to another. The remaining parts are parabolic, and stem almost entirely from the spring, as long as the minima of the disorder are sharp, i.e. have a high curvature as compared to the spring. This is rather natural, knowing that the disorder varies on microscopic scales, while the confining potential changes on macroscopic scales.

Taking the derivative of the potential leads to the force in figure 7 (lower left). It is characterized by almost linear pieces, and shocks (i.e. jumps). Let us now calculate the correlator of forces  $F(u) := -\nabla \hat{V}(u)$ ,

$$\Delta(w) := \overline{F(w')F(w'-w)^c}. \quad (97)$$

Here the average is over disorder realizations, or equivalently  $w'$ , on which it should not depend. Let us analyze its behavior at small distances,

$$\begin{aligned}\Delta(0) - \Delta(w) &= \frac{1}{2} \overline{[F(w') - F(w'-w)]^2} \\ &= \frac{1}{2} p_{\text{shock}}(w) \langle \delta F^2 \rangle + \mathcal{O}(w^2).\end{aligned}\quad (98)$$

As written, the leading contribution is proportional to the probability to have a shock (jump) inside the window of size  $w$ , times the expectation of the second moment of the force jump  $\delta F$ . If shocks are not dense, then the probability to have a shock is given by the density  $\rho_{\text{shock}}$  of shocks times the size  $w$  of the window, i.e.

$$p_{\text{shock}}(w) \simeq \rho_{\text{shock}}|w|. \quad (99)$$

Let us now relate  $\delta F$  to the change in  $u$ ; as the spring-constant is  $m^2$ ,

$$\delta F = m^2 \delta u \equiv m^2 S. \quad (100)$$

Here we have introduced the *avalanche size*  $S := \delta u$ . Putting everything together yields

$$\Delta(0) - \Delta(w) = \frac{m^4}{2} \langle S^2 \rangle \rho_{\text{shock}}|w| + \mathcal{O}(w^2). \quad (101)$$

We can eliminate  $\rho_{\text{shock}}$  by observing that on average the particle position  $u$  follows the spring, i.e.

$$w = \overline{u(w'+w) - u(w')} = \langle S \rangle \rho_{\text{shock}} w. \quad (102)$$

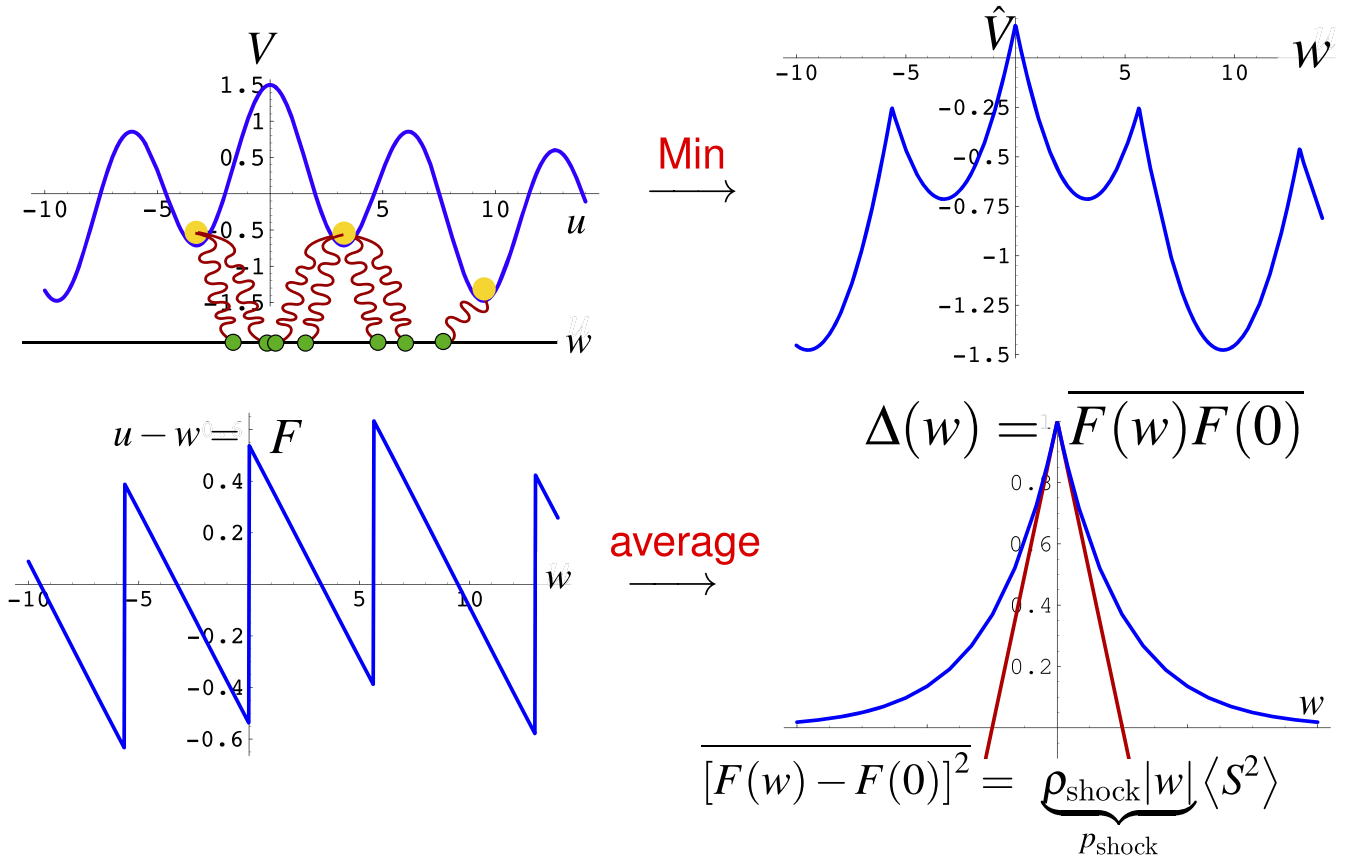


**Figure 7.** Generation of the cusp, as explained in the main text.

This yields

$$\rho_{\text{shock}} = \frac{1}{\langle S \rangle}. \quad (103)$$

Expanding equation (101) in  $w$ , and retaining only the term linear in  $w$  yields

$$-\Delta'(0^+) = m^4 \frac{\langle S^2 \rangle}{2 \langle S \rangle}. \quad (104)$$

We just showed that having a cusp non-analyticity in  $\Delta(w)$  is a necessity if the system under consideration has shocks or avalanches. The latter are a consequence of metastability (i.e. existence of local minima), thus metastability implies a cusp in  $\Delta(w)$ .

### 2.11. The effective disorder correlator in the field-theory

The above toy model can be generalized to the field theory [127]. Consider an interface in a random potential, as given by equations (4)–(6)

$$\mathcal{H}_{\text{tot}}^w[u] = \int_x \frac{m^2}{2} [u(x) - w]^2 + \mathcal{H}_{\text{el}}[u] + \mathcal{H}_{\text{dis}}[u]. \quad (105)$$

Physically, the role of the well is to forbid the interface to wander off to infinity. This avoids that observables are dominated by rare events. In each sample (i.e. disorder configuration), and given  $w$ , one finds the minimum-energy configuration. The

corresponding ground-state energy, or effective potential, is

$$\hat{V}(w) := \min_{u(x)} \mathcal{H}_{\text{tot}}^w[u]. \quad (106)$$

Let us call  $u_w^{\text{min}}(x)$  this configuration. Its center-of-mass position is

$$u_w := \frac{1}{L^d} \int_x u_w^{\text{min}}(x). \quad (107)$$

Both  $\hat{V}(w)$  and  $u_w$  vary with  $w$  as well as from sample to sample. Let us now look at their second cumulants. The effective potential  $\hat{V}(w)$  defines a function  $R(w)$ ,

$$R(w - w') := L^{-d} \overline{\hat{V}(w) \hat{V}(w')^c}. \quad (108)$$

This is the same function as computed in the field theory, defined there from the zero-momentum action. The factor of volume  $L^d$  is necessary. The interface is correlated over a length  $\xi = 1/m$ , while its width  $u^2$  is bounded by the confining well. This means that the interface is made of roughly  $(L/\xi)^d$  independent pieces of length  $\xi$ : equation (108) expresses the central-limit theorem and  $R(w)$  measures the second cumulant of the disorder seen by any one of the independent pieces.

The nice thing about equation (108) is that it can be measured. One varies  $w$  and computes (numerically) the new ground-state energy, finally averaging over disorder

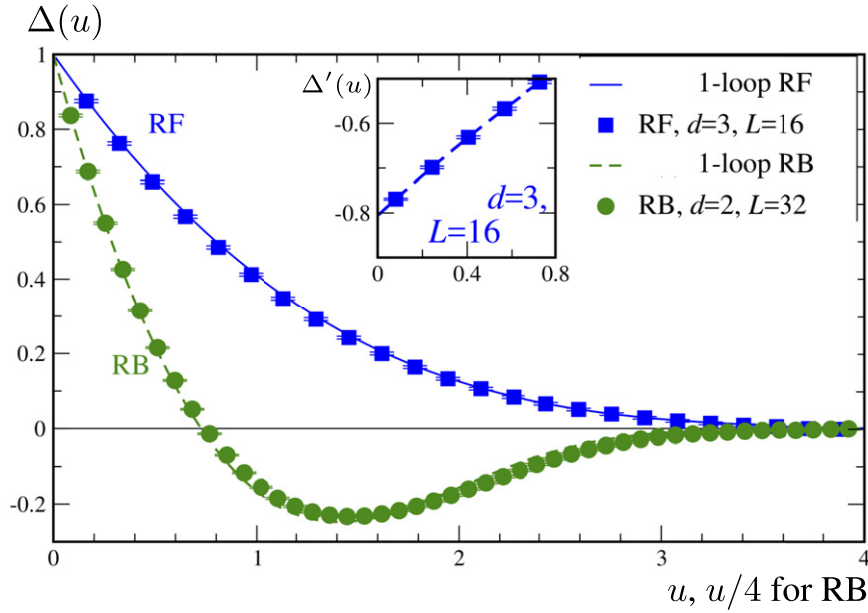


**Figure 8.** Filled symbols show numerical results for  $\Delta(u)$ , a normalized form of the interface displacement correlator  $-R''(u)$  (equation (111)), for  $D = 2 + 1$  RF and  $D = 3 + 1$  RB disorders. These suggest a linear cusp. The inset plots the numerical derivative  $\Delta'(u)$ , with intercept  $\Delta'(0^+) \approx -0.807$  from a quadratic fit (dashed line). The points are for confining wells with width given by  $m^2 = 0.02$ . Comparisons to one-loop FRG predictions (curves) are made with no adjustable parameters. Reprinted figure with permission from [128], Copyright (2007) by the American Physical Society.

realizations. In fact, what is even easier to measure are the fluctuations of the center-of-mass position  $u_w$ , related to the total force acting on the interface. To see this, write the condition for the interface to be in a minimum-energy configuration,

$$0 = -\frac{\delta\mathcal{H}[u]}{\delta u(x)} = \nabla^2 u(x) - m^2[u(x) - w] + F(x, u(x)),$$

$$F(x, u) = -\partial_u V(x, u). \quad (109)$$

Integrating over space, and using periodic boundary conditions, the term  $\sim \nabla^2 u(x)$  vanishes. At the minimum-energy configuration  $u_w^{\min}(x)$ , this yields

$$m^2(u_w - w) = \frac{m^2}{L^d} \int_x u_w^{\min}(x) - w$$

$$= \frac{1}{L^d} \int_x F(x, u_w^{\min}(x)) =: \hat{F}(w). \quad (110)$$

The last equation defines the effective force  $\hat{F}(w)$ . Its second cumulant reads

$$\overline{\hat{F}(w)\hat{F}(w')^c} \equiv m^4 \overline{[w - u_w][w' - u_{w'}]^c}$$

$$= L^{-d} \Delta(w - w'). \quad (111)$$

Taking two derivatives of equation (108), one verifies that the effective correlators for potential and force are related by  $\Delta(u) = -R''(u)$ , as in the microscopic relation (11). Equation (104) remains valid (without an additional factor of  $L^d$ ).

## 2.12. $\Delta(u)$ and the cusp in simulations

A numerical check has been performed in [128], using a powerful exact-minimization algorithm, which finds the ground state in a time polynomial in the system size. The result of these measurements is presented in figure 8. The function  $\Delta(u)$  is normalized to 1 at  $u = 0$ , and the  $u$ -axis is rescaled (to yield integral 1) to eliminate all non-universal scales. As a result, the plot is parameter free, thus what one compares is purely the shape. It has several remarkable features. Firstly, it shows that a linear cusp exists in all dimensions. Next it is very close to the one-loop prediction. Even more remarkably the statistics is good enough to reliably estimate the deviations from the two-loop predictions of [125], see figure 9.

While we vary the position  $w$  of the center of the well, it is not a real motion. Rather it means to find the new ground state given  $w$ . Literally *moving*  $w$  is another interesting possibility: it measures the universal properties of the so-called *depinning transition*, see section 3.

*A technical point.* A field theory is usually defined by its partition function  $\mathcal{Z}[J]$  in presence of an applied field  $J$ . To obtain the effective action  $\Gamma(u)$ , one evaluates the free energy  $\mathcal{F}[J] := -kT \ln \mathcal{Z}[J]$ , and then performs a Legendre transform from  $\mathcal{F}[J]$  to  $\Gamma[u]$ . The effective action, solution of the FRG flow equation, is the two-replica term in  $\Gamma[u]$ , and not  $\mathcal{F}[J]$  itself. When measuring the force-force correlations in equation (111), these are technically part of  $\mathcal{F}[J = m^2 w]$ . Passing from  $\mathcal{F}[J]$  to  $\Gamma[u]$  is achieved by amputating the correlation function. Due to the STS discussed in section 2.3, the latter does not renormalize. For the zero-mode (zero momentum) we consider, this amounts to multiplying twice with  $m^2$ ,

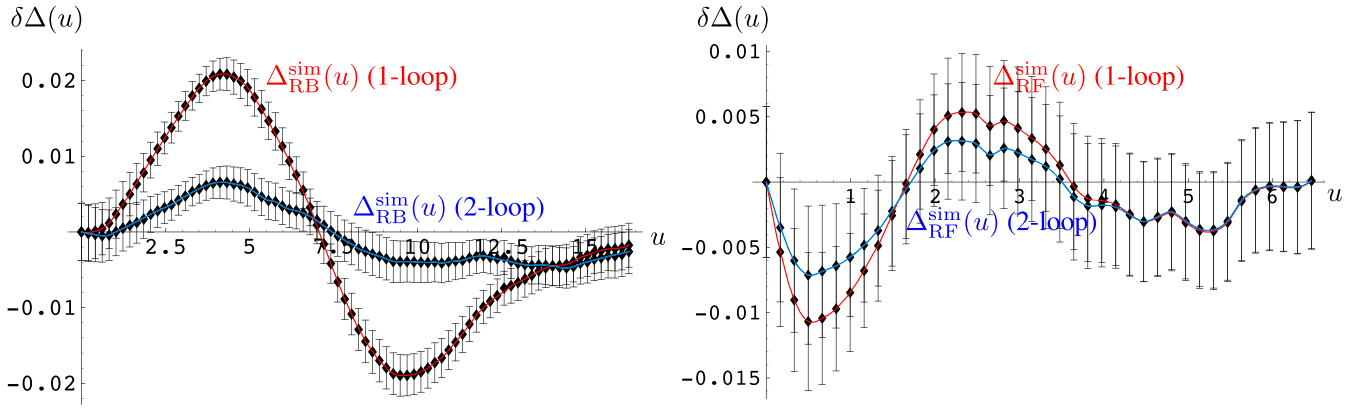


**Figure 9.** The measured  $\Delta(u)$  in equilibrium with the one-loop (red) and two-loop corrections (blue) subtracted. (Left) RB-disorder  $d = 2$ . (Right) RF-disorder  $d = 3$ . One sees that the two-loop corrections improve the precision, and that the second-order correction is stronger in  $d = 2$  than in  $d = 3$ .

resulting in the prefactor of  $m^4$  in equation (111). In the dynamics, this remains true in the limit of a vanishing driving velocity. These points are further discussed in [82, 127–131].

### 2.13. Beyond one-loop order

We have successfully applied functional renormalization at one-loop order. From a field theory, we demand more. Namely that it

- (a) be renormalizable<sup>15</sup>,
- (b) allows for systematic corrections beyond one-loop order,
- (c) and thus allows us to make universal predictions.

This has been a puzzle since 1986, and it was even suggested that the theory is not renormalizable due to the appearance of terms of order  $\epsilon^{\frac{3}{2}}$  [132]. Why is the next order so complicated? The reason is that it involves terms proportional to  $R'''(0)$ . A look at figure 5 or 8 explains the puzzle. Shall we use the symmetry of  $R(u)$  to conclude that  $R'''(0)$  is 0? Or shall we take the left-hand or right-hand derivatives, related by

$$R'''(0^+) := \lim_{u \rightarrow 0^+} R'''(u) = - \lim_{u \rightarrow 0^-} R'''(u) =: -R'''(0^-). \quad (112)$$

Below, we present the solution of this puzzle, obtained at two- and three-loop order. This is then extended to finite  $N$  (section 2.17), compared to large  $N$  (section 2.18), and the driven dynamics (section 3).

The flow-equation was first calculated at two-loop order without the anomalous terms  $\sim R'''(0^+)^2$  [133]. The full result with the necessary anomalous terms was first obtained at two-loop order [123, 125, 134–136], and later extended to three-loop order [40, 41]

$$\begin{aligned} \partial_t \tilde{R}(u) &= (\epsilon - 4\zeta) \tilde{R}(u) + \zeta u \tilde{R}'(u) \\ &+ \frac{1}{2} \tilde{R}''(u)^2 - \tilde{R}''(u) \tilde{R}''(0) \end{aligned}$$

<sup>15</sup> Renormalizability is a key concept of (perturbative) field theory about the organization of the leading divergences in perturbation theory, which imposes constraints on higher-order diagrams. These constraints were historically important to derive the RG equation at two-loop order [123, 125].

$$\begin{aligned} &+ \left( \frac{1}{2} + C_1 \epsilon \right) [(\tilde{R}''(u) - \tilde{R}''(0)) \tilde{R}'''(u)^2 - \tilde{R}'''(0^+)^2 \tilde{R}''(u)] \\ &+ C_4 \{ \tilde{R}''(u) [\tilde{R}'''(u)^2 \tilde{R}''''(u) - \tilde{R}'''(0^+)^2 \tilde{R}''''(0^+)] \\ &\quad - \tilde{R}''(0^+) \tilde{R}'''(u)^2 \tilde{R}''''(u) \} \\ &+ C_3 [\tilde{R}''(u) - \tilde{R}''(0^+)]^2 \tilde{R}''''(u)^2 \\ &+ C_2 [\tilde{R}'''(u)^4 - 2\tilde{R}'''(u)^2 \tilde{R}'''(0^+)^2] \end{aligned} \quad (113a)$$

$$C_1 = \frac{1}{36} \left[ 9 + 4\pi^2 - 6\psi' \left( \frac{1}{3} \right) \right] = -0.335976, \quad (113b)$$

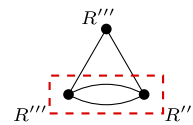
$$C_2 = \frac{3}{4} \zeta(3) + \frac{\pi^2}{18} - \frac{\psi' \left( \frac{1}{3} \right)}{12} = 0.608554, \quad (113c)$$

$$C_3 = \frac{\psi' \left( \frac{1}{3} \right)}{6} - \frac{\pi^2}{9} = 0.585977, \quad (113d)$$

$$C_4 = 2 + \frac{\pi^2}{9} - \frac{\psi' \left( \frac{1}{3} \right)}{6} = 1.414023. \quad (113e)$$

The first line contains the rescaling terms, the second line the result at one-loop order, already given in equation (64). The third line is new; setting there  $\epsilon = 0$  is the two-loop result. All remaining terms (proportional to  $C_1, \dots, C_4$ ) are three-loop contributions, which we put here for completeness.

Consider now the last term of the third line, which involves  $R'''(0^+)^2$  and which we call *anomalous*. The hard task is to fix the prefactor  $-1$ . There are different prescriptions to do this: the sloop-algorithm, recursive construction, reparametrization invariance, renormalizability, potentiality and exact RG [41, 123, 125]. For lack of space, let us consider only renormalizability, a *necessary* property for a field theory. The following two-loop diagram leads to the anomalous term



$$\longrightarrow \frac{1}{2} \left[ (R''(u) - R''(0)) R'''(u)^2 - R''(u) R'''(0^+)^2 \right]. \quad (114)$$

The momentum integral is

$$\triangle = \int_k \int_p \frac{1}{(k^2 + m^2)^2} \frac{1}{p^2 + m^2} \frac{1}{(k+p)^2 + m^2}. \quad (115)$$

In units where the one-loop integral (58) is  $1/\epsilon$ , it reads

$$\frac{\triangle}{[\epsilon \triangle]^2} = \frac{1}{2\epsilon^2} + \frac{1}{4\epsilon} + \mathcal{O}(\epsilon^0). \quad (116)$$

The integral (114) contains a sub-divergence, which is indicated by the red dashed box, and which yields the leading  $1/\epsilon^2$  term in equation (116). Renormalizability demands that this term be canceled by a one-loop counter-term. The latter is unique; it is obtained by replacing  $R(u)$  in the one-loop correction  $\delta R(u) = \frac{1}{2}R''(u)^2 - R''(u)R''(0)$  by  $\delta R(u)$  itself; the last term then yields

$$\delta R''(0) := \lim_{u \rightarrow 0} \delta R''(u) = \lim_{u \rightarrow 0} R'''(u)^2 = R'''(0^+)^2. \quad (117)$$

This fixes the prefactor of the last (anomalous) term in the third line of equation (113a).

A physical requirement is that the disorder correlations remain potential, i.e. that forces are derivatives of a potential. The force–force correlations being  $-R''(u)$ , this means that the flow of  $R'(0^+)$  has to vanish. (The simplest way to see this is to study a periodic potential.) From equation (113a) one can check that this does not remain true if one changes the prefactor of the last term in the third line of equation (113a); thus fixing it.

*RP disorder.* Let us give results for cases of physical interest. First of all, for a periodic potential (RP), which is relevant for CDWs, the fixed-point function can be calculated analytically. With the notations of equations (94) and (95) this reads (with the choice of period 1,  $u \in [0, 1]$ )

$$R_{\text{RP}}(u) = -u^2(1-u)^2 \frac{g}{24} + \text{const.}, \quad (118a)$$

$$\Delta_{\text{RP}}(u) = \frac{g}{12} - \frac{g}{2}u(1-u), \quad (118b)$$

$$g = \frac{\epsilon}{3} + \frac{2\epsilon^2}{9} + \frac{\epsilon^3}{81} \left[ 9 + 2\pi^2 - 18\zeta(3) - 3\psi' \left( \frac{1}{3} \right) \right] + \mathcal{O}(\epsilon^4). \quad (118c)$$

This gives a universal amplitude for the two-point function at two-loop [123] and three-loop order [40],

$$\overline{\ddot{u}(q)\ddot{u}(-q)}|_{q=0} = \frac{g}{6m^d}. \quad (119)$$

This in turn leads to a logarithmic growth of the two-point function in position space. The amplitude is more complicated to extract, as one needs to extract the asymptotic behavior of scaling functions involved in this transformation. Using

equations (4.13)–(4.18) of [40],<sup>16</sup> it can be written as

$$\frac{1}{2} \overline{[u(x) - u(0)]^2} = \frac{gB(d)}{6(4\pi)^{\frac{d}{2}} \Gamma(\frac{d}{2})} \ln \left( \frac{|x|}{L} \right), \quad (120a)$$

$$B(d) = \frac{1 + 0.134567\epsilon}{1 + 1.134567\epsilon} + \mathcal{O}(\epsilon^3). \quad (120b)$$

*RF disorder.* For RF disorder, the argument given in equation (82) is still valid, and  $\zeta = \frac{\epsilon}{3}$  remains valid, equivalent to the Flory estimate (22). The fixed-point function  $\Delta(u)$  changes, and can up to three-loop order be given analytically [40].

*RB disorder.* For RB disorder (short-ranged potential–potential correlation function) we have to solve equation (113a) numerically, order by order in  $\epsilon$ . The result is [40]

$$\zeta_{\text{RB}} = 0.20829804\epsilon + 0.006858\epsilon^2 - 0.01075\epsilon^3 + \mathcal{O}(\epsilon^4). \quad (121)$$

This compares well with numerical simulations, see figure 10. It is also surprisingly close to, but distinct from, the Flory estimate (21),  $\zeta = \epsilon/5$ . For  $d = 1$  ( $\epsilon = 3$ ) it gets close to the exact value [108]

$$\zeta_{\text{RB}}^{d=1} = \frac{2}{3}. \quad (122)$$

The fixed-point function  $\Delta(u)$  can be obtained up to three-loop order numerically [40].

## 2.14. Stability of the fixed point

Having found a fixed point,

$$\partial_t \Delta(u) = \beta[\Delta](u) = 0, \quad (123)$$

one has to ascertain that it is stable. Linear stability is analyzed by considering infinitesimal perturbations of the fixed point

$$\delta\beta[\Delta, z](u) := \frac{d}{d\kappa} \beta[\Delta + \kappa z](u) \Big|_{\kappa=0}. \quad (124)$$

Assuming that  $\Delta(u)$  is a solution of equation (123), the eigenvalue equation reads

$$\delta\beta[\Delta, z](u) = -\omega z(u). \quad (125)$$

The exponent  $\omega$ , if it exists, is the standard *correction-to-scaling exponent* [2] associated to the eigen-mode  $z(u)$ . In contrast to standard RG, more than one eigen-mode may exist. The solutions to equation (125) depend on the universality class.

First, for the periodic fixed point (118a), there is a discrete spectrum of solutions<sup>17</sup>,

$$\omega_{-1} = -\epsilon, \quad z_{-1}(u) = 1. \quad (126a)$$

$$\omega_1 = \epsilon - \frac{2}{3}\epsilon^2 + \frac{5 + 12\zeta(3)}{9}\epsilon^3 + \mathcal{O}(\epsilon^4), \quad (126b)$$

<sup>16</sup> Equation (4.15) of [40] should read  $F_d(0) = 1$ .

<sup>17</sup> As in [140] we use the high-energy-physics conventions with  $\omega > 0$  for an IR-attractive fixed point. This is opposite to some earlier work, as the leading solution given in [40].

$\zeta_{\text{eq}}$	1-loop	2-loop	3-loop	Padé-(2,1)	simulation and exact
$d = 3$	0.208	0.215	0.204	0.211	$0.22 \pm 0.01$ [137]
$d = 2$	0.417	0.444	0.358	0.423	$0.41 \pm 0.01$ [137], $0.42$ [138]
$d = 1$	0.625	0.687	0.396	0.636	$2/3$ [139]

**Figure 10.** Roughness exponent for RB disorder obtained by an  $\epsilon$ -expansion in comparison with exact results and numerical simulations. In the fourth column is an estimate value using a (2, 1)-Padé approximant of the three-loop result.

$$z_1(u) = 1 - 6u(1 - u).$$

$$\omega_2 = 4\epsilon - 5\epsilon^2 + \frac{5}{6}[13 + 12\zeta(3)]\epsilon^3 + \mathcal{O}(\epsilon^4), \quad (126c)$$

$$z_2(u) = 1$$

$$- \left\{ 15 + 5\epsilon - \frac{5}{6}\epsilon^2 \left[ 12\zeta(3) + 5 + 2\pi^2 - 3\psi' \left( \frac{1}{3} \right) \right] \right\} u(1 - u)$$

$$+ \left\{ 45 + 25\epsilon - \frac{25}{6}\epsilon^2 \left[ 12\zeta(3) + 5 + 2\pi^2 - 3\psi' \left( \frac{1}{3} \right) \right] \right\} [u(1 - u)]^2$$

$$\omega_3 = \frac{25\epsilon}{3} - \frac{140\epsilon^2}{9} + \frac{70}{9}[4\zeta(3) + 7]\epsilon^3 + \mathcal{O}(\epsilon^4) \quad (126d)$$

⋮

The first solution  $\omega_{-1} = -\epsilon$  is relevant, and comes with a constant perturbation for  $\Delta(u)$ . It is inadmissible in equilibrium, where  $\int_u \Delta(u) = 0$ , but shows up at depinning, see section 3. Thus the *leading* perturbation is  $z_1(u)$ , proportional to the fixed-point solution  $\Delta^*(u)$  itself. As the flow in this subspace can be represented by the flow of a single coupling constant  $g$ , the  $\beta$ -function must be a polynomial in  $g$ , and at leading order it is a parabola. This parabola has two fixed points, with slope  $-\epsilon$  at  $g = 0$  and consequently slope  $\epsilon$  at the non-trivial fixed point. This explains why the eigenvalue  $\omega_1$  starts with  $\epsilon$ , making the fixed point stable, exactly as in scalar  $\phi^4$  theory [2]. The following solutions  $z_n(u)$  can be classified by their maximal order in  $[u(1 - u)]^n$ . One sees that the larger  $n$ , the larger  $\omega_n$ . Thus this fixed point is perturbatively stable.

The analysis is more difficult for the non-periodic fixed points, i.e. those which allow for a non-trivial exponent  $\zeta > 0$ . The RB and RF fixed points above belong to this class. While a proof of stability even for the one-loop fixed point is still lacking, there are two analytical solutions which can be given ([50], section 7):

$$\omega_0 = 0 \quad (127)$$

$$z_0(u) = u\Delta'(u) - 2\Delta(u)$$

$$\omega_1 = \epsilon \quad (128)$$

$$z_1(u) = \zeta u\Delta'(u) + (\epsilon - 2\zeta)\Delta(u).$$

The first one is a redundant perturbation in the sense of Wegner [141]: it is a consequence of the invariance of the  $\beta$ -function under the rescaling  $\Delta(u) \rightarrow \kappa^{-2}\Delta(\kappa u)$ . In conformal field theory, redundant operators are associated to null states [142]. Their eigenvalues have no physical meaning. The dominant solution thus is  $\omega_1$ ,  $z_1(u)$ , which for  $\zeta = 0$  reduces (at leading order) to equation (126b). Subleading solutions can be constructed numerically.

To conclude, we believe that all the FRG fixed points discussed above are perturbatively stable, and that the leading eigenvalue, i.e. correction-to-scaling exponent is  $\omega_1 = \epsilon + \mathcal{O}(\epsilon^2)$ . Order- $\epsilon^2$  corrections depend on the universality class. Subleading solutions can be constructed manually [40].

### 2.15. Thermal rounding of the cusp

*Generalities.* As we have seen, a cusp non-analyticity necessarily arises at zero temperature, due to the jumps between metastable states. Interestingly, this cusp can be rounded by several effects: by a non-zero temperature  $T > 0$  (see below), *disorder chaos* as defined in section 2.16, or a non-zero driving velocity in the dynamics (section 3.11).

Let us start by a finite temperature, which is easy to include in the FRG equation [143]. The additional one-loop correction to  $R(u)$  is

$$\delta R(u) = T \left[ \text{diagram} \right] = TR''(u) \times \text{diagram}, \quad (129)$$

$$I_{\text{TP}} := \text{diagram} = \int_k \frac{1}{k^2 + m^2}. \quad (130)$$

The combinatorial factor is 2 for the two ends of the interaction, and  $1/2$  accompanying the second derivative; this can be checked for  $R(u_a - u_b) = (u_a - u_b)^2$ . The RG flow of the tadpole diagram is

$$-m\partial_m \left[ \text{diagram} \right] = 2m^2 \left[ \text{diagram} \right] = 2m^2 I_1, \quad (131)$$

with  $I_1$  given in equation (58). This leads to the  $\beta$ -function

$$\partial_\ell \tilde{R}(u) = (\epsilon - 4\zeta)\tilde{R}(u) + \zeta u\tilde{R}'(u) + \frac{1}{2}\tilde{R}''(u)^2 - \tilde{R}''(u)\tilde{R}''(0) + \tilde{T}_\ell \tilde{R}''(u). \quad (132)$$

The dimensionless temperature  $\tilde{T}_\ell$  is

$$\tilde{T}_\ell := \frac{2T}{\epsilon} (\epsilon I_1 |_{m=1}) m^\theta = \frac{2T}{\epsilon} (\epsilon I_1 |_{m=1}) e^{-\theta\ell}. \quad (133)$$

The power of  $m$  is obtained from equation (63) as the scaling of  $m^2 \tilde{R}''(u)$ , i.e.  $m^{2-\epsilon+2\zeta} = m^{d-2+2\zeta} = m^\theta$ . Although  $\tilde{T}_\ell$  finally flows to zero since  $\theta > 0$  (see equation (45)), in equation (132) it acts as a ‘diffusion’ term smoothening the cusp. In fact, at non-zero temperature there is no cusp, and  $R(u)$  remains analytic. The convergence to the fixed point is non-uniform. For  $u$  fixed,  $\tilde{R}(u)$  rapidly converges to the zero-temperature fixed point, except near  $u = 0$ , or more precisely in a boundary layer of size  $u \sim \tilde{T}_\ell$ , which shrinks to zero in the large-scale limit  $\ell \rightarrow \infty$ , i.e.  $m \rightarrow 0$ . Non-trivial consequences are:

the curvature blows up as  $R'''(0) \sim e^{\theta\ell}/T \sim L^\theta/T$ . We show in section 2.21 that this is related to the existence of thermal excitations, or *droplets* in the statics [144], and of *barriers* in the dynamics, which grow as  $L^\theta$  [145].

An analytic solution for the thermal boundary layer. Consider the flow equation (132) for RF disorder. Following section 2.5, we solve it analytically. Setting

$$-\tilde{R}''(u) \equiv \tilde{\Delta}(u) = \frac{\epsilon}{3}\kappa^{-2}y_t(\kappa u) \quad (134)$$

$$y_t(0) = 1, \quad \tilde{T}_\ell = \frac{\epsilon}{3}\kappa^{-2}t, \quad (135)$$

and taking two derivatives of equation (132) yields in generalization of equation (85)

$$\partial_u \left[ uy_t(u) - \frac{1}{2}\partial_u(y_t(u) - 1)^2 + ty_t'(u) \right] = 0. \quad (136)$$

The expression in the square brackets is a constant, fixed to 0 by considering the limit of  $u \rightarrow \infty$ . Simplifying gives

$$uy_t(u) + [t + 1 - y_t(u)]y_t'(u) = 0. \quad (137)$$

Dividing by  $y_t(u)$  and integrating once more we arrive at

$$\frac{u^2}{2} + (t + 1)\ln(y_t(u)) - y_t(u) = -1. \quad (138)$$

The integration constant was fixed by considering the limit of  $u \rightarrow 0, y_t \rightarrow 1$ . This is an explicit analytic solution, plotted on figure 11.

It is instructive to relate this to the solution at  $t = 0$ , which will guide us to a general finite- $T$  approximation. To this aim, rewrite equation (138) as

$$\frac{u^2}{2(1+t)} = -\ln(y_t(u)) - \frac{1 - y_t(u)}{1+t}. \quad (139)$$

It can be reduced to the solution  $y_0$  at  $t = 0$ , by setting  $y_t \rightarrow (1+t)y_0, u^2 \rightarrow u^2(1+t) - 2\ln(1+t)(1+t) + 2t$ . As a consequence,

$$y_t(u) = (1+t)y_0 \left( \sqrt{\frac{u^2 - 2t}{1+t}} + 2\ln(1+t) \right). \quad (140)$$

Finally using the rescaling invariance (134), we find yet another solution of the flow equation,

$$\tilde{y}_t(u) := \frac{1}{1+t'}y_{t'}(u\sqrt{1+t'}) \quad (141a)$$

$$t = \frac{t'}{1+t'} \iff t' = \frac{t}{1-t}. \quad (141b)$$

Using this and the rhs of equation (140) yields

$$\begin{aligned} \tilde{y}_t(u) &= y_0 \left( \sqrt{u^2 - \frac{2t}{t+1}} + 2\ln(t+1) \right) \\ &\approx y_0 \left( \sqrt{u^2 + t^2} \right). \end{aligned} \quad (142)$$

This solution, often in the approximate form of the second line, is commonly used in a *boundary-layer* analysis. The idea of

the latter is to match a solution in one range, say at small  $u$ , for which  $T\tilde{\Delta}''(u)$  is large but the non-linear terms in  $\partial_\ell\tilde{\Delta}(u)$  can be neglected, to a solution at large  $u$ , where the former can be neglected. As a consequence,

$$\lim_{t \rightarrow 0} \lim_{u \rightarrow 0} t \partial_u^2 \tilde{y}_t(u) = \lim_{u \rightarrow 0} \lim_{t \rightarrow 0} \partial_u \tilde{y}_t(u). \quad (143)$$

To rewrite this in terms of  $\tilde{\Delta}(u)$  is not immediate as we do not know the scale  $\kappa$ . However, we can derive a relation directly from the one-loop flow equation for  $\tilde{\Delta}(u)$ , obtained from equation (132) after taking two derivatives

$$\begin{aligned} \partial_\ell \tilde{\Delta}(u) &= (\epsilon - 2\zeta)\tilde{\Delta}(u) + \zeta u \tilde{\Delta}'(u) \\ &- \partial_u^2 \frac{1}{2} [\tilde{\Delta}(u) - \tilde{\Delta}(0)]^2 + \tilde{T}_\ell \tilde{\Delta}''(u). \end{aligned} \quad (144)$$

Suppose that the fixed point is attained and the lhs vanishes. Evaluating equation (144) once for  $\tilde{T}_\ell = 0$ , i.e.  $\tilde{T}_\ell \rightarrow 0$  and then  $u \rightarrow 0$ , and once for finite  $\tilde{T}_\ell$ , where the limit  $u \rightarrow 0$  is taken first, we obtain

$$(\epsilon - 2\zeta)\tilde{\Delta}(0) = \begin{cases} \tilde{\Delta}'(0^+)^2, & \tilde{T}_\ell = 0 \\ -\lim_{\tilde{T}_\ell \rightarrow 0} \tilde{T}_\ell \tilde{\Delta}''(0), & \tilde{T}_\ell > 0. \end{cases} \quad (145)$$

This implies

$$\tilde{\Delta}'(0^+)^2 \Big|_{\tilde{T}_\ell=0} = -\lim_{\tilde{T}_\ell \rightarrow 0} \tilde{T}_\ell \tilde{\Delta}''(0) \Big|_{\tilde{T}_\ell > 0}. \quad (146)$$

There is a large mathematics and physics literature on the subject. Relevant keywords are *boundary layer* (physics literature) or *singular perturbation theory* (mathematics literature); a few references to start with are [146–149].

Check for a toy model. Consider a particle subject to periodic disorder (CDW, RP universality class). Suppose that the minimum of the random potential is at  $u = u_0 + ni, i \in \mathbb{Z}$ , and that this minimum is rather sharp. Then for small  $m$ , the effective potential  $\hat{V}(w)$  is

$$\hat{V}(w) = -T \ln \left( \sum_{i \in \mathbb{Z}} \exp \left( -\frac{(w - i - u_0)^2 m^2}{2T} \right) \right). \quad (147)$$

The effective force is

$$\hat{F}(w) = -\partial_w \hat{V}(w). \quad (148)$$

We need the force–force correlator, which is obtained as

$$\Delta_T(w) = \langle \hat{F}(w)\hat{F}(0) \rangle^c = \int_0^1 du_0 \hat{F}(w)\hat{F}(0). \quad (149)$$

For  $T = 1$  we find at  $m = 1$

$$\Delta_0(w) = \frac{1}{12} - \frac{1}{2}w(1-w). \quad (150)$$

This solution is shown in blue in figure 11 (right). There is also the numerically evaluated integral (149) (red, dashed). Let us finally consider the FRG-equation for the rescaled disorder  $\tilde{\Delta}_T(w) := m^4 \Delta(w)$ ,

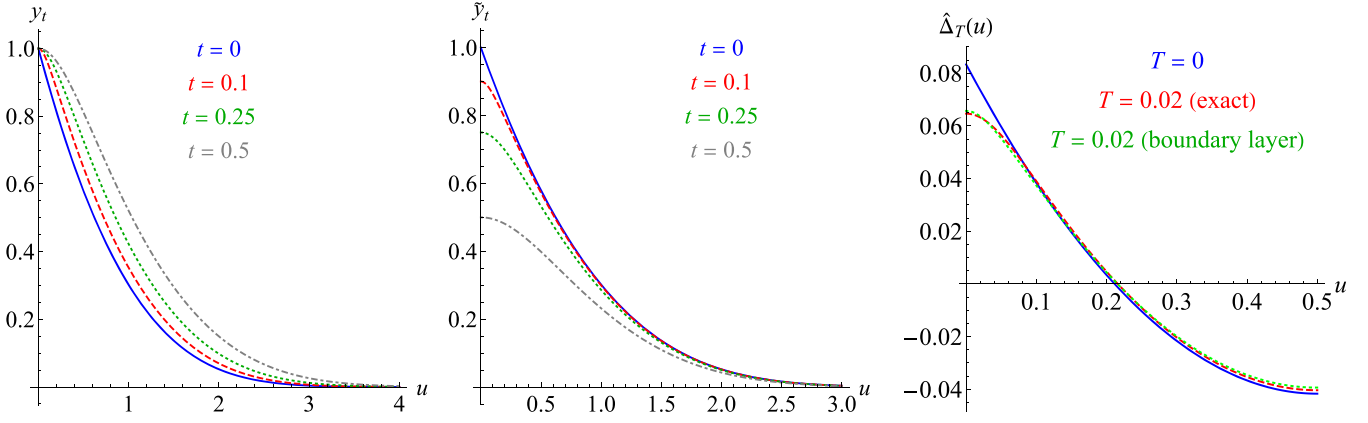


**Figure 11.** (Left) The RF-solution  $y_i$  given in equation (138). (Middle) The rescaled solution  $\tilde{y}_i$  given in equation (141a). (Right) Solution for the toy model. The blue line is the exact result at  $t = T = 0$ ; the red dashed line is the numerical integral (149) for  $t = T|_{m=1} = 0.02$ ; the green dotted line is the boundary-layer approximation (153).

$$\begin{aligned} \partial_\ell \tilde{\Delta}_T(w) &= 4\tilde{\Delta}_T(w) - 4\partial_u^2 \frac{1}{2} \left[ \tilde{\Delta}_T(w) - \tilde{\Delta}_T(0) \right]^2 \\ &\quad + 2Tm^2 \tilde{\Delta}_T''(w). \end{aligned} \quad (151)$$

The prefactors in their order of appearance are:  $\epsilon = 4$ ,  $4 = -m\partial_m \ln I_1$  from the one-loop diagram  $I_1$ , and  $2 = -m\partial_m \ln I_{\text{TP}}$  from the tadpole  $I_{\text{TP}}$  defined in equation (130). Thus the FP equation at  $m = 1$  is as above

$$0 = \tilde{\Delta}_T(w) - \partial_u^2 \frac{1}{2} \left[ \tilde{\Delta}_T(w) - \tilde{\Delta}_T(0) \right]^2 + \frac{T}{2} \tilde{\Delta}_T''(w). \quad (152)$$

At  $m = 1$ ,  $\tilde{\Delta}_T$  and  $\Delta$  coincide, resulting in

$$\tilde{\Delta}_T(w) = \Delta_T(w) \approx \Delta_0 \left( \sqrt{w^2 + \frac{T^2}{4}} \right) + \text{const.} \quad (153)$$

The constant is chosen s.t.  $\int_0^1 dw \Delta_T(w) = 0$ . This approximation works quite well, see figure 11, right.

For complementary descriptions of the high-temperature regime we refer to [151].

### 2.16. Disorder chaos

When changing the disorder slightly, e.g. by varying the magnetic field in a superconductor, the new ground state may change macroscopically, a phenomenon termed *disorder chaos* [128, 152, 153]. Not all types of disorder exhibit chaos. Using FRG, one studies a model with two copies,  $i = 1, 2$ , each seeing a slightly different potential  $V_i(x, u(x))$  in equation (6). The latter are mutually correlated Gaussian random potentials with correlation matrix

$$\overline{V_i(x, u)V_j(x', u')} = \delta^d(x - x')R_{ij}(u - u'). \quad (154)$$

At zero temperature, the FRG equations for  $R_{11}(u) = R_{22}(u)$  are the same as in equation (64). The one for the cross-correlator  $R_{12}(u)$  satisfies equation (132), with  $\tilde{T}_\ell$  replaced by  $\hat{T} := R_{12}''(0) - R_{11}''(0)$ . The flow of this fictitious temperature must be determined self-consistently from the FRG equations.

As for a real temperature the cusp is rounded, leading to a non-trivial cross-correlation function.

### 2.17. Finite $N$

Up to now, we have studied the functional RG for one component  $N = 1$ . The general case of  $N \neq 1$ , here termed *finite  $N$* , is more difficult to handle, since derivatives of the renormalized disorder now depend on the direction in which this derivative is taken. Define amplitude  $u := |\vec{u}|$  and direction  $\hat{u} := \vec{u}/|\vec{u}|$  of the field. Then deriving the latter variable leads to terms proportional to  $1/u$ , which are diverging in the limit of  $u \rightarrow 0$ . This poses problems in the calculation, and it is *a priori* not clear that the theory at  $N \neq 1$  exists, supposed this is the case for  $N = 1$ . At one-loop order everything is well-defined [132]. A consistent FRG-equation at two-loop order is [150]

$$\begin{aligned} \partial_\ell \tilde{R}(u) &= (\epsilon - 4\zeta)\tilde{R}(u) + \zeta u \tilde{R}'(u) \\ &\quad + \frac{1}{2} \tilde{R}''(u)^2 - \tilde{R}''(0)\tilde{R}''(u) \\ &\quad + \frac{N-1}{2} \frac{\tilde{R}'(u)}{u} \left[ \frac{\tilde{R}'(u)}{u} - 2\tilde{R}''(0) \right] \\ &\quad + \frac{1}{2} [\tilde{R}''(u) - \tilde{R}''(0)] \tilde{R}'''(u)^2 \\ &\quad + \frac{N-1}{2} \frac{[\tilde{R}'(u) - u\tilde{R}''(u)]^2}{u^5} [2\tilde{R}'(u) + u\tilde{R}''(u) - 3\tilde{R}''(0)] \\ &\quad - \tilde{R}'''(0^+)^2 \left[ \frac{N+3}{8} \tilde{R}''(u) + \frac{N-1}{4} \frac{\tilde{R}'(r)}{u} \right]. \end{aligned} \quad (155)$$

The first line is from rescaling, the next two lines are the one-loop contribution given in [132], with the third line containing additional contributions for  $N \neq 1$  as compared to equation (64). The last three lines represent the two-loop contributions, with the new anomalous terms proportional to  $\tilde{R}'''(0^+)^2$  in the last line.

The fixed-point equation (155) can be integrated numerically, order by order in  $\epsilon$ . The result, specialized to directed polymers, i.e.  $\epsilon = 3$  is plotted on figure 12. We see that the two-loop corrections are rather big at large  $N$ , so some doubt

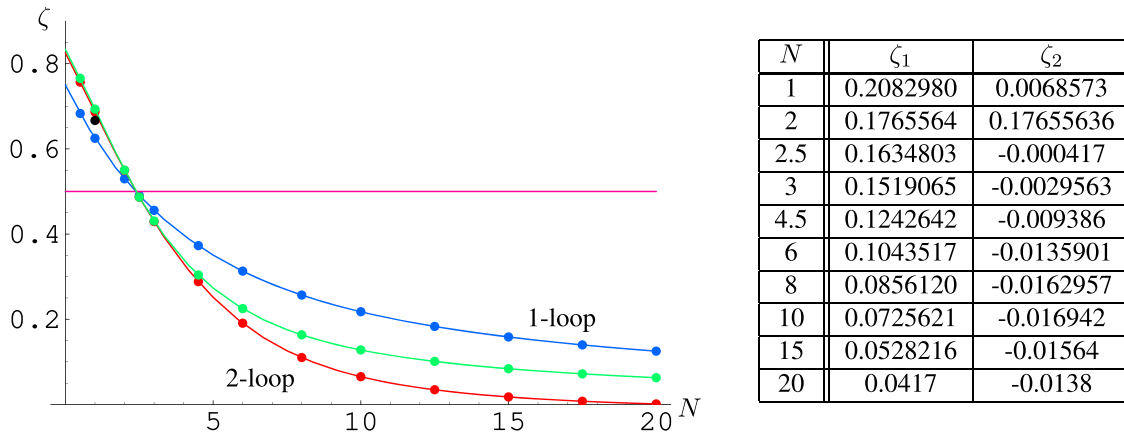


**Figure 12.** The roughness exponent  $\zeta$  as a function of the number of components  $N$ : 1 loop (blue), 2 loops (red), and a two-loop Padé-(1, 1) (green). Reprinted figure with permission from [150], Copyright (2005) by the American Physical Society.

on the applicability of the latter down to  $\epsilon = 3$  is advised. However both one- and two-loop results reproduce well the two known points on the curve:  $\zeta = 2/3$  for  $N = 1$  and  $\zeta = 0$  for  $N = \infty$ . The latter result will be given in section 2.18. As discussed in section 7, the directed polymer in  $N$  dimensions treated here, and the KPZ-equation of non-linear surface growth in  $N$  dimensions are related, identifying  $z_{\text{KPZ}} = 1/\zeta$ , see equation (783). Using the analytic solution for the latter in dimension  $N = 1$ ,  $\zeta_{\text{KPZ}}^{N=1} = 1/2$  (equation (817)), and the scaling relation  $z_{\text{KPZ}} + \zeta_{\text{KPZ}} = 2$  (equation (781)) leads to

$$\zeta_{d=1}^{N=1} = \frac{2}{3}. \quad (156)$$

The line  $\zeta = 1/2$  given on figure 12 plays a special role: in the presence of thermal fluctuations, we expect the roughness-exponent of the directed polymer to be bounded by  $\zeta \geq 1/2$ . In the KPZ-equation, this corresponds to a dynamic exponent  $z_{\text{KPZ}} = 1/\zeta \leq 2$ , which due to the scaling relation  $z_{\text{KPZ}} + \zeta_{\text{KPZ}} = 2$  is an upper bound in the strong-coupling phase. The results above suggest that there exists an upper critical dimension in the KPZ-problem, with  $d_{\text{uc}} \approx 2.4$ . Even though the latter value might be an underestimation, it is hard to imagine what can go wrong *qualitatively* with this scenario. The debate in the literature is far from settled, and we summarize it in section 7.11.

### 2.18. Large $N$

In the last sections we discussed renormalization in a loop expansion, i.e. an expansion in  $\epsilon = 4 - d$ . In order to check consistency, we now turn to a non-perturbative (NP) approach which can be solved analytically in the large- $N$  limit. The starting point is a straightforward generalization of equation (30),

$$\mathcal{H}[\vec{u}, \vec{j}] = \frac{1}{2T} \sum_{a=1}^n \int_x [\vec{u}_a(x) - \vec{w}](m^2 - \nabla^2)[\vec{u}_a(x) - \vec{w}] - \frac{1}{2T^2} \sum_{a,b=1}^n \int_x B((\vec{u}_a(x) - \vec{u}_b(x))^2), \quad (157)$$

$$B(u^2) = R(|u|). \quad (158)$$

For large  $N$  the saddle-point equation reads [49, 154]

$$\tilde{B}'(w_{ab}^2) = B'(w_{ab}^2 + 2TI_{\text{TP}} + 4I_1[\tilde{B}'(w_{ab}^2) - \tilde{B}'(0)]). \quad (159)$$

This equation gives the derivative of the effective (renormalized) disorder  $\tilde{B}$  as a function of the (constant) background field  $w_{ab}^2 = (\vec{w}_a - \vec{w}_b)^2$  in terms of: the derivative of the microscopic (bare) disorder  $B$ , the temperature  $T$  and the integrals  $I_1$  and  $I_{\text{TP}}$  defined in equations (58) and (130). The saddle-point equation can be turned into a closed functional renormalization group (FRG) equation for  $\tilde{B}$  by taking a derivative w.r.t.  $m$ . In analogy to equation (64), and with the same notation used there, one obtains [49, 154]

$$\partial_\ell \tilde{B}(x) := -\frac{m\partial}{\partial m} \tilde{B}(x) = (\epsilon - 4\zeta)\tilde{B}(x) + 2\zeta x \tilde{B}'(x) + \frac{1}{2} \tilde{B}'(x)^2 - \tilde{B}'(x)\tilde{B}'(0) + \frac{\epsilon T \tilde{B}'(x)}{\epsilon + \tilde{B}''(0)}. \quad (160)$$

This is a complicated nonlinear partial differential equation. It is surprising that one can find an analytic solution: the trick (reminding the RF-solution (88)) is to examine the flow-equation for the inverse function of  $y(x) := -\tilde{B}'(x)$ , which is the dominant term at large  $N$  for the force-force correlator<sup>18</sup>,

$$m\partial_m x(y) = (\epsilon - 2\zeta)yx'(y) + 2\zeta x(y) + y_0 - y + \frac{T_m}{1 - (\epsilon x'_0)^{-1}}. \quad (161)$$

Let us only give the results of this analytic solution: first of all, for LR correlated disorder of the form  $\tilde{B}'(x) \sim x^{-\gamma}$ , the exponent  $\zeta$  can be calculated analytically as  $\zeta = \frac{\epsilon}{2(1+\gamma)}$ . It agrees with the replica-treatment in [155], the one-loop treatment in [132], and the Flory estimate (23). For short-range correlated disorder,  $\zeta = 0$ . Second, it demonstrates that before reaching the Larkin-length,  $\tilde{B}(x)$  is analytic and dimensional reduction holds. Beyond the Larkin length,  $\tilde{B}''(0) = \infty$ , a cusp appears and dimensional reduction is broken. This shows again that the cusp is not an artifact of the perturbative expansion, but an

<sup>18</sup> The sign of the last term in equation (11) of [154] must be reversed.

important property of the exact solution of the problem (here for large  $N$ ).

### 2.19. Corrections at order $1/N$

In a graphical notation, we find [156]

$$\begin{aligned}
 \delta B^{(1)} = & \text{[Diagram 1]} + \text{[Diagram 2]} \\
 + & \text{[Diagram 3]} + \text{[Diagram 4]} + \text{[Diagram 5]} \\
 + T & \left[ \text{[Diagram 6]} + \text{[Diagram 7]} + \text{[Diagram 8]} \right] \\
 + & \text{[Diagram 9]} + \text{[Diagram 10]} + \text{[Diagram 11]} \\
 + T^2 & \left[ \text{[Diagram 12]} + \text{[Diagram 13]} + \text{[Diagram 14]} + \mathcal{A}^{T^2} \right]
 \end{aligned} \tag{162}$$

$$\begin{aligned}
 \text{[Diagram 15]} & = B''(\chi_{ab}) (1 - 4A_d I_2(p) B''(\chi_{ab}))^{-1}, \\
 \blacksquare & = B(\chi_{ab}),
 \end{aligned} \tag{163}$$

where  $\chi_{ab}$  is the argument of the rhs of equation (159). More explicit expressions are given in [156].

By varying the IR-regulator, one can derive a  $\beta$ -function at order  $1/N$  [156]. At  $T = 0$ , it is UV-convergent, and should allow one to find a NP fixed point. This goal has currently only been achieved to one-loop order [156]. Another open problem is the behavior at finite  $T$ .

### 2.20. Relation to replica symmetry breaking (RSB)

One of the key methods employed in disordered systems is a method termed RSB [57, 60–62, 157–162], sometimes referred to as *Gaussian variational ansatz*, or simply MF, since there is no tractable scheme to go beyond that limit. It is an interesting task to confront this alternative approach to the FRG. As we saw above, FRG works very well for the experimentally most relevant case of  $N = 1$ , whereas the RSB ansatz only holds in the limit of  $N \rightarrow \infty$  [155]. So what is the idea? [155] starts from equation (157) but *without* a source-term  $w$ , i.e. without an applied field, a relevant difference. In the limit of large  $N$ , a Gaussian variational energy of the form

$$\begin{aligned}
 \mathcal{H}_g[\vec{u}] = & \frac{1}{2T} \sum_{a=1}^n \int_x \vec{u}_a(x) (-\nabla^2 + m^2) \vec{u}_a(x) \\
 - & \frac{1}{2T^2} \sum_{a,b=1}^n \int_x \sigma_{ab} \vec{u}_a(x) \vec{u}_b(x)
 \end{aligned} \tag{164}$$

becomes exact. The art is to make an appropriate ansatz for  $\sigma_{ab}$ . The simplest possibility,  $\sigma_{ab} = \sigma$  for all  $a \neq b$  reproduces the

dimensional-reduction result, which we know to break down at the Larkin length. Beyond that scale, a replica-symmetry broken (RSB) ansatz for  $\sigma_{ab}$  is suggestive. To this aim, one breaks  $\sigma_{ab}$  into four blocks of equal size, and chooses two (variationally optimized) values for the diagonal and off-diagonal blocks. This is termed *one-step RSB*. One then iterates the procedure on the diagonal blocks, proceeding via a *two-step* to an *infinite-step* RSB. The final result has the form

$$\sigma_{ab} = \begin{pmatrix} \text{[Colorful Matrix]} \end{pmatrix}. \tag{165}$$

One finds that the more often one iterates, the more stable (to perturbations) and precise the result becomes. In fact, one has to repeat this procedure infinitely many times. This seems like a hopeless endeavor, but Parisi has shown [60] that the infinitely often replica symmetry broken matrix can be parameterized by a function  $[\sigma](z)$  with  $z \in [0, 1]$ . In the SK-model,  $z$  has the interpretation of an overlap between replicas. While there is no such simple interpretation for the model (164), we retain that  $z = 0$  describes distant states, whereas  $z = 1$  describes nearby states. The solution of the large- $N$  saddle-point equations leads to the curve depicted in figure 6. Knowing it, the two-point function is given by

$$\langle \vec{u}_k \vec{u}_{-k} \rangle = \frac{1}{k^2 + m^2} \left( 1 + \int_0^1 \frac{dz}{z^2} \frac{[\sigma](z)}{k^2 + [\sigma](z) + m^2} \right). \tag{166}$$

The important question is: what is the relation between the two approaches, which both declare to calculate the same two-point function? Comparing the analytical solutions, we find that the two-point function given by FRG is the same as that of RSB, if in the latter expression we only take into account the contribution from the most distant states, i.e. those for  $z$  between 0 and  $z_m$  (see figure 13). To understand why this is so, we have to remember that the two calculations are done under quite different assumptions: in contrast to the RSB-calculation, the FRG-approach calculates the partition function in presence of an external field  $w$ , which is then used to give via a Legendre transform the effective action. Even if the field  $w$  is finally tuned to 0, the system remembers its preparation, as does a magnet: preparing the system in presence of a magnetic field results in a magnetization which aligns with this field. The magnetization remains, even if finally the field is turned off. The same phenomenon happens here: by explicitly breaking the replica-symmetry through an applied field, all replicas settle into distant states, and the close states from the Parisi-function  $[\sigma](z) + m^2$  (which represent *spontaneous* RSB) will not contribute. However, the full RSB-result can be reconstructed by remarking that the part of the curve between  $z_m$  and  $z_c$  is independent of the infrared cutoff  $m$ . Integrating

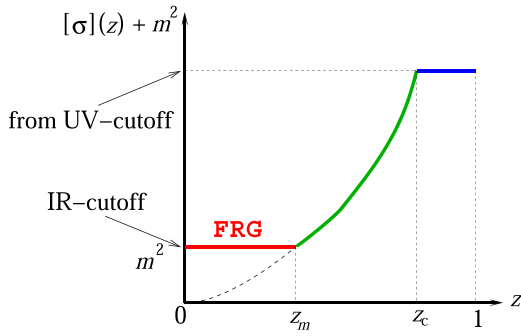


**Figure 13.** The function  $[\sigma](u) + m^2$ . Reproduced from [155]. CC BY 4.0.

over  $m$  [154] then yields ( $m_c$  is the mass corresponding to  $z_c$ )

$$\langle \tilde{u}_k \tilde{u}_{-k} \rangle \Big|_{k=0}^{\text{RSB}} = \frac{\tilde{B}'_m(0)}{m^4} + \int_m^{m_c} \frac{d\tilde{B}'_\mu(0)}{\mu^4} + \frac{1}{m_c^2} - \frac{1}{m^2}. \quad (167)$$

We also note that a similar effective action has been proposed in [126]. While it agrees qualitatively, it does not reproduce the correct FRG two-point function, as it should.

To go further, one needs to redo the analysis of [155] in presence of an applied field, a formidable task. A first step in this direction was taken in [126], building on the technique developed in [163]. However, the function  $R(u)$  defined in that work does not coincide with the one usually studied in field theory (there is an additional Legendre transform), making a precise comparison difficult. This goal was finally achieved in [164]. In summary, there are two distinct scaling regimes,

$$\tilde{B}(w^2) - \tilde{B}(0) = \begin{cases} L^{-d} \tilde{b}(w^2 L^d) & \text{for } w^2 \sim L^{-d}, \quad (\text{i}) \\ N b(w^2/N) & \text{for } w^2 \sim N, \quad (\text{ii}) \end{cases} \quad (168)$$

(i) a ‘single shock’ regime,  $w^2 \sim L^{-d}$  where  $L^d$  is the system’s volume, and (ii) a ‘thermodynamic’ regime, with  $w^2 \sim N$ , independent of  $L$ . In regime (i) all the equivalent RSB saddle points within the Gaussian variational approximation contribute, while in regime (ii) the effect of RSB enters only through a single anomaly. When RSB is continuous (e.g., for short-ranged disorder, in dimension  $2 \leq d \leq 4$ ), regime (ii) yields the large- $N$  FRG function shown above. In that case, the disorder correlator exhibits a cusp in both regimes, though with different amplitudes and of different physical origin. When the RSB solution is one-step and non-marginal (e.g. in  $d < 2$  for SR disorder), the correlator  $\tilde{R}(w) = \tilde{B}(w^2)$  in regime (ii) is considerably reduced, and exhibits no cusp.

*RSB at finite  $N$ .* The Gaussian variational ansatz with an infinite-step RSB is possible also at finite  $N$ , and termed the Gaussian variational model (GVM). For  $m = 0$ ,

$$[\sigma](u) \sim u^\alpha, \quad \alpha = \frac{4 + N}{d - N(1 - \frac{d}{2})}. \quad (169)$$

As a consequence,

$$\zeta_{\text{GVM}} = \frac{4 - d}{4 + N} \equiv \zeta_{\text{Flory}}^{\text{RB}}, \quad (170)$$

where  $\zeta_{\text{Flory}}^{\text{RB}}$  is the Flory estimate (21). How can this be explained? In the GVM solution [165], all power-laws can be deduced from dimensional considerations, leaving no room for a deviation from the Flory estimate (21). Deviations are possible with additional scales [166].

### 2.21. Droplet picture

The droplet picture was proposed [56, 167] for Ising spin glasses (more in [168–171]), as a conceptual alternative to the Parisi solution [60, 157–159] (more in [57, 61, 62, 160–162]) of the SK model [58, 59]. Using the concept of RSB, the latter yields infinitely many extremal Gibbs states at very low temperature, organized within an ultrametric topology, i.e. arrangeable as a tree. As temperature is raised, states at increasing distance coalesce until a unique state remains at  $T = T_c$ . Appropriate for the infinite-range SK model, its validity for short-ranged spin glasses as the Edwards–Anderson (EA) model [103] is disputed. The latter assumes an energy

$$\mathcal{H}_{\text{EA}} = \sum_{\langle i,j \rangle} J_{ij} S_i S_j \quad (171)$$

with uncorrelated random couplings  $J_{ij}$ , drawn from a probability distribution  $P(J)$ .

Existence of the spin-glass phase is detected by the EA order parameter

$$q_{\text{EA}}(T) := \overline{\langle S_i \rangle_t^2}, \quad (172)$$

where the overline denotes (as above) the disorder average (over  $J$ ), and  $\langle \dots \rangle_t$  the temporal average over an infinite time. One expects  $q_{\text{EA}}(T) = 0$  for  $T > T_c$ , and  $q_{\text{EA}}(T) > 0$  for  $T < T_c$ .

In contrast to the RSB scenario with a finite density of states at  $q = 0$ , the droplet picture proposes that the low-lying excitations which dominate the long-distance and long-time correlations are clusters of (nested) droplets of coherently flipped spins. Let us denote by  $\mathcal{F}_0$  the ground-state free energy, i.e. the infimum of all free energies  $\mathcal{F}_i$ ,

$$\mathcal{F}_0 := \inf_i (\mathcal{F}_i). \quad (173)$$

In a pure system at  $T = 0$ , the energy of a domain wall can be measured by imposing anti-periodic boundary conditions, which force a domain wall of size  $L^{d-1}$  and energy  $\mathcal{E}_L \simeq \Upsilon L^{d-1}$ . In a disordered system at  $T > 0$  this generalizes to

$$\mathcal{F}_L \simeq \Upsilon L^\theta, \quad (174)$$

with  $\theta < d - 1$ , where  $\mathcal{F}_L$  is the free energy at scale  $L$ . If one supposes that the free energies  $\mathcal{F}_L$  in the domain wall are uncorrelated, using the central-limit theorem improves the bound<sup>19</sup> to  $\theta \leq \frac{d-1}{2}$ . The probability of droplet excitations with

<sup>19</sup> One might argue that if a domain wall is rough, then its size scales as  $L^{d_f}$  with  $d - 1 \leq d_f \leq d$ , and we get a weaker bound for  $\theta$ . This is incorrect. While the minimum-energy domain wall may be larger, its energy is lower; otherwise the minimal-energy interface would be flat.

free-energy differences  $\mathcal{F}_L$ , given size  $L$ , has the scaling form

$$\rho(\mathcal{F}_L|L) = \frac{\rho(\mathcal{F}_L/\Upsilon L^\theta)}{\Upsilon L^\theta}, \quad \rho(0) > 0, \quad 0 < \theta \leq \frac{d-1}{2}. \quad (175)$$

Values of  $\theta$  satisfying the bound (175) have been reported [172].

Next consider an ensemble of independent (but possibly nested) droplets of size between  $L^d$  and  $(L + \delta L)^d$ . The probability that a spin is inside such a droplet is independent of  $L$ : while the probability that a spin is inside a droplet scales as  $L^d$ , the number of droplets scales as  $L^{-d}$ . Thus the measure for integration of  $\rho(\mathcal{F}_L|L)$  over  $L$  is

$$\rho(L)dL = \frac{dL}{L} \rho(\mathcal{F}_L|L). \quad (176)$$

Stated differently, a given spin has a finite,  $L$ -independent, probability to be inside a droplet of size  $L$ .

Only if both points  $i$  and  $i+r$  are inside a droplet, the connected spin-spin correlation function  $\langle S_i \rangle_t \langle S_{i+r} \rangle_t^c$ , is non-zero. To give a non-vanishing contribution to the space-dependent version of the EA order parameter (172), the droplet has to be bigger than  $r$ , leading to

$$q_{\text{EA}}(r) := \overline{\langle S_i \rangle_t \langle S_{i+r} \rangle_t^c} \sim r^{-\theta}, \quad \text{as } r \rightarrow \infty. \quad (177)$$

For higher-energy excitations, it is natural to suppose that their activation barriers scale with  $L$  as

$$\mathcal{F}_b \simeq \Delta L^\psi, \quad \theta \leq \psi \leq d-1. \quad (178)$$

The upper bound is given by the maximal energy needed to flip a flat wall. The lower bound insures that  $\mathcal{F}_L$  from equation (174) satisfies  $\mathcal{F}_L < \mathcal{F}_b$ .

To address dynamical properties, suppose a droplet persists for a time  $t = t_0 e^{\mathcal{F}_b/T}$ . The line of arguments used above implies that the autocorrelation function decays as

$$C(t) := \overline{\langle S_i(0) S_i(t) \rangle_t} \simeq \frac{q_{\text{EA}} T}{\Upsilon} \left[ \frac{\Delta}{T \ln(t/t_0)} \right]^{\frac{\theta}{\psi}}. \quad (179)$$

To conclude our excursion into the droplet picture for the EA-spin glass (for further reading see [56, 169–171, 173]), let us mention an interesting result due to Bovier and Fröhlich [167], who analyze EA-spin glasses with concepts from gauge theory. They state that for  $d = 2$  the Gibbs state is unique at all temperatures. In the language used here, this implies  $\theta < 0$ . The debate whether EA-spin glasses are better described by the droplet picture or RSB is still raging [174–181]. It is possible that depending on the dimension, the distance to  $T_c$ , and small modifications of the EA spin-glass energy (171), both phases are realized in some domains of the phase diagram, while in other domains, none of them is appropriate.

Let us finally apply the droplet ideas to the directed polymer [24], and more generally disordered elastic manifolds [127, 144, 145, 182]. First of all, the droplet exponent  $\theta$  as defined in equation (174) is the one given in equation (45)

$$\theta = d - 2 + 2\zeta. \quad (180)$$

The bound  $\theta \leq d/2$  translates into

$$\zeta \leq \zeta_{\text{droplet bound}} = \frac{4-d}{4}. \quad (181)$$

It is less clear what the exponent  $\psi$  is, but there is some evidence [183, 184] that

$$\psi = \theta, \quad (182)$$

up to logarithmic corrections, shown to exist at least in one case [184]. As an immediate generalization to equation (177), we expect that at finite temperature [182]

$$\langle [u(x) - u(y)]^{2n} \rangle \simeq T |x - y|^{2n\zeta - \theta}. \quad (183)$$

To build a consistent field theory is a challenge. Technically, one has to connect the thermal boundary layer of  $\Delta(w)$  (section 2.15) with the outer region. Physically, one needs to make the connection to the droplet picture. This problem is considered in [127, 144, 145, 182].

## 2.22. Kida model

In [187] Kida solved the problem how a random short-ranged correlated velocity field decays under action of the Burgers equation. As we discuss in sections 7.2–7.7, this is equivalent to minimizing the energy

$$\mathcal{H}_w(u) := \frac{m^2}{2} (u - w)^2 + V(u). \quad (184)$$

The random potential  $V(u)$  is defined for  $u \in \mathbb{Z}$ , and each  $V$  is drawn from a probability distribution  $P(V)$ . The effective potential is defined as in equation (96). Kida's solution for the  $\hat{V}(w)$  correlations, rephrased in [82, 188] for the minimization problem (184), is constructed in several steps: define

$$P_{<}(V) := \int_{-\infty}^V P(V') dV' \simeq e^{-A(-V)^\gamma} \quad \text{for } V \rightarrow -\infty. \quad (185)$$

The characteristic  $u$ -scale is

$$\rho_m = \left[ m^2 \gamma \ln(m^{-1})^{1-\frac{1}{\gamma}} A^{\frac{1}{\gamma}} \right]^{-\frac{1}{2}}. \quad (186)$$

For a standard Gaussian distribution,  $A = 1/2$ ,  $\gamma = 2$ , this can be simplified to

$$\rho_m^{\text{Gauss}} = \frac{1}{m} [\ln(m^{-2})]^{-\frac{1}{4}}, \quad \text{i.e. } \zeta_{\text{Kida}} = 1^-. \quad (187)$$

The  $u$ -distribution minimizing the energy (184) is

$$P(u) \approx \frac{1}{\rho_m \sqrt{2\pi}} e^{-\frac{1}{2}(u/\rho_m)^2}. \quad (188)$$

In order to proceed, define the auxiliary function

$$\Phi(x) := \int_0^\infty dy e^{-\frac{y^2}{2} + xy} = \sqrt{\frac{\pi}{2}} e^{\frac{x^2}{2}} \left[ \operatorname{erf}\left(\frac{x}{\sqrt{2}}\right) + 1 \right]. \quad (189)$$

The effective disorder force–force correlator  $\Delta(w)$  and  $R(w)$  are then given by

$$\Delta(u) = m^4 \rho_m^2 \tilde{\Delta}(w/\rho_m), \quad R(u) = m^4 \rho_m^4 \tilde{R}(w/\rho_m), \quad (190)$$

$$\tilde{\Delta}(w) = \frac{d}{dw} \int_0^\infty \frac{2w}{\Phi(\frac{w}{2} + x) + \Phi(\frac{w}{2} - x)} dx, \quad (191)$$

$$\tilde{R}(w) = \frac{\pi^2}{6} - \int_0^\infty \frac{2w^2 x \Phi(\frac{w}{2} - x)}{\Phi(\frac{w}{2} + x) + \Phi(\frac{w}{2} - x)} dx. \quad (192)$$

The solutions  $\tilde{\Delta}(w)$  and  $\tilde{R}(w)$  are compared in figure 14 to numerical simulations, and to the fixed point obtained by solving the one-loop FRG equation (79), for  $\zeta = \zeta_{\text{RB}}$ , equation (90). For reference we give for the Kida-solution

$$\begin{aligned} \tilde{\Delta}(0) &= 1, & \tilde{\Delta}'(0^+) &= -\frac{2}{\sqrt{\pi}}, & \tilde{\Delta}''(0^+) &= \frac{3^{\frac{3}{2}}}{\pi} - 1, \\ \frac{\Delta(0)\Delta''(0)}{\Delta'(0^+)^2} &\approx 0.5136. \end{aligned} \quad (193)$$

Using equation (104) the universal avalanche scale is

$$S_m := \frac{\langle S^2 \rangle}{2 \langle S \rangle} = \frac{2}{\sqrt{\pi}} \rho_m. \quad (194)$$

### 2.23. Sinai model

In 1983 Sinai asked: consider a RW  $X_n$ , which with probability  $p_n$  increases by 1 in step  $n$ , and with probability  $1 - p_n$  decreases by 1, assuming the  $p_n \in [0, 1]$  themselves to be (quenched) *independent random variables*. Sinai showed [189] that contrary to a normal RW, which has variance  $n$  after  $n$  steps, the process  $X_n$  defined above has a variance which grows as  $\ln^2(n)$ . Interpreting the  $p_n$  as RF disorder, Sinai's theorem shows that the walk is localized even at finite temperature.

Let us consider again the model defined in equation (184), but with a potential which itself is a RW,

$$\mathcal{H}_w(u) := \frac{m^2}{2}(u - w)^2 + V(u), \quad (195)$$

$$V(u) = - \int_0^u F(u') du', \quad (196)$$

$$\overline{F(u)F(u')} = \sigma \delta(u - u'). \quad (197)$$

Thus

$$\frac{1}{2} \overline{[V(u) - V(u')]^2} = \sigma |u - u'|. \quad (198)$$

Using the methods developed in [190], the renormalized disorder correlator  $\Delta(w)$  for the Sinai model has been obtained

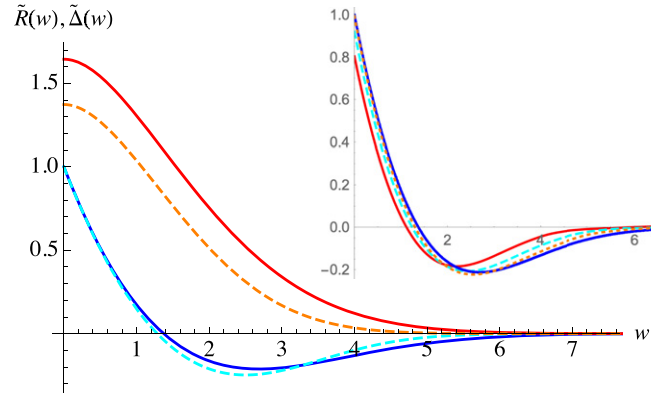


**Figure 14.** The force–force correlator  $\Delta(u)$  for the Kida model (blue solid), compared to the RB one-loop FRG result (cyan, dashed) already shown in figure 6 (right), rescaled to have the same value and slopes as equation (191). In solid red the potential–potential correlator  $\tilde{R}(w)$ , in dashed the corresponding one-loop FRG result. (Inset) Numerical simulations [185, 186] for  $m^2 = 10^{-1}$  (red solid),  $m^2 = 10^{-2}$  (cyan, dashed), and  $m^2 = 10^{-4}$  (orange dotted), compared to the theory curve (blue). Convergence is slow. Statistical errors are within the line thickness.

in [82]. Here we give a simplified version<sup>20</sup>:

$$\Delta(w) = m^4 \rho_m^2 \tilde{\Delta}(w/\rho_m), \quad (199)$$

$$R(w) = m^4 \rho_m^4 \tilde{R}(w/\rho_m), \quad (200)$$

$$\rho_m = 2^{\frac{2}{3}} m^{-\frac{4}{3}} \sigma^{\frac{1}{3}}. \quad (201)$$

The effective disorder correlator reads

$$\begin{aligned} \tilde{\Delta}(w) &= -\frac{e^{-\frac{w^2}{12}}}{4\pi^{\frac{3}{2}} \sqrt{w}} \int_{-\infty}^{\infty} d\lambda_1 \int_{-\infty}^{\infty} d\lambda_2 e^{-\frac{(\lambda_1 - \lambda_2)^2}{4w}} \\ &\times e^{i\frac{\pi}{2}(\lambda_1 + \lambda_2)} \frac{\operatorname{Ai}'(i\lambda_1)}{\operatorname{Ai}(i\lambda_1)^2} \frac{\operatorname{Ai}'(i\lambda_2)}{\operatorname{Ai}(i\lambda_2)^2} \\ &\times \left[ 1 + 2w \frac{\int_0^\infty dV e^{wV} \operatorname{Ai}(i\lambda_1 + V) \operatorname{Ai}(i\lambda_2 + V)}{\operatorname{Ai}(i\lambda_1) \operatorname{Ai}(i\lambda_2)} \right]. \end{aligned} \quad (202)$$

For reference we give

$$\begin{aligned} \tilde{\Delta}(0) &\approx 0.418375, & \tilde{\Delta}'(0^+) &\approx -0.566, \\ \tilde{\Delta}''(0^+) &\approx 0.52, & \frac{\Delta(0)\Delta''(0)}{\Delta'(0^+)^2} &\approx 0.68. \end{aligned} \quad (203)$$

Using equation (104), this predicts, among others, the universal avalanche scale,

$$S_m := \frac{\langle S^2 \rangle}{2 \langle S \rangle} = 0.566 \rho_m. \quad (204)$$

<sup>20</sup>We simplify the result of [82] such that the only appearance of  $a = 2^{-1/3}$  or  $b = 2^{2/3}$  is in the scale  $\rho_m$  of equation (201). We further correct several misprints: first, the formulas given for  $a$  and  $b$  in [82] can only be used for  $m = \sigma = 1$ , or one would have to rescale the term  $\sim w^3$  in the exponential as well. The factor of  $w$  in the innermost integral for  $\Delta$  is missing in equation (304) of [82], while it is there in equation (293) for  $R$ .

One can also give an explicit formula for the potential–potential correlator  $\tilde{R}(w)$

$$\begin{aligned} \tilde{R}(w) = & -\frac{\sqrt{w} e^{-\frac{w^3}{12}}}{16\pi^{\frac{3}{2}}} \int_{-\infty}^{\infty} d\lambda_1 \int_{-\infty}^{\infty} d\lambda_2 e^{-\frac{(\lambda_1 - \lambda_2)^2}{4w}} \\ & \times \frac{e^{i\frac{w}{2}(\lambda_1 + \lambda_2)}}{\text{Ai}(i\lambda_1)\text{Ai}(i\lambda_2)} \left[ 1 - \frac{(\lambda_1 - \lambda_2)^2}{2w} \right] \\ & \times \left[ 1 + 2w \frac{\int_0^{\infty} dV e^{\frac{w}{2}V} \text{Ai}(i\lambda_1 + V)\text{Ai}(i\lambda_2 + V)}{\text{Ai}(i\lambda_1)\text{Ai}(i\lambda_2)} \right] \\ & + \tilde{R}(0). \end{aligned} \quad (205)$$

We checked numerically that  $\tilde{\Delta}(w) = -\tilde{R}''(w)$ . We find that

$$\lim_{w \rightarrow \infty} \tilde{R}(0) - \tilde{R}(w) - \frac{w}{4} = 0.127\,689, \quad (206)$$

$$\lim_{w \rightarrow \infty} -R'(w) = \frac{m^4 \rho_m^3}{4} = \sigma. \quad (207)$$

The latter is a consequence of the FRG equation: it cannot renormalize the tail of  $R(w)$ , given for the microscopic disorder in equation (198). Finally note that if in the square brackets of the second line of equation (205) one only retains the ‘1’, then the dominant term  $w/4$  of equation (206) is obtained. A plot, a comparison to the one-loop FRG fixed point (79), and a numerical verification are presented in figure 15.

#### 2.24. Random-energy model (REM)

The random-energy model (REM) was introduced by Derrida in 1980 [55, 191] as an exactly soluble, albeit extreme simplification of a spin glass. It was further studied in [192–194]. Consider an Ising model with  $N$  spins. It has  $2^N$  distinct configurations, labeled by  $i = 1, \dots, 2^N$ . Suppose that the energy  $E_i$  of each state  $i$  is taken from a Gaussian distribution

$$P(E) = \frac{1}{\sqrt{\pi N}} e^{-E^2/N}. \quad (208)$$

Thus  $\langle E \rangle = 0$ , and  $\langle E^2 \rangle = N/2$ . The factor of  $N$  is chosen to obtain a non-trivial limit for  $N \rightarrow \infty$  below.

A sample of the REM consists of  $2^N$  random energies  $E_i$  drawn from equation (208). The partition function at temperature  $T = 1/\beta$ , and the occupation probabilities are

$$\mathcal{Z}_0 = \sum_{i=1}^{2^N} e^{-\beta E_i}, \quad p_i = \frac{e^{-\beta E_i}}{\mathcal{Z}_0}. \quad (209)$$

Consider the number  $\mathcal{N}(\epsilon, \epsilon + \delta)$  of states in the interval  $[N\epsilon, N(\epsilon + \delta)]$ . Setting

$$\mathcal{I}_\epsilon := \int_{N\epsilon}^{N(\epsilon + \delta)} P(x) dx \equiv \sqrt{\frac{N}{\pi}} \int_{\epsilon}^{\epsilon + \delta} e^{-y^2} dy, \quad (210)$$

the expectation and variance of  $\mathcal{N}(\epsilon, \epsilon + \delta)$  are

$$\langle \mathcal{N}(\epsilon, \epsilon + \delta) \rangle = 2^N \mathcal{I}_\epsilon, \quad (211)$$

$$\langle \mathcal{N}(\epsilon, \epsilon + \delta)^2 \rangle^c = 2^N \mathcal{I}_\epsilon (1 - \mathcal{I}_\epsilon). \quad (212)$$

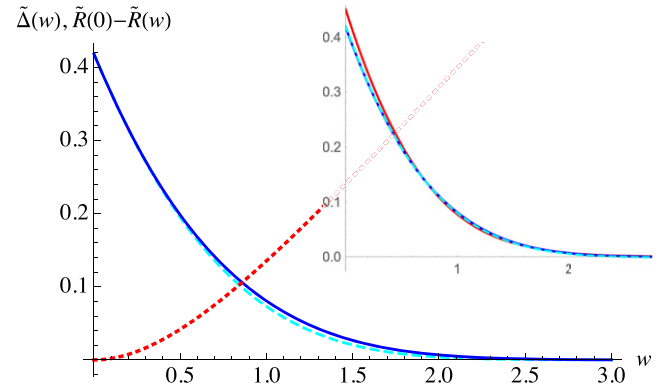


**Figure 15.**  $\tilde{\Delta}(w)$  for the Sinai model (blue), obtained by numerical integration of equation (202). In cyan dashed the solution (84)–(88) of the one-loop FRG equation, rescaled to the same value and slope at  $w = 0$ . In red, dotted  $\tilde{R}(0) - \tilde{R}(w)$ . (Inset) Numerical simulation [185, 186] for  $m^2 = 10^{-1}$  (red, solid), and  $m^2 = 10^{-2}$  (cyan, dashed), indistinguishable from the theory (blue solid). Statistical errors are within the line thickness.

This allows us to write the density of states  $\rho(\epsilon) \simeq \frac{1}{3} \mathcal{N}(\epsilon, \epsilon + \delta)$  as

$$\ln \rho(\epsilon) \simeq N [\ln(2) - \epsilon^2] + \frac{1}{2} \ln \left( \frac{N}{\pi} \right). \quad (213)$$

Define  $\epsilon_*$  s.t.

$$\ln \rho(\epsilon_*) = 0 \iff \epsilon_* = \sqrt{\ln 2} + \frac{\ln(N/\pi)}{4N\sqrt{\ln 2}} + \dots \quad (214)$$

It is instructive to run a simulation: as can be seen in figure 16, there is not a single state for  $|\epsilon| \geq \epsilon_*$ . Second, according to equations (211) and (212), relative fluctuations are suppressed,

$$\frac{\langle \mathcal{N}(\epsilon, \epsilon + \delta)^2 \rangle^c}{\langle \mathcal{N}(\epsilon, \epsilon + \delta) \rangle^2} = 2^{-N} \frac{1 - \mathcal{I}_\epsilon}{\mathcal{I}_\epsilon}. \quad (215)$$

To good precision one can therefore approximate at leading order in  $1/N$

$$\ln \rho(\epsilon) = N s(\epsilon), \quad s(\epsilon) = \begin{cases} \ln(2) - \epsilon^2, & |\epsilon| \leq \epsilon_* \\ -\infty, & |\epsilon| > \epsilon_*. \end{cases} \quad (216)$$

The quantity  $s(\epsilon)$  is interpreted as the entropy of the system;  $s(\epsilon) = -\infty$  means that the corresponding density  $\rho(\epsilon)$  vanishes. Note that the factor of  $N$  in equation (208) is introduced in order to render thermodynamic quantities as equation (216) extensive, i.e.  $\sim N$ .

We now proceed to other thermodynamic properties, notably the free energy

$$e^{-\beta N f(\epsilon)} = \mathcal{Z}_0 \simeq \int_{-\epsilon_*}^{\epsilon_*} d\epsilon e^{-N[\beta\epsilon - s(\epsilon)]}, \quad (217)$$

equivalent to

$$f(\epsilon) \simeq \min_{\epsilon \in [-\epsilon_*, \epsilon_*]} \left[ \epsilon - \frac{s(\epsilon)}{\beta} \right]. \quad (218)$$

This is a Legendre transform, typical of thermodynamic arguments; the restriction of  $\epsilon$  to  $[-\epsilon_*, \epsilon_*]$  is implicit in the definition (217), and allows us to use the parabolic form valid in that domain. An explicit calculation yields

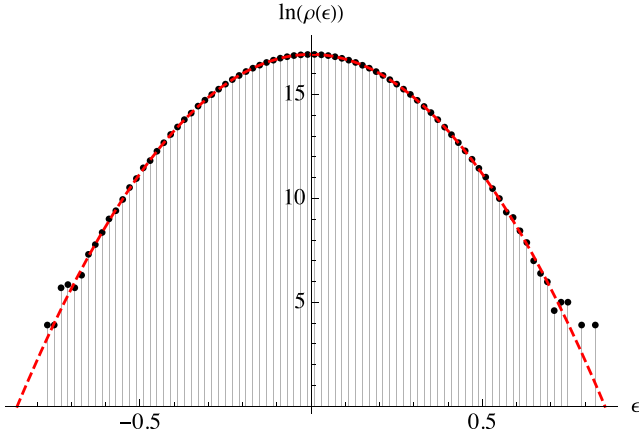


**Figure 16.** The log of the density of states  $\ln \rho(\epsilon)$  for the REM,  $n = 23$ . The maximal and minimal energies in this sample are 0.8376 and  $-0.7736$ , compared to  $\epsilon_* = 0.8582$ : the histogram vanishes for  $|\epsilon| \geq \epsilon_*$ .

$$f(\epsilon) = \begin{cases} -\frac{\beta}{4} - \frac{\ln(2)}{\beta}, & \beta \leq \beta_c, \\ -\sqrt{\ln(2)}, & \beta > \beta_c \end{cases}, \quad \beta_c = 2\sqrt{\ln(2)}. \quad (219)$$

Next define the *participation ratio* inspired by spin glasses [62, 195]

$$Y \equiv Y(\beta) = \frac{\sum_i e^{-2\beta E_i}}{\left[ \sum_i e^{-\beta E_i} \right]^2}. \quad (220)$$

It was shown [192] that all moments can be calculated analytically (see equations (10) and (11) of [192])

$$g(\mu) = \int_0^\infty (1 - e^{-u - \mu u^2}) u^{-\frac{T}{T_c} - 1} du, \quad (221)$$

$$\langle Y^n \rangle = \frac{(-1)^{n+1} T_c}{\Gamma(2n)} \frac{d^n}{d\mu^n} \ln g(\mu) \Big|_{\mu=0}. \quad (222)$$

The first moments read

$$\langle Y \rangle = 1 - \frac{T}{T_c}, \quad \langle Y^2 \rangle^c = \frac{1}{3} \frac{T}{T_c} \left( 1 - \frac{T}{T_c} \right). \quad (223)$$

Thus  $Y$  is a random variable, with rather large, non-selfaveraging fluctuations.

Finally, one can calculate the partition function in presence of a magnetic field [194], by generalizing its definition to

$$\mathcal{Z}(h) = \sum_{i=1}^{2^N} e^{-\beta E_i - \beta M_i h}, \quad (224)$$

where  $M_i$  is the total magnetization of the sample (the number of up spins minus the number of down spins). As the energies  $E_i$  are independent of the spin configuration  $\sigma_i$ , and its total magnetization  $M_i$ , the expectation value of  $\mathcal{Z}(h)$  factorizes,

$$\langle \mathcal{Z}(h) \rangle = \langle \mathcal{Z}_0 \rangle \times \langle e^{-\beta h M_1} \rangle_{\sigma_1}. \quad (225)$$

Using this factorization property (which also holds for SK), the partition function for two copies reads

$$\begin{aligned} \frac{\langle \mathcal{Z}(h_1) \mathcal{Z}(h_2) \rangle}{\mathcal{Z}_0^2} &= \sum_{i=j} \frac{1}{\mathcal{Z}_0^2} \langle e^{-\beta[2E_i + (h_1 + h_2)M_i]} \rangle \\ &+ \frac{1}{\mathcal{Z}_0^2} \sum_{i \neq j} \langle e^{-\beta[E_i + E_j + h_1 M_i + h_2 M_j]} \rangle \\ &= \langle Y \rangle \langle e^{-\beta(h_1 + h_2)M_1} \rangle_{\sigma_1} \\ &+ (1 - 2^{-N}) \langle e^{-\beta h_1 M_1} \rangle_{\sigma_1} \langle e^{-\beta h_2 M_1} \rangle_{\sigma_1}. \end{aligned} \quad (226)$$

The average over spin configurations factorizes<sup>21</sup>,

$$\langle e^{-\beta h M_1} \rangle_{\sigma_1} = \cosh(\beta h)^N. \quad (227)$$

In the high-temperature phase where  $\langle Y \rangle$  vanishes the partition function factorizes. In the low-temperature phase, the first term dominates for  $h_1 h_2 > 0$ , whereas the second one does for  $h_1 h_2 < 0$ . It leads to a non-analyticity of the effective action for  $T < T_c$ . This behavior is comparable to that of  $\Delta(w)$ , and different from that of  $R(w)$  (section 2.4). How can we understand this? The reason is that the disorder is *very strong*: flipping a single spin changes the energy as much as flipping a finite fraction of the spins. Thus there is no continuity in energy as for random manifolds, and shocks appear in the energy, rather than in the force. A cusp in the correlations of energy is a rather natural consequence.

## 2.25. Complex disorder and localization

*Motivation.* FRG is used with success to describe the statistics of elastic objects (this section 2) and depinning (next section 3), subjected to quenched *real* disorder. An interesting question is whether it can also be applied to systems with complex disorder (complex random potential or force), relevant in quantum mechanics. There is one study for quantum creep [198], but what we are after is a situation where interference becomes important.

Let us give a specific example. The hopping conductivity of electrons in disordered insulators in the strongly localized regime is described by the Nguyen–Spivak–Shklovskii (NSS) model [199]. The probability amplitude  $J(a, b)$  for a transition from  $a$  to  $b$  is the sum over interfering directed paths  $\Gamma$  from  $a$  to  $b$  [200–205]

$$J(a, b) := \sum_{\Gamma} \prod_{j \in \Gamma} \eta_j. \quad (228)$$

The conductivity between sites  $a$  and  $b$  is given by  $g(a, b) = |J(a, b)|^2$ . Each lattice site  $j$  contributes a random sign  $\eta_j = \pm 1$  (or, more generally a complex phase  $\eta_j = e^{i\theta_j}$ ).

Another example is the Chalker–Coddington model [206] for the quantum Hall (and spin quantum Hall) effect, where the transmission matrix  $J$  between two contacts  $a$  and  $b$  is given by [207, 208]

$$J(a, b) = \sum_{\Gamma} \prod_{(i,j) \in \Gamma} S_{(i,j)}. \quad (229)$$

<sup>21</sup> We refer to [194] for details.

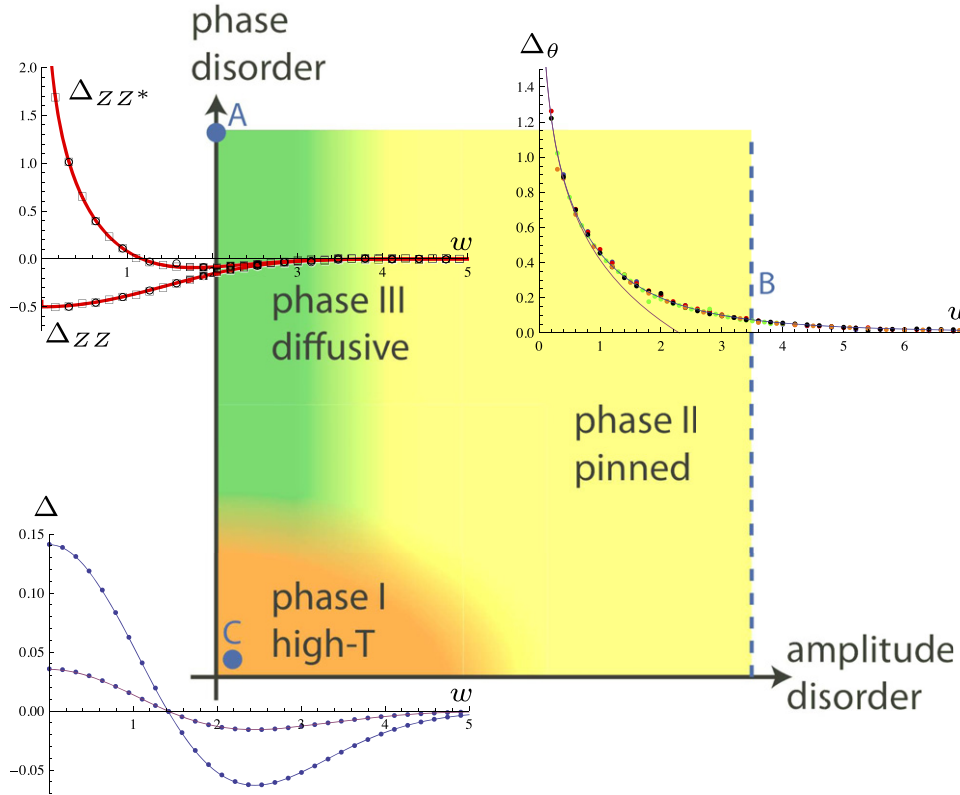


**Figure 17.** Phase portrait of the model defined in equation (230), following the conventions of [196]. The horizontal axis is the strength of  $V$ , the vertical axis the strength of  $\theta$ . The effective disorder correlators for points A (deep in the diffusive phase), B (deep in the pinned phase), C (infinitesimally small disorder) are shown as well. Symbols are from numerical simulations. Reprinted figure with permission from [196], Copyright (2011) by the American Physical Society.

The random variables  $S_{(i,j)}$  on every bond  $(i, j)$  are  $U(N)$  matrices, with  $N = 1$  for the charge quantum Hall effect and  $N = 2$  for the spin quantum Hall effect.  $\Gamma$  are paths subject to some rules imposed at the vertices. The conductance is given by  $g(a, b) = \text{tr}(J(a, b)^\dagger J(a, b))$ .

In both models, one would like to understand the dominating contributions to the sum  $Z$  over paths with random weights  $J(a, b)$ . In contrast to the thermodynamics of classical models, where all contributions are positive, contributions between paths with different phases can cancel. One is interested in the expected phase transitions.

*Definitions.* This is a complicated problem. In [197, 209–211] simplified models were considered. Here we consider the toy model of [197], which allows one to define the central objects of the FRG. The partition function at finite  $T = \beta^{-1}$  reads in generalization of equation (96)

$$\begin{aligned} Z(w) &= \sqrt{\frac{\beta m^2}{2\pi}} \int_{-\infty}^{\infty} dx e^{-\beta \left[ v(x) + \frac{m^2}{2}(x-w)^2 \right] - i\theta(x)} \\ &=: e^{-\beta \hat{V}(w) - i\hat{\theta}(w)}. \end{aligned} \quad (230)$$

One wishes to study the correlations

$$\Delta_V(w_1 - w_2) := \overline{\hat{V}'(w_1) \hat{V}'(w_2)}, \quad (231)$$

$$\Delta_\theta(w_1 - w_2) := \overline{\hat{\theta}'(w_1) \hat{\theta}'(w_2)}. \quad (232)$$

They are related to the correlations of  $\partial_w Z(w)$  and  $\partial_w Z^*(w)$  by

$$\Delta_{ZZ^*}(w) = \Delta_V(w) + \beta^{-2} \Delta_\theta(w), \quad (233)$$

$$\Delta_{ZZ}(w) = \Delta_V(w) - \beta^{-2} \Delta_\theta(w). \quad (234)$$

*Results.* As established by Derrida [196], there are three phases: high-temperature phase I, frozen phase II, and strong-interference phase III, depicted in the center of figure 17, accompanied by their correlation functions [197].

*Phase I.* For weak disorder (perturbative regime) one can evaluate the integral (230) by Taylor expanding to leading order in both  $V$  and  $\theta$ , to obtain

$$\Delta_V(w) \sim \Delta_\theta(w) \sim -\partial_w^2 e^{-\frac{m^2}{4} w^2}. \quad (235)$$

*Phase II.* This phase may be seen as a deformation of the localized phase, encountered for short-ranged disorder in the Kida model (section 2.22), or for long-ranged disorder in the Sinai model (section 2.23). The key change is a deformation of the shocks, which shows up in an additional logarithmic deformation of the force–force correlator inside a boundary layer of size  $w \sim T$ , see figure 17.

*Phase III.* Here  $V(u) = 0$ . This phase is the one most closely related to the NSS or Chalker–Coddington models. Contrary to the Kida or Sinai models which lead to a

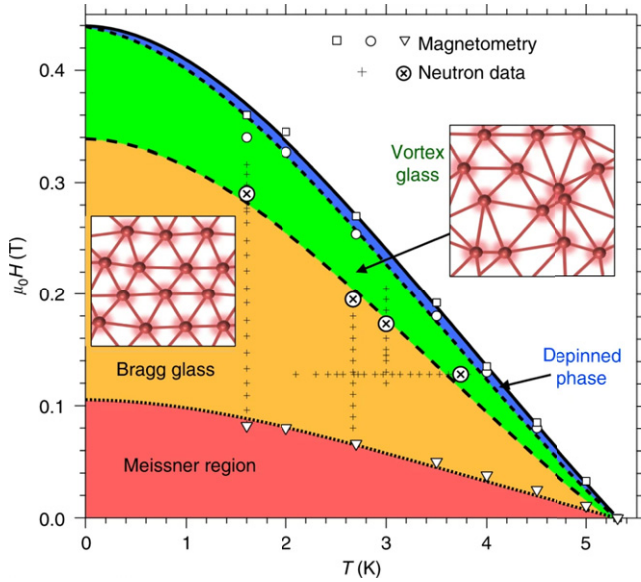


**Figure 18.** Phase diagram for vortices in a type-II superconductor. Reproduced from [212]. CC BY 4.0. From bottom to top these are the Meissner, vortex-free region (red), followed by the Bragg glass (orange) and a vortex glass (green and blue), above which super-conductivity vanishes (white).

localization of the path (the partition function is dominated by a minimizing path) fluctuations of  $Z$  are important, and zero-crossings are observed. They seem to be rather independent of the nature of the  $\theta$ -disorder, which we attribute to  $\theta$  being a compact variable. The zero crossings lead to a logarithmic divergence of the correlation functions (231) to (234), see figure 17.

### 2.26. Bragg glass and vortex glass

When the magnetic field  $H$  is increased in a pure type-II superconductor, there are two phase transitions: for low magnetic fields,  $H < H_1^c(T)$ , vortices are expelled due to the Meissner effect [213] (red region in figure 18). For  $H > H_1^c(T)$  flux-vortices appear. Increasing the magnetic field further, superconductivity breaks down for  $H > H_2^c(T)$  (white region in figure 18).

Let us now consider a dirty magnet. There has been a long debate whether the vortex lattice present for  $H_1^c(T) < H < H_2^c(T)$  can be described by a Bragg glass, or a vortex glass. In a Bragg glass favored by [21, 214–216], the Abrikosov lattice of vortices (see sketch in figure 3) is elastically deformed, but there are no topological defects and each vortex line retains six nearest neighbors. According to the theory of disordered elastic manifolds, the correlation function given in equation (120a) grows logarithmically with distance, preserving enough coherence to show up in a Bragg peak in neutron scattering experiments (hence the name). The alternative theory, termed vortex glass and favored (for sometimes quite different reasons) in [217–224], assumes that topological defects destroy the order, and as a consequence the Bragg peak in neutron scattering experiments.

The current experimental situation [212] shown in figure 18 favors, in agreement with intuition, a Bragg glass for smaller

fields, and a vortex glass for larger ones, with a transition at  $H_{B/V}^c(T)$ , with  $H_1^c(T) < H_{B/V}^c(T) < H_2^c(T)$ .

If the disorder contains columnar defects, it may exhibit [25, 225] a transverse Meissner effect, for which the tilt  $\vartheta$  to an applied field  $H$  vanishes up to  $H_{\text{tilt}}^c$ , after which it grows as  $\vartheta \sim |H - H_{\text{tilt}}^c|^\phi$ , with  $\phi < 1$ . One-dimensional quantum systems (Luttinger liquid) map to two-dimensional classical systems with columnar disorder, thus can be understood in the same framework [225], or alternatively [226–230] within the non-perturbative FRG (NPFGR) approach (section 9.1). One further encounters a rounding of the cusp through quantum fluctuations, similar to the quantum creep regime of [198].

There are also situations where one of the two phases is absent, as defects can destabilize the Bragg-glass phase [231]. Similar physics may be observed in CDWs [232]. For details we refer the reader to [19, 233]. Discussion of a moving vortex lattice is referred to section 3.25.

### 2.27. Bosons and fermions in $d = 2$ , bosonization

To proceed, we need to establish connections between theories in two dimensions, including relations between fermions and bosons, known as bosonization. Dimension  $d = 2$  is special as the Gaussian free field is dimensionless, allowing for a number of constructions of which we show some below. Our account is very condensed, and we refer to [3, 234–236] for background reading.

*Bosons.*

$$\mathcal{H}_{\text{boson}} = \frac{1}{8\pi} \int d^2\vec{z} [\nabla\Phi(\vec{z})]^2. \quad (236)$$

Appendix A.6 implies

$$\langle \Phi(\vec{z})\Phi(0) \rangle = -\ln|\vec{z}|^2 = -\ln z - \ln \bar{z}. \quad (237)$$

This suggests that one can decompose  $\Phi(\vec{z})$  into a holomorphic and antiholomorphic part,  $\Phi(\vec{z}) \equiv \Phi(z, \bar{z}) = \phi(z) + \bar{\phi}(\bar{z})$ , with

$$\begin{aligned} \langle \phi(z)\phi(w) \rangle &= -\ln(z-w), \\ \langle \bar{\phi}(\bar{z})\bar{\phi}(\bar{w}) \rangle &= -\ln(\bar{z}-\bar{w}), \\ \langle \phi(z)\bar{\phi}(\bar{w}) \rangle &= 0. \end{aligned} \quad (238)$$

Since  $\phi(z)$  has logarithmic correlations, an infinity of power-law correlated *vertex operators* can be constructed (the dots indicate normal ordering, i.e. exclusion of self-contractions at the vertex),

$$V_\alpha(z) = :e^{\alpha\phi(z)}: \quad (239)$$

$$\langle V_\alpha(z)V_\beta(w) \rangle = e^{-\alpha\beta \ln(z-w)} = (z-w)^{-\alpha\beta}. \quad (240)$$

*Majorana fermion.* Consider a Majorana (real) fermion, constructed from anti-commuting Grassman fields (section 8.2)

$$\mathcal{H}_{\text{Majorana}} = \frac{1}{2\pi} \int d^2\vec{z} [\bar{\psi}(\vec{z})\partial\bar{\psi}(\vec{z}) + \psi(z)\bar{\partial}\psi(z)]. \quad (241)$$

Its correlation-functions are obtained from equation (992) as

$$\langle \psi(z)\psi(w) \rangle = \frac{1}{z-w}, \quad (242)$$

$$\langle \bar{\psi}(\bar{z})\bar{\psi}(\bar{w}) \rangle = \frac{1}{\bar{z}-\bar{w}}. \quad (243)$$

As for the bosons above, the theory can be split into a holomorphic and an antiholomorphic part.

*Dirac fermion.* A Dirac (complex) fermion is made out of two Majorana-fermions  $\psi_1 = \psi_1^*$  and  $\psi_2 = \psi_2^*$ ,

$$\psi = \psi_1 + i\psi_2, \quad \psi^* = \psi_1 - i\psi_2. \quad (244)$$

Corresponding rules hold for the antiholomorphic fields. Choosing

$$\mathcal{H}_{\text{Dirac}} = \frac{1}{\pi} \int_z \bar{\psi}^*(\bar{z})\partial\bar{\psi}(\bar{z}) + \psi^*(z)\bar{\partial}\psi(z), \quad (245)$$

the correlation functions for the components  $\psi_1$  and  $\psi_2$  have an additional factor of 1/2 as compared to equations (241) and (242), resulting in

$$\langle \psi^*(z)\psi(w) \rangle = \langle \psi(z)\psi^*(w) \rangle = \frac{1}{z-w}, \quad (246)$$

$$\langle \psi(z)\psi(w) \rangle = \langle \psi^*(z)\psi^*(w) \rangle = 0. \quad (247)$$

Similar relations hold for the anti-holomorphic parts  $\bar{\psi}$ , and correlations vanish between  $\psi$  and  $\bar{\psi}$ .

*Bosonization.* Since a Dirac-fermion and a free boson have both central charge<sup>22</sup>  $c = 1$ , we may expect a closer relation between objects in these theories. Indeed setting

$$\psi(z) \hat{=} e^{i\phi(z)} : \quad \psi^*(z) \hat{=} e^{-i\phi(z)} : \quad (248)$$

$$\bar{\psi}(\bar{z}) \hat{=} e^{i\bar{\phi}(\bar{z})} : \quad \bar{\psi}^*(\bar{z}) \hat{=} e^{-i\bar{\phi}(\bar{z})} : \quad (249)$$

the (diverging part of the) fermion correlation functions are reproduced within the bosonic theory. Products of fermion operators are obtained from the point-split product

$$\begin{aligned} [\psi^*\psi](z) &:= \lim_{z \rightarrow w} \psi^*(w)\psi(z) = e^{-i\phi(w)}e^{i\phi(z)} \cdot \frac{1}{w-z} \\ &= \frac{1}{i} \partial\phi(z). \end{aligned} \quad (250)$$

<sup>22</sup> The conformal charge  $c$  is the amplitude of the leading term in the OPE of the stress–energy tensor with itself. It can be measured from the finite-size corrections of the free energy of a system [3, 234, 237, 238]. The central charge is often used to identify or distinguish systems. This has to be taken with some precaution, as the total central charge of non-interacting systems is the sum of the central charges of its components.

This rule allows one to decouple the four-fermion interaction as

$$\bar{\psi}^*(\bar{z})\bar{\psi}(\bar{z})\psi^*(z)\psi(z) \hat{=} \bar{\partial}\phi(\bar{z})\partial\phi(z). \quad (251)$$

Note that since there are two complex fermions, the only non-vanishing combination one can write down is the one given in equation (251). Introductory texts on bosonization techniques can be found in [235, 236].

*Thirring and sine-Gordon model.* The *Thirring model* introduced in [239] is the most general two-dimensional model with two independent families of fermions, and a kinetic term with a single derivative.

$$\begin{aligned} \mathcal{S}_{\text{Thirring}} &= \frac{1}{\pi} \int_z \left\{ \bar{\psi}^*(\bar{z})\partial\bar{\psi}(\bar{z}) + \psi^*(z)\bar{\partial}\psi(z) \right. \\ &\quad + \frac{\lambda}{2} [\bar{\psi}(\bar{z})\psi(z) + \bar{\psi}^*(\bar{z})\psi^*(z)] \\ &\quad \left. + \frac{g}{2} \bar{\psi}^*(\bar{z})\bar{\psi}(\bar{z})\psi^*(z)\psi(z) \right\}. \end{aligned} \quad (252)$$

Using the dictionary provided by equations (248), (249) and (251) shows equivalence to the *sine-Gordon model* [240]

$$\mathcal{H}_{\text{SG}} = \int d^2z \frac{1+g}{8\pi} [\nabla\Phi(\vec{z})]^2 + \frac{\lambda}{\pi} \cos(\Phi(\vec{z})). \quad (253)$$

## 2.28. Sine-Gordon model, Kosterlitz–Thouless transition

The sine-Gordon model can be treated in a perturbative expansion in  $\lambda$ . The leading-order correction comes at second order, and corrects  $g$ . Noting

$$T := \frac{1}{1+g}, \quad (254)$$

it can be written as<sup>23</sup>

$$\begin{aligned} &\left(\frac{\lambda}{2\pi}\right)^2 \int_{x,y} :e^{i\Phi(x)}: :e^{-i\Phi(y)}: \\ &= \left(\frac{\lambda}{2\pi}\right)^2 \int_{x,y} :e^{i[\Phi(x)-\Phi(y)]}: |x-y|^{-2T} \\ &\simeq \left(\frac{\lambda}{2\pi}\right)^2 \int_{x,y} \left\{ 1 - \frac{1}{2} :[\Phi(x)-\Phi(y)]^2: + \dots \right\} |x-y|^{-2T} \\ &\simeq \left(\frac{\lambda}{2\pi}\right)^2 \int_{x,y} \left\{ 1 - \frac{1}{2} : \left[ (x-y)\nabla\Phi\left(\frac{x+y}{2}\right) \right]^2 : + \dots \right\} \\ &\quad \times |x-y|^{-2T} \\ &\simeq \left(\frac{\lambda}{2\pi}\right)^2 \int_{x,y} \left\{ 1 - \frac{(x-y)^2}{4} : \left[ \nabla\Phi\left(\frac{x+y}{2}\right) \right]^2 : + \dots \right\} \\ &\quad \times |x-y|^{-2T}. \end{aligned} \quad (255)$$

<sup>23</sup> Combinatorial factors are obtained from  $\cos(\Phi) = \frac{1}{2}(e^{i\Phi} + e^{-i\Phi})$ , leaving two combinations with overall charge neutrality, which cancel against the 1/2! from the expansion of  $e^{-\mathcal{H}_{\text{SG}}}$ . The dots denote normal-ordering, the change in  $\lambda$  being absorbed therein. Vector notation is suppressed for simplicity. For an introduction into the technique see [118].

The first term yields a correction to the free energy; it necessitates a relevant counter term (UV divergent, IR finite), but does not enter into IR properties of the theory. The second term is a correction to  $g$ ,

$$\delta g = \lambda^2 \int_0^L \frac{dz}{z} z^{4-2T} = \lambda^2 \frac{L^{4-2T}}{4-2T}. \quad (256)$$

Defining the dimensionless couplings as  $\tilde{g} \equiv g_{\text{eff}} = g + \delta g$ ,  $\tilde{\lambda} := \lambda_{\text{eff}} L^{2-T}$ , with  $\lambda_{\text{eff}} = \lambda + \mathcal{O}(\lambda^3)$ , one obtains the  $\beta$  functions<sup>24</sup>

$$\beta_{\tilde{g}}(\tilde{\lambda}, \tilde{g}) = \tilde{\lambda}^2 + \dots \quad (257a)$$

$$\beta_{\tilde{\lambda}}(\tilde{\lambda}, \tilde{g}) = (2-T)\tilde{\lambda} + \dots = \left(2 - \frac{1}{1+\tilde{g}}\right)\tilde{\lambda} + \dots \quad (257b)$$

Subdominant corrections are down by a factor of  $\tilde{\lambda}^2$ . Rewritten in terms of  $\tilde{\lambda}$  and  $\tilde{T} = 1/(1+\tilde{g})$ , this yields

$$\beta_{\tilde{T}}(\tilde{T}, \tilde{\lambda}) = -\tilde{T}^2 \tilde{\lambda}^2 + \dots = -\tilde{T}_c^2 \tilde{\lambda}^2 + \dots \quad (258a)$$

$$\beta_{\tilde{\lambda}}(\tilde{T}, \tilde{\lambda}) = (\tilde{T}_c - \tilde{T})\tilde{\lambda} + \dots \quad (258b)$$

The reader will mostly see these equations expanded around  $\tilde{T}_c = 2$ , as done above. The schematic flow chart is shown in figure 19.

There is a line of fixed points for  $\tilde{T} > \tilde{T}_c$  (red in figure 19). All these fixed points have  $\tilde{\lambda} = 0$ , thus are Gaussian theories. Below  $\tilde{T}_c$ , the flow is to strong coupling. Physically,  $e^{i\Phi}$  and  $e^{-i\Phi}$  are interpreted as vortices and anti-vortices, topological defects with charge  $\pm 1$ , chemical potential  $\lambda$ , interacting via Coulomb interactions. For  $\tilde{T} > \tilde{T}_c$  they are bound, and only a finite number is present. For  $\tilde{T} < \tilde{T}_c$  they are unbound, gaining enough entropy to overcome the energetic costs for their core. The transition at  $\tilde{T} = \tilde{T}_c$  is known as the Kosterlitz–Thouless transition [241].

Higher-loop calculations can be performed, both in the Thirring model (241), as in the sine-Gordon model (253). As our treatment shows, they are rather straight-forward, and one should be able to go at least to three-loop order in sine-Gordon, and to even higher order in the fermionic model. It is therefore surprising to read about massive contradictions in the literature at two-loop order [242], confirming the original 1980 result of [243], but declaring later calculations in [244–246] as well as [247] to be incorrect.

<sup>24</sup> Definition of the  $\beta$  functions are as in section 2.2. Equations (252) and (253) were tuned to have the simplest coefficients later.

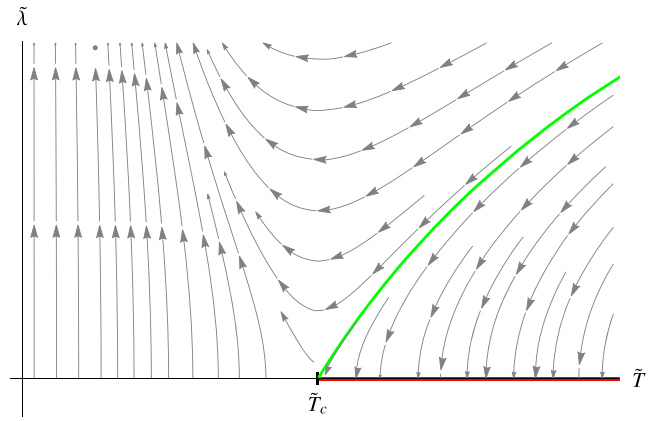


**Figure 19.** Flow diagram of the Kosterlitz–Thouless transition: all trajectories starting from the green line are attracted to  $\tilde{\lambda} = 0$ , and  $\tilde{T} > \tilde{T}_c$  (line of fixed points), the remaining ones to the strong-coupling regime with  $\tilde{\lambda} \gg 1$ .

What the RG approach cannot reach is the strong-disorder fixed point  $\tilde{\lambda} \gg 1$ . The latter has been studied in the Wegner flow-equation approach [248], and via NPF RG [249].

## 2.29. Random-phase sine-Gordon model

The sine-Gordon model (253) with quenched disorder coupling to  $e^{i\Phi}$  reads (writing  $\vec{z} \rightarrow z$ )

$$\mathcal{H}_{\text{rpsG}} = \int_z \frac{[\nabla\Phi(z)]^2}{8\pi T} + \xi(z) : e^{i\Phi(z)} : + \xi^*(z) : e^{-i\Phi(z)} : \\ \overline{\xi(z)\xi^*(z')} = \frac{\lambda}{2\pi} \delta^2(z-z'). \quad (259)$$

After replication (see section 1.5), the effective action reads

$$\mathcal{S}_{\text{rpsG}} = \int_z \sum_{\alpha} \frac{[\nabla\Phi_{\alpha}(z)]^2}{8\pi T} - \frac{\lambda}{2\pi} \int_{z_{\alpha \neq \beta}} : e^{i[\Phi_{\alpha}(z) - \Phi_{\beta}(z)]} : \\ - \frac{\sigma}{4\pi} \int_{z_{\alpha \neq \beta}} \nabla\Phi_{\alpha}(z) \nabla\Phi_{\beta}(z). \quad (260)$$

We added an additional off-diagonal term in the second line, since it is generated under RG; we will see this shortly.

Perturbation theory is performed with

$$\langle \Phi_{\alpha}(x)\Phi_{\beta}(y) \rangle_0 = -T\delta_{\alpha\beta} \ln(|x-y|^2). \quad (261)$$

*First diagram (one loop).* We use the graphical notation

$$\alpha \bullet \text{---} \ominus_{\beta} = : e^{i[\Phi_{\alpha}(x) - \Phi_{\beta}(x)]} : \quad (262)$$

The contributions to the effective action are  $\delta S_i \equiv \int_x \delta s_i$ . The first one is (an ellipse encloses the same replica)

$$-\delta s_1 = \begin{array}{c} x \\ \bullet \text{---} \ominus_{\beta} \\ y \end{array} \\ = \frac{1}{2!} \left( \frac{\lambda}{2\pi} \right)^2 \sum_{\alpha \neq \beta} \int_y : e^{i[\Phi_{\alpha}(x) - \Phi_{\beta}(x) - \Phi_{\alpha}(y) + \Phi_{\beta}(y)]} : \\ \times e^{-4T \ln|x-y|}. \quad (263)$$

This term contains a strongly UV-divergent contribution to the free energy (which we do not need) and the sub-dominant term

$$\begin{aligned}
-\delta s_1 &\approx -\frac{1}{4} \left( \frac{\lambda}{2\pi} \right)^2 \sum_{\alpha \neq \beta} \int_y |x-y|^{-4T} \\
&\times :[(x-y) \cdot \nabla \Phi_\alpha(x) - (x-y) \cdot \nabla \Phi_\beta(x)]^2: \\
&= -\frac{1}{4} \left( \frac{\lambda}{2\pi} \right)^2 \sum_{\alpha \neq \beta} \int_y |x-y|^{2-4T} \\
&\times :[\nabla \Phi_\alpha(x) - \nabla \Phi_\beta(x)]^2: \quad (264)
\end{aligned}$$

It corrects  $\sigma$ ,

$$\delta\sigma = \frac{1}{2} \lambda^2 \times I_1, \quad (265a)$$

$$I_1 = \frac{1}{2\pi} \int dy^2 |y|^{2-2T} \Theta(|y| < L) = \frac{L^{4\tau}}{4\tau}, \quad (265b)$$

$$\tau := 1 - T. \quad (265c)$$

Second diagram (one loop).

$$\begin{aligned}
-\delta s_2 &= \bullet \text{---} \bigcirc \text{---} \bullet \\
&= \frac{2}{2!} \left( \frac{\lambda}{2\pi} \right)^2 \sum_{\alpha \neq \beta \neq \gamma} \int_y :e^{i[\Phi_\alpha(x) - \Phi_\gamma(y)]} : : e^{-i[\Phi_\beta(x) - \theta_\beta(y)]} : \\
&\quad \times e^{-2T \ln|x-y|}. \quad (266)
\end{aligned}$$

Projecting onto the interaction yields

$$-\delta s_2 \approx \left( \frac{\lambda}{2\pi} \right)^2 \times (n-2) \sum_{\alpha \neq \gamma} :e^{i[\Phi_\alpha(x) - \Phi_\gamma(x)]} : I_2, \quad (267)$$

$$I_2 = \frac{1}{2\pi} \int d^2y |y|^{-T} \Theta(|y| < L) = \frac{L^{2\tau}}{2\tau}. \quad (268)$$

Setting the number of replicas  $n \rightarrow 0$ , we get

$$\delta\lambda = -2\lambda^2 \times I_2. \quad (269)$$

Defining the  $\beta$ -functions as the variation with respect to the large-scale cutoff  $L$ , keeping the bare coupling  $\lambda$ , one obtains after some algebra

$$\beta_{\tilde{\lambda}}(\tilde{\lambda}) := L \frac{\partial}{\partial L} \tilde{\lambda} = 2\tau \tilde{\lambda} - 2\tilde{\lambda}^2 + \tilde{\lambda}^3 + \mathcal{O}(\tilde{\lambda}^4), \quad (270a)$$

$$\beta_\sigma(\tilde{\lambda}) := L \frac{\partial}{\partial L} \sigma = \frac{1}{2} \tilde{\lambda}^2 + \mathcal{O}(\tilde{\lambda}^4). \quad (270b)$$

The additional two-loop coefficients are obtained in [257]. What are the physical consequences of these  $\beta$ -functions? First of all, there is a non-trivial fixed point for  $\tilde{\lambda}$  at

$$\tilde{\lambda}_c = \tau + \frac{1}{2} \tau^2 + \mathcal{O}(\tau^3). \quad (271)$$

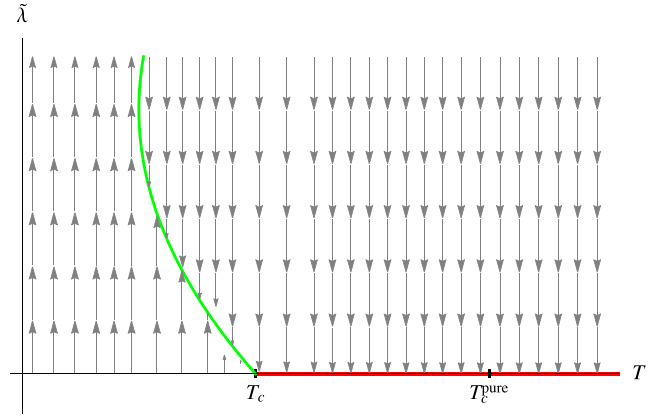


Figure 20. The RG flow for  $\tilde{\lambda}$  as a function of  $T$ .

Second, integrating the  $\beta$ -function for  $\sigma$ , starting at a microscopic scale  $a$ , yields, see figure 20

$$\sigma = \frac{1}{2} \tilde{\lambda}_c^2 \ln\left(\frac{L}{a}\right) + \dots = \left[ \frac{\tau^2}{2} + \frac{\tau^3}{2} + \mathcal{O}(\tau^4) \right] \ln\left(\frac{L}{a}\right), \quad (272)$$

equivalent to

$$\sigma(k) \simeq - \left[ \frac{\tau^2}{2} + \frac{\tau^3}{2} + \mathcal{O}(\tau^4) \right] \ln(ak). \quad (273)$$

This allows us to obtain the  $k$  dependent two-point function as

$$\overline{\langle \tilde{\Phi}_1(k) \tilde{\Phi}_2(-k) \rangle} = \left( \frac{4\pi T}{k^2} \right)^2 \frac{\sigma(k) k^2}{2\pi}. \quad (274)$$

As a consequence<sup>25</sup>,

$$\overline{\langle \Phi(x) - \Phi(0) \rangle^2} = \mathcal{A} \ln(x/a)^2 + \mathcal{O}(\ln(x/a)), \quad (275)$$

$$\begin{aligned}
\mathcal{A} &= 2(1-\tau)^2 [\tau^2 + \tau^3 + \mathcal{O}(\tau^4)] \\
&= 2\tau^2 - 2\tau^3 + \mathcal{O}(\tau^4). \quad (276)
\end{aligned}$$

A numerical test [254] using a combinatorial algorithm growing polynomial in system size (the concept behind this achievement is discussed in section 2.31) are shown in figure 21.

The result (276) was obtained in a perturbative expansion in  $T - T_c$ . Even if one could calculate the following orders, and resum them properly, one wonders whether the expansion remains correct down to  $T = 0$ . This is unlikely: we know from

<sup>25</sup> Intermediate steps are

$$\begin{aligned}
\overline{\langle \Phi_1(x) \Phi_1(0) \rangle} - \overline{\langle \Phi_1(x) \Phi_2(0) \rangle} &= \int \frac{d^2k}{(2\pi)^2} \frac{4\pi T}{k^2} e^{ikx} \\
&= -2T \ln|x/a|.
\end{aligned}$$

$$\begin{aligned}
\overline{\langle \Phi_1(x) \Phi_2(0) \rangle} &= \int \frac{d^2k}{(2\pi)^2} \left( \frac{4\pi T}{k^2} \right)^2 \frac{\sigma(k) k^2}{2\pi} e^{ikx} \\
&= -[\tau^2 + \tau^3 + \mathcal{O}(\tau^4)] T^2 \ln^2|x/a|.
\end{aligned}$$

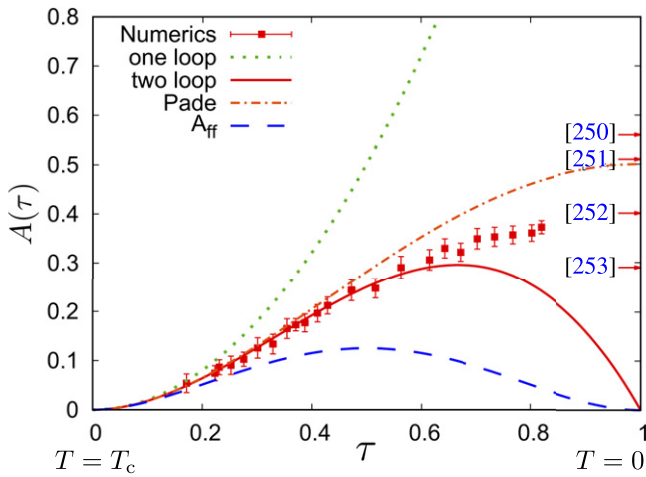


**Figure 21.** The amplitude  $A(\tau)$ , characterizing the super-rough phase. Reprinted figure with permission from [254], Copyright (2012) by the American Physical Society. The squares are numerical estimates using the algorithm of [255]. ‘One loop’ indicates the one-loop result  $A(\tau) = 2\tau^2$  while ‘two loop’ refers to equation (276), (a Padé resummation of it is shown as well).  $A_{\text{ff}}$  is the result of [256]. We also show values obtained numerically at  $T = 0$  in the corresponding references.

the  $\epsilon$ -expansion, see equation (94), that the fixed-point at  $T = 0$  has to all orders in  $\epsilon$  the form (with  $\mathcal{C}$  a constant)

$$\Delta(\Phi) = \mathcal{C} \left[ \frac{2\pi^2}{3} - \Phi(2\pi - \Phi) \right] \equiv 4\mathcal{C} \sum_{q=1}^{\infty} \frac{\cos(q\Phi)}{q^2}. \quad (277)$$

It contains an infinity of subdominant modes indexed by  $q$ , which one can try to incorporate into the perturbative result. Naively one expects the mode  $q$  to show up at  $T_c(q) = T_c/q^2$ , and it is likely to increase the perturbative result. Attempts to do so have been undertaken in [258–261].

### 2.30. Multifractality

Consider an observable  $\mathcal{O}(\ell)$  such as the field difference between two points a distance  $\ell$  apart. Its  $n$ th moment reads

$$\langle \mathcal{O}(\ell)^n \rangle \sim \ell^{\zeta_n}. \quad (278)$$

Generically there are two possibilities

- (a)  $\zeta_n = n\zeta$ : fractal
- (b)  $\zeta_n \neq n\zeta$ : multifractal

In some cases, e.g. in the critical dimension, one has

$$\langle \mathcal{O}(\ell)^n \rangle \sim \ell^{\zeta_n} = e^{\zeta_n \ln(\ell)} \rightarrow \zeta_n \ln(\ell), \quad (279)$$

i.e. the universal anomalous dimension appears as the amplitude of the log, see e.g. equation (120a) and section 3.8. We still think of these systems as fractal or multifractal, depending on which of the two choices above applies.

Most pure critical systems are fractals. Famous multifractal systems are Navier–Stokes turbulence [262–264], or the more tractable passive advection of particles, the *passive scalar* [265–271], or its generalization to the advection of extended elastic objects [272].

An important question is whether systems with *quenched disorder* show multifractality. A prominent example is the wave-function statistics at a delocalization transition, such as the Anderson metal–insulator transition at the mobility edge in three spatial dimensions, or the integer quantum-Hall plateau transition in two dimensions. Here one considers (see [273] for a concise introduction or the classic [274])

$$P_q(\epsilon_i) := \int_{L^d} d^d r |\psi_i(r)|^{2q} \sim L^{-\tau(q)}, \quad (280)$$

where  $\epsilon_i$  is the energy of the state  $i$ , and  $\psi_i(r)$  its wave function. Note that normalization imposes  $\tau(1) = 0$ . For extended states inside a band  $\tau(q) = d(q - 1)$ , while for localized states  $\tau(q) = 0$ . At the band edge  $\tau(q)$  is non-trivial. Define by  $f(\alpha)$  its Legendre transform,

$$\text{Legendre}_{\alpha \leftrightarrow q} \quad f(\alpha) + \tau(q) = \alpha q. \quad (281)$$

Then the set of points at which an eigenfunction takes the value  $|\psi(r)|^2 = \mathcal{A}L^{-\alpha}$  has weight  $L^{f(\alpha)}$ . Both  $f(\alpha)$  and  $\tau(q)$  are convex.

The question relevant for this review is whether disordered elastic manifolds show multifractality. As long as the roughness exponent  $\zeta > 0$ , this does not seem to be the case. The situation is different for  $\zeta = 0$ , i.e. CDWs or vortex lattices. Technically, it can be accessed either via a  $4 - \epsilon$  expansion [275] or directly in two dimensions [276].

*Multifractality of the random-phase sine-Gordon model in dimension  $d = 2$ .* The random-phase sine-Gordon model was introduced above in section 2.29. The object to be considered is

$$C(q, r) := \overline{\langle e^{iq[\Phi(r) - \Phi(0)]} \rangle}. \quad (282)$$

It was shown in [276] that with  $\mathcal{A}$  given in equation (276),

$$C(q, r) \simeq \left(\frac{a}{r}\right)^{\eta(q)} \exp\left(-\frac{1}{2}\mathcal{A}q^2 \ln^2(r/a)\right). \quad (283)$$

The anomalous exponent  $\eta$  defined in equation (283) reads

$$\eta(q) = 2q^2(1 - \tau)[1 + 2(1 - \tau)\sigma'] + \tau^2\eta_g(q) + \mathcal{O}(\tau^3). \quad (284)$$

Its nontrivial part  $\eta_g$  is [276]

$$\eta_g(q) = \begin{cases} q^2[1 - 2\gamma_E - \psi(q) - \psi(-q)], & q < 1 \\ -2, & q = 1. \end{cases} \quad (285)$$

Here  $\gamma_E$  is Euler’s constant. The result for the correlation function (282) enables one to calculate the leading large-distance behavior of all higher powers of the connected correlation

functions in the super-rough phase, i.e., for  $T < T_c$  ( $\tau > 0$ , see figure 20). Using

$$\eta_g(q) = q^2 + 2 \sum_{n=2}^{\infty} \zeta(2n-1) q^{2n}, \quad (286)$$

one sees that odd moments vanish, the second moment is given by equations (275) and (276), and higher even moments by

$$\frac{(-1)^n}{(2n)!} \overline{[\Phi(r) - \Phi(0)]^{2n}}_c = -2\tau^2 \zeta(2n-1) \ln\left(\frac{r}{a}\right) + \dots \quad (287)$$

This system is multifractal.

FRG in dimension  $4 - \epsilon$ . Following [275], define

$$\mathcal{G}[\lambda] := \overline{\langle e^{\int_x \lambda(x) u_1(x)} \rangle}_S, \quad (288)$$

$$\lambda(x) = iq[\delta(x) - \delta(x+r)]. \quad (289)$$

This can be calculated with methods similar to [277], using from the action (30) only the cubic vertex,

$$\begin{aligned} & \frac{1}{2T^2} \int_x \sum_{a,b} R(u_a(x) - u_b(x)) \\ & \rightarrow \frac{\sigma}{12T^2} \sum_{a,b} |u_a(x) - u_b(x)|^3, \quad \sigma = R'''(0^+). \end{aligned} \quad (290)$$

The connected part of  $\mathcal{G}[\lambda]$  reads (the correlation function  $C(x)$  is defined in equation (33a))

$$\begin{aligned} \ln(\mathcal{G}[\lambda]) &= \text{diagram 1} - \frac{1}{2} \text{diagram 2} + \frac{1}{3} \text{diagram 3} + \dots \\ &= \ln\left(\frac{\det(-\nabla^2 + \sigma U(x) + m^2)}{\det(-\nabla^2 + m^2)}\right) \end{aligned} \quad (291)$$

$$U(x) = \int_y C(x-y)\lambda(y). \quad (292)$$

Calculating the determinant (291) is a formidable task, usually only possible in perturbation theory in  $\sigma$ . Here we give analytical results, using three consecutive tricks:

- (a) Solve the problem for a spherically symmetric source  $\lambda(y)$ , assuming a uniformly distributed positive unit charge on a circle of radius  $a$ , and a compensating negative charge on a circle of radius  $L \gg a$ . The potential is  $U(x) = (r^{-2} - L^{-2})/(2\pi)^2$  for  $a \leq r \leq L$ , and constant beyond.

- (b) Write the Laplacian in distance and angle variables,

$$-\nabla^2 \rightarrow \mathcal{H}_l := -\frac{d^2}{dr^2} + \frac{(l + \frac{d-3}{2})(l + \frac{d-1}{2})}{r^2}. \quad (293)$$

- (c)  $\ln(\mathcal{G}[\lambda])$  is written as a sum of the logarithms of the one-dimensional determinant ratios  $\mathcal{B}_l$  for partial waves, weighted with the degeneracy of angular momenta  $l$ ,

$$\ln(\mathcal{G}[\lambda]) = \sum_{l=0}^{\infty} \frac{(2l+d-2)(l+d-3)!}{l!(d-2)!} \ln(\mathcal{B}_l). \quad (294)$$

- (d) The Gel'fand–Yaglom method [278] explained in appendix A.8 gives the ratio of the one-dimensional functional determinants for each partial wave  $l$  as

$$\mathcal{B}_l := \frac{\det[\mathcal{H}_l + \sigma U(r) + m^2]}{\det[\mathcal{H}_l + m^2]} = \frac{\psi_l(L)}{\tilde{\psi}_l(L)}. \quad (295)$$

Here  $\psi_l(r)$  is the solution of

$$[\mathcal{H}_l + \sigma U(r) + m^2] \psi_l(r) = 0, \quad (296)$$

satisfying  $\psi_l(r) \sim r^{l+(d-1)/2}$  for  $r \rightarrow 0$ ;  $\tilde{\psi}_l(r)$  is the solution for  $\sigma = 0$ .

- (e) After some pages of algebra, one finds (modulo odd terms which cancel below)

$$\ln(\mathcal{G}[\lambda]) = \mathcal{F}\left(\frac{\sigma q}{(2\pi)^2}\right) + \text{terms odd in } \sigma \quad (297)$$

$$\begin{aligned} \mathcal{F}(s) &= -\sum_{l=0}^{\infty} (l+1)^2 \left( \sqrt{(l+1)^2 + s} - (l+1) \right. \\ & \quad \left. - \frac{s}{2(l+1)} + \frac{s^2}{8(l+1)^3} \right). \end{aligned} \quad (298)$$

Resummation yields (dropping odd terms)

$$\mathcal{F}(s) = \sum_{n=2}^{\infty} \frac{s^{2n} \Gamma(2n - \frac{1}{2}) \zeta(4n-3)}{2\sqrt{\pi} (2n)!}. \quad (299)$$

- (f) In a last step one proves perturbatively that all  $n$ -point functions remain unchanged if one moves the charge on the sphere at  $|r| = L$  to a single point at distance  $L$  from the origin. The combinatorial analysis yields an additional factor of 2.

Using the FRG fixed point (95),  $s = \frac{\epsilon}{3}q$ , the  $2n$ (th) cumulant of relative displacements is obtained as

$$\overline{[u(r) - u(0)]^{2n}}_c \simeq \mathcal{A}_{2n} \ln(r/a) \quad (300)$$

$$\mathcal{A}_{2n} = -\left(\frac{\epsilon}{3}\right)^{2n} \frac{\Gamma(2n - \frac{1}{2}) \zeta(4n-3)}{\sqrt{\pi}}, \quad n \geq 2. \quad (301)$$

This correlation function is multifractal.

### 2.31. Simulations in equilibrium: polynomial versus NP-hard

Finding the ground state of a disordered system is in general a very difficult problem, often even NP-hard, meaning no algorithm exists which is guaranteed to find the ground state in polynomial time, i.e. within a time which does not grow faster than  $N^p$ , with  $N$  the system size, and  $p$  a finite number. This statement should be viewed as ‘state of the art’: e.g. we know of no algorithm to find the ground state of the SK model in polynomial time; but this does not imply that no such algorithm can exist. What computer scientists have proven is that if one

day an algorithm is found to solve one NP-hard problem, all other NP-hard problems can be solved as well. We refer the reader to the textbooks [279, 280] and collection [281] for a more precise definition and further information on the subject.

While many ground-state calculations are considered NP-hard, there are some notable exceptions: for the RNA-folding problem [282] a polynomial algorithm exists [283], which evaluates the partition function at all temperatures in a time growing as  $N^3$ , allowing one not only to find the ground state but even the phase transition from a frozen to a molten phase [284–286].

Another notable exception are disordered elastic manifolds, or more specifically the ground state of an Ising ferromagnet coupled to either RB or RF disorder. It can be solved by the *minimum-cut algorithm* [287]. This has been used in numerous publications: to find the roughness exponent  $\zeta$  in dimensions 2 and 3 [137], see figure 10; to measure the FRG-fixed point function [128], see figure 8 or avalanche-size distributions in equilibrium [288], see figure 51. Further for flux lines in a disordered environment [289, 290]; or solid-on-solid models with disordered substrates [250].

### 2.32. Experiments in equilibrium

There are few experiments which really are in equilibrium. The main reason is that in most cases the exponent  $\theta$  defined in equation (45) is positive, restricting the energy fluctuations which according to equation (47) grow as  $L^\theta$ . As a consequence, there is a maximal length  $L_T^{\max}$  up to which the system can equilibrate, i.e. find the minimum-energy configuration. Let us give a list of notable exceptions.

- (a) *Domain walls in thin magnetic films* with RB disorder have long been interpreted [84, 291, 292] as showing the roughness exponent of  $\zeta_{\text{RB}}^{d=1} = 2/3$  given in equation (122). This interpretation probably holds only on small scales, see the discussion in section 3.21.
- (b) *Hairpin unzipping* reported in [293] is consistent with a roughness exponent  $\zeta = 4/3$ , in agreement with the value predicted for a single degree of freedom, i.e.  $d = 0$  or  $\epsilon = 4$  in equation (83). We discuss this experiment in detail in section 3.17. There it is confronted with an experiment using the much softer peeling mode, placing it in the different depinning universality class with  $\zeta = 2^-$ .
- (c) Vortex lattices (section 2.26).

## 3. Dynamics, and the depinning transition

### 3.1. Phenomenology

Another important class of phenomena for elastic manifolds in disorder is the so-called *depinning transition*: applying a constant force to the elastic manifold, e.g. a constant magnetic field to the ferromagnet mentioned in the introduction, the latter will move if, and only if, a certain critical threshold force  $f_c$  is surpassed, see figure 22. (This is fortunate, since otherwise the magnetic domain walls in the hard-disc drive onto which this article is stored would move, with the effect of deleting all information, depriving you from your reading.)

At  $f = f_c$ , the so-called depinning transition, the manifold has a roughness exponent  $\zeta$  (see equation (7)), distinct from the equilibrium ( $f = 0$ ). The equation describing the movement of the interface is

$$\partial_t u(x, t) = (\nabla^2 - m^2)u(x, t) + F(x, u(x, t)) + f(x, t), \quad (302)$$

$$F(x, u) = -\partial_u V(x, u). \quad (303)$$

There are two main driving protocols, depending on whether one controls the applied force, or the mean driving velocity.

*Force-controlled depinning.* Let us impose a driving force  $f(x, t) = f$ , and set  $m \rightarrow 0$ . For  $f > f_c$ , the manifold then moves with velocity  $v$ . Close to the transition, new critical exponents appear:

- a velocity-force relation given by (see figure 22)

$$v \sim |f - f_c|^\beta \quad \text{for } f > f_c, \quad (304)$$

- a *dynamic* exponent  $z$  relating correlation functions in space and time

$$t \sim x^z. \quad (305)$$

Thus if one has a correlation or response function  $R(x, t)$ , it will be for short times and distances be a function of  $t/x^z$  only,

$$R(x, t) \simeq R(t/x^z). \quad (306)$$

- a correlation length  $\xi$  set by the distance to  $f_c$

$$\xi = \xi_f \sim |f - f_c|^{-\nu}. \quad (307)$$

Remarkably, this relation holds on both sides of the transition: for  $f < f_c$ , it describes how starting from a flat or equilibrated configuration, the correlation length  $\xi$ , which can be interpreted as the avalanche extension (defined below in equation (470)), increases as one approaches  $f_c$ . Arriving at  $f_c$ , each segment of the interface has moved. Above  $f_c$ , the interface is always moving, and the correlation length  $\xi$  (which now decreases upon an increase in  $f$ ) gives the size of coherently moving pieces.

- The new exponents  $z$ ,  $\beta$  and  $\nu$  are not independent, but related [294]. Suppose that  $f > f_c$ , and we witness an avalanche of extension  $\xi$ . Then its mean velocity scales as

$$\begin{aligned} v \sim \frac{u}{t} &\sim \frac{\xi^\zeta}{\xi^z} \sim |f - f_c|^{-\nu(\zeta-z)} \\ \implies \beta &= \nu(z - \zeta). \end{aligned} \quad (308)$$

One can make the same argument below  $f_c$ , by slowing increasing  $f$  to  $f_c$ .

- Suppose that below  $f_c$  the manifold is in a pinned configuration. Increasing  $f$  leads to an avalanche, of extension  $\xi$ , and a change of elastic force (per site)  $\sim \xi^{\zeta-2}$ . This has to be balanced by the driving force, i.e.

$$\xi^{\zeta-2} \sim |f - f_c| \implies \nu = \frac{1}{2 - \zeta}. \quad (309)$$

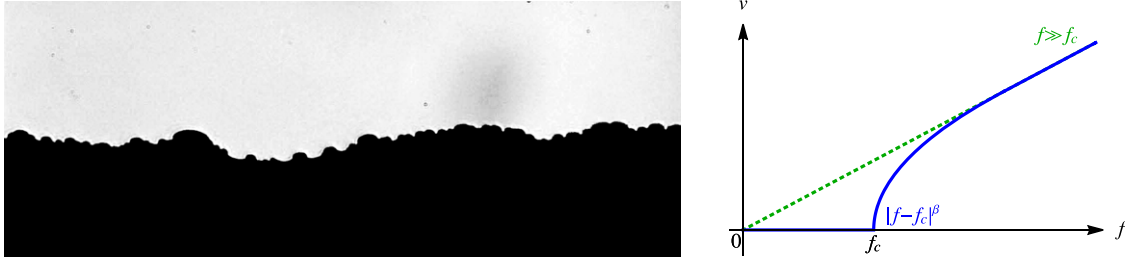


**Figure 22.** (Left) Snapshot of a contact-line at depinning, courtesy Rolley (movie). Observables derived from this system are shown in figures 32 and 48. (Right) Velocity of a pinned interface as a function of the applied force.  $f = 0$ : equilibrium.  $f = f_c$ : depinning. For an experimental confirmation of the  $v(f)$  curve in a thin magnetic film, see figure 43.

*Velocity-controlled depinning.* If  $m > 0$ , then we can rewrite the equation of motion (302) as

$$\begin{aligned} \partial_t u(x, t) &= (\nabla^2 - m^2)[u(x, t) - w] + F(x, u(x, t)), \\ w &= vt. \end{aligned} \quad (310)$$

The phenomenology changes:

- The driving force acting on the interface is fluctuating as well as the velocity, while the mean driving velocity is fixed

$$\overline{\dot{u}(x, t)} = v, \quad f = \frac{1}{L^d} \int_x \overline{F(x, u(x, t))}. \quad (311)$$

- The correlation length  $\xi$  is set by the confining potential,

$$\xi = \xi_m = \frac{1}{m}. \quad (312)$$

### 3.2. Field theory of the depinning transition, response function

We can enforce the equation of motion (310) with an auxiliary field  $\tilde{u}(x, t)$ <sup>26</sup>

$$\mathcal{S}[u, \tilde{u}, F] = \int_{x,t} \tilde{u}(x, t) \left[ (\partial_t - \nabla^2 + m^2) (u(x, t) - w) - F(x, u(x, t)) - f(x, t) \right]. \quad (313)$$

We need to average over disorder, to obtain the disorder-averaged action  $e^{-\mathcal{S}[u, \tilde{u}]} := e^{-\mathcal{S}[u, \tilde{u}, F]}$ , with

$$\begin{aligned} \mathcal{S}[u, \tilde{u}] &= \int_{x,t} \tilde{u}(x, t) [(\partial_t - \nabla^2 + m^2)[u(x, t) - w] - f(x, t)] \\ &- \frac{1}{2} \int_{x,t,t'} \tilde{u}(x, t) \Delta(u(x, t) - u(x, t')) \tilde{u}(x, t'). \end{aligned} \quad (314)$$

We remind the definition of the force–force correlator given in equation (10).

*Response function and the free theory.* The response of a system is defined as the answer of the system given a perturbation  $f(x, t)$ . The response can be any observable, as the

<sup>26</sup> This trick is known as the MSR formalism [295–299]. It is the generalization to a field of the relation  $\int_k e^{ikx} = \delta(x)$ : the response field  $\tilde{u}(x, t)$  enforces the Langevin equation (310) for each  $x$  and  $t$ . A short introduction is given in appendix A.4.

avalanche-size distribution defined below in equation (472), but the simplest one is the response of the field  $u(x', t')$  itself,

$$R_f(x', t'|x, t) := \frac{\delta}{\delta f(x, t)} \overline{u(x', t')} = \langle u(x', t') \tilde{u}(x, t) \rangle. \quad (315)$$

In a translationally invariant system,  $R_f(x', t'|x, t)$  does only depend on  $x' - x$  and  $t' - t$ , and is denoted

$$R(x' - x, t' - t) := R_f(x', t'|x, t). \quad (316)$$

In the second equality of equation (315) we used the average provided by the action (314). The formalism is explained in appendix A.4, see equation (969) and following. The most convenient representation is the spatial Fourier transform calculated for the free theory in equation (983),

$$R(k, t) = \langle u(k, t + t') \tilde{u}(-k, t') \rangle = e^{-(k^2 + m^2)t} \Theta(t). \quad (317)$$

We could introduce response functions as the answer to different perturbations, e.g. increasing  $w$  instead of  $f$ ,

$$R_w(k = 0, t) := \frac{d}{dw} \langle u(k = 0, t) \rangle = m^2 R(k = 0, t). \quad (318)$$

This changes the normalization,

$$\int_t R_w(k = 0, t) = 1. \quad (319)$$

While equation (318) is the free-theory result, corrected in perturbation theory, equation (319) is by construction exact.

### 3.3. Middleton theorem

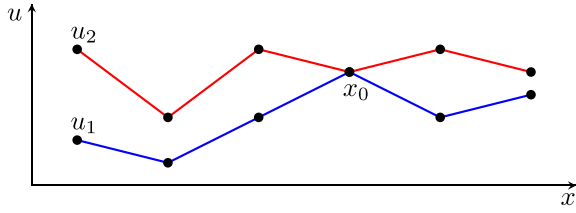
We now state the famous Middleton theorem [300].

**Middleton theorem.** *If  $F(x, u)$  is continuous in  $u$ , and  $\dot{u}(x, t) \geq 0$ , then  $\dot{u}(x, t') \geq 0$  for all  $t' \geq t$ . Moreover, if two configurations are ordered,  $u_2(x, t) \geq u_1(x, t)$ , then they remain ordered for all times, i.e.  $u_2(x, t') \geq u_1(x, t')$  for all  $t' \geq t > t$ .*

**Proof.** Consider an interface discretized in  $x$ . The trajectories  $u(x, t)$  are a function of time. Suppose that there exists  $x$  and  $t' > t$  s.t.  $\dot{u}(x, t') < 0$ . Define  $t_0$  as the first time when this happens,  $t_0 := \inf_x \inf_{t' > t} \{\dot{u}(x, t') < 0\}$ , and  $x_0$  the corresponding position  $x$ . By continuity of  $F$  in  $u$ , the velocity  $\dot{u}$  is continuous in time, and  $\dot{u}(x_0, t_0) = 0$ . This implies that the disorder force acting on  $x_0$  does not change in the next (infinitesimal) time step, and the only changes in force can come from a

change in the elastic terms. Since by assumption no other point has a negative velocity, this change in force cannot be negative, contradicting the assumption.

To prove the second part of the theorem, consider the following configuration at time  $t_0$ :



Here the red configuration is ahead of the blue one, except at position  $x_0$ , where they coincide. As in the first part of the proof, we wish to bring to a contradiction the hypothesis that at some later time  $u_1(x_0)$  (blue) is ahead of  $u_2(x_0)$  (red). For this reason, we have chosen  $t_0$  the infimum of times contradicting the theorem,  $t_0 := \inf_{t' > t} \{u_1(x_0, t') > u_2(x_0, t')\}$ . Consider the equation of motion equation (310) for the difference between  $u_1$  and  $u_2$ ,

$$\begin{aligned} \partial_t [u_2(x_0, t) - u_1(x_0, t)]|_{t=t_0} \\ = \nabla^2 [u_2(x_0, t_0) - u_1(x_0, t_0)]. \end{aligned} \quad (320)$$

The disorder force terms have canceled as well as the term of order  $m^2$ , since by assumption  $u_2(x_0, t_0) = u_1(x_0, t_0)$ . By construction, the rhs is positive, leading to the desired contradiction.

**Remark.** Uniqueness of perturbation theory. As in the statics, one encounters terms proportional to  $\Delta'(0^+) \equiv -R'''(0^+)$ . Here the sign problem can uniquely be solved by observing that due to Middleton's theorem the manifold only moves forward,

$$t' > t \implies u(x, t') - u(x, t) \geq 0. \quad (321)$$

Thus the argument of  $\Delta(u(x, t') - u(x, t))$  has a well-defined sign, allowing us to interpret derivatives at vanishing arguments correctly. Practically this means that when evaluating diagrams containing  $\Delta(u(x, t) - u(x, t'))$ , one splits them into two pieces, one with  $t < t'$  and one with  $t > t'$ . Both pieces are well defined, even in the limit of  $t \rightarrow t'$ .

### 3.4. Loop expansion

Consider the field theory defined by the action (314). To appreciate the problem, let us remind that in equilibrium a model is defined by its Boltzmann weight. As long as the system is ergodic, it can be sampled with the help of a Langevin equation, and equilibrium expectations can be evaluated as expectations in the dynamic field theory. This goes hand in hand with identical renormalizations, as is e.g. known for the effective coupling in  $\phi^4$  theory. On the other hand, it does not fix the dynamics. It is indeed well-known that a different dynamics leads to a different *dynamic universality class*,

as exemplified by the Hohenberg–Halperin classification of dynamical critical phenomena [301], leading to the zoo of models A, B, C, ..., F, and J. We might therefore not be surprised if below we find the same renormalization for the disorder in the driven dynamics. On the other hand, equilibrium and out-of-equilibrium are two distinct phenomena, and may have distinct critical exponents. As we will see below, at one-loop order all comparable observables are identical, whereas differences are manifest at two-loop order.

Let us start by rederiving the corrections to the renormalized disorder correlator at one-loop order. The replica diagram in equation (54) is one of the two contributions to the effective potential–potential correlator  $R(u)$  given in equation (60). In the dynamics, the disorder term in equation (314) is the bare (microscopic) *force–force correlator*  $\Delta_0(u)$ , which we note graphically as

$$\begin{aligned} \int_{x, t_1, t_2} \tilde{u}(x, t_1) \tilde{u}(x, t_2) \Delta_0(u(x, t_1) - u(x, t_2)) \\ = \begin{array}{c} t_2 \bullet \longrightarrow \\ | \\ t_1 \bullet \longrightarrow \\ x \end{array} \end{aligned} \quad (322)$$

The arrows are the response fields  $\tilde{u}(x, t_1) \tilde{u}(x, t_2)$ ; some authors represent them by a wiggly line. Since the response function has a direction in time, the static diagram (54) has two *descendants* in the dynamic formulation,

$$\begin{array}{c} \bullet \longrightarrow \bullet \\ | \quad | \\ x \quad y \end{array} \longrightarrow \begin{array}{c} \bullet \longrightarrow \bullet \longrightarrow \bullet \\ | \quad | \quad | \\ x \quad y \quad y \end{array} + \begin{array}{c} \bullet \longrightarrow \bullet \\ | \quad | \\ \bullet \longleftarrow \bullet \\ | \quad | \\ x \quad y \end{array} \quad (323)$$

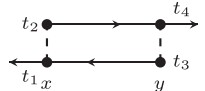
The first descendant with the corresponding times is

$$\begin{aligned} \begin{array}{c} t_2 \bullet \longrightarrow \bullet t_4 \\ | \quad | \\ t_1 \bullet \longrightarrow \bullet t_3 \\ x \quad y \end{array} \\ = - \int_{t_1, t_2, x} R(x - y, t_4 - t_2) R(x - y, t_3 - t_1) \\ \times \Delta_0(u(x, t_2) - u(x, t_1)) \Delta_0''(u(y, t_4) - u(y, t_3)) \\ \times \tilde{u}(y, t_3) \tilde{u}(y, t_4) \\ \simeq - \int_k \int_{t_1 < t_3, t_2 < t_4} e^{-(k^2 + m^2)(t_4 - t_2)} e^{-(k^2 + m^2)(t_3 - t_1)} \\ \times \Delta_0(u(y, t_4) - u(y, t_3)) \Delta_0''(u(y, t_4) - u(y, t_3)) \\ \times \tilde{u}(y, t_3) \tilde{u}(y, t_4) \\ = - \int_k \frac{1}{(k^2 + m^2)^2} \Delta_0(u(y, t_4) - u(y, t_3)) \\ \times \Delta_0''(u(y, t_4) - u(y, t_3)) \tilde{u}(y, t_3) \tilde{u}(y, t_4). \end{aligned} \quad (324)$$

Some remarks are in order: this is a correction to  $\Delta$ , and we have not written the integrations over  $t_3$ ,  $t_4$  and  $y$ . The derivatives of  $\Delta$  come from the Wick contractions as in equation (52). The global minus sign in the first line originates from the derivatives acting once on the field at time  $t_3$ , and once at time  $t_4$ . Going to the second line, we have in the argument of  $\Delta$  replaced fields at time  $t_2$  by those at time  $t_4$ , and fields at time  $t_1$  by those at time  $t_3$ ; this is justified since the response function  $R$  decays rapidly in time. In the argument of

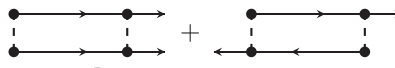
$\Delta$  we have also replaced  $x$  by  $y$ , as we did in the statics after arriving at equation (55). The remaining two times  $t_3$  and  $t_4$  can be taken arbitrarily far apart, thus this diagram encodes a contribution to the effective disorder.

The second descendant gives after the same steps



$$\simeq - \int_k \frac{1}{(k^2 + m^2)^2} \Delta'_0(u(y, t_4) - u(y, t_3))^2 \times \tilde{u}(y, t_3) \tilde{u}(y, t_4). \quad (325)$$

We used that  $\Delta'(u)$  is odd in  $u$ . Together, these two diagrams give with  $I_1$  defined in equation (58)



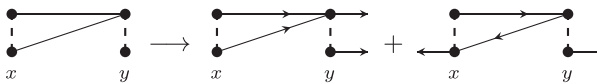
$$\simeq -I_1 \left[ \Delta_0(u(y, t_4) - u(y, t_3)) \Delta''_0(u(y, t_4) - u(y, t_3)) + \Delta'_0(u(y, t_4) - u(y, t_3))^2 \right] \tilde{u}(y, t_3) \tilde{u}(y, t_4). \quad (326)$$

Taking care of the combinatorial factors, and the factors of  $1/2$  in the action, we read off their contribution to the effective disorder  $\Delta(u)$ ,

$$\begin{aligned} \delta_1 \Delta(u) &= - \left[ \Delta_0(u) \Delta''_0(u) + \Delta'_0(u)^2 \right] I_1 \\ &= - \partial_u^2 \frac{1}{2} \Delta_0(u)^2 I_1. \end{aligned} \quad (327)$$

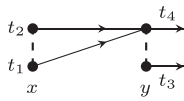
This is the same contribution as given by the diagram in equation (54), noting that  $\Delta_0(u) = -R''_0(u)$ , and using the combinatorial factor  $1/2$  reported in equation (60).

To complete our analysis, consider the second diagram; it also has two descendants,

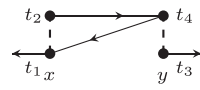


$$(328)$$

After time-integration this yields



$$\simeq \int_k \frac{1}{(k^2 + m^2)^2} \Delta_0(0) \Delta''_0(u(y, t_4) - u(y, t_3)). \quad (329)$$



$$\simeq \int_k \frac{1}{(k^2 + m^2)^2} \Delta'_0(0^+) \Delta'_0(u(y, t_4) - u(y, t_3)). \quad (330)$$

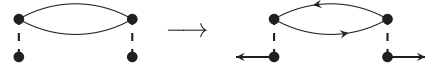
The last diagram contains a first factor of  $\Delta'(0^+)$ ; the definite sign results from the causality of the response functions ensuring  $t_2 < t_1$ . It is asymmetric under exchange of  $t_3$  and  $t_4$ , thus vanishes after integrating over these times. (B.t.w., inserted into a two-loop diagram, it is this diagram which is responsible for the differences seen there, especially for the two-loop

contribution to  $\zeta$ .) Together, they give a second contribution to the effective disorder

$$\delta_2 \Delta(u) = \Delta_0(0) \Delta''_0(u) I_1 = \partial_u^2 [\Delta_0(0) \Delta_0(u)] I_1. \quad (331)$$

This is the same contribution as given by equation (55).

The last diagram we drew for the equilibrium was given in equation (56). Its descendant reads



$$(332)$$

While the static diagram on the lhs does not contribute to the effective disorder since it is a three-replica term (three independent sums over replicas), the dynamic diagram on the rhs does not contribute due to the acausal loop, as it does not allow for any time integration, thus vanishes.

For completeness, we write the effective disorder-force correlator at one-loop order,

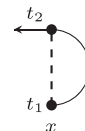
$$\Delta(u) = \Delta_0(u) - \partial_u^2 \left[ \frac{1}{2} \Delta_0(u)^2 - \Delta_0(0) \Delta_0(u) \right] I_1. \quad (333)$$

This result is the same as when applying  $-\partial_u^2$  to equation (60). We thus recover the same flow equation for the renormalized dimensionless force-force correlator as given in equation (69) and first derived in [121, 122, 294, 302]

$$\begin{aligned} \partial_\ell \tilde{\Delta}(u) &= (\epsilon - 2\zeta) \tilde{\Delta}(u) + \zeta u \tilde{\Delta}'(u) \\ &\quad - \partial_u^2 \frac{1}{2} [\tilde{\Delta}(u)^2 - \tilde{\Delta}(0)]^2. \end{aligned} \quad (334)$$

While this might not be surprising on a formal level, it is *very surprising* on a physical level: the effective disorder (60) is for the minimum energy state, while the derivation given above is for a state at depinning. We will see in the next section 3.5 that there are indeed corrections at two-loop order which account for this difference, and which are important to reconcile the physically observed differences in exponents and other observables with the theoretical prediction.

Before going there, let us complete our analysis with two additional contributions not present in the statics, and which we will interpret as the critical force at depinning, and a renormalization of friction, leading to a non-trivial dynamical exponent  $z$ , as defined in equation (305). The diagram in question is



$$\begin{aligned} &= \tilde{u}(x, t_2) \int_{t_1, k} \Delta'_0(u(x, t_2) - u(x, t_1)) e^{-(t_2 - t_1)(k^2 + m^2)} \\ &\quad \times \Theta(t_1 < t_2) \\ &\simeq \tilde{u}(x, t_2) \int_{t_1, k} \left[ \Delta'_0(0^+) + \Delta''_0(0^+) (t_2 - t_1) \dot{u}(x, t_2) + \dots \right] \\ &\quad \times e^{-(t_2 - t_1)(k^2 + m^2)} \Theta(t_1 < t_2) \\ &= \tilde{u}(x, t_2) \int_k \frac{\Delta'_0(0^+)}{k^2 + m^2} + \frac{\Delta''_0(0^+)}{(k^2 + m^2)^2} \dot{u}(x, t_2) + \dots \end{aligned} \quad (335)$$

The first term corresponds to a constant driving force  $f$  in equation (302), and can be interpreted as the threshold force below which the manifold will not move. In terms of the renormalized disorder, it reads

$$f_c = -\Delta'(0^+)I_{\text{TP}}, \quad (336)$$

$$I_{\text{TP}} = \textcircled{\bullet} = \int_k \frac{1}{k^2 + m^2}. \quad (337)$$

Its value is non-universal, but gives us a pretty good idea how strong we have to drive. In the driving protocol with a parabola centered at  $w$  as given in equation (310), it gives us the size of the *hysteresis loop*, illustrated in figure 25,

$$m^2 [\overline{u_w - w}^{\text{forward}} - \overline{u_w - w}^{\text{backward}}] = 2f_c. \quad (338)$$

Let us now turn to the second term in equation (335). Restoring the friction coefficient  $\eta$  in front of  $\partial_t u(x, t)$  in the equation of motion (310) yields

$$\eta_{\text{eff}} = 1 - \Delta''_0(0^+)I_1 + \dots \quad (339)$$

The dynamical exponent  $z$ , expressed in terms of the renormalized disorder, is then obtained as

$$z = 2 - m\partial_m \ln \eta_{\text{eff}} = 2 - \tilde{\Delta}''(0^+) + \dots \quad (340)$$

Taking one derivative of equation (79), or equivalently of equation (334) at the fixed point  $\partial_\ell \tilde{\Delta}(u) = 0$ , and evaluating it in the limit of  $u \rightarrow 0$  allows us to conclude that

$$\tilde{\Delta}''(0^+) = \frac{\epsilon - \zeta}{3}. \quad (341)$$

This depends on the universality class,

$$z = 2 - \frac{\epsilon - \zeta}{3} + \dots = \begin{cases} 2 - \frac{\epsilon}{3} + \dots & \text{RP disorder} \\ 2 - \frac{2\epsilon}{9} + \dots & \text{RF disorder.} \end{cases} \quad (342)$$

We do not give a value of  $z$  for the RB fixed point, as the latter is unstable under RG, as we will see in the next section.

### 3.5. Depinning beyond leading order

Renormalization at the depinning transition was first treated at one-loop order by Natterman *et al* [294], soon followed by Narayan and Fisher [303]. As we have seen, the one-loop flow-equations are identical to those of the statics. This is surprising, since equilibrium and depinning are quite different phenomena. There was even a claim by [303], that the roughness exponent in the RF universality class is  $\zeta = \epsilon/3$  also at depinning. After a long debate among numerical physicists, the issue is now resolved: the roughness is significantly larger, and reads e.g. for the driven polymer  $\zeta = 1.25 \pm 0.005$  [53, 304], and possibly exactly  $\zeta = \frac{5}{4}$  [305]; this should be contrasted to  $\zeta = 1$  at equilibrium, see equation (83). Clearly, a two-loop analysis is necessary to resolve these issues. The latter was performed in [124, 125]. At the

**Table 1.** Critical exponents at the depinning transition for short-ranged elasticity ( $\alpha = 2$ ). One-loop and two-loop results compared to estimates based on three Padé approximants, scaling relations and common sense.

	$d$	$\epsilon$	$\epsilon^2$	Estimate	Simulation
$\zeta$	3	0.33	0.38	$0.38 \pm 0.02$	$0.355 \pm 0.01$ [307]
	2	0.67	0.86	$0.82 \pm 0.1$	$0.753 \pm 0.002$ [307]
	1	1.00	1.43	$1.2 \pm 0.2$	5/4 [305]
$z$	3	1.78	1.73	$1.74 \pm 0.02$	$1.75 \pm 0.15$ [294]
	2	1.56	1.38	$1.45 \pm 0.15$	$1.56 \pm 0.06$
	1	1.33	0.94	$1.35 \pm 0.2$	10/7 [305]
$\beta$	3	0.89	0.85	$0.84 \pm 0.01$	$0.84 \pm 0.02$ [294]
	2	0.78	0.62	$0.53 \pm 0.15$	$0.64 \pm 0.02$
	1	0.67	0.31	$0.2 \pm 0.2$	5/21 [305]
$\nu$	3	0.58	0.61	$0.62 \pm 0.01$	
	2	0.67	0.77	$0.85 \pm 0.1$	$0.77 \pm 0.04$ [308]
	1	0.75	0.98	$1.25 \pm 0.3$	4/3 [305]

depinning transition, the two-loop FRG flow equation reads [124, 125]

$$\begin{aligned} \partial_\ell \tilde{\Delta}(u) &= (\epsilon - 2\zeta)\tilde{\Delta}(u) + \zeta u \tilde{\Delta}'(u) - \frac{1}{2} \partial_u^2 [\tilde{\Delta}(u) - \tilde{\Delta}(0)]^2 \\ &+ \frac{1}{2} \partial_u^2 \left\{ [\tilde{\Delta}(u) - \tilde{\Delta}(0)] \tilde{\Delta}'(u)^2 + \tilde{\Delta}'(0^+)^2 \tilde{\Delta}(u) \right\}. \end{aligned} \quad (343)$$

Compared to the FRG-equation (113a) for the statics, the only change is in the last sign on the second line of equation (343), given in bold. This ‘small change’ has important consequences for the physics. First of all, the roughness exponent  $\zeta$  for the RF universality class changes: integrating equation (343) the last term yields a boundary term at  $u = 0$ , and due to the different sign it no longer cancels with the preceding one, resulting in

$$0 = (\epsilon - 3\zeta) \int_0^\infty \tilde{\Delta}(u) du - \tilde{\Delta}'(0^+)^3 + \mathcal{O}(\epsilon^3). \quad (344)$$

Inserting the one-loop fixed point (84)–(88) leads to<sup>27</sup>

$$\zeta_{\text{RF}}^{\text{dep}} = \frac{\epsilon}{3}(1 + 0.143317\epsilon + \dots). \quad (345)$$

Other critical exponents mentioned above can also be calculated. The dynamical exponent  $z$  reads [124, 125]

$$\zeta_{\text{RF}}^{\text{dep}} = 2 - \frac{2}{9}\epsilon - 0.04321\epsilon^2 + \dots \quad (346)$$

The remaining exponents are related via the scaling relations (308) and (309). That the method works well quantitatively can be inferred from table 1.

The RB fixed point is unstable and renormalizes to the RF universality class. This might physically be expected: since the manifold only moves forward, each time it advances it experiences a new disorder configuration, and it has no way to ‘know’ whether this disorder is derived from a potential or not. This

<sup>27</sup> For details see [124], section 4.1.

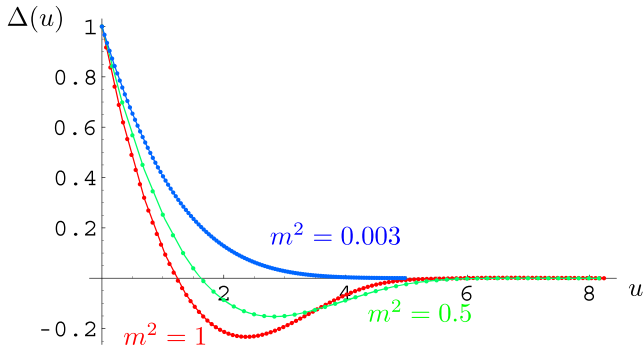


**Figure 23.** Doing RG in a simulation: crossover from RB disorder to RF for a driven particle. Reprinted figure with permission from [128], Copyright (2007) by the American Physical Society.

can be seen from the integrated FRG equation (344): according to equation (89), an RB fixed point is characterized by a vanishing of the integral in equation (344), but this does not solve equation (344). The instability of the RB fixed point can already be seen for a toy model with a single particle, measuring the renormalized disorder correlator at a scale  $\ell = 1/m$  set by the confining potential, see figure 23. Generalizing the arguments of section 2.11 one shows [129] that equation (111) remains valid in the limit of  $w = vt$ ,  $v \rightarrow 0$ . It was confirmed numerically for a string that both RB and RF disorder flow to the RF fixed point [306], and that this fixed point is close to the analytic solution of equation (343), see figure 24.

The non-potentiality of the depinning fixed point is also observed in the RP universality class, relevant for CDWs. The fixed point for a periodic disorder of period one reads (remember  $\tilde{\Delta}(u) = -\tilde{R}''(u)$ )

$$\tilde{\Delta}(u) = \frac{\epsilon}{36} + \frac{\epsilon^2}{108} - \left( \frac{\epsilon}{6} + \frac{\epsilon^2}{9} \right) u(1-u) + \mathcal{O}(\epsilon^3). \quad (347)$$

Integrating over a period, we find

$$\int_0^1 du \tilde{\Delta}(u) \equiv \int_0^1 du \overline{\tilde{F}(u)\tilde{F}(u')} = -\frac{\epsilon^2}{108}. \quad (348)$$

In equilibrium, this correlator vanishes since potentiality requires  $\int_0^1 du \tilde{F}(u) \equiv 0$ . Here, there are non-trivial contributions at two-loop order,  $\mathcal{O}(\epsilon^2)$ , violating this condition and rendering the system non-potential.

If an additional constant term  $\tilde{\Delta}_0$  cannot be excluded as is the case in equilibrium, then according to equation (343) it flows as

$$\partial_t \tilde{\Delta}_0 = (\epsilon - 2\zeta)\tilde{\Delta}_0. \quad (349)$$

It acts as a *Larkin term* leading to a roughness exponent [122, 124, 309]

$$\zeta_{\text{obs}}^{\text{CDW}} = \zeta_{\text{Larkin}} = \frac{4-d}{2}. \quad (350)$$

For the dynamic exponent  $z$ , one can go further [140, 310–312], using the equivalence to  $\phi^4$ -theory discussed in

section 8.9,

$$\begin{aligned} z = & 2 - \frac{\epsilon}{3} - \frac{\epsilon^2}{9} + \left[ \frac{2\zeta(3)}{9} - \frac{1}{18} \right] \epsilon^3 \\ & - \left[ \frac{70\zeta(5)}{81} - \frac{\zeta(4)}{6} - \frac{17\zeta(3)}{162} + \frac{7}{324} \right] \epsilon^4 \\ & - \left[ \frac{541\zeta(3)^2}{162} + \frac{37\zeta(3)}{36} + \frac{29\zeta(4)}{648} + \frac{703\zeta(5)}{243} \right. \\ & \left. + \frac{175\zeta(6)}{162} - \frac{833\zeta(7)}{216} + \frac{17}{1944} \right] \epsilon^5 \\ & - 11.7939\epsilon^6 + \mathcal{O}(\epsilon^7). \end{aligned} \quad (351)$$

### 3.6. Stability of the depinning fixed points

The stability analysis at depinning is done as in section 2.14 for the equilibrium.

*RP fixed point.* The RP fixed point at depinning is stable perturbatively, (appendix I of [124]). The leading three modes are

$$\omega_{-1} = -\epsilon, \quad z_{-1}(u) = 1. \quad (352a)$$

$$\omega_1 = \epsilon + \frac{7}{3}\epsilon^2 + \mathcal{O}(\epsilon^3), \quad (352b)$$

$$z_1(u) = 1 - (6 + 4\epsilon)u(1-u). \quad (352c)$$

$$\omega_2 = 2\epsilon + 4\epsilon^2 + \mathcal{O}(\epsilon^3),$$

$$z_2(u) = 1 - (15 + 20\epsilon)u(1-u) + (45 + 85\epsilon)[u(1-u)]^2,$$

$$\omega_3 = \frac{25}{3}\epsilon + \frac{140}{9}\epsilon^2 + \mathcal{O}(\epsilon^3). \quad (352d)$$

*RF fixed point.*

$$\omega = \epsilon + 0.0186\epsilon^2 + \mathcal{O}(\epsilon^3). \quad (353a)$$

The fixed-point function is

$$z(u, \epsilon) = \epsilon z_1(u) + \epsilon^2 z_2(u) + \mathcal{O}(\epsilon^3), \quad (353b)$$

$$z_1(u) = \zeta u \Delta'(u) + (\epsilon - 2\zeta)\Delta(u)|_{\epsilon=1}. \quad (353c)$$

While the first-order term can rather instructively be expressed in terms of the fixed point  $\Delta(u)$  itself, the higher-order terms are more complicated (section 6.5 of [40]).

### 3.7. Non-perturbative FRG

The fixed points discussed above are also present in the non-perturbative functional renormalization group (NP-FRG) approach [313], leading to slightly varying numerical predictions in the values of the critical exponents. The result of NP-FRG for the RF class is  $z = 1.69$  ( $d = 3$ ),  $z = 1.33$

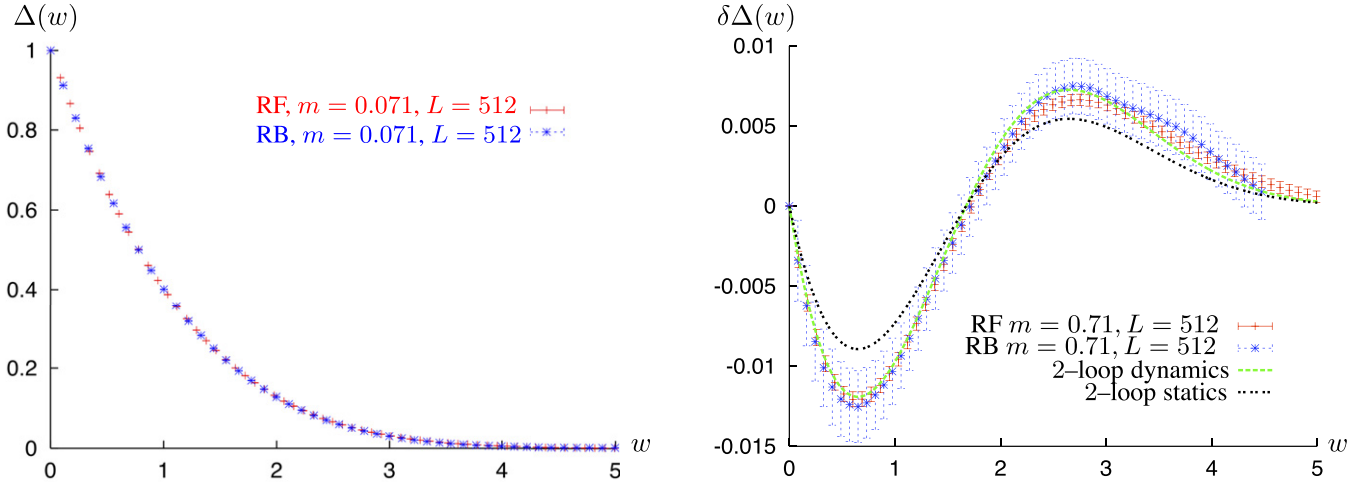


**Figure 24.** (Left) The fixed point  $\Delta(w)$  for the force–force correlations in  $d = 1$ , rescaled s.t.  $\Delta(0) = 1$ , and  $\int_w \Delta(w) = 1$ , starting both from RB and RF initial condition. Reprinted figure with permission from [306], Copyright (2007) by the American Physical Society. (Right) Residual error  $\delta\Delta(w)$  after subtracting the one-loop correction. The measured difference is consistent with the depinning fixed point, but not the static one.

( $d = 2$ ), and  $z = 0.97$  ( $d = 1$ ). For the roughness at depinning this yields  $\zeta = 0.37$  ( $d = 3$ ),  $\zeta = 0.76$  ( $d = 2$ ), and  $\zeta = 1.15$  ( $d = 1$ ).

### 3.8. Behavior at the upper critical dimension

[50, 314] consider depinning at the upper critical dimension. To derive this, note that the integral  $I_1$  defined in equation (58) has a well-defined limit for  $\epsilon \rightarrow 0$ , if one introduces as in equation (57) an UV-cutoff  $\Lambda \sim 1/a$ ,

$$I_1 := \text{---} \text{---} = \int^\Lambda \frac{d^d k}{(2\pi)^d} \frac{1}{(k^2 + m^2)^2} \quad (354)$$

$$= \frac{m^{-\epsilon} - \Lambda^{-\epsilon} 2\Gamma(1 + \frac{\epsilon}{2})}{\epsilon} \xrightarrow{(4\pi)^{d/2}} \frac{\ln(\Lambda/m)}{8\pi^2}.$$

This suggests as scale for the RG flow

$$\ell := \ln(\Lambda/m). \quad (355)$$

Let us make in generalization of equation (63) the ansatz

$$\Delta(u) = 8\pi^2 \ell^{2\zeta_1 - 1} \tilde{\Delta}_\ell(u\ell^{-\zeta_1}), \quad (356)$$

$$\zeta = \zeta_1 \epsilon + \zeta_2 \epsilon^2 + \dots \quad (357)$$

Then  $\tilde{\Delta}_\ell(u)$  satisfies the flow equation [50, 314]

$$\partial_\ell \tilde{\Delta}_\ell(u) = (1 - 2\zeta_1) \tilde{\Delta}_\ell(u) + \zeta_1 u \tilde{\Delta}'_\ell(u) - \frac{1}{2} \partial_u^2 [\tilde{\Delta}_\ell(u) - \tilde{\Delta}_\ell(0)]^2 + \sum_{n>1} \ell^{1-n} \beta_n(u), \quad (358)$$

where  $\beta_n(u)$  are the  $n$ -loop contributions to the  $\beta$ -function. As a consequence,

$$\overline{u_q \tilde{u}_{-q}}|_{q \ll m} \simeq \frac{\Delta(0)}{m^4} [1 + \mathcal{O}(\ell^{-1})] \simeq \frac{8\pi^2 \ln(\Lambda/m)^{2\zeta_1 - 1}}{m^4} + \dots \quad (359a)$$

This formula is valid both in equilibrium and at depinning. For RF disorder,  $\zeta_1 = 1/3$ , leading to an additional factor of  $\ln(\Lambda/m)^{1/3}$  in the 2-point function (359a) as compared to naive expectations. In position space this reduces the expected  $\ln x$  behavior to

$$\overline{[u(x) - u(0)]^2} \sim (\ln x)^{2/3}. \quad (359b)$$

Thus mean field is invalid at the upper critical dimension.

### 3.9. Extreme-value statistics: the discretized particle model (DPM)

For a single particle, there is a nice geometrical construction to obtain the particle trajectories, indicated in figure 25: for given  $w$ , draw a line  $m^2(u - w)$ . For forward driving,  $u(w)$  is the leftmost intersection with the pinning force  $F(u)$ , while for backward driving it is the rightmost such intersection. As indicated by the arrows, this is equivalent to shining light with slope  $m^2$ , either from the left for forward driving, or from the right for backward driving. Parts in the shadow are never visited, while illuminated ones are. The jumps are the avalanches of section 2.10 and are further discussed in section 4.

Using this construction, one can obtain both the distribution of critical forces, as well as the renormalized disorder force–force correlator  $\Delta(w)$  analytically [315]. The distribution of threshold forces corresponds to the three main classes of extreme-value statistics. Let us according to equation (111) define

$$\Delta(w - w') := m^4 \overline{[w - u(w)][w' - u(w')]^c}. \quad (360)$$

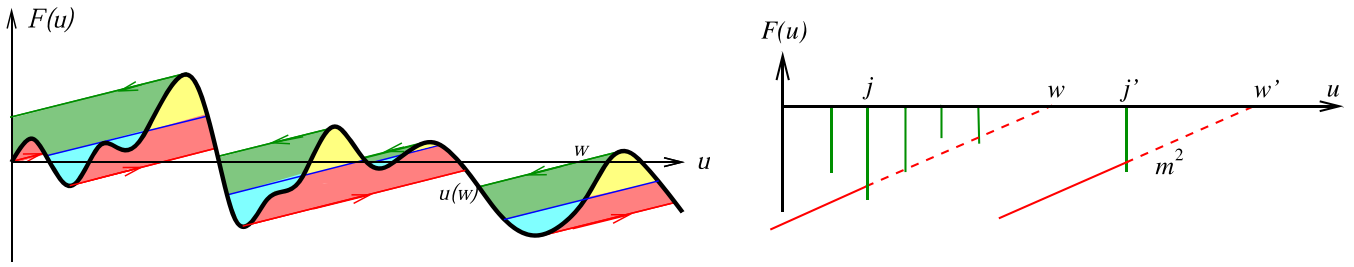


**Figure 25.** Construction of  $u(w)$  in  $d = 0$ , for the pinning force  $F(u)$  (bold black line). The two quasi-static motions driven to the right and to the left are indicated by red and green arrows, and exhibit jumps (‘dynamical shocks’). The position of the shocks in the statics is shown for comparison, based on the Maxwell construction (equivalence of light blue and yellow areas, both bright in black and white). The critical force is  $1/(2m^2)$  times the area bounded by the hull of the construction. (Right) The needles of the discretized particle model (DPM). Reprinted figure with permission from [315], Copyright (2009) by the American Physical Society.  $u_w$  as a function of  $w$  is given by the left-most intersection of  $m^2(u - w)$  with a needle, here  $u_w = j$ , and  $u_w' = j'$ .

Each class (discussed below), has its own exponent  $\zeta$ , setting a scale  $\rho_m \sim m^{-\zeta}$ . At small  $m$ , force–force correlations are universal, given by

$$\Delta(w) = m^4 \rho_m^2 \tilde{\Delta}(w/\rho_m). \quad (361)$$

The fixed-point function  $\tilde{\Delta}(w)$  depends on the universality class. The three classes are distinguished by the distribution of the random forces  $F$  for the *most blocking* forces.

*Gumbel class.*

$$P(F) \simeq e^{-A(-F)^\gamma}, \quad \text{as } F \rightarrow -\infty. \quad (362)$$

The threshold forces  $f_c$  are distributed according to a *Gumbel* distribution (tested in [131]),

$$P_G(a) = \exp(-a)\Theta(a), \quad (363)$$

$$f_c = \left[ \frac{-\ln(m^2 a)}{A} \right]^{1/\gamma} = f_c^0 - \ln(a)m^2 \rho_m + \dots \quad (364)$$

The constant  $f_c^0$ , the scale  $\rho_m$ , and the exponent  $\zeta$  are

$$\begin{aligned} f_c^0 &= A^{-1/\gamma} (\ln m^{-2})^{1/\gamma}, \\ \rho_m^{-1} &= \gamma A^{1/\gamma} m^\zeta (\ln m^{-2})^{1-1/\gamma}, \quad \zeta = 2^-. \end{aligned} \quad (365)$$

The effective disorder correlator reads

$$\tilde{\Delta}_G(w) = \frac{w^2}{2} + \text{Li}_2(1 - e^w) + \frac{\pi^2}{6}. \quad (366)$$

Its first derivatives are

$$\begin{aligned} \tilde{\Delta}_G(0) &= \frac{\pi^2}{6}, & \tilde{\Delta}'_G(0) &= -1, & \tilde{\Delta}''_G(0) &= \frac{1}{2}, \\ \frac{\tilde{\Delta}_G(0)\tilde{\Delta}'_G(0)}{\tilde{\Delta}'_G(0)^2} &= \frac{\pi^2}{12} = 0.822467. \end{aligned} \quad (367)$$

It can be compared to the FRG fixed point for the RF class at depinning, see figure 26, and discussed below around equation (376).

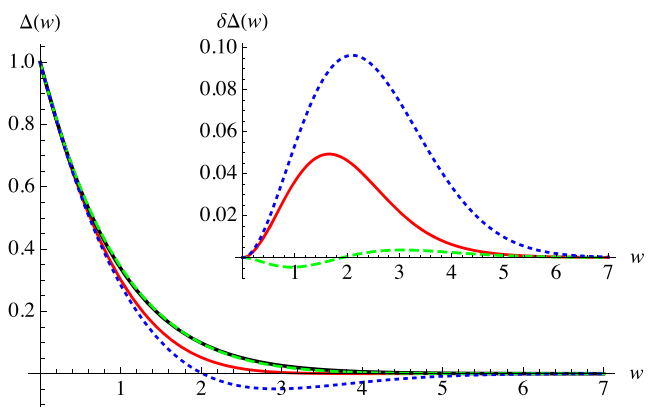


**Figure 26.** (Main plot) The function (366) rescaled s.t.  $\Delta(0) = -\Delta'(0^+) = 1$  (in black). This is compared to the similarly rescaled one-loop prediction (88) (in red), and the straightforward two-loop prediction obtained from equation (343) (blue dashed). To improve convergence, we have used a Padé-(1, 1) resummation (green, dashed), defined in equation (376). (Inset) The same functions with the black curve subtracted. We see that the one-loop result is decent, and that the Padé-resummed two-loop result strongly improves on it.

*Fréchet class.*

$$P(F) \simeq A\alpha(\alpha + 1)(-F)^{-2-\alpha}\Theta(-F) \quad \text{as } F \rightarrow -\infty. \quad (368)$$

The threshold forces  $f_c$  are distributed according to a *Fréchet* distribution ( $\alpha > 0$ ),

$$f_c = xm^2 \rho_m, \quad P_F(x) = \alpha x^{-\alpha-1} e^{-x^{-\alpha}} \Theta(x). \quad (369)$$

The mean pinning force  $f_c$ , the scale  $\rho_m$ , and the exponent  $\zeta$  are

$$\begin{aligned} \bar{f}_c &= \Gamma\left(1 - \frac{1}{\alpha}\right) m^2 \rho_m, & \rho_m &= A^{1/\alpha} m^{-\zeta}, \\ \zeta &= 2 + \frac{2}{\alpha}. \end{aligned} \quad (370)$$

The effective disorder correlator can be written as an integral, and is ill-defined for  $\alpha < 2$ , where the second moment of the

force–force fluctuations vanishes. For  $\alpha > 2$  it has a cusp at small  $w$ , and decays algebraically at large  $w$ ,

$$\begin{aligned}\tilde{\Delta}_F(w) &\simeq \Gamma\left(\frac{\alpha-2}{\alpha}\right) - \Gamma\left(1 - \frac{1}{\alpha}\right)^2 + \frac{1}{\alpha^2}\Gamma\left(-\frac{1}{\alpha}\right)w \\ &\quad + \frac{\alpha w^2}{4\alpha+2} + \dots \quad \text{for } w \rightarrow 0, \\ \tilde{\Delta}_F(w) &\simeq \frac{w^{2-\alpha}\alpha}{(\alpha-2)(\alpha-1)} + \dots \quad \text{for } w \rightarrow \infty.\end{aligned}\quad (371)$$

*Weibull class.* In this class, the random forces are bounded from below, growing as a power law above the threshold, here chosen to be zero,

$$P(F) = A\alpha(\alpha-1)F^{\alpha-2}\theta(F), \quad \alpha > 1. \quad (372)$$

The threshold forces are distributed according to a *Weibull* distribution

$$\begin{aligned}f_c &= xm^2\rho_m, \\ P_W(x) &= \alpha(-x)^{\alpha-1}e^{-(-x)^\alpha}\Theta(-x).\end{aligned}\quad (373)$$

The mean pinning force  $\overline{f_c}$ , the scale  $\rho_m$ , and the exponent  $\zeta$  are

$$\begin{aligned}\overline{f_c} &= -A^{-\frac{1}{\alpha}}m^{\frac{2}{\alpha}}\Gamma\left(1 + \frac{1}{\alpha}\right), \\ \rho_m &= A^{-\frac{1}{\alpha}}m^{-\zeta}, \quad \zeta = 2 - \frac{2}{\alpha}.\end{aligned}\quad (374)$$

The most important class is the box distribution with minimum at 0 ( $\alpha = 2$ ). Its force–force correlator is

$$\begin{aligned}\tilde{\Delta}_W^{\alpha=2}(w) &= \frac{e^{-w^2}}{4w} \left[ 2w - e^{w^2} \sqrt{\pi} (2w^2 + 1) \operatorname{erfc}(w) + \sqrt{\pi} \right] \\ &\quad + \frac{1}{2} \sqrt{\pi} \left[ w e^{-w^2} - \Gamma\left(\frac{3}{2}, w^2\right) \right].\end{aligned}\quad (375)$$

*Comparison to the  $\epsilon$ -expansion.* An interesting question is whether one of the cases discussed above can be related to the  $\epsilon$ -expansion. The most natural candidate is the Gumbel class with  $\gamma = 2$ , as field theory assumes bare Gaussian disorder. In that case  $\zeta = 2^-$ , close to the two-loop result (345), i.e.  $\zeta(\epsilon = 4) = 2.098$ . While a straightforward  $\epsilon$ -expansion for  $\tilde{\Delta}(w)$  is not satisfactory at two-loop order, we can use a Padé approximant,

$$\tilde{\Delta}^{\text{Padé}}(w) = \frac{\tilde{\Delta}_1(w) + \alpha\epsilon\tilde{\Delta}_2(w)}{1 + (\alpha-1)\epsilon\tilde{\Delta}_2(w)/\tilde{\Delta}_1(w)}. \quad (376)$$

A comparison between equations (366) and (376), rescaled s.t.  $\tilde{\Delta}(0) = 1$ , and  $\int_0^\infty dw \tilde{\Delta}(w) = 1$ , is shown on figure 26. As can be seen there,  $\alpha = 0.35$  yields a good approximation, making it a strong candidate to compare to numerical simulations or experiments in  $d = 1$  and  $d = 2$ . Note however, that the functions (366), (371) and (375) are close, so that the  $\epsilon$  expansion might not be able to discriminate between them.

*Avalanches and waiting times.* For simplicity we restrict ourselves to the Gumbel class, where both the *waiting distances*  $w$  between jumps as well as the avalanches size  $S$  have a pure exponential distribution, (for definitions see section 4),

$$P(w) = \rho_m^{-1} \exp(-w/\rho_m), \quad (377)$$

$$P(S) = \rho_m^{-1} \exp(-S/\rho_m). \quad (378)$$

*Dynamics.* The model defined in [315] and discussed in this section advances instantaneously. The easiest way to endow it with a dynamics is to consider a Langevin equation [131],

$$\eta\partial_t u(t) = m^2[w - u(t)] + F(u(t)). \quad (379)$$

If the disorder is needle-like as on the right of figure 25 (the original construction of [315]), then either the particle is at rest, blocked by a needle, or it moves, and the only force acting on it comes from the spring. Neglecting that the spring gets shorter during the movement, the response-function is then given by  $R(t) \sim P(S/v)$ , where  $\eta v = f_c$ , resulting for Gaussian disorder (Gumbel class with  $\gamma = 2$ ,  $A = 1/2$ ) into

$$R(t) = \tau_m^{-1} e^{-t/\tau_m}, \quad \tau_m = \frac{\eta}{2m^2 \ln(m^{-2})}. \quad (380)$$

### 3.10. Mean-field theories

The framework of disordered elastic manifolds covers many experiments, from contact-line depinning over magnetic domain walls to earthquakes. Many of these experiments, or at least aspects thereof, are successfully described by MF *theory*. For driven disordered systems the first question to pose is: what is meant by MF? Let us define MF *theory as a theory which reduces an extended system to a single degree of freedom*<sup>28</sup>, in general its center of mass  $u$ . For depinning,  $u$  then follows the equation of motion (302), reduced to a single degree of freedom,

$$\partial_t u(t) = m^2[w - u(t)] + F(u(t)). \quad (381)$$

Specifying the correlations of  $F(u)$  selects one MF theory. However, when the reader encounters the term ‘MF theory’ in the literature, it is quite generally employed for a model where the forces perform a RW,

$$\partial_u F(u) = \xi(u), \quad (382)$$

$$\langle \xi(u)\xi(u') \rangle = 2\sigma\delta(u - u'). \quad (383)$$

This model was introduced in 1990 by Alessandro, Beatrice, Bertotti and Montorsi (ABBM) [316, 317] to describe magnetic domain walls. There  $F(u)$  are the ‘coercive magnetic

<sup>28</sup> In the literature, the term MF is used with varying meanings: it was coined for magnetic systems, when each spin interacts with all the other spins, the *mean field*. This approximation is valid in Ginzburg–Landau theory above a critical dimension and MF theory is often equated with the minimum of the Ginzburg–Landau free energy. In the bootstrap approach to CFT, Gaussian theories with long-range interactions are termed MF. In the context of avalanches, MF equates with the ABBM model introduced below. The term MF is further used for the Gaussian variational ansatz to replica-symmetry breaking (section 2.20), and in dynamical systems (section 6.7).

fields' pinning the domain wall, which were observed experimentally [318] to change with a *seemingly* uncorrelated function  $\xi(u)$ . The decision of ABBM [316] to model  $\xi(u)$  in equation (383) as a white noise is a strong assumption, *a posteriori* justified by the applicability to experiments [317]. It means that  $F(u)$  has the statistics of a RW.

Field theory [123–125] gives a more differentiated view: first of all, MF theory should be applicable (with additional logarithmic corrections, see section 3.8) in  $d = d_c$  [50, 314], which contains magnets with strong dipolar interactions [319], earthquakes [80], and micro-pillar shear experiments [320]. As  $F(u)$  has the statistics of a RW, the (microscopic) force–force correlator of equations (382) and (383) is

$$\Delta(0) - \Delta(u - u') = \frac{1}{2} \langle [F(u) - F(u')]^2 \rangle = \sigma |u - u'|. \quad (384)$$

Our argument for RF-disorder in section 1.2, the strongest microscopic disorder at our disposal, predicts such a behavior for the correlator  $R(0) - R(u) = \frac{1}{2} \langle [V(u) - V(0)]^2 \rangle$  of the potential, but not of the force. On the other hand, the effective (renormalized) force–force correlator  $\Delta(u)$  has a cusp, so equation (384) with  $\sigma = |\Delta'(0^+)|$  is an approximation, valid for small  $u$ . The ABBM model (381)–(383) should then be viewed as an effective theory, arriving *after renormalization*.

If indeed the microscopic disorder has the statistics of a RW, then the force–force correlator (384) does not change under renormalization, as is easily checked by inserting it into the one-loop (334) or two-loop (343) flow equation. Counting of derivatives for higher-order corrections proves that this statement persists to all orders in perturbation theory. Thus even an extended (non-MF) system where each degree of freedom sees a random force which performs a RW, the BFM, introduced in [321] and further discussed in section 4.5, is stable under renormalization, and has an a roughness exponent  $\zeta_{\text{ABBM}} = \epsilon$ .<sup>29</sup>

Our discussion shows that the ABBM model (382) and (383) is adequate only at small distances, but fails at larger ones, where the force–force correlator decorrelates. We therefore expect that at large distances it crosses over to the DPM of section 3.9. ter Burg *et al* [131] proposed to model the crossover by replacing the RW equation (382) by an Ornstein–Uhlenbeck process,

$$\partial_u F(u) = -F(u) + \xi(u). \quad (385)$$

This equation is solved by

$$F(u) = \int_{-\infty}^u du_1 e^{-(u-u_1)} \xi(u_1). \quad (386)$$

<sup>29</sup> This was indirectly numerically verified in [322].

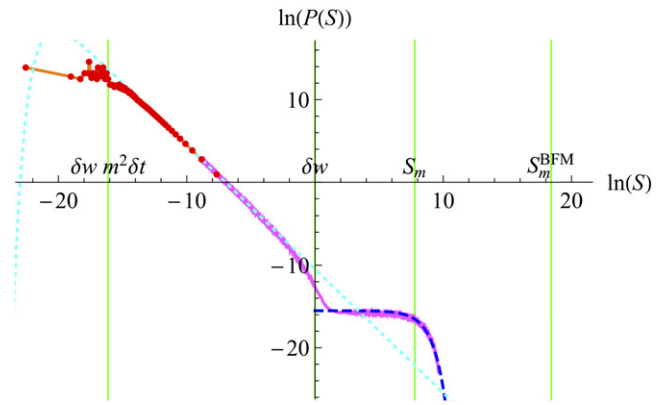


**Figure 27.** Avalanche-size distribution  $P(S)$  for a particle evolving due to equation (379), with forces  $F(u)$  modeled by the Ornstein–Uhlenbeck process (385). The theoretical curves are the kicked ABBM model as given by equation (527) (cyan dotted), and the discrete particle model as given by equation (378) (blue, dashed).  $m^2 = 10^{-4}$ ,  $\delta w = \mathcal{A} = \rho = 1$ ,  $\delta t = 10^{-4}$ ,  $S_m = \langle S^2 \rangle / (2 \langle S \rangle) = 2408.89$ ,  $\rho_m = 2329.95$ ,  $10^8$  samples. Reprinted figure with permission from [131], Copyright (2021) by the American Physical Society.

It leads to microscopic correlations

$$\begin{aligned} \Delta(u - u') &= \overline{F(u)F(u')} \\ &= \int_{-\infty}^u du_1 \int_{-\infty}^{u'} du_2 e^{-(u+u'-u_1-u_2)} \overline{\xi(u_1)\xi(u_2)} \\ &= 2\sigma \int_{-\infty}^{\min(u,u')} d\tilde{u} e^{-(u+u'-2\tilde{u})} \\ &= \sigma e^{-|u-u'|}. \end{aligned} \quad (387)$$

The small-distance behavior of  $\Delta(u - u')$  is as in equation (384). The crossover was confirmed numerically [131], and in experiments on magnetic domain walls [323] and knitting [324]. On figure 27 we show a simulation for the crossover in the avalanche-size distribution (section 4) from  $\tau = 3/2$  for ABBM, given in equation (527), to  $\tau = 0$  as given by equation (378).

Equation (385) also serves as an effective theory for the crossover observed in systems of linear size  $L$ , from a regime with  $mL \gg 1$  described by an extended elastic manifold (section 3.4), to a single-particle regime as described by the DPM model (section 3.9). This crossover has indeed been seen in numerical simulations for a line with periodic disorder [325–327].

### 3.11. Effective disorder, and rounding of the cusp by a finite driving velocity

Suppose the system is driven quasi-statically, such that whenever we measure, almost surely  $\partial_t u(x, t) = 0$ . Then the condition (109) derived for equilibrium is valid too. As is illustrated in figure 25, the chosen minimum is not the global minimum, but the leftmost stable one (driving from left to right), as obtained by the construction contained in Middleton's theorem of section 3.2. Thus there are three relevant local minima: from

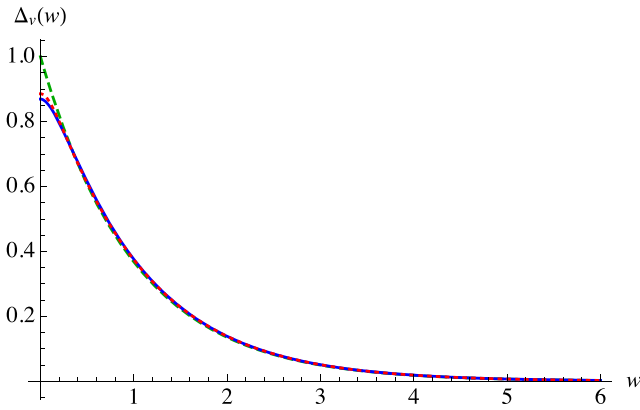


**Figure 28.** Rounding of  $\Delta(w)$  (green, dashed) at finite  $v$  to  $\Delta_v(w)$  (blue solid) given by equation (390) and the boundary-layer approximation (393) (red dotted).

left to right these are the (local) depinning minimum, the equilibrium one, and finally the (local) depinning minimum for driving the system in the opposite direction. The arguments in the construction entering equations (109)–(111) remain valid, and equation (111) is the prescription to measure  $\Delta(w)$  at depinning. Defining with  $w = vt$ ,  $w' = vt'$

$$\Delta_v(w - w') := L^d m^4 \overline{[w - u_w][w' - u_{w'}]^c}, \quad (388)$$

the renormalized force–force correlator is

$$\Delta(w - w') = \lim_{v \rightarrow 0} \Delta_v(w - w'). \quad (389)$$

In an experiment, the driving velocity  $v$  is finite, and it is impossible to take the limit of  $v \rightarrow 0$ . However, the observable (388) can be calculated as [131]

$$\Delta_v(w) = \int_0^\infty dt \int_0^\infty dt' \Delta(w - vt + vt') R_w(t) R_w(t'), \quad (390)$$

where  $R_w(t)$  is the response (318) of the center of mass to an increase in  $w$ , and  $\int_t R_w(t) = 1$ . This implies that the integral of  $\Delta_v(w)$  is independent of  $v$ . An example is shown in figure 28.

As an illustration, consider  $\Delta(w) = \Delta(0)e^{-|w|/\xi}$ , and  $R_w(t) = \tau^{-1}e^{-t/\tau}$ . Then

$$\Delta_v(w) = \Delta(0) \frac{e^{-|w|/\xi} - \frac{\tau v}{\xi} e^{-|w|/(\tau v)}}{1 - \left(\frac{\tau v}{\xi}\right)^2}. \quad (391)$$

This is a superposition of two exponentials, with the natural scales  $\xi$  and  $\tau v$ . Since

$$\Delta'_v(0^+) = 0, \quad (392)$$

the cusp is rounded. This can be proven in general from equation (390). However,  $\Delta_v(w)$  is *not* analytic, contrary to the thermal rounding discussed in section 2.15. As long as  $\tau v \ll \xi$ , the second term decays much faster than the first, allowing us to perform a boundary-layer analysis, already encountered for the thermal rounding of the cusp in equation (142). Equation (390) is approximated by the boundary-layer ansatz

$$\Delta_v(w) \simeq \mathcal{A}_v \Delta\left(\sqrt{w^2 + (\delta_w^{\text{BL}})^2}\right), \quad (393)$$

$$\delta_w^{\text{BL}} = v\tau, \quad \tau := \int_0^\infty dt R_w(t)t, \quad (394)$$

$$\mathcal{A}_v = \frac{\int_0^\infty dw \Delta(w)}{\int_0^\infty dw \Delta(\sqrt{w^2 + (\delta_w^{\text{BL}})^2})}. \quad (395)$$

The amplitude  $\mathcal{A}_v$  ensures normalization. While the response function  $R_w(t)$  (and possibly  $\Delta(w)$ ) in equation (390) may depend on  $v$ , our considerations using the zero-velocity expressions in equation (390) yield at least the correct small-velocity behavior [131].

If in an experiment the response function is unavailable, its characteristic time scale  $\tau$  can be reconstructed approximately from  $\Delta_v(w)$  as

$$\tau \simeq \frac{1}{v} \frac{\lim_{w \rightarrow 0} \Delta'(w)}{\Delta_v''(0)}. \quad (396)$$

In the numerator we have written  $\lim_{w \rightarrow 0} \Delta'(w)$ , which is obtained by extrapolating  $\Delta'_v(w)$  from outside the boundary layer, i.e.  $w \geq \delta_w^{\text{BL}} = v\tau$ , to  $w = 0$ .

There are two other, and more precise, strategies to obtain  $\tau$ , and at the same time reconstruct the zero-velocity correlator:

- use the boundary-layer formula (393) to plot the measured  $\Delta_v(w)$  against  $\sqrt{w^2 + (v\tau)^2}$ ; find the best  $\tau$  which removes the curvature of  $\Delta_v(w)$ . This yields  $\tau$ , and by extrapolation to  $w = 0$  the full  $\Delta(w)$ .
- Use that  $(\tau \partial_t + 1)R_w(t) = \delta(t)$  to remove the response functions in equation (390),

$$\Delta_{v=0}(w) = \left[1 - \left(\tau v \frac{d}{dw}\right)^2\right] \Delta_v(w). \quad (397)$$

In both approaches, the fitting parameter  $\tau$  can rather precisely be obtained by plotting  $-\Delta'_{v=0}(w)/\Delta_{v=0}(w)$ , and optimizing to render the plot as straight as possible for small  $w$ , i.e. inside the boundary layer  $w \leq \delta_w^{\text{BL}} = v\tau$ . While equation (397) is more precise, and reconstructs  $\Delta_{v=0}(w)$  down to  $w = 0$ , the boundary analysis is more robust for noisy data [131, 323].

### 3.12. Simulation strategies

In order to test the predictions of the field theory, one needs efficient simulation algorithms. There are three categories.

- Cellular automata* are simple to implement, either directly for the elastic manifold, or for one of the related sandpile models (section 5). Direct implementations for the elastic manifold are tricky, as extended moves are necessary [328].
- Langevin dynamics* is the most realistic approach, and the best approach to access the dynamics [304]; even though dynamical simulations are sometimes performed in cellular automata.
- Critical configurations* in a continuous setting can be sampled most efficiently by the Rosso–Krauth algorithm [329, 330], termed by the authors variant Monte Carlo.

The idea is simple: when updating the position of a single site, the latter site can be moved as far ahead as the equation of motion permits, without updating at the same time its neighbors. Since Middleton’s theorem guarantees that the such generated configuration cannot surpass the next pinning configuration, the algorithm converges to the latter. This fictitious dynamics is much faster than the Langevin one, and gives precise estimates for the roughness  $\zeta$  in dimension  $d = 1$  [53], and higher [307].

### 3.13. Characterization of the one-dimensional string

**Scaling variables.** To keep a system translationally invariant, simulations are usually performed with periodic boundary conditions. Trying to extract critical exponents by plotting simulation results against distance yields poor results. There are two natural scaling variables:

- (a) *Polymer scaling.* For a non-interacting polymer of size  $x$ , or RW of time  $x$ , the probability that monomers 0 and  $x$  come close in  $d$ -dimensional space is  $P(x) = \mathcal{A}x^{-d/2}$ . The probability that a ring polymer of size  $L$  has monomers 0 and  $x$  close together equals the probability to have two rings of sizes  $x$  and  $L - x$ ,

$$P(x|L) = P(x)P(L - x) = \mathcal{A}^2[x(L - x)]^{-\frac{d}{2}}. \quad (398)$$

This identifies the natural scaling variables

$$x_p^{(1)} := \frac{4x(L - x)}{L^2}, \quad x_p^{(2)} := (x_p^{(1)})^2. \quad (399)$$

- (b) *Conformal invariance.* The conformal mapping from the line  $z = 1 + iy$  to the circle of diameter 1 as shown in figure 29 and known as an *inversion at the circle*, maps

$$z = 1 + iy \rightarrow z' = \frac{1}{1 - iy} = \frac{1}{2} (1 + e^{i\phi}). \quad (400)$$

This implies (for details see [331])

$$y = \tan(\phi/2). \quad (401)$$

Suppose the two-point function on the infinite axis is

$$\langle \mathcal{O}(y_1)\mathcal{O}(y_2) \rangle = \frac{1}{|y_1 - y_2|^{2\Delta}}. \quad (402)$$

Conformal invariance [234, 332, 333] implies that on the circle

$$\begin{aligned} \langle \mathcal{O}(\phi_1)\mathcal{O}(\phi_2) \rangle &= \left( \frac{\partial y_1}{\partial \phi_1} \right)^\Delta \left( \frac{\partial y_2}{\partial \phi_2} \right)^\Delta \langle \mathcal{O}(y_1)\mathcal{O}(y_2) \rangle \\ &= t_{12}^{-2\Delta}. \end{aligned} \quad (403)$$

Here  $t_{12}$  is the chordal distance between the two points parameterized by  $\phi_1$  and  $\phi_2$ , i.e.

$$t_{12} = t(\phi_1 - \phi_2) = |e^{i\phi_1} - e^{i\phi_2}| = 2 \left| \sin \left( \frac{\phi_1 - \phi_2}{2} \right) \right|. \quad (404)$$

Similarly, for the three-point function of scalar operators of dimension  $\Delta$ , conformal invariance implies

$$\langle \mathcal{O}(\phi_1)\mathcal{O}(\phi_2)\mathcal{O}(\phi_3) \rangle = \mathcal{A}(t_{12}t_{13}t_{23})^{-\Delta}. \quad (405)$$

An anomalously large roughness  $\zeta = 5/4$ . Consider the standard definition of the two-point function

$$\langle u^{(2)}(x) \rangle := \frac{1}{2} \langle [u(x) - u(0)]^2 \rangle. \quad (406)$$

We expect that  $\langle u^{(2)}(x) \rangle \sim |x|^{2\zeta}$ . This is not possible for  $\zeta > 1$ , as is shown by the following simple argument [334]:

$$\begin{aligned} &\frac{1}{2} \langle [u(x) - u(0)]^2 \rangle \\ &= \frac{1}{2} \sum_{i=1}^x \sum_{j=1}^x \langle [u(i) - u(i-1)][u(j) - u(j-1)] \rangle. \end{aligned} \quad (407)$$

The expression inside the expectation value depends on  $i - j$ , and is maximal for  $i = j$ . Thus

$$\frac{1}{2} \langle [u(x) - u(0)]^2 \rangle \leq \frac{x^2}{2} \langle [u(1) - u(0)]^2 \rangle. \quad (408)$$

As can be seen on the middle of figure 30, the bound is almost saturated. Thus, we expect

$$\frac{1}{2} \langle [u(x) - u(0)]^2 \rangle \approx \mathcal{A}x_p^{(2)}L^{2\zeta} \simeq 4\mathcal{A}x^2L^{2\zeta-2}, \quad x \ll L. \quad (409)$$

The roughness exponent  $\zeta$  can be observed in the overall scaling, evaluating  $\langle u^{(2)}(x) \rangle$  at its maximum  $x = L/2$ , in Fourier space, or by measuring correlations of the discrete derivative of  $u(x)$ . We expect that

$$\begin{aligned} \langle \partial u^{(2)}(x) \rangle &:= \frac{1}{2} \left\langle \left[ (u(x+1) - u(x)) - (u(1) - u(0)) \right]^2 \right\rangle \\ &= \mathcal{B}(x^{(2)})^{\zeta-1} \simeq 4\mathcal{B}x^{2\zeta-2}, \quad x \ll L. \end{aligned} \quad (410)$$

This is indeed satisfied, see the middle of figure 30. The exponent is consistent with  $\zeta = 5/4$ , as conjectured in [305], see section 5.4.

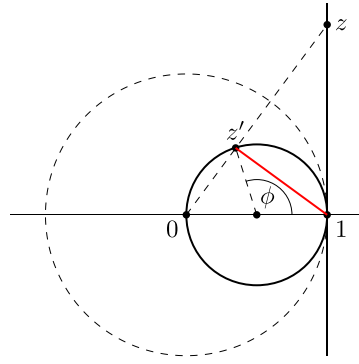


**Figure 29.** The conformal transformation  $z \rightarrow z'$  as given in equation (400).

**Skewness.** In equilibrium the connected three-point function  $\langle u(x)u(y)u(z) \rangle^c$  vanishes, due to the symmetry  $u \rightarrow -u$ . At depinning this symmetry may be broken, but no signs were found yet [335, 336].

On figure 31 we show non-vanishing simulation results for the three-point function [331]

$$\langle u^{(3)}(x) \rangle := \langle [u(x) - u(0)]^2 [u(-x) - u(0)] \rangle. \quad (411)$$

Note that the more symmetric-looking variant

$$\langle [u(x) - u(y)][u(y) - u(z)][u(z) - u(x)] \rangle^c = 0 \quad (412)$$

vanishes as indicated, which can be shown by expansion. The simplest symmetric, non-vanishing combination is

$$\begin{aligned} \langle u^{(3)}(x, y, z) \rangle &:= \frac{1}{6} \langle \Delta u(x, y, z) \Delta u(y, z, x) \Delta u(z, x, y) \rangle^c, \\ \Delta u(x, y, z) &:= u(x) + u(y) - 2u(z). \end{aligned} \quad (413)$$

It is related to the combination in equation (411) by

$$\langle u^{(3)}(x, 0, -x) \rangle \equiv \langle u^{(3)}(x) \rangle. \quad (414)$$

From scaling, we expect that

$$\langle u^{(3)}(x) \rangle \sim |x|^{3\zeta}, \quad x \ll L, \quad (415)$$

as long as we escape the argument that leads to equation (409). Figure 31 shows that this is the case. What is tested there in addition is whether conformal invariance holds. According to equation (405), conformal invariance implies that

$$\langle u^{(3)}(x) \rangle = \mathcal{A}(x^{(3)})^\zeta, \quad (416)$$

$$x^{(3)} = t(x)^2 t(2x). \quad (417)$$

with  $t(x)$  introduced in equation (404). While this does not hold conformal symmetry may be present in a different observable.

### 3.14. Theory and numerics for long-range elasticity: contact-line depinning and fracture

Contact-line depinning can be treated by a modification of the theory for disordered elastic manifolds, using the LR elasticity introduced in section 1.3, equation (15). The theory was

developed to  $\mathcal{O}(\epsilon)$  in [338] and to  $\mathcal{O}(\epsilon^2)$  in [124, 125]. Key predictions for  $\alpha = 1$  are [124]

$$\epsilon = 2 - d, \quad (418)$$

$$\zeta = \frac{\epsilon}{3} (1 + 0.39735\epsilon^2) + \mathcal{O}(\epsilon^3), \quad (419)$$

$$z = 1 - \frac{2}{9}\epsilon - 0.1132997\epsilon^2 + \mathcal{O}(\epsilon^3). \quad (420)$$

The other exponents are obtained via scaling,  $\nu = 1/(1 - \zeta)$ , and  $\beta = \nu(z - \zeta)$ . Simulation results are

$$\zeta = 0.388 \pm 0.002 \text{ [330]}, \quad (421)$$

$$z = 0.770 \pm 0.005 \text{ [338]}, \quad (422)$$

$$\beta = 0.625 \pm 0.005 \text{ [338]}. \quad (423)$$

For arbitrary  $\alpha$  the roughness reads [339]

$$\zeta(\alpha) = \frac{\epsilon}{3} + \frac{\psi(\alpha) - 2\psi(\frac{\alpha}{2}) - \gamma_E}{20.9332} \epsilon^2 + \mathcal{O}(\epsilon^3). \quad (424)$$

For the exponent  $z$ , expressions are more involved, and we only give an additional value for  $\alpha = 3/2$  [339],

$$z(\alpha = 3/2) = \frac{3}{2} - \frac{2}{9}\epsilon - 0.0679005\epsilon^2. \quad (425)$$

Numerical values both for the  $\epsilon$ -expansion and for simulations are collected on figure 32.

### 3.15. Experiments on contact-line depinning

Contact lines are a nice experimental realization of depinning, as one can watch and film them to extract not only their roughness, but also dynamical properties. The value of the roughness exponent, given as  $\zeta = 0.51$  in [85], but observed smaller  $\zeta \approx 1/3$  in earlier work [340], is still debated [341], and many effective exponents are found in the literature. Our own theoretical work [94, 95] does not allow to exclude an exponent of  $\zeta > \zeta_{\text{dep}}^{\text{LR}} = 0.38$ , but we do not believe this to be likely.

Contact-line depinning is also the first system where the renormalized disorder correlator  $\Delta(w)$  was measured, both for liquid hydrogen on a disordered cesium substrate, and for isobutanol on a randomly silanized silicon wafer [71]. Earlier experiments with water on a glass plate with randomly deposited chromium islands [85] turned out to have LR correlated correlations, both due to the impurity of water as of the inhomogeneity of glass. Measurements of the renormalized force-force correlator  $\Delta(w)$  as defined in equation (111) are shown in figure 33, using the cleaner of the two systems, liquid hydrogen on a disordered cesium substrate. The agreement is satisfactory.

### 3.16. Fracture

There are two main types of fracture experiments: fracture along a fault plane [329, 342–345], and fracture of a bulk material [73, 74, 346–351].

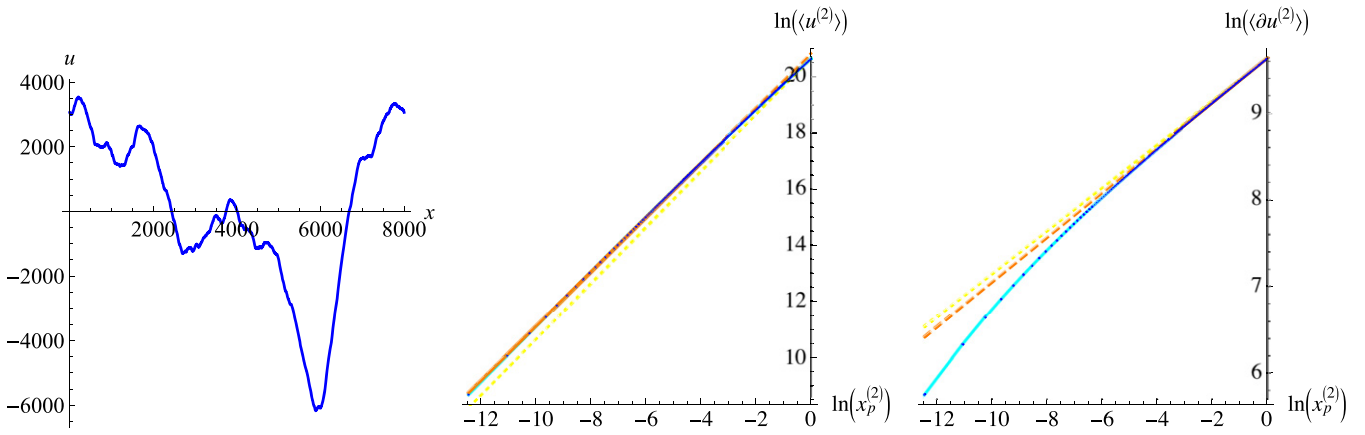


**Figure 30.** (Left) A critical string at depinning,  $L = 8000$ ,  $mL = 1$ . (Middle and right) The two-point function for  $L = 2000$ ,  $mL = 1$ . The measured slopes (in orange) are 0.970, and 0.259, confirming the theoretically expected 1, and 0.25 (in yellow).

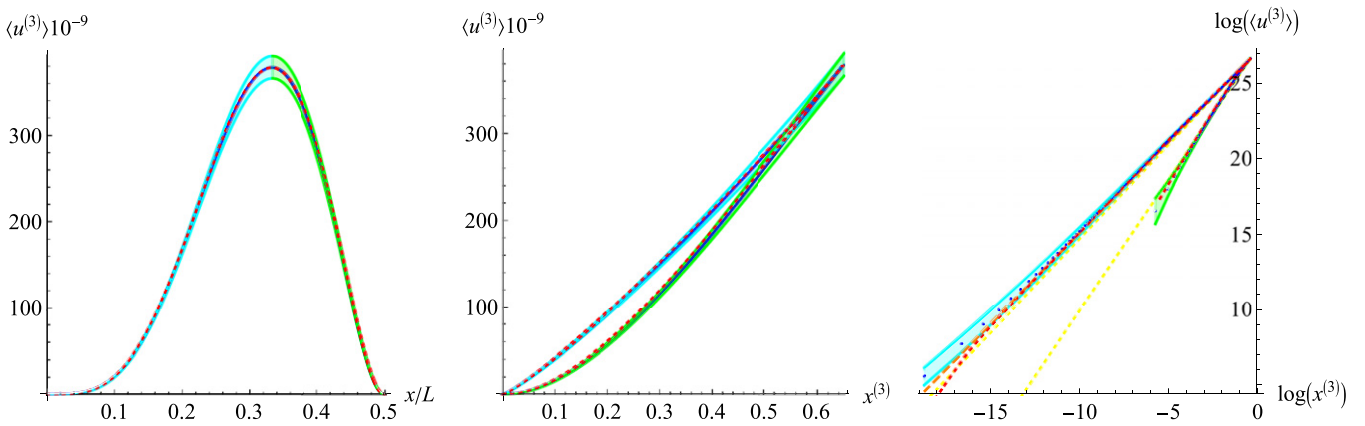


**Figure 31.** The three-point function  $\langle u^{(3)} \rangle$  for  $L = 2000$ ,  $mL = 1$ . The measured slope is  $1.21 \pm 0.04$  (orange, dashed), as compared to the expected  $\zeta = 1.25$  (in yellow). The descending branch of the last curve has slope  $3\zeta - 2 = 1.75$ . The red dotted curves are the theoretical prediction from [331].

	$\epsilon$	$\epsilon^2$	estimate	simulation
$\zeta$	0.33	0.47	$0.47 \pm 0.1$	$0.388 \pm 0.002$ [330]
$\beta$	0.78	0.59	$0.6 \pm 0.2$	$0.625 \pm 0.005$ [338]
$z$	0.78	0.66	$0.7 \pm 0.1$	$0.770 \pm 0.005$ [338]
$\nu$	1.33	1.58	$2 \pm 0.4$	$1.634 \pm 0.005$ [330]

**Figure 32.** Exponents for the depinning of a line with LR elasticity, ( $\alpha = 1$ ) relevant for contact-line depinning and fracture. The last exponent  $\nu$  was obtained from  $\nu = 1/(1 - \zeta)$ .

*Fracture along a fault plane.* Let us start with the conceptually simpler fracture along a fault plane. It is characterized by a roughness exponent  $\zeta \equiv \zeta_{\parallel}$  in the propagation direction. A beautiful example is the *Oslo experiment* [342, 345], where two transparent plexiglas plates are sandblasted rendering them opaque. Sintered together the sandwich becomes transparent. Breaking the crack open along the fault plane between the two plates, the damaged parts become again opaque, allowing one to observe and film the advancing crack, see the inset of figure 34. Below a characteristic scale  $\delta_0 \approx 100 \mu\text{m}$ , which also is the correlation length of the disorder, the roughness exponent is  $\zeta_{\parallel} \approx 0.63$ , which

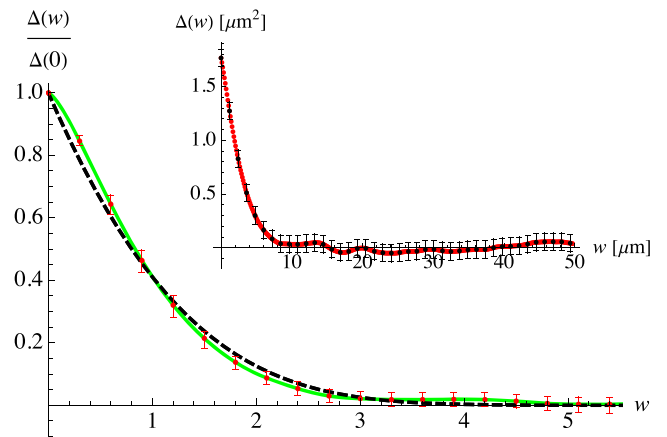


**Figure 33.** (Inset) The disorder correlator  $\Delta(w)$  for contact-line depinning  $\text{H}_2/\text{Cs}$ , with error bars estimated from the experiment. (Main plot) The rescaled disorder correlator (green/solid) with error bars (red). The dashed line is the one-loop result. Reproduced from [71]. © IOP Publishing Ltd. All rights reserved. Note that the boundary layer due to the finite driving velocity (section 3.11) is not deconvoluted.

is interpreted [342] as the roughness exponent in directed percolation (DP)  $\zeta = 0.632613(3)$ , see equation (670). (For

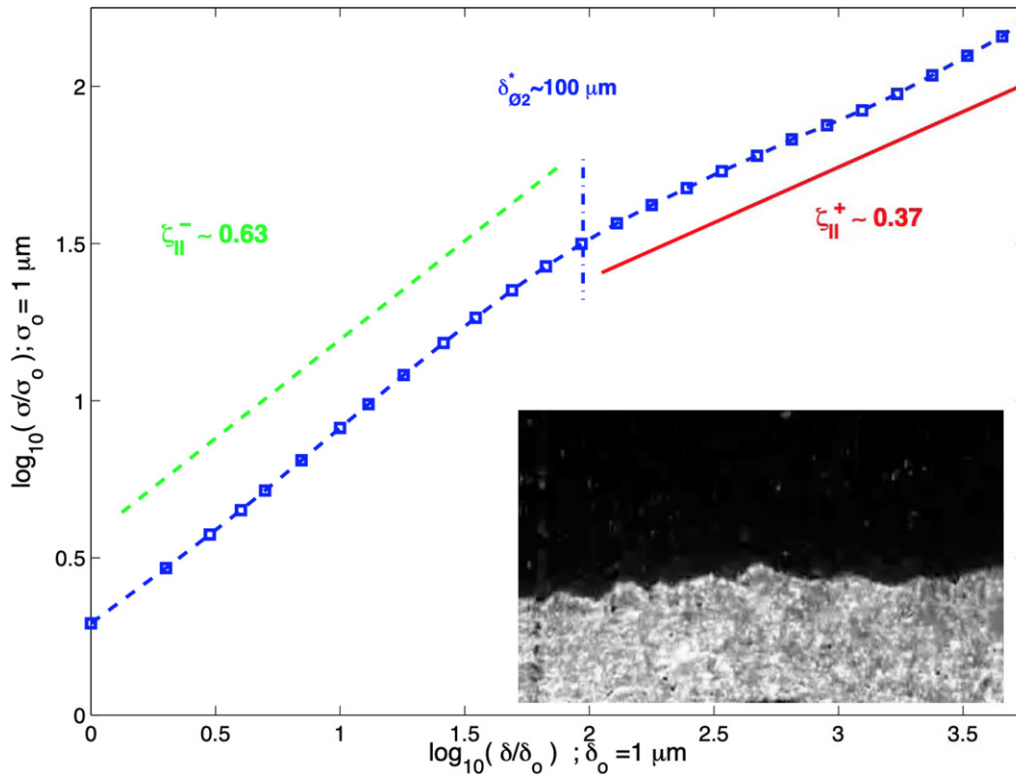
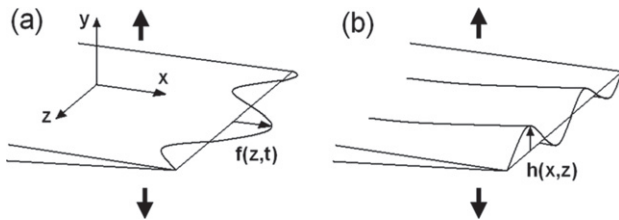


**Figure 34.** Scaling behavior of the height–height correlations with two different roughness exponents  $\zeta_{||} \approx 0.63$  below the critical scale  $\delta^* = 100 \mu\text{m}$  and  $\zeta_{||} \approx 0.37$  above. Reproduced from [342]. © IOP Publishing Ltd. All rights reserved. The inset shows the fracture front, moving from bottom to top.

reasons discussed in section 5.7, DP is also relevant for anisotropic depinning.) For larger scales, the roughness crosses over to a smaller exponent of  $\zeta_{||} \approx 0.37$ , consistent with the roughness exponent for depinning of a line with long-ranged elasticity,  $\zeta = 0.388 \pm 0.002$  see equation (421) [329]. (LR elasticity is explained in section 1.3.) For fracture it was introduced in [93]. Finally, interface configurations are non-Gaussian [352].

*Fracture of bulk material.* Fracture of a bulk material is more complicated. To get the notations straight, we show the coordinate system favored in the fracture community (drawing of [350]).



Applying stress in the direction of the fat arrows, the crack advances on average in the  $x$  direction. The crack front as a function of time is parameterized by

$$x(z, t) = w + f(z, t), \tag{426}$$

$$y(z, t) = \hat{h}(z, t) = h(x(z, t), z). \tag{427}$$

The quantity  $w = vt$  is the external control parameter (used throughout this review). Several critical exponents can be defined. Denote

$$\delta h(\delta x, \delta z)^2 := \langle [h(x + \delta x, z + \delta z) - h(x, z)]^2 \rangle, \tag{428}$$

where the average is taken over all  $x$  and  $z$  (and samples, if possible). The critical exponents  $\hat{\beta}$  and  $\zeta$  defined in the literature are (we changed  $\beta \rightarrow \hat{\beta}$  in order to avoid confusion with the exponent  $\beta$  defined in equation (304))

$$\delta h(\delta x, 0) \sim \delta x^{\hat{\beta}}, \quad \delta h(0, \delta z) \sim \delta z^{\zeta}. \tag{429}$$

Scaling implies that equation (428) can be written as

$$\delta h(\delta x, \delta z) = \delta x^{\hat{\beta}} f\left(\frac{\delta z}{\delta x^{1/\zeta}}\right), \tag{430}$$

$$f(u) \sim u^{\zeta}, \quad \text{for } u \text{ large, and } \zeta = \hat{\beta}\zeta. \tag{431}$$

A third exponent  $\zeta_{||}$  can be defined by the fluctuations of  $f$ ,

$$\delta f \sim \delta z^{\zeta_{||}}. \tag{432}$$

As measurements are in general *post-mortem*,  $\zeta_{||}$  is inaccessible, except if the broken material is transparent, and one can observe the crack front advancing. It has been measured in a clever experiment where a crack was filled with color, and broken open after the color had dried, confirming the small-scale regime  $\zeta_{||} \approx 0.6$  [353]. Numerical simulations suggest [354] that a smaller exponent  $\zeta_{||} \approx 0.38$  should hold at larger scales;

an experimental confirmation is outstanding [354]. One imaging option is to use a synchrotron; this challenging experiment has to our knowledge not been attempted. Common values for materials as diverse as silica glass, aluminum, mortar or wood give  $\hat{\beta} \approx 0.6$ , and  $\zeta \approx 0.75$  to 0.8 [350, 353]. The question arises whether there is a connection to fracture along a fault plane, and depinning.

To make contact to the latter, we first observe that fracture is irreversible, a crucial point for depinning. To proceed, note the 2D vector

$$\vec{u}(z, t) = \left( f(z, t), h(z, t) \right). \quad (433)$$

Knowing the elastic kernel (18) for LR elasticity with  $\alpha = 1$  [93], the only Langevin equation linear in  $u(z, t)$  one can write down is (see e.g. [355, 356])

$$\partial_t \vec{u}(z, t) = \frac{\gamma}{2\pi} \int_{z'} \frac{\vec{u}(z', t) - \vec{u}(z, t)}{(z - z')^2} + \eta(\vec{u}(z, t), z), \quad (434)$$

$$\overline{\eta(x, y, z)\eta(x', y', z')} = \sigma \delta(x - x') \delta(y - y') \delta(z - z'). \quad (435)$$

Assuming that the scenario of [357, 358] holds for long-ranged elasticity, *at large scales* the longitudinal exponent  $\zeta_{\parallel}$  should be that of a contact line, with according to equations (421)–(423) an exponent  $\zeta_{\parallel} = 0.388$ . The transversal roughness  $\zeta_{\perp}$  should be *thermal*, which for  $\alpha = 1$  means logarithmically rough ( $\int_k e^{ikz}/|k| \sim \ln z$ ). This agrees with [355], and was experimentally verified in [359].

The question arises whether this LR universality class, and especially the roughness exponent  $\zeta = 0.38$  can be seen in an experiment. The first such experiment is in [73], using a very brittle material. The authors of this study conjecture that [73] ‘both critical scaling regimes can be observed in all heterogeneous materials’: for length scales smaller than the process zone, the larger exponents ( $\zeta \approx 0.75$ ,  $\hat{\beta} \approx 0.6$ ,  $z = \zeta/\hat{\beta} \approx 1.2$ ) should be relevant, and the fracture surface was reported to be multi-fractal [360]. For larger scales the exponents are those of depinning ( $\zeta \approx 0.4$ ,  $\hat{\beta} = 0.5$ ,  $z = \zeta/\hat{\beta} \approx 0.8$ ). However, these observations were made for the transversal roughness, accessible post-mortem, whereas according to the scenario proposed above it should hold for the longitudinal roughness which is less accessible in experiments. The emerging consensus [354] of the community seems to be that the large-scale roughness in the longitudinal direction is  $\zeta_{\parallel} \approx 0.38$ , whereas the transversal roughness  $\zeta_{\perp} = 0$  (logarithmic rough), as observed in [359]; and that whenever a roughness of  $\zeta_{\perp} \approx 0.38$  has been observed, it has to do with physics related to short scales (damage zone).

What is the *process-zone* mentioned above? The standard theory for fracture is based on work by Griffith [361], with a crucial improvement by Irwin [362]. The idea of Griffith [361] was to write an energy balance between the stress released by the crack, and the surface energy necessary to create it. Irwin [362] realized that for ductile material, part of the released energy goes into a plastic deformation, i.e. heat, at the crack

front. The size of the zone affected is the *process zone*. It ranges from  $\xi = 50 \pm 9 \mu\text{m}$  for ceramics, over  $\xi = 170 \pm 12 \mu\text{m}$  for aluminum to  $\xi = 450 \pm 35 \mu\text{m}$  for mortar [360].

*Fracture in thin sheets.* In thin sheets, very different roughness exponents have been reported:  $\zeta = 0.48 \pm 0.05$  for polystyrene, and  $\zeta = 0.67 \pm 0.05$  for paper [364]. We may speculate that the larger one is related to DP (section 5.8).

*Random fuse models.* Random fuse models, a.k.a. *damage percolation*, have been proposed [365] as a model for fracture: consider a regular lattice, where on each bond is placed a fuse of unit resistance, and a random maximum carrying capacity  $i_c$  (maximal current), in most studies drawn from a uniform distribution,  $i_c \in [0, 1]$ . The system may be two or three-dimensional, with a voltage applied in one direction. To avoid finite-size effects due to the electrodes, it is advantageous to use periodic boundary conditions [366], with an additional voltage gain  $V$  in one dimension. The voltage is then ramped up from 0, until one of the fuses exceeds its carrying capacity, at which point it is considered broken, i.e. having an infinite resistance. One then recalculates the current distribution and checks whether another fuse breaks. If not, one increases the applied voltage.

This is an interesting model for fracture: (i) by solving the Laplace equation to find the current distribution, it incorporates the elasticity of the bulk of the material, providing an effective LR elasticity; (ii) when a part of the material is broken, it is removed. It incorporates ingredients found in Laplacian walks (section 8.9) and DLA (solving in both cases the Laplace equation to determine the most likely point of action), and cellular automata as **TL92** (section 5.7).

A roughness exponent of the fracture surface in  $d = 2 + 1$  was reported to be  $\zeta = 0.62 \pm 0.05$  [366], apparently not too different from some experiments [366]. Other authors focused on the distribution of strength, or broken fuses upon failure [367–369]. A variant is the fiber-bundle model [370, 371].

### 3.17. Experiments for peeling and unzipping

There are two ways to open a double helix made out of two complementary RNA or DNA strands, or one RNA and its complementary DNA strand: peeling and unzipping. In both cases beads are fixed to the molecules, and then pulled in an optical or magnetic trap. In the literature, the word *peeling* is used for the setup of figure 35, where forces act along the helical axis from opposite extremities of a duplex, and one of the two strands peels off. *Unzipping* denotes an alternative setup where the right bead of figure 35 is attached to the free end of the upper strand. As the reader can easily verify with a twisted thread, unzipping is much easier to accomplish than peeling. Let us start with peeling [363], for which a typical force-extension curve is shown in figure 36. The stationary regime is the plateau part (in red). Averaging over about 400 samples, the effective disorder  $\Delta(w)$  defined in equation (111) is measured. The resulting curve, including error bars for the shape [363], is shown in gray in figure 37, where it is compared to three theoretical curves: an exponentially decaying function (red, dotted, top curve), the DPM solution (366) for the Gumbel class (blue, dashed, middle curve), and the one-loop

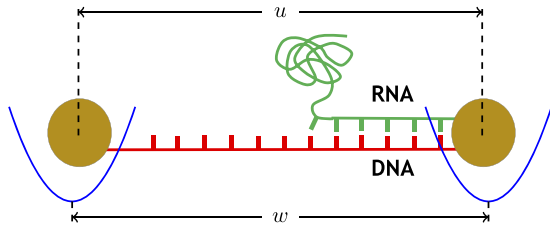


**Figure 35.** Peeling of an RNA-DNA double strand. The RNA sequence is from subunit 23S of the ribosome in *Escherichia coli*, prolonged to attach the beads (brown circles, with a much larger radius than drawn here). The DNA sequence is its complement. The beads sit in an optical trap (blue), at a distance  $w$ . (Drawing not to scale.) Reproduced from [363]. CC BY 4.0.

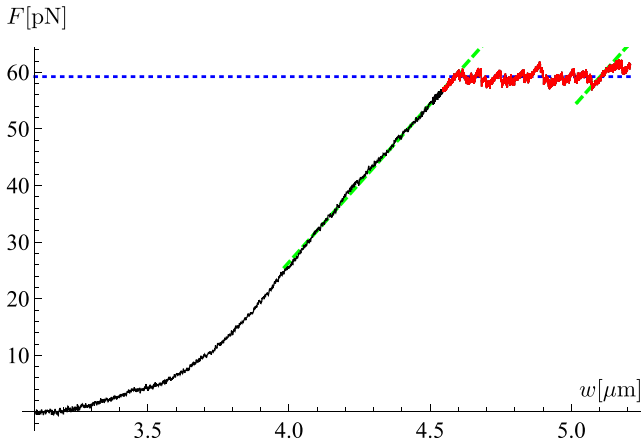


**Figure 36.** (Left) A sample force-extension curve. For the data-analysis only the last plateau part of the curve is used (in red). The effective stiffness  $m^2$  in equation (302) is estimated from the slope of the green dashed lines as  $m^2 = 55 \pm 5 \text{ pN } \mu\text{m}^{-1}$  at the beginning of the plateau, which remains at least approximately correct at the end of the plateau. The driving velocity is about  $7 \text{ nm s}^{-1}$ . Reproduced from [363]. CC BY 4.0.

FRG solution given by equations (84) and (88), all rescaled to have the same value and slope at  $u = 0$ . The experiment clearly favors the DPM solution, best seen in the inset of figure 36. While this is expected, it is a nice confirmation of the theory in a delicate experiment.

One should be able to extract  $\Delta(w)$  also from the unzipping of a hairpin. Interestingly, experiments report that the scaling of equation (365) is replaced by [293]

$$\rho_m \sim m^{-4/3}, \quad \text{i.e. } \zeta = \frac{4}{3}. \quad (436)$$

This is a clear signature of a different universality class, namely ‘RF’ disorder in equilibrium, for which the roughness exponent (83) to all orders in  $\epsilon$  reads  $\zeta = \epsilon/3$ ; setting  $\epsilon = 4$  leads to equation (436). An analytic solution is given in section 2.23. This scenario is possible through the much larger effective stiffness  $m^2$  there, which manifests itself in correlation lengths of  $\xi = 1$  to 35 base pairs, as compared to  $\xi = 186$  base pairs for peeling. Equilibrium is observed experimentally [293] through a vanishing hysteresis curve.

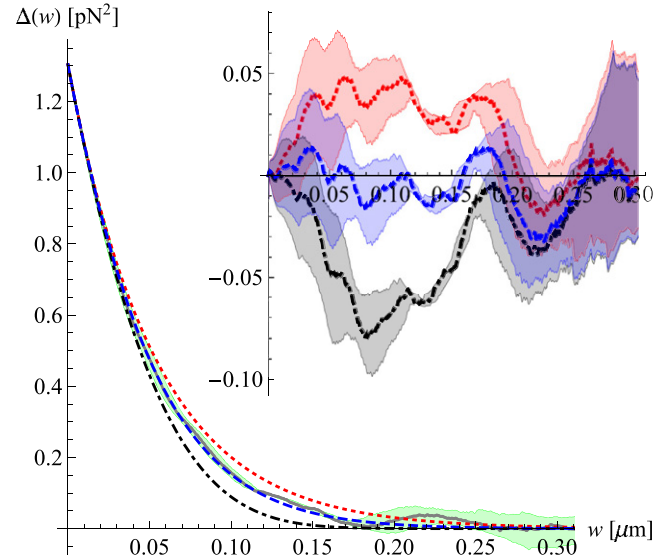


**Figure 37.** Measurements of  $\Delta(w)$  (in gray), with one- $\sigma$  error bars (green shaded), compared to three theoretical curves: pure exponential decay (dotted red), one-loop FRG, equation (84) (black dot-dashed), and DPM, equation (366) (blue dashed), all rescaled to have the same value and slope at  $u = 0$ . Inset: theoretical curves with the data subtracted (same color code). The blue curve is the closest to the data. The correlation length estimated from  $\Delta(w)$  is  $\xi = 0.055 \pm 0.005 \mu\text{m} \simeq 186$  base pairs. Reproduced from [363]. CC BY 4.0.

### 3.18. Creep, depinning and flow regime

In section 1.7, equations (45) and (47), we had argued that in equilibrium the elastic energy scales as

$$\mathcal{E}_{\text{el}}(\ell) \sim \ell^\theta, \quad \theta = 2\zeta_{\text{eq}} + d - \alpha, \quad (437)$$

and as long as  $\theta > 0$  the temperature  $T$  is irrelevant at large scales. On the other hand, if the driving velocity  $v = 0$ , and leaving the system enough time to equilibrate, it is in equilibrium. As sketched in figure 38, there are three different fixed points: equilibrium ( $v = f = 0$ ,  $T \rightarrow 0$ ), depinning ( $T = 0$ ,  $v \rightarrow 0$  or  $f \rightarrow f_c$ ), and large  $v$  or  $f$ , for which we expect  $\eta v = f$ . Let us now consider perturbations of the equilibrium fixed point, i.e.  $T$  small, and  $f \ll f_c$ , commonly referred to as the *creep regime*. Scaling arguments first proposed by Ioffe and Vinokur [372], and Nattermann [373], were later put on more solid ground via FRG [143, 374]. Scaling arguments compare the elastic energy (437) with the energy gained through the advance of the interface, i.e. an avalanche of size  $S$ ,

$$\mathcal{E}_f(\ell) = -f \int_x \delta u(x) \equiv -fS \sim -f\ell^{d+\zeta_{\text{eq}}}. \quad (438)$$

As  $\zeta_{\text{eq}} < \alpha$ , the energy  $\mathcal{E}_f(\ell)$  dominates over  $\mathcal{E}_{\text{el}}(\ell)$  for large  $\ell$ , and the *optimal fluctuation* is obtained for  $\partial_\ell[\mathcal{E}_{\text{el}}(\ell) + \mathcal{E}_f(\ell)] \stackrel{!}{=} 0$ , resulting in  $\ell_{\text{opt}}^{\zeta_{\text{eq}} - \alpha} \sim f$ , or

$$\ell_{\text{opt}} \sim f^{-\nu_{\text{eq}}}, \quad \nu_{\text{eq}} = \frac{1}{\alpha - \zeta_{\text{eq}}}, \quad (439)$$

$$\mathcal{E}_{\text{opt}} \sim f^{-\mu_{\text{eq}}}, \quad \mu_{\text{eq}} = \nu_{\text{eq}}\theta = \frac{2\zeta_{\text{eq}} + d - \alpha}{\alpha - \zeta_{\text{eq}}}. \quad (440)$$

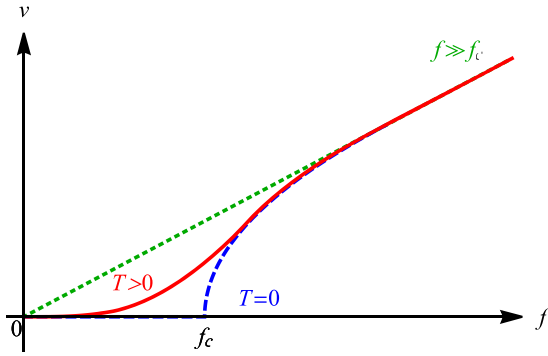


**Figure 38.** Sketch of velocity force curve at vanishing ( $T = 0$ , depinning) and finite temperature ( $T > 0$ , creep). For an experimental test see figure 43.

This identifies the *creep law* as

$$v(f, T) = v_0 e^{-\frac{T}{T^*} \left(\frac{f}{T}\right)^{\mu_{\text{eq}}}}, \quad f \ll f_c. \quad (441)$$

We remind that for depinning (see equations (304) and (308))

$$v \sim (f - f_c)^\beta, \quad f \geq f_c, \quad (442)$$

and that for large  $f$

$$v \simeq \frac{f}{\eta}, \quad f \gg f_c. \quad (443)$$

There are thus three regimes, sketched in figure 38:  $f \ll f_c$ , the creep regime discussed above, governed by the  $T = 0$  equilibrium fixed point;  $T = 0$ , and  $f \approx f_c$ , the depinning fixed point; and the large- $f$  and large- $v$  regime, where the disorder resembles a thermal white noise, with amplitude proportional to  $1/v$ . The latter can be understood from the relation

$$\Delta^{\text{RF}}(w) \simeq \delta(w) = \delta(vt) = \frac{1}{v} \delta(t). \quad (444)$$

More precisely, for RF it looks like a thermal noise with temperature

$$T^{\text{RF}} = \frac{1}{v} \int_0^\infty dw \Delta(w). \quad (445)$$

For RB disorder, the noise decays as  $T^{\text{RB}} \sim 1/v^3$  [359].

*Creep in simulations.* In  $d = 1$ , the creep law (441) was verified numerically [327, 376–380] both for RB and RF disorder, and short-ranged elasticity ( $\alpha = 2$ ):

$$\zeta_{\text{eq}}^{\text{RB}} = \frac{2}{3} \implies \mu_{\text{eq}}^{\text{RB}} = \frac{1}{4}, \quad (446)$$

$$\zeta_{\text{eq}}^{\text{RF}} = 1 \implies \mu_{\text{eq}}^{\text{RF}} = 1. \quad (447)$$

The numerical work [327, 376, 378–380] was possible through the realization that for  $T \rightarrow 0$  the sequence of states, in which the interface rests, becomes deterministic, and can be found by a clever enumeration of all possible saddle points.

*Creep in experiments.* The exponent  $\mu_{\text{eq}}^{\text{RB}} = 1/4$  was first found experimentally in [84], see figure 39, and later con-

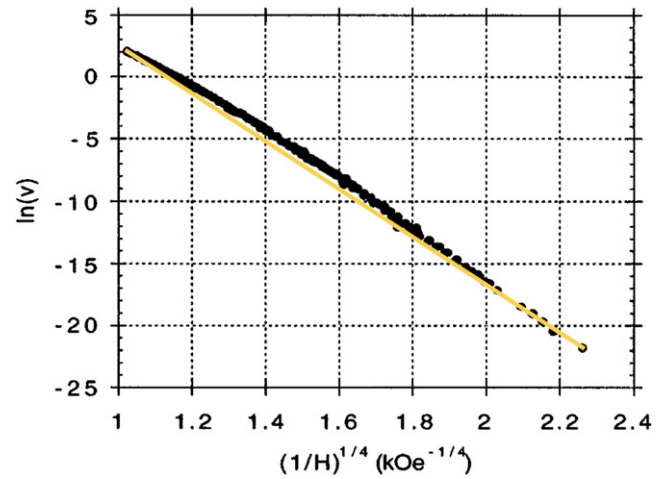


**Figure 39.** Experimental confirmation of the creep-law  $\ln(v) \sim f^{-\mu}$  in an ultrathin PtCoPt film [84]. Tested is the hypothesis  $\mu_{\text{eq}}^{\text{RB}} = 1/4$ ; as the added orange line shows, a larger value of  $\mu_{\text{eq}} \approx 1/3$  should improve the fit, consistent with a value of  $\zeta > 2/3$ . One might see the beginning of the large-scale regime with  $\zeta = \zeta_{\text{dep}} = 5/4$ , see e.g. [375]. A recent experiment is shown in figure 43.

firmed in numerous other magnetic domain-wall experiments [47, 381–384]. These experiments use a Kerr microscopic to image the domain wall; a sample image is given in figure 1. At large scales, the domain-wall roughness is expected to cross over to  $\zeta_{\text{qKPZ}} = 0.63$  or  $\zeta_{\text{dep}} = 1.25$ , see the discussion in section 3.21.

Creep motion was in less depth studied in vortex lattices [385], fracture experiments [386, 387], and quantum systems [198, 388, 389].

For  $f = f_c$  (critical driving), [390] claims that for periodic disorder

$$v(T, f = f_c) \sim T^\chi, \quad \chi = \frac{d+2}{6-d}. \quad (448)$$

In the fixed-velocity ensemble, the scaling (304) suggests

$$\lim_{v \rightarrow 0} [\langle f(0, v) \rangle - \langle f(T, v) \rangle] \sim T^{\chi/\beta}. \quad (449)$$

### 3.19. Quench

In most of this review we studied situations where the system is equilibrated, either in its ground state, or in the steady state. One may ask how it reacts to a quench. This question was first considered for model A (Langevin dynamics for  $\phi^4$ -theory, classification of [301]) in [391]. There one starts with a system at  $T \gg T_c$ , where correlations vanish. At  $t = 0$  one *quenches* it to  $T = T_c$ . The response function  $R(q, t_w, t)$  then depends on  $t$  where one measures the field, and a *waiting time*  $t_w < t$  at which a small kick was performed. For disordered elastic manifolds, the state with vanishing correlations is a flat interface. It can be obtained by imposing  $u(x, t = 0) = 0$ , by moving the interface with a very large velocity  $v \gg 1$  up to  $t = 0$ , or by switching on the disorder at time  $t = 0$ . Scaling

implies that  $R$  takes the form<sup>30</sup>

$$R(q, t_w, t) = \left(\frac{t}{t_w}\right)^{\theta_R} (t - t_w)^{\frac{2-\zeta}{z}} f_R(q^\zeta(t - t_w), t/t_w),$$

$$f_R(x, y) \rightarrow \text{const} \quad \forall x \rightarrow 0, \quad \text{or } y \rightarrow \infty. \quad (450)$$

A similar ansatz holds for the correlation function. Equation (450) would simplify if

$$\theta_R \stackrel{?}{=} \frac{z-2}{z}. \quad (451)$$

In model A,  $\theta_R$  violates equation (451) at two-loop order [391].<sup>31</sup> For disordered elastic manifolds at depinning, equation (451) is satisfied at two-loop order [393, 394], but may be violated in simulations in  $d = 1$  [394]; to decide the matter, larger systems need to be simulated [336].

Technically, the two calculations are rather different: imposing  $\phi(x, t = 0) = 0$  in model A amounts to using Dirichlet boundary conditions. New divergences then appear between fields  $\phi(x, t)$ , and their mirror images at  $t < 0$ . For disordered elastic manifolds no mirror images appear, and one can simply switch on the disorder at  $t = 0$ , reducing the possibility for independent divergences; it may thus well be that relation (451) remains valid at all orders.

The situation simplifies in the limit of  $t_w \rightarrow 0$ . Standard power counting then implies that (see section 3.1)

$$\langle \dot{u}(t) \rangle \sim t^{-\frac{\beta}{\nu z}} \equiv t^{\frac{\zeta}{z}-1}. \quad (452)$$

Similarly, the squared interface width grows as

$$\left\langle L^{-2d} \int_{x,y} [u(x) - u(y)]^2 \right\rangle \rightarrow t^{\frac{2\zeta}{z}}. \quad (453)$$

In [304] these relations were used in simulations of system sizes up to  $L = 2^{25}$  to give the most precise (direct) estimation of the two independent exponents  $\zeta$  and  $z$  in dimension  $d = 1$ , yielding  $\zeta = 1.25 \pm 0.005$ ,  $\nu = 1.333 \pm 0.007$ ,  $\beta = 0.245 \pm 0.006$ , and  $z = 1.433 \pm 0.007$ . This should be compared to the values conjectured to be exact reported in table 1.

A quench has also been studied in the Manna model (MM) [395–397], and interpreted as a dependence of the dynamical exponent  $z$  on the initial condition. As  $z$  is a bulk property, this is hard to believe. It seems [336] that the systems used in the simulations are too small to be in the asymptotic regime.

### 3.20. Barkhausen noise in magnets ( $d = 2$ )

To our knowledge, domain walls in bulk magnets are the only system to realize depinning of a two-dimensional manifold. Two universality classes need to be distinguished [319, 398]:

- magnets with short-ranged elastic interactions, as the Ising model, for which  $\alpha = 2$  (notations as in section 1.3), and  $\epsilon = 2$ .
- Magnets with strong dipolar interactions, which have LR elasticity with  $\alpha = 1$ , thus  $d_c = 2$  is the upper critical dimension (see section 3.14).

For dynamic properties the influence of eddy currents, which varies from sample to sample, needs to be taken into account. A simple model is discussed in section 4.21. Here we consider the renormalized disorder correlator, for which eddy currents are less important. The signal obtained experimentally is the current induced in a pickup coil, which we identify as  $\dot{u}(t)$ , the velocity of the center of mass of the interface. Integrating once yields  $u(w = vt)$ .  $\Delta_v(w)$  is its auto-correlation function defined in equation (388). Using the deconvolution procedure of equation (397) (section 3.11), allows one to extract the zero-velocity limit  $\Delta(w)$ . The latter is plotted in figure 40 for the SR sample, and in figure 41 for the LR sample. For the SR sample, we expect  $\Delta(w)$  to be closest to the resummed loop expansion at  $\epsilon = 2$ , as given in equation (376). For the LR sample, we expect the FRG-fixed point at the upper critical dimension (section 3.8), equivalent to the one-loop FRG fixed point (84)–(88). In both cases, the agreement is very good, and clearly allows us to distinguish between the different universality classes. Let us stress that while the LR sample has critical exponents consistent with the ABBM model [319], the disorder correlator  $\Delta(w)$  is clearly distinct<sup>32</sup> from the one in ABBM, given in equation (493).

The measured  $\Delta(w)$  can be compared to the correlator for RNA-DNA peeling in figure 37 ( $d = 0$ ), and to contact-line depinning ( $d = 1$ ,  $\alpha = 1$ ) in figure 33. Note that for the latter the boundary layer due to the finite driving velocity (section 3.11) was not deconvoluted.

### 3.21. Experiments on thin magnetic films ( $d = 1$ )

Thin magnetic films are appealing, as the position of the domain wall can be visualized using Kerr microscopy, see figure 1. There is a long and somewhat controversial interpretation of the results, which we summarize (figure 44):

- Guided by a theoretical framework based on creep, the first experiments were interpreted as a perturbation of the RB equilibrium fixed point with  $\zeta = 2/3$  [84], even though configurations seem to be frozen.
- Creep exponents are reported [382, 384, 401] without a measurement of the roughness.
- A roughness exponent of  $\zeta \approx 0.6$  was reported [402] together with a plateau of the two-point function for large distances due to the confining potential, here a consequence of dipolar interactions. (The plateau was interpreted as a smaller roughness  $\zeta \approx 0.17$ , a conclusion we do not share.)

<sup>30</sup> The dimension is  $R(q, t) \sim t^{\frac{2-\zeta}{z}} \sim 1/(q^2 t)$ , s.t.  $\int_t R(q, t) \sim q^{-2}$ , reflecting the non-renormalization of the elasticity (STS, section 2.3).

<sup>31</sup> Janssen *et al* [391] does not state the  $\epsilon$  expansion for  $\theta_R$ , but for a related object  $\eta_0$ . The missing relation is  $\theta_R = -\frac{\eta_0}{2z}$ , confirmed in [392].

<sup>32</sup> As  $\Delta(w)$  for ABBM is not renormalized, we should measure it if the microscopic disorder were of the ABBM type.

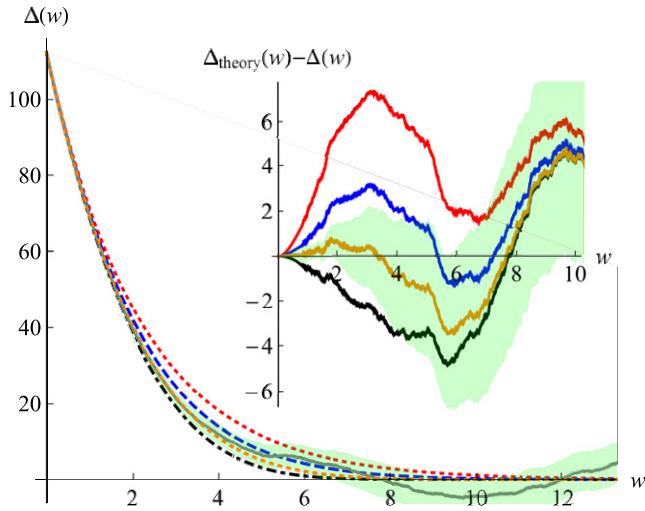


**Figure 40.** Measured force–force correlator  $\Delta(w)$  for a 200 nm ribbon of FeSiB, a bulk magnet with SR elasticity [323] (in gray, with error bars in shaded green, arbitrary units), after correcting for the finite driving velocity (section 3.11). This is compared to several theoretical curves (from top to bottom): an exponential function (red, dotted), the DPM correlator (366) (blue, dashed), FRG resummation (376) for  $\epsilon = 2$  (orange, dashed), and one-loop (black, dot-dashed). Error bars are at 68% confidence level. The inset shows theory minus measurement, favoring the FRG fixed point at  $\epsilon = 2$  (with error bars for this curve only).

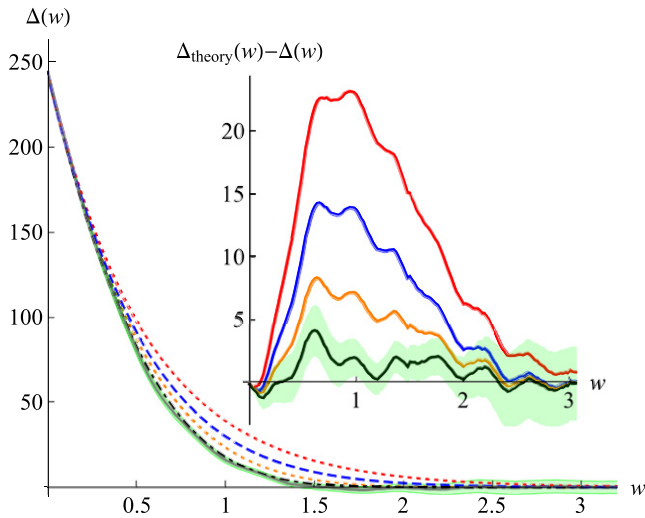


**Figure 41.** Measured force–force correlator  $\Delta(w)$  as in figure 40, for FeSi 7.8%, a bulk magnet with strong dipolar interactions, making the elasticity long-ranged [323]. The FRG prediction for  $\Delta(w)$  is the one-loop fixed point (section 3.8). For better visibility, error bars are at 90% confidence level, not accounting for a remaining oscillation from the power grid with period in  $w$  of about 0.4.

- (d) Bound pairs of domain walls are reported [403], with no clear theoretical interpretation in terms of the phenomena discussed here.
- (e) Moon *et al* [404] shows clear evidence for the negative quenched KPZ (qKPZ) class for current induced depinning, and for the positive qKPZ class for field-induced depinning. We discuss this experiment in section 5.12.

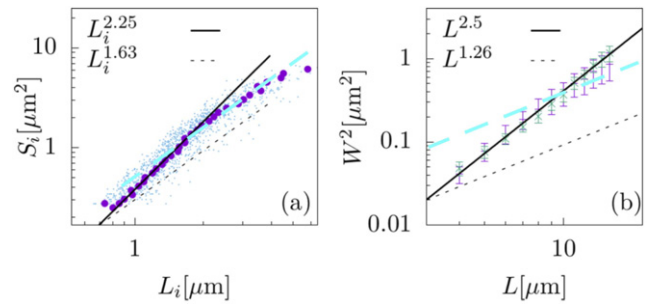


**Figure 42.** Experimentally observed scaling of avalanche sizes (left) and squared width (right) for magnetic domain walls in ferromagnetic Pt/Co/Pt thin films. The solid lines indicate the exponent expected from depinning ( $\zeta = 1.25$ ), whereas dashed lines are for qKPZ ( $\zeta = 0.63$ ). Reprinted figure with permission from [399], Copyright (2018) by the American Physical Society.

- (f) The authors of [291, 292] give the most complete analysis of the roughness exponent to date. The beautiful image shown in figure 45 qualitatively confirms the findings of [404]. Note the strong up-down asymmetry which is inconsistent with an equilibrated systems (see section 3.13). Nevertheless, the equilibrium RB fixed point with  $\zeta_{\text{eq}} = 2/3$  is still the key theoretical class the experiments are compared to. In the case of faceting as in figure 45, the analysis is applied to fluctuations of the facets itself.
- (g) For a thin antiferromagnetic GdFeCo film, exponents consistent with the one-dimensional RF depinning class were found:  $\beta = 0.30 \pm 0.03$  and  $\nu = 1.3 \pm 0.3$  [400], see figure 43. In particular the determination of  $\beta$  is remarkable. The sample in question has a vanishing mass,  $m^2 \approx 0$ . Direct confirmation of a roughness  $\zeta > \zeta_{\text{qKPZ}}$  is more tentative [399], see figure 42.
- (h) Experiments for alternating drive [405].
- (i) More experimental results can be found in [406].

To conclude: evidence for the equilibrium RB universality class with  $\zeta = 2/3$  (sections 2.5 and 2.13) seems to evaporate in favor of the quenched KPZ class with  $\zeta = 0.63$  (section 5.7). At small scales depinning without KPZ-terms is visible [399], but remains to be confirmed. Our conclusion is that at short scales KPZ terms are absent, leading to the RF-depinning class with  $\zeta = 1.25$ . At larger scales, the KPZ term becomes relevant, and one crosses over to one of the qKPZ classes: positive qKPZ for field-induced driving, and negative qKPZ for current-induced driving, see figures 45 and 64 (page 82).

### 3.22. Hysteresis

As we have seen in sections 3.1, 3.4 and 3.9, hysteresis in a driven disordered system is a sign of a non-vanishing force at depinning. In a real magnet the overall magnetization is bounded, thus the critical force depends on where one is on the hysteresis loop. This allows one to invent a plethora of protocols: one can try to get as close as possible into equilibrium by ramping up and down the magnetic field, while reducing the amplitude of the field in each cycle. One can also study *sub-loops*, by varying the applied field in a much smaller range than

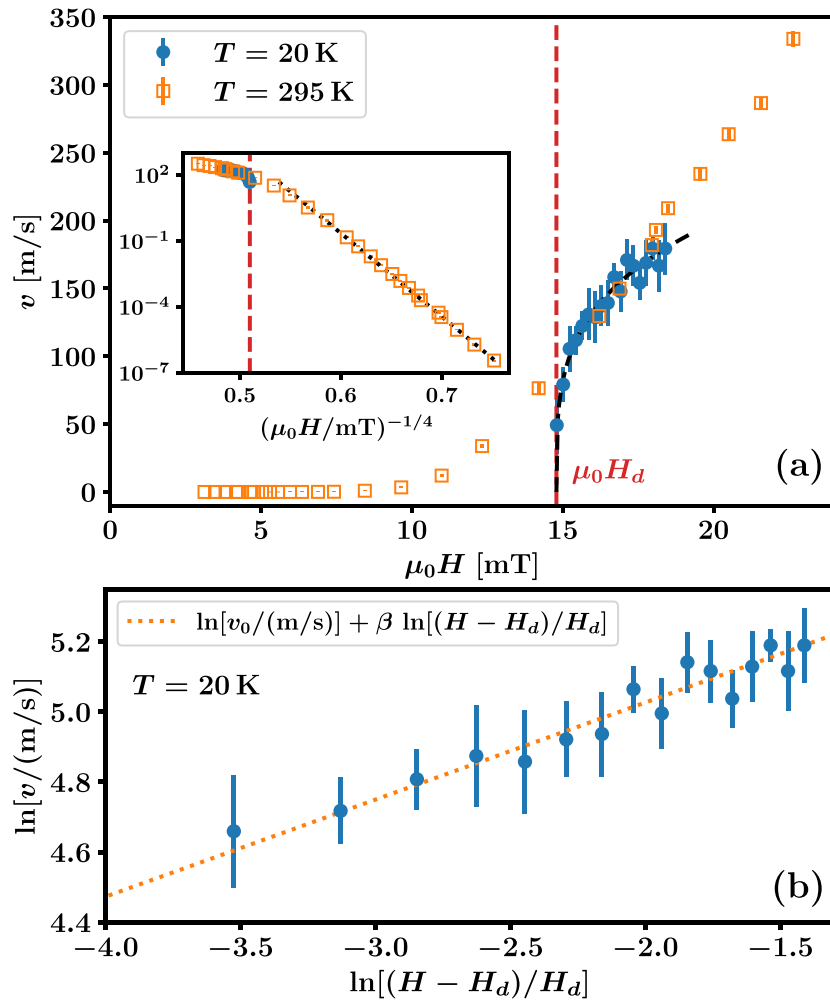


**Figure 43.** The velocity as a function of applied force  $f = \mu_0 H$  for a thin GdFeCo film (top). The sharp transition at  $T = 20$  K is rounded at  $T = 295$  K. The bottom plot shows the quality of the determination of  $\beta = 0.3 \pm 0.03$ . The inset shows the creep law (441) with  $\mu_{eq} = 1/4$ . Reprinted figure with permission from [400], Copyright (2021) by the American Physical Society.

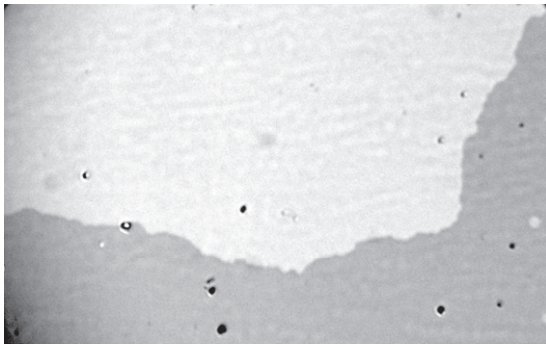


**Figure 44.** PMOKE image of a domain wall in the GdFeCo sample used for figure 43. Reproduced with permission from [407].

necessary for a full magnetization reversal. The reader wishing to enter the *Science of Hysteresis* can find a book with this title [398], or one of the many original research articles [408–411]. There are few analytical result, a notable exception being the hysteresis curve in the ABBM model [412].

### 3.23. Inertia, and a large-deviation function

Inertia plays an important role in everyday-life with depinning: when we were children, we pulled a block or a cart with the help of an elastic string, observing stick-slip motion, with a certain periodicity. At a higher frequency stick-slip motion may be observed when breaking a bike or opening a door, often amplified by a resonance excited in the surrounding medium. Despite its ubiquity in everyday life, stick-slip motion is absent in the avalanche phenomenology discussed above. The reason for this absence is the modeling of the equation of motion (302) or (310) via an overdamped Langevin equation, neglecting inertia.

This is a good occasion to remind us how the overdamped Langevin equation (310) is derived from Newton’s equation of motion for depinning ( $w = vt$ ):

$$M \partial_t^2 u(x, t) = -\eta \partial_t u(x, t) + (\nabla^2 - m^2)[u(x, t) - w] + F(x, u(x, t)). \quad (454)$$

Inertia  $M$  times acceleration  $\partial_t^2 u(x, t)$  are balanced by friction  $-\eta \partial_t u(x, t)$ , forces exerted by the elasticity of the interface

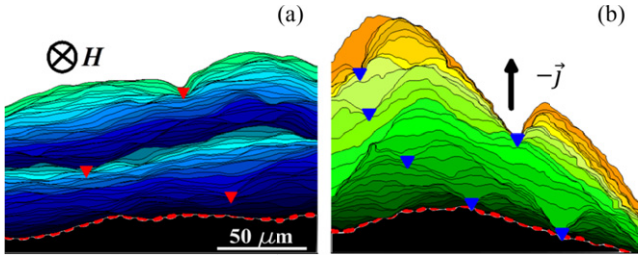


**Figure 45.** Reprinted figure with permission from [291], Copyright (2019) by the American Physical Society, showing the time evolution of the domain-wall shape. (a) Successive positions at  $T = 28$  K, driven by a magnetic field ( $H = 0.16$  mT, delay between images  $t = 0.5$  s, total duration 60 s). (b) Successive positions at  $T = 28$  K, driven by an electric current ( $j \approx 0.5$  GA  $\text{m}^{-2}$ ,  $t = 0.5$  s, total duration 16 s) observed at the same sample location. The DW moves in the direction opposite to the current density, which is indicated by the arrow. The initial DW position is underlined by a thick dashed line. The triangles indicate the strongest DW pinning positions.

( $\sim \nabla^2 u(x, t)$ ), the confining well  $m^2[u(x, t) - w]$  and disorder  $F(x, u)$ . Neglecting inertia, i.e. setting  $M \rightarrow 0$  yields back the standard equation of motion (310), written there with  $\eta = 1$ .

Assuming an exponential behavior  $u(t) \sim e^{-t/\tau}$ , the time scale  $\tau$  satisfies

$$M\tau^{-2} - \eta\tau^{-1} + m^2 = 0. \quad (455)$$

The solution for  $M \rightarrow 0$  starts with  $\tau = \eta/m^2$ ; when  $M$  reaches

$$M_c = \left(\frac{\eta}{2m}\right)^2 \quad (456)$$

this solutions splits into two complex ones, and movement becomes oscillatory. This can be interpreted as a dynamical phase transition. One may conjecture that this remains valid for an extended elastic system. This was indeed observed in MF theory [413]. A careful scaling analysis shows that this extends to systems below the upper critical dimension, where MF theory is no longer valid. Analytic progress was made [414] for various toy models generalizing ABBM (section 4.3), i.e. quenched forces which have the statistics of a RW. All these models share a common *large-deviation function* (a concept discussed below) for a large driving velocity  $v$ . They differ in how returns, which are difficult to incorporate in the field theory, are treated. If instead of returning on the same quenched disorder, new random forces are generated with the same statistics of a RW, then despite dissipation one finds a new active steady state in the limit of a vanishing driving velocity  $v \rightarrow 0$ .

*Large-deviation function.* An interesting concept, well studied in the literature of driven systems, is the large-deviation function, see e.g. [414–418]. Set  $F_v(x)$  and  $Z_v(\lambda)$  to be

$$\mathcal{F}_v(x) := -\frac{\ln(P(xv))}{v}, \quad Z_v(\lambda) := \frac{\ln(\overline{e^{\lambda \dot{u}}})}{v}. \quad (457)$$

Define  $\mathcal{F}(x)$  and  $Z(\lambda)$  as the large- $v$  limits, if they exist, of the above functions,

$$\mathcal{F}(x) := \lim_{v \rightarrow \infty} \mathcal{F}_v(x), \quad Z(\lambda) := \lim_{v \rightarrow \infty} Z_v(\lambda). \quad (458)$$

The existence of the second limit can be shown in field theory. In simple models,  $Z_v(\lambda)$  is even independent of  $v$ , see equation (522) in a simpler setting. Supposing the latter, we obtain

$$\begin{aligned} \overline{e^{\lambda \dot{u}}} &= e^{vZ(\lambda)} = \int_0^\infty d\dot{u} e^{\lambda \dot{u}} P(\dot{u}) \\ &= v \int_0^\infty dx e^{v[\lambda x - \mathcal{F}_v(x)]}. \end{aligned} \quad (459)$$

If  $v$  is large, the latter integral can be approximated by its saddle point with  $\lambda = \partial_x \mathcal{F}_v(x)$ . We recognize a Legendre transform,

$$Z(\lambda) + \mathcal{F}(x) = \lambda x, \quad \lambda = \partial_x \mathcal{F}(x), \quad x = \partial_\lambda Z(\lambda). \quad (460)$$

As by assumption  $Z(\lambda)$  does not depend on  $v$ , this shows that also the first limit in equation (458) exists, and  $\mathcal{F}_v(x) \equiv \mathcal{F}(x)$ , independent of  $v$ . The large-deviation function for the FBM model defined in section 4.5 with an additional inertia term as in equation (454) can then be constructed. Setting for simplicity  $m = \eta = 1$ , it reads [414]

$$\begin{aligned} \mathcal{F}(x, M) &= x - \ln(x) - 1 + M \left[ \frac{x}{2} - \frac{1}{2x} - \ln(x) \right] + \mathcal{O}(M^2), \\ &= \frac{(1-x)^2}{2} + \frac{(1-x)^3}{3} (1+M) + \dots, \end{aligned} \quad (461)$$

where on the second line terms of order  $(1-x)^4$  have been dropped. Units are restored by [414]

$$P_{v \gg 1}(\dot{u}) \simeq e^{-v \frac{\eta m^2}{\sigma} \mathcal{F}(\frac{\dot{u}}{v}, \frac{M m^2}{\eta^2})}. \quad (462)$$

A similar form holds for the joint distribution of velocities and accelerations.

### 3.24. Plasticity

Most systems and their deformations discussed so far are *elastic*, indicating that conformational changes are reversible, and nearest-neighbor relations fixed. When the experiment is repeated, it passes through the same configurations, as given by Middleton's theorem (section 3.3). There are numerous systems where this is not the case, as in sheared colloidal systems, termed *plastic* for their irreversible deformations. The question relevant for us is how much of the phenomenology and methodology developed for disordered elastic manifolds carries over to plastic systems. The gap has not been bridged yet, but efforts have been undertaken starting from disordered elastic manifolds [419–427], and plastic (mostly sheared colloidal) systems [428–431]. A good starting point for the latter is the review [432].

### 3.25. Depinning of vortex lines or charge-density waves, columnar defects, and non-potentiality

A vortex line in 3-dimensional space, driven through quenched disorder, has the statistics of a depinning line in the driving direction ( $\zeta_{\parallel} = 5/4$ , section 3.13) and Gaussian fluctuations ( $\zeta_{\perp} = 1/2$ ) in the transversal direction [357–359]. While the

dynamical exponent  $z_{\parallel} = 10/7$  in the driving direction seems to be unchanged, the perpendicular dynamical exponent is argued to be larger,

$$z_{\perp} = z_{\parallel} + 2 - \zeta = \frac{61}{28} = 2.17857 \dots \quad (463)$$

Note that we updated the values for the exponents of [357, 358] to today's best estimates (section 3.13).

A defect line binds a vortex line more strongly than point disorder. Tilting the sample such that the columnar defect no longer aligns with the magnetic field, one observes an unbinding transition of the vortex line, known as the *transverse Meissner effect* [25, 225, 433–435]. This is also observed as an effective model for sliding CDWs [436].

In the above setting, forces are assumed to be derivatives of a potential, i.e. conservative. If they are non-conservative, as e.g. in presence of stable advecting currents, then a new universality class is reached, accessible perturbatively [437–439].

In section 2.26 we had shown experimental and theoretical evidence for the existence of an ordered phase in vortex lattices (Bragg glass) at weak disorder. The authors of [440, 441] argue that the Bragg-glass phase is stable w.r.t. slow driving, with the lattice responding by flowing through well-defined, elastically coupled, static channels. If the lattice is preserved, then after it has moved by a full lattice constant, it comes back to its original configuration. In this case, one expects the velocity to be periodic in time [442].

In [443] it was found that translational order in the driving direction can be destroyed.

### 3.26. Other universal distributions

Exponents are not the only interesting observables: in experiments and simulations, often whole distributions can be measured, as e.g. the width distribution of an interface at depinning [50, 444, 445]. Be  $\langle u \rangle$  its spatial average for a *given* disorder configuration, then the width

$$w^2 := \frac{1}{L^d} \int_x (u(x) - \langle u \rangle)^2 \quad (464)$$

is a random variable, with distribution  $P(w^2)$ . The rescaled function  $\Phi(z)$ , defined by

$$P(w^2) = 1/w^2 \Phi(w^2/w^2) \quad (465)$$

is expected to be universal, i.e. independent of microscopic details and the size of the system.

Supposing  $u(x)$  to be Gaussian,  $\Phi(z)$  was calculated analytically to leading order. It depends on two parameters, the roughness exponent  $\zeta$  and the dimension  $d$ . Numerical simulations [50, 444] displayed in figure 46 show agreement between analytical and numerical results. The distribution is distinct from a Gaussian.

There are more observables of which distributions have been calculated within FRG, or measured in simulations. Let us mention fluctuations of the elastic energy [446], and of the depinning force [48, 277].

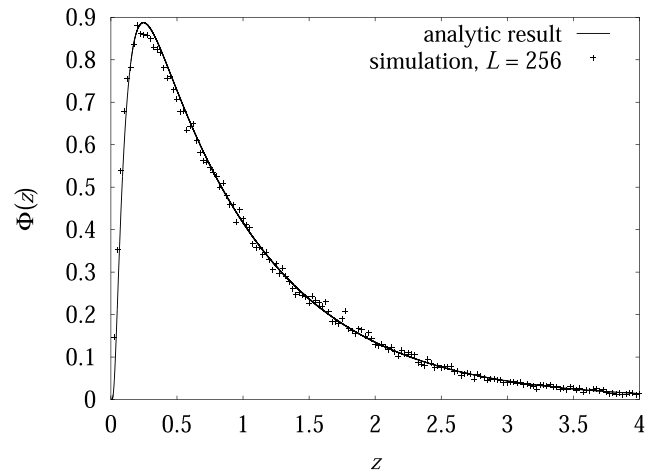


**Figure 46.** Scaling function  $\Phi(z)$  for the  $(1+1)$ -dimensional harmonic model, compared to the Gaussian approximation for  $\zeta = 1.25$ . Reprinted figure with permission from [444], Copyright (2003) by the American Physical Society.

## 4. Shocks and avalanches

### 4.1. Observables and scaling relations

When slowly driving a system, according to equation (310), long times of inactivity are followed by bursts of activity, which on these long time scales look instantaneous. To be specific, we start with the system at rest, and instantaneously increase  $w \rightarrow w + \Delta w$ . Observables of interest are

- center-of-mass position

$$u(t) := \frac{1}{L^d} \int_x u(x, t), \quad (466)$$

- center-of-mass velocity

$$\dot{u}(t) := \partial_t u(t), \quad (467)$$

- duration  $T$ , see figure 48. This quantity is well-defined, as every avalanche stops at some point when it is no longer driven (see section 4.4), so

$$T := \inf_t \{t, \dot{u}(t) > 0\} < \infty. \quad (468)$$

- shape  $\langle \dot{u}(t) \rangle$ .

- Avalanche size  $S$ ,

$$S := \int_x \delta u(x) = \int_x u_2(x) - u_1(x), \quad (469)$$

where  $u_1(x)$  is the interface position before, and  $u_2(x)$  after an avalanche, see figures 47 and 48.

- The avalanche extension  $\ell$ ,

$$\ell := \sup_{x,y} \{|x - y|, \delta u(x) > 0, \delta u(y) > 0\}. \quad (470)$$

These are the main observables. Setting and language here are for depinning. Some observables, as the avalanche-size distribution can also be formulated in the statics: these *static avalanches*, also termed *shocks*, are the changes in the ground-state configuration upon a change in the applied field, i.e. the position  $w$  of the confining potential. We will comment

**Table 2.** Scaling relations discussed in the main text, specifying to SR elasticity ( $\alpha = 2$ ), and standard LR elasticity  $\alpha = 1$ .

	$\rho(S)$	$\rho(S_\phi)$	$\rho(T)$	$\rho(\dot{u})$	$\rho(\dot{u}_\phi)$	$\rho(\ell)$
	$S^{-\tau}$	$S_\phi^{-\tau_\phi}$	$T^{-\tilde{\alpha}}$	$\dot{u}^{-a}$	$\dot{u}_\phi^{-a_\phi}$	$\ell^{-k}$
SR elasticity	$\tau = 2 - \frac{2}{d+\zeta}$	$\tau_\phi = 2 - \frac{2}{d_\phi+\zeta}$	$\tilde{\alpha} = 1 + \frac{d-2+\zeta}{z}$	$a = 2 - \frac{2}{d+\zeta-z}$	$a_\phi = 2 - \frac{2}{d_\phi+\zeta-z}$	$k = d + \zeta - 1$
LR elasticity	$\tau = 2 - \frac{1}{d+\zeta}$	$\tau_\phi = 2 - \frac{1}{d_\phi+\zeta}$	$\tilde{\alpha} = 1 + \frac{d-1+\zeta}{z}$	$a = 2 - \frac{1}{d+\zeta-z}$	$a_\phi = 2 - \frac{1}{d_\phi+\zeta-z}$	$k = d + \zeta$

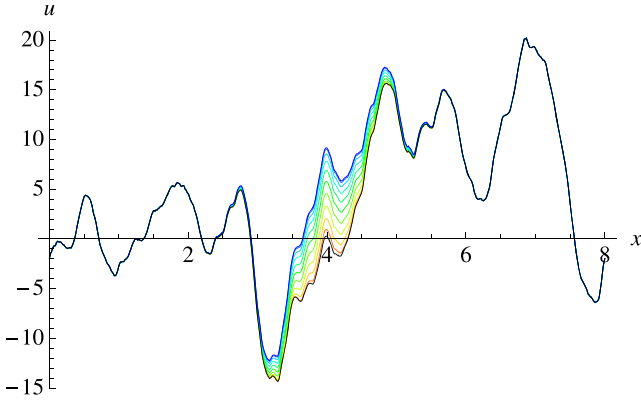


**Figure 47.** Temporal evolution of an avalanche starting at  $x = 4$  at  $t = 0$ , evolving to the top until time  $T$ . Interface positions at intermediate times  $t = iT/10$  are shown for  $i = 1, 2, \dots, 10$ . Reprinted figure with permission from [321], Copyright (2013) by the American Physical Society.

on differences between these two concepts at the appropriate positions. Key points are

- avalanches are the response of the system to an increase in force. They have a typical size

$$S_m := \frac{\langle S^2 \rangle}{2 \langle S \rangle} \sim \xi^{d+\zeta} \sim m^{-(d+\zeta)}. \quad (471)$$

In the literature one sometimes finds the notation  $D = d + \zeta$  for the fractal dimension of an avalanche.

- The *avalanche-size distribution* per unit force  $\delta f = m^2 \delta w$ ,

$$\rho_f(S) := \frac{\delta N(S)}{\delta f} \simeq S^{-\tau} f_S(S/S_m) g_S(S/S_0), \quad (472)$$

$$S_0 \ll S_m,$$

has a large-scale cutoff  $S_m$  defined in equation (471) due to the confining potential, and a small-scale cutoff  $S_0$  due to the size of the kick or discretization effects (as in a spin system). The scaling functions are expected to have a finite limit when  $m \rightarrow 0$ , i.e.  $\lim_{x \rightarrow 0} f_S(x) = \text{const}$ , and  $\lim_{x \rightarrow \infty} g_S(x) = 1$ .

- An increase  $\delta f$  in the total integrated force is then on average given by an increase  $\delta u(x)$  in  $u$ , which integrated over space gives  $S$ . On the other hand, we can integrate equation (472) over  $S$ . Together, these relations give

$$\delta f = m^2 \int_x \langle \delta u(x) \rangle = m^2 \langle S \rangle$$

$$= \delta f m^2 \int_0^\infty dS S \rho_f(S) \sim \delta f m^2 [S_m^{2-\tau} - \mathcal{O}(S_0^{2-\tau})]. \quad (473)$$

As we will see below  $\tau < 2$ , and the last term can be dropped due to the assumption of  $S_0 \ll S_m$  in equation (472). This gives

$$m^2 \sim S_m^{\tau-2}. \quad (474)$$

Inserting  $S_m$  from equation (471) yields

$$\tau_{\text{SR}} = 2 - \frac{2}{d + \zeta}. \quad (475)$$

In  $d = 1$  and with  $\zeta = 5/4$  this gives

$$\tau_{\text{SR}}^{d=1} = \frac{10}{9} = 1.111 \dots \quad (476)$$

- *LR-elasticity.* Here one replaces  $m^2 \rightarrow m^\alpha$ , leading to

$$\tau_\alpha = 2 - \frac{\alpha}{d + \zeta}. \quad (477)$$

- *Alternative scaling argument.* In [447] it was suggested in the context of sandpile models (see section 6.6) that a single grain performs a RW which has to reach the boundary, implying that  $\langle S \rangle \sim L^2$ . Using  $\langle S \rangle \sim S_m^{2-\tau}$ , and  $L \sim m^{-1}$  leads to  $(2 - \tau)(d + \zeta) = 2$ , equivalent to equation (475).
- *Boundary driving.* When a (SR-elastic) system is driven at the boundary (tip driving [448]) there is a drift (advection) away from this boundary<sup>33</sup>, leading to a linear scaling,  $\langle S \rangle \sim L$ , and as a consequence  $(2 - \tau)(d + \zeta) = 1$  [448–450],

$$\tau_{\text{SR}}^{\text{tip}} = 2 - \frac{1}{d + \zeta}. \quad (478)$$

In  $d = 1$  and for  $\zeta = 5/4$  this gives

$$\tau_{\text{SR}}^{\text{tip},d=1} = \frac{14}{9} = 1.555 \dots > \frac{3}{2}. \quad (479)$$

- the distribution of avalanche sizes in a submanifold  $\phi$  of dimension  $d_\phi$ ,

$$\rho_f^\phi(S^\phi) \sim S^{-\tau_\phi}, \quad S_m^\phi \gg S^\phi \gg S_0^\phi, \quad (480)$$

$$\tau_\phi = 2 - \frac{\alpha}{d_\phi + \zeta}.$$

The derivation proceeds as for equations (475) and (477).

<sup>33</sup> We do not understand the first-return-to-the-origin argument of [449].

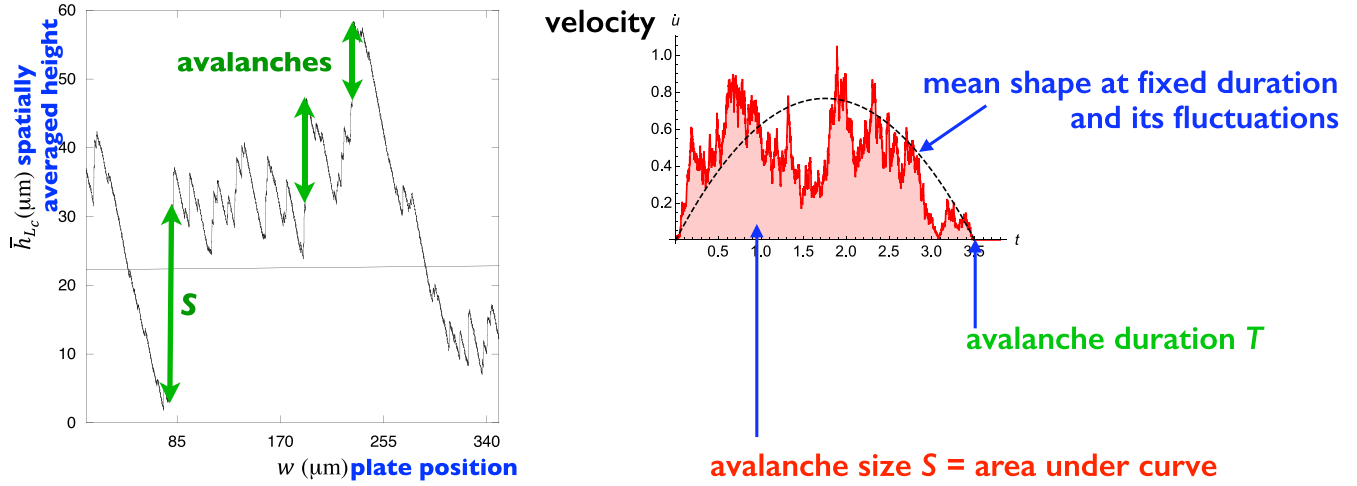


**Figure 48.** (Left) The mean spatial height in the contact-line depinning experiment of figure 22. (Right) Increasing the time resolution to resolve a single avalanche (jump, marked by the arrow), the velocity inside a single avalanche can be viewed as a RW with absorbing boundary conditions at vanishing velocity. This allows us to define observables as the mean avalanche shape, the size  $S$  (area under the curve), or its duration  $T$ .

- Avalanche size and duration are related via

$$S_m \sim T_m^\gamma, \quad \gamma = \frac{d + \zeta}{z}. \quad (481)$$

This is obtained from the scaling relations  $S_m \sim m^{-d-\zeta}$ , and  $T_m \sim m^{-z}$ .

- The (unnormalized) duration distribution per unit force is<sup>34</sup>

$$\rho_f(T) \sim T^{-\tilde{\alpha}}, \quad T_m \gg T \gg T_0, \quad T_m = \frac{\langle T^3 \rangle}{\langle T^2 \rangle}. \quad (482)$$

The integral relation  $\rho(S)dS = \rho(T)dT$  implies  $S_m^{1-\tau} \sim T_m^{1-\tilde{\alpha}}$ . Using  $S_m \sim m^{-(d+\zeta)}$ , and  $T_m \sim m^{-z}$  yields with the help of equation (477)

$$\tilde{\alpha} = 1 + \frac{d + \zeta - \alpha}{z}. \quad (483)$$

- the (unnormalized) velocity distribution

$$\rho_f(\dot{u}) \sim \dot{u}^{-a}, \quad \dot{u}_m \gg \dot{u} \gg \dot{u}_0, \quad \dot{u}_m = \frac{S_m}{T_m}. \quad (484)$$

The exponent  $a$  is obtained from arguments similar to those used in the derivation of equations (475) and (480), with the result that in the denominator the dimension of the observable in question appears. For the velocity distribution it yields

$$a = 2 - \frac{\alpha}{d + \zeta - z}. \quad (485)$$

- avalanche extension: in general, avalanches have a well-defined spatial extension  $\ell$ , allowing us to define their distribution  $\rho_f(\ell)$ . If  $\ell \ll \xi = 1/m$ , then  $\ell$ , and not  $\xi$  is the

relevant scale, and  $S \sim \ell^{d+\zeta}$ . Writing  $\rho_f(S)dS = \rho_f(\ell)d\ell$  allows us to conclude [451] that for extensions between the lattice cutoff  $a$  and  $\xi = 1/m$ ,

$$\rho_f(\ell) \sim \ell^{-k}, \quad a \ll \ell \ll \frac{1}{m},$$

$$k = d + \zeta + 1 - \alpha. \quad (486)$$

- avalanche volume: in higher dimensions, it is difficult to define the spatial extension of an avalanche, while its volume is well-defined. Using  $\rho_f(V)dV = \rho_f(S)dS$ , and  $S \sim \ell^{d+\zeta}$ ,  $V \sim \ell^d$  we arrive at

$$\rho_f(V) \sim V^{-k_V}, \quad a^d \ll V \ll \frac{1}{m^d}, \quad (487)$$

$$k_V = 2 - \frac{\alpha - \zeta}{d}.$$

- differences between static avalanches (shocks) and avalanches at depinning: a conceptually and practically important question is whether static avalanches and avalanches at depinning are in the same universality class. As the roughness exponent  $\zeta$  differs from one class to the other, equation (475) implies that they also have a different avalanche-size exponent  $\tau$ , and thus must be different. We will see below that this difference is not visible at one-loop order, but shows up at two-loop order.

- *Phenomenology, and a warning:* for magnetic domain walls, where avalanche phenomena were first observed as *Barkhausen noise* [68], one distinguishes in general SR samples ( $\alpha = 2$ ) from LR samples ( $\alpha = 1$ ), and samples with noticeable eddy currents from those without. A good review is [319]. The reader should realize that the ABBM model (section 4.3) is often equated with the LR class or MF, even though this is not true [131, 323]. The line of theory we develop below starts with the ABBM model, generalizes it to the BFM (section 4.5), and then proceeds to short-range correlated disorder (section 4.6).

<sup>34</sup> We note the exponent as  $\tilde{\alpha}$  instead of the standard notation  $\alpha$  to avoid confusion with  $\alpha$  for the exponent of LR elasticity in equation (16), and here present in equations (480), (483), (485)–(487).

#### 4.2. A theory for the velocity

Up to now, our modeling of depinning was based on the equation of motion (310) for the position of the interface. This formulation makes it difficult to extract observables involving the velocity. For this purpose it is better to take a time derivative of equation (310), to get an equation of motion for the velocity  $\dot{u}(x, t)$ ,

$$\partial_t \dot{u}(x, t) = (\nabla^2 - m^2) [\dot{u}(x, t) - \dot{w}(t)] + \partial_t F(x, u(x, t)). \quad (488)$$

#### 4.3. ABBM model

The field theory to be constructed below gives a quantitative description of avalanches in a force field  $F(x, u)$ , with short-ranged correlations in both the  $x$  and  $u$ -directions. We start with a toy model for a single degree of freedom, and then proceed in two steps to short-range correlated forces for an interface.

The toy model in question is the ABBM model, introduced in 1990 by Alessandro, Beatrice, Bertotti and Montorsi [316, 317], see also [452, 453]. Setting  $w(t) = vt$ , it reads

$$\partial_t \dot{u}(t) = m^2 [v - \dot{u}(t)] + \partial_t F(u(t)), \quad (489)$$

$$\partial_t F(u(t)) = \sqrt{\dot{u}(t)} \xi(t), \quad (490)$$

$$\langle \xi(t) \xi(t') \rangle = 2\sigma \delta(t - t'). \quad (491)$$

The last equation implies that  $F(u)$  is a RW, as can be seen as follows: as  $\dot{u}$  is non-negative,  $t$  is an increasing function of  $u$ , and we can change variables from  $t$  to  $u$ ,

$$\partial_u F(u) = \bar{\xi}(u), \quad \langle \bar{\xi}(u) \bar{\xi}(u') \rangle = 2\sigma \delta(u - u'). \quad (492)$$

As a RW,  $F(u)$  has correlations

$$\Delta(0) - \Delta(u - u') \equiv \frac{1}{2} \langle [F(u) - F(u')]^2 \rangle = \sigma |u - u'|. \quad (493)$$

In the language introduced above, the (bare) disorder has a cusp, with amplitude  $|\Delta'(0^+)| = \sigma$ .

The ABBM model is traditionally treated [316, 317, 452] via the associated Fokker–Planck equation (944) (for a derivation see appendix A.3),

$$\partial_t P(\dot{u}, t) = \sigma \frac{\partial^2}{\partial \dot{u}^2} [\dot{u} P(\dot{u}, t)] + m^2 \frac{\partial}{\partial \dot{u}} [(\dot{u} - v) P(\dot{u}, t)]. \quad (494)$$

This approach is difficult for time-dependent quantities, but efficient for observables in the steady state. As an example, consider the steady-state distribution of velocities, obtained by solving  $\partial_t P(\dot{u}, t) = 0$ ,

$$P(\dot{u}) = \frac{\dot{u}^{\frac{m^2 v}{\sigma} - 1} e^{-\dot{u} \frac{m^2}{\sigma}} \left(\frac{m^2}{\sigma}\right)^{\frac{m^2 v}{\sigma}}}{\Gamma\left(\frac{m^2 v}{\sigma}\right)}. \quad (495)$$

Setting  $\sigma = m = 1$  to simplify the expressions yields

$$P(\dot{u}) = \frac{\dot{u}^{v-1} e^{-\dot{u}}}{\Gamma(v)}. \quad (496)$$

#### 4.4. End of an avalanche, and an efficient simulation algorithm

It is important to remark that an avalanche stops at a given well-defined time. To see this, we solve equations (489) and (490) for  $m = 0$ , given that at time  $t = 0$  the velocity is  $\dot{u}_0$ . The associated Fokker–Planck equation is

$$\partial_t P(\dot{u}, t) = \partial_{\dot{u}}^2 [\sigma \dot{u} P(\dot{u}, t)]. \quad (497)$$

It can be solved analytically, for given initial distribution  $P(\dot{u}, 0) = \delta(\dot{u} - \dot{u}_0)$ , as

$$P(\dot{u}, t) = \delta(\dot{u}) \exp\left(-\frac{\dot{u}_0}{\sigma t}\right) + \frac{\exp\left(-\frac{\dot{u}_0 + \dot{u}}{\sigma t}\right)}{\sigma t} \sqrt{\frac{\dot{u}_0}{\dot{u}}} I_1\left(\frac{2\sqrt{\dot{u}_0 \dot{u}}}{\sigma t}\right). \quad (498)$$

( $I_1$  is the Bessel-function of the first kind.) This can be checked by inserting the solution into the differential equation (497). Equation (498) teaches us that for an initial velocity  $\dot{u}_0$ , with a finite probability  $\exp(-\frac{\dot{u}_0}{\sigma t})$  the velocity will be (strictly) zero after time  $t$ . It also means that the end of an avalanche is well defined in time, which is crucial to define its duration. This would not be the case for a particle in a smooth potential: linearizing the potential close to the endpoint of the avalanche assumed to be  $u(t = \infty) = 0$  yields

$$\partial_t u(t) \simeq -\alpha u(t) \implies u(t) \simeq u_0 e^{-\alpha t}. \quad (499)$$

Equation (498) can serve as an efficient simulation algorithm, replacing  $t$  by the time-discretization step  $\delta t$ , and alternately integrating the forcing term  $\delta \dot{u}(t) = m^2 [v - \dot{u}(t)] \delta t$  and the stochastic process according to equation (498). This is not straightforward, due to the appearance of multiplicative noise [454]. We can use an additional trick [455]: observe that the solution (498) can be written as

$$P(\dot{u}, t) = \delta(\dot{u}) \exp\left(-\frac{\dot{u}_0}{\sigma t}\right) + \sum_{n=1}^{\infty} \frac{\left(\frac{\dot{u}_0}{\sigma t}\right)^n \exp\left(-\frac{\dot{u}_0}{\sigma t}\right)}{n!} \times \frac{1}{\sigma t} \frac{\left(\frac{\dot{u}}{\sigma t}\right)^{n-1} \exp\left(-\frac{\dot{u}}{\sigma t}\right)}{(n-1)!} = \sum_{n=0}^{\infty} p_n \frac{1}{\sigma t} P_n\left(\frac{\dot{u}}{\sigma t}\right). \quad (500)$$

Here,  $p_n$  is a normalized probability vector, i.e.  $\sum_{n=0}^{\infty} p_n = 1$ , and each probability  $P_n(x)$  is normalized,  $\int_0^{\infty} dx P_n(x) = 1$ . Explicitly, we have

$$p_n = \frac{\left(\frac{\dot{u}_0}{\sigma t}\right)^n \exp\left(-\frac{\dot{u}_0}{\sigma t}\right)}{n!}, \quad (501)$$

$$P_0(x) = \delta(x), \quad (502)$$

$$P_n(x) = \frac{x^{n-1} \exp(-x)}{(n-1)!}, \quad n \geq 1. \quad (503)$$

Given  $\dot{u}_0$ , one obtains  $\dot{u}$  with probability  $P(\dot{u}, t)$  as follows:

- (a) draw an integer random number  $n$ , from the Poisson distribution  $p_n$ ; the latter has parameter  $\dot{u}_0/(\sigma t)$ ,
- (b) if  $n = 0$ , return  $\dot{u} = 0$ ,
- (c) else draw a positive real random number  $x$ , from the Gamma distribution with parameter  $n$ .
- (d) Return  $\dot{u} = \sigma t x$ ,

Contrary to a naive integration of the stochastic differential equation which yields  $\partial_t F(u(t)) \delta t = \xi_t \sqrt{\delta t}$ ,  $\langle \xi_t \xi_{t'} \rangle = \delta_{t,t'}$ , this algorithm is linear in  $\delta t$ .

This allows us to define the distribution of durations, given below in equation (546), and the mean temporal shape (552), without introducing an (arbitrary) small-velocity cutoff.

#### 4.5. Brownian force model (BFM)

The model defined in equations (489) and (490) is a model for a single degree of freedom, not for an interface. A model for an interface can be defined by [321]

$$\partial_t \dot{u}(x, t) = \nabla^2 u(x, t) + m^2 [v - \dot{u}(x, t)] + \partial_t F(x, u(x, t)), \quad (504)$$

$$\partial_t F(x, u(x, t)) = \sqrt{\dot{u}(x, t)} \xi(x, t), \quad (505)$$

$$\langle \xi(x, t) \xi(x', t') \rangle = 2\sigma \delta(t - t') \delta^d(x - x'). \quad (506)$$

Since each degree of freedom sees a force which is a RW, this model is termed the BFM [321].

#### 4.6. Short-ranged rough disorder

Both the ABBM model as its spatial generalization, the BFM model, are pathologic in the sense that the force–force correlator grows for all distances instead of saturating as expected in short-ranged correlated systems, and as is reflected in the FRG fixed points discussed in section 2.5. To remedy this, one can keep the equation of motion (504), but add an additional damping term in the evolution equation (505) of the force,

$$\partial_t F(x, u(x, t)) = -\gamma \dot{u}(x, t) F(x, u(x, t)) + \sqrt{\dot{u}(x, t)} \xi(x, t), \quad (507)$$

$$\langle \xi(x, t) \xi(x', t') \rangle = 2\sigma \delta(t - t') \delta^d(x - x'). \quad (508)$$

As  $\dot{u}(x, t) \geq 0$ , the equation of motion for the force is equivalent to

$$\partial_u F(x, u) = -\gamma F(x, u) + \tilde{\xi}(x, u), \quad (509)$$

$$\langle \tilde{\xi}(x, u) \tilde{\xi}(x', u') \rangle = 2\sigma \delta(u - u') \delta^d(x - x'). \quad (510)$$

This system has the force–force correlator

$$\langle F(x, u) F(x', u') \rangle^c = \sigma \delta^d(x - x') \frac{e^{-\gamma|u-u'|}}{\gamma}, \quad (511)$$

derived in equation (387). For  $u \ll \gamma$ , we recover the correlations (493).

#### 4.7. Field theory

Consider the equation of motion (488) with generic short-ranged force–force correlators. The dynamical action is

obtained by multiplying the equation of motion with  $\tilde{u}(x, t)$ , and averaging over disorder<sup>35</sup>,

$$\mathcal{S} = \int_{x,t} \tilde{u}(x, t) \left[ (\partial_t - \nabla^2) \dot{u}(x, t) + m^2 (\dot{u}(x, t) - \dot{w}) \right] - \frac{1}{2} \int_{x,t,t'} \tilde{u}(x, t) \tilde{u}(x, t') \partial_t \partial_{t'} \Delta(u(x, t) - u(x, t')). \quad (512)$$

The second line contains

$$\begin{aligned} & \partial_t \partial_{t'} \Delta(u(x, t) - u(x, t')) \\ &= \dot{u}(x, t) \partial_{t'} \Delta'(u(x, t) - u(x, t')) \\ &= \dot{u}(x, t) [\Delta'(0^+) \partial_{t'} \text{sign}(t - t') - \Delta''(0^+) \dot{u}(x, t') + \dots] \\ &= -2\dot{u}(x, t) \Delta'(0^+) \delta(t - t') \\ &\quad - \Delta''(0^+) \dot{u}(x, t) \dot{u}(x, t') + \dots \end{aligned} \quad (513)$$

The terms dropped in this expansion are higher derivatives of  $\Delta(u)$ , and they come with higher powers of  $\dot{u}(x, t)$ , and its time-integral  $u(x, t) - u(x, t') = \int_{t'}^t d\tau \dot{u}(x, \tau)$ , reminding that  $\dot{u}(x, t)$  and not  $u(x, t)$  is the variable for which we wrote down the equation of motion.

This expression is quite remarkable: the leading term is proportional to  $\delta(t - t')$ , rendering the last term in equation (512) *local* in time. It is therefore appropriate to start our analysis of the theory with this term only. The action we obtain is

$$\begin{aligned} \mathcal{S}_{\text{BFM}}[\dot{u}, \tilde{u}] &= \int_{x,t} \tilde{u}(x, t) \left[ (\partial_t - \nabla^2) \dot{u}(x, t) + m^2 (\dot{u}(x, t) - \dot{w}(x, t)) \right] \\ &\quad + \Delta'(0^+) \tilde{u}(x, t)^2 \dot{u}(x, t). \end{aligned} \quad (514)$$

This is the action of the BFM introduced in equations (504)–(506): as  $\Delta(u)$  only has a first non-vanishing derivative, all subsequent terms in equation (513) vanish. Corrections are obtained by adding the omitted terms perturbatively. The subleading term is

$$\begin{aligned} \mathcal{S}[\dot{u}, \tilde{u}] &= \mathcal{S}_{\text{BFM}}[\dot{u}, \tilde{u}] \\ &\quad + \frac{\Delta''(0^+)}{2} \int_{x,t,t'} \tilde{u}(x, t) \tilde{u}(x, t') \dot{u}(x, t) \dot{u}(x, t') + \dots \end{aligned} \quad (515)$$

We show below on page 68 several theorems, indicating that at the upper critical dimension the action (512) leads to the results of the BFM model, and that the additional term in equation (515) is sufficient for the one-loop corrections, of order  $\epsilon = d_c - d$ .

<sup>35</sup> The response field  $\tilde{u}(x, t)$  is different from that in equations (313) and (314). One can derive equation (512) by substituting in equation (314)  $\tilde{u}(x, t) \rightarrow -\partial_t \tilde{u}(x, t)$ , and then integrating by parts in time.

#### 4.8. FRG and scaling

The FRG equation (343) for the disorder has the following structure

$$\partial_t \tilde{\Delta}(u) = (\epsilon - 2\zeta) \tilde{\Delta}(u) + \zeta u \tilde{\Delta}'(u) + \sum_{n=1}^{\infty} \partial_u^{2n} [\tilde{\Delta}(u) - \tilde{\Delta}(0)]^{n+1}. \quad (516)$$

The  $n$ -loop terms are highly symbolic, since the derivatives can be distributed in different ways on the  $n + 1$  disorder correlators, and we have dropped all prefactors. We now assume that the microscopic disorder has the form (493), thus  $\tilde{\Delta}(0) - \tilde{\Delta}(u)$  has only a term linear in  $u$ . This implies that the term of order  $n = 1$  may contribute a constant to equation (516), while terms with  $n \geq 2$  vanish. Thus to all orders, the roughness exponent is given by

$$\zeta_{\text{BFM}} = \epsilon = 4 - d. \quad (517)$$

As a consequence, the unrescaled disorder is scale independent (does not renormalize), and

$$\Delta_{\text{BFM}}(0) - \Delta_{\text{BFM}}(u) \equiv \sigma |u|. \quad (518)$$

Note that  $\Delta(0)$  is not well-defined, since random forces grow unboundedly.

Similarly, the dynamical exponent  $z$  has corrections proportional to  $\Delta''(0)$ , which vanish. As a consequence,  $z = 2$ , and all exponents can be obtained analytically,

$$\begin{aligned} z_{\text{BFM}} &= 2, & \beta_{\text{BFM}} &= \mathbf{a}_{\text{BFM}} = 1, & \gamma_{\text{BFM}} &= \alpha_{\text{BFM}} = 2, \\ \tau_{\text{BFM}} &= \frac{3}{2}, & \kappa_{\text{BFM}} &= 3. \end{aligned} \quad (519)$$

#### 4.9. Instanton equation

We want to construct observables for the BFM such as

$$\begin{aligned} Z[\lambda, w] &:= \left\langle e^{\int_{x,t} \lambda(x,t) \dot{u}(x,t)} \right\rangle \\ &= \int \mathcal{D}[\dot{u}] \mathcal{D}[\tilde{u}] e^{\int_{x,t} \lambda(x,t) \dot{u}(x,t) - S_{\text{BFM}}[\dot{u}, \tilde{u}]}. \end{aligned} \quad (520)$$

This includes the avalanche-size distribution with  $\lambda(x, t) = \lambda$ , the velocity distribution with  $\lambda(x, t) = \lambda \delta(t)$ , the local avalanche-size distribution with  $\lambda(x, t) = \lambda \delta(x)$ , a.s.o.

The key observation is that  $\dot{u}(x, t)$  appears linearly in the exponent, thus the path integral over  $\dot{u}$  can be performed *exactly*, enforcing an *instanton equation* for  $\tilde{u}(x, t)$ ,

$$(-\partial_t - \nabla^2 + m^2) \tilde{u}_{\text{inst}}(x, t) - \sigma \tilde{u}_{\text{inst}}(x, t)^2 = \lambda(x, t). \quad (521)$$

Here  $\sigma \equiv -\Delta'(0^+) > 0$ , see e.g. equations (493) and (511). The expectation (520) simplifies to

$$Z[\lambda, w] = e^{\int_{x,t} m^2 \dot{w}(x,t) \tilde{u}(x,t)} \Big|_{\tilde{u}=\tilde{u}_{\text{inst}}}. \quad (522)$$

The term with  $\dot{w}(x, t)$  in the exponential is the only one not proportional to  $\dot{u}(x, t)$ ; the latter vanish due to the instanton equation (521). Let us consider some examples.

#### 4.10. Avalanche-size distribution

The simplest example is the avalanche-size distribution. Noting that  $S = \int_{x,t} \dot{u}(x, t)$ , we have to solve the instanton equation (521) for  $\lambda(x, t) = \lambda$ . The solution for  $\tilde{u} = \tilde{u}_{\text{inst}}$  will be constant in space and time, thus the instanton equation (521) reduces to

$$m^2 \tilde{u} - \sigma \tilde{u}^2 = \lambda. \quad (523)$$

This quadratic equation has two solutions. The relevant one vanishing at  $\lambda = 0$  reads

$$\tilde{u} = \frac{m^2 - \sqrt{m^4 - 4\lambda\sigma}}{2\sigma}. \quad (524)$$

We now insert this solution into equation (522). As  $\tilde{u}(x, t)$  is constant in space and time, the integral on the rhs of equation (522) is  $\tilde{u}$  times

$$w := \int_{x,t} \dot{w}(x, t) > 0. \quad (525)$$

This yields with  $\tilde{u}$  given in equation (524)

$$\langle e^{\lambda S} \rangle = e^{m^2 w \tilde{u}}. \quad (526)$$

Taking the inverse Laplace transform gives

$$P_w^S(S) = m^2 w \frac{e^{-\frac{m^4(S-w)^2}{4\sigma S}}}{2\sqrt{\pi\sigma S^{3/2}}}. \quad (527)$$

One checks that  $P_w^S(S)$  is normalized,  $\langle 1 \rangle_w = \int_0^\infty dS P_w^S(S) = 1$ , and that the first avalanche-size moment is  $\langle S \rangle_w = \int_0^\infty dS S P_w^S(S) = w$ . If  $w(x, t)$  is constant in  $x$ , then  $\langle S \rangle_w = w$  is nothing but the displacement of the confining parabola.

$P_w(S)$  is the response of the system to a displacement  $w$ , or equivalently to a *force kick*  $\delta f = m^2 w$ . We now take the limit of an infinitesimally small displacement  $w$ , and to this purpose define

$$\begin{aligned} P^S(S) &:= \lim_{w \rightarrow 0} \frac{\langle S \rangle_w}{w} P_w^S(S) \\ &= \langle S \rangle m^2 \frac{e^{-\frac{m^4 S}{4\sigma}}}{2\sqrt{\pi\sigma S^{3/2}}} \equiv \langle S \rangle \frac{e^{-\frac{S}{4S_m}}}{2\sqrt{\pi S_m S^{3/2}}}, \end{aligned} \quad (528)$$

$$\tau = \tau_{\text{ABBM}} = \frac{3}{2}, \quad (529)$$

$$S_m := \frac{\langle S^2 \rangle}{2 \langle S \rangle} = \frac{\sigma}{m^4}. \quad (530)$$

Since  $\langle S \rangle_w = w$ , by construction all moments which do not necessitate a small- $S$  cutoff, i.e.  $\langle S^n \rangle_w$  with  $n \geq 1$  have a well-defined small- $w$  limit, given by Equation (528). What one loses when taking the limit of  $w \rightarrow 0$  is normalizability, as formally  $\langle 1 \rangle = \lim_{w \rightarrow 0} w^{-1} = \infty$ .

#### 4.11. Watson–Galton process, and first-return probability

The avalanche size-exponent  $\tau = 3/2$  observed in the ABBM model appears in many contexts: it was first studied in the survival probability of a noble man's name (male descendents)

[456]. The latter has the equations of motion (489)–(491), where  $\dot{u}(t)$  is the number of descendants in a generation,  $v = 0$ , and  $m^2$  the mean relative decrease in male descendants in a generation (which could be negative),

$$\partial_t u(t) = -m^2 \dot{u}(t) + \sqrt{\dot{u}(t)} \xi(t), \quad (531)$$

$$\langle \xi(t) \xi(t') \rangle = 2\sigma \delta(t - t'). \quad (532)$$

As  $\dot{u}(t) > 0$ , the total number of descendants  $u(t)$  is monotonically increasing, allowing us to write  $\dot{u}(t) \equiv \dot{u}(u(t))$ . The equation of motion (531) then becomes

$$\partial_t \dot{u}(u(t)) = \dot{u}(u) \partial_u \dot{u}(u) = -m^2 \dot{u}(u) + \sqrt{\dot{u}(u)} \xi(t). \quad (533)$$

As long as  $\dot{u} > 0$ , we can divide both sides by  $\dot{u}$  to arrive at

$$\partial_u \dot{u}(u) = -m^2 + \tilde{\xi}(u), \quad (534)$$

$$\langle \tilde{\xi}(u) \tilde{\xi}(u') \rangle = 2\sigma \delta(u - u'). \quad (535)$$

Note the change of argument in the noise. Thus  $\dot{u}(u)$  performs a RW in ‘time’  $u$  with drift  $-m^2$  and absorbing boundary conditions at  $\dot{u} = 0$ . In absence of an absorbing wall, the probability that  $\dot{u}(u)$  starts close to zero at  $u = 0$ , and returns to zero behaves for large  $u$  as

$$P_{\text{return}}(u) \sim \frac{e^{-m^2 u}}{\sqrt{u}}. \quad (536)$$

In presence of an absorbing wall, we need the probability to arrive at zero for the first ‘time’  $u$ . The latter is obtained by taking a ‘time’, i.e.  $u$ -derivative of  $P_{\text{return}}(u)$ ,

$$P_{\text{first}}(u) = -\partial_u P_{\text{return}}(u) \sim \frac{e^{-m^2 u}}{u^{\frac{3}{2}}}. \quad (537)$$

This is again the ABBM avalanche-size distribution (528) with  $\tau = 3/2$ , interpreted as first-return probability of a RW.

#### 4.12. Velocity distribution

To simplify further considerations, we set

$$m^2 \rightarrow 1, \quad -\Delta'(0^+) \equiv \sigma \rightarrow 1. \quad (538)$$

To obtain the instantaneous velocity distribution, we evaluate equations (520)–(522) for  $\lambda(x, t) = \lambda \delta(t)$ , setting  $\dot{w}(x, t) = v$  (uniform driving). The instanton equation to be solved is

$$-\partial_t \tilde{u}(t) + \tilde{u}(t) - \tilde{u}(t)^2 = \lambda \delta(t). \quad (539)$$

To impose proper boundary conditions, look at the rhs of equation (522): driving at times  $t > 0$  does not affect the velocity distribution at  $t = 0$ , thus the instanton solution  $\tilde{u}(t)$  must vanish for positive times. Equation (539) with this constraint is solved by

$$\tilde{u}(t) = \frac{\lambda \Theta(-t)}{\lambda + (1 - \lambda) e^{-t}}. \quad (540)$$

With the above solution equation (522) reduces to

$$\begin{aligned} \left\langle e^{\lambda \int_x \dot{u}(x,0)} \right\rangle &= e^{v L^d \int_t \tilde{u}(t)} = e^{-v L^d \ln(1-\lambda)} \\ &= (1 - \lambda)^{-v L^d}. \end{aligned} \quad (541)$$

The inverse Laplace transform for the integrated velocity  $\dot{u} = \int_x \dot{u}(x, 0)$  is

$$P_{v,L}^{\dot{u}}(\dot{u}) = \frac{\dot{u}^{v L^d - 1} e^{-\dot{u}}}{\Gamma(v L^d)}. \quad (542)$$

Apart from the source  $v L^d$ , this result is independent of the dimension  $d$ , and agrees with the ABBM result equation (495), there derived for a single degree of freedom. We can take the limit of  $v \rightarrow 0$ , and define

$$P^{\dot{u}}(\dot{u}) := \lim_{v \rightarrow 0} \frac{P_{v,L}^{\dot{u}}(\dot{u})}{v L^d} = \frac{e^{-\dot{u}}}{\dot{u}}. \quad (543)$$

#### 4.13. Duration distribution

The probability that the avalanche has velocity zero at time 0 after a kick of size  $w$  at time  $t = -T$ , with  $T > 0$ , can be obtained from the central result (522) with the instanton (540) as

$$\begin{aligned} P(\dot{u}(x, 0) = 0 \forall x) &= \lim_{\lambda \rightarrow -\infty} \left\langle e^{\lambda \int_x \dot{u}(x,0)} \right\rangle \\ &= \lim_{\lambda \rightarrow -\infty} e^{w \tilde{u}(-T)} = \exp\left(-\frac{w}{e^T - 1}\right). \end{aligned} \quad (544)$$

This is also the probability that the duration following a kick of size  $w$  is smaller than  $T$ . The distribution of durations is obtained by taking a derivative w.r.t.  $T$ ,

$$\begin{aligned} P_w^{\text{duration}}(T) &= \partial_T \exp\left(-\frac{w}{e^T - 1}\right) \\ &= w \exp\left(-\frac{w}{e^T - 1}\right) \frac{e^{-T}}{(e^{-T} - 1)^2} \\ &= w \exp\left(-\frac{w}{e^T - 1}\right) \frac{1}{[2 \sinh(T/2)]^2}. \end{aligned} \quad (545)$$

This distribution is normalized. As at the end of section 4.10, let us define the (unnormalized) probability density in the limit of  $w \rightarrow 0$ ,

$$P^{\text{duration}}(T) := \lim_{w \rightarrow 0} \frac{P_w^{\text{duration}}(T)}{w} = \frac{1}{[2 \sinh(T/2)]^2}. \quad (546)$$

#### 4.14. Temporal shape of an avalanche

In order to obtain the temporal shape of an avalanche, we need to solve the instanton equation

$$-\partial_t \tilde{u}(t) + \tilde{u}(t) - \tilde{u}(t)^2 = \lambda \delta(t_f - t) + \eta \delta(t - t_m), \quad (547)$$

where  $t_f$  is the final time (where the avalanche stops) and  $t_m$  the time at which the velocity is measured. Since we only need its

first moment, we can construct  $\tilde{u}(t)$  perturbatively in  $\eta$ . To that purpose write

$$\begin{aligned} \tilde{u}(t) &= \tilde{u}_0(t) + \eta \tilde{u}_1(t) + \eta^2 \tilde{u}_2(t) + \mathcal{O}(\eta^3), \\ \tilde{u}_0(t) &= \frac{\Theta(t_f - t)}{1 - e^{t_f - t}}. \end{aligned} \quad (548)$$

The solution  $\tilde{u}_0(t)$  is the solution (540), translated to stop at  $t = t_f$ , in the limit of  $\lambda \rightarrow -\infty$ . Inserting equation (548) into equation (547) and collecting terms of order  $\eta$  yields

$$-\partial_t \tilde{u}_1(t) + \tilde{u}_1(t) - 2\tilde{u}_1(t)\tilde{u}_0(t) = \delta(t - t_m). \quad (549)$$

The solution is

$$\tilde{u}_1(t) = \frac{\sinh^2(\frac{t_f - t_m}{2})}{\sinh^2(\frac{t_f - t}{2})} \theta(t_m - t). \quad (550)$$

Performing a kick of size  $w$  at  $t = 0$ , and constraining the avalanche to stop at time  $t_f = T$ , the shape can be written as

$$\begin{aligned} \langle \dot{u}(t_m) \rangle &= \partial_\eta \Big|_{\eta=0} \ln \left( \partial_{t_f} e^{w\tilde{u}(t)} \right) \Big|_{T=t_f} \\ &= 4w \frac{\sinh^2(\frac{T-t_m}{2})}{\sinh^2(\frac{T}{2})} + 4 \frac{\sinh(\frac{T-t_m}{2}) \sinh(\frac{t_m}{2})}{\sinh(\frac{T}{2})}. \end{aligned} \quad (551)$$

Consider now the limit of  $w \rightarrow 0$ , for which the first term vanishes: for short durations  $T$ ,  $\langle \dot{u}(m) \rangle$  converges to a parabola,

$$\langle \dot{u}(t_m) \rangle = 2 \frac{t_m(T - t_m)}{T}. \quad (552)$$

For long durations, it settles on a plateau at  $\langle \dot{u}(t) \rangle = 2$ , see figure 49.

Pursuing to the next order, one finds for the connected average

$$\begin{aligned} \langle \dot{u}(t_m)^2 \rangle^c &= 4w \frac{\sinh^3(\frac{T-t_m}{2}) \sinh(\frac{t_m}{2})}{\sinh^3(\frac{T}{2})} \\ &+ 8 \frac{\sinh^2(\frac{T-t_m}{2}) \sinh^2(\frac{t_m}{2})}{\sinh^2(\frac{T}{2})}. \end{aligned} \quad (553)$$

At  $w = 0$ , quite remarkably the ratio

$$\frac{\langle \dot{u}(t_m)^2 \rangle}{\langle \dot{u}(t_m) \rangle^2} = \frac{3}{2} \quad (554)$$

is time independent.

Further observables, as well as loop corrections are obtained in [412, 457], and compared to experiments in [70].

#### 4.15. Local avalanche-size distribution

We now consider avalanches on a codimension-1 hyperplane, i.e. at a point for a line, or on a line for a 2D interface, a.s.o., by choosing

$$\lambda(x, \vec{x}_\perp) = \lambda \delta(x). \quad (555)$$

As a consequence,  $\vec{x}_\perp$  drops from the instanton equation. Setting again  $\sigma = m^2 = 1$ , one arrives at

$$\tilde{u}(x) - \tilde{u}''(x) - \tilde{u}(x)^2 = \lambda \delta(x). \quad (556)$$

The only solution which vanishes at infinity and satisfies the instanton equation at  $\lambda = 0$  is

$$\tilde{u}(x) = \frac{3}{1 + \cosh(x + x_0)}. \quad (557)$$

It can be promoted to a solution at  $\lambda \neq 0$  by setting  $\tilde{u}(-x) = \tilde{u}(x)$ . The parameter  $x_0 = x_0(\lambda)$  has to be chosen to satisfy the instanton equation at  $x = 0$ . Integrating equation (556) within a small domain around  $x = 0$  yields

$$\lambda = -2\tilde{u}'(0^+) = \frac{6 \sinh(x_0)}{[1 + \cosh(x_0)]^2}. \quad (558)$$

On the other hand, the generating function is

$$Z := \int_{-\infty}^{\infty} dx \tilde{u}(x) = \frac{12}{1 + e^{x_0}}. \quad (559)$$

Solving equation (559) for  $x_0$  and inserting into equation (558) yields

$$\lambda = \frac{Z(Z - 6)(Z - 12)}{72}. \quad (560)$$

The inverse Laplace transform is *a priori* difficult to perform, as  $Z(\lambda)$  is a complicated function of  $\lambda$ . The trick is to write

$$\begin{aligned} P_w(S_0) &:= \langle e^{\lambda S_0} \rangle = \int_{-i\infty}^{i\infty} \frac{d\lambda}{2\pi i} e^{-\lambda S_0} e^{wZ(\lambda)} \\ &= \int_{-i\infty}^{i\infty} \frac{dZ}{2\pi i} \frac{d\lambda(Z)}{dZ} e^{-\lambda(Z)S_0 + wZ} \\ &= -\frac{1}{S_0} \int_{-i\infty}^{i\infty} \frac{dZ}{2\pi i} e^{wZ} \frac{d}{dZ} e^{-\lambda(Z)S_0} \\ &= \frac{w}{S_0} \int_{-i\infty}^{i\infty} \frac{dZ}{2\pi i} e^{wZ} e^{-\lambda(Z)S_0} \\ &= \frac{6 e^{6w}}{\pi S_0} \int_0^{\infty} dx \cos(3x(S_0 x^2 + S_0 + 2w)) \\ &= \frac{2 e^{6w} w \sqrt{S_0 + 2w}}{\pi S_0^{3/2}} K_{\frac{1}{3}} \left( \frac{2(S_0 + 2w)^{3/2}}{\sqrt{3} S_0} \right). \end{aligned} \quad (561)$$

This can also be written in terms of the Airy function (formula (21) of [451]). In the limit of  $w \rightarrow 0$ , it reduces to

$$P(S_0) = \frac{2}{\pi S_0} K_{\frac{1}{3}} \left( \frac{2S_0}{\sqrt{3}} \right). \quad (562)$$

One can also give analytical expressions for the joint distribution of avalanche size  $S$  and local size  $S_0$ , as well as of size  $S$  and spatial extension  $\ell$ . The interested reader finds this in [451].

#### 4.16. Spatial shape of avalanches

We now turn to the spatial shape of avalanches [322]. We remind that avalanches have a well-defined extension  $\ell$ , beyond which there is no movement. For a given avalanche, denote its advance by  $S(x)$ , and its size by  $S = \int_x S(x)$ . We call

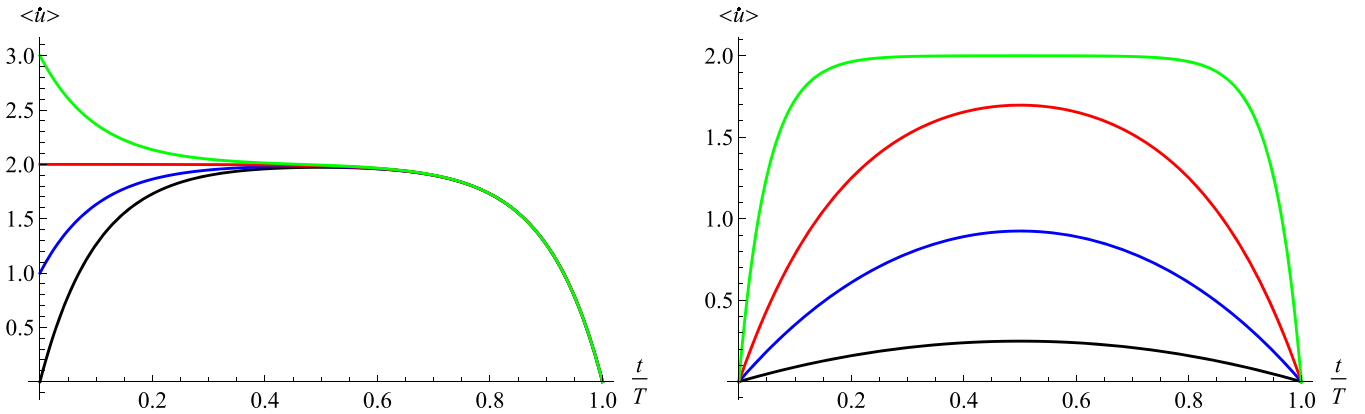


**Figure 49.** Expectation  $\langle \dot{u}(t) \rangle$ . (Left)  $T = 10$ , and from bottom to top  $w = 0, 1, 2$ , and  $3$ . (Right)  $w = 0$  (infinitesimal kick), and from bottom to top  $T = \frac{1}{2}, 2, 5$ , and  $20$ . Reprinted figure with permission from [321], Copyright (2013) by the American Physical Society.

avalanche extension  $\ell$  the size of the smallest ball into which we can fit the avalanche. As long as  $\ell \ll m^{-1}$ ,

$$\langle S(x) \rangle_\ell = \ell^\zeta g(x/\ell), \quad (563)$$

where  $g(x)$  is non-vanishing in the unit ball. Integrating over space yields  $S \sim \ell^{d+\zeta}$ , the canonical scaling relation between size and extension of avalanches, confirming the ansatz (563).

We now want to deduce how  $g(x)$  behaves close to the boundary. For simplicity of notations, we write our argument for the left boundary in  $d = 1$ , which we place at  $x = -\ell/2$ . Imagine the avalanche dynamics for a discretized system. The avalanche starts at some point, which in turn may trigger an advance of its neighbors, a.s.o. This leads to a shock front propagating outwards from the seed to the left and to the right. As long as the elasticity is local, the dynamics of these two shock fronts is local: if one conditions on the position of the  $i$ th point away from the front, with  $i$  being much smaller than the total extension  $\ell$  of the avalanche (in fact, we only need that the avalanche started right of this point), then we expect that the joint probability distribution for the advance of points  $1$  to  $i - 1$  depends on  $i$ , but is independent of the size  $\ell$ . Thus we expect that in this discretized model the shape  $\langle S(x - r_1) \rangle$  close to the left boundary  $r_1$  is independent of  $\ell$ . Let us now turn to avalanches of large size  $\ell$ , so that we are in the continuum limit studied in the field theory. Our argument then implies that the shape  $\langle S(x - r_1) \rangle$  measured from the left boundary  $r_1 = -\ell/2$ , is independent of  $\ell$ . In order to cancel the  $\ell$ -dependence in equation (563) this in turn implies that [322]

$$g(x) = \mathcal{B} \times (x - 1/2)^\zeta, \quad (564)$$

with some amplitude  $\mathcal{B}$ . For the BFM in  $d = 1$ , the roughness exponent is  $\zeta_{\text{BFM}} = 4 - d = 3$ , and one can further show that  $\mathcal{B} = \sigma/21$  [322].

On the left of figure 50, we show twenty realizations of avalanches, with mean given by the thick black line. On the right we compare numerical averages with the theory sketched below. Note that the latter indeed has a cubic behavior close to the boundary, as predicted by equation (564).

We now turn to the theory: in order to get the spatial avalanche shape, one needs to construct a solution of the instanton equation (521), with a source

$$\lambda(x) = -\lambda_1 \delta(x - r_1) - \lambda_2 \delta(x - r_2) + \eta \delta(x - x_c), \quad (565)$$

$$\lambda_1, \lambda_2 \rightarrow \infty.$$

Looking at our central result (522), this choice implies that the avalanche kicked at  $x = x_0$  does not extend to  $x = r_{1,2}$ . To simplify matters further, one replaces  $m^2 w(x) \rightarrow f(x)$ , and considers the response to a kick in the force. This allows us to take the limit of  $m \rightarrow 0$ . Setting further  $\sigma = 1$ , the instanton equation to be solved is

$$\tilde{u}''(x) + \tilde{u}(x)^2 = -\lambda(x). \quad (566)$$

The source  $\eta$  generates moments of the avalanche size at  $x_c$ . While unsolvable for arbitrary  $\eta$ , equation (566) can be solved perturbatively in  $\eta$ , allowing us to construct moments of the spatial avalanche shape. This solution has the form

$$\tilde{u}(x) = \tilde{u}_0(x) + \eta \tilde{u}_1(x) + \eta^2 \tilde{u}_2(x) + \dots, \quad (567)$$

$$\tilde{u}_0(x) = \frac{1}{(r_2 - r_1)^2} f\left(\frac{2x - r_1 - r_2}{2(r_2 - r_1)}\right), \quad (568)$$

$$f(x) = -6\mathcal{P}\left(x + 1/2; g_2 = 0, g_3 = \frac{\Gamma(\frac{1}{3})^{18}}{(2\pi)^6}\right). \quad (569)$$

Here  $\mathcal{P}$  is the Weierstrass-P function, diverging at  $x = 0$  and  $x = 1$ . The subdominant terms in  $\eta$  are obtained by realizing that if  $f(x)$  is solution of the instanton equation (566), so is  $\kappa^2 f(\kappa x + c)$ . The details of this calculation are cumbersome, and can be found in [322]. On the right of figure 50 we show  $\langle S(X) \rangle$  predicted by the theory, and its numerical test.

Note that the shape of very large avalanches does not scale as  $\ell^3$  but  $\ell^4$ ; it also has a different shape [458].

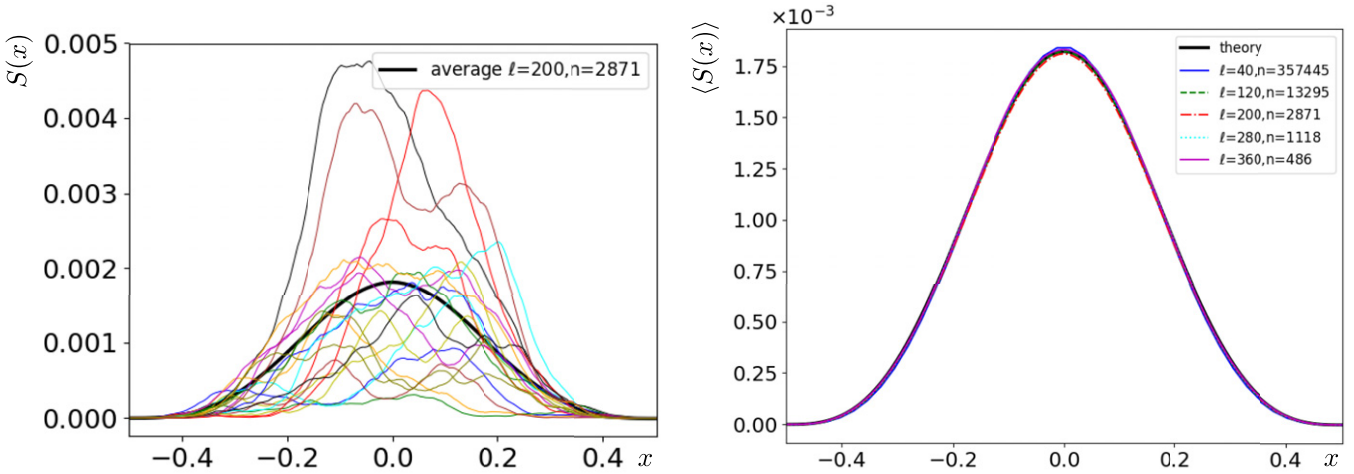


**Figure 50.** (Left) 20 avalanches with extension  $\ell = 200$ , rescaled to  $\ell = 1$ .  $n = 2871$  is the number of samples used for the average. (Right) The shape  $\langle S(x) \rangle \equiv \langle S(x/\ell) \rangle_\ell / \ell^3$  averaged for all avalanches with a given  $\ell$  between 40 and 360. To reduce statistical errors, we have symmetrized this function. Reprinted figure with permission from [322], Copyright (2017) by the American Physical Society.

#### 4.17. Some theorems

Inspired by the calculations done so far, one can show the following theorems [321]:

**Theorem 1.** *The zero-mode  $\dot{u}(t) := \frac{1}{L^d} \int_x \dot{u}(x, t)$  of the BFM field theory (514) is the same random process as in the ABBM model, equation (489).*

**Theorem 2.** *The field theory of this process is the sum of all tree diagrams, involving  $\Delta'(0^+)$  as a vertex.*

**Theorem 3.** *Tree diagrams are relevant at the upper critical dimension  $d_c$ . Corrections involve loops and can be constructed in a controlled  $\epsilon$ , i.e. loop, expansion around the upper critical dimension  $d_c$ .*

*Sketch of proof.* One first constructs the generating function for a spatially constant observable, as the velocity or the size in the BFM model. As we saw, these generating functions involve instanton solutions constant in space, thus independent of the dimension. Graphically this can be understood by constructing  $\tilde{u}$  perturbatively, with vertices proportional to  $\sigma = -\Delta'(0^+)$ , and lines which are response functions, possibly integrated over time. Since by assumption external observable vertices are at zero momentum, all response functions are at zero momentum. This proves theorems 1 and 2.

We now consider models with one of the fixed points studied above, be it RB, RF or periodic disorder, at equilibrium or at depinning. Since each vertex is proportional to  $\epsilon$ , the leading order is again given by trees constructed from  $\Delta'(0^+)$ . The only thing which can be added are loops. Each loop comes with an additional factor of  $\epsilon$  from the additional vertex, of which the leading one is given in equation (515). As long as the ensuing momentum integrals are finite, thus do not yield a factor of  $1/\epsilon$ , these additional contributions are of order  $\epsilon^n$ , where  $n$  is the number of loops. That the momentum integrals are finite can be checked; it reflects the fact that the theory is renormalizable, i.e. that all divergences which can possibly

appear have already been taken care of by the counter terms introduced earlier, see section 3.4 for depinning.

#### 4.18. Loop corrections

Loop corrections are cumbersome to obtain, and prone to errors. To avoid the latter, one should check the obtained results by explicitly constructing them perturbatively in  $\Delta(u)$ , and  $\lambda$ . This is done in the relevant research literature [321, 412, 459, 460]. Here we sketch the generally applicable method of [321], to which we refer for details.

*Simplified model.* Consider the action (515). To leading order, we can decouple the term in addition to the BFM via

$$e^{-S[\tilde{u}, \tilde{u}]} = \langle e^{-S_\eta[\tilde{u}, \tilde{u}]} \rangle_\eta \tag{570}$$

$$S_\eta[\tilde{u}, \tilde{u}] = S_{\text{BFM}}[\tilde{u}, \tilde{u}] + \int_{x,t} \eta(x) \tilde{u}(x, t) \dot{u}(x, t). \tag{571}$$

$\eta(x)$  is an (imaginary) Gaussian disorder to be averaged over, with correlations

$$\langle \eta(x) \eta(x') \rangle_\eta = -\Delta''(0) \delta^d(x - x'). \tag{572}$$

For each realization  $\eta(x)$ , the theory has the same form as in the preceding sections. In particular, the total action (including the sources) is linear in the velocity field, and the only change is an additional term in the instanton equation (521),

$$\begin{aligned} (-\partial_t - \nabla^2 + m^2) \tilde{u}(x, t) - \sigma \tilde{u}(x, t)^2 \\ = \lambda(x, t) + \eta(x) \tilde{u}(x, t). \end{aligned} \tag{573}$$

Our central result (522) remains unchanged.

*Perturbative solution.* To simplify notations, we set  $m = \sigma = 1$ . We expand the solution of equation (573) in powers of  $\eta(x)$ , denoting by  $\tilde{u}^{(n)}(x, t)$  the term of order  $\eta^n$ ,

$$\tilde{u}(x, t) = \tilde{u}^{(0)}(x, t) + \tilde{u}^{(1)}(x, t) + \tilde{u}^{(2)}(x, t) + \dots \tag{574}$$

The hierarchy of equations to be solved is

$$[-\partial_t - \nabla_x^2 + 1] \tilde{u}^{(0)}(x, t) = \lambda(x, t) + \tilde{u}^{(0)}(x, t)^2, \tag{575}$$

$$[-\partial_t - \nabla_x^2 + 1 - 2\tilde{u}^{(0)}(x, t)] \tilde{u}^{(1)}(x, t) = \eta_x \tilde{u}^{(0)}(x, t), \tag{576}$$

$$[-\partial_t - \nabla_x^2 + 1 - 2\tilde{u}^{(0)}(x, t)] \tilde{u}^{(2)}(x, t) = \tilde{u}^{(1)}(x, t)^2 + \eta(x) \tilde{u}^{(1)}(x, t). \tag{577}$$

The first line is the usual instanton equation (521). Let us introduce the dressed response kernel

$$[-\partial_t - \nabla_x^2 + 1 - 2\tilde{u}^{(0)}(x, t)] \mathbb{R}_{x't',xt} = \delta^d(x - x') \delta(t - t'). \tag{578}$$

It has the usual causal structure of a response function, and obeys a backward evolution equation. It allows us to rewrite the solution of the system of equations (575) to (577) as

$$\tilde{u}^{(1)}(x, t) = \int_{x'} \int_{t' > t} \eta(x') \tilde{u}^{(0)}(x', t') \mathbb{R}_{x't',xt}, \tag{579}$$

$$\tilde{u}^{(2)}(x, t) = \int_{x'} \int_{t' > t} [\tilde{u}^{(1)}(x', t')^2 + \eta(x') \tilde{u}^{(1)}(x', t')] \times \mathbb{R}_{x't',xt}. \tag{580}$$

Consider now the average (572) over  $\eta(x)$ . Since  $\langle \tilde{u}^{(1)}(x, t) \rangle_\eta = 0$ , the lowest-order correction is given by the average of  $\tilde{u}^{(2)}(x, t)$ ,

$$Z[\lambda] = Z_{\text{tree}}[\lambda] + \int_{xt} \langle \tilde{u}^{(2)}(x, t) \rangle_\eta + \dots \tag{581}$$

Inserting equation (579) into equation (580), and performing the average over  $\eta$ , one finds

$$\begin{aligned} \langle \tilde{u}^{(2)}(x, t) \rangle_\eta &= -\Delta''(0) \int_{t < t_1 < t_2, t_3} \int_{x_1, x'} \tilde{u}^{(0)}(x', t_2) \tilde{u}^{(0)}(x', t_3) \\ &\quad \times \mathbb{R}_{x't_2, x_1 t_1} \mathbb{R}_{x't_3, x_1 t_1} \mathbb{R}_{x_1 t_1, xt} \\ &- \Delta''(0) \int_{t < t_1 < t_2} \int_{x'} \tilde{u}^{(0)}(x', t_2) \mathbb{R}_{x't_2, x' t_1} \mathbb{R}_{x' t_1, xt}. \end{aligned} \tag{582}$$

It admits the following graphical representation

$$\langle \tilde{u}^{(2)}(x, t) \rangle_\eta = \text{[Tree Diagram]} + \text{[Loop Diagram]}. \tag{583}$$

The symbols are as follows: (i) a wiggly line represents  $\tilde{u}^{(0)}(x, t)$ , the MF solution; (ii) a double solid line is a dressed response function  $\mathbb{R}$ , advancing in time following the arrow

(upwards), thus times are ordered from bottom to top. We now define the combination

$$\Phi(x', x, t) := \int_{t' > t} \tilde{u}^{(0)}(x', t') \mathbb{R}_{x't',xt}, \tag{584}$$

in terms of which

$$\begin{aligned} \langle \tilde{u}^{(2)}(x, t) \rangle_\eta &= \int_{t', x'} \left[ \int_y \Phi(y, x', t')^2 + \Phi(x', x', t') \right] \mathbb{R}_{x't',xt}. \end{aligned} \tag{585}$$

There are several additional terms: (i) a counter-term for the disorder, showing up in a change of  $\Delta'(0^+)$  to its renormalized value. (ii) A counter-term to friction. (iii) A missed boundary term, due to the replacement of  $\Delta''(u_t - u_{t'})$  which decays to zero for large times by  $\Delta''(0)$ , which does not.

*One-loop corrections to the avalanche-size distribution.*

Let us construct the one-loop corrections to the avalanche-size distribution, following the formalism developed above. For  $\lambda(x, t) = \lambda$ , the solution of the unperturbed instanton equation was given in equation (524). For  $m = \sigma = 1$ , it reads

$$Z_{\text{MF}}(\lambda) \equiv \tilde{u}^{(0)} = \frac{1}{2} \left( 1 - \sqrt{1 - 4\lambda} \right). \tag{586}$$

The dressed response kernel in Fourier representation becomes

$$\mathbb{R}_{k, t_2, t_1} = e^{-(k^2 + 1 - 2\tilde{u}^{(0)})(t_2 - t_1)} \theta(t_2 - t_1). \tag{587}$$

It is the bare response function up to the replacement  $m^2 \rightarrow m^2 - 2\tilde{u}^{(0)}(\lambda)$ . The combination in the exponential simplifies,

$$k^2 + 1 - 2\tilde{u}^{(0)} = k^2 + \sqrt{1 - 4\lambda}. \tag{588}$$

Formula (584) then gives

$$\Phi(k, t_1) = \tilde{u}^{(0)} \int_{t_1 < t_2} \mathbb{R}_{k, t_2, t_1} = \frac{\tilde{u}^{(0)}}{k^2 + 1 - 2\tilde{u}^{(0)}}. \tag{589}$$

With the additional integral over  $\mathbb{R}$  in equation (585), the latter becomes

$$\begin{aligned} \langle \tilde{u}^{(2)} \rangle_\eta &= -\frac{\Delta''(0^+)}{1 - 2\tilde{u}^{(0)}} \\ &\times \int_k \left( \frac{\tilde{u}^{(0)}}{k^2 + 1 - 2\tilde{u}^{(0)}} \right)^2 + \frac{\tilde{u}^{(0)}}{k^2 + 1 - 2\tilde{u}^{(0)}}. \end{aligned} \tag{590}$$

Adding the proper counter-terms, and replacing the bare disorder by the renormalized one [321], the full generating function is

$$\begin{aligned} Z(\lambda) \equiv \tilde{u} &= \tilde{u}^{(0)} - \frac{\tilde{\Delta}''(0^+)}{1 - 2\tilde{u}^{(0)}} \frac{1}{\epsilon I_1} \\ &\int k \left[ \left( \frac{\tilde{u}^{(0)}}{k^2 + 1 - 2\tilde{u}^{(0)}} \right)^2 + \frac{\tilde{u}^{(0)}}{k^2 + 1 - 2\tilde{u}^{(0)}} - \frac{\tilde{u}^{(0)}}{k^2 + 1} - \frac{3(\tilde{u}^{(0)})^2}{(k^2 + 1)^2} \right]. \end{aligned} \tag{591}$$

*Avalanche-size distribution at one-loop order.* The generating function (591) can be inverted analytically [459]. The

result for avalanches larger than a microscopic cutoff  $S_0$  is to  $\mathcal{O}(\epsilon)$

$$P(S) = \frac{\langle S \rangle}{2\sqrt{\pi}} S_m^{\tau-2} A S^{-\tau} \exp\left(C\sqrt{\frac{S}{S_m}} - \frac{B}{4}\left[\frac{S}{S_m}\right]^\delta\right). \quad (592)$$

The coefficients are to  $\mathcal{O}(\epsilon)$

$$\begin{aligned} A &= 1 + \frac{1}{8}(2 - 3\gamma_E)\alpha, & B &= 1 - \alpha\left(1 + \frac{\gamma_E}{4}\right), \\ C &= -\frac{\sqrt{\pi}}{2}\alpha, & \alpha &= \frac{\zeta - \epsilon}{3}, \end{aligned} \quad (593)$$

and  $\gamma_E = 0.577216$  is Euler's number. The exponent  $\tau$  is consistent with the scaling relation (475), while the new exponent  $\delta$  reads

$$\delta = 1 + \frac{\epsilon - \zeta}{12}. \quad (594)$$

#### 4.19. Simulation results and experiments

*Avalanche-size distribution.* The result for the avalanche-size distribution has been verified numerically, both for the statics [288] as for depinning [461].

For the statics (equilibrium) [288], we show plots on figure 51. The simulations are for a three-dimensional RF magnet, with weak disorder s.t. only a single domain wall appears, yielding  $d = 2$ ,  $\epsilon = 2$ , and  $\zeta = \zeta_{\text{RF}} = 2/3$ . The generating function  $Z(\lambda)$  is verified with high precision. For the avalanche-size distribution, the agreement is good, even though there is appreciable noise due to binning, which is absent from the generating function  $Z(\lambda)$ .

At depinning, avalanches are simulated for an elastic string in  $d = 1$  [461]. The results for system sizes up to  $L = 4000$  are shown on figure 52. The statistics is good, allowing to verify equation (592) in the tail region, with  $\delta = 7/6$ .

*The temporal avalanche shape at fixed duration  $T$ .* The temporal shape at fixed duration  $T$  is predicted by the theory [412, 457] as

$$\begin{aligned} \langle \dot{u}(t = \vartheta T) \rangle_T &= 2\mathcal{N}[T\vartheta(1 - \vartheta)]^{\gamma-1} \\ &\times \exp\left(-\frac{16\epsilon}{9d_c}\left[\text{Li}_2(1 - \vartheta) - \text{Li}_2\left(\frac{1 - \vartheta}{2}\right) + \frac{\vartheta \ln(2\vartheta)}{\vartheta - 1}\right.\right. \\ &\quad \left.\left.+ \frac{(\vartheta + 1)\ln(\vartheta + 1)}{2(1 - \vartheta)}\right]\right). \end{aligned} \quad (595)$$

The exponent  $\gamma$  is given in equation (481). The temporal shape is well approximated by

$$\langle \dot{u}(t = \vartheta T) \rangle_T \simeq [T\vartheta(1 - \vartheta)]^{\gamma-1} \exp\left(\mathcal{A}\left[\frac{1}{2} - \vartheta\right]\right). \quad (596)$$

The asymmetry  $\mathcal{A} \approx -0.336(1 - d/d_c)$  is negative for  $d$  close to  $d_c$ , skewing the avalanche toward its end, as observed in numerical simulations in  $d = 2$  and 3 [462]. For  $d = 1$  the asymmetry is positive in numerical simulations [463]. In experiments on magnetic avalanches (Barkhausen noise), and in fracture experiments, the asymmetry is difficult to see [463].

*The temporal avalanche shape at fixed size  $S$ .* The temporal shape can also be calculated at fixed size  $S$ . Scaling suggests that

$$\langle \dot{u}(t) \rangle_S = \frac{S}{\tau_m} \left(\frac{S}{S_m}\right)^{-\frac{1}{\gamma}} f\left(\frac{t}{\tau_m} \left(\frac{S_m}{S}\right)^{\frac{1}{\gamma}}\right), \quad (597)$$

with  $\int_0^\infty dt f(t) = 1$ , where  $f(t)$  may depend on  $S/S_m$ . In MF, the scaling function  $f(t)$  is independent of  $S/S_m$  [464], and reads

$$f_0(t) = 2t e^{-t^2}, \quad \gamma = 2. \quad (598)$$

To one loop one obtains  $f(t) = f_0(t) - \frac{\epsilon}{9}\delta f(t)$ . Expressions for arbitrary  $S/S_m$  are lengthy. The universal small- $S$  limit reads

$$\begin{aligned} \delta f(t) &\simeq \frac{f_0(t)}{4} \left[ \pi(2t^2 + 1) \text{erfi}(t) + 2\gamma_E(1 - t^2) - 4 \right. \\ &\quad \left. - 2t^2(2t^2 + 1) {}_2F_2\left(1, 1; \frac{3}{2}, 2; t^2\right) \right. \\ &\quad \left. - 2e^{t^2} \left(\sqrt{\pi}t \text{erfc}(t) - \text{Ei}(-t^2)\right) \right]. \end{aligned} \quad (599)$$

It satisfies  $\int_0^\infty dt \delta f(t) = 0$ . The asymptotic behaviors are

$$f(t) \simeq_{t \rightarrow 0} 2At^{\gamma-1}, \quad A = 1 + \frac{\epsilon}{9}(1 - \gamma_E), \quad (600)$$

$$f(t) \simeq_{t \rightarrow \infty} 2A't^\beta e^{-Ct^\delta}, \quad \delta = 2 + \frac{\epsilon}{9}, \quad \beta = 1 - \frac{\epsilon}{18},$$

$$A' = 1 + \frac{\epsilon}{36}(5 - 3\gamma_E - \ln 4), \quad C = 1 + \frac{\epsilon}{9} \ln 2. \quad (601)$$

The amplitude  $A$  leads to the same universal short-time behavior as in equation (595). To properly extrapolate to larger values of  $\epsilon$ , we use

$$f(t) \approx 2t e^{-Ct^\delta} \mathcal{N} \exp\left(-\frac{\epsilon}{9}\left[\frac{\delta f(t)}{f_0(t)} - t^2 \ln(2t)\right]\right), \quad (602)$$

with the normalization  $\mathcal{N}$  chosen s.t.  $\int_0^\infty dt f(t) = 1$ . Equation (602) is exact to  $\mathcal{O}(\epsilon)$  and satisfies the asymptotic expansions (600) and (601).

This result has beautifully been measured in the Barkhausen noise experiment of [70], see figure 53.

*The spatial avalanche shape (in  $d = 1$ ).* The spatial avalanche shape for the BFM was shown on figure 50. For systems with SR-correlated disorder, it was measured for two different driving protocols: tip driven (driving at a single point), and spatially homogeneous driving by the parabola, the protocol used above. For tip-driven avalanches at the non-driven end, as well as for homogeneously driven avalanches, equation (564) predicts that the avalanche shape at fixed extension  $\ell$  grows close to the boundary point  $b$  as

$$\langle S(x) \rangle_\ell \sim |x - b|^\zeta. \quad (603)$$

For  $\zeta = 1.25$  one thus expects this curve to have a slightly positive curvature at these points, consistent with plots 3 and 5 of [448].

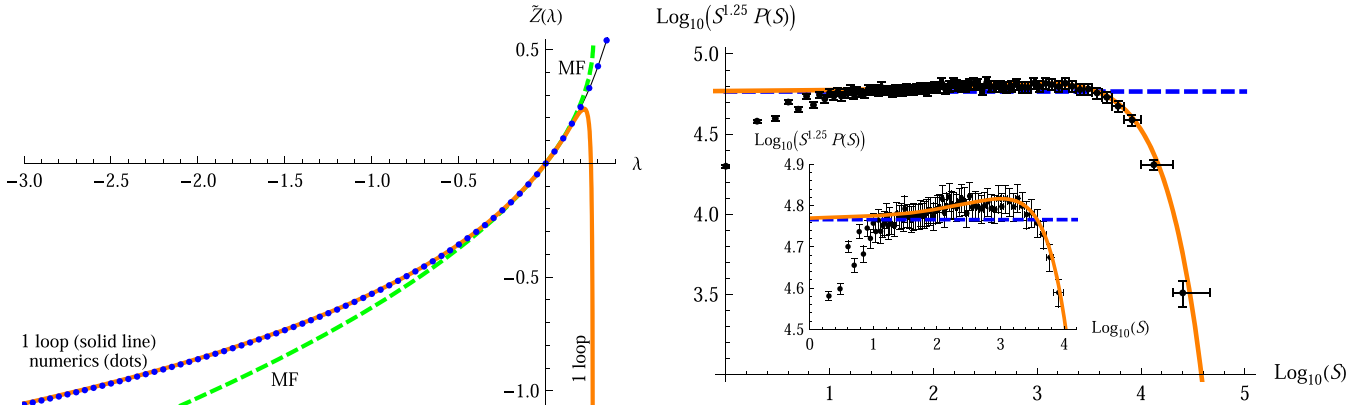


**Figure 51.** Results of [288] for RF disorder,  $d = 2$ . (Left) Numerically measured  $\tilde{Z}(\lambda)$  (blue dots). MF result (586) (green dashed), one-loop result (591) (orange solid). The latter is rather precise, almost up to the singularity at  $\lambda = 1/4$ . (Right) Avalanche-size distribution  $P(S)$ , multiplied by  $S^\tau$  with  $\tau = 1.25$  from equation (475) (dots). The orange solid curve is the prediction from equation (592). The dashed line is a constant (guide to the eye). (Inset) Blow-up of main plot.

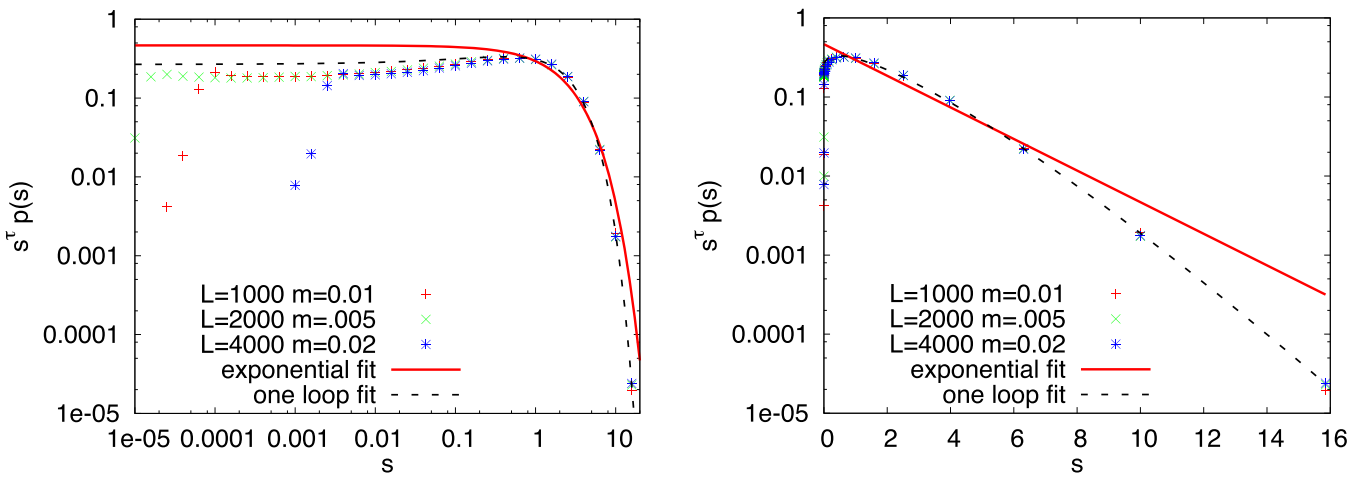


**Figure 52.** (Left) Avalanche-size distribution for RF in  $d = 1$  at depinning. The variable  $s = S/S_m$ . Blow up of the power-law region. The red solid curve is given by the MF result equation (528), the black dashed line by equation (592), with  $A = 0.947$ ,  $B = 1.871$  and  $C = 0.606$ . (Right) The same for the tail. Reprinted figure with permission from [461], Copyright (2009) by the American Physical Society.

Let us also mention the studies of [458] for avalanches with a large aspect ratio in the BFM which are rare, and with fixed seed position [465] which are difficult to realize in an experiment.

*The velocity distribution.* The velocity distribution was analytically obtained in [321, 467], and numerically checked in [466]. The scaling relation of equation (485) actually predicts a negative exponent  $a = -10/23$ , implying  $P(\dot{u}) \sim \dot{u}^{10/23}$ . Despite the change in sign, this is beautifully verified in figure 54.

#### 4.20. Correlations between avalanches

In section 2.10, we had asked how avalanche moments are encoded in  $\Delta(w)$ , and found the key relation (104). We can further ask how avalanches at  $w_1$  and  $w_2$  are correlated. This can be evaluated along the same lines [468]: on one hand,

$$\overline{[u_{w_1+\delta w_1} - u_{w_1}][u_{w_2+\delta w_2} - u_{w_2}]} = \langle S_{w_1} S_{w_2} \rangle \delta w_1 \delta w_2 \rho_2(w_1 - w_2) + \mathcal{O}(\delta w^3), \quad (604)$$

where  $\rho_2(w)$  is the probability density to have two shocks a distance  $w$  apart. On the other hand,

$$\begin{aligned} & \overline{[u_{w_1+\delta w_1} - u_{w_1}][u_{w_2+\delta w_2} - u_{w_2}]} - \delta w_1 \delta w_2 \\ &= \frac{1}{m^4 L^d} [\Delta(w_1 + \delta w_1 - w_2 - \delta w_2) - \Delta(w_1 - w_2 - \delta w_2) \\ & \quad - \Delta(w_1 + \delta w_1 - w_2) + \Delta(w_1 - w_2)] \\ &= -\delta w_1 \delta w_2 \frac{\Delta''(w_1 - w_2)}{m^4 L^d} + \mathcal{O}(\delta w^3). \end{aligned} \quad (605)$$

Using equation (99) in equation (604), and comparing to equation (605) for small  $\delta w$  implies

$$\frac{\langle S_{w_1} S_{w_2} \rangle^c}{\langle S \rangle^2} \equiv \frac{\langle S_{w_1} S_{w_2} \rangle}{\langle S \rangle^2} - 1 = -\frac{\Delta''(w_1 - w_2)}{m^4 L^d}. \quad (606)$$

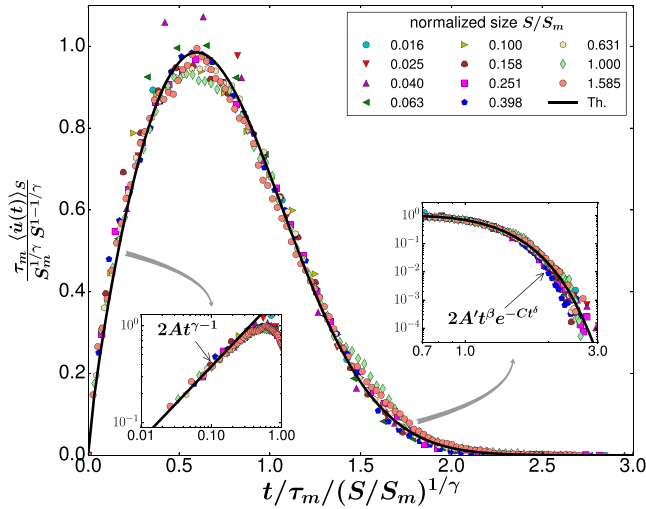


**Figure 53.** Scaling collapse of the average shape at fixed avalanche sizes  $\langle \dot{u}(t) \rangle_S$ , according to equation (597), in the FeSiB thin film. The continuous line is the prediction for the universal SR scaling function of equation (602). The insets show comparisons of the tails of the data with the predicted asymptotic behaviors of equations (600) and (601), setting  $\epsilon = 2$ , with  $A = 1.094$ ,  $A' = 1.1$ ,  $\beta = 0.89$ ,  $C = 1.15$ , and  $\delta = 2.22$ . Consistent with scaling relations, the measured  $\gamma = 1.76$ . Reprinted figure with permission from [70], Copyright (2016) by the American Physical Society.

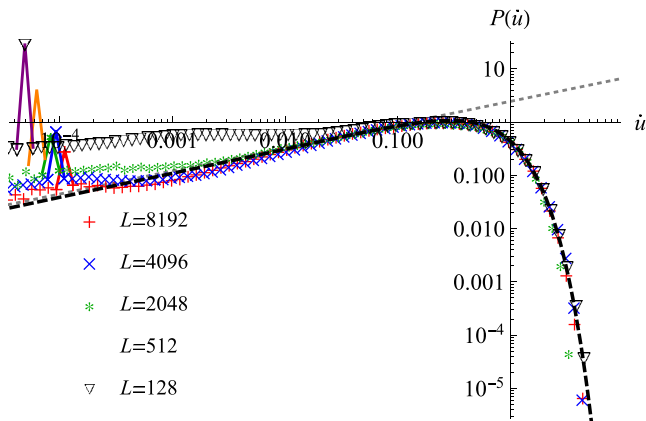


**Figure 54.** The center-of-mass velocity distribution  $P(\dot{u})$ . The weight of the peak at  $\dot{u} = v_{\text{kick}}$  is  $\frac{\delta t}{T} \sim L^{-z} \sim m^z$ , where  $T$  is the duration of an avalanche and  $\delta t$  the time discretization step. The analytic result (black dashed line) is from equation (385) of [321], the dotted gray line the pure power law  $P(\dot{u}) \sim \dot{u}^{-a}$ , with  $a = -\frac{10}{23} = -0.435$  as given in equation (485). There is no adjustable (fitting) parameter, thus convergence to the theory including all scales is read off from the plot. Plot from [466].

Since  $\langle S_{w_1} S_{w_2} \rangle \geq 0$ , the rhs is bounded from below by  $-1$ , or

$$\frac{\Delta''(w)}{m^4 L^d} \leq \frac{\Delta''(0^+)}{m^4 L^d} \leq 1. \quad (607)$$

For the Kida and Sinai models, this yields the bounds  $\tilde{\Delta}''(0^+) \leq 1$ , which are indeed satisfied by equations (191)

and (203). At depinning, the DPM has  $\tilde{\Delta}''(0^+) = 0.5$ , see equation (367). In the perturbative FRG, equations (63) and (341), extended by the two-loop results of [124], imply

$$\frac{\Delta''(0^+)}{m^4 L^d} \simeq \left( \frac{2}{9} + 0.107533\epsilon + \mathcal{O}(\epsilon^2) \right) \frac{1}{m^4 L^d I_1}. \quad (608)$$

The diagram  $I_1$  defined in equation (58) as an integral, here depends both on  $m$  and  $L$ , and is evaluated as a discrete sum over momenta  $k_i = n_i 2\pi/L$ ,  $n_i \in \mathbb{Z}$ . One shows that  $m^4 L^d I_1 \geq 1$ , the bound is saturated for  $mL \rightarrow 0$ , and deviations from the bound remain smaller than 10% for  $mL \leq 3.2$  in  $d = 1$ ,  $mL \leq 2.4$  in  $d = 2$ ,  $mL \leq 1.8$  in  $d = 3$ , and  $mL \leq 0.6$  in  $d = 4$ , indicating optimal choices for the sample size. The experiments [323] shown on figure 55 satisfy (606), and almost saturate the bound (608). Further relations are studied in [468, 469].

#### 4.21. Avalanches with retardation

In magnetic systems, a change in the magnetization induces an *eddy current*, which in turn can reignite an avalanche which had already stopped [470]. The simplest model exhibiting this phenomenon, and which remains analytically solvable [464] reads

$$\partial_t u(t) = F(u(t)) + m^2 [w(t) - u(t)] - ah(t), \quad (609)$$

$$\tau \partial_t h(t) = \partial_t u(t) - h(t). \quad (610)$$

While many observables can be obtained analytically [464] and measured, e.g. the temporal shape given  $S$ , other ones are not well-defined, as the duration of an avalanche. As due to the eddy current  $h(t)$ , an avalanche can restart, this complicates the data-analysis in real magnets [319].

#### 4.22. Power-law correlated random forces, relation to fractional Brownian motion

Fractional Brownian motion (fBm) is the unique Gaussian process  $X_t$  which is scale and translationally invariant, see e.g. [471–474]. It is uniquely characterized by its two-point function

$$\langle X_t X_s \rangle = \sigma (t^{2H} + s^{2H} - |s - t|^{2H}). \quad (611)$$

The Hurst exponent  $H$  may take values between 0 and 1,

$$0 < H \leq 1. \quad (612)$$

Note that  $X_t$  is non-Markovian, since the two-time correlations of increments at times  $t \neq s$

$$\langle \partial_t X_t \partial_s X_s \rangle = 2H(2H - 1)\sigma |s - t|^{2H-2} \quad (613)$$

do not vanish, except for  $H = 1/2$ , for which the fBm reduces to standard Brownian motion.

Since  $X_t$  is a Gaussian process, many observables can be calculated analytically. This is interesting, since one can access

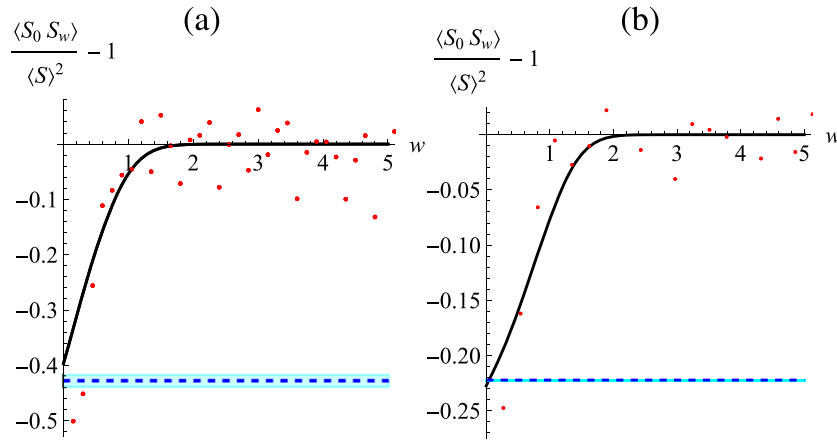


**Figure 55.** Anticorrelation of avalanches as a function of  $w$ , for two samples with eddy currents, SR (a), and LR (b). The solid line is the prediction for  $-\Delta''(w)/(m^4 L^d)$  from equation (606), as obtained from the experiment. The dashed lines are bounds on the maximally achievable reduction from the  $\epsilon$ -expansion (608), with error bars in cyan for SR. There are no fitting parameters.

analytically, in an expansion in  $H - 1/2$ , most variables of interest for extremal statistics [474–484]. An example of such an observable is the maximum relative height of elastic interfaces in a random medium [485]. fBm is also the simplest choice if one only knows the scaling dimension  $H$  of a process, without further insight into higher correlation functions.

Returning to depinning, suppose that random forces are Gaussian and correlated as a fBm

$$\Delta(0) - \Delta(u) = \sigma |u|^{2H}. \quad (614)$$

Solving equation (343), and realizing that loop corrections are subdominant<sup>36</sup> in the tail for  $H < 1$ , we obtain similar to the derivation of equation (517)

$$\zeta = \frac{\epsilon}{2(1-H)}. \quad (615)$$

As a consequence of equation (475), the avalanche-size exponent is

$$\tau = 2 - \frac{2}{d + \zeta} = 2 - \frac{4(1-H)}{4 + d(1-2H)}. \quad (616)$$

Interestingly, in  $d = 0$ , i.e. for a particle, this reduces to

$$\tau|_{d=0} = 1 + H. \quad (617)$$

This is consistent with the first-return probability derived in [474, 476]. Indeed, the probability to return to the origin of a fBm  $X_t$  with Hurst exponent  $H$  is  $P(t) = \langle \delta(X_t) \rangle \sim t^{-H}$ , equivalent to equation (40) of [476]. The probability to return for the first time is  $\partial_t P(t) \sim t^{-(1+H)}$ , equivalent to Equation (617). These considerations generalize those leading to equations (536) and (537), and in  $d = 0$  confirm equations (615) and (616).

<sup>36</sup> Corrections in the FRG equation (69) are  $\delta[\Delta(0) - \Delta(u)] \sim u^{4H-2} \ll u^{2H}$  for  $u \rightarrow \infty$ .

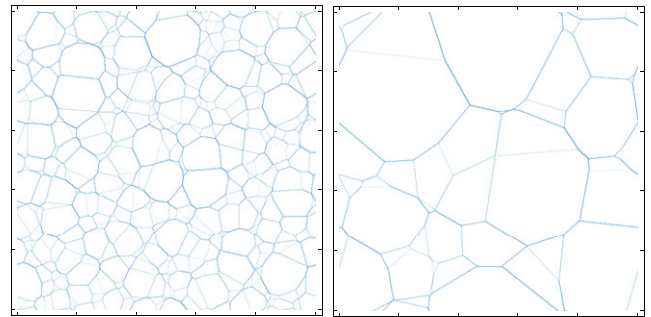


**Figure 56.** Shocks in a two-dimensional system with short-ranged correlated disorder, size  $L = 500$ , and periodic boundary conditions, for two different masses  $m^2 = 10^{-3}$  (left) and  $m^2 = 10^{-4}$  (right). Decreasing  $m^2$ , shocks merge. Shock fronts are almost straight.

#### 4.23. Higher-dimensional shocks

Little is known about higher-dimensional shocks or avalanches. As in our understanding of the cusp, the two-dimensional toy model (96) is helpful here, with  $V(u)$  drawn as uncorrelated Gaussian random variables with variance 1 on a unit grid. On figure 56 we show the shocks, i.e. the locations where the minimizer  $u$  in equation (96) changes discontinuously. Principle properties are

- (a)  $\hat{V}(u)$  can be interpreted as a decaying KPZ height field, and  $\hat{F}(u) := -\nabla \hat{V}(u)$  as a decaying Burgers velocity, see section 7.7.
- (b) Decreasing  $m^2$ , i.e. increasing time  $t \sim m^{-2}$  in the KPZ/Burgers formulation, shocks merge and annihilate.
- (c) Shock fronts are straight lines.
- (d) When crossing a shock line, the minimizer  $u$  of equation (96) jumps perpendicular to the shock.

Properties (c) and (d) suggest to write (with  $S = |\vec{S}|$ ) [486]

$$P(\vec{S}) dS_1 dS_2 = \mathbb{P}(S) dS \cos(\theta) d\theta. \quad (618)$$

Using  $dS_1 dS_2 = S dS d\theta$  yields

$$P(S_1, S_2) = \frac{\mathbb{P}(S)}{S} \cos(\theta). \quad (619)$$

On the other hand, one can again solve the problem in the MF limit [486, 487], valid if the microscopic disorder  $R(0) - R(u) \sim |u|^3$ . In this limit, shocks are *an infinitely divisible process* [460]. As a consequence,

$$\overline{e^{\vec{\lambda}[\vec{u}(\vec{w}) - u(\vec{0}) - \vec{w}]}} = e^{wZ(\vec{\lambda})} = \int d^N \vec{S} e^{\vec{\lambda} \vec{S}} P(\vec{S}, \vec{w}). \quad (620)$$

As in section 3.23, the *large-deviation function*  $F(\vec{x})$  can be defined as

$$F(\vec{x}) := - \lim_{w \rightarrow \infty} \frac{\ln P(\vec{x}w, \vec{w})}{w}. \quad (621)$$

Inserting this expression into equation (620) yields

$$e^{wZ(\vec{\lambda})} = w^N \int d^N \vec{x} e^{w[\vec{\lambda} \vec{x} - F(\vec{x})]}. \quad (622)$$

This shows that the generating function  $Z(\vec{\lambda})$  and the large-deviation function  $F(\vec{w})$  are Legendre-transforms of each other,

$$Z(\vec{\lambda}) + F(\vec{x}) = \vec{\lambda} \vec{x}, \quad (623)$$

$$\lambda_i = \frac{\partial}{\partial x_i} F(\vec{x}), \quad x_i = \frac{\partial}{\partial \lambda_i} Z(\vec{\lambda}). \quad (624)$$

It is non-trivial to show [486, 487] that

$$F(x_1, x_2) = \frac{2x_2^2 + [x_2^2 + (x_1 - 1)x_1]^2}{4(x_1^2 + x_2^2)^{3/2}}. \quad (625)$$

Measuring only a single component, equivalent to setting  $x_2 = \lambda_2 = 0$ , this reduces to

$$F(x, 0) = \frac{(1-x)^2}{4x}, \quad Z(\lambda, 0) = \frac{1}{2} \left( 1 - \sqrt{1-4\lambda} \right). \quad (626)$$

This is the same generating function as in equation (524), thus the probability distribution for the longitudinal component  $S_1$  is as given in equation (527) (standard Watson–Galton process [315, 456]). The transversal avalanche-size distribution is more involved, but a parametric representation for  $\tilde{Z}_2(\lambda) := Z(0, \lambda)$  can be given [487],

$$\lambda(\theta) = \sin(\theta) \frac{\sqrt{5 - \cos(4\theta)} + 2}{[1 - \cos(2\theta) + \sqrt{5 - \cos(4\theta)}]^2}, \quad (627)$$

$$\tilde{Z}_2(\theta) = \frac{\cos(\theta)}{2} \frac{\sqrt{5 - \cos(4\theta)} - 2}{1 - \cos(2\theta) + \sqrt{5 - \cos(4\theta)}}.$$

This allows one to obtain the graph of  $\tilde{Z}_2(\lambda)$ , and even to Laplace-invert it. The results and numerical tests are shown in figure 57.

#### 4.24. Clusters of avalanches in systems with long-range elasticity

When elasticity is long-ranged, avalanches can nucleate away from the part of the avalanche including the first point to have moved. This is an old problem, with many references, see e.g. [488–493].

Suppose that each avalanche of size  $S$  is composed of  $N_c(S)$  clusters, distributed as

$$P(S_c | S) \sim S_c^{-\tau_c} \Theta(S_c < S), \quad \tau_c < 2. \quad (628)$$

Then the typical size of clusters, given avalanche size  $S$ , is

$$\langle S_c \rangle_S = \int_0^S dS_c S_c P(S_c | S) \sim S^{2-\tau_c}. \quad (629)$$

There are

$$N_c(S) \simeq \frac{S}{\langle S_c \rangle} \sim S^{\tau_c-1} \quad (630)$$

clusters. Suppose that the number of clusters scales as

$$P(N_c) \sim N_c^{-\mu} \Theta(N_c < N_c(S)). \quad (631)$$

On dimensional grounds,  $P(S)dS \sim P(N_c)dN_c$ . Inserting the above relations yields

$$\tau_c - 1 = \frac{\tau - 1}{\mu - 1}. \quad (632)$$

If one further supposes [491–493] that the generation of a new cluster is a Galton–Watson process (section 4.11), then

$$\mu = 3/2, \quad (633)$$

simplifying equation (632) to [491–493]

$$\tau_{\text{cluster}} = 2\tau - 1. \quad (634)$$

Numerically it was checked [491, 492] that this scaling relation works for all  $0 \leq \alpha < 2$ ; it might actually continue to work for  $\alpha = 2$ , if one keeps a finite value for  $\mathcal{A}_d^\alpha$  in equation (17b) avoiding to reduce the power-law kernel to short-ranged correlations in that limit (see section 1.3). These results have recently been questioned [494].

#### 4.25. Earthquakes

Gutenberg and Richter [75, 97] first reported that the magnitude of earthquakes in California follows a power-law, equivalent to an avalanche-size exponent<sup>37</sup> of  $\tau = 3/2$ . Due to its enormous impact on society, much research is done in the domain, both by geophysicists with the aim of predicting the next big earthquake, and by theoretical physicists, trying to put earthquakes into the framework of disordered elastic manifolds. The latter is successful to a certain extend:

- the elastic object depinning is a two-dimensional fault plane, to which the relative movement is confined, often with sub-mm precision (*localization*),

<sup>37</sup>Geophysicist usually consider the cumulative distribution of magnitude. The magnitude was originally defined as ‘proportional to the log of the maximum amplitude on a standard torsion seismometer’ [495].

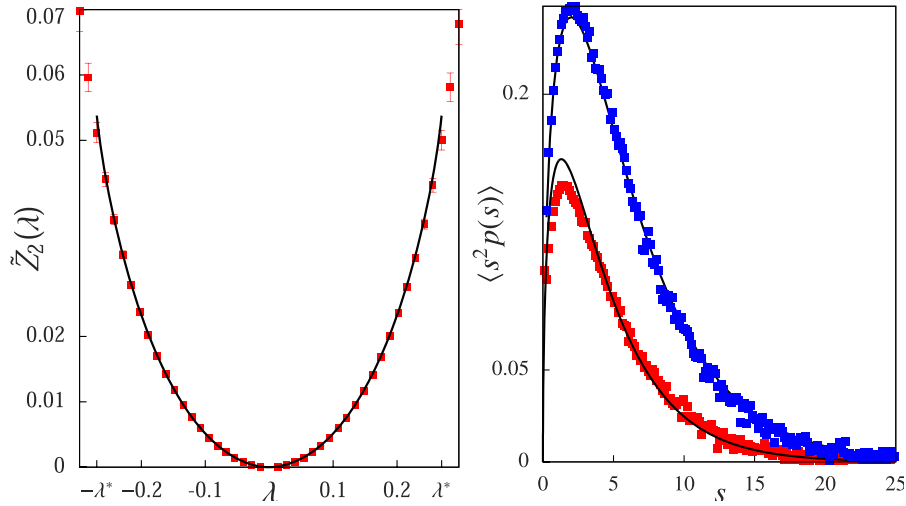


**Figure 57.** (Left) Measured  $\tilde{Z}_2(\lambda)$  (squares) compared to the prediction (627) (solid line). (Right) Plot of  $s_x^2 p_1(s_x)$  (top curve) and  $s_x^2 [p_2(s_x) + p_2(-s_x)]$  (bottom curve). Solid lines represents the analytical predictions. Reproduced from [487]. © IOP Publishing Ltd. All rights reserved.

- driving is through the tectonic plates, equivalent to the parabolic confining potential of equation (5),
- the elastic interactions on the fault plane are long-ranged since elasticity is mediated by the bulk. The calculation is essentially the same as for contact lines in section 1.3, and yields  $\alpha = 1$  in equation (16),
- the critical dimension  $d_c(\alpha) = 2\alpha = 2$  is the dimension of the fault plane. The system is in its critical dimension. As a consequence  $\zeta = 0$ ,  $z = 2$ , and  $\tau = 3/2$ , which correctly predicts the Gutenberg–Richter law.

But there is an additional element: after an earthquake, the fault is *damaged*, rendering it less resistant to further movement before the damage is *healed*, which happens on a much longer time scale (see e.g. [496]). As a consequence, immediately after a big earthquake, the likelihood of another earthquake is increased. It is indeed found that the probability for an *after-shock* to appear decays (roughly) as  $1/t$  in time  $t$ , known today as Omori’s law [497].

For further reading, we refer to the original literature [80, 496, 498–509] and to some of the relevant concepts discussed in this review, LR correlated elasticity (section 4.24), and inertia (section 3.23).

#### 4.26. Avalanches in the SK model

The ABBM model, the BFM, or any other approach based on a RW, and commonly summarized as ‘MF’ gives an avalanche-size exponent  $\tau = 3/2$  (defined in equation (472)), bounding from above all experiments and simulations on disordered elastic manifolds

$$\zeta_{\text{ABBM}} = \zeta_{\text{BFM}} = \zeta_{\text{MF}} = \frac{3}{2} \geq \zeta_{\text{dep}}^d \equiv 2 - \frac{2}{d + \zeta} > 1. \quad (635)$$

On the other hand, since  $d + \zeta > 2$ , even in dimension  $d = 1$ , there seems to be a lower bound on  $\tau$  as well, indicated above. Note that for  $\tau \leq 1$  the avalanche-size distribution becomes non-integrable at large  $S$  in absence of an IR cutoff.

It is thus quite surprising to learn that in the SK model [59] the exponent  $\tau$  is smaller [510, 511],

$$\tau_{\text{SK}}^{\text{equilibrium}} = \tau_{\text{SK}}^{\text{dynamic}} = 1. \quad (636)$$

This result for the equilibrium was obtained [510, 511] within a full-RSB scheme, relevant for SK. Curiously, exactly the same exponent is found in numerical simulations [512] out of equilibrium, where one simply increases the magnetic field until one spin becomes unstable, which is then flipped. While finding the ground-state is an NP-hard problem, this dynamic algorithm is trivial to implement. Still, the exponent  $\tau$  is the same. It is also counterintuitive to learn that avalanches in the SK model involve a finite fraction of its  $N$  spins, changing the magnetization on average by  $\sqrt{N}$  for an increase in external field by order  $1/\sqrt{N}$ , i.e.

$$S_{\text{typ}} := \frac{\langle S^2 \rangle}{\langle 2S \rangle} = \sqrt{N}. \quad (637)$$

This means that on the complete hysteresis curve each spin flips on average an order of  $\sqrt{N}$  times. This is very different from magnetic domain walls, where each spin flips exactly once. It is compatible with the non-integrable tail in the size distribution,  $P(S) \sim 1/S$ , knowing that there is no natural IR cutoff other than the system size.

## 5. Sandpile models, and anisotropic depinning

### 5.1. From charge-density waves to sandpiles

While nowadays sandpile models constitute a domain of statistical physics and mathematics on their own, it is worth reminding that they originated in the study of CDWs. In the seminal paper [513], the authors considered an array of rotating pendula elastically coupled to their neighbors via weak torsion springs, a mechanical analogue of a CDW. In any equilibrium state the pendulum will almost point down. Consider a decomposition of the positions  $u_i$  of the pendula, into their integer part

$\bar{u}(i)$  and a rest  $\delta u(i)$ ,

$$u(i) = \bar{u}(i) + \delta u(i), \quad \bar{u}(i) \in \mathbb{Z}. \quad (638)$$

The limit considered in [513] is that of weak springs as compared to the gravitational forces, implying that  $\delta u(i)$  is small. The forces acting on pendulum  $i$  are

$$\begin{aligned} z(i) &= g \cos(2\pi u(i)) + \sum_{j \in \text{nn}(i)} u(j) - u(i) + F(i) \\ &= g \cos(2\pi \delta u(i)) + \sum_{j \in \text{nn}(i)} \bar{u}(j) - \bar{u}(i) \\ &\quad + \sum_{j \in \text{nn}(i)} \delta u(j) - \delta u(i) + F(i). \end{aligned} \quad (639)$$

$F(i)$  are  $u$ -independent applied forces, and  $g$  is the gravitational constant (with mass and length of the pendula set to 1). The sum runs over the nearest neighbors  $j$  of  $i$ , denoted  $\text{nn}(i)$ . If a pendulum becomes unstable,  $\bar{u}(i) \rightarrow \bar{u}(i) + 1$ . The model (639) can also be viewed as a CDW at depinning (sections 1.2, 2.9 and 3.5).

Supposing that the  $\delta u(i)$  are small, the update rule for  $z(i)$  can be written as

$$\begin{aligned} z(i) &\rightarrow z(i) - 2d, \\ z(j) &\rightarrow z(j) + 1, \quad \text{for } j \in \text{nn}(i). \end{aligned} \quad (640)$$

Again neglecting  $\delta u(i)$ , the condition for the event (640) is

$$z(i) > z_c, \quad (641)$$

with  $z_c = g$ .

### 5.2. Bak–Tang–Wiesenfeld, or Abelian sandpile model

The Bak–Tang–Wiesenfeld (BTW) model [513], also known as the Abelian sandpile model (ASM), uses the update rules (640) combined with

$$z_c = 2d. \quad (642)$$

It is interpreted as a sandpile of height  $z(i)$ . A site *topples*, i.e. the rule (640) is performed, when its height exceeds  $z_c$ . If several sites become unstable at the same time, one has to choose an order of the topplings. Considering the original model in terms of the  $u(i)$ , and using Middleton's theorem, it is clear that the final state is independent of the order of updates. Stated differently, the topplings commute. For this reason the model is also referred to as the ASM. Its algebra was studied in detail, especially by Dhar [514–517].

In this model, one starts from  $z(i) = 0$  for all  $i$ , chosen to belong to a finite lattice with open boundaries, as a chess board. Grains are added at random sites. If a site becomes unstable, it topples. If this toppling renders one of its neighbors unstable, it topples in turn. Grains fall off at the boundary. When topplings have stopped, a new grain is added.

In the interface formulation, grains falling off at the boundary correspond to an interface where  $u(i) = 0$  outside the finite lattice ('on the boundary'). As a result, the system is automatically in a critical state. This phenomenon called self-organized



**Figure 58.** Stable configuration in a rice pile experiment. (Photo by the author.) The grains are between two glass plates 5 mm apart. The pile was prepared by slowly increasing the inclination of the plates from horizontal to vertical. Brighter grains sit at the top and are more likely to topple.

criticality, made the BTW model [513] popular. It is now recognized that if a system can become critical, slowly driving it achieves criticality. In the language developed in this review, it is *velocity-controlled depinning*, instead of *force-controlled depinning* (section 3.1). Many natural phenomena are self-organized critical, and a large literature exists on the topic [54, 83, 356, 512, 513, 515–540].

Configurations in the ASM can be classified as recurrent or not. Recurrent configurations can be realized in the steady state, while non-recurrent ones cannot. An example for a non-recurrent configuration is the initial state  $u(i) = 0$ . Recurrent configurations can be mapped one-to-one onto uniform spanning trees (USTs), and the  $q$ -states Potts model in the limit of  $q \rightarrow 0$ . There further is an injection onto LERWs. We discuss this in more depth in section 8.9. We refer the reader to the cited literature and especially [83, 515] for details.

### 5.3. Oslo model

Albeit we used the term 'sandpile', we did not yet motivate its use. To this aim, consider figure 58. The system is in a stable configuration, characterized by a mean slope, plus fluctuations. A grain may start to slide, depending on the local slope, the friction between the neighbors, and its orientation. The ASM does not contain any randomness, but instead is deterministic. Randomness enters only through the driving, i.e. the order in which grains are added. Any realistic model for a sandpile must contain some randomness. A simple one-dimensional model to accomplish this is the Oslo model.

It is defined as follows [533, 541]: consider the height function  $h(i)$  of the sand or rice pile as shown in figure 59. To each height profile  $h(i)$  is associated a stress field  $z(i)$  defined by

$$z(i) := h(i) - h(i + 1). \quad (643)$$

A toppling is invoked if  $z(i) > z_c(i)$ ,  $i > 1$ . The toppling rules are equivalent to those of equation (640),

$$z(i) \rightarrow z(i) - 2, \quad z(i \pm 1) \rightarrow z(i \pm 1) + 1. \quad (644)$$

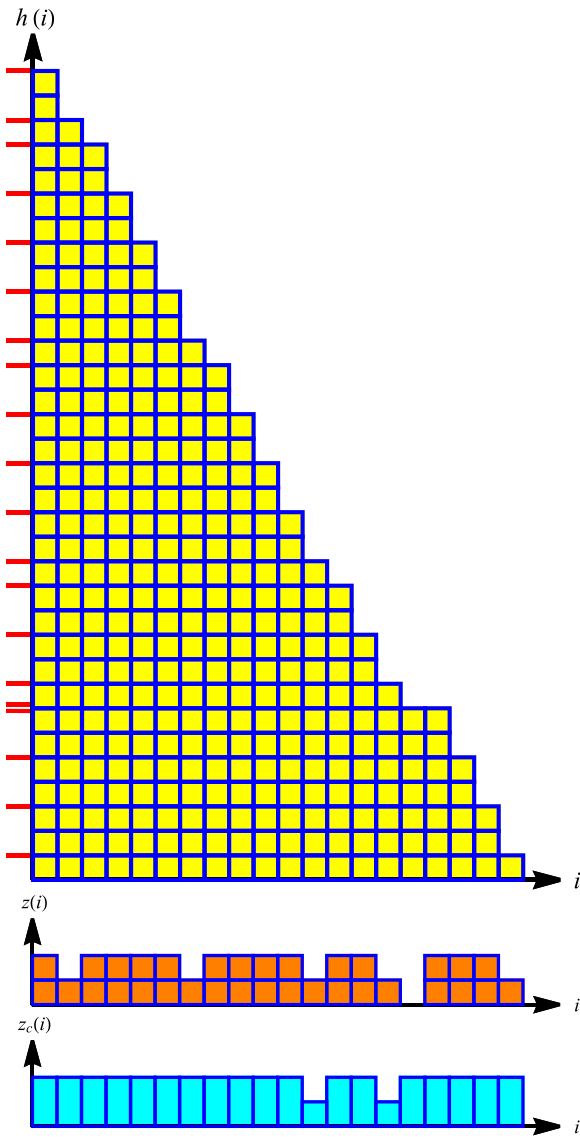


**Figure 59.** A stable configuration of the Oslo model. The latter is a cellular automaton version of the right half of the rice pile in figure 58. The red lines indicate the particle positions of particles used in section 5.4. Note that there is one plateau where two particles sit on top of each other, drawn here slightly apart.

They can be interpreted as moving a grain from the top of the pile at site  $i$  to the top of the pile at site  $i + 1$ ,

$$h(i) \rightarrow h(i) - 1, \quad h(i + 1) \rightarrow h(i + 1) + 1. \quad (645)$$

After such a move, the threshold  $z_c(i)$  for site  $i$  is updated,

$$z_c(i) \rightarrow \text{new random number}. \quad (646)$$

In its original version, the random number is 1 or 2 with probability 1/2. To obtain figure 59 we used a random number drawn uniformly from the interval  $[0, 2]$ . This reduces the critical slope, and the result looks closer to the experiment in figure 58.

The function  $h(i)$  is not one of the usual random-manifold coordinates. If we use the interpretation in equation (640) that  $z(i)$  is the discrete Laplacian of the interface position  $u(i)$ , then

the interface position  $u(i)$  is given by

$$h(i) = u(i - 1) - u(i). \quad (647)$$

The random force sits in the threshold  $z_c$ . The variable  $u(0)$  can be identified as the total number of grains added to the pile. The Oslo model can thus be viewed as an elastic string, pulled at  $i = 0$ . Its average profile is parabolic,

$$\langle u(i) \rangle \approx \frac{\langle z \rangle}{2}(L - i)^2 + \#\{\text{grains fallen off at the right}\}. \quad (648)$$

As the disorder is renewed after each displacement, it falls into the RF universality class.

Is this model realistic for the rice pile of figure 58? According to [534], this depends on the shape of the grains and their friction. If the grains are round, the system goes into a self-organized critical state, described by the Oslo model. On the other hand, if the grains are longish (as on our photo), this does not work. It appears that the direction of the grains is a relevant variable, to be incorporated.

For further reading on the Oslo model, we refer to [305, 524, 542–544].

#### 5.4. Single-file diffusion, and $\zeta_{d=1}^{\text{dep}} = 5/4$

Let us consider the heights  $h(i)$  of the plateaus in figure 59. They are marked on the left as red lines, which we interpret as particles. If a plateau has length  $n \geq 2$ , then  $n$  particles are at the same position. (In the figure there is one plateau of length 2, for which we have drawn the two particle positions slightly apart.) As  $h(i)$  is a monotonically decreasing function,  $h(i) \geq h(i + 1)$ . This induces a half-order  $h(i) \succeq h(i + 1)$  on the particle positions. We can extend this to an order by the convention that if  $i < i + 1$ , and  $h(i) \geq h(i + 1)$ , then  $h(i) \succ h(i + 1)$ . Topplings preserve this order. If we identify this process as single-file diffusion [545–547], then its Hurst exponent is  $H_{\text{SFD}} = 1/4$ . The additional advection term (grains always topple to the right) converts the temporal correlations into spatial ones, resulting into  $\langle [h(i) - h(j)]^2 \rangle^c \sim |i - j|^{2H_{\text{SFD}}}$ . Using that according to equation (647)  $h$  is the discrete gradient of  $u$ , we conclude that [548]

$$\langle [u(i) - u(j)]^2 \rangle^c \sim |i - j|^{2\zeta}, \quad (649)$$

$$\zeta_{d=1}^{\text{dep}} = 1 + H_{\text{SFD}} = \frac{5}{4}. \quad (650)$$

A roughness exponent  $\zeta_{d=1}^{\text{dep}} = 5/4$  is indeed conjectured in [305].

#### 5.5. Manna model

We introduced the ASM with toppling rules (640), i.e. if  $z(i) \geq 2d$ , then one grain is moved to each of the  $2d$  neighbors of site

*i*. In 1991, Manna [537] proposed a stochastic variant<sup>38</sup>

$$z(i) \geq 2 : \text{move 2 grains to randomly chosen neighbors.} \quad (651)$$

The chosen neighbors may be identical. Again, we wish to introduce a random-manifold variable  $u(i)$ , s.t. a toppling on site  $i$  corresponds to  $u(i) \rightarrow u(i) + 1$ , while the remaining  $u(j)$  remain unchanged. To do so, let us define the discrete Laplacian of  $u(i)$  as

$$\nabla^2 u(i) := \sum_{j \in \text{nn}(i)} u(j) - u(i). \quad (652)$$

Write

$$z(i) := \frac{1}{d} [\nabla^2 u(i) + F(i)]. \quad (653)$$

Suppose two grains from site  $i$  go to sites  $i_1$  and  $i_2$ , possibly identical. Then choose for the site  $i$  and its nearest neighbors  $j$

$$u(i) \rightarrow u(i) + 1, \quad F(i) \text{ unchanged}, \quad (654)$$

$$F(j) \rightarrow F(j) + \delta F(j), \quad (655)$$

$$\delta F(j) = d(\delta_{j,i_1} + \delta_{j,i_2}) - 1. \quad (656)$$

The total random force remains constant,  $\sum_{j \in \text{nn}(i)} \delta F(j) = 0$ . We may think of this process as distributing  $2d$  grains onto the  $2d$  neighbors, but instead of doing this uniformly as in the ASM, twice  $d$  grains are moved collectively to a randomly chosen neighbor. Equations (651) and (653) imply that the interface position  $u(i)$  increases by 1 if the rhs of equation (653) is larger than 2. This can be interpreted as a cellular automaton for the equation of motion (302), if  $F(i)$  has the statistics of a random force. One can show that in any dimension  $d$

$$\delta F(i) = \nabla[\dot{u}(i)\bar{\eta}(i)], \quad (657)$$

where  $\bar{\eta}(i)$  is a white noise in space and time<sup>39</sup>.

As a result, for each  $i$  the variable  $F(i)$  performs a RW, which due to equation (657), and the equation of motion, cannot grow unboundedly. This suggests that the MM is in the same universality class as disordered elastic manifolds. In section 6.6 we give a more formal two-step mapping of the MM onto disordered elastic manifolds.

### 5.6. Hyperuniformity

Consider a stationary random point process on the line. It is said to be *hyperuniform* [305], if the number  $n_L$  of points in an interval of size  $L$  has a variance which scales with  $L$  as

$$\text{var}(n_L) \sim L^{\zeta_h}, \quad 0 \leq \zeta_h \leq 1. \quad (658)$$

A Poisson process has  $\zeta = 1$ , a periodic function  $\zeta = 0$ .

For sandpile models, this property was first observed in [549], and later verified in [550–552]. Recent references analyzing or using hyperuniformity include [305, 553, 554].

<sup>38</sup> The original version moves *all* the grains to randomly selected neighbors. This version is not Abelian, whereas equation (651) is. Some authors call it the Abelian Manna model.

<sup>39</sup> In  $d = 1$  it is uncorrelated in space and time, whereas in  $d = 2$  it has a non-trivial spatial structure, but remains short-ranged correlated.

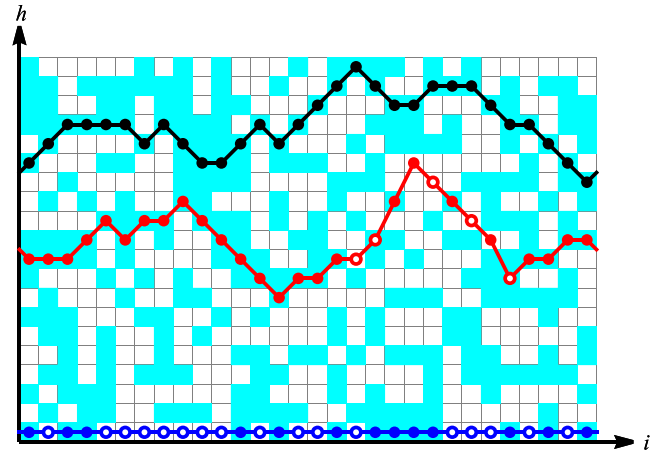


**Figure 60.** The cellular automaton model **TL92**. Blocking cells, i.e. cells above the threshold are drawn in cyan; those below in white. The initial configuration is the string at height 1 (dark blue). The interface moves up. An intermediate configuration is shown in red, the final configuration in black. Open circles represent unstable points, i.e. points which can move forward; closed circles are stable.

Hyperuniformity renders simulations much better convergent, allowing for results from the Manna or Oslo model to exceed in size those obtained directly for the depinning of a disordered elastic manifold.

### 5.7. A cellular automaton for fluid invasion, and related models

There are intriguing connections between invasion of porous media, directed percolation (DP), and depinning of disordered elastic manifolds when the nearest-neighbor interactions grow stronger than linearly. Let us start our considerations with the cellular automaton model proposed in [555]. Variants of this model can be found in [556], where it is applied to experiments on fluid invasion, both numerically and experimentally; see also [557].

The model **TL92** proposed in [555] uses a square lattice as shown in figure 60. To each cell  $(i, j)$  is assigned a random variable  $f(i, j) \in [0, 1]$ . If  $f(i, j) < f_c$ , the cell is considered closed (blocking), drawn in cyan. Open cells (not blocking) are drawn in white. The interface starts as a flat configuration at the bottom (dark blue in figure 60). A point  $(i, h(i))$  on this interface is unstable and can move forward by 1,  $h(i) \rightarrow h(i) + 1$ , according to the following rule in meta code:

```

unstable(i)
# links cannot be longer than 2
if h(i) - h(neighbor) ≥ 2 return false
# move forward if open
if f(i, h(i)) > f_c return true
# move forward if a neighbor is 2 ahead
if h(neighbor) - h(i) ≥ 2 return true
end
    
```

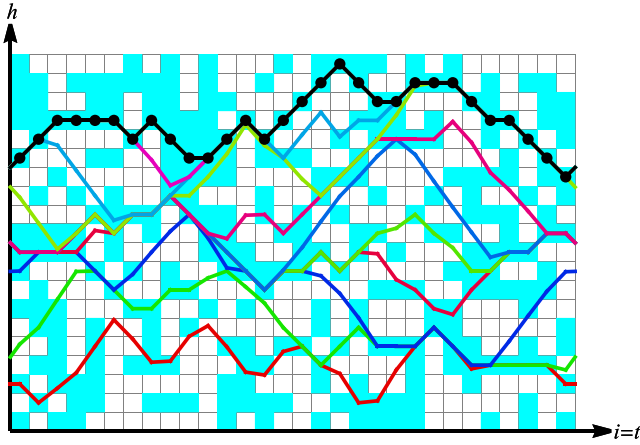


**Figure 61.** Simulation of the continuous version of the cellular automaton model **TL92**. The continuous configurations (in color) converge reliably against the DP solution (black, with filled circles).

This cellular automaton models a fluid invading a porous medium. Invasion takes place if a cell is open (second ‘if’ above), or can be invaded from the side (third ‘if’). The process stops if all points  $(i, h(i))$  are stable. As is illustrated in figure 60, this stopped configuration is a directed path from left to right passing only through blocked sites, commonly referred to as a DP path. One can convince oneself that upon stopping the algorithm yields the lowest-lying DP path. This can be implemented both for open and periodic boundary conditions. The latter are chosen in figure 60. The automaton **TL92** can straightforwardly be generalized to higher dimensions [558], but there is *a priori* no DP process in the orthogonal direction.

Two continuous equations of motion may be associated with this surface growth. The first is the (massive) quenched KPZ equation,

$$\partial_t u(x, t) = c \nabla^2 u(x, t) + \lambda [\nabla u(x, t)]^2 + m^2 [w - u(x, t)] + F(x, u(x, t)). \quad (659)$$

This is almost the equation of motion (302) for a disordered elastic interface; the additional non-linear term proportional to  $\lambda$  is referred to as a KPZ-term, due to its appearance in the famous KPZ equation of non-linear surface growth [560]. The latter accounts for the surface growing in its normal direction, and not in the direction of  $h$ . For a derivation see section 7.1. For an early reference see [561]. In the present context it was first observed in simulations [562], where an increase in the drift-velocity was found upon tilting the interface.

The second model one can associate with the automaton **TL92** is depinning of an elastic interface (figure 61). As **TL92** makes no distinction between nearest-neighbor distances 0 or  $\pm 1$ , has strong interactions at distance 2, and forbids larger distances, the corresponding elastic energy  $\mathcal{H}_{\text{el}}[u]$  must be strongly anharmonic. Our choice is (with  $u(L+1) = u(1)$ )

$$\mathcal{H}_{\text{el}}[u] = \sum_{i=1}^L \mathcal{E}_{\text{el}}(u(i) - u(i+1)), \quad (660)$$

$$\mathcal{E}_{\text{el}}(u) = \begin{cases} 0, & |u| \leq 1 \\ \frac{1}{24}(u^2 - 1)^2, & |u| > 1. \end{cases} \quad (661)$$

This implies an elastic nearest-neighbor force

$$f_{\text{el}}(u) := -\partial_u \mathcal{E}_{\text{el}}(u) = \begin{cases} 0, & |u| \leq 1 \\ -\frac{1}{6}u(u^2 - 1), & |u| > 1. \end{cases} \quad (662)$$

It evaluates to  $-1$  at  $u = 2$ , which is sufficient to overcome any obstacle; and to  $-4$  at  $u = 3$ , making the latter unattainable. The full equation of motion for site  $i$  then reads

$$\partial_t u(i, t) = f_{\text{el}}(u(i, t) - u(i+1, t)) + f_{\text{el}}(u(i, t) - u(i-1, t)) + F(i, u(i, t)). \quad (663)$$

The last term is the disorder force, which we choose to be  $f(i, j) - f_c$  if  $u$  is within  $\delta$  close to  $j$ . Thus disorder acts as an obstacle close to an integer  $h$ . To mimic **TL92**, we wish the manifold to advance freely between obstacles, setting there  $F = f_+$ . Formally

$$F(i, u) := \begin{cases} f(i, j) - f_c, & \exists j, |u - j| < \delta, \\ f_+, & \text{else.} \end{cases} \quad (664)$$

The  $f(i, j)$  are the threshold forces of **TL92**. The parameter  $\delta$  is a regulator. One checks that  $\delta = 10^{-3}$ , and  $f_+ = 2$  reproduces the time evolution of **TL92**, if movement is restricted to a single degree of freedom  $i$ , and one stops when  $u(i)$  hits the next barrier. This is not how Langevin evolution works: the latter being parallel, we cannot expect trajectories to go through the same states. However, due to Middleton’s theorem (see section 3.2), the blocking configurations of both algorithms are the same. We have verified with numerical simulations that the Langevin equation of motion finds exactly the same blocking configurations as the cellular automaton **TL92**. This proves that the critical configurations of the former are states of DP.

While this statement was proven above for a specific non-linearity, we expect that it is more generic, and applies to any convex elastic energy which at large distances grows stronger than a parabola. This was numerically verified for several anharmonicities in [53].

### 5.8. Brief summary of directed percolation

DP is a mature domain of statistical physics [543, 563, 564]. Consider figure 62. Sites are empty or full with probability  $p$ , which in our discussion above equals  $p = f_c$ . A site  $(i, h)$  is said to be connected to the left boundary, if it is occupied, and at least one of its three left neighbors  $(i-1, h)$ ,  $(i-1, h \pm 1)$  is connected to the left boundary. The system is said to percolate, if at least one point on the right boundary is connected to the left boundary. For small  $p$ , this is unlikely, whereas for large  $p$  this is likely. There is a transition at  $p = p_c$ . What is commonly considered are the three independent exponents  $\beta$ ,  $\nu_{\parallel}$ , and  $\nu_{\perp}$ ,

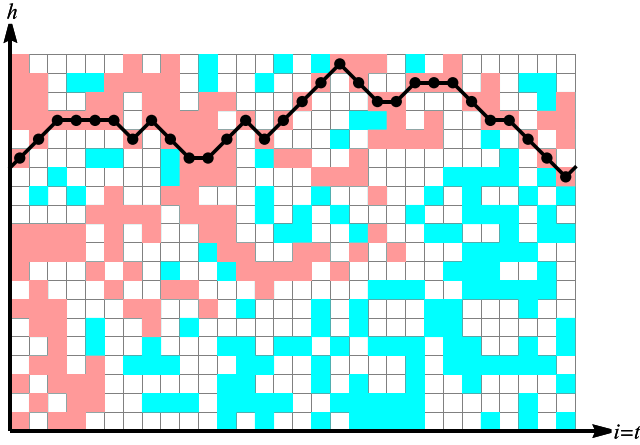


**Figure 62.** DP from left to right. A site  $(i, h)$  is defined to be *connected* if it is occupied, and at least one of its left neighbors  $(i - 1, h), (i - 1, h \pm 1)$  is connected. The index  $i$  takes the role of time  $t$ .

defined via

$$\rho(t) := \left\langle \frac{1}{H} \sum_h s_h(t) \right\rangle \xrightarrow{t \rightarrow \infty} \rho^{\text{stat}}, \quad (665)$$

where  $s_h(t) = 1$  if site  $(t, h)$  is occupied and 0 else.

$$\rho^{\text{stat}} \sim (p - p_c)^\beta, \quad p > p_c, \quad (666)$$

$$\xi_{\parallel} = |p - p_c|^{-\nu_{\parallel}}, \quad (667)$$

$$\xi_{\perp} = |p - p_c|^{-\nu_{\perp}}. \quad (668)$$

The last two relations imply

$$\xi_{\perp} \sim \xi_{\parallel}^{\zeta}, \quad \zeta := \frac{\nu_{\perp}}{\nu_{\parallel}}. \quad (669)$$

Hinrichsen [543] gives in  $d = 1$ :

$$\begin{aligned} \nu_{\parallel} &= 1.733847(6), & \nu_{\perp} &= 1.096854(4), \\ \beta &= 0.276486(8), & \Rightarrow \zeta &= 0.632613(3). \end{aligned} \quad (670)$$

In  $d = 2$ :

$$\nu_{\parallel} = 1.295(6), \quad \nu_{\perp} = 0.734(4), \quad \beta = 0.584(4). \quad (671)$$

In  $d = 3$ :

$$\nu_{\parallel} = 1.105(5), \quad \nu_{\perp} = 0.581(5), \quad \beta = 0.81(1). \quad (672)$$

For **TL92** ( $d = 1$ ), the exponent  $\zeta$  is interpreted as the roughness exponent. Simulations in dimensions  $d = 1$  to 4 yield [543]:

$$\zeta = \frac{\nu_{\perp}}{\nu_{\parallel}} = \begin{cases} 0.632613(3), & d = 1 \\ 0.566(7), & d = 2 \\ 0.526(7), & d = 3 \\ 0.5, & d \geq 4 \end{cases} \quad (673)$$

Field-theory for DP is derived in section 6.5. At two-loop order [565–568] it reads<sup>40</sup>

$$\nu_{\parallel} = 1 + \frac{\epsilon}{12} + \frac{\epsilon^2 [109 - 110 \ln(\frac{4}{3})]}{3456} + \mathcal{O}(\epsilon^3), \quad (674)$$

$$\nu_{\perp} = \frac{1}{2} + \frac{\epsilon}{16} + \frac{\epsilon^2 [107 - 34 \ln(\frac{4}{3})]}{4608} + \mathcal{O}(\epsilon^3), \quad (675)$$

$$\beta = 1 - \frac{\epsilon}{6} + \frac{\epsilon^2 [11 - 106 \ln(\frac{4}{3})]}{1728} + \mathcal{O}(\epsilon^3). \quad (676)$$

This yields

$$\zeta := \frac{\nu_{\perp}}{\nu_{\parallel}} = \frac{1}{2} + \frac{\epsilon}{48} + \frac{\epsilon^2 [79 + 118 \ln(\frac{4}{3})]}{13824} + \mathcal{O}(\epsilon^3). \quad (677)$$

In  $d = 1$  ( $\epsilon = 3$ ), these values are in decent agreement with those of equation (670).

### 5.9. Fluid invasion fronts from directed percolation

To avoid confusion, let us define

$$\langle [u(x, t) - u(0, t)]^2 \rangle \sim \begin{cases} |x - x'|^{2\zeta} & \text{for } |x - x'| \ll \xi_m, \\ m^{-2\zeta_m} & \text{for } |x - x'| \gg \xi_m. \end{cases} \quad (678)$$

In  $d = 1$ , the scaling of  $x$  and  $u$  as a function of  $p - p_c$  is

$$x \sim \xi_{\parallel} \sim |p - p_c|^{-\nu_{\parallel}}, \quad (679)$$

$$u \sim \xi_{\perp} \sim |p - p_c|^{-\nu_{\perp}}. \quad (680)$$

This implies

$$u \sim x^{\zeta}, \quad \zeta = \frac{\nu_{\perp}}{\nu_{\parallel}}. \quad (681)$$

The exponent  $\nu$  defined for depinning in equation (307) is identified from equation (680) as

$$\nu \equiv \nu_{\text{dep}} = \nu_{\parallel}. \quad (682)$$

If we drive with a parabolic confining potential,

$$m^2 u \simeq |p - p_c|. \quad (683)$$

This yields

$$u \sim m^{-\zeta_m}, \quad \zeta_m = \frac{2\nu_{\perp}}{1 + \nu_{\perp}}. \quad (684)$$

Let us define the correlation length  $\xi_m$  as the  $x$ -scale at which the crossover between the two regimes of equation (678) takes place. This yields

$$\xi_m \sim m^{-\frac{\zeta_m}{\zeta}}, \quad \frac{\zeta_m}{\zeta} = \frac{2\nu_{\parallel}}{1 + \nu_{\perp}}. \quad (685)$$

<sup>40</sup>Note that the notations in these papers are somehow contradictory. The dynamical critical exponent  $z$  is related to our roughness  $\zeta$  via  $z = 1/\zeta$ . The  $z$  defined in [566, 567, 569] is in Reggeon field theory, and equals  $z_{\text{Reggeon}} = 2\zeta$ . Partial results at three-loop order are reported in [570].

**Table 3.** The exponents of qKPZ.

	$d = 1$	$d = 2$	$d = 3$
$\zeta$	0.63 [555]	0.45	?
$z$	1 [555]	$1.15 \pm 0.05$ [571]	$1.36 \pm 0.05$ [571]

(We remind that in contrast for qEW  $\zeta = \zeta_m$ , and  $\xi_m = 1/m$ , see equation (312).) The avalanche-size exponent also changes. An avalanche scales as

$$S_m = \xi_m^{d+\zeta} \equiv \xi_m^d m^{-\zeta_m}. \quad (686)$$

Since equation (474) was derived under the sole assumption that the avalanche density has a finite IR-independent limit for  $m \rightarrow 0$ , it remains valid, implying

$$\tau = 2 - \frac{2}{d + \zeta} \frac{\zeta}{\zeta_m}. \quad (687)$$

In dimension  $d = 1$ , the dynamical exponent  $z = 1$  (see below). The depinning scaling relation (308) can be rewritten with equation (681) and  $z = 1$  as

$$\beta_{\text{dep}} = \nu_{\parallel}(z - \zeta) \equiv \nu_{\parallel} - \nu_{\perp}. \quad (688)$$

Using the values of [543] combined with the above scaling relations, the numerical values in  $d = 1$  are

$$\nu_{\text{dep}} \equiv \nu_{\parallel} = 1.733847(6) \quad (689)$$

$$\nu_{\perp} = 1.096854(4) \quad (690)$$

$$\zeta = 0.632613(3), \quad (691)$$

$$\zeta_m = 1.04619(2), \quad (692)$$

$$\frac{\zeta_m}{\zeta} = 1.47955(3), \quad (693)$$

$$\tau = 1.259246(2), \quad (694)$$

$$\beta_{\text{dep}} = 0.636993(7), \quad (695)$$

$$z = 1. \quad (696)$$

*The dynamic exponent  $z$ .* In [571] it was proposed that the dynamical exponent  $z$  is related to the fractal dimension  $d_{\text{min}}$  of the shortest path connecting two points a distance  $r$  apart in a percolation cluster. Denoting its length by  $\ell \sim r^{d_{\text{min}}}$ , the conjecture is

$$z = d_{\text{min}}. \quad (697)$$

This relation was confirmed numerically, and yielded the dynamical exponents  $z$  reported in table 3. Curiously, the upper critical dimension of percolation is  $d = 6$ , whereas the theory for DP used in the preceding section has an upper critical dimension of  $d = 4$ . As a consequence, constructing a field theory encompassing both seems challenging.

### 5.10. Anharmonic depinning and FRG

Let us finally study anharmonic depinning within FRG, and to this purpose consider the standard elastic energy (4),

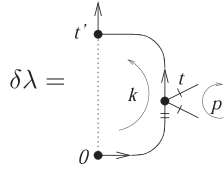
supplemented by an additional anharmonic (quartic) term,

$$\mathcal{H}_{\text{el}}[u] = \int_x \frac{1}{2} [\nabla u(x)]^2 + \frac{c_4}{4} [(\nabla u(x))^2]^2. \quad (698)$$

The corresponding equation of motion reads

$$\partial_t u(x, t) = \nabla^2 u(x, t) + c_4 \nabla \{ \nabla u(x, t) [\nabla u(x, t)]^2 \} + F(x, u(x, t)) + f. \quad (699)$$

Since the rhs of equation (699) is a total derivative, it is surprising that a KPZ-term can be generated in the limit of a *vanishing* driving-velocity. This puzzle was solved in [572], where the KPZ term arises by contracting the non-linearity with one disorder, following the rules of section 3.4 (setting  $m = 0$ ):



$$\delta\lambda = -\frac{c_4}{p^2} \int_{t>0} \int_{t'>0} \int_k e^{-(t+t')k^2} (k^2 p^2 + 2(kp)^2) \times \Delta'(u_{x,t+t'} - u_{x,0}). \quad (700)$$

As  $u(x, t + t') - u(x, 0) \geq 0$ , equation (700) can be written as

$$\delta\lambda = -\frac{c_4}{p^2} \int_t \int_{t'} \int_k e^{-(t+t')k^2} (k^2 p^2 + 2(kp)^2) \Delta'(0^+). \quad (701)$$

Integrating over  $t, t'$  and using the radial symmetry in  $k$  yields

$$\delta\lambda = -c_4 \left(1 + \frac{2}{d}\right) \int_k \frac{\Delta'(0^+)}{k^2}. \quad (702)$$

This shows that in the FRG a KPZ term is generated from the non-linearity. Field theory does not yet permit to calculate the ensuing roughness exponent, nor explain the mapping onto DP, even though a mechanism for the generation of a branching-like process was found [572].

### 5.11. Other models in the same universality class

Many models nowadays are recognized as being in the universality class of DP. This started with work by Janssen [565] and Grassberger [574], who conjectured that the findings ‘suggest another type of universality, comprising all critical points with an absorbing state and a single order parameter in one universality class’ [574]. As a general rule, a model belongs to the universality class of DP, as long as it has no additional symmetry. A notable exception is the MM (see section 6.6). Note that additional conserved quantities are not enough, as exemplified by DP with many absorbing states [518, 575–578]. The reader wishing to explore the large literature further can find a lot of material in the context of *phase transitions into absorbing states*, see [299, 543] for review, as well as [518, 528, 576, 579–582].

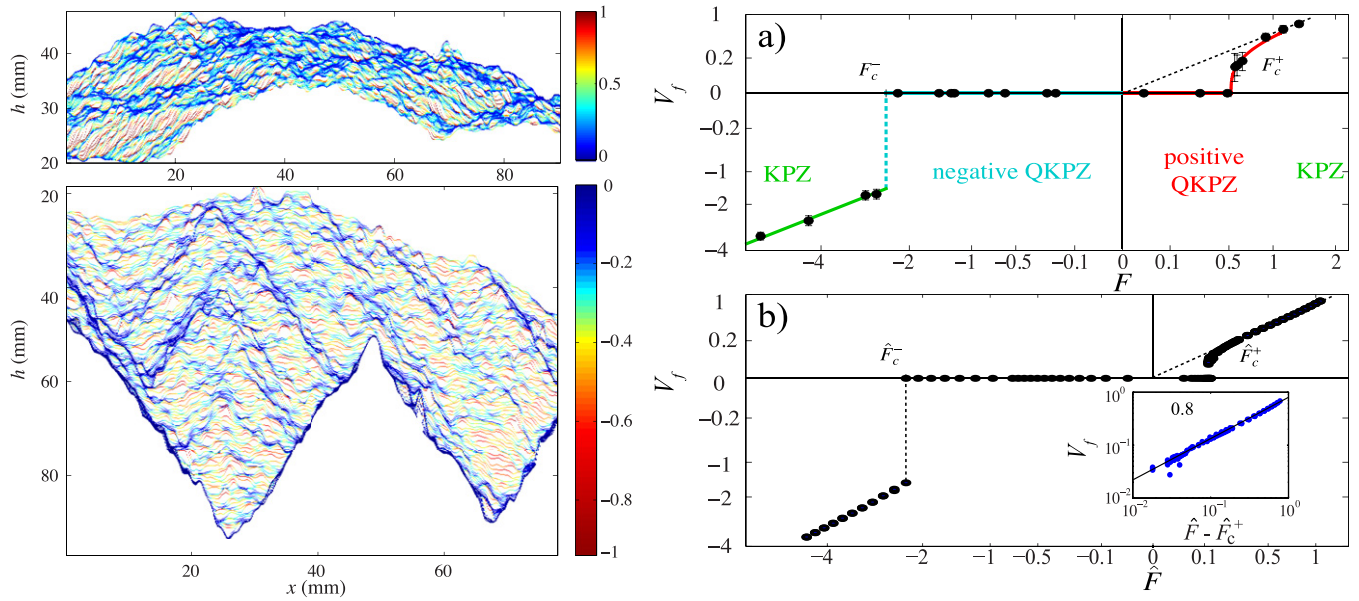


**Figure 63.** (Left) Successive experimental fronts at constant time intervals in a self-sustained reaction, propagating in a disordered environment made by polydisperse beads [573]. Color represents local front velocity. (Top left) Upward propagating front near  $F_c^-$ . (Bottom left) Backward propagating front near  $F_c^+$ . (Right) Front velocity  $V_f$  versus the applied force  $F$ , in adverse flow. (a) Experiments (black dots with error bars), (b) numerics. Dashed lines are a linear extrapolation of the advancing branch. To put all data on one plot, axes are rescaled according to  $F \rightarrow F/|F|^{1/2}$ ,  $V_f \rightarrow V_f/|V_f|^{1/2}$ . (Inset) Log-log plot of front velocity versus  $\hat{F} - \hat{F}_{c^+}$ . The continuous line corresponds to  $v(\hat{F}) \propto (\hat{F} - \hat{F}_{c^+})^{0.8 \pm 0.05}$ . Reprinted figure with permission from [573], Copyright (2015) by the American Physical Society.

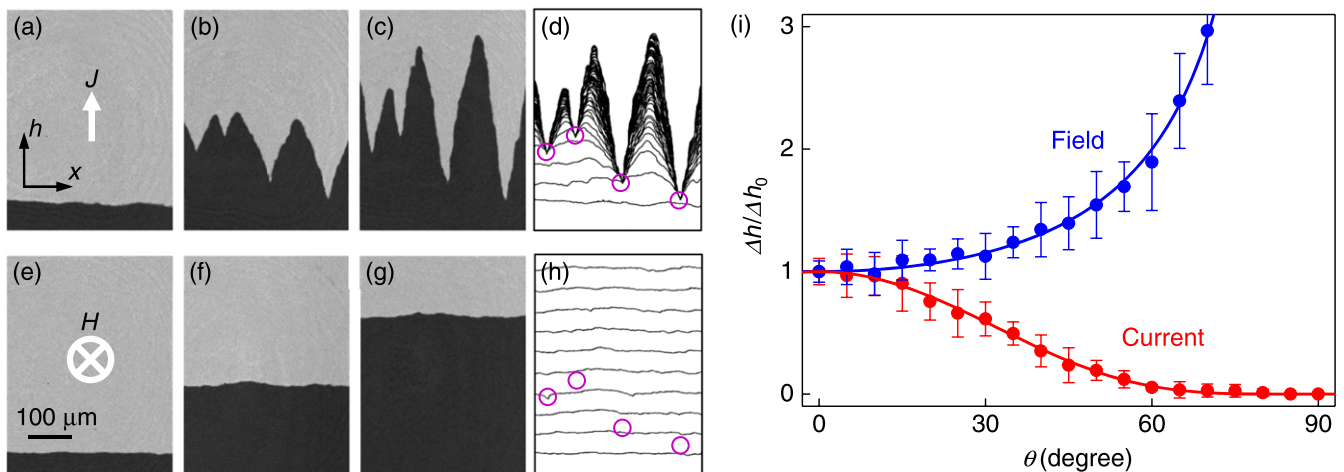


**Figure 64.** Magnetic domain walls in a two-dimensional Pt-Co-Pt thin film. (a)–(d) Images for current-driven walls at increasing times. (e)–(h) Images for field-driven walls at increasing times. (i) Measurement of the angle-dependent force as extracted from an analysis of the creep laws. Reprinted figure with permission from [404], Copyright (2013) by the American Physical Society.

### 5.12. Quenched KPZ with a reversed sign for the non-linearity

As long as the disorder  $F(x, u)$  is statistically invariant under  $u \rightarrow -u$ , the qKPZ equation (659) is invariant under  $u \rightarrow -u$ ,  $\lambda \rightarrow -\lambda$ , and  $f \rightarrow -f$ . This leads to two distinct cases:  $\lambda f > 0$  the *positive qKPZ* class, and  $\lambda f < 0$  the *negative qKPZ* class. Consider  $f > 0$ , and  $\lambda > 0$ , then the KPZ term facilitates depinning. In the opposite case, assuming a tilted configuration allows the interface to remain pinned for larger applied forces. It then assumes a sawtooth shape, with the bottom kinks at the strongest pinning centers, and the slope

given by  $f \approx (-\lambda)(\nabla u)^2$ . This was first observed numerically [583, 584], and later confirmed experimentally [404, 573], as beautifully illustrated in figures 63 and 64, and discussed in the next section.

### 5.13. Experiments for directed percolation and quenched KPZ

Experiments for DP seem to be scarce [543]. A notable exception is [585, 586], where a transition between two topologically different turbulent states, called dynamic scattering modes 1 and 2 (DSM1 and DSM2), is observed upon an

increase in the applied voltage. This allows them to measure directly the exponent  $\beta$  as

$$\beta_{\text{DP}}^{d=2} = 0.59(4). \quad (703)$$

The remaining exponents are obtained from a quench. Citing only the most precise values,

$$\nu_{\parallel} = 1.18_{-(21)}^{+(14)}, \quad (704)$$

$$\nu_{\perp} = 0.77(7). \quad (705)$$

The theory values are given in equation (671).

More experiments have been done for the qKPZ class. A particularly nice example are self-sustained reaction fronts propagating in a disordered environment made by polydisperse beads [573], as depicted on figure 63. The measured spatial and temporal fluctuations are consistent with three distinct universality classes in dimension  $d = 1 + 1$ , controlled by a single parameter, the mean (imposed) flow velocity. The three classes are

- (a) the KPZ class for fast advancing or receding fronts, with a roughness exponent of  $\zeta \approx 0.5$ , see equation (817). (Purely diffusive motion with the same roughness exponent is excluded by the temporal correlations.)
- (b) The quenched Kardar–Parisi–Zhang class (positive-qKPZ) when the mean-flow velocity almost cancels the reaction rate. It has a roughness of  $\zeta \approx 0.63$ , in agreement with our discussion in section 5.9. A depinning transition with a non-linear velocity-force characteristics,  $v \sim |F - F_c|^\beta$  is observed, see figure 63.
- (c) The negative-qKPZ class for receding fronts, close to the lower depinning threshold  $\hat{F}_{c-}$ . One observes characteristic saw-tooth shapes, see figure 63, bottom left.

To our knowledge, this system is the only one where all three KPZ universality classes have been observed in a single experiments.

The qKPZ phenomenology is also observed in domain walls in thin magnetic films [404] (see section 3.21), either driven by an applied field (positive qKPZ) or a current (negative qKPZ). The experiment performed in [404] cleverly extracts the slope-dependent mean force as a function of the angle, see figure 64 (right). This firmly establishes the relevance of the two qKPZ classes for domain wall experiments. It would be interesting to drive the system both with a magnetic field and a current, chosen s.t. the two effects cancel.

## 6. Modeling discrete stochastic systems

### 6.1. Introduction

In *discrete stochastic processes* the elementary degrees of freedom are discrete variables. This can be the number of colloids in a suspension, the number of bacteria, fishes and their predators in the ocean, or the grains in sandpile models. There are two powerful methods to treat these systems (for a pedagogical introduction see [587])

- (a) the coherent-state path integral [587–591],

- (b) effective stochastic equations of motion.

The first method, the coherent-state path integral, is an exact method, and as such a natural starting point in a field-theoretic setting, i.e. to construct a dynamic action, similar to the Martin–Siggia–Rose action (appendix A.4). As we will see in the next section 6.2, despite the fact that it is an exact method, or maybe due to it, it has its problems. They arrive when decoupling the non-linear terms via an auxiliary noise. This noise is in general imaginary, leading to problems both in the interpretation, as in simulations. As a caveat to the reader, let us mention that things sometimes get messed up in the literature: starting with the coherent-state path integral, one sees emerging an effective stochastic equation of motion with real noise. We show below why this is in general *not possible*.

Real noise appears in a different modeling of stochastic systems, via *effective stochastic equations of motion*. Here the noise stems from the fact that one tries to approximate a *discrete* random process by a *continuous* one, and one has to add back the appropriate *shot noise*.

Another important question we need to deal with is the notion of the MF approximation in stochastic equations. We will give a simple and precise definition of the latter. To our astonishment, we have not found a discussion of this in the literature prior to [588].

### 6.2. Coherent-state path integral, imaginary noise and its interpretation

The coherent-state path-integral [587–591] is constructed by using creation and annihilation operators familiar from quantum mechanics,

$$[\hat{a}, \hat{a}^\dagger] = 1, \quad |n\rangle := (\hat{a}^\dagger)^n |0\rangle. \quad (706)$$

The state  $|n\rangle$  is interpreted as  $n$ -times occupied. Eigenstates of  $\hat{a}$  are coherent states. They are the building blocks of the formalism, giving it its name

$$|\phi\rangle := e^{\phi \hat{a}^\dagger} |0\rangle \quad \Rightarrow \quad \hat{a} |\phi\rangle = \phi |\phi\rangle. \quad (707)$$

Taylor expanding  $e^{\phi \hat{a}^\dagger} |0\rangle$ , one sees that coherent states are Poisson distributions with  $n$ -fold occupation probability given by

$$p(n) = e^{-\phi} \frac{\phi^n}{n!}. \quad (708)$$

Note that  $\langle n \rangle = \langle n^2 \rangle^c = \phi$ , thus the parameter  $\phi$  characterizing a coherent state is both its mean and variance.

Consider the reaction–diffusion process with diffusion constant  $D$  and reaction rate  $A + A \xrightarrow{\nu} A$ . The action, see (equation (112) of [587]) reads

$$\begin{aligned} \mathcal{S}'[\phi^*, \phi] &= \int_{x,t} \phi^*(x,t) [\partial_t \phi(x,t) - D \nabla^2 \phi(x,t)] \\ &+ \int_{x,t} \frac{\nu}{2} [\phi^*(x,t) \phi(x,t)^2 + \phi^*(x,t)^2 \phi(x,t)^2]. \end{aligned} \quad (709)$$

The first two terms are similar to those appearing in the Martin–Siggia–Rose (MSR) formalism for diffusion, identifying the tilde fields there with star fields here. The next term  $\phi^*(x, t)\phi(x, t)^2$  is also intuitive: two particles are destroyed, and one is created. The only surprising term is the last one. It appears in the formalism to ensure that the probability is conserved, and can be interpreted as a first-passage time problem [587]. If the last term were not there, then we could interpret the action as an equation of motion for  $\phi(x, t)$ . To include the latter, let us decouple the quartic term by introducing an auxiliary field  $\xi(x, t)$ , to be integrated over in the path integral,

$$\begin{aligned} \mathcal{S}'[\phi^*, \phi, \xi] = & \int_{x,t} \phi^*(x, t) \left[ \partial_t \phi(x, t) - D \nabla^2 \phi(x, t) \right. \\ & \left. + \frac{\nu}{2} \phi(x, t)^2 - i\sqrt{\nu} \xi(x, t) \phi(x, t) \right] + \frac{1}{2} \xi(x, t)^2. \end{aligned} \quad (710)$$

The corresponding equation of motion and noise correlations are

$$\begin{aligned} \partial_t \phi(x, t) = & -\frac{\nu}{2} \phi(x, t)^2 + D \nabla^2 \phi(x, t) \\ & + i\sqrt{\nu} \phi(x, t) \xi(x, t), \end{aligned} \quad (711)$$

$$\langle \xi(x, t) \xi(x', t') \rangle = \delta(t - t') \delta(x - x'). \quad (712)$$

This noise is imaginary. It has puzzled many researchers whether this is unavoidable [579, 592–594], or could even be beneficial [595].

For the moment, let us restrict our considerations to a single site, starting at time  $t = t_i$  with the initial state,  $\phi_{t_i} = \phi_i$ ,

$$\begin{aligned} \partial_t \phi(t) = & -\frac{\nu}{2} \phi(t)^2 + i\sqrt{\nu} \phi(t) \xi(t), \\ \langle \xi(t) \xi(t') \rangle = & \delta(t - t'). \end{aligned} \quad (713)$$

This equation is integrated from  $t = t_i$  to  $t_f$ . On the left of figure 65 we show the result for  $\phi_{t_f}$  for different realizations of the noise  $\xi(t)$ . Since  $\phi_{t_f}$  is complex, the question is how to interpret these states. The answer is that the probability distribution is given, in generalization of equation (708), by [587]

$$P_i^{\text{SEM}}(n) := \left\langle e^{-\phi_i} \frac{\phi_i^n}{n!} \right\rangle_{\xi}. \quad (714)$$

A complex  $\phi(t)$  is necessary, since the final distribution is narrower than a Poissonian<sup>41</sup>. The problem with the stochastic average (714) is that when  $\arg(\phi_i)$  grows in time, it is dominated by those  $\phi_i$  with the smallest real part, and the estimate (714) breaks down. A stochastic equation of motion for the coherent-state path integral is thus not a valid simulation tool. This is similar to what happens in the REM model (section 2.24): in both cases rare events give a substantial contribution to the observable we want to calculate, which is missed in any finite sample or simulation.

<sup>41</sup> First, large particle numbers have a higher probability to annihilate, thus the tail of the distribution is suppressed, making it decay faster than an exponential. Second, it is impossible to construct a probability distribution which is narrower than a Poissonian by a superposition of Poissonians with positive coefficients.

In the next sections, we follow a different strategy: we give up on the discreteness of the number  $n(t)$  of particles, and replace it by a continuous variable  $\hat{n}(t)$ . In exchange we need to introduce a stochastic noise.

### 6.3. Stochastic noise as a consequence of the discreteness of the state space

We want to derive a stochastic differential equation with real noise. To this aim let us simulate directly the random process  $A + A \xrightarrow{\nu} A$ . Each simulation run gives one possible realization of the process, in the form of an integer-valued monotonically decreasing function  $n(t)$ . Averaging over these runs, one samples the final distribution  $P_f(n)$ , or, equivalently, moments of  $n_f$ . We ask the question: is there a continuous random process  $\hat{n}(t)$  which has the same statistics as  $n(t)$ ?

Let us consider a more general problem: be  $n(t)$  the number of particles at time  $t$ . With rate  $r_+$  the number of particles increases by one, and with rate  $r_-$  it decreases by one. This implies that after one time step, as long as  $r_{\pm} \delta t$  are small,

$$\langle n(t + \delta t) - n(t) \rangle = (r_+ - r_-) \delta t, \quad (715)$$

$$\langle [n(t + \delta t) - n(t)]^2 \rangle = (r_+ + r_-) \delta t. \quad (716)$$

The following continuous random process  $\hat{n}(t)$  has the same first two moments as  $n(t)$ ,<sup>42</sup>

$$d\hat{n}(t) = (r_+ - r_-) dt + \sqrt{r_+ + r_-} \xi(t) dt, \quad (717)$$

$$\langle \xi(t) \xi(t') \rangle = \delta(t - t'). \quad (718)$$

This procedure can be modified to include higher cumulants of  $n(t + \delta t) - n(t)$ , leading to more complicated noise correlations. Results along these lines were obtained in [568] by considering cumulants generated in the effective field theory.

### 6.4. Reaction-annihilation process

For the reaction-annihilation process, the rate  $r_+ = 0$ , and  $r_- = \frac{\nu}{2} \hat{n}(t)(\hat{n}(t) - 1)$ ; the latter, in principle, is only defined on integer  $\hat{n}(t)$ , but we will use it for all  $\hat{n}(t)$ . Thus the best we can do to replace the discrete stochastic process with a continuous one is to write

$$\frac{d\hat{n}(t)}{dt} = -\frac{\nu}{2} \hat{n}(t)(\hat{n}(t) - 1) + \sqrt{\frac{\nu}{2} \hat{n}(t)(\hat{n}(t) - 1)} \xi(t), \quad (719)$$

$$\langle \xi(t) \xi(t') \rangle = \delta(t - t').$$

Using  $n_i = 15$ , and  $\nu = 1$ , we have shown two typical trajectories on figure 65 (right), one for the process  $n(t)$  (red, with jumps), and one for the process  $\hat{n}_t$  (blue-grey, rough). While by construction both processes have (almost) the same first two moments, clearly  $\hat{n}(t)$  looks different: it is continuous, which  $n(t)$  is not, and it can increase in time, which  $n(t)$  cannot.

<sup>42</sup> Despite our best efforts, we have not been able to locate a source for this simple argument in the literature prior to [588]. It is applied in [565], but the cited source [596] drily states ‘our whole work depends on the use of stochastic master equations, which, we believe, have a better conceptual and intuitive basis than the fluctuating force formalism of Langevin equations’.

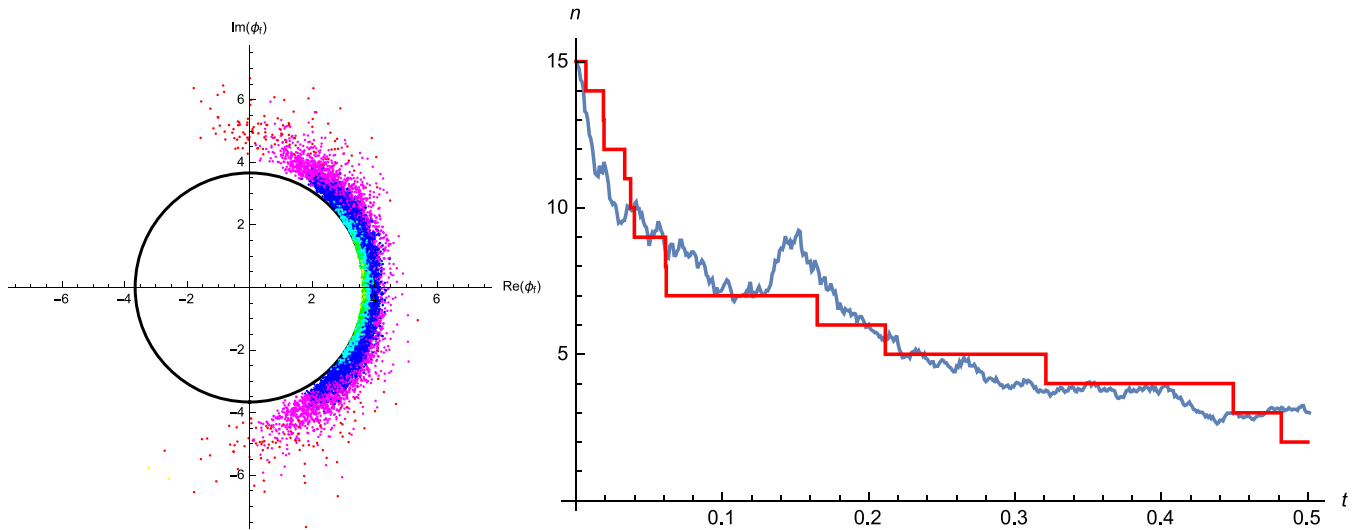


**Figure 65.** (Left) Result of the integration of equation (558), with  $\nu = 1$ , total time  $t_f - t_i = 0.5$ , and initial state  $\phi_i = 15$ . The black circle has radius  $\phi_f = 3.6614$ , obtained by integrating the drift term  $\partial_t \phi_t = -\phi_t^2 + \phi_t + t/2$ . Using an algorithm which splits points which are likely to contribute more to the final result, the color codes less probable values, from yellow over green, cyan, blue, magenta to red. (Thus a red point has  $2^{-5}$  times the weight of a yellow point.) (Right) One trajectory each for process  $n_t$ , i.e. a direct numerical simulation of  $A + A \rightarrow A$  (red, with jumps), and  $\hat{n}_t$ , equation (719) (blue-grey, continuous, rough). The rate is  $\nu = 1$ . We have chosen two trajectories which look ‘similar’. Note that  $\hat{n}_t$  is not monotonically decreasing. Reprinted figure with permission from [587], Copyright (2016) by the American Physical Society.

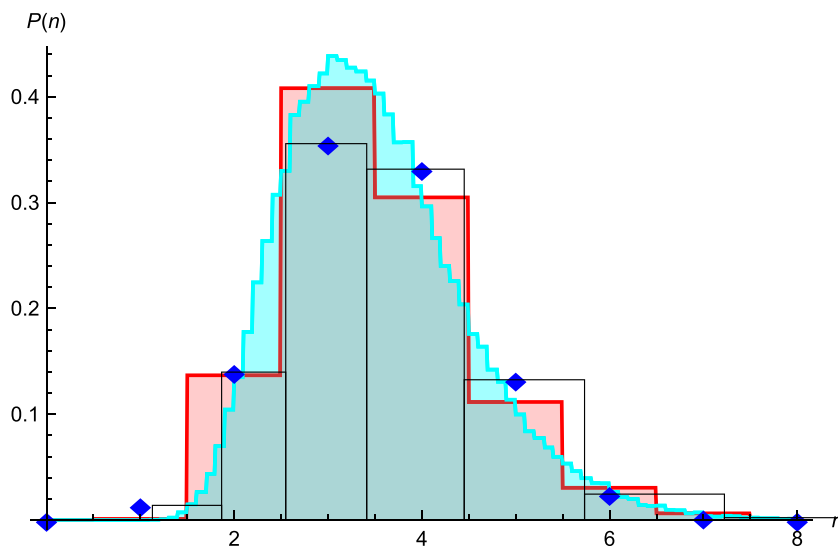


**Figure 66.** Result of a numerical simulation, starting with  $n_i = 15$  particles, and evolving for  $t_f - t_i = 0.025$ . Blue diamonds: direct numerical simulation of the process  $A + A \rightarrow A$  with rate  $\nu = 1$ . Cyan: distribution of the continuous RW (719). Red: the latter distribution, when rounding  $n_f$  to the nearest integer. Black boxes: the size of the boxes in  $n$ -direction to obtain the result of the direct numerical simulation of the process  $A + A \rightarrow A$ . Both processes have first moment  $3.511 \pm 0.001$ , and second connected moment  $1 \pm 0.05$ ; the third connected moments already differ quite substantially, 0.75 versus 0.2. Reprinted figure with permission from [587], Copyright (2016) by the American Physical Society.

not. One can also compare the distribution for  $t_f - t_i = 0.5$ , see figure 66. While the distribution of  $n_f$  is discrete (blue diamonds), the one for  $\hat{n}_f$  is continuous (cyan). Rounding  $n_f$  to the nearest integer gives a different distribution (red). We have also drawn (black lines) the size of the boxes which would produce  $p(n)$  from  $p(\hat{n})$ . Clearly, there are differences. On the other hand, it is also evident that these differences diminish when increasing  $n_i$ .

### 6.5. Field theory for directed percolation

There are several paths to a field theory for reaction–diffusion or DP. A beautiful derivation is given by Cardy and Sugar [567]. The authors start from an exact microscopic modelization, before introducing an auxiliary field resulting into the action given below in equation (726). They then use perturbative results obtained for the equivalent action in Reggeon

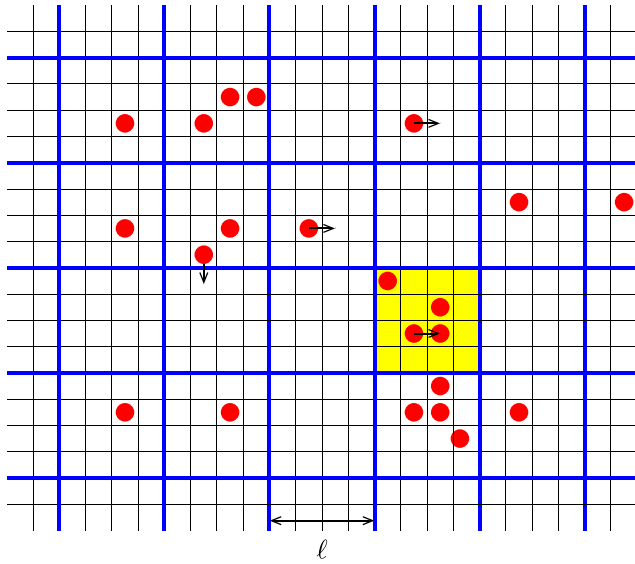


**Figure 67.** A coarse-grained lattice with box-size  $\ell = 4$ . The yellow box contains  $n = 4$  particles. Reprinted figure with permission from [587], Copyright (2016) by the American Physical Society.

field theory. The latter is an effective theory for deep-inelastic scattering [569], quantum gravity (simplicial gravity) [597], vortices in He-II [598], and many more<sup>43</sup>.

For pedagogic reasons, we apply the formalism developed in section 6.3 [339]: denote  $n \equiv n(x, t)$  the number of particles inside a box located around  $(x, t)$  with size  $\ell^d$ , see figure 67. There we could draw time as coming out of the plane.

In figure 62 a different view is taken: here  $n(x, t)$  is the coarse-grained number of occupied sites connected to the left border, there drawn in red. Going one step in  $t$  to the right,  $n$  grows with rate

$$n \xrightarrow{r_+} n + 1, \quad r_+ = \alpha_+ n, \quad (720)$$

$$\alpha_+ \approx 3p. \quad (721)$$

Here 3 is the number of left neighbors per site, and  $p$  is the probability that the site itself is not empty, and thus can be connected. The rate to reduce  $n$  by one is given by

$$n \xrightarrow{r_-} n - 1, \quad r_- = \alpha_- n + \beta n^2, \quad (722)$$

$$\alpha_- = 1 - p, \quad \beta \approx \frac{1}{\ell^d}. \quad (723)$$

The first term takes into account that if the site itself is empty, it cannot be connected. The second term proportional to  $n^2$  ensures that the fraction of connected sites cannot grow beyond 1. According to equation (717), this leads to the stochastic equation of motion

$$\begin{aligned} \partial_t \hat{n}(x, t) &= \nabla^2 \hat{n}(x, t) + (\alpha_+ - \alpha_-) \hat{n}(x, t) - \beta \hat{n}(x, t)^2 \\ &+ \sqrt{\hat{n}(x, t)} \sqrt{\alpha_+ + \alpha_- + \beta \hat{n}(x, t)} \xi(x, t). \end{aligned} \quad (724)$$

<sup>43</sup> Note however, that different theories are associated with the name ‘Regge’: sometimes the cubic vertex is an antisymmetrized combination of a field with two field derivatives, as in [598].

Note that we have added a diffusive term (rescaling  $x$  if necessary to set its prefactor to 1). In DP (figure 62) it arises since the left neighbor to which a site is connected can be one up or down on the lattice.

Multiplying equation (724) with a response field  $\tilde{n}(x, t)$ , and averaging over the noise  $\xi(x, t)$  yields the dynamic action

$$\begin{aligned} S[\tilde{n}, \hat{n}] &= \int_{x,t} \tilde{n}(x, t) [\partial_t \hat{n}(x, t) - \nabla^2 \hat{n}(x, t) + (\alpha_- - \alpha_+) \hat{n}(x, t)] \\ &+ \int_{x,t} \beta \tilde{n}(x, t) \hat{n}(x, t)^2 \\ &- \int_{x,t} \frac{1}{2} [\alpha_+ + \alpha_- + \beta \hat{n}(x, t)] \tilde{n}(x, t)^2 \hat{n}(x, t). \end{aligned} \quad (725)$$

Let us rewrite this action. As one can see from the equation of motion, the combination  $m^2 := \alpha_- - \alpha_+$  measures the distance to criticality (without perturbative corrections). The term proportional to  $\beta$  in the last line gives a quartic term, which is irrelevant. Finally, one can change normalization of the fields, setting  $\hat{n} \rightarrow \lambda \phi$ ,  $\tilde{n} \rightarrow \lambda^{-1} \tilde{\phi}$ , which leaves the quadratic terms invariant, but changes the relative magnitude of the two cubic terms. As a result, we obtain the action with coupling const  $g = \sqrt{\beta(\alpha_+ + \alpha_-)}/2$ ,

$$\begin{aligned} S[\tilde{n}, \hat{n}] &= \int_{x,t} \tilde{\phi}(x, t) [\partial_t \phi(x, t) - \nabla^2 \phi(x, t) + m^2 \phi(x, t)] \\ &+ \int_{x,t} g [\tilde{\phi}(x, t) \phi(x, t)^2 - \tilde{\phi}(x, t)^2 \phi(x, t)]. \end{aligned} \quad (726)$$

Note the relative sign change w.r.t. equation (709). It has four renormalizations, one for each of the three quadratic terms, plus one for the coupling constant  $g$ . This leads to three independent exponents given in section 5.8. Results at two-loop order can be found in [565–568]. Partial three-loop results are given in [570]. The action (726), known as Regge field theory [569], is also used as an effective field theory for deep inelastic scattering. There  $\phi$  and  $\tilde{\phi}$  are interpreted as particle annihilation and creation operators<sup>43</sup>.

## 6.6. State variables of the Manna model

In this section, we apply our considerations to a non-trivial example, the stochastic Manna model, following [587]. We will see that our formalism permits a systematic derivation of its effective stochastic equations of motion. While the result is known in the literature [518, 525, 580, 599], it is there derived by symmetry principles, which are convincing ‘up to a certain degree’. Furthermore, they leave undetermined all coefficients. While many of them can be eliminated by rescaling, our derivation ‘lands’ on a particular line of parameter space, characterized by the absence of additional memory terms, see section 6.9.

The MM, introduced in 1991 by Manna [537], is a stochastic version of the BTW sandpile [513]. Let us recall its definition given in section 5.5:

*Manna model (MM).* Randomly throw grains on a lattice. If the height at one point is greater or equal to two, then with

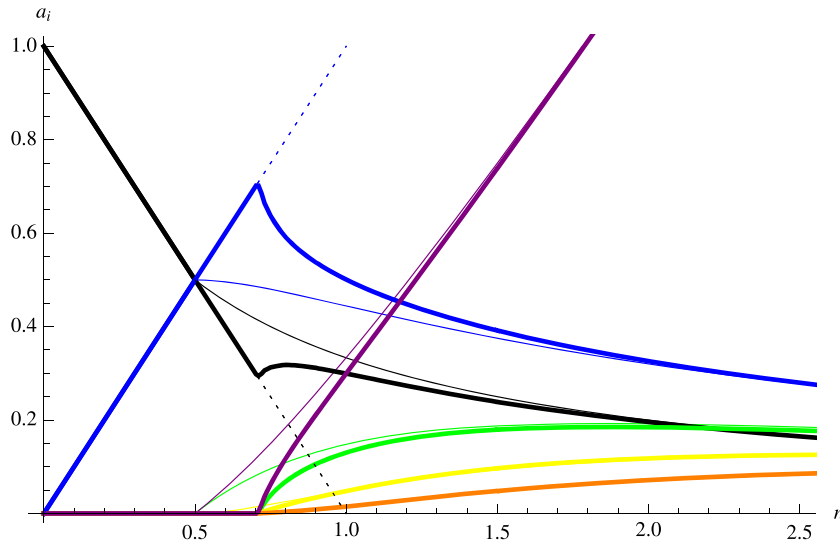


**Figure 68.** (Thick lines) The order parameters of the MM, as a function of  $n$ , the average number of grains per site, obtained from a numerical simulation of the stochastic MM on a grid of size  $150 \times 150$  with periodic boundary conditions. We randomly update a site for  $10^7$  iterations, and then update the histogram 500 times every  $10^5$  iterations. Plotted are the fraction of sites that are: unoccupied (black), singly occupied (blue), double occupied (green), triple occupied (yellow), quadruple occupied (orange). The activity  $\rho = \sum_{i>1} a_i(i - 1)$  is plotted in purple. No data were calculated for  $n < 0.5$ , where  $a_0 = e = 1 - n$ ,  $a_1 = n$ , and  $a_{i>2} = 0$  (inactive phase). Note that before the transition,  $a_0 = 1 - n$  and  $a_1 = n$ . The transition is at  $n = n_c = 0.702$ . (Thin lines) The MF phase diagram, as given by equation (736) and the following equations. For  $n \leq \frac{1}{2}$ , and by equation (737) ff. for  $n \geq \frac{1}{2}$ . We checked the latter with a direct numerical simulation. Reprinted figure with permission from [587], Copyright (2016) by the American Physical Society.

rate 1 move two grains from this site to randomly chosen neighboring sites. Both grains may end up on the same site.

We start by analyzing the phase diagram. We denote by  $a_i$  the fraction of sites with  $i$  grains. It satisfies the sum rule

$$\sum_i a_i = 1. \tag{727}$$

In these variables, the number of grains  $n$  per site can be written as

$$n := \sum_i a_i i. \tag{728}$$

The empty sites are

$$e := a_0. \tag{729}$$

The fraction of active sites is

$$a := \sum_{i \geq 2} a_i. \tag{730}$$

We also define the (weighted) activity as

$$\rho := \sum_{i \geq 2} a_i(i - 1). \tag{731}$$

Note that  $\rho$  satisfies the sum rule

$$n - \rho + e = 1. \tag{732}$$

In order to take full advantage of this sum rule, we change the toppling rules of the MM to those of the

*Weighted Manna model (wMM)*. If a site contains  $i \geq 2$  grains, randomly move these grains to neighboring sites with rate  $(i - 1)$ .

On figure 68 (thick lines), we show a numerical simulation of the MM in a two-dimensional system of size  $L \times L$ ,

with  $L = 150$ . There is a phase transition at  $n = n_c = 0.702$ . Close to  $n_c$ , the fraction of doubly occupied sites  $a_2$  grows linearly with  $n - n_c$ , and higher occupancy is small. Indeed, we checked numerically that for  $n > n_c$  the probability  $p_i$  to find  $i$  grains on a site decays exponentially with  $i$ , i.e.  $p_i \sim \exp(-\alpha_n i)$ , where  $\alpha_n$  depends on  $n$ , see figure 69. This is to be contrasted with the initial condition, where we randomly distribute  $n \times L^2$  grains on the lattice of size  $L \times L$ . It yields a Poisson distribution, the coherent state  $|n\rangle$ , for the number of grains on each site, see inset of figure 69 (left). This result suggests that coherent states may not be the best representation for this system. It further implies that close to the transition,  $\rho \approx a$ , and we expect that the wMM and the original MM have the same critical behavior. We come back to this question below.

### 6.7. Mean-field solution of the Manna model

In order to make analytical progress, we now study the *topple-away* or MF solution of the stochastic Manna sandpile, which we can solve analytically:

*Mean-field Manna model (MF-MM)*. If a site contains two or more grains, move these grains to any randomly chosen sites of the system.

The rate equations are, setting for convenience  $a_{-1} := 0$ :

$$\partial_t a_i = -a_i \Theta(i \geq 2) + a_{i+2} + 2 \left[ \sum_{j \geq 2} a_j \right] (a_{i-1} - a_i). \tag{733}$$

Using the sum rule (727), they can be rewritten as

$$\partial_t a_i = -a_i \Theta(i \geq 2) + a_{i+2} + 2(1 - a_0 - a_1)(a_{i-1} - a_i). \tag{734}$$

We are interested in the steady state  $\partial_t a_i = 0$ . One can solve these equations by introducing a generating function.

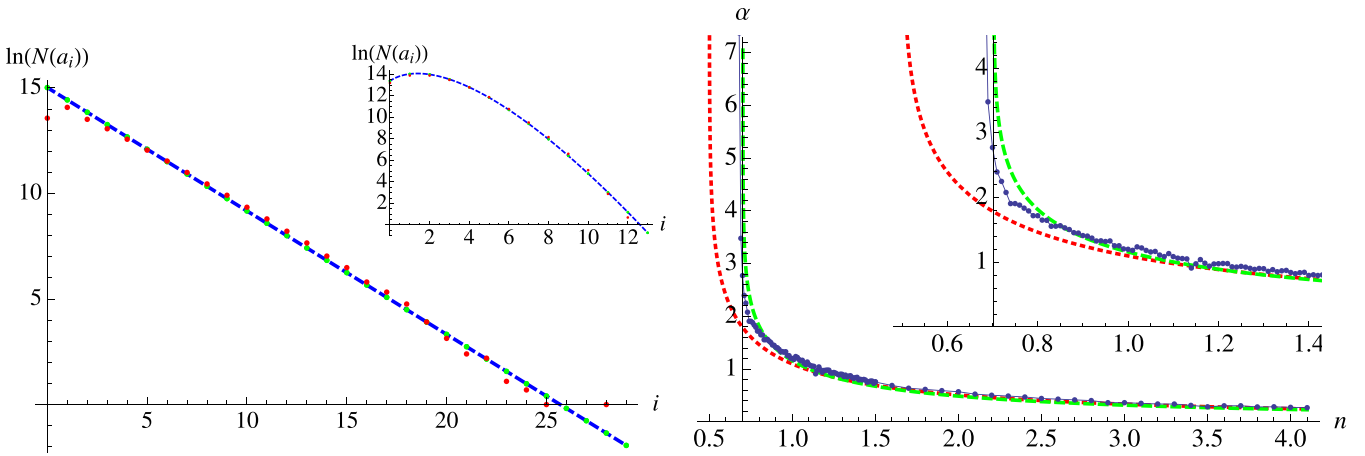


**Figure 69.** (Left) (Unnormalized) histogram after many topplings for  $n = 2$ ; the probability that a site has  $i$  grains decays as  $e^{-0.585i}$ , for all  $i \geq 1$ . (Inset) The initial distribution, a Poissonian. (Right) The exponential decay coefficient  $\alpha$  as a function of  $n$ . The dots are from a numerical simulation. The dashed red line is the MF result (738). The green dashed line is a fit corresponding to  $\alpha \approx \frac{2}{3} \ln \left( \frac{n + n_c}{n - n_c} \right)$ . (Inset) Blow-up of main plot. Reprinted figure with permission from [587], Copyright (2016) by the American Physical Society.

An simpler approach consists in realizing that for  $i \geq 2$ , equation (734) admits a steady-state solution of the form

$$a_i = a_2 \kappa^{i-2}, \quad i > 2. \quad (735)$$

This reduces the number of independent equations  $\partial_t a_i = 0$  in equation (734) from infinity to three. Furthermore, there are the equations  $\sum_{i=0}^{\infty} a_i = 1$ , and  $\sum_{i=0}^{\infty} i a_i = n$ . Thus there are five equations for the four variables  $a_0, a_1, a_2$ , and  $\kappa$ . The reason we apparently have one redundant equation is due to the fact that we already used the normalization condition (727) to go from equation (733) to equation (734).

These equations have two solutions: for  $0 < n < 1$ , there is always the solution for the *inactive* or *absorbing state*,

$$a_0 = 1 - n, \quad a_1 = n, \quad a_{i \geq 2} = 0. \quad (736)$$

For  $n > 1/2$ , there is a second non-trivial solution,

$$a_0 = \frac{1}{1 + 2n}, \quad a_{i > 0} = \frac{4n \left( \frac{2n-1}{2n+1} \right)^i}{4n^2 - 1}. \quad (737)$$

(Note that  $a_2/a_1$  has the same geometric progression as  $a_{i+1}/a_i$  for  $i > 2$ , which we did not suppose in our ansatz.) Thus the probability to find  $i > 0$  grains on a site is given by the exponential distribution

$$p(i) = \frac{4n}{4n^2 - 1} \exp(-i\alpha_n), \quad \alpha_n = \ln \left( \frac{2n + 1}{2n - 1} \right). \quad (738)$$

Using these two solutions, we get the MF phase diagram plotted on figure 68 (thin lines). This has to be compared with the simulation of the MM on the same figure (thick lines). One sees that for  $n \geq 2$ , MF solution and simulation are almost indistinguishable. We also checked with simulations that the MM has a similar exponentially decaying distribution of grains per site, with a decay-constant  $\alpha$  plotted on the right of figure 69.

### 6.8. Effective equations of motion for the Manna model: CDP theory

In this section, we give the effective equations of motion for the MM. Let us start from the MF equations for  $\rho(t)$  and  $n(t)$ . For simplicity we use the wMM. The physics close to the transition should not depend on it. Let us start from the hierarchy of MF equations for the wMM. These are similar to equation (734), and can be rewritten as

$$\partial_t a_i = (1 - i)a_i \Theta(i \geq 2) + (i + 1)a_{i+2} + 2\rho(a_{i-1} - a_i). \quad (739)$$

Let us write explicitly the rate equation for the fraction of empty sites  $e \equiv a_0$ ,

$$\partial_t e = a_2 - 2\rho e. \quad (740)$$

The first term, the gain  $r_+ = a_2$  comes from the sites with two grains, toppling away, and leaving an empty site. The second term, the loss term, is the rate at which one of the toppling grains lands on an empty site,  $r_- = 2\rho e$ .

The formalism developed in section 6.3, equations (715)–(718), demands to add an additional noise:

$$\partial_t e = a_2 - 2\rho e + \sqrt{a_2 + 2\rho e} \bar{\xi}_t, \quad (741)$$

where  $\langle \bar{\xi}_t \bar{\xi}_{t'} \rangle = \delta(t - t')/\ell^d$ , and  $\ell$  is the size of the box which we consider. Close to the transition,  $a_2 \approx \rho$ . Inserting this into the above equation, we arrive at

$$\partial_t e \approx \rho(1 - 2e) + \sqrt{\rho} \sqrt{1 + 2e} \bar{\xi}_t. \quad (742)$$

Next we approximate  $\sqrt{1 + 2e}$  by the value of  $e$  at the transition, i.e.  $e \rightarrow e_c^{\text{MF}} = \frac{1}{2}$ , see the MF phase diagram in figure 68, leading to

$$\partial_t e \approx \rho(1 - 2e) + \sqrt{2\rho} \bar{\xi}_t. \quad (743)$$

This equation consistently gives back  $e_c^{\text{MF}} = \frac{1}{2}$ , used above in the simplification of the noise term.

As the number  $n$  of grains is conserved, with the help of the sum rule  $n + e = \rho + 1$  we can write two more equations,

$$\partial_t n = 0, \quad \partial_t \rho = \partial_t e. \quad (744)$$

Finally, we do not have a single box of size  $\ell$ , but a lattice of boxes, indexed by a  $d$ -dimensional label  $x$ . Each toppling moves two grains from a site to neighboring sites, equivalent to a current

$$J(x, t) = -D\nabla\rho(x, t) + \sqrt{2D\rho(x, t)}\xi(x, t). \quad (745)$$

The diffusion constant is  $D = 2 \times \frac{1}{2d} = \frac{1}{d}$ . The first factor of 2 is due to the fact that two grains topple. The factor of  $\frac{1}{2d}$  is due to the fact that each grain can topple in any of the  $2d$  directions, thus the rate  $D$  per direction is  $\frac{1}{2d}$ , resulting into  $D = 1/d$ . As discussed above, we drop the noise term as subdominant.

This current corrects both the activity  $\rho(x, t)$ , as the number of grains  $n(x, t)$ , resulting into the same contribution for both  $\partial_t \rho(x, t)$ , and  $\partial_t n(x, t)$ . It does not couple to the density of empty sites. This is consistent with the sum-rule (732)  $n - \rho + e = 1$ , which implies that  $\partial_t \rho(x, t) \equiv \partial_t n(x, t) + \partial_t e(x, t)$ .

In conclusion, we have the set of equations

$$\partial_t e(x, t) = [1 - 2e(x, t)]\rho(x, t) + \sqrt{2\rho(x, t)}\xi(x, t), \quad (746)$$

$$\partial_t \rho(x, t) = \frac{1}{d}\nabla^2 \rho(x, t) + \partial_t e(x, t), \quad (747)$$

$$\langle \xi(x, t)\xi(x', t') \rangle = \delta^d(x - x')\delta(t - t'). \quad (748)$$

Instead of writing coupled equations for  $e(x, t)$  and  $\rho(x, t)$ , with the help of the sum rule (732) we can also write coupled equations for  $\rho(x, t)$  and  $n(x, t)$ :

$$\begin{aligned} \partial_t \rho(x, t) &= \frac{1}{d}\nabla^2 \rho(x, t) + [2n(x, t) - 1]\rho(x, t) - 2\rho(x, t)^2 \\ &\quad + \sqrt{2\rho(x, t)}\xi(x, t), \end{aligned} \quad (749)$$

$$\partial_t n(x, t) = \frac{1}{d}\nabla^2 \rho(x, t). \quad (750)$$

Equations (749) and (750) are known as the equations of motion for the conserved directed percolation (C-DP) class. They were obtained in the literature [518, 525, 580, 599] by means of symmetry principles. This leaves all coefficients undefined, and does not ensure that equation (746) is *local*. This locality will prove essential in the next section. The derivation above is due to [587].

### 6.9. Mapping of the Manna model to disordered elastic manifolds

It had been conjectured for a long time that the MM and depinning of disordered elastic manifolds are equivalent, and much work was devoted to clarify this connection [518, 520, 600]. The identification of fields which finally led to a simple proof of this equivalence is given in [601], followed by [602],

$$\rho(x, t) = \partial_t u(x, t) \quad (\text{the velocity of the interface}), \quad (751)$$

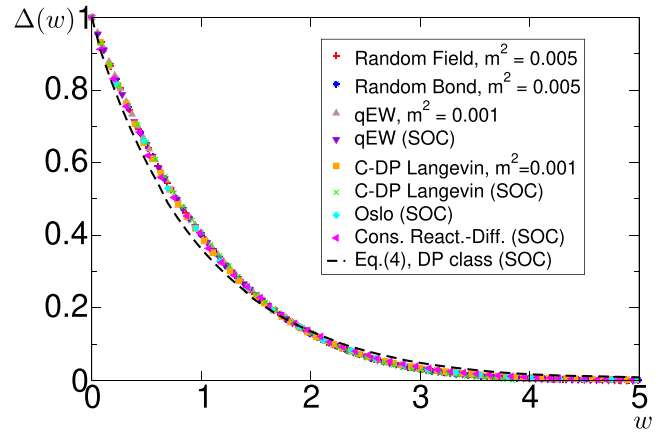


**Figure 70.** The renormalized disorder correlator  $\Delta(u)$ , rescaled to  $\Delta(0) = 1$  and  $\int_u \Delta(u) = 1$ , for several situations: RF and RB disorder for a disordered elastic manifolds, the Oslo and MMs, as well as C-DP, all in  $d = 1$ . Reprinted figure with permission from [518], Copyright (2009) by the American Physical Society.

$$e(x, t) = \mathcal{F}(x, t) \quad (\text{the force acting on it}). \quad (752)$$

The second equation (747) is the time derivative of the equation of motion of an interface, subject to a random force  $\mathcal{F}(x, t)$ ,

$$\partial_t u(x, t) = \frac{1}{d}\nabla^2 u(x, t) + \mathcal{F}(x, t). \quad (753)$$

Since  $\rho(x, t)$  is positive for each  $x$ ,  $u(x, t)$  is monotonously increasing. Instead of parameterizing  $\mathcal{F}(x, t)$  by space  $x$  and time  $t$ , it can be written as a function of space  $x$  and *interface position*  $u(x, t)$ . Setting  $\mathcal{F}(x, t) \rightarrow F(x, u(x, t))$ , the first equation (746) becomes

$$\begin{aligned} \partial_t \mathcal{F}(x, t) &\rightarrow \partial_t F(x, u(x, t)) \\ &= \partial_u F(x, u(x, t)) \partial_t u(x, t) \\ &= [1 - 2F(x, u(x, t))] \partial_t u(x, t) \\ &\quad + \sqrt{2\partial_t u(x, t)}\xi(x, t). \end{aligned} \quad (754)$$

For each  $x$ , this equation is equivalent to the Ornstein–Uhlenbeck [603] process  $F(x, u)$ , defined by

$$\partial_u F(x, u) = 1 - 2F(x, u) + \sqrt{2}\xi(x, u), \quad (755)$$

$$\langle \xi(x, u)\xi(x', u') \rangle = \delta^d(x - x')\delta(u - u'). \quad (756)$$

It is a Gaussian Markovian process with mean  $\langle F(x, u) \rangle = 1/2$ , and variance in the steady state of, see equation (387)

$$\begin{aligned} &\left\langle \left[ F(x, u) - \frac{1}{2} \right] \left[ F(x', u') - \frac{1}{2} \right] \right\rangle \\ &= \frac{1}{2} \delta^d(x - x') e^{-2|u - u'|}. \end{aligned} \quad (757)$$

Writing the equation of motion (753) as

$$\partial_t u(x, t) = \frac{1}{d}\nabla^2 u(x, t) + F(x, u(x, t)), \quad (758)$$

it is interpreted as the motion of an interface with *position*  $u(x, t)$ , subject to a disorder force  $F(x, u(x, t))$ . The latter is

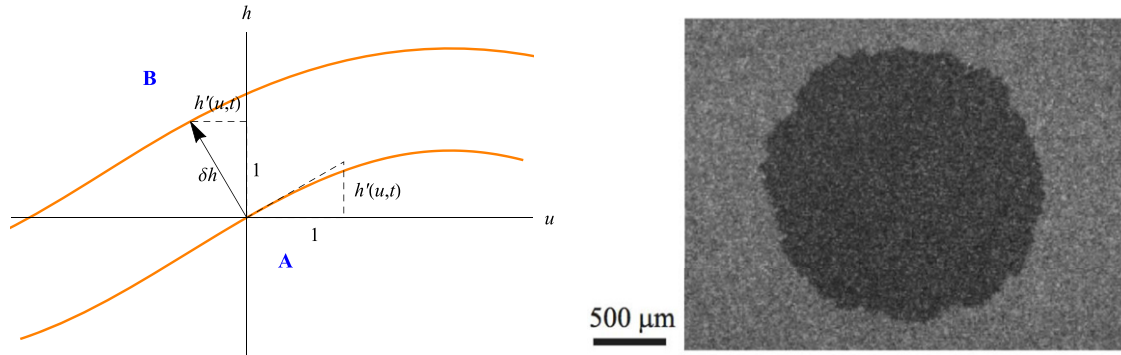


**Figure 71.** (Left) An interface growing in its normal direction, with phase A invading phase B. (Right) An experimental realization using two phases of a nematic liquid crystal. Reprinted by permission from Springer Nature Customer Service Centre GmbH: Springer. J. Stat. Phys. [606] (c) 2012.

$\delta$ -correlated in the  $x$ -direction, and short-ranged correlated in the  $u$ -direction. In other words, this is a disordered elastic manifold subject to RF disorder. As a consequence, the field-theoretic results of sections 3.2–3.5 are also valid for the MM.

Equation (749) has a quite peculiar property, namely the factor of 2 in front of both  $n(x, t)\rho(x, t)$  and  $-\rho(x, t)^2$ . As a consequence, equation (746) does not contain a term  $\sim \rho^2(x, t)$ , which would spoil the simple mapping presented above. The absence of this term *cannot* be induced on symmetry arguments only. How this additional term, if present, can be treated is discussed in [601].

The mapping of the MM on disordered elastic manifolds implies that properties of the latter should be measurable in the former. As we discussed in sections 2.5 to 2.11, and sections 3.2 to 3.5, a key feature of the theory of disordered elastic manifolds is the existence of a renormalized disorder correlator with a cusp. Its existence in the MM, and equivalence to the one measured at depinning was established in the beautiful work [518]. The resulting (rescaled) disorder correlators  $\Delta(w)$  are shown in figure 70: it confirms the equivalence of depinning with both RB and RF disorder, C-DP, Oslo, and several sandpile automata.

*Remarks on the short-time dynamics of the Manna model.* The short-time dynamics of the MM has been measured in several publications [395–397], and was interpreted as the dynamical exponent  $z$  depending on the initial condition. We cannot follow this logic: the critical exponent  $z$  is a bulk property of the system, and as such is defined only after memory of the initial state is erased. What is possible is that the initial-time critical exponent discussed in section 3.19 depends on the initial condition. Simulations for much larger systems are needed to settle this question.

## 7. KPZ, Burgers, and the directed polymer

In this section we review basic properties for the non-linear surface growth known as the KPZ equation [560]. KPZ matters for disordered systems and the subject of this review for its multiple connections:

- mapping of the  $N$ -dimensional KPZ equation to the  $N$ -component directed polymer (random manifold with  $d = 1$ ),

- mapping of the  $N$ -dimensional decaying Burgers or KPZ equation to a particle (formally a random manifold with  $d = 0$ ) in  $N$  dimensions,
- non-linear surface growth terms à la KPZ appear for disordered systems, producing the distinct quenched KPZ class discussed in section 5.7.

For further reading on non-linear surface growth we refer to the 1997 review by Krug [604]. A short summary of modern developments can be found in [605].

*Notation.* We use  $N$  for the dimension of the KPZ equation instead of  $d$ , keeping  $d$  for the random-manifold dimension with  $N$  components, i.e. living in  $N$  dimensions. The  $N$ -dimensional KPZ equation will be shown to be equivalent to the directed polymer ( $d = 1$ ) in  $N$  dimensions.

### 7.1. Non-linear surface growth: KPZ equation

Consider figure 71. What is seen is an interface between two phases, A and B. Phase A is stable, while phase B is unstable. The interface grows with a velocity  $\lambda(u, t)$  in its normal direction, increasing phase A, while diminishing phase B. Using the Monge representation  $\{u, h(u, t)\}$ ,  $u \in \mathbb{R}^N$  the growth in  $h$  direction is given by (see figure)

$$\delta h = \sqrt{1 + [\nabla h(u, t)]^2} \lambda(u, t) \delta t. \quad (759)$$

Assume that the growth is due to a discrete process. Following the prescription in section 6.3, the growth velocity  $\lambda(u, t)$  has a mean  $\lambda$  plus fluctuations  $\eta(u, t)$ ,

$$\begin{aligned} \lambda(u, t) &= \lambda + \eta(u, t), \\ \langle \eta(u, t) \eta(u', t') \rangle &= 2D \delta(t - t') \delta^N(u - u'). \end{aligned} \quad (760)$$

This leads to

$$\partial_t h(u, t) = \lambda + \frac{\lambda}{2} [\nabla h(u, t)]^2 + \eta(u, t) + \dots, \quad (761)$$

where the dots indicate higher-order terms in  $(\nabla h)^2$ . This is (almost) the famous KPZ [560] equation. To derive the latter, we first subtract the growth for a flat interface, setting  $h \rightarrow h - \lambda t$ , and finally add one more term to the equation

$$\partial_t h(u, t) = \nu \nabla^2 h(u, t) + \frac{\lambda}{2} [\nabla h(u, t)]^2 + \eta(u, t). \quad (762)$$

The additional term proportional to  $\nu$  describes diffusion along the interface, rendering it smoother.

One typically measures the two-point function

$$\langle [h(x, t) - h(x', t')]^2 \rangle \simeq |x - x'|^{2\zeta_{\text{KPZ}}} f(x^{\zeta_{\text{KPZ}}}/t), \quad (763)$$

where  $f$  goes to a constant for  $t \rightarrow 0$  ( $x \rightarrow \infty$ ), and together with its prefactor becomes independent of  $x$  for  $x \rightarrow 0$ . This defines two exponents, the roughness  $\zeta_{\text{KPZ}}$  and the dynamic exponent  $z_{\text{KPZ}}$ . The added index allows us to distinguish it from the exponents of the directed polymer, especially since we will see later that  $z_{\text{KPZ}} = 1/\zeta_{\text{directed polymer}}$ .

## 7.2. Burgers equation

Taking one spatial derivative of equation (762) yields Burgers' equation [607]. Define

$$v(u, t) := \nabla h(u, t). \quad (764)$$

Burgers' equation reads

$$\partial_t v(u, t) = \nu \nabla^2 v(u, t) + \frac{\lambda}{2} \nabla [v(u, t)^2] + \nabla \eta(u, t), \quad (765)$$

$$\langle \eta(u, t) \eta(u', t') \rangle = 2D \delta(t - t') \delta^N(u - u'). \quad (766)$$

The non-linear term satisfies the identity

$$\begin{aligned} \frac{1}{2} \sum_i \partial_j [v_i(u, t)^2] &\equiv \frac{1}{2} \sum_i \partial_j [\partial_i h(u, t)^2] \\ &= \sum_i [\partial_i h(u, t)] [\partial_j \partial_i h(u, t)] \equiv \sum_i [v_i(u, t) \partial_i] v_j(u, t). \end{aligned} \quad (767)$$

Equation (765) can be written as

$$\partial_t v(u, t) = \nu \nabla^2 v(u, t) + \lambda [v(u, t) \cdot \nabla] v(u, t) + \nabla \eta(u, t). \quad (768)$$

This is identical to Navier–Stokes' equation for incompressible fluids, with the crucial difference that Burgers' velocity is a total derivative,  $v(u, t) = \nabla h(u, t)$ , whereas for Navier–Stokes it is divergence free,  $\nabla \cdot v(u, t) = 0$ . For this reason, Burgers equation does not describe turbulence encountered e.g. in a fast-flowing river. It has, however, applications to the large-scale structure of galaxies [608–610].

## 7.3. Cole–Hopf transformation

Consider the  $N$ -dimensional KPZ equation (762) in Itô discretization, with noise as given in Equation (760). We can eliminate the non-linear term by the so-called *Cole–Hopf transformation* [611, 612]

$$\begin{aligned} Z(u, t) &:= e^{\frac{\lambda}{2\nu} h(u, t) - D \frac{\lambda^2}{4\nu^2} t} \\ \iff h(u, t) &= \frac{2\nu}{\lambda} \ln Z(u, t) + \frac{D\lambda}{2\nu} t. \end{aligned} \quad (769)$$

(The reader might see this transformation without the term  $-D\lambda^2 t/(4\nu^2)$ ; this is then done in mid-point, i.e. Stratonovich

discretization [2, 298, 299], see appendix A.4). Using Itô calculus (appendix A.2), we obtain

$$\begin{aligned} dZ(u, t) &= \frac{\lambda}{2\nu} Z(u, t) dh(u, t) + \frac{\lambda^2}{8\nu^2} Z(u, t) dh(u, t)^2 \\ &\quad - \frac{D\lambda^2}{4\nu^2} Z(u, t) dt \\ &= \frac{\lambda}{2\nu} Z(u, t) \left\{ \left( \nu \nabla^2 h(u, t) + \frac{\lambda}{2} [\nabla h(u, t)]^2 \right) dt \right. \\ &\quad \left. + d\eta(u, t) \right\} \\ &= \nu \nabla^2 Z(u, t) dt + Z(u, t) \frac{\lambda}{2\nu} d\eta(u, t). \end{aligned} \quad (770)$$

Noting  $\lambda \eta(u, t) \equiv V(u, t)$  this can be written as

$$\partial_t Z(u, t) = \nu \nabla^2 Z(u, t) + \frac{1}{2\nu} V(u, t) Z(u, t), \quad (771)$$

$$\langle V(u, t) V(u', t') \rangle = \delta(t - t') R(u - u'), \quad (772)$$

$$R(u) = 2\lambda^2 D \delta^N(u). \quad (773)$$

## 7.4. KPZ as a directed polymer

The equation of motion (771) can be solved by

$$Z(u, t|V) = \int_{u(t_i)=u_i}^{u=u(t)} \mathcal{D}[u] e^{-\frac{1}{2} \int_{t_i}^t d\tau \frac{1}{2} u'(\tau)^2 - V(u(\tau), \tau)}, \quad (774)$$

$$T = 2\nu.$$

This is the path integral of a directed polymer in the quenched random potential  $V(u)$ , also referred to as the Feynman–Kac formula [613, 614]. To average over disorder, we use the formalism with  $n$  replicas introduced in section 1.5,

$$\begin{aligned} Z(u_1, \dots, u_n, t) &= \prod_{\alpha=1}^n \int_{u_\alpha(t_i)=u_{\alpha,i}}^{u_\alpha(t)=u_\alpha} \mathcal{D}[u_\alpha] \int \mathcal{D}[V] \\ &\quad \times e^{-\frac{1}{2} \int_{t_i}^t d\tau \sum_{\alpha=1}^n \left[ \frac{1}{2} u'_\alpha(\tau)^2 + V(u_\alpha(\tau)) \right]} e^{-\frac{1}{4\lambda^2 D} \int_{u,\tau} V(u, \tau)^2} \\ &= \prod_{\alpha=1}^n \int_{u_\alpha(t_i)=u_{\alpha,i}}^{u_\alpha(t)=u_\alpha} \mathcal{D}[u_\alpha] \\ &\quad \times e^{-\int_{t_i}^t d\tau \sum_{\alpha} \frac{1}{2T} u'_\alpha(\tau)^2 - \frac{1}{2T^2} \sum_{\alpha, \beta} R(u_\alpha(\tau) - u_\beta(\tau))}. \end{aligned} \quad (775)$$

We had discussed its solution in the  $T \rightarrow 0$ -limit in section 1.5, see equation (30).

Using equations (774) and (769), the free energy of a directed polymer is related to the KPZ height field  $h(u, t)$  via

$$\mathcal{F}(u, t) := -T \ln Z(u, t) \equiv -\lambda h(u, t) + \frac{D\lambda^2}{2\nu} t. \quad (776)$$

Apart from the (last) drift term which is due to the discretization scheme and which can always be subtracted, this relation is valid in the inviscid limit  $\nu \rightarrow 0$ , equivalent to  $T \rightarrow 0$ , i.e. for

the ground state of the directed polymer. For further reading we refer to [615].

### 7.5. Galilean invariance, and scaling relations

A scaling analysis of the KPZ equation (762) starts at [604]

$$\tilde{h}(u, t) = b^{-\zeta_{\text{KPZ}}} h(bu, b^{z_{\text{KPZ}}} t) \quad (777)$$

with a roughness exponent  $\zeta_{\text{KPZ}}$  and a dynamical exponent  $z_{\text{KPZ}}$  defined in equation (763). The rescaled field  $\tilde{h}$  satisfies a KPZ equation (762) with rescaled coefficients

$$\begin{aligned} \tilde{\nu} &= b^{z_{\text{KPZ}}-2} \nu, & \tilde{D} &= b^{z_{\text{KPZ}}-d-2\zeta_{\text{KPZ}}} D, \\ \tilde{\lambda} &= b^{z_{\text{KPZ}}+\zeta_{\text{KPZ}}-2} \lambda. \end{aligned} \quad (778)$$

If  $\lambda = 0$ , the scaling of the diffusion equation  $\zeta_{\text{KPZ}} = (2 - N)/2$ , and  $z_{\text{KPZ}} = 2$  yields a fixed point of the coarse graining transformation (777). For  $\lambda \neq 0$ , the non-linearity  $\lambda$  grows if the combination  $\zeta_{\text{KPZ}} + z_{\text{KPZ}} - 2 \rightarrow \frac{2-N}{2}$  is positive. This is always the case in dimension  $N < 2$ . As we will see below in section 7.8 for dimension  $N > 2$  there is a transition between a weak-coupling and a strong-coupling regime.

The KPZ equation has an important invariance in any dimension  $N$  [560, 604, 616]. Consider the tilt transformation parameterized by an  $N$ -dimensional vector  $c$ ,

$$h'(u, t) = h(u + \lambda ct, t) + cu + \frac{\lambda}{2} c^2 t. \quad (779)$$

For  $\lambda \rightarrow 0$ , this reduces to the STS (66). It is reminiscent of the full rotational invariance of the growing surface before passing to the Monge representation (759). As a consequence, we expect the KPZ equation to remain invariant under this transformation. Indeed,  $h'$  satisfies the same KPZ equation (762) as  $h$ , with a shifted noise

$$\eta'(u, t) = \eta(u + \lambda ct, t). \quad (780)$$

As long as the temporal correlations of  $\eta$  are sufficiently short ranged, the shift does not affect the statistical properties of the noise [617], and the statistics of  $h$  is invariant under the transformation (779). In the literature this property is referred to as Galilean invariance, as in the context of the stirred Burgers equation (765), where it was first discussed in [616], it appears as a shift in the velocity,  $v \rightarrow v' = v + \lambda c$ .

As the tilt transformation explicitly contains the non-linearity  $\lambda$ , the latter should not change under rescaling. From equation (778) we conclude that at a fixed point with  $\lambda \neq 0$  [617–619]

$$\zeta_{\text{KPZ}} + z_{\text{KPZ}} = 2. \quad (781)$$

To make contact with the scaling properties of the directed polymer, we remind the exponent relation (47) for the free energy of an elastic manifold,  $\mathcal{F} \sim L^\theta$ , with  $\theta = d - 2 + 2\zeta$ . The directed polymer has internal dimension  $d = 1$ . Using that according to equation (769) the free energy identifies with  $h$ , and that the length  $L$  of the directed polymer is the time in the KPZ equation, we arrive at  $h \hat{=} \mathcal{F} \sim L^\theta \hat{=} t^\theta$ . On the other hand

$h \sim u^{\zeta_{\text{KPZ}}}$  and  $u \sim t^{1/z_{\text{KPZ}}}$ , such that

$$\theta = 2\zeta - 1 = \frac{\zeta_{\text{KPZ}}}{z_{\text{KPZ}}} = \frac{2 - z_{\text{KPZ}}}{z_{\text{KPZ}}}, \quad (782)$$

where for the last identity equation (781) was used. This implies that

$$z_{\text{KPZ}} = \frac{1}{\zeta}. \quad (783)$$

While the notations in the literature are somehow divergent, the prevailing ones seem to be

$$\alpha \equiv \chi \equiv \zeta_{\text{KPZ}}, \quad \beta = \frac{\zeta_{\text{KPZ}}}{z_{\text{KPZ}}} \equiv \theta, \quad z = z_{\text{KPZ}} \equiv \frac{1}{\zeta}. \quad (784)$$

### 7.6. A field theory for the Cole–Hopf transform of KPZ

Another possibility to obtain a field theory for equations (771)–(773) is to write the partition function for the  $n$ -times replicated field  $Z_\alpha$ ,  $\alpha = 1, \dots, n$ , i.e.  $Z \in \mathbb{R}^n$ , as

$$\mathcal{Z} = \int \mathcal{D}[Z] \mathcal{D}[\tilde{Z}] \mathcal{D}[V] e^{-\mathcal{S}_{\text{CH}}[Z, \tilde{Z}, V]}, \quad (785)$$

$$\begin{aligned} \mathcal{S}_{\text{CH}}[Z, \tilde{Z}, V] &= \int_{u,t} \tilde{Z}(u, t) \left[ \partial_t Z(u, t) - \nu \nabla^2 Z(u, t) - \frac{1}{2\nu} V(u, t) Z(u, t) \right] \\ &+ \frac{1}{4\lambda^2 D} \int_{u,t} V(u, t)^2. \end{aligned} \quad (786)$$

Performing the integral over  $V$  we obtain

$$\mathcal{Z} = \int \mathcal{D}[Z] \mathcal{D}[\tilde{Z}] e^{-\mathcal{S}_{\text{CH}}[Z, \tilde{Z}]}, \quad (787)$$

$$\begin{aligned} \mathcal{S}_{\text{CH}}[Z, \tilde{Z}] &= \int_{u,t} \tilde{Z}(u, t) \left[ \partial_t Z(u, t) - \nu \nabla^2 Z(u, t) \right] \\ &- \frac{\lambda^2 D}{4\nu^2} \left[ \tilde{Z}(u, t) Z(u, t) \right]^2. \end{aligned} \quad (788)$$

Replacing  $t \rightarrow t/\nu$ , we arrive at

$$\begin{aligned} \mathcal{S}_{\text{CH}}[Z, \tilde{Z}] &= \int_{u,t} \tilde{Z}(u, t) \left[ \partial_t Z(u, t) - \nabla^2 Z(u, t) \right] \\ &- \frac{g}{2} \left[ \tilde{Z}(u, t) Z(u, t) \right]^2, \end{aligned} \quad (789)$$

$$g = \frac{\lambda^2 D}{2\nu^3}. \quad (790)$$

Note that we do not need to take the limit of  $n \rightarrow 0$  at the end. This is allowed as in Itô calculus the partition function  $\mathcal{Z} = 1$ . To study the flow of the effective coupling constant  $g$ , we need at least two distinct ‘replicas’, which can be thought of as ‘worldlines’ of two particles, starting at different initial positions.

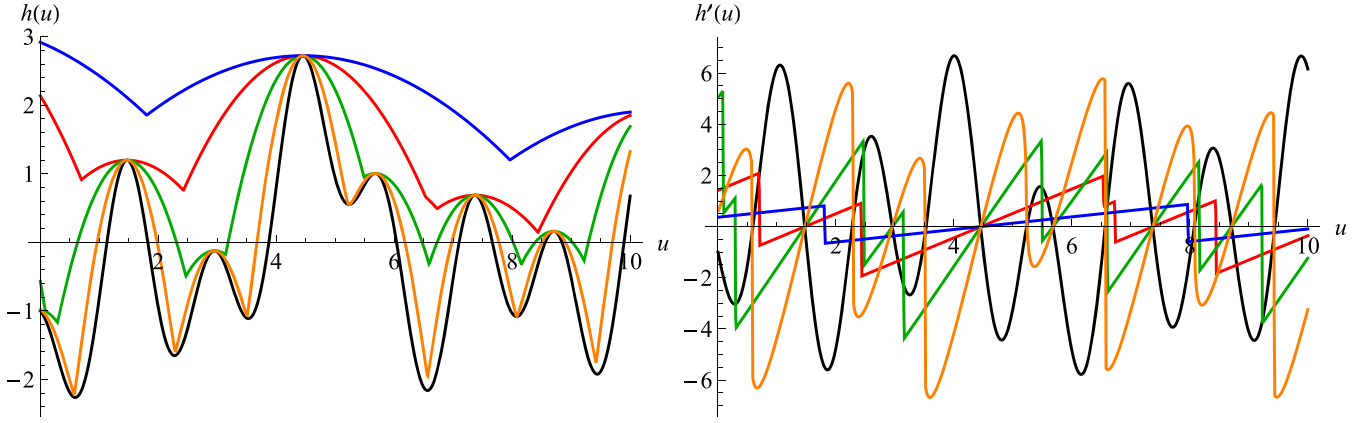


**Figure 72.** (Left) Evolution of a random initial condition (black) at times  $\lambda t = 0$  (black, bottom),  $1/16$  (orange),  $1/4$  (green),  $1$  (red), and  $4$  (blue). (Right) Evolution of a random initial condition (black) at times  $\lambda t = 0$  (black, bottom) for the Burgers velocity  $v(u) := h'(u)$ .

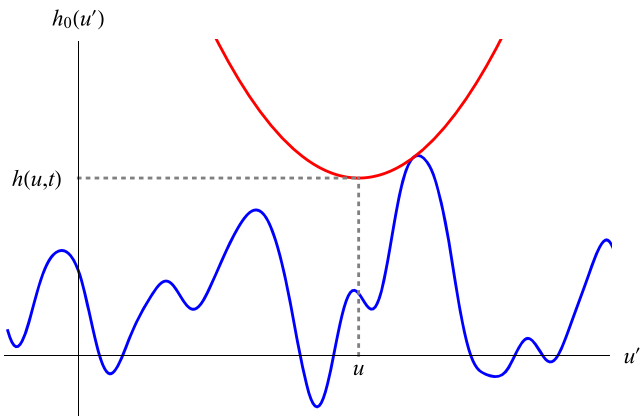


**Figure 73.** A geometrical solution to equation (793) is obtained by moving a parabola of curvature  $1/(2\lambda t)$  and centered at  $u$  (in red) down until it hits  $h_0(u')$  in blue. Its minimum is then at  $h(u, t)$ . (This construction is already discussed in the 1979 paper by Kida [187].)

7.7. Decaying KPZ, and shocks

To better understand the behavior of the KPZ equation (762), let us consider equation (762) for given initial condition  $h_0(u) := h(u, t = 0)$ , in absence of the noise  $\eta(u, t)$ , i.e.  $D = 0$ . The Cole–Hopf transformed KPZ equation (771) reduces to a diffusion equation, solved as

$$Z(u, t) = \int_{u'} \frac{e^{-\frac{(u-u')^2}{4\nu t}}}{(4\pi\nu t)^{d/2}} Z(u', 0). \tag{791}$$

Putting back the definition (769) of  $Z$  in terms of  $h_0(u) := h(u, t = 0)$ , we obtain, since  $D = 0$ ,

$$e^{\frac{\lambda}{2\nu} h(u, t)} = \int_{u'} \frac{e^{\frac{\lambda}{2\nu} \left[ h_0(u') - \frac{(u-u')^2}{2\lambda t} \right]}}{(4\pi\nu t)^{d/2}}. \tag{792}$$

It is interesting to consider the limit of  $\nu \rightarrow 0$ , equivalent to  $T \rightarrow 0$  for the directed polymer (774). Then the solution to equation (792) is

$$h(u, t) = \max_{u'} \left[ h_0(u') - \frac{(u - u')^2}{2\lambda t} \right]. \tag{793}$$

This solution is formally equivalent to the solution (96) of the toy model introduced in section 2.10, replacing

$$-h_0(u) \rightarrow V(u) \quad (\text{microscopic disorder}) \tag{794}$$

$$\frac{1}{\lambda t} \rightarrow m^2 \tag{795}$$

$$-h(u, t) \rightarrow \hat{V}(u) \quad (\text{effective disorder at scale } m^2 = \frac{1}{\lambda t}). \tag{796}$$

As observed there and shown in figure 72 for a random initial condition, the function  $h(u, t)$  is composed of almost parabolic pieces, continuous everywhere but not differentiable at the junctures. Geometrically, this can be obtained by approaching a parabola of curvature  $m^2 = 1/(\lambda t)$  from the top, and reporting as a function of its center  $u$  the position  $h(u, t)$  at which it first touches the initial condition  $h_0(u')$ . This construction is shown in figure 73. More can be learned via this approach, see [82].

7.8. All-order  $\beta$ -function for KPZ

As we had seen after equation (778), the Gaussian fixed point ( $\lambda = 0$ ) is stable for weak disorder as long as the number  $N$  of dimensions is larger than 2. We now show that for  $N > 2$  there exists a phase transition between the weak-coupling phase (Gaussian fixed point), and a strong-coupling phase. This transition is accessible to a standard perturbative RG treatment, contrary to the strong-coupling phase which is not.

Perturbative RG treatments of the KPZ equation are numerous, starting with the original work [560]. They were extended to two-loop order in [620–624], leading to some controversy finally resolved in [625]. The treatment is much easier for the Cole–Hopf transformed version [626, 627], allowing us to resum perturbation theory to all orders. We now calculate the  $\beta$ -function associated to the model (789) and (790), following [627]. To this aim we introduce the graphical notation

$$\text{[Diagram]} := \int_{u, t} \left[ \tilde{Z}(u, t) Z(u, t) \right]^2. \tag{797}$$

Then the only diverging diagrams are chains of , of the form , and so on. Higher-order vertices are irrelevant in perturbation theory. As a result, the effective coupling constant is

$$g_{\text{eff}} \text{ (loop) } = g \text{ (loop) } + g^2 \text{ (chain of 2 loops) } + g^3 \text{ (chain of 3 loops) } + g^4 \text{ (chain of 4 loops) } + \dots + \text{higher order vertices.} \quad (798)$$

In Fourier-representation with incoming momentum  $p$  and frequency  $\omega$ , each chain in equation (798) factorizes, i.e. can be written as a product of the vertex  times a power of the elementary loop diagram (which is a function of  $p$  and  $\omega$ ):

$$\begin{aligned} & \xrightarrow{p, \omega} \underbrace{\text{(chain of } n \text{ loops)}}_{n \text{ loops}} \\ & = \left( \text{(loop)}_{p, \omega} \right)^n \text{ (loop)}_{p, \omega}. \end{aligned} \quad (799)$$

Equation (798) is a geometric sum which yields the effective four-point function

$$g_{\text{eff}} = \Gamma_{ZZ\bar{Z}\bar{Z}}|_{p, \omega} = \frac{g}{1 - g \text{ (loop)}_{p, \omega}}. \quad (800)$$

The elementary diagram is

$$\begin{aligned} & \xrightarrow{p, \omega} \text{(loop)}_{p, \omega} \\ & = \int \frac{d^N k}{(2\pi)^N} \int \frac{d\nu}{2\pi} \frac{1}{\left(\frac{p}{2} + k\right)^2 + i\left(\frac{\omega}{2} + \nu\right)} \frac{1}{\left(\frac{p}{2} - k\right)^2 + i\left(\frac{\omega}{2} - \nu\right)} \\ & = a \left(\frac{1}{2}p^2 + i\omega\right)^{N/2-1}, \quad a = \frac{1}{(8\pi)^{N/2}} \Gamma\left(1 - \frac{N}{2}\right). \end{aligned} \quad (801)$$

This integral is divergent for any  $p$  and  $\omega$  when  $N \rightarrow 2$ . Renormalization means to absorb this divergence into a reparametrization of the coupling constant  $g$ : we claim that the four-point function (the effective coupling  $g_{\text{eff}}$ ) is finite (renormalized) as a function of  $g_r$  instead of  $g$ , upon setting

$$g = Z_g g_r \mu^{-\varepsilon}, \quad Z_g = \frac{1}{1 + a g_r}, \quad \varepsilon = N - 2. \quad (802)$$

$\mu$  is an arbitrary scale, the *renormalization scale*. As a function of  $g_r$ , the four-point function reads

$$\Gamma_{ZZ\bar{Z}\bar{Z}}|_{p, \omega} = \frac{g_r \mu^{-\varepsilon}}{1 + (a - \mu^{-\varepsilon} \text{ (loop)}_{p, \omega}) g_r}. \quad (803)$$

Since  $\frac{1}{\varepsilon} \left(\frac{1}{2}p^2 + i\omega\right)^{\varepsilon/2} \mu^{-\varepsilon}$  is finite for  $\varepsilon > 0$  as long as the combination  $\frac{1}{2}p^2 + i\omega$  is finite, it can be read off from equation (803) that  $\Gamma_{ZZ\bar{Z}\bar{Z}}|_{p, \omega}$  is finite even in the limit of  $\varepsilon \rightarrow 0$ . (If useful, either  $p = 0$  or  $\omega = 0$  may safely be taken.) This completes the proof. Note that this ensures that the model is renormalizable to all orders in perturbation-theory, what is normally a formidable task to show [112–115, 118, 628, 629].

The  $\beta$ -function that we calculate now is exact to all orders in perturbation theory. It is defined as the variation of the renormalized coupling constant, keeping the bare one fixed

$$\beta(g_r) = -\mu \frac{\partial}{\partial \mu} \Big|_g g_r. \quad (804)$$

From equation (803) we see that it gives the dependence of the four-point function on  $p$  and  $\omega$  for fixed bare coupling. The relation between  $g$  and  $g_r$  is

$$g = \frac{g_r \mu^{-\varepsilon}}{1 + a g_r} \Leftrightarrow g_r = \frac{g}{\mu^{-\varepsilon} - a g}, \quad (805)$$

and hence

$$\beta(g_r) = -\varepsilon g_r (1 + a g_r). \quad (806)$$

Using  $a$  from equation (801), our final result is

$$\beta(g_r) = (2 - N)g_r + \frac{2}{(8\pi)^{N/2}} \Gamma\left(2 - \frac{N}{2}\right) g_r^2. \quad (807)$$

This equation has a perturbative, IR repulsive, fixed point at

$$g_r^* = \frac{2(8\pi)^{N/2}}{(N - 2)\Gamma\left(2 - \frac{N}{2}\right)}. \quad (808)$$

For  $N > 2$  it describes the phase transition between the weak-coupling phase where the KPZ term is irrelevant ( $g = 0$ ), and a strong coupling phase, for which  $g \rightarrow \infty$ . This is the only fixed point available for  $N \leq 2$ ; especially, the perturbative treatment above does not describe KPZ in dimension  $N = 1$ .

As a consequence, standard perturbation theory fails to produce a strong-coupling fixed point, a result which cannot be overemphasized. This means that any treatment of the strong coupling regime has to rely on NP *methods*. The FRG approach discussed above qualifies as NP in this sense, since FRG follows more than the flow of a single coupling constant. It does of course not rule out the possibility to find an exactly solvable model, distinct from KPZ, for which it is possible to expand toward the strong-coupling regime of KPZ.

Let us also note that the  $\beta$ -function is divergent at  $N = 4$ , and therefore our perturbation expansion breaks down at  $N = 4$ . To cure the problem, a lattice regularized version of equation (771) may be used. However, then the lattice cut-off  $a$  will enter into the equations and the result is no longer model-independent. This may be interpreted as  $N = 4$  being the upper critical dimension of KPZ, or as a sign for a simple technical problem. See [412, 630], and the discussion in section 7.11.

### 7.9. Anisotropic KPZ

A special case is the anisotropic KPZ equation in two dimensions, for which the KPZ-nonlinearity is positive in one direction, and negative in the other. This competition produces a perturbative fixed point [631].

### 7.10. KPZ with spatially correlated noise

When the noise  $\eta(u, t)$  in equation (762) is LR correlated,

$$\langle \eta(u, t) \eta(u', t') \rangle = \delta(t - t') |u - u'|^{2\rho - N}, \quad \rho > 0, \quad (809)$$

**Table 4.** Growth exponent estimates of the  $d$ -mer model ( $d$ -mer) [656]; the results in  $d = 1$  are exact. The last column represents the results for the RSOS model, always taking the most recent and precise values [643–645, 647, 648, 657]. At least some of the error bars seem overly optimistic.

$d$	$\zeta_{\text{KPZ}}(d\text{-mer})$	$\frac{\zeta_{\text{KPZ}}}{\zeta_{\text{KPZ}}}(d\text{-mer})$	$z_{\text{KPZ}}(d\text{-mer})$	$\zeta_{\text{KPZ}}(\text{RSOS})$
1	1/2	1/3	3/2	1/2
2	0.395(5)	0.245(5)	1.58(10)	0.393(3)
3	0.29(1)	0.184(5)	1.60(10)	0.3135(15)
4	0.245(5)	0.15(1)	1.91(10)	0.2537(8)
5	0.22(1)	0.115(5)	1.95(15)	0.205(15)

a different exponent is expected. Using equation (23) with  $\gamma = N - 2\rho$  and  $d = 1$ , we find  $\zeta_{\text{Flory}}^{\text{LR}} = \frac{3}{4+N-2\rho}$ , and as a consequence of equation (783) and (781)

$$\zeta_{\text{KPZ}}^{\text{LR}} = \frac{4 + N - 2\rho}{3}, \quad \zeta_{\text{KPZ}}^{\text{LR}} = \frac{2 - N + 2\rho}{3}. \quad (810)$$

This LR fixed point, which is exact as long as the disorder does not get renormalized, is in competition with the SR (RB) fixed point for which disorder renormalizes. As a rule of thumb, the fixed point with the larger  $\zeta$  or  $\zeta_{\text{KPZ}}$ , and smaller  $z_{\text{KPZ}}$  dominates. In dimension  $N = 1$  where  $\zeta_{\text{KPZ}} = 1/2$ , the LR fixed point dominates for  $\rho > \rho_c = \frac{1}{4}$ . These results can already be found in [632, 633], and were reanalyzed via RG in [634, 635].

### 7.11. An upper critical dimension for KPZ?

A lot of work has been devoted to either proving or disproving the existence of an upper critical dimension  $N_c \approx 4$ . The arguments in favor are via *proof by consistency or contradiction* [636–638],  $N_c = 4$ , or mode-coupling:  $N_c = 4$  [639–641],  $N_c = 3.7$  or  $N_c = 4.3$ , depending on the UV regularization [642]. If these are wrong, presumably one of the underlying assumptions fails.

The arguments against are mostly from numerical simulations, either directly on the KPZ in its rigid-solid-on-solid (RSOS) representation [643–648] or on the directed polymer [649]. The criticism voiced is that they are not in the asymptotic regime, or break the rotational symmetry of the KPZ equation. Mode-coupling solutions without an upper critical dimension have been proposed [650], as well as approximate RG schemes [651], or NPRG [652].

The issue is far from settled, and only few distinct arguments can be found: FRG for the directed polymer favors a critical dimension  $N_c \approx 2.5$  [150], approximately also found in [653]. While the work by [626, 627] indicates the necessity for an UV-cutoff in dimension  $N = 4$  (see above), an additional scale may appear at all even  $N$ , i.e.  $N = 6, 8$ , etc [412]. Closure relations in CFT lead to simple fractions for the critical exponents [654, 655], not favored by numerical simulations. From the newer developments, let us mention the mapping to  $d$ -mer diffusion [656], which seems to give rather precise numerical estimates, see table 4. Let us conclude with a quote from the recent review [605]: the ‘equation proposed nearly three decades ago by Kardar, Parisi and Zhang continues to inspire, intrigue and confound its many admirers’.

**7.11.1. Quenched KPZ.** The quenched KPZ equation was discussed in section 5.7.

### 7.12. The KPZ equation in dimension $d = 1$

The KPZ equation (762) is formally a Langevin equation. The corresponding Fokker–Planck equation for the evolution of its measure  $P_t[h]$ , derived in equation (946), reads

$$\partial_t P_t[h] = D \int_u \frac{\delta^2}{\delta h(u)^2} P_t[h] - \int_u \frac{\delta}{\delta h(u)} \left( \nu \nabla^2 h(u) + \frac{\lambda}{2} [\nabla h(u)]^2 P_t[h] \right). \quad (811)$$

At least for  $\lambda = 0$ , a steady-state solution can be found by asking that

$$D \frac{\delta}{\delta h(u)} P_t[h] = \nu \nabla^2 h(u) P_t[h]. \quad (812)$$

This is solved by<sup>44</sup>

$$P_t[h] = \mathcal{N} \exp \left( -\frac{\nu}{2D} \int_u [\nabla h(u)]^2 \right). \quad (813)$$

Unsurprisingly, this is the measure for a diffusing elastic string. What are the additional terms for  $\lambda \neq 0$ ? Inserting the measure (813) into equation (811) yields

$$\begin{aligned} \partial_t P_t[h] &= - \int_u \frac{\delta}{\delta h(u)} \left( \frac{\lambda}{2} [\nabla h(u, t)]^2 P_t[h] \right) \\ &= \frac{\lambda \nu}{2D} \int_u [\nabla h(u)]^2 \nabla^2 h(u) P_t[h]. \end{aligned} \quad (814)$$

While written in continuous notation, the calculation should be made on the discretized version, with proper symmetrization of the  $[\nabla h]^2$  term. To go to the second line, we dropped the direct derivative of the latter, as it integrates to 0. In dimension  $N = 1$ , the integrand is a total derivative, thus integrates to zero. In higher dimensions, this is not the case. The simplest explicit counterexample for periodic boundary conditions ( $L = 2\pi$ ) in dimension  $N = 2$  we found is  $h(u_1, u_2) = [a + \cos(u_1)][b + \cos(u_2)]$ , for which the last integral in equation (814) evaluates to  $-abL^2$ .

The measure (813) implies that equal-time correlation functions of the nonlinear ( $\lambda > 0$ ) theory are given by those of the linear theory ( $\lambda = 0$ ), first in Fourier and then in real space,

$$\langle \tilde{h}(q) \tilde{h}(q') \rangle = 2\pi \delta(q + q') \frac{Dq^2}{\nu} \quad (815)$$

$$\Leftrightarrow \langle [h(x) - h(x')]^2 \rangle = \frac{D}{\nu} |x - x'|^{2\zeta_{\text{KPZ}}}, \quad (816)$$

$$\zeta_{\text{KPZ}}^{d=1} = \frac{1}{2}. \quad (817)$$

<sup>44</sup>Note that some authors [604] use a different normalization for equation (760)  $2D_{\text{here}} = D_{\text{there}}$ , reflected in the invariant measure.

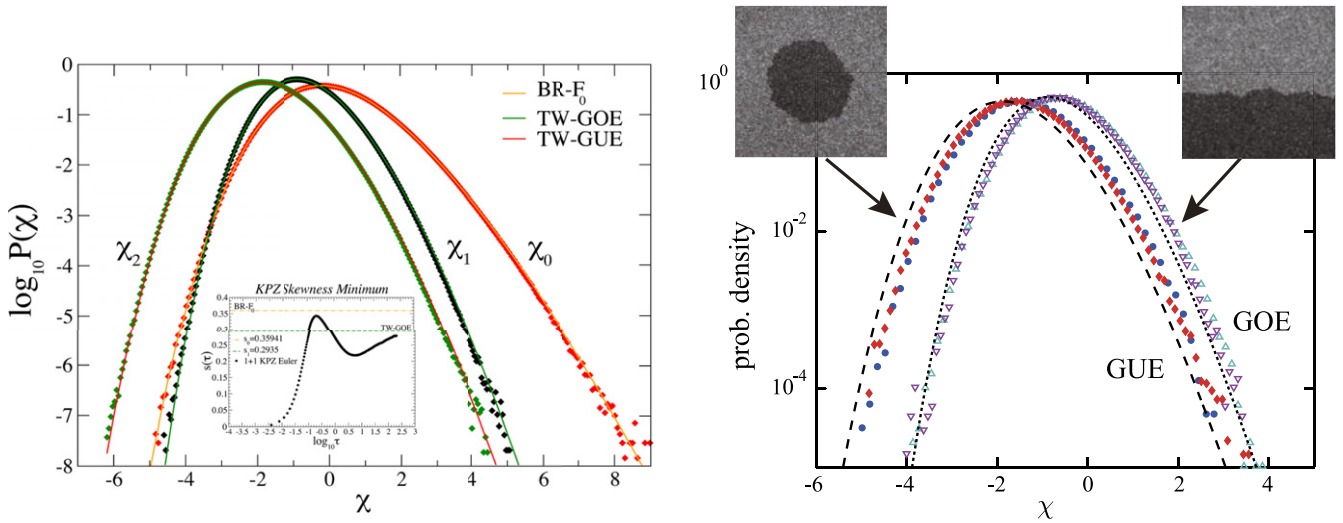


**Figure 74.** (Left) Numerical verification of the universal distributions for KPZ in one dimension as explained in the text. Reprinted by permission from Springer Nature Customer Service Centre GmbH: Springer. J. Stat. Phys. [605] (c) 2015. (Right) Experimental verification in [606]. The blue circles and red diamonds display the histograms for the circular interfaces at  $t = 10$  s and 30 s, respectively, while the turquoise up-triangles and purple down-triangles are for the flat interfaces at  $t = 20$  s and 60 s, respectively.

Moreover, the measure (813) is Gaussian. This can be viewed as due to a fluctuation-dissipation theorem [658]. Equation (781) further implies

$$\zeta_{\text{KPZ}}^{d=1} = \frac{3}{2}. \tag{818}$$

As a consequence,

$$\zeta_{\text{RB}}^{d=1} = \frac{1}{\zeta_{\text{KPZ}}^{d=1}} = \frac{2}{3} \tag{819}$$

is the roughness exponent of a directed polymer in  $1 + 1$  dimensions, and the roughness of domain walls in dirty 2D magnets. Their energy-fluctuation exponent is

$$\theta = d - 2 + 2\zeta = \frac{1}{3}. \tag{820}$$

This can also be obtained via Bethe ansatz [108, 617].

**7.13. KPZ, polynuclear growth, Tracy–Widom and Baik–Rains distributions**

Since the introduction of the KPZ equation in 1986 [560], much progress has been made in one dimension. This started in 2000 with the groundbreaking work by Prähofer and Spohn [659–661] introducing the polynuclear growth (PNG) model: one starts from a flat configuration. Steps of vanishing size are deposited as a Poisson process upon the already constructed surface. Steps then grow with unit velocity at both ends. When steps meet, they merge. Heuristically it seems clear that this process belongs to the KPZ universality class, similar to its discrete cousin, the RSOS model. Independently, Johansson introduced the single-step model [662], relating surface growth to the combinatorial problem of finding the longest increasing subsequence in a random permutation [663] and random matrix theory [664], relating to older work in this domain [665]. The key observables are constructed from the

spatially averaged mean height  $h(t)$ , which for large times is assumed to grow with velocity  $v_\infty$ ,  $\lim_{t \rightarrow \infty} \langle h(t) \rangle - v_\infty t = \text{const}$ . As the mean height is proportional to the free energy of a directed polymer, see equation (776), results for the height fluctuation have an immediate interpretation in terms of free-energy fluctuations of a directed polymer.

Key observables are

$$\chi_0 = \frac{h(t_0 + t) - h(t_0) - v_\infty t}{\left(\frac{D^2 \lambda}{2\nu^2} t\right)^{1/3}}, \tag{821}$$

$$\chi_1 = \frac{h(t) - v_\infty t}{\left(\frac{D^2 \lambda}{2\nu^2} t\right)^{1/3}}, \quad (\text{flat initial conditions}), \tag{822}$$

$$\chi_2 = \frac{h(t) - v_\infty t}{\left(\frac{D^2 \lambda}{2\nu^2} t\right)^{1/3}}, \quad (\text{circular initial conditions}). \tag{823}$$

Each of these observables has a unique universal distribution:

- $\chi_0$  is distributed according to the Baik–Rains  $F_0$  distribution,
- $\chi_1$  is distributed according to the Tracy–Widom (TW) Gaussian orthogonal ensemble distribution,
- $\chi_2$  is distributed according to the TW Gaussian unitary ensemble distribution.

The reader wishing to test these laws himself can find a Mathematica implementation online [666].

The Bethe-ansatz for the directed polymer was introduced in 1987 by Kardar to obtain the roughness exponent of a directed polymer,  $\zeta = 2/3$  and  $\theta = 1/3$ . A revival started in 2010, when physicists succeeded [667–671] to first reproduce the work of [659–661] via the Bethe ansatz, and then extend it to other situations [672]. At the same time, a new generation of mathematicians developed complementary tools [673–676], joining the work of Sasamoto and Spohn [677, 678].

Extraordinarily, Takeuchi and Sano [606, 679] succeeded to extract the universal distributions from a turbulent liquid-crystal experiment. A snapshot is shown in figure 71, and the two Tracey–Widom distributions for circular and flat initial conditions in figure 74.

Let us conclude by mentioning pedagogical presentations [680–682], as well as attempts to port this at least numerically to higher dimensions [683, 684].

#### 7.14. Models in the KPZ universality class, and experimental realizations

In all dimensions:

- KPZ [560],
- PNG [659–661],
- RSOS models [643–648].
- Directed polymer in quenched disorder (section 7.4).

In one dimension:

- longest growing subsequence in a random permutation [663],
- the asymmetric simple exclusion process [685–687].

Experimental realizations (one dimension only):

- slow combustion of paper [688, 689],
- turbulent liquid crystals [606, 679],
- particle deposition (with crossover to qKPZ) [690],
- bacterial growth [691],
- chemical reaction fronts [573].

#### 7.15. From Burgers' turbulence to Navier–Stokes turbulence?

In Burgers' turbulence velocity profiles are locally linear (see e.g. the right of figure 72), interrupted by jumps. Phenomenologically it is similar to the force field in disordered systems. This implies that, if non-vanishing, at small distances

$$\langle [v(u, t) - v(u', t)]^n \rangle \simeq \mathcal{A}_n |u - u'|^{\zeta_n}, \quad (824)$$

and for Burger  $\zeta_n = 1$ , independent of  $n$ . In Navier–Stokes turbulence, the exponent  $\zeta_3 = 1$ , as predicted by Kolmogorov in 1941 [692]. Other moments obey

$$\zeta_n = \frac{n}{3} + \delta\zeta_n, \quad (825)$$

where  $\delta\zeta_n$  is small. Calculating  $\delta\zeta_n$  analytically is the outstanding problem of turbulence research. One can try to use FRG for this problem [693], but something crucial is missing: while FRG correctly deals with shocks, the weaker singularities responsible for equation (825) are not captured by FRG. (It may work in dimension  $d = 2$ , though [693].) It is possible that the FRG fixed point which typically has a cusp, and which usually is implemented for the second cumulant, instead applies to the third cumulant, as  $\zeta_3 = 1$ . How to implement this idea remains an open problem.

## 8. Links between loop-erased random walks, CDWs, sandpiles, and scalar field theories

### 8.1. Supermathematics

*Supermathematics*, introduced in [694] and nicely reviewed in [695] is an alternative way to average over disorder. In this technique, additional fermionic or *Grassmannian* degrees of freedom are introduced to normalize the partition function to  $\mathcal{Z} = 1$ , even before averaging over disorder. We start by reviewing basic properties of Grassmann variables, before using them for disorder averages. Most of the material is standard, and the reader familiar with it, or wishing to advance may safely do so.

Two points should be retained: while *supermathematics* is usually referred to as *supersymmetry technique*, this is a misnomer as supersymmetry is broken at the Larkin scale, i.e. when a cusp appears. The name is due to historical reasons, stemming from a time when people believed that supersymmetry is not broken. To avoid this confusion, we prefer the term *supermathematics*.

Braking of supersymmetry, and the cusp, can be found in this framework, as long as one considers at least two physically distinct copies. The technical reason is that to assess the  $n$ th cumulant of a distribution, one needs at least  $n$  distinct copies. Even when supposing the disorder to be Gaussian distributed, the variance, i.e. the second cumulant needs to be assessed, thus two distinct replicas.

Apart from these more formal considerations, the technique has proven powerful in the mapping of CDWs onto a  $\phi^4$ -type theory (section 8.6).

### 8.2. Basic rules for Grassmann variables

Grassmann variables are anticommuting variables which allow one to write a path-integral for fermions, in the same way as one does for bosons. There are only few rules to remember. If  $\chi$  and  $\psi$  are Grassmann variables, then

$$\chi\psi = -\psi\chi. \quad (826)$$

This immediately implies that

$$\chi^2 = 0. \quad (827)$$

One introduces derivatives, and integrals through the same formula, known as Berezin integral [694],

$$\int d\chi\chi \equiv \frac{d}{d\chi}\chi = 1. \quad (828)$$

One checks that they satisfy the usual properties associated to 'normal' derivatives, and integrals. An important property is

$$\int d\bar{\chi} d\chi e^{-a\bar{\chi}\chi} = a. \quad (829)$$

This is easily proven upon Taylor expansion. The minus sign in the exponential cancels the minus sign obtained when exchanging  $\bar{\chi}$  with  $\chi$ , which is necessary since an integral

or derivative is defined to act directly on the variable following it. Equation (829) can be generalized to integrals over an  $n$ -component pair of vectors  $\vec{\chi}$ , and  $\vec{\bar{\chi}}$ :

$$\int d\vec{\chi} d\vec{\bar{\chi}} e^{-\vec{\bar{\chi}}\mathbb{A}\vec{\chi}} := \prod_{a=1}^n \int d\bar{\chi}^a d\chi^a e^{-\vec{\bar{\chi}}\mathbb{A}\vec{\chi}} = \det(\mathbb{A}). \quad (830)$$

It is proven by changing coordinates s.t.  $\mathbb{A}$  becomes diagonal. For comparison we give the corresponding formula for normal (bosonic) fields, noting  $\phi^a := \phi_x^a + i\phi_y^a$ ,  $\bar{\phi}^a := \phi_x^a - i\phi_y^a$ ,

$$\int d\bar{\phi} d\phi e^{-\bar{\phi}\mathbb{A}\phi} := \prod_{a=1}^n \int \frac{d\phi_x^a d\phi_y^a}{\pi} e^{-\bar{\phi}\mathbb{A}\phi} = \frac{1}{\det(\mathbb{A})}. \quad (831)$$

When combining normal and Grassmannian integrals over the same number of variables into a product, the contributions from equations (830) and (831) cancel. This will be used below.

### 8.3. Disorder averages with bosons and fermions

The above formulas permit a different approach to average over disorder. For concreteness, define

$$\mathcal{H}[u, V] = \int_x \left\{ \frac{1}{2} [\nabla u(x)]^2 + \frac{m^2}{2} u(x)^2 + \mathcal{U}(u(x)) + V(x, u(x)) \right\}. \quad (832)$$

The disorder-average of an observable  $\mathcal{O}$  is defined as

$$\overline{\mathcal{O}[u]} := \frac{\int \prod_{a=1}^r \mathcal{D}[u_a] \mathcal{O}[u_1] e^{-\frac{1}{r} \mathcal{H}[u_a, V]}}{\int \prod_{a=1}^r \mathcal{D}[u_a] e^{-\frac{1}{r} \mathcal{H}[u_a, V]}}. \quad (833)$$

The function  $\mathcal{U}(u)$  is an arbitrary potential, e.g. the non-linearity in  $\phi^4$ -theory,  $\mathcal{U}(u) = gu^4$ . The random potential  $V(x, u)$  is the same one used in section 1.2, with correlations given by equation (9). Its average is indicated by the overline. We remind that the difficulty in evaluating (833) comes from the denominator. The replica trick used in section 1.5 allowed us to set  $r = 0$ , effectively discarding the denominator. Here we follow a different strategy.

In the limit of  $T \rightarrow 0$  only configurations which minimize the energy survive. These configurations satisfy  $\frac{\delta \mathcal{H}[u_a, V]}{\delta u_a(x)} = 0$ , and we want to insert a  $\delta$ -distribution enforcing this condition into the path-integral. This has to be accompanied by a factor of  $\det \left[ \frac{\delta^2 \mathcal{H}[u_a, V]}{\delta u_a(x) \delta u_a(y)} \right]$ , such that the path integral is normalized to 1. The latter can be achieved by an additional integral over Grassmann variables, i.e. fermionic degrees of freedom, using that

$$\det \left( \frac{\delta^2 \mathcal{H}[u, V]}{\delta u(x) \delta u(y)} \right) = \int \mathcal{D}[\bar{\psi}_a] \mathcal{D}[\psi_a] \exp \left( - \int_x \bar{\psi}(x) \frac{\delta^2 \mathcal{H}[u, V]}{\delta u(x) \delta u(y)} \psi(x) \right). \quad (834)$$

This allows us to write the disorder average of any observable  $\mathcal{O}[u]$  as

$$\overline{\mathcal{O}[u]} = \int \prod_{a=1}^r \mathcal{D}[\tilde{u}_a] \mathcal{D}[u_a] \mathcal{D}[\bar{\psi}_a] \mathcal{D}[\psi_a] \mathcal{O}[u] \times \exp \left[ - \int_x \tilde{u}_a(x) \frac{\delta \mathcal{H}[u_a]}{\delta u_a(x)} + \bar{\psi}_a(x) \frac{\delta^2 \mathcal{H}[u_a]}{\delta u_a(x) \delta u_a(y)} \psi_a(y) \right]. \quad (835)$$

This method was first introduced in [32, 696]. An alternative derivation and insight are offered by Cardy [697–699], see also [700, 701].

Averaging over disorder with the force–force correlator  $\Delta(u) := -R''(u)$  yields

$$\begin{aligned} \overline{\mathcal{O}[u]} &= \int \prod_a \mathcal{D}[u_a] \mathcal{D}[\tilde{u}_a] \mathcal{D}[\bar{\psi}_a] \mathcal{D}[\psi_a] \\ &\quad \exp(-\mathcal{S}[u_a, \tilde{u}_a, \bar{\psi}_a, \psi_a]), \\ \mathcal{S}[\tilde{u}_a, u_a, \bar{\psi}_a, \psi_a] &= \int_x \sum_{a=1}^r \left\{ \tilde{u}_a(x) \left[ (-\nabla^2 + m^2) u_a(x) + \mathcal{U}'(u_a(x)) \right] \right. \\ &\quad \left. + \bar{\psi}_a(x) \left[ -\nabla^2 + m^2 + \mathcal{U}''(u_a(x)) \right] \psi_a(x) \right\} \\ &\quad - \sum_{a,b=1}^r \left[ \frac{1}{2} \tilde{u}_a(x) \Delta(u_a(x) - u_b(x)) \tilde{u}_b(x) \right. \\ &\quad \left. - \tilde{u}_a(x) \Delta'(u_a(x) - u_b(x)) \bar{\psi}_b(x) \psi_b(x) \right. \\ &\quad \left. - \frac{1}{2} \bar{\psi}_a(x) \psi_a(x) \Delta''(u_a(x) - u_b(x)) \bar{\psi}_b(x) \psi_b(x) \right]. \end{aligned} \quad (836)$$

We first analyze the special case of  $n = 1$ . Suppose that  $\Delta(u)$  is even and analytic to start with, then few terms survive from equation (836),

$$\begin{aligned} \mathcal{S}_{\text{Susy}}[u, \tilde{u}, \bar{\psi}, \psi] &= \int_x \left\{ \tilde{u}(x) \left[ (-\nabla^2 + m^2) u(x) + \mathcal{U}'(u(x)) \right] \right. \\ &\quad \left. + \bar{\psi}(x) \left[ -\nabla^2 + m^2 + \mathcal{U}''(u(x)) \right] \psi(x) - \frac{1}{2} \tilde{u}(x) \Delta(0) \tilde{u}(x) \right\}. \end{aligned} \quad (837)$$

(We have used that  $\bar{\psi}_a^2 = \psi_a^2 = 0$  to eliminate the four-fermion-term.) A particularly simple case are random manifolds, for which  $\mathcal{U}(u) = 0$ . Then bosons  $\tilde{u}$  and  $u$ , and fermions  $\bar{\psi}$  and  $\psi$  do not interact, all expectation values are Gaussian, perturbation theory gives equation (38), and dimensional reduction holds. When  $\mathcal{U}(u) \neq 0$ , things are more complicated, but as we will see in the next section, dimensional reduction still holds, at least formally.

The reason is that the action (837) possesses an apparent supersymmetry, made manifest by grouping all fields into a

(bosonic) superfield,

$$\Phi(x, \bar{\Theta}, \Theta) := u(x) + \bar{\Theta}\psi(x) + \bar{\psi}(x)\Theta - \bar{\Theta}\Theta\tilde{u}(x). \quad (838)$$

Both  $\bar{\Theta}$  and  $\Theta$  are Grassmann numbers. The action (837) can then be written with the super Laplacian  $\Delta_s$  as

$$\mathcal{S}_{\text{Susy}} = \int d\bar{\Theta}d\Theta \int_x \frac{1}{2} \Phi(x, \bar{\Theta}, \Theta)(-\Delta_s + m^2)\Phi(x, \bar{\Theta}, \Theta) + \mathcal{U}(\Phi(x, \bar{\Theta}, \Theta)), \quad (839)$$

$$\Delta_s := \nabla^2 + \Delta(0) \frac{\partial}{\partial \bar{\Theta}} \frac{\partial}{\partial \Theta}. \quad (840)$$

As we will see in section 8.5, the action is invariant under the two supergenerators

$$\begin{aligned} Q &:= x \frac{\partial}{\partial \bar{\Theta}} - \frac{2}{\Delta(0)} \bar{\Theta} \nabla, & \bar{Q} &:= x \frac{\partial}{\partial \Theta} + \frac{2}{\Delta(0)} \Theta \nabla, \\ \{Q, \bar{Q}\} &= 0. \end{aligned} \quad (841)$$

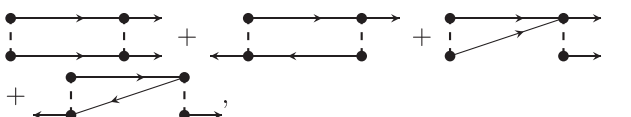
This is sufficient to ‘prove’ dimensional reduction.

#### 8.4. Renormalization of the disorder

For more than  $r = 1$  replicas, the theory is richer, and we can recover the renormalization of  $\Delta(u)$  itself. To simplify matters, set  $\mathcal{U}(u) = 0$ , and write

$$\begin{aligned} \mathcal{S}[\tilde{u}_a, u_a, \bar{\psi}_a, \psi_a] &= \sum_a \int_x \left[ \tilde{u}_a(x)(-\nabla^2 + m^2)u_a(x) \right. \\ &\quad \left. + \bar{\psi}_a(x)(-\nabla^2 + m^2)\psi_a(x) - \frac{1}{2} \tilde{u}_a(x)\Delta(0)\tilde{u}_a(x) \right] \\ &\quad - \sum_{a \neq b} \int_x \left[ \frac{1}{2} \tilde{u}_a(x)\Delta(u_a(x) - u_b(x))\tilde{u}_b(x) \right. \\ &\quad \left. - \tilde{u}_a(x)\Delta'(u_a(x) - u_b(x))\bar{\psi}_b(x)\psi_b(x) \right. \\ &\quad \left. - \frac{1}{2} \bar{\psi}_a(x)\psi_a(x)\Delta''(u_a(x) - u_b(x))\bar{\psi}_b(x)\psi_b(x) \right]. \end{aligned} \quad (842)$$

Corrections to  $\Delta(u)$  are constructed by remarking that the interaction term quadratic in  $\tilde{u}$  is almost identical to the treatment of the dynamics in the static limit (i.e. after integration over times). The diagrams in question are



$$(843)$$

where an arrow indicates the correlation-function,  $x \rightarrow y = \langle \tilde{u}(x)u(y) \rangle = C(x - y)$ . This leads to (in the order given above)

$$\begin{aligned} \delta\Delta(u) &= [-\Delta(u)\Delta''(u) - \Delta'(u)^2 + \Delta''(u)\Delta(0)] \\ &\quad \times \int_{x-y} C(x - y)^2. \end{aligned} \quad (844)$$

The last term of equation (843) is odd, and vanishes. Equation (844) is equal to the results of equations (323)–(331).

A non-trivial ingredient is the cancellation of the acausal loop (332) in the dynamics, equivalent to the three-replica term in the statics:



$$(845)$$

The first diagram comes from the contraction of two terms proportional to  $\tilde{u}_a\Delta(u_a - u_b)\tilde{u}_b$ . The second is obtained from contracting all fermions in two terms proportional to  $\tilde{u}_a\Delta'(u_a - u_b)\bar{\psi}_b\psi_b$ . Since the fermionic loop (oriented wiggly line in the second diagram) contributes a factor of  $-1$ , both cancel.

One can treat the interacting theory completely in a superspace formulation. The action is

$$\begin{aligned} \mathcal{S}[\Phi] &= \sum_a \int_{\bar{\Theta}, \Theta} \int_x \frac{1}{2} \Phi_a(x, \bar{\Theta}, \Theta)(-\Delta_s + m^2)\Phi_a(x, \bar{\Theta}, \Theta) \\ &\quad - \frac{1}{2} \sum_{a \neq b} \int_x \int_{\bar{\Theta}, \Theta, \bar{\Theta}', \Theta'} R(\Phi_a(x, \bar{\Theta}, \Theta) - \Phi_b(x, \bar{\Theta}', \Theta')). \end{aligned} \quad (846)$$

‘Non-locality’ in replica-space or in time is replaced by ‘non-locality’ in superspace. Corrections to  $R(u)$  all stem from *superdiagrams*, which result into bilocal interactions in superspace, not trilocal, or higher. The latter find their equivalent in three-local terms in replica-space in the replica-formulation, and three-local terms in time, in the dynamic formulation.

Supersymmetry is broken, once  $\Delta(0)$  changes, i.e. at the Larkin length. A seemingly ‘effective supersymmetry’, or ‘scale-dependent supersymmetry’ appears, in which the parameter  $\Delta(0)$ , which appears in the Susy-transformation, changes with scale, according to the FRG flow equation (64) for  $\Delta(u)$ , continued to  $u = 0$ .

#### 8.5. Supersymmetry and dimensional reduction

Let us study invariants of the action. Since total derivatives both in  $x$  and  $\theta$  or  $\bar{\theta}$  vanish, the crucial term to focus on is the super-Laplacian. To simplify notations, we set

$$\rho := \Delta(0). \quad (847)$$

By explicit inspection, we find that the two generators of supertranslations

$$Q := x \frac{\partial}{\partial \bar{\Theta}} + \frac{2}{\rho} \bar{\Theta} \nabla, \quad \bar{Q} := x \frac{\partial}{\partial \Theta} - \frac{2}{\rho} \Theta \nabla \quad (848)$$

both commute with the super-Laplacian, and anti-commute with each other,

$$[\Delta_s, Q] = [\Delta_s, \bar{Q}] = 0, \quad \{Q, \bar{Q}\} = 0. \quad (849)$$

The following combination is invariant under the action of  $Q$  and  $\bar{Q}$ ,

$$\bar{Q} \left( x^2 + \frac{4}{\rho} \bar{\Theta} \Theta \right) = Q \left( x^2 + \frac{4}{\rho} \bar{\Theta} \Theta \right) = 0. \quad (850)$$

Applying the super-Laplacian (840) gives<sup>45</sup>

$$\Delta_s \left( x^2 + \frac{4}{\rho} \bar{\Theta} \Theta \right) = 2(d-2). \quad (851)$$

To obtain the super-propagator, inverse of the super-Laplacian plus mass term in equation (839), we remark that

$$\begin{aligned} & \left( m^2 - \nabla^2 - \rho \frac{\partial}{\partial \bar{\Theta}} \frac{\partial}{\partial \Theta} \right) \left( m^2 - \nabla^2 + \rho \frac{\partial}{\partial \bar{\Theta}} \frac{\partial}{\partial \Theta} \right) \\ &= (m^2 - \nabla^2)^2. \end{aligned} \quad (852)$$

This implies that

$$(m^2 - \Delta_s)^{-1} = \frac{m^2 - \nabla^2 + \rho \frac{\partial}{\partial \bar{\Theta}} \frac{\partial}{\partial \Theta}}{(m^2 - \nabla^2)^2}. \quad (853)$$

Therefore

$$\begin{aligned} & C(x-x', \Theta - \Theta', \bar{\Theta} - \bar{\Theta}') \\ &= \frac{m^2 - \nabla^2 + \rho \frac{\partial}{\partial \bar{\Theta}} \frac{\partial}{\partial \Theta}}{(m^2 - \nabla^2)^2} \delta(x-x') \delta(\Theta - \Theta') \delta(\bar{\Theta} - \bar{\Theta}'). \end{aligned} \quad (854)$$

The Grassmanian  $\delta$ -functions are defined as

$$\int d\Theta \delta(\Theta - \Theta') f(\Theta) = f(\Theta'). \quad (855)$$

By direct calculation one finds

$$\delta(\Theta - \Theta') = \Theta' - \Theta = \int d\bar{\chi} e^{\bar{\chi}(\Theta' - \Theta)}. \quad (856)$$

One can transform (854) into a representation in dual spaces of momentum ( $k$ -space) and super-coordinates ( $\chi$ -space) as

$$\begin{aligned} C(k, \bar{\chi}, \chi) &= \frac{m^2 + k^2 + \rho \bar{\chi} \chi}{(m^2 + k^2)^2} \equiv \frac{1}{m^2 + k^2 + \rho \chi \bar{\chi}} \\ &\equiv \int_0^\infty ds e^{-s(m^2 + k^2 + \rho \chi \bar{\chi})}. \end{aligned} \quad (857)$$

The final proof of dimensional reduction is performed with this representation of the super-correlator<sup>46</sup>. Any diagram can be written as

$$\int_{k_1} \int_{\bar{\chi}_1 \chi_1} \dots \int_{k_n} \int_{\bar{\chi}_n \chi_n} \prod_{i=1}^n \left[ \int_0^\infty ds_i e^{-s_i(m^2 + k_i^2 + \rho \chi_i \bar{\chi}_i)} \right], \quad (858)$$

where some  $\delta$ -distributions have already been used to eliminate integrations over  $k$ 's, i.e. some of the  $k_i$ 's appearing in the exponential are not independent variables, but linear combinations of other  $k_j$ 's, and the same holds for the corresponding

$\chi_i$  and  $\bar{\chi}_i$ . The product of exponential factors can be written as

$$\begin{aligned} \prod_{i=1}^n \left[ e^{-s_i(m^2 + k_i^2 + \rho \chi_i \bar{\chi}_i)} \right] &= \exp \left( - \begin{pmatrix} k_1 \\ k_2 \\ \dots \\ k_n \end{pmatrix} \mathbb{W} \begin{pmatrix} k_1 \\ k_2 \\ \dots \\ k_n \end{pmatrix} \right) \\ &\times \exp \left( - \begin{pmatrix} \chi_1 \\ \chi_2 \\ \dots \\ \chi_n \end{pmatrix} \mathbb{W} \begin{pmatrix} \bar{\chi}_1 \\ \bar{\chi}_2 \\ \dots \\ \bar{\chi}_n \end{pmatrix} \right). \end{aligned} \quad (859)$$

Integration over the  $k$ 's gives

$$\int_{k_1} \dots \int_{k_n} e^{-\bar{k} \cdot \mathbb{W} \cdot \vec{k}} = \left( \frac{1}{4\pi} \right)^{ld/2} \det(\mathbb{W})^{-d/2}, \quad (860)$$

where  $l$  is the number of loops. Integration over  $\bar{\chi}$  and  $\chi$  gives

$$\int_{\bar{\chi}_1 \chi_1} \dots \int_{\bar{\chi}_n \chi_n} e^{-\rho \bar{\chi} \cdot \mathbb{W} \cdot \bar{\chi}} = (\rho)^l \det(\mathbb{W}). \quad (861)$$

The product of the two factors (860) and (861) is the same as for a standard bosonic diagram in dimension  $d-2$ . Remark that the expansion is in powers of  $T$ , and combining these relations, we obtain after integration over the  $s_i$ :

$$\begin{aligned} & l\text{-loop super-diagram in dimension } d \\ &= \left( \frac{\rho}{4\pi T} \right)^l \times l\text{-loop standard-diagram in dimension } d-2. \end{aligned} \quad (862)$$

This implies that for any observable  $\mathcal{O}(T)$

$$\mathcal{O}_{\text{disordered}}^d(\rho) = \mathcal{O}_{\text{thermal}}^{d-2} \left( T = \frac{\rho}{4\pi} \right). \quad (863)$$

The above proof can be extended to theories with derivative couplings. The rules are as follows: consider  $\mathcal{H}_s[\Phi]$  given in equation (839). To this we can add an interaction in derivatives, for a total of

$$\begin{aligned} \mathcal{H}_s[\Phi] &= \int_{\bar{\Theta}, \Theta} \int_x \left[ \frac{1}{2} \Phi(x, \bar{\Theta}, \Theta) (-\Delta_s + m^2) \Phi(x, \bar{\Theta}, \Theta) \right. \\ &\quad + \mathcal{U}(\Phi(x, \bar{\Theta}, \Theta)) \\ &\quad \left. + \mathcal{A}_1(\Phi(x, \bar{\Theta}, \Theta)) (-\Delta_s + m^2) \mathcal{A}_2(\Phi(x, \bar{\Theta}, \Theta)) \right]. \end{aligned} \quad (864)$$

This theory is supersymmetric: calculating diagrams in perturbation theory, we get additional vertices. The corresponding diagrams can be calculated from the same type of generating function (859). The trick is to use instead of an integral w.r.t.  $s$  a derivative w.r.t.  $s$ , taken at  $s=0$ ,

$$(m^2 + k^2 + \rho \chi \bar{\chi}) = - \frac{d}{ds} \Big|_{s=0} e^{-s(m^2 + k^2 + \rho \chi \bar{\chi})}. \quad (865)$$

<sup>45</sup> This relation comes out incorrectly in [32].

<sup>46</sup> Note that one can also work in position-space [32]. Then the super-correlator is explicitly  $d$ -dependent, and one should check that this  $d$ -dependence comes out correctly.

8.6. CDWs and their mapping onto  $\phi^4$ -theory with two fermions and one boson

Consider the fixed point (94) for CDWs. It has the form

$$\Delta(u) = \frac{g}{12} - \frac{g}{2}u(1-u) = \frac{g}{2}u^2 + \text{lower-order terms in } u. \tag{866}$$

The renormalization, encoded in  $g$ , can be gotten by retaining only terms of order  $u^2$ , and dropping lower-order terms which do not feed back into terms of order  $u^2$ . To this aim, consider the action (842) with *two replicas*, replacing  $\Delta(u) \rightarrow \frac{g}{2}u^2$ . We further go to center-of-mass coordinates for the bosons by introducing

$$\begin{aligned} u_1(x) &= u(x) + \frac{1}{2}\phi(x), & u_2(x) &= u(x) - \frac{1}{2}\phi(x), \\ \tilde{u}_1(x) &= \frac{1}{2}\tilde{u}(x) + \tilde{\phi}(x), & \tilde{u}_2(x) &= \frac{1}{2}\tilde{u}(x) - \tilde{\phi}(x). \end{aligned} \tag{867}$$

$$\tag{868}$$

The action (836) can then be rewritten as

$$\begin{aligned} \mathcal{S} &= \int_x \tilde{\phi}(x)(-\nabla^2 + m^2)\phi(x) + \tilde{u}(x)(-\nabla^2 + m^2)u(x) \\ &\quad + \sum_{a=1}^2 \bar{\psi}_a(x)(-\nabla^2 + m^2)\psi_a(x) \\ &\quad + \frac{g}{2}\tilde{u}(x)\phi(x) [\bar{\psi}_2(x)\psi_2(x) - \bar{\psi}_1(x)\psi_1(x)] \\ &\quad - \frac{g}{8}\tilde{u}(x)^2\phi(x)^2 \\ &\quad + \frac{g}{2}[\tilde{\phi}(x)\phi(x) + \bar{\psi}_1(x)\psi_1(x) + \bar{\psi}_2(x)\psi_2(x)]^2. \end{aligned} \tag{869}$$

Note that only  $\tilde{u}(x)$ , but not the center-of-mass  $u(x)$  appears in the interaction. While  $u(x)$  may have non-trivial expectations, it does not contribute to the renormalization of  $g$ , and the latter can be obtained by considering solely the first and last line of equation (869): this is a  $\phi^4$ -type theory, with one complex bosonic, and two complex fermionic fields. It can equivalently be viewed as complex  $\phi^4$ -theory at  $N = -1$ , or real  $\phi^4$ -theory with  $n = -2$  [310].

8.7. Supermathematics: a critical discussion

When supersymmetry was first proposed [32, 696], it was believed to produce an exact result, namely dimensional reduction. While the latter was found earlier [101, 104, 106] by inspection of diagrams and a combinatorial analysis, supermathematics proved to be a clever tool to show it efficiently. Supermathematics got *discredited* when it was realized that dimensional reduction breaks down at the Larkin scale. As a remedy, breaking of replica symmetry was invoked, or FRG. As we have seen in section 2.20, RSB and FRG fit together, and the applied field inherent to FRG explicitly breaks replica symmetry, and as a consequence supersymmetry. As shown in section 8.4, supermathematics can be used to obtain the FRG

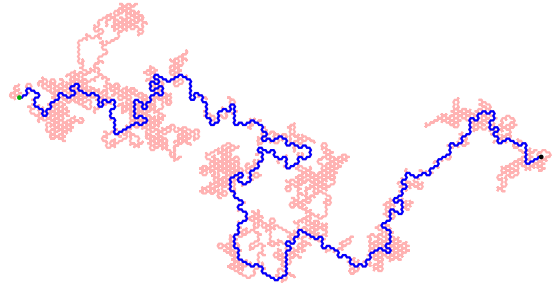


Figure 75. Example of a LERW on the hexagonal lattice with 3000 steps, starting at the black point to the right and arriving at the green point to the left.

flow equation for the disorder. Thus dimensional reduction beyond the Larkin length is not a problem of supermathematics, but of its improper application.

It has been argued that equation (835) is inappropriate as it sums over all saddle points, not only the minima, and for this reason it fails. The objection *per se* can not be discarded. But does it invalidate the formalism put in place above? We believe not: the formalism makes numerous predictions, especially for such non-trivial observables as the FRG fixed-point function  $\Delta(w)$  (sections 2.2–2.13). Our intuition is that each RG step merges pairs of close minima, without invoking any of the higher-lying states present in the above argument. And that by this the objection becomes irrelevant.

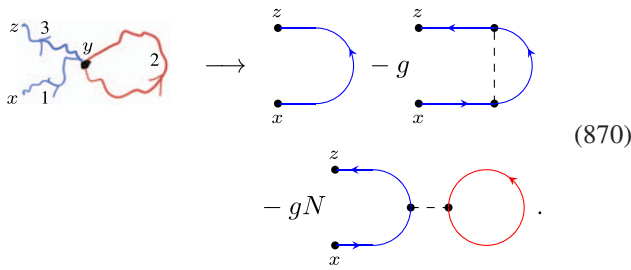
8.8. Mapping loop-erased random walks onto  $\phi^4$ -theory with two fermions and one boson

*Introduction.* A LERW is defined as the trajectory of a RW in which any loop is erased as soon as it is formed [702]. An example is shown on figure 75, where the underlying RW is drawn in red, and the LERW remaining after erasure in blue. Similar to a self-avoiding walk it has a scaling limit in all dimensions, e.g. the end-to-end distance  $R$  scales with the intrinsic length  $\ell$  as  $R \sim \ell^{1/z}$ , where  $z$  is the fractal dimension [703]. It is crucial to note that while both LERWs and SAWs are non-selfintersecting, their fractal dimensions do not agree since they have a different statistics on the same set of allowed trajectories. LERWs appear in many combinatorial problems, e.g. the shortest path on a UST is an LERW. We have collected the many connections in figure 77, together with other identities, which we discuss in the next section.

In contrast to SAWs, LERWs have no obvious field-theoretic description. In three dimensions LERWs have been studied numerically [704–707], while in two dimensions they are described by SLE with  $\kappa = 2$  [708, 709], predicting a fractal dimension  $z_{\text{LERW}}(d = 2) = \frac{5}{4}$ . Coulomb-gas techniques link this to the 2d  $O(n)$ -model at  $n = -2$  [163, 710]. It was recently shown that LERWs can be mapped *in all dimensions* to the theory of two complex fermions and one complex boson, equivalent to the  $O(n)$  model at  $n = -2$  [310–312, 711].

*Perturbative argument.* This mapping was first established perturbatively [310, 311]. Consider perturbation theory for the

complex  $N$ -component  $\phi^4$  theory



The drawing on the lhs of equation (870) is an LERW starting at  $x$ , ending in  $z$ , and passing through the segments numbered 1 to 3. Due to the crossing at  $y$ , the loop labeled 2 is erased; we draw it in red. The rhs of equation (870) gives all diagrams of  $\phi^4$  theory up to order  $g^5$ . The first term is the free-theory result, proportional to  $g^0$ . The second term  $\sim g$  cancels the first term, if one puts  $g \rightarrow 1$ . Here it is crucial to have the same regularization for the interaction as for the conditioning. The third term is proportional to  $N$ , due to the loop, indicated in red. Setting  $N \rightarrow -1$  compensates for the subtracted second term. Thus setting  $g \rightarrow 1$  and  $N \rightarrow -1$ , the probability to go from  $x$  to  $z$  remains unchanged as compared to the free theory. This is a necessary condition to be satisfied. Since the first two terms cancel, what remains is the last diagram, corresponding to the drawing for the trajectory of the LERW we started with.

Continuing to higher orders, one establishes a one-to-one correspondence between traces of LERWs and diagrams in perturbation theory. We still need an observable which is 1 when inserted into a blue part of the trace, and 0 within a red part. This can be achieved by the operator

$$\mathcal{O}(y) := \Phi_1^*(y)\Phi_1(y) - \Phi_2^*(y)\Phi_2(y). \tag{871}$$

When inserted into a loop, it cancels, whereas inserted into the backbone (LERW, blue), it yields one for each point. The fractal dimension  $z$  of an LERW is extracted from the length of the walk after erasure (blue part) as

$$\frac{\left\langle \int_{y,z} \Phi_1^*(x)\mathcal{O}(y)\Phi_1(z) \right\rangle}{\left\langle \int_z \Phi_1^*(x)\Phi_1(z) \right\rangle} \equiv m^2 \left\langle \int_{y,z} \Phi_1^*(x)\mathcal{O}(y)\Phi_1(z) \right\rangle \sim m^{-z}. \tag{872}$$

*Proof via Viennot's theorem.* This section is a shortened version of [312], itself inspired by [711]. The main tool is a combinatorial theorem due to Viennot [712]. It is part of the general theory of *heaps of pieces* (online lectures [713]). Here it reduces to a relation between LERWs, and collections of loops. To state the theorem, we need some definitions.

Consider a RW on a directed graph  $\mathcal{G}$ . The walk moves from vertex  $x$  to  $y$  with rate  $\beta_{xy}$ , and dies out with rate  $\lambda_x = m_x^2$ . The coefficients  $\{\beta_{xy}\}_{x,y \in \mathcal{G}}$  are weights on the graph. In particular, when  $\beta_{xy}$  is positive,  $\mathcal{G}$  contains an edge from  $x$  to  $y$ . Denote by  $r_x := \lambda_x + \sum_y \beta_{xy}$  the total rate at which the walk exits from vertex  $x$ .

A *path* is a sequence of vertices, denoted  $\omega = (\omega_1, \dots, \omega_n)$ . The probability  $\mathbb{P}(\omega)$  that the RW selects the path  $\omega$  and then

stops is

$$\mathbb{P}(\omega) = \frac{\lambda_{\omega_n} q(\omega)}{r_{\omega_n}}, \tag{873}$$

$$q(\omega) = \frac{\beta_{\omega_1\omega_2}}{r_{\omega_1}} \frac{\beta_{\omega_2\omega_3}}{r_{\omega_2}} \dots \frac{\beta_{\omega_{n-1}\omega_n}}{r_{\omega_{n-1}}}. \tag{874}$$

A *loop* is a path  $\omega = (\omega_1, \dots, \omega_{n-1}, \omega_n = \omega_1)$  where the first and last points are identical, and all other vertices distinct, so it cannot be decomposed into smaller loops. Loops obtained from each other via cyclic permutations are considered identical.

A *collection of disjoint loops* is a set  $L = \{C_1, C_2, \dots\}$  of mutually non-intersecting loops. We denote the *set of all such collections* by  $\mathcal{L}$ .

To formulate the theorem, fix a self-avoiding<sup>47</sup> path  $\gamma$ . Define the set  $\mathcal{L}_\gamma$  to consist of all collections of disjoint loops in which no loop intersects  $\gamma$ . Then Viennot's theorem can be written as ( $|L|$  being the number of loops)

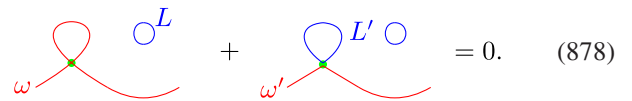
$$\mathcal{A}(\gamma) := q(\gamma) \sum_{L \in \mathcal{L}_\gamma} (-1)^{|L|} \prod_{C \in L} q(C) = \mathcal{P}(\gamma) \times \mathcal{Z}, \tag{875}$$

$$\mathcal{P}(\gamma) = \sum_{\omega: \mathcal{L}(\omega) = \gamma} q(\omega), \tag{876}$$

$$\mathcal{Z} = \sum_{L \in \mathcal{L}} (-1)^{|L|} \prod_{C \in L} q(C). \tag{877}$$

For  $\mathcal{A}(\gamma)$  one sums over the ensemble of collections of loops which do not intersect  $\gamma$ , giving each collection a weight  $(-1)^{|L|} \prod_{C \in L} q(C)$ . The rhs contains two factors. The first,  $\mathcal{P}(\gamma)$ , is the weight to find the LERW path  $\gamma$ , our object of interest. The second is the partition function  $\mathcal{Z}$ . Conditioning the walk to stop at  $x$ , this relation can be read as  $\mathcal{P}(\gamma) = \mathcal{A}(\gamma)/\mathcal{Z}$ .

To prove equation (875) consider a pair  $\{\omega, L\}$  constructed as follows: take a path  $\omega$  such that  $\mathcal{L}(\omega) = \gamma$  and an *arbitrary* collection  $L$  of disjoint loops. Our goal is to construct another pair  $\{\omega', L'\}$  by transferring a loop from  $L$  to  $\omega$  or vice versa, depending on where the loop originally was. For example,



In the first drawing, the left loop is part of  $\omega$ , whereas in the second one it is part of  $L'$ . These terms cancel, as  $(-1)^{|L|} = -(-1)^{|L'|}$ , and all other factors are identical. After each such pair is canceled, we are left with the terms in which it is impossible to transfer a loop from  $\omega$  to  $L$  or vice versa. These are exactly the terms on the lhs of equation (875).

For this procedure to work we need to ensure that we cannot obtain the same pair  $\{\omega', L'\}$  starting from two different pairs  $\{\omega, L\}$ . In order to achieve this, we use the following prescription. Start walking along  $\omega$ , until

<sup>47</sup> **Warning:** a *self-avoiding path* is a combinatorial object. The loop-erased random walk is one possible distribution on the set of self-avoiding paths. It should not be confused with the *self-avoiding walk* or *self-avoiding polymer*, a distinct distribution on the same set of self-avoiding paths.

- (a) we reach a vertex  $\omega_i$  that belongs to some  $C = (\omega_i = c_1, c_2 \dots, c_m = \omega_i) \in L$ , or
- (b) we reach a vertex  $\omega_i$  that does not belong to any  $C$ , but that we have already seen before, i.e.,  $\omega_j = \omega_i$  for  $j < i$ .

In the first case, we transfer  $C$  to  $\omega$ , i.e.,

$$\begin{aligned} \omega' &= (\omega_1, \dots, \omega_i, c_2, \dots, c_{m-1}, \omega_i, \dots, \omega_n), \\ L' &= L \setminus \{C\}. \end{aligned} \tag{879}$$

In the second case, we apply the one-loop erasure to  $\omega$ , and transfer the erased loop to  $L$ ,

$$\begin{aligned} \omega' &= (\omega_1, \dots, \omega_j, \omega_{j+1}, \dots, \omega_n), \\ L' &= L \cup \{(\omega_j, \omega_{j+1}, \dots, \omega_i = \omega_j)\}. \end{aligned} \tag{880}$$

Note that disjointness of the loop collections is preserved under the transfer, and that the loop erasure of  $\omega'$  remains  $\gamma$ . This completes the proof. For examples see [312].

A lattice action with two complex fermions and one complex boson. Our goal is to write a lattice action which generates  $\mathcal{A}(\gamma)$ , the lhs of equation (875). This can be achieved with an action based on one pair of complex conjugate fermionic fields. While this theory sums over all paths  $\gamma$ , yielding back the RW propagator, it contains no information on the erasure. In order to answer whether the resulting loop-erased path passes through a given point  $y$  it is necessary to use more fields. The simplest such setting consists of two pairs of complex conjugate fermionic fields  $(\phi_1, \phi_1^*)$ , and  $(\phi_2, \phi_2^*)$ , as well as a pair of complex conjugate bosonic fields  $(\phi_3, \phi_3^*)$ . When appearing in a loop, the latter cancels one of the fermions.

We define the action as

$$\phi^*(y)\phi(x) := \sum_{i=1}^3 \phi_i^*(y)\phi_i(x), \tag{881}$$

$$e^{-S} = \prod_x e^{-r_x \phi^*(x)\phi(x)} \left[ 1 + \sum_y \beta_{xy} \phi^*(y)\phi(x) \right]. \tag{882}$$

The path integral is defined by integrating over the  $n_f = 2$  families of fermionic fields,  $(\phi_i^*, \phi_i)$ ,  $i = 1, 2$ , and  $n_b = 1$  family of bosonic fields,  $i = 3$ . For  $\beta_{xy} = 0$ , we obtain

$$Z_0 = \prod_x r_x^{n_f - n_b} = \prod_x r_x. \tag{883}$$

Define (normalized) expectation values  $\langle \mathcal{O}(\phi^*, \phi) \rangle$  w.r.t. the action (882) and the (normalized) partition function  $Z$  as

$$\langle \mathcal{O}(\phi^*, \phi) \rangle := \frac{1}{Z_0} \int \mathcal{D}[\phi] \mathcal{D}[\phi^*] e^{-S} \mathcal{O}(\phi^*, \phi), \tag{884}$$

$$Z := \langle 1 \rangle. \tag{885}$$

Calculating  $Z$  by expansion in  $\beta_{xy}$  is best done graphically: due to the square bracket in equation (882), at each  $x$  one can place exactly one outgoing arrow to one of the neighbors  $y$ , with color  $i$ , or no arrow. Summing over all possible colorings and all graphs, we obtain  $\mathcal{Z}$  as given in equation (877).

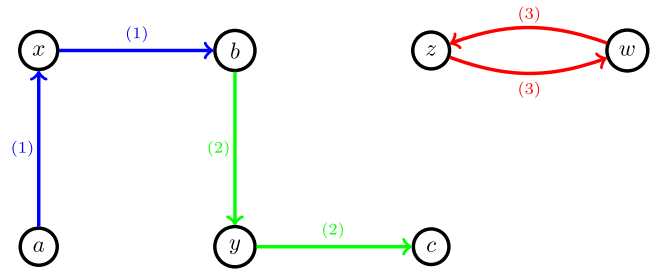


**Figure 76.** An example of a diagram that contributes to  $U$ . Our coloring conventions are blue for  $(\phi_1, \phi_1^*)$ , green for  $(\phi_2, \phi_2^*)$ , and red for  $(\phi_3, \phi_3^*)$ . Reproduced from [312]. CC BY 4.0.

In order to assess whether a point  $b$  belongs to a LERW from  $a$  to  $c$  after erasure, we fix the three vertices  $a, b$  and  $c$ , and consider the observable

$$U(a, b, c) = \lambda_c r_b^2 r_c \langle \phi_2(c)\phi_2^*(b)\phi_1(b)\phi_1^*(a) \rangle, \tag{886}$$

defined by equation (884).

The graphs that contribute consist of a self-avoiding path  $\gamma$  and a collection  $L$  of disjoint self-avoiding colored loops such that (see figure 76):

- (a)  $\gamma$  is a path from  $a$  to  $c$  passing through  $b$ . The edges of  $\gamma$  between  $a$  and  $b$  have color 1, and the edges between  $b$  and  $c$  have color 2.
- (b) Fix  $C \in L$ . If the color of  $C$  is 2 then it cannot intersect  $\gamma$ . If its color is 1 or 3, it can only intersect  $\gamma$  at the (final) point  $c$ .

In the latter case, the contribution to  $U(a, b, c)$  is

$$(-1)^{\#\text{fermionic loops}} q(\gamma) \prod_{C \in L} q(C). \tag{887}$$

We now sum over all possible colorings of the loops. Since loops that intersect  $c$  may have either color 1 or 3, one fermionic and one bosonic, they cancel, leaving only graphs in which loops do not intersect  $\gamma$ . The other loops, as before, give a factor of  $-1$ . We therefore established that

$$U(a, b, c) = \sum_{\gamma \in \text{SA}(a, b, c)} q(\gamma) \sum_{L \in \mathcal{L}_\gamma} (-1)^{|L|} \prod_{C \in L} q(C), \tag{888}$$

where the sum is over all self-avoiding paths from  $a$  to  $c$  passing through  $b$ , and denoted  $\text{SA}(a, b, c)$ . In view of equation (875) this can be written as

$$U(a, b, c) = \sum_{\gamma \in \text{SA}(a, b, c)} \mathcal{A}(\gamma). \tag{889}$$

It implies that our object of interest, the probability that an LERW starting at  $a$  and ending in  $c$  passes through  $b$  is

$$\sum_{\gamma \in \text{SA}(a, b, c)} \mathcal{P}(\gamma) = \frac{U(a, b, c)}{Z}. \tag{890}$$

*Continuous limit of the lattice action.* Let us rewrite the action  $\mathcal{S}$  explicitly,

$$\mathcal{S} = \sum_x \left[ r_x \phi^*(x) \phi(x) - \ln \left( 1 + \sum_y \beta_{xy} \phi^*(y) \phi(x) \right) \right]. \tag{891}$$

The leading term in  $\mathcal{S}$  reads

$$\begin{aligned} & \sum_x \left[ r_x \phi^*(x) \phi(x) - \sum_y \beta_{xy} \phi^*(y) \phi(x) \right] \\ &= \sum_x \phi^*(x) [m_x^2 - \nabla_\beta^2] \phi(x), \\ m_x^2 &= r_x - \sum_y \beta_{yx}, \quad \nabla_\beta^2 \phi(x) = \sum_y \beta_{yx} [\phi(y) - \phi(x)]. \end{aligned} \tag{892}$$

The subleading term in  $\mathcal{S}$  is

$$\begin{aligned} & \frac{1}{2} \sum_x \left[ \sum_y \beta_{xy} \phi^*(y) \phi(x) \right]^2 = \frac{g}{2} \sum_x [\phi^*(x) \phi(x)]^2 + \dots \\ g &:= \left[ \sum_y \beta_{xy} \right]^2, \end{aligned} \tag{893}$$

where the dropped terms contain at least one lattice Laplacian  $\nabla_\beta^2$ . Standard arguments [2] show that the latter are irrelevant in an RG analysis, as are higher-order terms in the expansion of the  $\ln$  in equation (891). Taking the continuum limit, we arrive at the theory defined in equation (869), setting there  $u, \tilde{u} \rightarrow 0$ , and identifying  $(\bar{\psi}_i, \psi_i)$ ,  $i = 1, 2$  there with  $(\phi_i^*, \phi_i)$  here, and  $(\tilde{\phi}, \phi)$  there with  $(\phi_3^*, \phi_3)$  here.

*Perturbative results.* Using  $\phi^4$ -theory at  $n = -2$  allows us to obtain an extremely precise estimate of the fractal dimension  $z$ , which can be compared to an even more precise Monte Carlo simulation,

$$z = 1.6243(10) \quad (6 \text{ loops}) \quad [140], \tag{894}$$

$$z = 1.62400(5) \quad (\text{Monte Carlo}) \quad [708]. \tag{895}$$

The agreement is quite impressive.

### 8.9. Other models equivalent to loop-erased random walks, and CDWs

There is a plethora of further relations relating CDWs or LERWs to other critical systems, see figure 77. Let us discuss at least some of them: while LERWs are non-Markovian RWs, their traces are equivalent to those of the *Laplacian RW* [715, 719], which is Markovian, if one considers the whole trace as the variable of state. It is constructed on the lattice by solving the Laplace equation  $\nabla^2 \Phi(x) = 0$  with boundary conditions  $\Phi(x) = 0$  on the already constructed curve, and  $\Phi(x) = 1$  at the destination of the walk, either a chosen point, or infinity. The walk then advances from its tip  $x$  to a neighboring point  $y$ , with probability proportional to  $\Phi(y)$ . As  $\Phi(x) = 0$ ,

$\Phi(y) \equiv \Phi(y) - \Phi(x)$  can be interpreted as the *electric field* of the *potential*  $\Phi(y)$ .

In a variant of this model growth is allowed not only from the tip, but from any point on the already constructed object, with a probability  $\sim \Phi(y)$ . This is known as the *dielectric breakdown model* [720], the simplest model for lightning. The same construction pertains to diffusion-limited aggregation [721].

The shortest path on a UST is an LERW [714]. The latter are equivalent to Eulerian circuits [715], and Abelian sandpiles [718]. Abelian sandpiles are equivalent to the Potts-model in the limit of  $q \rightarrow 0$  [514]. Many of these exact mappings can be found in the lecture [515]. It was conjectured long ago that Abelian sandpiles map on CDWs [120]. A test on the FRG field theory was performed in [717], and validated in [706].

It would be interesting to generalize loops to higher-dimensional surfaces, as was done for self-avoiding manifolds in [722, 723].

### 8.10. Conformal field theory for critical curves

In  $d = 2$ , all critical exponents should be accessible via conformal field theory (CFT). The latter is based on ideas proposed in the 80s by Belavin *et al* [724]. They constructed a series of minimal models, indexed by an integer  $m \geq 3$ , starting with the Ising model at  $m = 3$ . These models are conformally invariant and unitary, equivalent to reflection positive in Euclidean theories. For details, see one of the many excellent textbooks on CFT [234, 237, 238, 725]. Their conformal charge<sup>48</sup> is given by

$$c = 1 - \frac{6}{m(m+1)}. \tag{896}$$

The list of conformal dimensions for allowed operators at a given  $m$  is given by the Kac formula with integers  $r, s$

$$h_{r,s} = \frac{[r(m+1) - sm]^2 - 1}{4m(m+1)}, \quad 1 \leq r < m, \quad 1 \leq s \leq m. \tag{897}$$

It was later realized that other values of  $m$  also correspond to physical systems, in particular  $m = 1$  (LERWs), and  $m = 2$  (self-avoiding walks). These values can further be extended to non-integer  $n$  and  $m$ , using the identification

$$n = 2 \cos \left( \frac{\pi}{m} \right). \tag{898}$$

More strikingly, the table of dimensions allowed by equation (897) has to be extended to half-integer values, including 0. This yields: the fractal dimension of the propagator line [726–728]

$$d_f = 2 - 2h_{1,0} = 1 + \frac{\pi}{2 \left( \arccos \left( \frac{n}{2} \right) + \pi \right)}. \tag{899}$$

<sup>48</sup>The conformal charge is the coefficient in the leading term of the OPE of the stress-energy tensor. It also gives the amplitude of finite-size corrections [3].

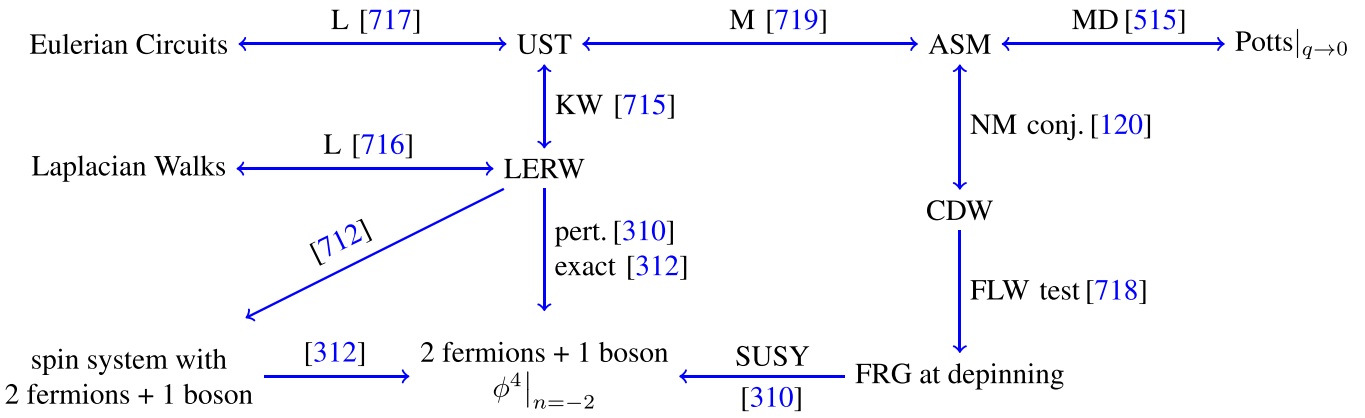


**Figure 77.** Relations between Laplacian walks, LERW, USTs, Eulerian circuits, the ASM, the Potts-model in the limit of  $q \rightarrow 0$ , CDWs at depinning, mapping onto the FRG field theory at depinning, reducing to  $\phi^4$ -theory at  $n = -2$ , and equivalent to an interacting theory of two complex fermions and one complex boson.

$\nu$ , i.e. the inverse fractal dimension of all lines, be it propagator or loops ([728], inline after equation (2))

$$\nu = \frac{1}{2 - 2h_{1,3}} = \frac{1}{4} \left( 1 + \frac{\pi}{\arccos(\frac{n}{2})} \right). \quad (900)$$

For  $\eta$ , there are two suggestive candidates from the Ising model,  $\eta = 4h_{1,2} = 4h_{2,2}$ , which do not work for other values of  $n$ ; instead [726–728]

$$\eta = 4h_{\frac{1}{2},0} = \frac{5}{4} - \frac{3 \arccos(\frac{n}{2})}{4\pi} - \frac{\pi}{\arccos(\frac{n}{2}) + \pi}. \quad (901)$$

It has a square-root singularity both for  $n = -2$  and  $n = 2$ . There is no clear candidate for the exponent  $\omega$  [140]. The crossover exponent  $\phi_c$  [1, 140, 729] (explained in [140], page 7) becomes

$$\phi_c = \nu d_f = \frac{1 - h_{1,0}}{1 - h_{1,3}} = \frac{1}{4} + \frac{3\pi}{8 \arccos(\frac{n}{2})}. \quad (902)$$

To conclude, we remark that ideas identifying symplectic fermions with the ASM [730] are overly simplistic, as they do not catch any of the above exponents.

## 9. Further developments and ideas

### 9.1. Non-perturbative RG (NPRG)

The renormalization transformation originally proposed by Wilson and Kogut [117] consists in integrating out a specific range of fast modes, and following the effective action of the remaining modes under this transformation. While this procedure is exact by construction, its implementation is infeasible, and one has to rely on approximation schemes. Several such schemes have been proposed:

- (a) expansion in  $\epsilon = 4 - d$  [111]. This scheme produces a divergent, albeit Borel-resummable series in  $\epsilon$ , with high predictive power [2, 140, 731, 732].
- (b) Expansion in the number of components  $N$  [2, 733]. This works in general well for  $N \gtrsim 5$ , but gives mostly qualitative information at  $N = 1$ .

- (c) The non-perturbative RG (NPRG) approach. This technique can be formulated for the free energy  $\mathcal{F}(J) = \ln \mathcal{Z}(J)$  [734], or the effective action  $\Gamma[\phi]$  [735]. For the effective action it has the structure

$$\partial_\ell \Gamma[\phi] = \frac{1}{2} \text{tr} \left[ \left( \frac{\delta^2 \Gamma[\phi]}{\delta \phi^2} + R_\ell \right)^{-1} \partial_\ell R_\ell \right]. \quad (903)$$

The function  $R_\ell$  is a momentum cutoff function, optimized for convergence. The simplest truncation of equation (903) is the local potential approximation, sometimes followed by a gradient expansion. (For historical work and a recent review see [734–740].)

The FRG technique used in this review is perturbative in  $\epsilon = 4 - d$ ; keeping the exact field dependence is crucial. The NPRG is an approximation (truncation) in the momentum dependence. Based on a numeric integration of the flow equations, keeping only the leading orders in the field is often sufficient and accelerates the implementation. The NPFRG (used for the RF Ising model in section 9.2) is approximate in the momentum, but aims at keeping the full field dependence as does perturbative FRG. One sometimes encounters the term *exact RG* instead of NPRG, a notion better reserved for the concept of RG than any of its approximate implementations. The Heidelberg school [735] now uses FRG instead of NPRG, a notion we reserve to situations when the exact functional form is required.

### 9.2. Random-field magnets

Another domain of application of the Functional RG are spin models in a RF (for an introduction see [741]). The model usually studied is

$$\mathcal{H} = \int d^d x \frac{1}{2} (\nabla \vec{S})^2 + \vec{h}(x) \vec{S}(x), \quad (904)$$

where  $\vec{S}(x)$  is a unit vector with  $N$ -components, and  $\vec{S}(x)^2 = 1$ . This is the so-called  $O(N)$  sigma model, to which has been added a RF, which can be taken Gaussian  $\vec{h}_i(x) \vec{h}_j(x')$  =

$\sigma \delta_{ij} \delta^d(x - x')$ . In the absence of disorder the model has a ferromagnetic phase for  $T < T_f$  and a paramagnetic phase above  $T_f$ . The lower critical dimension is  $d = 2$  for any  $N \geq 2$ , meaning that below  $d = 2$  no ordered phase exists. In  $d = 2$  solely a paramagnetic phase exists for  $N > 2$ ; for  $N = 2$  (XY model) quasi LR order exists at low temperature, with  $\vec{S}(x)\vec{S}(x')$  decaying as a power law of  $x - x'$ . This is the RP fixed point of sections 2.9 and 2.28. Here we wish to study the model directly at  $T = 0$ . The first step is to rewrite the hard-spin constraint  $\vec{S}(x)^2 = 1$  as a field theory. This yields an energy before disorder-averaging

$$\mathcal{H} = \int d^d x \frac{1}{2} \left[ \nabla \vec{\phi}(x) \right]^2 + \mathcal{V}(\vec{\phi}(x)) + \vec{h}(x) \vec{\phi}(x). \quad (905)$$

The potential  $\mathcal{V}(\vec{\phi})$  is the typical double-well potential, as e.g.  $\mathcal{V}(\vec{\phi}) \simeq (\vec{\phi}^2 - 1)^2$ . The dimensional-reduction theorem in section 1.6, written for this energy indicates that the effect of a quenched RF in dimension  $d$  equals the one for a pure model at a temperature  $T \sim \sigma$  in dimension  $d - 2$ . Hence one expects a transition from a ferromagnetic phase to a disordered phase at  $\sigma_c$  as the disorder increases in any dimension  $d > 4$ , and no order for  $d < 4$  and  $N \geq 2$ . Not surprisingly, this is again incorrect, as can be seen using FRG.

It was noticed by Fisher [742] that an infinity of relevant operators are generated. These operators, which correspond to an infinite set of random anisotropies, are irrelevant by naive power counting near  $d = 6$  [743, 744], the naive upper critical dimension (corresponding to  $d = 4$  for the pure  $O(N)$  model via dimensional reduction). Indeed many early studies concentrating on  $d$  around  $d = 6$  missed the anisotropies mentioned above.

A controlled  $\epsilon$ -expansion using FRG can be constructed around dimension  $d = 4$ , the naive lower critical dimension, using the reformulation of the Hamiltonian (904) in terms of a non-linear  $\sigma$ -model, first at one-loop order [742–744], and then extended to two loops [33, 38]. The FRG includes all operators which are marginal in  $d = 4$ . Its action in replicated form reads

$$\mathcal{S} = \int d^d x \frac{1}{2T} \sum_a \left[ \nabla \vec{S}_a(x) \right]^2 - \frac{1}{2T^2} \sum_{ab} \hat{R} \left( \vec{S}_a(x) \vec{S}_b(x) \right). \quad (906)$$

The function  $\hat{R}(z)$  parameterizes the disorder. The term  $\hat{R}(z) \sim z$  is a direct result of the disorder average of equation (905); higher-order terms are generated within perturbation theory. The FRG flow equation has been obtained to order  $R^2$  (one loop) [742–744] and  $R^3$  (two loops) [33, 38]. It is best parameterized in terms of the variable  $\phi$ , the angle between the two replicas, defining  $R(\phi) = \hat{R}(z = \cos \phi)$ . Since the vectors are of unit norm,  $z = \cos \phi$  lies in the interval  $[-1, 1]$ .

$$\begin{aligned} \partial_\ell R(\phi) = & \epsilon R(\phi) + \frac{1}{2} R'(\phi)^2 - R''(0) R'(\phi) \\ & + (N - 2) \left[ \frac{1}{2} \frac{R'(\phi)^2}{\sin^2 \phi} - \cot \phi R'(\phi) R''(0) \right] \end{aligned}$$

$$\begin{aligned} & + \frac{1}{2} [R''(\phi) - R''(0)] R'''(\phi)^2 \\ & + (N - 2) \left[ \frac{\cot \phi}{\sin^4 \phi} R'(\phi)^3 - \frac{5 + \cos 2\phi}{4 \sin^4 \phi} R'(\phi)^2 R''(\phi) \right. \\ & + \frac{1}{2 \sin^2 \phi} R''(\phi)^3 - \frac{1}{4 \sin^4 \phi} R''(0) \left( 2(2 + \cos 2\phi) R'(\phi)^2 \right. \\ & \left. \left. - 6 \sin 2\phi R'(\phi) R''(\phi) + (5 + \cos 2\phi) \sin^2 \phi R''(\phi)^2 \right) \right] \\ & - \frac{N + 2}{8} R'''(0)^2 R''(\phi) - \frac{N - 2}{4} \cot \phi R'''(0)^2 R'(\phi) \\ & - 2(N - 2) [R''(0) - R''(0)^2 + \gamma_a R'''(0)^2] R(\phi). \quad (907) \end{aligned}$$

The last factor proportional to  $R(\phi)$  takes into account the renormalization of temperature, absent in the manifold problem<sup>49</sup>. The full analysis of this equation is quite involved. The key observation is that under FRG again a cusp develops near  $z = 1$ . Analysis of the FRG fixed points shows interesting features already at one-loop order. For  $N = 2$ , the fixed point corresponds to the Bragg-glass phase of the XY model with quasi-long range order accessible via a  $d = 4 - \epsilon$  expansion below  $d = 4$  [745]. Hence for  $N = 2$  the lower critical dimension is  $d_{lc} < 4$ , and conjectured to be  $d_{lc} < 3$  [745]. On the other hand Feldman [743, 744] found that for  $N = 3, 4, \dots$  there is a fixed point in dimension  $d = 4 + \epsilon > 4$ . This fixed point has exactly one unstable direction, corresponding to the ferromagnetic-to-disorder transition. The situation at one loop is thus rather strange: for  $N = 2$ , only a stable FP which describes a *unique* phase exists, while for  $N = 3$  only an unstable FP exists, describing the transition between two phases. The question is: where does the disordered phase go as  $N$  decreases? The complete analysis at two-loop order [33] shows that there is a critical value of  $N$ ,  $N_c = 2.8347408$ , below which the lower critical dimension  $d_{lc}$  of the quasi-ordered phase plunges below  $d = 4$ , resulting into two new fixed points below  $d = 4$ . This is schematically shown in figure 78. For  $N > N_c$  a ferromagnetic phase exists with lower critical dimension  $d_{lc} = 4$ . For  $N < N_c$  one finds the expansion

$$d_{lc}^{\text{RF}} = 4 - \epsilon_c \approx 4 - 0.1268(N - N_c)^2 + \mathcal{O}(N - N_c)^3. \quad (908)$$

One can then compute the critical exponents at this fixed point [33, 38, 743, 744].

The expansions discussed above were either in  $d = 6 - \epsilon$ , neglecting by construction FRG corrections of the disorder with the physics of the cusp, or in  $d = 4 + \epsilon$ , neglecting amplitude fluctuations in  $\vec{\phi}(x) := \int_{\text{box}} \vec{S}(x)$ , as they were formulated in terms of a non-linear  $\sigma$ -model. To find a consistent RG treatment in the full  $(N, d)$ -plane is much more complicated, and can to date only be achieved within the non-perturbative FRG approach (NP-FRG), i.e. the RG must be both non-perturbative (NP) and functional (FRG). For this formalism to work, and to correctly encounter shocks, i.e. the physics of the cusp, one has to allow for a cusp in the effective disorder correlator. It

<sup>49</sup> The constant  $\gamma_a$  is discussed in [33].

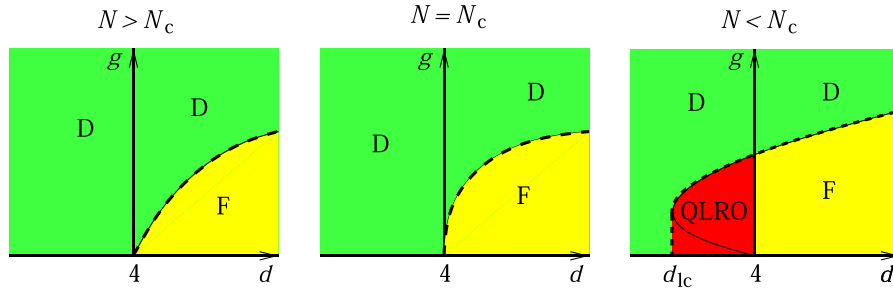


**Figure 78.** Phase diagram of the RF non-linear sigma model. D = disordered, F = ferromagnetic, QLRO = quasi long-range order. Reprinted figure with permission from [33], Copyright (2006) by the American Physical Society.

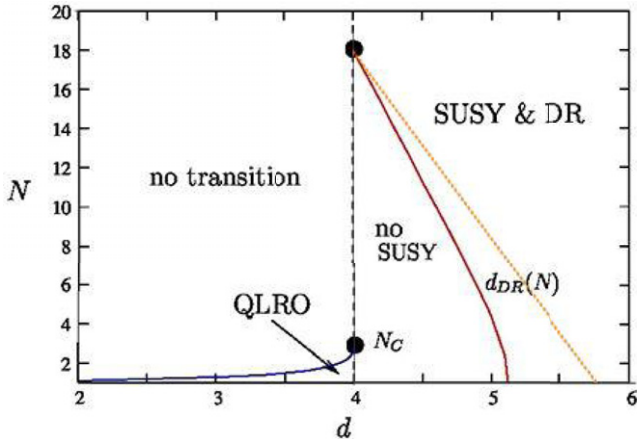


**Figure 79.** The phase diagram of Tarjus and Tissier. Reprinted by permission from Springer Nature Customer Service Centre GmbH: Springer. Eur. Phys. J. (c) 2020. The added line given by equation (909) qualitatively agrees with the NP-FRG prediction.

is the merit of Tarjus and Tissier to have transformed this general idea into a predictive framework [34–37, 39, 746]. We show in figure 79 their phase diagram. The behavior in the region around  $d = 4$  and  $N = N_c$  was obtained above from the non-linear  $\sigma$  model. A novel prediction is that for  $d = 4 + \epsilon$  and  $N > N^* = 18$  there is a solution without cusp, and as a consequence dimensional reduction and super-symmetry are restored [34, 747–749]. The critical line starting at  $d = 4$  and  $N^* = 18$  can be obtained in an  $\epsilon$ -expansion [38, 750],

$$N^*(d) = 18 - \frac{49}{5}(d - 4) + \mathcal{O}(d - 4)^2. \quad (909)$$

The FRG in its perturbative and NP versions can be applied to a variety of disordered systems in and out of equilibrium, see e.g. [746]. In particular,  $O(N)$  models with a random anisotropy can be treated. For this universality class, details of the phase diagram, the critical exponents, and the many subtleties involved, the reader is referred to [33–39, 746, 750–753].

For RF, the NP-FRG solution qualitatively agrees with the perturbative FRG solution, but systematically predicts a smaller  $N^*(d)$ , terminating for  $N = 1$  at  $d = 5.1$ , while the analytic solution favors  $d = 5.74$ . We remind that NP-FRG is based on a truncation of the functional form of the effective action. By construction it includes loop corrections at all orders, but in an approximate way beyond one loop. Thus for

the Ising model, dimensional reduction is valid near dimension  $d = 6$ , whereas a non-trivial ordered phase exists down to  $d = 2$ . This has been confirmed numerically in [27, 754–756], the most remarkable test being the comparison of diverse correlation functions in the five-dimensional RF model, as compared to their pure three-dimensional counterparts at  $T = T_c$  [756].

There is renewed interest into the RF Ising model [700, 701]. The authors follow the proposition of Cardy [698] to use  $n$  bosonic replicas  $\phi_i, i = 1, \dots, n$ , to introduce fields

$$u := \frac{1}{2} [\phi_1 + (n - 1)^{-1}(\phi_2 + \dots + \phi_n)], \quad (910)$$

$$\tilde{u} := \frac{1}{2} \left[ \phi_1 - \frac{T}{\Delta(0)}(n - 1)^{-1}(\phi_2 + \dots + \phi_n) \right], \quad (911)$$

together with  $(n - 2)$  fields  $\psi_j$  which are linear combinations of  $\frac{T}{\Delta(0)}(\phi_2, \dots, \phi_n)$  chosen to be orthogonal to  $\phi_2 + \dots + \phi_n$ . As Cardy showed, this choice of fields allows one to write an action which (apart from terms irrelevant in  $6 - \epsilon$  dimensions) is *formally* equivalent to equation (837), but containing more fields, thus a breaking of super-symmetry becomes possible. The authors then identify [701] such perturbations which destabilize the supersymmetric dimensional-reduction fixed point below  $d_c \approx 4.2$ . In section 8.4 we showed that in order to see the renormalization of the disorder, one needs more than one physical copy. To be precise, the cusp appears in the renormalized disorder correlations, as a function of the difference between the two physical copies. In such a calculation, the critical dimension moves up to  $d_c \approx 4.6$  [757]. We do not see how this difference between replicas is present in the above choice of coordinates, but we believe that by doubling the set of Cardy variables this can be achieved.

We would like to conclude by some general remarks on the form of the effective action necessary for a proper RG treatment of the RF Ising model. As in all disordered systems, it should *at least* contain a one-replica *and* a two-replica contribution. Its general form should be as given in equation (30) in a replica formulation, in equation (314) in a dynamical formulation, or in equation (836) in the Susy formulation. While the one-replica part may contain an arbitrary function of  $u$  and  $\nabla u$ , let us concentrate on the two-replica part parameterizing the disorder correlations. For disordered elastic manifolds, this is achieved by the function  $\Delta(u_1 - u_2)$ , where we remind that  $\Delta(u_1 - u_2)$  has only one argument due to the STS (66). As the latter is absent for the RF Ising model, one needs to make a

more general ansatz, see e.g. [37, 752],

$$\Delta(u_1, u_2) = \hat{\Delta}(\bar{u}, \delta u), \quad (912)$$

$$\bar{u} := \frac{1}{2}(u_1 + u_2), \quad \delta u := |u_2 - u_1|. \quad (913)$$

The absolute value appears since  $\Delta(u_1, u_2) = \Delta(u_2, u_1)$ . Let us apply as in sections 2.10 and 2.11 a field  $h = m^2 w$ , and denote  $u_i \equiv u(w_i)$  the expectation of  $u$  given  $w_i$ . Both in the statics and at depinning  $u(w_i)$  is unique. The connected correlation function  $\langle u_1 u_2 \rangle^c$  is

$$\overline{u(w_1)u(w_2)}^c = \Gamma_1''(u_1)^{-1} \Delta(u_1, u_2) \Gamma_1''(u_2)^{-1}. \quad (914)$$

Here  $\Gamma_1''(u)$  is the second (functional) derivative of the one-replica contribution to the effective action. Formally, the lhs which depends on  $w_1$  and  $w_2$  is the Legendre transform of the second cumulant  $\Delta(u_1, u_2)$  in the effective action depending on  $u_1$  and  $u_2$ . Graphically, the prescription amounts to amputating the one-particle irreducible contributions to (914). The key point is that the observable on the lhs can be measured. For small  $w_1 - w_2 > 0$  it behaves with  $\bar{w} := (w_1 + w_2)/2$  as

$$\frac{1}{2} \overline{[u(w_1) - u(w_2)]^2}^c \simeq \mathcal{A}(\bar{w}) |w_1 - w_2| + \mathcal{O}(w_1 - w_2)^2, \quad (915)$$

$$\mathcal{A}(\bar{w}) := \left. \frac{\langle S^2 \rangle}{2 \langle S \rangle} \right|_{\bar{w}} \times \overline{u'(\bar{w})}. \quad (916)$$

As indicated, the ratio  $\langle S^2 \rangle / (2 \langle S \rangle)$  depends on  $\bar{w}$ . These relations are derived similar to equation (104), except that when writing equation (102) as

$$\overline{u(w_1) - u(w_2)} = \langle S \rangle \rho_{\text{shock}} |w_1 - w_2| + \mathcal{O}(w_1 - w_2)^2, \quad (917)$$

the lhs becomes

$$\overline{u(w_1) - u(w_2)} \simeq \overline{u'(\bar{w})} (w_1 - w_2) + \mathcal{O}(w_1 - w_2)^2. \quad (918)$$

Solving equation (914) for  $\Delta(u_1, u_2)$  proves that it has a cusp as a function of  $u_1 - u_2$ , with amplitude given in equation (916).

### 9.3. Dynamical selection of critical exponents

Evaluating the partition function of a field theory in presence of a potential  $\mathcal{V}_0(u)$  at constant background field  $u$  to one-loop order, and normalizing with its counterpart at  $\mathcal{V}_0 = 0$ , one typically gets a partition function of the form

$$\ln \left( \frac{Z[u]}{Z_0[u]} \right) = - \int^{\Lambda} \frac{d^d k}{(2\pi)^d} \ln \left( 1 + \frac{\mathcal{V}_0''(u)}{k^2 + m^2} \right). \quad (919)$$

We have explicitly written an UV cutoff  $\Lambda$ . This equation is at the origin of *non-perturbative* renormalization group (NPRG) schemes (section 9.1). To leading order, the effective action is  $\Gamma(u) = - \ln(Z[u]/Z_0[u])$ , and denoting its local part by  $\mathcal{V}(u)$ , we arrive at the following *functional* flow equation for the *renormalized* potential  $\mathcal{V}(u)$

$$-m\partial_m \mathcal{V}(u) = -m\partial_m \int^{\Lambda} \frac{d^d k}{(2\pi)^d} \ln \left( 1 + \frac{\mathcal{V}_0''(u)}{k^2 + m^2} \right). \quad (920)$$

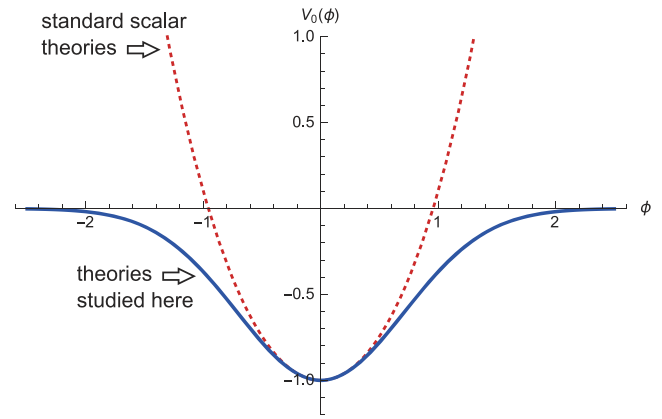


**Figure 80.** The function  $\mathcal{V}_0(\phi)$ , for  $\phi^4$  theory (top, red, dashed), and a bounded potential (bottom, blue, solid). Reprinted figure with permission from [758], Copyright (2016) by the American Physical Society.

Keeping only the leading non-linear term [758] leads to the simple flow equation

$$-m\partial_m \mathcal{V}(u) = -m^{d-4} \frac{1}{2} \mathcal{V}''(u)^2 + \dots \quad (921)$$

Note that this equation is very similar to the FRG flow equation (61) for disordered elastic manifolds. It reproduces the standard RG-equation for  $\phi^4$  theory; indeed, setting

$$\mathcal{V}(u) = m^{4-d} \frac{u^4}{72} g, \quad (922)$$

we arrive with  $\epsilon := 4 - d$  at

$$-m\partial_m g = \epsilon g - g^2 + \dots \quad (923)$$

This is the standard flow equation of  $\phi^4$  theory, with fixed point  $g_* = \epsilon$ . One knows that the potential (922) at  $g = g_*$  is attractive, i.e. perturbing it with a perturbation  $\phi^{2n}$ ,  $n > 2$ , the flow brings it back to its fixed-point form.

This fixed point, and its treatment with the projected simplified flow equation (923) is relevant in many situations, the most famous being the Ising model. The form of its microscopic potential, which is plotted in figure 80 (red dashed curve), grows unboundedly for large  $\phi$ . This is indeed expected for the Ising model, for which the spin, of which  $\phi$  is the coarse-grained version, is bounded.

There are, however, situations, where this is not the case. An example is the attraction of a domain wall by a defect. In this situation, one expects that the potential at large  $\phi$  vanishes, as plotted on figure 80 (solid blue line). The question to be asked is then: where does the RG flow lead?

As one sees from figure 80, the *bounded* potential  $\mathcal{V}_0$  is negative. In order to deal with positive quantities, set  $\mathcal{V}(u) \equiv -\mathcal{R}(u)$ . The flow equation to be studied is

$$-m\partial_m \mathcal{R}(u) = m^{-\epsilon} \frac{1}{2} \mathcal{R}''(u)^2 + \dots \quad (924)$$

As shown in [758], for generic smooth initial conditions as plotted on figure 80:

- (a) The flow equation (924) develops a cusp at  $u = 0$ , and a cubic singularity at  $u = u_c > 0$ .
- (b) The rescaled flow equation for the dimensionless function  $\tilde{R}(u)$  (to be compared to equation (64))

$$-m\partial_m\tilde{R}(u) = (\epsilon - 4\zeta)\tilde{R}(u) + \zeta u\tilde{R}'(u) + \frac{1}{2}\tilde{R}''(u)^2 + \dots \quad (925)$$

has an infinity of fixed points  $-m\partial_m\tilde{R}(u) = 0$ , indexed by  $\zeta \in [\frac{\epsilon}{4}, \infty]$ .

- (c) The solution chosen dynamically when starting from smooth initial conditions is  $\zeta = \frac{\epsilon}{3}$ . Its analytic expression for  $0 \leq u \leq 1$  reads

$$\tilde{R}_{\zeta=\frac{\epsilon}{3}}(u) = \epsilon \left[ \frac{1}{18}(1-u)^3 - \frac{1}{72}(1-u)^4 \right]. \quad (926)$$

It vanishes for  $u > 1$ , and is continued symmetrically to  $u < 0$ .

This scenario is quite unusual: normally, the perturbatively accessible fixed points of the RG flow have only one fixed point. In the few cases where there is more than one fixed point, the spectrum of fixed points is at least *discrete*. In contrast, here is a spectrum of fixed points. On the other hand, only one of them seems to be chosen. Thus experiments would only see this one fixed point.

It is yet not clear to which physical system it applies. As discussed in the literature [759–764], experiments describing wetting are usually attributed to a flow equation *linear* in  $R(u)$ . Is a nonlinear fixed point possible? Let me cite Thierry Giamarchi, one of the pioneers of FRG: ‘whenever there is a simple equation, it is somewhere realized in nature’.

#### 9.4. Conclusion and perspectives

The aim of this review was to give a thorough overview over the physics of disordered elastic manifolds, with its numerous connections to systems as diverse as sandpiles and LERWs. We covered all theoretical tools developed to date, including FRG, replicas, RSB, MSR dynamics, and super-symmetry. We put emphasis on applications, giving experimentalists the necessary tools to verify the theoretical concepts, and going beyond critical exponents.

Our aim at completeness was seriously challenged by the sheer amount of publications on the subject, and we apologize for any omissions. Please let us know, and we will try to remedy.

While the presented methods are powerful, fundamental questions remain: can FRG be applied to other systems such as spin glasses, sheared colloids, real glasses, or Navier–Stokes turbulence? Can FRG be applied beyond the elastic limit, i.e. to systems with overhangs or topological defects, or to fractal curves that cannot be represented by directed interfaces?

The author is looking forward to exciting new discoveries, and the contributions of today’s PhD students and postdocs. As for this review, it needs to stop here.

## Acknowledgments

It is a pleasure to thank all my collaborators over the past years: Pierre Le Doussal for introducing me to the subject and all his enthusiasm in the many projects we undertook together. A Rosso, A Kolton, L Laurson, and A Middleton for putting the theoretical concepts to test. M Müller for all his insights in the connection to RSB. Many thanks go to my students M Delorme, A Dobrinevski, C ter Burg, G Mukerjee, T Thierry, Z Zhu, and postdocs C Husemann, A Petkovic, Z Ristivojevic and A Shapira, for their help and pertinent questions. I am grateful to A A Fedorenko for the many enjoyable common projects. S Atis, F Bohn, M Correa, A Douin, A K Dubey, G Durin, F Lechenault, S Moulinet, M R Pastó, F Ritort, P Rissone, E Rolley, D Salin, R Sommer, and L Talon were essential in testing the concepts in experiments. I have benefitted from collaborations with L Aragon, C Bachas, P Chauve, R Golestanian, E Jagla, M Kardar, M Kompaniets, W Krauth, A Ludwig, C Marchetti, A Perret, E Raphael, G Schehr and J Vannimenus. Many thanks for discussions go to M Alava, C Aron, E Brézin, L Balents, E Bouchaud, J P Bouchaud, J Cardy, F David, H W Diehl, T Giamarchi, P Goldbart, D Gross, F Haake, A Hartmann, J Jacobsen, J Krug, S Majumdar, M Mézard, T Nattermann, G Parisi, H Rieger, L Ponson, S Rychkov, S Santucci, L Schäfer, S Stepanov, L Sütterlin, G Tarjus, M Tissier, F Wegner, J Zinn-Justin and A Zippelius. This review is based on lecture notes for the ICTP master program at ENS, and I thank all students for their feedback.

## Data availability statement

All data that support the findings of this study are included within the article (and any supplementary files).

## Appendix A. Basic tools

### A.1. Markov chains, Langevin equation, inertia

In Markov chains the state at time  $t_N := N\tau$  is given by the product of *transition probabilities*

$$\mathcal{P}(x_N, x_{N-1}, \dots, x_1, x_0) = \prod_{i=1}^N \mathcal{P}_\tau(x_i | x_{i-1}). \quad (927)$$

Transition probabilities are drawn from a Gaussian distribution. The probability to be at  $x$  (the variable) given  $x'$  (prime as previous), reads

$$\mathcal{P}_\tau(x|x') = \frac{1}{\sqrt{4\pi\tau D(x')}} e^{-\frac{[\eta(x-x') - \tau F(x')]^2}{4\eta\tau D(x')}}. \quad (928)$$

Both  $F$  and  $D$  depend on the previous position (Itô discretization). As a stochastic process, this reads

$$\eta(x_{i+1} - x_i) = \tau F(x_i) + \sqrt{\tau} \xi_i, \quad (929)$$

$$\langle \xi_i \rangle = 0, \quad \langle \xi_i \xi_j \rangle = 2\delta_{ij} \eta D(x_i). \quad (930)$$

The formal limit of  $\tau \rightarrow 0$  is the *Itô–Langevin equation*,

$$\eta \dot{x}(t) = F(x(t)) + \xi(t), \quad (931)$$

$$\langle \xi(t) \rangle = 0, \quad \langle \xi(t) \xi(t') \rangle = 2\eta \delta(t - t') D(x(t)). \quad (932)$$

The factor of  $\eta$  is the friction coefficient in Newton's equation of motion. Indeed, for the problem at hand the latter reads

$$M \partial_t \dot{x}(t) = F(x(t)) + \xi(t) - \eta \dot{x}(t). \quad (933)$$

On the lhs is the mass  $M$  (or inertia) of the particle (not to be confounded with the mass  $m$  in field theory), times its acceleration. This defines a characteristic time scale

$$\tau_M = \frac{M}{\eta}. \quad (934)$$

For times  $t \gg \tau_M$ , inertia plays no role,  $M$  can be set to 0, and we arrive at equation (931).

The situation is different, when the noise is correlated on a time scale  $\tau \gg \tau_M$ . Then in the equation of motion  $F(x(t))$  changes, since  $x(t)$  changes, and it is better to discretize this limit as

$$\eta(x_{i+1} - x_i) = \tau F\left(\frac{x_i + x_{i+1}}{2}\right) + \sqrt{\tau} \xi_i. \quad (935)$$

This prescription is known as mid-point or Stratonovich discretization.

Let us finally rescale time,  $t \rightarrow \eta t$ , which effectively sets  $\eta \rightarrow 1$ . The friction coefficient  $\eta$  can always be restored by multiplying each time derivative with  $\eta$ .

### A.2. Itô calculus

Consider (with  $\eta = 1$ )

$$\begin{aligned} g(x_{i+1}) - g(x_i) &= g(x_i + \tau F(x_i) + \sqrt{\tau} \xi_i) - g(x_i) \\ &= g'(x_i) [\tau F(x_i) + \sqrt{\tau} \xi_i] + \frac{1}{2} g''(x_i) \tau \xi_i^2 + \mathcal{O}(\tau^{3/2}) \\ &= g'(x_i) [\tau F(x_i) + \sqrt{\tau} \xi_i] + g''(x_i) \tau D(x_i) + \mathcal{O}(\tau^{3/2}). \end{aligned} \quad (936)$$

The last relation is justified since in any time slice maximally two powers of  $\xi_i$  can appear. (If there could be 4 then one would have to use Wick's theorem to decouple them pairwise.) It is implicitly understood that the noise is independent of  $x$ , thus  $\langle g(x_i) \xi_i \rangle = 0$ , and  $\langle g(x_i) \xi_i^2 \rangle = 2g(x_i) D(x_i) dt$ .

Mathematicians prefer setting  $x_i \rightarrow x$ ,  $\tau \rightarrow dt$ ,  $\xi_i \sqrt{\tau} \rightarrow d\xi$ , and write the Langevin equation as

$$dx = F(x) dt + d\xi, \quad (937)$$

$$\langle d\xi \rangle = 0, \quad \langle d\xi^2 \rangle = \langle d\xi^2 \rangle = 2D(x) dt. \quad (938)$$

The stochastic evolution of a function  $g(x)$  can then be written with these 'differentials' as

$$\begin{aligned} dg(x) &= g'(x) dx + \frac{1}{2} g''(x) dx^2 + \dots \\ &= g'(x) [F(x) dt + d\xi] + \frac{1}{2} g''(x) [F(x) dt + d\xi]^2 + \dots \\ &= [g'(x) F(x) + g''(x) D(x)] dt + g'(x) d\xi. \end{aligned} \quad (939)$$

This is known as *Itô calculus*. The rule of thumb to remember is that when expanding to first order in the time differential  $dt$ , as  $d\xi \sim \sqrt{dt}$ , one has to keep all terms up to second order in  $d\xi$ .

### A.3. Fokker–Planck equation

Derivation of (forward) Fokker–Planck equation using Itô's formalism: the forward Fokker–Planck equation can be derived from Itô's formalism. Consider the expectation of a test function  $g(x)$  at time  $t$ :

$$\langle g(x_t) \rangle \equiv \int_x g(x) P_t(x). \quad (940)$$

Taking the expectation of the first line of equation (939) yields

$$\langle dg(x_t) \rangle = \langle g'(x_t) dx \rangle + \frac{1}{2} \langle g''(x_t) dx^2 \rangle + \dots \quad (941)$$

Averaging over the noise gives

$$\frac{d}{dt} \langle g(x_t) \rangle = \langle g'(x_t) F(x_t) \rangle + \langle g''(x_t) D(x_t) \rangle. \quad (942)$$

Expressing the expectation values with the help of equation (940), we obtain

$$\begin{aligned} &\int_x g(x) \partial_t P_t(x) \\ &= \int_x g'(x) F(x) P_t(x) + g''(x) D(x) P_t(x). \end{aligned} \quad (943)$$

Integrating by part, and using that  $g(x)$  is an arbitrary test function, we obtain the *forward Fokker–Planck equation*

$$\partial_t P_t(x) = \frac{\partial^2}{\partial x^2} (D(x) P_t(x)) - \frac{\partial}{\partial x} (F(x) P_t(x)). \quad (944)$$

Our derivation is valid for any initial condition, thus the propagator  $P(x_f, t_f | x_i, t_i)$  also satisfies the forward Fokker Planck equation as a function of  $x = x_f$ ,  $t = t_f$ .

If there are several degrees of freedom  $x_u$ ,  $u = 1, \dots, L$ , then equation (944) generalizes to an equation for the joint probability  $P_t[x] \equiv P_t(x_1, x_2, \dots, x_L)$

$$\partial_t P_t[x] = \sum_{u=1}^L \frac{\partial^2}{\partial x_u^2} (D_u[x] P_t[x]) - \frac{\partial}{\partial x_u} (F_u[x] P_t[x]). \quad (945)$$

Passing to the continuum limit, this yields the functional Fokker–Planck equation

$$\begin{aligned} \partial_t P_t[x] &= \int du \frac{\delta^2}{\delta x(u)^2} \left( D_u[x] P_t[x] \right) - \frac{\delta}{\delta x(u)} \left( F_u[x] P_t[x] \right). \end{aligned} \quad (946)$$

The backward Fokker–Planck equation: let us study  $P(x_f, t_f | x_i, t_i)$  as a function of its initial time and position. To this purpose, write down the exact equation, using the notations of equation (937),

$$P(x_f, t_f | x, t) = \langle P(x_f, t_f | x + dx, t + dt) \rangle. \quad (947)$$

The average is over all realizations of the noise  $\eta$  during a time step  $dt$ . Expanding inside the expectation value to first order in  $dt$  and second order in  $dx$ , and taking the expectation, we find

$$\begin{aligned} \langle P(x_f, t_f | x + dx, t + dt) \rangle &= \left\langle P(x_f, t_f | x, t) + dt \partial_t P(x_f, t_f | x, t) \right. \\ &\quad \left. + dx \partial_x P(x_f, t_f | x, t) + \frac{dx^2}{2} \partial_x^2 P(x_f, t_f | x, t) \right\rangle \\ &= P(x_f, t_f | x, t) + dt \left[ \partial_t P(x_f, t_f | x, t) \right. \\ &\quad \left. + F(x) \partial_x P(x_f, t_f | x, t) + D(x) \partial_x^2 P(x_f, t_f | x, t) \right]. \end{aligned} \quad (948)$$

Comparing to equation (947) implies that the term of order  $dt$  vanishes, thus

$$\begin{aligned} - \partial_t P(x_f, t_f | x, t) &= F(x) \frac{\partial}{\partial x} P(x_f, t_f | x, t) + D(x) \frac{\partial^2}{\partial x^2} P(x_f, t_f | x, t). \end{aligned} \quad (949)$$

This is the *backward Fokker–Planck equation*. Note that contrary to the forward equation, all derivatives act on  $P(x_f, t_f | y, t)$ , not on  $F$  or  $D$ .

*Remark on consistency.* The form of the backward and forward equations is constraint by an important consistency relation: using that the process is Markovian, we can write the *Chapman–Kolmogorov equation*

$$P(x_f, t_f | x_i, t_i) = \int_x P(x_f, t_f | x, t) P(x, t | x_i, t_i). \quad (950)$$

This relation must hold for all  $t$  between  $t_i$  and  $t_f$ . Taking a  $t$  derivative and using the backward Fokker–Planck equation for the first propagator  $P(x_f, t_f | x, t)$ , and the forward equation for the second  $P(x, t | x_i, t_i)$ , we find cancelation of all terms upon partial integration in  $x$ , due to the specific arrangement of the derivatives in equations (944) and (949).

*Remark on steady state.* Let us find a steady-state solution of equation (944), i.e. a solution which does not depend on

time. Integrating once and dropping the time argument yields

$$\frac{\partial}{\partial x} [D(x)P(x)] = F(x)P(x) + \text{const.} \quad (951)$$

Let us suppose that the probability  $P(x)$  vanishes when  $x \rightarrow \infty$ . This implies that the constant vanishes. The solution is obtained as ( $x_0$  is arbitrary)

$$P(x) = \frac{\mathcal{N}}{D(x)} \exp \left( \int_{x_0}^x \frac{F(y)}{D(y)} dy \right), \quad (952)$$

$$\mathcal{N}^{-1} = \int_{-\infty}^{\infty} dx \frac{1}{D(x)} \exp \left( \int_{x_0}^x \frac{F(y)}{D(y)} dy \right). \quad (953)$$

The simplest case is obtained for thermal noise, i.e.  $D(x) = T$ , and when the force  $F(x)$  is the derivative of a potential,  $F(x) = -V'(x)$ . Equation (952) can then be written as

$$P(x) = \mathcal{N} e^{-V(x)/T}, \quad \mathcal{N}^{-1} = \int_{-\infty}^{\infty} dx e^{-V(x)/T}. \quad (954)$$

This is Boltzmann's law [765].

#### A.4. Martin–Siggia–Rose (MSR) formalism

*The path integral.* The transition probability (928) from  $x'$  to  $x$  was

$$\mathcal{P}_\tau(x|x') dx = \frac{dx}{\sqrt{4\pi\tau D(x')}} e^{-\frac{[x-x'-\tau F(x')]^2}{4\tau D(x')}}. \quad (955)$$

This is ugly: our standard field-theory calculations work with polynomials in the exponential. We therefore rewrite this measure as

$$\mathcal{P}_\tau(x|x') dx = dx \int_{-\infty}^{\infty} \frac{d\tilde{x}}{2\pi i} e^{-\mathcal{S}_\tau[x, \tilde{x}]}, \quad (956)$$

$$\mathcal{S}_\tau[x, \tilde{x}] = \tilde{x} (x - x' - \tau F(x')) - \tau \tilde{x}^2 D(x'). \quad (957)$$

The term  $\mathcal{S}_\tau[x, \tilde{x}]$  is termed *action*. Reassembling all time slices, it is normally written in the limit of  $\tau \rightarrow 0$  as

$$\mathcal{P}(x|x_0) = \int_{x(0)=x_0}^{x(N)=x} \mathcal{D}[x] \mathcal{D}[\tilde{x}] e^{-\mathcal{S}[x, \tilde{x}]}, \quad (958)$$

$$\mathcal{S}[x, \tilde{x}] = \int_t \tilde{x}(t) [\dot{x}(t) - F(x(t))] - \tilde{x}(t)^2 D(x(t)), \quad (959)$$

$$\mathcal{D}[x] \mathcal{D}[\tilde{x}] = \prod_{i=1}^N \int_{-\infty}^{\infty} dx_i \int_{-\infty}^{\infty} \frac{d\tilde{x}_i}{2\pi i}. \quad (960)$$

This is known as the MSR formalism (Martin–Siggia–Rose) [295], the action also as Martin–Siggia–Rose–Janssen–DeDominicis action, in honor of their respective work [296–298, 766].

*Changing the discretization.* Let us turn back to a single time slice, as given in equation (956). The variables  $\tilde{x}$  and  $x$  are conjugate, i.e.

$$\begin{aligned} & \int \frac{dx d\tilde{x}}{2\pi i} e^{-\tilde{x}(x-x')} \tilde{x}^n f(x, \tilde{x}) \\ &= \int \frac{dx d\tilde{x}}{2\pi i} e^{-\tilde{x}(x-x')} \partial_{\tilde{x}}^n f(x, \tilde{x}), \end{aligned} \quad (961)$$

$$\begin{aligned} & \int \frac{dx d\tilde{x}}{2\pi i} e^{-\tilde{x}(x-x')} (x-x')^n f(x, \tilde{x}) \\ &= \int \frac{dx d\tilde{x}}{2\pi i} e^{-\tilde{x}(x-x')} \partial_{\tilde{x}}^n f(x, \tilde{x}). \end{aligned} \quad (962)$$

We can thus change our discretization scheme, i.e. replace  $F(x') \rightarrow F(\bar{x})$ ,  $D(x') \rightarrow D(\bar{x})$ , where

$$\bar{x} = \alpha x + (1 - \alpha)x', \quad 0 \leq \alpha \leq 1. \quad (963)$$

There are cases where this change is advantageous. On the other hand, the microscopic dynamics may be such that  $F$  and  $D$  depend on  $\bar{x}$  instead of  $x'$  (see end of appendix A.1).

The consequences of the reparametrization (963) is understood from the following example: expand  $e^{\tau \bar{x} F(\bar{x})} - 1$  to linear order in  $\tau$ ,

$$\begin{aligned} & \tau \int \frac{dx d\tilde{x}}{2\pi i} e^{-\tilde{x}(x-x')} \tilde{x} F(\bar{x}) f(x, \tilde{x}) \\ &= \tau \int \frac{dx d\tilde{x}}{2\pi i} e^{-\tilde{x}(x-x')} \partial_x [F(\bar{x}) f(x, \tilde{x})]. \end{aligned} \quad (964)$$

As the derivative acts on  $F(\bar{x})$ , this depends on  $\alpha$ , as  $\partial_x \bar{x} = \alpha$ . Luckily, we can compensate this by an explicit  $x$  derivative: wherever we change  $x \rightarrow \bar{x}$ , we also replace  $\tilde{x}$  by  $\tilde{x} - \partial_x$ . This yields for the action of a single time slice

$$\begin{aligned} S_\tau[x, \tilde{x}] &= \tilde{x} (x - x') - \tau(\tilde{x} - \partial_x)F(\bar{x}) - \tau(\tilde{x} - \partial_x)^2 D(\bar{x}) \\ &= \alpha \tau F'(\bar{x}) - \alpha^2 \tau D''(\bar{x}) \\ &\quad + \tilde{x} [x - x' - \tau F(\bar{x}) + 2\alpha \tau D'(\bar{x})] - \tau \tilde{x}^2 D(\bar{x}). \end{aligned} \quad (965)$$

The noise-correlator  $D(x)$  did not change, but there is an additional contribution to the force

$$F(x') \rightarrow F(\bar{x}) - 2\alpha D'(\bar{x}). \quad (966)$$

The first two terms,  $\alpha F'(\bar{x}) - \alpha^2 D''(\bar{x})$  can be interpreted as a change in the integration measure. Let us stress that the change in the action *leaves the physics of the problem invariant*. One may arrive at  $\alpha = \frac{1}{2}$  also when the bath is evolving more slowly than the time scale set by viscosity (see end of appendix A.1). Then the choice  $\alpha = 1/2$ , known as *Stratonovich discretization*, is natural; one can use the above procedure to get back to Itô's discretization.

*Interpretation of the field  $\tilde{x}(t)$ .* Let us now turn to an interpretation of the two fields  $x(t)$  and  $\tilde{x}(t)$ , and modify equation (931) to

$$\dot{x}(t) = F(x(t)) + \xi(t) + f\delta(t - t_0). \quad (967)$$

Thus at time  $t = t_0$ , we kick the system with an infinitely small force  $f$ . Then, the probability changes by

$$\begin{aligned} \partial_f \Big|_{f=0} \mathcal{P}(x|x_0) &= \partial_f \Big|_{f=0} \int_{x(0)=x_0}^{x(t)=x} \mathcal{D}[x] \mathcal{D}[\tilde{x}] e^{-S[x, \tilde{x}]} \\ &= \int_{x_0=x(0)}^{x(t)=x} \mathcal{D}[x] \mathcal{D}[\tilde{x}], \tilde{x}(t_0) e^{-S[x, \tilde{x}]}. \end{aligned} \quad (968)$$

Multiplying with  $x(t)$  and integrating over all final configurations, we obtain

$$R(t, t_0) = \partial_f \Big|_{f=0} \langle x(t) \rangle = \langle x(t) \tilde{x}(t_0) \rangle. \quad (969)$$

The expectation is w.r.t. the measure  $\mathcal{D}[x] \mathcal{D}[\tilde{x}] e^{-S[x, \tilde{x}]}$ . As equation (969) is the response of the system to a change in force,  $\tilde{x}$  is called *response field*, and  $R(t, t_0)$  *response function*. *Correlation functions* are similarly obtained as

$$C(t, t') = \langle x(t)x(t') \rangle. \quad (970)$$

Since the probability is normalized,

$$\int \mathcal{P}(x|x_0) dx = 1, \quad (971)$$

for all forces, one shows by taking derivatives w.r.t. forces at different times that expectations of the sole response field vanish,

$$\langle \tilde{x}(t) \rangle = \langle \tilde{x}(t) \tilde{x}(t') \rangle = \langle \tilde{x}(t) \tilde{x}(t') \tilde{x}(t'') \rangle = \dots = 0. \quad (972)$$

#### A.5. Gaussian theory with spatial degrees of freedom

Consider theories with spatial dependence, and let us suppose that the energy is given by

$$\mathcal{H}[u] = \int_x \frac{1}{2} [\nabla u(x)]^2 + \frac{m^2}{2} u(x)^2. \quad (973)$$

This corresponds to an elastic manifold inside a confining potential of curvature  $m^2$ . The *elastic forces* acting on a piece of the manifold at position  $x$  are given by

$$F(x) = -\frac{\delta \mathcal{H}[u]}{\delta u(x)} = (\nabla^2 - m^2) u(x). \quad (974)$$

Its Langevin dynamics reads

$$\partial_t u(x, t) = (\nabla^2 - m^2) u(x, t) + \xi(x, t), \quad (975)$$

$$\langle \xi(t) \xi(t') \rangle = 2T \delta(t - t') \delta(x - x'). \quad (976)$$

The action in Itô discretization is

$$S[u, \tilde{u}] = \int_{x,t} \tilde{u}(x, t) [\partial_t - \nabla^2 + m^2] u(x, t) - T \tilde{u}(x, t)^2. \quad (977)$$

It can be diagonalized in momentum and frequency space,

$$\begin{aligned}
 S[u, \tilde{u}] &= \int_{k, \omega} \tilde{u}(-k, -\omega) [i\omega + k^2 + m^2] u(k, \omega) \\
 &\quad - T \tilde{u}(-k, -\omega) \tilde{u}(k, \omega) \\
 &= \frac{1}{2} \int_{k, \omega} \begin{pmatrix} u(-k, -\omega) \\ \tilde{u}(-k, -\omega) \end{pmatrix} \mathcal{M} \begin{pmatrix} u(k, \omega) \\ \tilde{u}(k, \omega) \end{pmatrix}, \quad (978)
 \end{aligned}$$

$$\mathcal{M} = \begin{pmatrix} 0 & -i\omega + k^2 + m^2 \\ i\omega + k^2 + m^2 & -2T \end{pmatrix}. \quad (979)$$

This implies

$$\mathcal{M}^{-1} = \begin{pmatrix} \frac{2T}{(i\omega + k^2 + m^2)(-i\omega + k^2 + m^2)} & \frac{1}{i\omega + k^2 + m^2} \\ \frac{1}{-i\omega + k^2 + m^2} & 0 \end{pmatrix}. \quad (980)$$

As a consequence,

$$R(k, \omega) := \langle u(-k, -\omega) \tilde{u}(k, \omega) \rangle = \frac{1}{i\omega + k^2 + m^2}, \quad (981)$$

$$C(k, \omega) := \langle u(-k, -\omega) u(k, \omega) \rangle = \frac{2T}{|i\omega + k^2 + m^2|^2}. \quad (982)$$

Inverse Fourier transforming  $R$  leads to

$$\begin{aligned}
 R(k, t) &= \langle u(-k, t) \tilde{u}(k, 0) \rangle \\
 &= \int_{-\infty}^{\infty} \frac{d\omega}{2\pi} \frac{e^{i\omega t}}{i\omega + k^2 + m^2} = e^{-(k^2 + m^2)t} \Theta(t). \quad (983)
 \end{aligned}$$

We used the residue theorem to evaluate the integral: there is a pole at  $\omega = i(k^2 + m^2)$ , i.e. in the upper complex half-plane. If  $t > 0$ , then the integral converges in the upper half plane, and closing the contour there yields the residuum as written. For  $t < 0$ , one has to close the path in the lower half-plane, and there is no contribution, thus the  $\Theta(t)$ .

The response function (983) satisfies the *massive diffusion equation*,

$$(\partial_t + k^2 + m^2)R(k, t) = \delta(t). \quad (984)$$

Performing one more inverse Fourier transform yields the response function in real space, a.k.a. the diffusion kernel (we complete the square)

$$\begin{aligned}
 R(x, t) &= \int_{-\infty}^{\infty} \frac{d^d k}{(2\pi)^d} e^{ikx - (k^2 + m^2)t} \Theta(t) \\
 &= \frac{e^{-m^2 t - \frac{x^2}{4t}}}{(4\pi t)^{d/2}} \Theta(t). \quad (985)
 \end{aligned}$$

Setting  $d = 1$  this is identical to equation (955) (setting there  $\eta = D = 1, F = x' = 0$ , and  $\tau = t$ ). Correlation functions can be obtained as

$$\begin{aligned}
 C(k, t - t') &= \langle u(k, t) u(-k, t') \rangle \\
 &= 2T \int_{-\infty}^{\infty} d\tau R(k, t - \tau) R(k, t' - \tau) \\
 &= 2T \int_{-\infty}^{\min(t, t')} d\tau e^{-(k^2 + m^2)(t + t' - 2\tau)} \\
 &= \frac{T}{k^2 + m^2} e^{-(k^2 + m^2)|t - t'|}. \quad (986)
 \end{aligned}$$

For equal times one recovers the equilibrium correlator,

$$C(k, 0) = \langle u(k, t) u(-k, t) \rangle = \frac{T}{k^2 + m^2}. \quad (987)$$

The correlation function (986) satisfies the differential equation

$$\partial_t C(k, t - t') = T [R(k, t' - t) - R(k, t - t')]. \quad (988)$$

This relation is known as fluctuation–dissipation theorem. It is more generally valid, see e.g. [298, 766].

#### A.6. The inverse of the Laplace operator

$$\nabla^2 \left[ \frac{1}{(2-d)S_d} |\vec{z}|^{2-d} \right] = \delta^d(\vec{z}), \quad (989)$$

where the volume of the unitsphere is defined as

$$S_d = \frac{2\pi^{d/2}}{\Gamma(d/2)}. \quad (990)$$

**Proof.**  $\nabla^2 |\vec{z}|^{2-d+\eta} = (2-d+\eta)\eta |\vec{z}|^{-d+\eta}$ . Integrating the last term against a test function  $f(\vec{z})$  yields  $(2-d+\eta)S_d f(0)$ . Taking the limit of  $\eta \rightarrow 0$  completes the proof.

*The inverse Laplacian in  $d = 2$ .* In  $d = 2$ , we set  $\vec{z} := (x, y)$ , and  $z = x + iy, \bar{z} = x - iy$ . Equation (989) reduces to

$$\nabla^2 \frac{\ln(\bar{z}^2)}{4\pi} = \delta^2(\vec{z}). \quad (991)$$

Our notations imply  $\ln(\bar{z}^2) = \ln(z\bar{z}) = \ln z + \ln \bar{z}$ . Since  $\bar{\partial}\partial = \frac{1}{4}\nabla^2$  (check of norm:  $\partial\bar{\partial}(z\bar{z}) = 1, \nabla^2(x^2 + y^2) = 4$ ),

$$\frac{1}{\partial} = 4 \frac{\bar{\partial}}{\nabla^2} = \frac{\bar{\partial} \ln(z\bar{z})}{\pi} = \frac{1}{\pi\bar{z}}. \quad (992)$$

As a consequence

$$\partial \frac{1}{\pi\bar{z}} = \bar{\partial} \frac{1}{\pi z} = \delta^2(\vec{z}) \equiv \delta(x)\delta(y). \quad (993)$$

#### A.7. Extreme-value statistics: Gumbel, Weibull and Fréchet distributions

*Generalities.* Consider a random variable  $x$  with probability distribution  $P(x)$ , and cumulative distributions

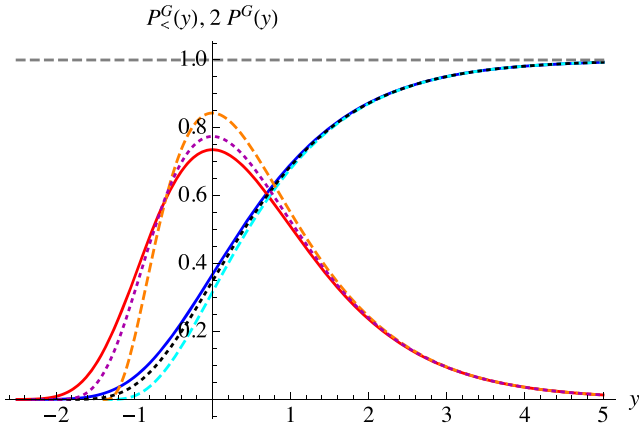


**Figure 81.** The cumulative Gumbel distribution  $P_{\leq}^G(y)$  (blue, solid) and its derivative  $P^G(y)$  (red, solid, rescaled by a factor of 2 for better readability). This is compared to the law exact law (997) for  $N = 4$  (dashed, note the bounded support) and  $N = 10$  (dotted). For  $N = 100$  no difference would be visible on this plot.

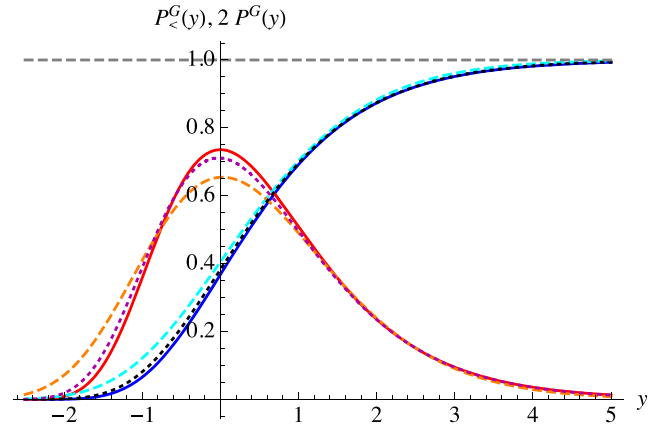


**Figure 82.** The cumulative Gumbel distribution  $P_{\leq}^G(y)$  (blue, solid) and its derivative  $P^G(y)$  (red, solid). This is compared to the exact law (997) for a Gauss-distribution, using the equality in equation (1004), for  $N = 100$  (dashed) and  $N = 10^{13}$  (dotted).

$$P_{>}(x) := \int_x^{\infty} P(y)dy, \tag{994}$$

$$P_{<}(x) := \int_{-\infty}^x P(y)dy = 1 - P_{>}(x). \tag{995}$$

Suppose  $x_i, i = 1, \dots, N$  are drawn from the measure  $P(x)$ . We are interested in the law of their maximum  $m$ ,

$$m := \max(x_1, \dots, x_N). \tag{996}$$

The probability that the maximum is smaller than  $m$  is equivalent to the probability that  $x_i < m$  for all  $i$ ,

$$P_{<}^{\max}(m) = P_{<}(m)^N = [1 - P_{>}(m)]^N. \tag{997}$$

For large  $N$ , this can be approximated by

$$P_{<}^{\max}(m) \simeq e^{-NP_{>}(m)}, \tag{998}$$

with density

$$P^{\max}(m) = \partial_m P_{<}^{\max}(m) \simeq NP(m)e^{-NP_{>}(m)}. \tag{999}$$

*Gumbel distribution.* Suppose that

$$P(x) = e^{-x}\Theta(x) \Leftrightarrow P_{>}(x) = e^{-x}\Theta(x). \tag{1000}$$

This implies that for large  $N$

$$P_{<}^{\max}(m) \simeq e^{-Ne^{-m}} \Theta(m) = e^{-e^{-m+\ln(N)}} \Theta(m). \tag{1001}$$

The variable

$$y = m - \ln(N) \tag{1002}$$

is distributed according to a Gumbel distribution [767]

$$P_{<}^G(y) = e^{-e^{-y}}, \quad P^G(y) = \partial_y P_{<}^G(y) = e^{-y-e^{-y}}. \tag{1003}$$

A plot elucidating the convergence is shown in figure 81. The Gumbel class has a large basin of attraction, encompassing all distributions which decay as  $P_{>}(m) \sim e^{-x^\alpha}$ ,  $\alpha > 0$ , including in particular the Gauss distribution. The idea is that a particular

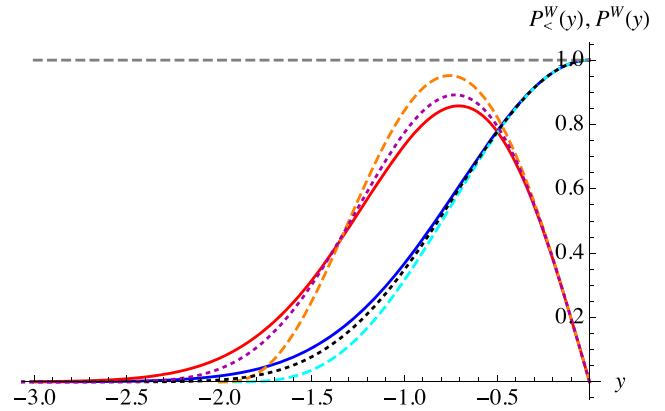


**Figure 83.** The cumulative Weibull distribution  $P_{\leq}^W(y)$  (blue, solid) and its derivative  $P^W(y)$  (red, solid) for  $\alpha = 2$ . This is compared to the exact law (997) for  $N = 4$  (dashed) and  $N = 10$  (dotted). For  $N = 100$  virtually no difference would be visible on this plot.

point  $x_c$  in the distribution of  $P(x)$  will dominate  $P^{\max}(m)$ ; it then suffices to approximate  $\ln P_{>}(x)$  by a linear fit at  $m = m_c$ . For the standard Gauss-distribution (figure 82)

$$P(x) = \frac{e^{-x^2/2}}{\sqrt{2\pi}}, \tag{1004}$$

$$P_{>}(x) = \frac{1}{2} \operatorname{erfc}\left(\frac{x}{\sqrt{2}}\right) \simeq \frac{e^{-x^2/2}}{\sqrt{2\pi}x}. \tag{1005}$$

A strategy is to replace  $x^{-1} e^{-x^2/2} \rightarrow x_c^{-1} e^{-x_c^2/2 - xx_c}$ , and then to find the best  $x_c$  to eliminate the  $N$ -dependence. This yields after some algebra

$$y \simeq x\sqrt{\ln(N^2)} - \ln(N^2) + \frac{1}{2} \ln(2\pi \ln(N^2)). \tag{1006}$$

A numerical check reveals a very slow convergence to the asymptotic form: while the right tail and the center of the density are correct even for small  $N$ , the left tail converges very slowly (from above), while the peak amplitude converges slowly from below. Note that this could not be repaired by

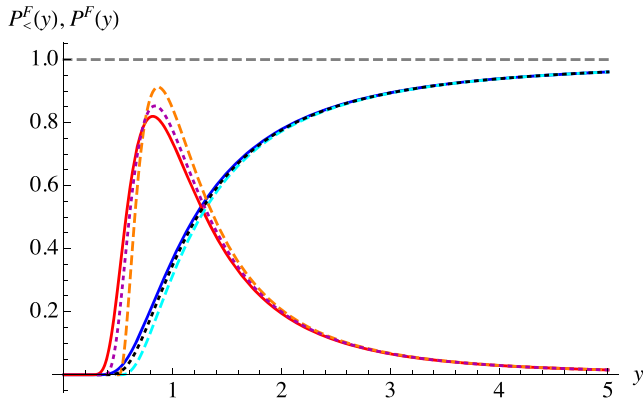


**Figure 84.** The cumulative Fréchet distribution  $P_{\le}^W(y)$  (blue, solid) and its derivative  $P_{\le}^W(y)$  (red, solid) for  $\alpha = 2$ . This is compared to the exact law (997) for  $N = 4$  (dashed) and  $N = 10$  (dotted). For  $N = 100$  virtually no difference would be visible on this plot.

changing the parameters in equation (1006), which work for the peak-position and the right tail.

*Weibull distribution.* Suppose that  $P(x)$  is distributed according to a power-law, bounded from above by  $x = 0$ ,

$$P(x) = \alpha(-x)^{\alpha-1}\Theta(-1 \leq x \leq 0), \quad (1007)$$

$$P_{>}(x) = (-x)^{\alpha}\Theta(-1 \leq x \leq 0). \quad (1008)$$

This implies that for large  $N$  (we suppress the lower bound at  $x = -1$  for compactness of notation, and since it does not matter in the final result)

$$\begin{aligned} P_{\le}^{\max}(m) &\simeq e^{-N(-m)^{\alpha}}\Theta(m), \\ &= \exp\left(-\left[-mN^{\frac{1}{\alpha}}\right]^{\alpha}\right)\Theta(-m). \end{aligned} \quad (1009)$$

The variable

$$y = mN^{\frac{1}{\alpha}} \quad (1010)$$

is distributed according to a Weibull distribution [768] with index  $\alpha$  (figure 83)

$$P_{\alpha, <}^W(y) = e^{-(-y)^{\alpha}}\Theta(-y), \quad (1011)$$

$$P_{\alpha}^W(y) = \partial_y P_{\le}^W(y) = \alpha(-y)^{\alpha-1} e^{-(-y)^{\alpha}}\Theta(-y). \quad (1012)$$

*Fréchet distribution.* Suppose that  $P(x)$  is distributed according to an unbounded power law,  $\alpha > 0$ ,

$$P(x) = \alpha x^{\alpha-1}\Theta(x > 1), \quad (1013)$$

$$P_{>}(x) = x^{-\alpha}\Theta(x > 1). \quad (1014)$$

This implies that for large  $N$

$$\begin{aligned} P_{\le}^{\max}(m) &\simeq e^{-Nm^{-\alpha}}\Theta(m > 1) \\ &= \exp\left(-\left[mN^{-\frac{1}{\alpha}}\right]^{-\alpha}\right)\Theta(m > 1). \end{aligned} \quad (1015)$$

The variable

$$y = mN^{-\frac{1}{\alpha}} \quad (1016)$$

is distributed according to a Fréchet distribution [769] with index  $\alpha$  (figure 84),

$$P_{\alpha, <}^F(y) = e^{-y^{-\alpha}}\Theta(y), \quad (1017)$$

$$P_{\alpha}^F(y) = \partial_y P_{\le}^W(y) = \alpha y^{-\alpha-1} e^{-y^{-\alpha}}\Theta(y). \quad (1018)$$

Note that  $P_{\alpha, <}^F(y)$  has an algebraic tail  $\sim y^{-\alpha}$ , thus decays much more slowly than the Gumbel distribution for large  $y$ .

### A.8. Gel'fand Yaglom method

We want to compute functional determinants of the form

$$f(\alpha, m^2) := \frac{\det[-\nabla^2 + \alpha V(x) + m^2]}{\det[-\nabla^2 + m^2]}, \quad (1019)$$

with Dirichlet boundary conditions at  $x = 0$  and  $x = L$ , at  $\alpha = 1$ . In order for the problem to be well-defined,  $-\nabla^2 + \alpha V(x) + m^2$  must have a discrete spectrum.

In dimension  $d = 1$ , this can efficiently be calculated using the Gel'fand Yaglom method [278]. Consider solutions of the ODE

$$[-\nabla^2 + \alpha V(x) + m^2]\psi_{\alpha}(x) = 0, \quad (1020)$$

with boundary conditions

$$\psi_{\alpha}(0) = 0, \quad \psi'_{\alpha}(0) = 1. \quad (1021)$$

Define

$$g(\alpha, m^2) := \frac{\psi_{\alpha}(L)}{\psi_0(L)}. \quad (1022)$$

Then the ratio of determinants is given by

$$f(\alpha, m^2) = g(\alpha, m^2). \quad (1023)$$

**Proof.** Set  $\Lambda_{\alpha} := -\nabla^2 + \alpha V(x) + m^2$ . Call its eigenvalues  $\lambda_i(\alpha)$ , ordered, and non-degenerate. Consider the analytic structure of  $f(\alpha, m^2 - \lambda)$  and  $g(\alpha, m^2 - \lambda)$ , as a function of  $\lambda$ . By definition  $f$  is a product over eigenvalues,

$$f(\alpha, m^2 - \lambda) = \prod_i \frac{\lambda_i(\alpha) - \lambda}{\lambda_i(0) - \lambda}. \quad (1024)$$

Note that for large  $i$  the ratio  $\lambda_i(\alpha)/\lambda_i(0)$  goes to 1, thus the product should converge; that was the reason why the ratio of determinants was introduced in the first place. If we want to make the proof rigorous, we can put the system on a lattice, replacing the Laplacian by its lattice version. Then the spectrum is finite, and the product converges. As a consequence of equation (1024),  $f(\alpha, m^2 - \lambda)$  is an analytic function of  $\lambda$ , which vanishes at  $\lambda = \lambda_i(\alpha)$ . Now consider  $g(\alpha, m^2 - \lambda)$ . If  $\lambda$  is an eigenvalue,  $\lambda = \lambda_i(\alpha)$ , then the solution of equation (1020) vanishes at  $x = L$ . Playing around with solutions of differential equations, we can convince ourselves that for  $\lambda - \lambda_i(\alpha) \rightarrow 0$ ,

$$\psi_{\alpha}(L) \sim \lambda - \lambda_i(\alpha). \quad (1025)$$

We further expect  $g$  to be analytic in  $\lambda$ . Thus, as a function of  $\lambda$ ,  $f$  and  $g$  have the same analytic structure, i.e. the same zeros and poles. The latter cancel in the ratio

$$r(\lambda) := \frac{f(\alpha, m^2 - \lambda)}{g(\alpha, m^2 - \lambda)}. \quad (1026)$$

The only possibility for a zero or a pole we have to check is for  $|\lambda| \rightarrow \infty$ .  $\square$

Consider  $f$  in the limit of  $\lambda \rightarrow -\infty$ : each factor in (1024) will go to 1, s.t. also  $f$  goes to 1. (For the discretized version, this is evident, and does not depend on the phase of  $\lambda$ ; for the continuous version one has to work a little bit, and take the limit away from the positive real axes, where the spectrum lies.)

Now consider the differential equation (1020) with  $m^2 \rightarrow m^2 - \lambda$ , in the same limit  $\lambda \rightarrow -\infty$ . In this case, one can convince oneself that both solutions grow exponentially, and that  $V(x)$  is a small perturbation, s.t. again  $g(\alpha, m^2 - \lambda) \rightarrow 1$ . Thus  $r(\lambda)$  is a function in the complex plane which has no poles. As a consequence,  $r(\lambda)$  is bounded. According to Liouville's theorem it is a constant. This constant can be extracted from both limits  $\lambda \rightarrow \infty$  and  $\lambda = 0$ , which shows that  $r(\lambda) = 1$ . This concludes our proof.

A more rigorous proof can be found in [770]: the idea there is to show that  $\partial_\alpha f(\alpha, m^2) = \partial_\alpha g(\alpha, m^2)$  for all  $\alpha$ , as both can be written as Green functions at the given value of  $\alpha$ . A proof similar to ours, using Fredholm-determinant theory, can be found in section 7, appendix 1 of [771].

## ORCID iDs

Kay Jörg Wiese  <https://orcid.org/0000-0002-9270-4990>

## References

- [1] Amit D J and Martin-Mayor V 2005 *Field Theory, The Renormalization Group, and Critical Phenomena* 3rd edn (Singapore: World Scientific)
- [2] Zinn-Justin J 1989 *Quantum Field Theory and Critical Phenomena* (Oxford: Oxford University Press)
- [3] Cardy J 1996 *Scaling and Renormalization in Statistical Physics* (Cambridge: Cambridge University Press)
- [4] Kardar M 2007 *Statistical Physics of Fields* (Cambridge: Cambridge University Press)
- [5] Brézin E 2010 *Introduction to Statistical Field Theory* (Cambridge: Cambridge University Press)
- [6] Vasil'ev A N 2004 *The Field Theoretic Renormalization Group in Critical Behavior Theory and Stochastic Dynamics* (Boca Raton, FL: CRC Press)
- [7] Parisi G 1988 *Statistical Field Theory (Frontiers in Physics)* (Reading, MA: Addison-Wesley)
- [8] Pelissetto A and Vicari E 2002 Critical phenomena and renormalization-group theory *Phys. Rep.* **368** 549–727
- [9] El-Showk S, Paulos M F, Poland D, Rychkov S, Simmons-Duffin D and Vichi A 2014 Solving the 3D Ising model with the conformal bootstrap: II.  $c$ -minimization and precise critical exponents *J. Stat. Phys.* **157** 869–914
- [10] El-Showk S, Paulos M F, Poland D, Rychkov S, Simmons-Duffin D and Vichi A 2012 Solving the 3D Ising model with the conformal bootstrap *Phys. Rev. D* **86** 025022
- [11] Chester S M, Landry W, Liu J, Poland D, Simmons-Duffin D, Su N and Vichi A 2019 Carving out OPE space and precise  $O(2)$  model critical exponents (arXiv:1912.03324)
- [12] Ferrenberg A M, Xu J and Landau D P 2018 Pushing the limits of Monte Carlo simulations for the three-dimensional Ising model *Phys. Rev. E* **97** 043301
- [13] Clisby N and Dünweg B 2016 High-precision estimate of the hydrodynamic radius for self-avoiding walks *Phys. Rev. E* **94** 052102
- [14] Clisby N 2017 Scale-free Monte Carlo method for calculating the critical exponent  $\gamma$  of self-avoiding walks *J. Phys. A: Math. Theor.* **50** 264003
- [15] Lipa J A, Swanson D R, Nissen J A, Geng Z K, Williamson P R, Stricker D A, Chui T C P, Israelsson U E and Larson M 2000 Specific heat of helium confined to a 57  $\mu\text{m}$  planar geometry near the lambda point *Phys. Rev. Lett.* **84** 4894–7
- [16] Hasenbusch M 2019 Monte Carlo study of an improved clock model in three dimensions *Phys. Rev. B* **100** 224517
- [17] Franz S, Jacquin H, Parisi G, Urbani P and Zamponi F 2012 Quantitative field theory of the glass transition *Proc. Natl Acad. Sci. USA* **109** 18725–30
- [18] Müller M and Wyart M 2014 Marginal stability in structural, spin, and electron glasses *Annu. Rev. Condens. Matter Phys.* **6** 177–200
- [19] Nattermann T and Scheidl S 2000 Vortex-glass phases in type-II superconductors *Adv. Phys.* **49** 607–704
- [20] Kierfeld J, Nattermann T and Hwa T 1997 Topological order in the vortex-glass phase of high-temperature superconductors *Phys. Rev. B* **55** 626–9
- [21] Carpentier D, Le Doussal P and Giamarchi T 1996 Stability of the Bragg glass phase in a layered geometry *Europhys. Lett.* **35** 379–84
- [22] Cule D and Shapir Y 1995 Nonergodic dynamics of the two-dimensional random-phase sine-Gordon model: applications to vortex-glass arrays and disordered-substrate surfaces *Phys. Rev. B* **51** 3305
- [23] Hwa T and Fisher D S 1994 Vortex glass phase and universal susceptibility variations in planar arrays of flux lines *Phys. Rev. Lett.* **72** 2466–9
- [24] Hwa T and Fisher D S 1994 Anomalous fluctuations of directed polymers in random media *Phys. Rev. B* **49** 3136–54
- [25] Balents L 1993 Localization of elastic layers by correlated disorder *Europhys. Lett.* **24** 489–94
- [26] Feldman D E 2002 Critical exponents of the random-field  $O(N)$  model *Phys. Rev. Lett.* **88** 177202
- [27] Middleton A A and Fisher D S 2002 Three-dimensional random-field Ising magnet: interfaces, scaling, and the nature of states *Phys. Rev. B* **65** 134411
- [28] Dahmen K A, Sethna J P, Kuntz M C and Perković O 2001 Hysteresis and avalanches: phase transitions and critical phenomena in driven disordered systems *J. Magn. Magn. Mater.* **226–230** 1287–92
- [29] Dahmen K A, Sethna J P and Perkovic O 2000 Hysteresis, Barkhausen noise, and disorder induced critical behavior *IEEE Trans. Magn.* **36** 3150–4
- [30] Bricmont J and Kupiainen A 1987 Lower critical dimension for the random-field Ising model *Phys. Rev. Lett.* **59** 1829–32
- [31] Imbrie J Z 1984 Lower critical dimension of the random-field Ising model *Phys. Rev. Lett.* **53** 1747–50
- [32] Parisi G and Sourlas N 1979 Random magnetic fields, supersymmetry, and negative dimensions *Phys. Rev. Lett.* **43** 744–5
- [33] Le Doussal P and Wiese K J 2006 Random field spin models beyond one loop: a mechanism for decreasing the lower critical dimension *Phys. Rev. Lett.* **96** 197202

- [34] Tissier M and Tarjus G 2011 Supersymmetry and its spontaneous breaking in the random field Ising model *Phys. Rev. Lett.* **107** 041601
- [35] Tarjus G and Tissier M 2008 Nonperturbative functional renormalization group for random field models and related disordered systems: I. Effective average action formalism *Phys. Rev. B* **78** 024203
- [36] Tissier M and Tarjus G 2008 Nonperturbative functional renormalization group for random field models and related disordered systems: II. Results for the random field  $O(N)$  model *Phys. Rev. B* **78** 024204
- [37] Tarjus G and Tissier M 2006 Unified picture of ferromagnetism, quasi-long range order and criticality in random field models *Phys. Rev. Lett.* **96** 087202
- [38] Tarjus G and Tissier M 2006 Two-loop functional renormalization group of the random field and random anisotropy  $O(N)$  models *Phys. Rev. B* **74** 214419
- [39] Tarjus G and Tissier M 2004 Nonperturbative functional renormalization group for random-field models: the way out of dimensional reduction *Phys. Rev. Lett.* **93** 267008
- [40] Husemann C and Wiese K J 2018 Field theory of disordered elastic interfaces at three-loop order: critical exponents and scaling functions *Nucl. Phys. B* **932** 589–618
- [41] Wiese K J, Husemann C and Le Doussal P 2018 Field theory of disordered elastic interfaces at three-loop order: the  $\beta$ -function *Nucl. Phys. B* **932** 540–88
- [42] Wiese K J and Le Doussal P 2007 Functional renormalization for disordered systems: basic recipes and gourmet dishes *Markov Process. Relat. Fields* **13** 777–818 (arXiv:cond-mat/0611346)
- [43] Hui S and Tang L-H 2006 Ground state and glass transition of the RNA secondary structure *Eur. Phys. J. B* **53** 77–84
- [44] Fedorenko A, Le Doussal P and Wiese K J 2006 Statics and dynamics of elastic manifolds in media with long-range correlated disorder *Phys. Rev. E* **74** 061109
- [45] Wiese K J 2005 Supersymmetry breaking in disordered systems and relation to functional renormalization and replica-symmetry breaking *J. Phys.: Condens. Matter* **17** S1889–98
- [46] Wiese K J 2005 Why one needs a functional renormalization group to survive in a disordered world *Pramana* **64** 817–27
- [47] Repain V, Bauer M, Jamet J-P, Ferré J, Mouglin A, Chappert C and Bernas H 2004 Creep motion of a magnetic wall: avalanche size divergence *Europhys. Lett.* **68** 460–6
- [48] Bolech C J and Rosso A 2004 Universal statistics of the critical depinning force of elastic systems in random media *Phys. Rev. Lett.* **93** 125701
- [49] Le Doussal P and Wiese K J 2003 Functional renormalization group at large  $N$  for disordered elastic systems, and relation to replica symmetry breaking *Phys. Rev. B* **68** 174202
- [50] Le Doussal P and Wiese K J 2003 Higher correlations, universal distributions and finite size scaling in the field theory of depinning *Phys. Rev. E* **68** 046118
- [51] Wiese K J 2003 The functional renormalization group treatment of disordered systems: a review *Ann. Henri Poincaré* **4** 473–96
- [52] Wiese K J 2002 Disordered systems and the functional renormalization group: a pedagogical introduction *Acta Phys. Slovaca* **52** 341 (arXiv:cond-mat/0205116)
- [53] Rosso A and Krauth W 2001 Origin of the roughness exponent in elastic strings at the depinning threshold *Phys. Rev. Lett.* **87** 187002
- [54] Cule D and Hwa T 1998 Static and dynamic properties of inhomogeneous elastic media on disordered substrate *Phys. Rev. B* **57** 8235–53
- [55] Derrida B 1980 Random-energy model: limit of a family of disordered models *Phys. Rev. Lett.* **45** 79–82
- [56] Fisher D S and Huse D A 1986 Ordered phase of short-range Ising spin-glasses *Phys. Rev. Lett.* **56** 1601–4
- [57] Mézard M, Parisi G and Virasoro M A 1987 *Spin Glass Theory and Beyond* (Singapore: World Scientific)
- [58] Kirkpatrick S and Sherrington D 1978 Infinite-ranged models of spin-glasses *Phys. Rev. B* **17** 4384–403
- [59] Sherrington D and Kirkpatrick S 1975 Solvable model of a spin-glass *Phys. Rev. Lett.* **35** 1792–6
- [60] Parisi G 1979 Infinite number of order parameters for spin-glasses *Phys. Rev. Lett.* **43** 1754–6
- [61] Mézard M, Parisi G, Sourlas N, Toulouse G and Virasoro M 1984 Nature of the spin-glass phase *Phys. Rev. Lett.* **52** 1156–9
- [62] Mézard M, Parisi G and Virasoro M A 1985 Random free energies in spin glasses *J. Physique Lett.* **46** 217–22
- [63] Cugliandolo L F and Kurchan J 1993 Analytical solution of the off-equilibrium dynamics of a long-range spin-glass model *Phys. Rev. Lett.* **71** 173–6
- [64] Guerra F 2003 Broken replica symmetry bounds in the mean field spin glass model *Commun. Math. Phys.* **233** 1–12
- [65] Talagrand M 2011 *Mean Field Models for Spin Glasses: Volume I: Basic Examples* (Berlin: Springer)
- [66] Talagrand M 2011 *Mean Field Models for Spin Glasses: Volume II: Advanced Replica-Symmetry and Low Temperature* (Berlin: Springer)
- [67] Panchenko D 2013 *The Sherrington–Kirkpatrick Model* (Berlin: Springer)
- [68] Barkhausen H 1919 Zwei mit Hilfe der neuen Verstärker entdeckte Erscheinungen *Phys. Ztschr.* **20** 401–3
- [69] Cizeau P, Zapperi S, Durin G and Stanley H E 1997 Dynamics of a ferromagnetic domain wall and the Barkhausen effect *Phys. Rev. Lett.* **79** 4669–72
- [70] Durin G, Bohn F, Correa M A, Sommer R L, Le Doussal P and Wiese K J 2016 Quantitative scaling of magnetic avalanches *Phys. Rev. Lett.* **117** 087201
- [71] Le Doussal P, Wiese K J, Moulinet S and Rolley E 2009 Height fluctuations of a contact line: a direct measurement of the renormalized disorder correlator *Europhys. Lett.* **87** 56001
- [72] Ponson L, Bonamy D and Bouchaud E 2007 Method and system for determining the propagation path of at least one crack from one or more fracture surfaces created by said crack(s) *French Patent* FR:2892811
- [73] Bonamy D, Ponson L, Prades S, Bouchaud E and Guillot C 2006 Scaling exponents for fracture surfaces in homogenous glass and glassy ceramics *Phys. Rev. Lett.* **97** 135504
- [74] Ponson L, Bonamy D and Bouchaud E 2006 Two-dimensional scaling properties of experimental fracture surfaces *Phys. Rev. Lett.* **96** 035506
- [75] Gutenberg B and Richter C F 1956 Earthquake magnitude, intensity, energy, and acceleration *Bull. Seismol. Soc. Am.* **46** 105–45
- [76] Binder K and Young A P 1986 Spin glasses: experimental facts, theoretical concepts, and open questions *Rev. Mod. Phys.* **58** 801
- [77] McKane A, Droz M, Vannimenus J and Wolf D (ed) 1995 *Scale Invariance, Interfaces, and Non-Equilibrium Dynamics (NATO ASI Series vol 344)* (Berlin: Springer)
- [78] Kardar M 1998 Nonequilibrium dynamics of interfaces and lines *Phys. Rep.* **301** 85–112
- [79] Giamarchi T and Le Doussal P 1997 Statics and dynamics of disordered elastic systems *Spin Glasses and Random Fields* ed A P Young (Singapore: World Scientific) (arXiv:cond-mat/9705096)
- [80] Fisher D S 1998 Collective transport in random media: from superconductors to earthquakes *Phys. Rep.* **301** 113–50
- [81] Brazovskii S and Nattermann T 2004 Pinning and sliding of driven elastic systems: from domain walls to charge density waves *Adv. Phys.* **53** 177–252
- [82] Le Doussal P 2009 Exact results and open questions in first principle functional RG *Ann. Phys., NY* **325** 49–150

- [83] Pruessner G 2012 *Self-Organised Criticality: Theory, Models and Characterisation* (Cambridge: Cambridge University Press)
- [84] Lemerle S, Ferré J, Chappert C, Mathet V, Giamarchi T and Le Doussal P 1998 Domain wall creep in an Ising ultrathin magnetic film *Phys. Rev. Lett.* **80** 849
- [85] Moulinet S, Guthmann C and Rolley E 2002 Roughness and dynamics of a contact line of a viscous fluid on a disordered substrate *Eur. Phys. J. E* **8** 437–43
- [86] Peierls R E 1955 *Quantum Theory of Solids* (Oxford: Oxford University Press)
- [87] Fukuyama H and Lee P A 1978 Dynamics of the charge-density wave: I. Impurity pinning in a single chain *Phys. Rev. B* **17** 535
- [88] Lee P A and Rice T M 1979 Electric-field depinning of charge-density waves *Phys. Rev. B* **19** 3970–80
- [89] Grüner G 1988 The dynamics of charge-density waves *Rev. Mod. Phys.* **60** 1129–81
- [90] Monceau P 2012 Electronic crystals: an experimental overview *Adv. Phys.* **61** 325
- [91] Kardar M 1996 Lectures on directed paths in random media *Fluctuating Geometries in Statistical Mechanics and Field Theory* (*École d'Été de Physique Théorique* vol 62) ed F David, P Ginsparg and J Zinn-Justin (Amsterdam: Elsevier) (arXiv:cond-mat/9411022)
- [92] Brochard F and De Gennes P G 1991 Collective modes of a contact line *Langmuir* **7** 3216–8
- [93] Rice J R 1985 First-order variation in elastic fields due to variation in location of a planar crack front *J. Appl. Mech.* **52** 571–9
- [94] Bachas C, Le Doussal P and Wiese K J 2007 Wetting and minimal surfaces *Phys. Rev. E* **75** 031601
- [95] Le Doussal P, Wiese K J, Raphael E and Golestanian R 2006 Can non-linear elasticity explain contact-line roughness at depinning? *Phys. Rev. Lett.* **96** 015702
- [96] Le Doussal P and Wiese K J 2010 Elasticity of a contact-line and avalanche-size distribution at depinning *Phys. Rev. E* **82** 011108
- [97] Gutenberg B and Richter C F 1944 Frequency of earthquakes in California *Bull. Seismol. Soc. Am.* **34** 185
- [98] Zapperi S, Cizeau P, Durin G and Stanley H E 1998 Dynamics of a ferromagnetic domain wall: avalanches, depinning transition, and the Barkhausen effect *Phys. Rev. B* **58** 6353–66
- [99] Flory P J 1953 *Principles of Polymer Chemistry* (Ithaca, NY: Cornell University Press)
- [100] Harris A B 1974 Effect of random defects on the critical behaviour of Ising models *J. Phys. C: Solid State Phys.* **7** 1671–92
- [101] Imry Y and Ma S-k 1975 Random-field instability of the ordered state of continuous symmetry *Phys. Rev. Lett.* **35** 1399–401
- [102] Brout R 1959 Statistical mechanical theory of a random ferromagnetic system *Phys. Rev.* **115** 824–35
- [103] Edwards S F and Anderson P W 1975 Theory of spin glasses *J. Phys. F: Met. Phys.* **5** 965–74
- [104] Aharony A, Imry Y and Ma S-k 1976 Lowering of dimensionality in phase transitions with random fields *Phys. Rev. Lett.* **37** 1364–7
- [105] Efetov K B and Larkin A I 1977 Charge-density wave in a random potential *Sov. Phys. - JETP* **45** 1236
- [106] Young A P 1977 On the lowering of dimensionality in phase transitions with random fields *J. Phys. C: Solid State Phys.* **10** L257–6
- [107] Ising E 1925 Beitrag zur Theorie des Ferromagnetismus *Z. Phys.* **31** 253–8
- [108] Kardar M 1987 Replica Bethe ansatz studies of two-dimensional interfaces with quenched random impurities *Nucl. Phys. B* **290** 582–602
- [109] Larkin A I 1970 *Sov. Phys. - JETP* **31** 784
- [110] Nattermann T 1985 Ising domain wall in a random pinning potential *J. Phys. C: Solid State Phys.* **18** 6661–79
- [111] Wilson K G and Fisher M E 1972 Critical exponents in 3.99 dimensions *Phys. Rev. Lett.* **28** 240–3
- [112] Bogoliubov N N and Parasiuk O S 1957 Über die Multiplikation der Kausalfunktionen in der Quantentheorie der Felder *Acta Math.* **97** 227
- [113] Hepp K 1966 Proof of the Bogoliubov–Parasiuk theorem on renormalization *Commun. Math. Phys.* **2** 301–26
- [114] Zimmermann W 1969 Convergence of Bogoliubov's method of renormalization in momentum space *Commun. Math. Phys.* **15** 208–34
- [115] Bergere M C and Lam Y M P 1976 Bogoliubov–Parasiuk theorem in the  $\alpha$ -parametric representation *J. Math. Phys.* **17** 1546–57
- [116] Rivasseau V 1991 *From Perturbative to Constructive Renormalization* (Princeton, NJ: Princeton University Press)
- [117] Wilson K and Kogut J 1974 The renormalization group and the  $\epsilon$ -expansion *Phys. Rep.* **12** 75–199
- [118] Wiese K J 1999 Polymerized membranes, a review *Phase Transitions and Critical Phenomena* vol 19 (London: Academic)
- [119] Fisher D S 1986 Interface fluctuations in disordered systems:  $5 - \epsilon$  expansion expansion and failure of dimensional reduction *Phys. Rev. Lett.* **56** 1964–7
- [120] Narayan O and Middleton A A 1994 Avalanches and the renormalization-group for pinned charge-density waves *Phys. Rev. B* **49** 244–56
- [121] Narayan O and Fisher D S 1992 Critical behavior of sliding charge-density waves in  $4 - \epsilon$  dimensions *Phys. Rev. B* **46** 11520–49
- [122] Narayan O and Fisher D S 1992 Dynamics of sliding charge-density waves in  $4 - \epsilon$  dimensions *Phys. Rev. Lett.* **68** 3615–8
- [123] Le Doussal P, Wiese K J and Chauve P 2004 Functional renormalization group and the field theory of disordered elastic systems *Phys. Rev. E* **69** 026112
- [124] Le Doussal P, Wiese K J and Chauve P 2002 Two-loop functional renormalization group theory of the depinning transition *Phys. Rev. B* **66** 174201
- [125] Chauve P, Le Doussal P and Wiese K J 2001 Renormalization of pinned elastic systems: how does it work beyond one loop? *Phys. Rev. Lett.* **86** 1785–8
- [126] Balents L, Bouchaud J-P and Mézard M 1996 The large scale energy landscape of randomly pinned objects *J. Physique I* **6** 1007–20
- [127] Le Doussal P 2006 Finite-temperature functional RG, droplets and decaying Burgers turbulence *Europhys. Lett.* **76** 457–63
- [128] Middleton A A, Le Doussal P and Wiese K J 2007 Measuring functional renormalization group fixed-point functions for pinned manifolds *Phys. Rev. Lett.* **98** 155701
- [129] Le Doussal P and Wiese K J 2007 How to measure functional RG fixed-point functions for dynamics and at depinning *Europhys. Lett.* **77** 66001
- [130] Wiese K J and Le Doussal P 2008 How to measure the effective action for disordered systems *Path Integrals—New Trends and Perspectives* ed W Janke and A Pelster (Singapore: World Scientific) arXiv:0712.4286
- [131] ter Burg C and Wiese K J 2021 Mean-field theories for depinning and their experimental signatures *Phys. Rev. E* **103** 052114
- [132] Balents L and Fisher D S 1993 Large- $N$  expansion of  $(4 - \epsilon)$ -dimensional oriented manifolds in random media *Phys. Rev. B* **48** 5949–63
- [133] Wagner O S, Geshkenbein V B, Larkin A I and Blatter G 1999 Renormalization-group analysis of weak collective pinning in type-II superconductors *Phys. Rev. B* **59** 11551–62
- [134] Scheidl S private communication about two-loop calculations for the random manifold problem 2000–2004

- [135] Dincer Y 1999 Zur Universalität der Struktur elastischer Mannigfaltigkeiten in Unordnung *Master's Thesis* Universität Köln
- [136] Chauve P and Le Doussal P 2001 Exact multilocal renormalization group and applications to disordered problems *Phys. Rev. E* **64** 051102
- [137] Middleton A A 1995 Numerical results for the ground-state interface in a random medium *Phys. Rev. E* **52** R3337–40
- [138] Alava M J and Duxbury P M 1996 Disorder-induced roughening in the three-dimensional Ising model *Phys. Rev. B* **54** 14990–3
- [139] Kardar M, Huse D A, Henley C L and Fisher D S 1985 Roughening by impurities at finite temperatures *Phys. Rev. Lett.* **55** 2923
- [140] Kompaniets M and Wiese K J 2019 Fractal dimension of critical curves in the  $O(n)$ -symmetric  $\phi^4$ -model and crossover exponent at six-loop order: loop-erased random walks, self-avoiding walks, Ising, XY and Heisenberg models *Phys. Rev. E* **101** 012104
- [141] Wegner F J 1974 Some invariance properties of the renormalization group *J. Phys. C: Solid State Phys.* **7** 2098–108
- [142] Poland D, Rychkov S and Vichi A 2019 The conformal bootstrap: theory, numerical techniques, and applications *Rev. Mod. Phys.* **91** 015002
- [143] Chauve P, Giamarchi T and Le Doussal P 2000 Creep and depinning in disordered media *Phys. Rev. B* **62** 6241–67
- [144] Balents L and Le Doussal P 2005 Thermal fluctuations in pinned elastic systems: field theory of rare events and droplets *Ann. Phys., NY* **315** 213–303
- [145] Balents L and Le Doussal P 2004 Broad relaxation spectrum and the field theory of glassy dynamics for pinned elastic systems *Phys. Rev. E* **69** 061107
- [146] Wasow W 1965 *Asymptotic Expansions for Ordinary Differential Equations (Pure and Applied Mathematics vol 14)* (New York: Wiley)
- [147] Bogolyubov (originator) N N Jr 2011 *Encyclopedia of Mathematics: Perturbation Theory*
- [148] Smith D R 1985 *Singular-Perturbation Theory* (Cambridge: Cambridge University Press)
- [149] Hairer E and Wanner G 1996 *Solving Ordinary Differential Equations II: Stiff and Differential-Algebra Problems* (Berlin: Springer)
- [150] Le Doussal P and Wiese K J 2005 Two-loop functional renormalization for elastic manifolds pinned by disorder in  $N$  dimensions *Phys. Rev. E* **72** 035101(R)
- [151] Rosso A, Bustingorry S and Le Doussal P 2010 Universal high temperature regime of pinned elastic objects *Phys. Rev. B* **82** 140201
- [152] Le Doussal P 2006 Chaos and residual correlations in pinned disordered systems *Phys. Rev. Lett.* **96** 235702
- [153] Duemmer O and Le Doussal P 2007 Chaos in the thermal regime for pinned manifolds via functional RG (arXiv:0709.1378)
- [154] Le Doussal P and Wiese K J 2002 Functional renormalization group at large  $N$  for random manifolds *Phys. Rev. Lett.* **89** 125702
- [155] Mézard M and Parisi G 1991 Replica field theory for random manifolds *J. Physique I* **1** 809–36
- [156] Le Doussal P and Wiese K J 2004 Derivation of the functional renormalization group  $\beta$ -function at order  $1/N$  for manifolds pinned by disorder *Nucl. Phys. B* **701** 409–80
- [157] Parisi G 1980 A sequence of approximated solutions to the S-K model for spin glasses *J. Phys. A: Math. Gen.* **13** L115–21
- [158] Parisi G 1980 The order parameter for spin glasses: a function on the interval 0–1 *J. Phys. A: Math. Gen.* **13** 1101–12
- [159] Parisi G 1980 Magnetic properties of spin glasses in a new mean field theory *J. Phys. A: Math. Gen.* **13** 1887–95
- [160] Parisi G and Toulouse G 1980 A simple hypothesis for the spin glass phase of the infinite-ranged SK model *J. Physique Lett.* **41** 361–4
- [161] Parisi G and Toulouse G 1981 A simple hypothesis for the spin glass phase of the infinite-ranged SK model *J. Physique Lett.* **42** 71 (erratum)
- [162] Mézard M, Parisi G, Sourlas N, Toulouse G and Virasoro M 1984 Replica symmetry breaking and the nature of the spin glass phase *J. Physique* **45** 843–54
- [163] Duplantier B 1992 Loop-erased self-avoiding walks in two dimensions: exact critical exponents and winding numbers *Physica A* **191** 516–22
- [164] Le Doussal P, Müller M and Wiese K J 2007 Cusps and shocks in the renormalized potential of glassy random manifolds: how functional renormalization group and replica symmetry breaking fit together *Phys. Rev. B* **77** 064203
- [165] Agoritsas E and Lecomte V 2017 Power countings versus physical scalings in disordered elastic systems—case study of the one-dimensional interface *J. Phys. A: Math. Theor.* **50** 104001
- [166] Agoritsas E and Lecomte V unpublished
- [167] Bovier A and Fröhlich J 1986 A heuristic theory of the spin glass phase *J. Stat. Phys.* **44** 347–91
- [168] Fisher D S and Huse D A 1987 Absence of many states in realistic spin glasses *J. Phys. A: Math. Gen.* **20** L1005–10
- [169] Huse D A and Fisher D S 1987 Dynamics of droplet fluctuations in pure and random Ising systems *Phys. Rev. B* **35** 6841–6
- [170] Fisher D S and Huse D A 1988 Equilibrium behavior of the spin-glass ordered phase *Phys. Rev. B* **38** 386–411
- [171] Fisher D S and Huse D A 1988 Nonequilibrium dynamics of spin glasses *Phys. Rev. B* **38** 373–85
- [172] Bray A J and Moore M A 1985 Critical behavior of the three-dimensional Ising spin glass *Phys. Rev. B* **31** 631–3
- [173] Newman C M and Stein D L 1997 Metastate approach to thermodynamic chaos *Phys. Rev. E* **55** 5194–211
- [174] Moore M A, Bokil H and Drossel B 1998 Evidence for the droplet picture of spin glasses *Phys. Rev. Lett.* **81** 4252–5
- [175] Marinari E, Parisi G, Ruiz-Lorenzo J and Ritort F 1996 Numerical evidence for spontaneously broken replica symmetry in 3D spin glasses *Phys. Rev. Lett.* **76** 843–6
- [176] Marinari E, Parisi G, Ricci-Tersenghi F, Ruiz-Lorenzo J J and Zuliani F 2000 Replica symmetry breaking in short-range spin glasses: theoretical foundations and numerical evidences *J. Stat. Phys.* **98** 973–1074
- [177] Aspelmeier T, Wang W, Moore M A and Katzgraber H G 2016 Interface free-energy exponent in the one-dimensional Ising spin glass with long-range interactions in both the droplet and broken replica symmetry regions *Phys. Rev. E* **94** 022116
- [178] Charbonneau P and Yaida S 2017 Nontrivial critical fixed point for replica-symmetry-breaking transitions *Phys. Rev. Lett.* **118** 215701
- [179] Moore M A 2019 Why replica symmetry breaking does not occur below six dimensions in Ising spin glasses (arXiv:1902.07099)
- [180] Yeo J and Moore M A 2020 Possible instability of one-step replica symmetry breaking in p-spin Ising models outside mean-field theory *Phys. Rev. E* **101** 032127
- [181] Höller J and Read N 2020 One-step replica-symmetry-breaking phase below the de Almeida–Thouless line in low-dimensional spin glasses *Phys. Rev. E* **101** 042114
- [182] Balents L and Le Doussal P 2004 Field theory of statics and dynamics of glasses: rare events and barrier distributions *Europhys. Lett.* **65** 685–91
- [183] Drossel B and Kardar M 1995 Scaling of energy barriers for flux lines and other random systems *Phys. Rev. E* **52** 4841–52

- [184] Mikheev L V, Drossel B and Kardar M 1995 Energy barriers to motion of flux lines in random media *Phys. Rev. Lett.* **75** 1170–3
- [185] ter Burg C 2021 To appear *PhD Thesis* PSL Research University
- [186] ter Burg C and Wiese K J unpublished
- [187] Kida S 1979 Asymptotic properties of Burgers turbulence *J. Fluid Mech.* **93** 337–77
- [188] Bouchaud J-P and Mézard M 1997 Universality classes for extreme-value statistics *J. Phys. A: Math. Gen.* **30** 7997–8015
- [189] Sinai Y G 1983 The limiting behaviour of a one-dimensional random walk in a random environments *Theory Probab. Appl.* **27** 256–68
- [190] Le Doussal P and Monthus C 2003 Exact solutions for the statistics of extrema of some random 1D landscapes, application to the equilibrium and the dynamics of the toy model *Physica A* **317** 140–98
- [191] Derrida B 1981 Random-energy model: an exactly solvable model of disordered systems *Phys. Rev. B* **24** 2613–26
- [192] Derrida B and Toulouse G 1985 Sample to sample fluctuations in the random energy model *J. Physique Lett.* **46** 223–8
- [193] Ruelle D 1987 A mathematical reformulation of Derrida's REM and GREM *Commun. Math. Phys.* **108** 225–39
- [194] Mukaida H 2015 Non-differentiability of the effective potential and the replica symmetry breaking in the random energy model *J. Phys. A: Math. Theor.* **49** 045002
- [195] Gross D J and Mezard M 1984 The simplest spin glass *Nucl. Phys. B* **240** 431–52
- [196] Derrida B 1991 The zeroes of the partition function of the random energy model *Physica A* **177** 31–7
- [197] Dobrinevski A, Le Doussal P and Wiese K J 2011 Interference in disordered systems: a particle in a complex random landscape *Phys. Rev. E* **83** 061116
- [198] Gorokhov D A, Fisher D S and Blatter G 2002 Quantum collective creep: a quasiclassical Langevin equation approach *Phys. Rev. B* **66** 214203
- [199] Nguen V L, Spivak B Z and Shklovskii B I 1985 Tunnel hopping in disordered systems *J. Exp. Theor. Phys.* **62** 1021
- [200] Medina E and Kardar M 1991 Spin-orbit scattering and magnetoconductance of strongly localized electrons *Phys. Rev. Lett.* **66** 3187–90
- [201] Medina E and Kardar M 1992 Quantum interference effects for strongly localized electrons *Phys. Rev. B* **46** 9984–10006
- [202] Medina E, Kardar M, Shapir Y and Wang X R 1989 Interference of directed paths in disordered systems *Phys. Rev. Lett.* **62** 941–4
- [203] Medina E, Kardar M, Shapir Y and Wang X R 1990 Magnetic-field effects on strongly localized electrons *Phys. Rev. Lett.* **64** 1816–9
- [204] Somoza A M, Ortuño M and Prior J 2007 Universal distribution functions in two-dimensional localized systems *Phys. Rev. Lett.* **99** 116602
- [205] Prior J, Somoza A M and Ortuño M 2009 Conductance distribution in two-dimensional localized systems with and without magnetic fields *Eur. Phys. J. B* **70** 513–21
- [206] Chalker J T and Coddington P D 1988 Percolation, quantum tunnelling and the integer Hall effect *J. Phys. C: Solid State Phys.* **21** 2665–79
- [207] Cardy J 2010 Quantum network models and classical localization problems *Int. J. Mod. Phys. B* **24** 1989–2014
- [208] Beamond E J, Cardy J and Chalker J T 2002 Quantum and classical localization, the spin quantum Hall effect, and generalizations *Phys. Rev. B* **65** 214301
- [209] Cook J and Derrida B 1990 Lyapunov exponents of large, sparse random matrices and the problem of directed polymers with complex random weights *J. Stat. Phys.* **61** 961–86
- [210] Derrida B 1991 Mean field theory of directed polymers in a random medium and beyond *Phys. Scr.* **T38** 6–12
- [211] Derrida B, Evans M R and Speer E R 1993 Mean field theory of directed polymers with random complex weights *Commun. Math. Phys.* **156** 221–44
- [212] Toft-Petersen R, Abrahamsen A B, Balog S, Porcar L and Laver M 2018 Decomposing the Bragg glass and the peak effect in a type-II superconductor *Nat. Commun.* **9** 901
- [213] Meissner W and Ochsenfeld R 1933 Ein neuer Effekt bei Eintritt der Supraleitfähigkeit *Naturwissenschaften* **21** 787–8
- [214] Giamarchi T and Le Doussal P 1994 Elastic theory of pinned flux lattices *Phys. Rev. Lett.* **72** 1530–3
- [215] Giamarchi T and Le Doussal P 1996 Variational theory of elastic manifolds with correlated disorder and localization of interacting quantum particles *Phys. Rev. B* **53** 15206
- [216] Klein T, Joumard I, Blanchard S, Marcus J, Cubitt R, Giamarchi T and Le Doussal P 2001 A Bragg glass phase in the vortex lattice of a type II superconductor *Nature* **413** 404–6
- [217] Fisher M P A 1989 Vortex-glass superconductivity: a possible new phase in bulk high- $T_c$  oxides *Phys. Rev. Lett.* **62** 1415–8
- [218] Koch R H, Foglietti V, Gallagher W J, Koren G, Gupta A and Fisher M P A 1989 Experimental evidence for vortex-glass superconductivity in Y–Ba–Cu–O *Phys. Rev. Lett.* **63** 1511–4
- [219] Reger J D, Tokuyasu T A, Young A P and Fisher M P A 1991 Vortex-glass transition in three dimensions *Phys. Rev. B* **44** 7147–50
- [220] Moser A, Hug H J, Parashikov I, Stiefel B, Fritz O, Thomas H, Baratoff A, Güntherodt H-J and Chaudhari P 1995 Observation of single vortices condensed into a vortex-glass phase by magnetic force microscopy *Phys. Rev. Lett.* **74** 1847–50
- [221] Balents L, Marchetti M C and Radzihovsky L 1998 Nonequilibrium steady states of driven periodic media *Phys. Rev. B* **57** 7705–39
- [222] Aranson I S, Scheidl S and Vinokur V M 1998 Nonequilibrium dislocation dynamics and instability of driven vortex lattices in two dimensions *Phys. Rev. B* **58** 14541–7
- [223] Scheidl S and Vinokur V 1998 Driven dynamics of periodic elastic media in disorder *Phys. Rev. E* **57** 2574–93
- [224] Pfeiffer F O and Reiger H 1999 Numerical study of the strongly screened vortex-glass model in an external field *Phys. Rev. B* **60** 6304–7
- [225] Fedorenko A A 2008 Elastic systems with correlated disorder: response to tilt and application to surface growth *Phys. Rev. B* **77** 094203
- [226] Dupuis N 2019 Glassy properties of the Bose-glass phase of a one-dimensional disordered Bose fluid *Phys. Rev. E* **100** 030102
- [227] Dupuis N and Daviet R 2020 Bose-glass phase of a one-dimensional disordered Bose fluid: metastable states, quantum tunneling, and droplets *Phys. Rev. E* **101** 042139
- [228] Dupuis N 2020 Is there a Mott-glass phase in a one-dimensional disordered quantum fluid with linearly confining interactions? *Europhys. Lett.* **130** 56002
- [229] Daviet R and Dupuis N 2020 Mott-glass phase of a one-dimensional quantum fluid with long-range interactions *Phys. Rev. Lett.* **125** 235301
- [230] Daviet R and Dupuis N 2021 Chaos in the Bose-glass phase of a one-dimensional disordered Bose fluid (arXiv:2101.12487)
- [231] Emig T and Nattermann T 2006 Effect of planar defects on the stability of the Bragg glass phase of type-II superconductors *Phys. Rev. Lett.* **97** 177002
- [232] Emig T and Nattermann T 1997 A new disorder-driven roughening transition of charge-density waves and flux-line lattices *Phys. Rev. Lett.* **79** 5090–3
- [233] Le Doussal P 2010 Novel phases of vortices in superconductors *Int. J. Mod. Phys. B* **24** 3855–914
- [234] Di Francesco P, Mathieu P and Sénéchal D 1997 *Conformal Field Theory* (New York: Springer)

- [235] von Delft J and Schoeller H 1998 Bosonization for beginners—refermionization for experts *Ann. Phys., Lpz.* **7** 225–305
- [236] Giamarchi T 2004 *Quantum Physics in One Dimension* (Oxford: Oxford University Press)
- [237] Dotsenko V S Série de cours sur la théorie conforme *Lecture Notes* Universités Paris VI and VII
- [238] Henkel M 1999 *Conformal Invariance and Critical Phenomena* (Berlin: Springer)
- [239] Thirring W E 1958 A soluble relativistic field theory *Ann. Phys., NY* **3** 91–112
- [240] Coleman S 1975 Quantum sine-Gordon equation as the massive Thirring model *Phys. Rev. D* **11** 2088–97
- [241] Kosterlitz J M and Thouless D J 1973 Ordering, metastability and phase transitions in two-dimensional systems *J. Phys. C: Solid State Phys.* **6** 1181–203
- [242] Balog J and Hegedus Á 2000 Two-loop beta-functions of the sine-Gordon model *J. Phys. A: Math. Gen.* **33** 6543
- [243] Amit D J, Goldschmidt Y Y and Grinstein S 1980 Renormalisation group analysis of the phase transition in the 2D Coulomb gas, sine-Gordon theory and XY-model *J. Phys. A: Math. Gen.* **13** 585
- [244] Lovelace C 1986 Stability of string vacua: (I). A new picture of the renormalization group *Nucl. Phys. B* **273** 413–67
- [245] Boyanovsky D 1989 Field-theoretical renormalisation and fixed-point structure of a generalised Coulomb gas *J. Phys. A: Math. Gen.* **22** 2601–14
- [246] Naik S 1993 The exact mass gap of the chiral  $SU(n) \times SU(n)$  model *Nucl. Phys. B* **30** 232–5
- [247] Konik R M and LeClair A 1996 Short-distance expansions of correlation functions in the sine-Gordon theory *Nucl. Phys. B* **479** 619–53
- [248] Kehrein S 2001 Flow equation approach to the sine-Gordon model *Nucl. Phys. B* **592** 512–62
- [249] Daviet R and Dupuis N 2019 Nonperturbative functional renormalization-group approach to the sine-Gordon model and the Lukyanov–Zamolodchikov conjecture *Phys. Rev. Lett.* **122** 155301
- [250] Rieger H and Blasum U 1997 Ground-state properties of solid-on-solid models with disordered substrates *Phys. Rev. B* **55** R7394–7
- [251] Zeng C, Middleton A A and Shapir Y 1996 Ground-state roughness of the disordered substrate and flux lines in  $d = 2$  *Phys. Rev. Lett.* **77** 3204–7
- [252] Kenyon R 2001 Dominos and the Gaussian free field *Ann. Probab.* **29** 1128–37
- [253] Le Doussal P and Schehr G 2007 Disordered free fermions and the Cardy–Ostlund fixed line at low temperature *Phys. Rev. B* **75** 184401
- [254] Perret A, Ristivojevic Z, Le Doussal P, Schehr G and Wiese K J 2012 Super-rough glassy phase of the random field XY model in two dimensions *Phys. Rev. Lett.* **109** 157205
- [255] Propp J 2003 Generalized domino-shuffling *Theor. Comput. Sci.* **303** 267–301
- [256] Guruswamy S, LeClair A and Ludwig A W W 2000  $gl(N|N)$  super-current algebras for disordered Dirac fermions in two dimensions *Nucl. Phys. B* **583** 475–512
- [257] Ristivojevic Z, Le Doussal P and Wiese K J 2012 Super-rough phase of the random-phase sine-Gordon model: two-loop results *Phys. Rev. B* **86** 054201
- [258] Carpentier D and Le Doussal P 1998 Disordered XY models and Coulomb gases: renormalization via traveling waves *Phys. Rev. Lett.* **81** 2558–61
- [259] Carpentier D and Le Doussal P 2000 Topological transitions and freezing in XY models and Coulomb gases with quenched disorder: renormalization via traveling waves *Nucl. Phys. B* **588** 565–629
- [260] Carpentier D and Le Doussal P 2001 Glass transition of a particle in a random potential, front selection in nonlinear renormalization group, and entropic phenomena in Liouville and sinh-Gordon models *Phys. Rev. E* **63** 026110
- [261] Carpentier D and Le Doussal P 2008 Electromagnetic Coulomb gas with vector charges and ‘elastic’ potentials: renormalization group equations *Nucl. Phys. B* **795** 491–518
- [262] Frisch U 1995 *Turbulence* (Cambridge: Cambridge University Press)
- [263] Lesieur M 1995 *Turbulence in Fluids* 3rd edn (Dordrecht: Kluwer)
- [264] Gawędzki K 2008 Stochastic processes in turbulent transport (arXiv:0806.1949)
- [265] Kraichnan R H, Yakhot V and Chen S 1995 Scaling relations for a randomly advected passive scalar field *Phys. Rev. Lett.* **75** 240–3
- [266] Gawędzki K and Kupiainen A 1995 Anomalous scaling of the passive scalar *Phys. Rev. Lett.* **75** 3834
- [267] Bernard D, Gawędzki K and Kupiainen A 1998 Slow modes in passive advection *J. Stat. Phys.* **90** 519–69
- [268] Antonov N V 1999 Anomalous scaling regimes of a passive scalar advected by the synthetic velocity field *Phys. Rev. E* **60** 6691–707
- [269] Adzhemyan L T, Antonov N V and Vasil’ev A N 1998 Renormalization group, operator product expansion, and anomalous scaling in a model of advected passive scalar *Phys. Rev. E* **58** 1823–35
- [270] Adzhemyan L T, Antonov N V, Barinov V A, Kabrits Y S and Vasil’ev A N 2001 Anomalous exponents to order  $\varepsilon^3$  in the rapid-change model of passive scalar advection *Phys. Rev. E* **63** 025303
- [271] Adzhemyan L T, Antonov N V, Barinov V A, Kabrits Y S and Vasil’ev A N 2001 Anomalous exponents to order  $\varepsilon^3$  in the rapid-change model of passive scalar advection *Phys. Rev. E* **64** 019901 (erratum)
- [272] Wiese K J 2000 The passive polymer problem *J. Stat. Phys.* **101** 843–91
- [273] Foster M S, Ryu S and Ludwig A W W 2009 Termination of typical wave-function multifractal spectra at the Anderson metal–insulator transition: field theory description using the functional renormalization group *Phys. Rev. B* **80** 075101
- [274] Halsey T C, Jensen M H, Kadanoff L P, Procaccia I and Shraiman B I 1986 Fractal measures and their singularities: the characterization of strange sets *Phys. Rev. A* **33** 1141–51
- [275] Fedorenko A A, Le Doussal P and Wiese K J 2014 Non-Gaussian effects and multifractality in the Bragg glass *Europhys. Lett.* **105** 16002
- [276] Le Doussal P, Ristivojevic Z and Wiese K J 2013 Exact form of the exponential correlation function in the glassy super-rough phase *Phys. Rev. B* **87** 214201
- [277] Fedorenko A, Le Doussal P and Wiese K J 2006 Universal distribution of threshold forces at the depinning transition *Phys. Rev. E* **74** 041110
- [278] Gel’fand I M and Yaglom A M 1960 Integration in functional spaces and its applications in quantum physics *J. Math. Phys.* **1** 48
- [279] Hartmann A K and Rieger H 2002 *Optimization Algorithms in Physics* (New York: Wiley-VCH)
- [280] Krauth W 2006 *Statistical Mechanics: Algorithms and Computations* (Oxford: Oxford University Press)
- [281] Hartmann A K and Rieger H (ed) 2002 *New Optimization Algorithms in Physics* (New York: Wiley-VCH)
- [282] Tinoco I and Bustamante C 1999 How RNA folds *J. Mol. Biol.* **293** 271–81
- [283] McCaskill J S 1990 The equilibrium partition function and base pair binding probabilities for RNA secondary structure *Biopolymers* **29** 1105–19

- [284] Bundschuh R and Hwa T 1999 RNA secondary structure formation: a solvable model of heteropolymer folding *Phys. Rev. Lett.* **83** 1479–82
- [285] Higgs P G 2000 RNA secondary structure: physical and computational aspects *Quart. Rev. Biophys.* **33** 199
- [286] Baez W D, Wiese K J and Bundschuh R 2019 Behavior of random RNA secondary structures near the glass transition *Phys. Rev. E* **99** 022415
- [287] Sedgewick R 1990 *Algorithms in C* (Reading, MA: Addison-Wesley)
- [288] Le Doussal P, Middleton A A and Wiese K J 2009 Statistics of static avalanches in a random pinning landscape *Phys. Rev. E* **79** 050101(R)
- [289] Rieger H 1998 Ground state properties of fluxlines in a disordered environment *Phys. Rev. Lett.* **81** 4488–91
- [290] Jae N D and Rieger H 2001 Disorder-driven critical behavior of periodic elastic media in a crystal potential *Phys. Rev. Lett.* **87** 176102
- [291] Díaz Pardo R, Moisan N, Alborno L J, Lemaître A, Curiale J and Jeudy V 2019 Common universal behavior of magnetic domain walls driven by spin-polarized electrical current and magnetic field *Phys. Rev. B* **100** 184420
- [292] Diaz Pardo R 2018 Universal behaviors of magnetic domain walls in thin ferromagnets *PhD Thesis* Université Paris Saclay
- [293] Huguet J M, Forns N and Ritort F 2009 Statistical properties of metastable intermediates in DNA unzipping *Phys. Rev. Lett.* **103** 248106
- [294] Nattermann T, Stepanow S, Tang L-H and Leschhorn H 1992 Dynamics of interface depinning in a disordered medium *J. Physique II* **2** 1483–8
- [295] Martin P C, Siggia E D and Rose H A 1973 Statistical dynamics of classical systems *Phys. Rev. A* **8** 423–37
- [296] Janssen H-K 1976 On a Lagrangean for classical field dynamics and renormalization group calculations of dynamical critical properties *Z. Phys. B* **23** 377–80
- [297] De Dominicis C 1976 Techniques de renormalisation de la théorie des champs et dynamique des phénomènes critiques *J. Phys. Colloq.* **37** 247–53
- [298] Janssen H K 1985 Feldtheoretische methoden in der Statistischen mechanik *Vorlesungsmanuskript* Universität Düsseldorf
- [299] Täuber U 2012 *Critical Dynamics: A Field Theory Approach to Equilibrium and Non-equilibrium Scaling Behavior* (Cambridge: Cambridge University Press)
- [300] Middleton A A 1992 Asymptotic uniqueness of the sliding state for charge-density waves *Phys. Rev. Lett.* **68** 670–3
- [301] Hohenberg P C and Halperin B I 1977 Theory of dynamic critical phenomena *Rev. Mod. Phys.* **49** 435
- [302] Leschhorn H, Nattermann T, Stepanow S and Tang L-H 1997 Driven interface depinning in a disordered medium *Ann. Phys., Lpz.* **509** 1–34
- [303] Narayan O and Fisher D S 1993 Threshold critical dynamics of driven interfaces in random media *Phys. Rev. B* **48** 7030–42
- [304] Ferrero E E, Bustingorry S and Kolton A B 2013 Non-steady relaxation and critical exponents at the depinning transition *Phys. Rev. E* **87** 032122
- [305] Grassberger P, Dhar D and Mohanty P K 2016 Oslo model, hyperuniformity, and the quenched Edwards–Wilkinson model *Phys. Rev. E* **94** 042314
- [306] Rosso A, Le Doussal P and Wiese K J 2007 Numerical calculation of the functional renormalization group fixed-point functions at the depinning transition *Phys. Rev. B* **75** 220201
- [307] Rosso A, Hartmann A K and Krauth W 2003 Depinning of elastic manifolds *Phys. Rev. E* **67** 021602
- [308] Roters L, Hucht A, Lübeck S, Nowak U and Usadel K D 1999 Depinning transition and thermal fluctuations in the random-field Ising model *Phys. Rev. E* **60** 5202
- [309] Kaspar D C and Mungan M 2013 Subthreshold behavior and avalanches in an exactly solvable charge density wave system *Europhys. Lett.* **103** 46002
- [310] Wiese K J and Fedorenko A A 2019 Field theories for loop-erased random walks *Nucl. Phys. B* **946** 114696
- [311] Wiese K J and Fedorenko A A 2019 Depinning transition of charge-density waves: mapping onto  $O(n)$  symmetric  $\phi^4$  theory with  $n \rightarrow -2$  and loop-erased random walks *Phys. Rev. Lett.* **123** 197601
- [312] Shapira A and Wiese K J 2020 An exact mapping between loop-erased random walks and an interacting field theory with two fermions and one boson *SciPost Phys.* **9** 063
- [313] Balog I, Tarjus G and Tissier M 2019 Benchmarking the non-perturbative functional renormalization group approach on the random elastic manifold model in and out of equilibrium *J. Stat. Mech.* 103301
- [314] Fedorenko A and Stepanow S 2003 Depinning transition at the upper critical dimension *Phys. Rev. E* **67** 057104
- [315] Le Doussal P and Wiese K J 2009 Driven particle in a random landscape: disorder correlator, avalanche distribution and extreme value statistics of records *Phys. Rev. E* **79** 051105
- [316] Alessandro B, Beatrice C, Bertotti G and Montorsi A 1990 Domain-wall dynamics and Barkhausen effect in metallic ferromagnetic materials: I. Theory *J. Appl. Phys.* **68** 2901
- [317] Alessandro B, Beatrice C, Bertotti G and Montorsi A 1990 Domain-wall dynamics and Barkhausen effect in metallic ferromagnetic materials: II. Experiments *J. Appl. Phys.* **68** 2908
- [318] Vergne R, Cotillard J C and Porteseil J L 1981 Quelques aspects statistiques des processus d'aimantation dans les corps ferromagnétiques. Cas du déplacement d'une seule paroi de Bloch à  $180^\circ$  dans un milieu monocristallin aléatoirement perturbé *Rev. Phys. Appl.* **16** 449–76
- [319] Durin G and Zapperi S 2006 The Barkhausen effect *The Science of Hysteresis* ed G Bertotti and I Mayergoyz (Amsterdam: Elsevier) p 51
- [320] Csikor F F, Motz C, Weygand D, Zaiser M and Zapperi S 2007 Dislocation avalanches, strain bursts, and the problem of plastic forming at the micrometer scale *Science* **318** 251–4
- [321] Le Doussal P and Wiese K J 2013 Avalanche dynamics of elastic interfaces *Phys. Rev. E* **88** 022106
- [322] Zhu Z and Wiese K J 2017 The spatial shape of avalanches *Phys. Rev. E* **96** 062116
- [323] ter Burg C, Bohn F, Durin G, Sommer R L and Wiese K J 2021 Force-force correlations in disordered magnets (arXiv:2109.01197)
- [324] Douin A, ter Burg C, Lechenault F and Wiese K J unpublished
- [325] Bustingorry S, Kolton A B and Giamarchi T 2010 Random-manifold to random-periodic depinning of an elastic interface *Phys. Rev. B* **82** 094202
- [326] Bustingorry S and Kolton A 2010 Anisotropic finite-size scaling of an elastic string at the depinning threshold in a random-periodic medium *Pap. Phys.* 020008
- [327] Kolton A B, Bustingorry S, Ferrero E E and Rosso A 2013 Uniqueness of the thermodynamic limit for driven disordered elastic interfaces *J. Stat. Mech.* P12004
- [328] Rosso A and Krauth W 2001 Monte Carlo dynamics of driven strings in disordered media *Phys. Rev. B* **65** 012202
- [329] Rosso A and Krauth W 2002 Roughness at the depinning threshold for a long-range elastic string *Phys. Rev. E* **65** 025101
- [330] Rosso A 2002 Dépiéage de variétés élastiques en milieu aléatoire *PhD Thesis* Université Pierre et Marie Curie <https://tel.archives-ouvertes.fr/tel-00002097>

- [331] Sparfel J and Wiese K J 2021 Skewness at depinning, and conformal invariance unpublished
- [332] Ginsparg P 1988 Applied conformal field theory *Fields, Strings and Critical Phenomena (École d'Été de Physique Théorique LesHouches vol 49)* ed E Brézin and J Zinn-Justin (Amsterdam: North Holland)
- [333] Cardy J 1987 *Conformal Invariance (Phase Transitions and Critical Phenomena vol 11)* (London: Academic) pp 55–126
- [334] Leschhorn H and Tang L-H 1993 Comment on 'Elastic string in a random potential' *Phys. Rev. Lett.* **70** 2973
- [335] Rosso A and Krauth W private communication
- [336] Kolton A B private communication
- [337] Dümmer O and Krauth W 2007 Depinning exponents of the driven long-range elastic string *J. Stat. Mech.* **P01019**
- [338] Ertas D and Kardar M 1994 Critical dynamics of contact line depinning *Phys. Rev. E* **49** R2532
- [339] Wiese K J Original research done for this review yet unpublished
- [340] Rolley E, Guthmann C, Gombrowicz R and Repain V 1998 Roughness of the contact line on a disordered substrate *Phys. Rev. Lett.* **80** 2865–8
- [341] Iliev P, Pesheva N and Iliev S 2018 Roughness of the contact line on random self-affine rough surfaces *Phys. Rev. E* **98** 060801
- [342] Santucci S, Grob M, Toussaint R, Schmittbuhl J, Hansen A and Maløy K J 2010 Fracture roughness scaling: a case study on planar cracks *Europhys. Lett.* **92** 44001
- [343] Ramanathan S and Fisher D S 1997 Dynamics and instabilities of planar tensile cracks in heterogeneous media *Phys. Rev. Lett.* **79** 877–80
- [344] Katzav E, Adda-Bedia M, Ben Amar M and Boudaoud A 2007 Roughness of moving elastic lines: crack and wetting fronts *Phys. Rev. E* **76** 051601
- [345] Santucci S, Måløy K J, Delaplace A, Mathiesen J, Hansen A, Bakke J Ø H, Schmittbuhl J, Vanel L and Ray P 2007 Statistics of fracture surfaces *Phys. Rev. E* **75** 016104
- [346] Bouchaud E, Lapasset G and Planès J 1990 Fractal dimension of fractured surfaces: a universal value? *Europhys. Lett.* **13** 73–9
- [347] Lawn B 1993 *Fracture of Brittle Solids* 2nd edn (Cambridge: Cambridge University Press)
- [348] Parisi A, Caldarelli G and Pietronero L 2000 Roughness of fracture surfaces *Europhys. Lett.* **52** 304–10
- [349] Arndt P F and Nattermann T 2001 Criterion for crack formation in disordered materials *Phys. Rev. B* **63** 134204
- [350] Ponson L 2007 Crack propagation in disordered materials: how to decipher fracture surfaces *Ann. Phys., Paris* **32** 1–120
- [351] Ponson L 2009 Depinning transition in failure of inhomogeneous brittle materials *Phys. Rev. Lett.* **103** 055501
- [352] Tallakstad K T, Toussaint R, Santucci S and Måløy K J 2013 Non-Gaussian nature of fracture and the survival of fat-tail exponents *Phys. Rev. Lett.* **110** 145501
- [353] Bouchaud E 1997 Scaling properties of cracks *J. Phys.: Condens. Matter* **9** 4319–44
- [354] Ponson L private communication
- [355] Ramanathan S, Ertaş D and Fisher D S 1997 Quasistatic crack propagation in heterogeneous media *Phys. Rev. Lett.* **79** 873–6
- [356] Bonamy D, Santucci S and Ponson L 2008 Crackling dynamics in material failure as the signature of a self-organized dynamic phase transition *Phys. Rev. Lett.* **101** 045501
- [357] Ertas D and Kardar M 1994 Anisotropic scaling in depinning of a flux line *Phys. Rev. Lett.* **73** 1703–6
- [358] Ertas D and Kardar M 1996 Anisotropic scaling in threshold critical dynamics of driven directed lines *Phys. Rev. B* **53** 3520–42
- [359] Dalmas D, Lelarge A and Vandembroucq D 2008 Crack propagation through phase-separated glasses: effect of the characteristic size of disorder *Phys. Rev. Lett.* **101** 255501
- [360] Vernède S, Ponson L and Bouchaud J-P 2015 Turbulent fracture surfaces: a footprint of damage percolation? *Phys. Rev. Lett.* **114** 215501
- [361] Griffith A A 1921 The phenomena of rupture and flow in solids *Phil. Trans. R. Soc. A* **221** 163–98
- [362] Irwin G R 1957 Analysis of stresses and strains near the end of a crack traversing a plate *J. Appl. Mech.* **24** 361–4
- [363] Wiese K J, Bercy M, Melkonyan L and Bizebard T 2020 Universal force correlations in an RNA-DNA unzipping experiment *Phys. Rev. Res.* **2** 043385
- [364] Ponson L 2016 Statistical aspects in crack growth phenomena: how the fluctuations reveal the failure mechanisms *Int. J. Fract.* **201** 11–27
- [365] de Arcangelis L, Redner S and Herrmann H J 1985 A random fuse model for breaking processes *J. Physique Lett.* **46** 585–90
- [366] Batrouni G G and Hansen A 1998 Fracture in three-dimensional fuse networks *Phys. Rev. Lett.* **80** 325–8
- [367] Nukala P K V V, Imunovi S and Zapperi S 2004 Percolation and localization in the random fuse model *J. Stat. Mech.* **P08001**
- [368] Zapperi S, Nukala P K V V and Šimunović S 2005 Crack avalanches in the three-dimensional random fuse model *Physica A* **357** 129–33
- [369] Zapperi S and Nukala P K V V 2006 Fracture statistics in the three-dimensional random fuse model *Int. J. Fract.* **140** 99–111
- [370] Gjerden K S, Stormo A and Hansen A 2014 Local dynamics of a randomly pinned crack front: a numerical study *Front. Phys.* **2** 66
- [371] Stormo A, Lengliné O, Schmittbuhl J and Hansen A 2016 Soft-clamp fiber bundle model and interfacial crack propagation: comparison using a non-linear imposed displacement *Front. Phys.* **4** 18
- [372] Ioffe L B and Vinokur V M 1987 Dynamics of interfaces and dislocations in disordered media *J. Phys. C: Solid State Phys.* **20** 6149–58
- [373] Nattermann T 1990 Scaling approach to pinning: charge density waves and giant flux creep in superconductors *Phys. Rev. Lett.* **64** 2454–7
- [374] Chauve P, Giamarchi T and Le Doussal P 1998 Creep via dynamical functional renormalization group *Europhys. Lett.* **44** 110–5
- [375] Ferrero E E, Foini L, Giamarchi T, Kolton A B and Rosso A 2020 Creep motion of elastic interfaces driven in a disordered landscape *Annu. Rev. Condens. Matter Phys.* **12** 111–34
- [376] Kolton A B, Rosso A and Giamarchi T 2005 Creep motion of an elastic string in a random potential *Phys. Rev. Lett.* **94** 047002
- [377] Kolton A B, Rosso A, Giamarchi T and Krauth W 2006 Dynamics below the depinning threshold in disordered elastic systems *Phys. Rev. Lett.* **97** 057001
- [378] Kolton A B, Rosso A, Giamarchi T and Krauth W 2009 Creep dynamics of elastic manifolds via exact transition pathways *Phys. Rev. B* **79** 184207
- [379] Ferrero E E, Bustingorry S, Kolton A B and Rosso A 2013 Numerical approaches on driven elastic interfaces in random media *C. R. Phys.* **14** 641–50
- [380] Ferrero E E, Foini L, Giamarchi T, Kolton A B and Rosso A 2017 Spatiotemporal patterns in ultraslow domain wall creep dynamics *Phys. Rev. Lett.* **118** 147208
- [381] Metaxas P J, Jamet J P, Mougina A, Cormier M, Ferré J, Baltz V, Rodmacq B, Dieny B and Stamps R L 2007 Creep

- and flow regimes of magnetic domain-wall motion in ultrathin Pt/Co/Pt films with perpendicular anisotropy *Phys. Rev. Lett.* **99** 217208
- [382] Gorchon J, Bustingorry S, Ferré J, Jeudy V, Kolton A B and Giamarchi T 2014 Pinning-dependent field-driven domain wall dynamics and thermal scaling in an ultrathin Pt/Co/Pt magnetic film *Phys. Rev. Lett.* **113** 027205
- [383] Jeudy V, Mougou A, Bustingorry S, Savero Torres W, Gorchon J, Kolton A B, Lemaître A and Jamet J-P 2016 Universal pinning energy barrier for driven domain walls in thin ferromagnetic films *Phys. Rev. Lett.* **117** 057201
- [384] Diaz Pardo R, Savero Torres W, Kolton A B, Bustingorry S and Jeudy V 2017 Universal depinning transition of domain walls in ultrathin ferromagnets *Phys. Rev. B* **95** 184434
- [385] Troyanovski A M, Aarts J and Kes P H 1999 Collective and plastic vortex motion in superconductors at high flux densities *Nature* **399** 665–8
- [386] Tallakstad K T, Toussaint R, Santucci S, Schmittbuhl J and Måløy K J 2011 Local dynamics of a randomly pinned crack front during creep and forced propagation: an experimental study *Phys. Rev. E* **83** 046108
- [387] Vincent-Dospital T, Cochard A, Santucci S, Maloy K J and Toussaint R 2020 Thermally activated intermittent dynamics of creeping crack fronts along disordered interfaces (arXiv:2010.06865)
- [388] Nattermann T, Giamarchi T and Le Doussal P 2003 Variable-range hopping and quantum creep in one dimension *Phys. Rev. Lett.* **91** 056603
- [389] Andreanov A and Fedorenko A A 2014 Localization of spin waves in disordered quantum rotors *Phys. Rev. B* **90** 014205
- [390] Kolton A B and Jagla E A 2020 Thermally rounded depinning of an elastic interface on a washboard potential (arXiv:2008.00534)
- [391] Janssen H K, Schaub B and Schmittmann B 1989 New universal short-time scaling behaviour of critical relaxation processes *Z. Phys. B* **73** 539–49
- [392] Chen Y, Guo S H, Li Z B, Marculescu S and Schülke L 2000 The short-time critical behaviour of the Ginzburg–Landau model with long-range interaction *Eur. Phys. J. B* **18** 289–96
- [393] Schehr G and Le Doussal P 2005 Functional renormalization for pinned elastic systems away from their steady states *Europhys. Lett.* **71** 290–6
- [394] Kolton A B, Schehr G and Le Doussal P 2009 Universal non-stationary dynamics at the depinning transition *Phys. Rev. Lett.* **103** 160602
- [395] Dickman R, Alava M, Muñoz M A, Peltola J, Vespignani A and Zapperi S 2001 Critical behavior of a one-dimensional fixed-energy stochastic sandpile *Phys. Rev. E* **64** 056104
- [396] Kwon S and Kim J M 2016 Critical behavior for random initial conditions in the one-dimensional fixed-energy Manna sandpile model *Phys. Rev. E* **94** 012113
- [397] Tapader D, Pradhan P and Dhar D 2020 Density relaxation in conserved Manna sandpiles (arXiv:2011.01173)
- [398] Bertotti G and Mayergoyz I (ed) 2005 *The Science of Hysteresis* vol 1–3 (Amsterdam: Elsevier)
- [399] Grassi M P, Kolton A B, Jeudy V, Mougou A, Bustingorry S and Curiale J 2018 Intermittent collective dynamics of domain walls in the creep regime *Phys. Rev. B* **98** 224201
- [400] Albornoz L J, Ferrero E E, Kolton A B, Jeudy V, Bustingorry S and Curiale J 2021 Universal critical exponents of the magnetic domain wall depinning transition (arXiv:2101.06555)
- [401] Jeudy V, Díaz Pardo R, Savero Torres W, Bustingorry S and Kolton A B 2018 Pinning of domain walls in thin ferromagnetic films *Phys. Rev. B* **98** 054406
- [402] Shibauchi T, Krusin-Elbaum L, Vinokur V M, Argyle B, Weller D and Terris B D 2001 Deroughening of a 1D domain wall in an ultrathin magnetic film by a correlated defect *Phys. Rev. Lett.* **87** 267201
- [403] Bauer M, Mougou A, Jamet J P, Repain V, Ferré J, Stamps R L, Bernas H and Chappert C 2005 Deroughening of domain wall pairs by dipolar repulsion *Phys. Rev. Lett.* **94** 207211
- [404] Moon K-W, Kim D-H, Yoo S-C, Cho C-G, Hwang S, Kahng B, Min B-C, Shin K-H and Choe S-B 2013 Distinct universality classes of domain wall roughness in two-dimensional Pt/Co/Pt films *Phys. Rev. Lett.* **110** 107203
- [405] Domenichini P, Quinteros C P, Granada M, Collin S, George J-M, Curiale J, Bustingorry S, Capeluto M G and Pasquini G 2019 Transient magnetic-domain-wall ac dynamics by means of magneto-optical Kerr effect microscopy *Phys. Rev. B* **99** 214401
- [406] Ferré J, Metaxas P J, Mougou A, Jamet J-P, Gorchon J and Jeudy V 2013 Universal magnetic domain wall dynamics in the presence of weak disorder *C. R. Phys.* **14** 651–66
- [407] Albornoz L J 2021 Dynamics and morphology of driven domain walls in magnetic thin films from the standpoint of statistical physics *PhD Thesis* Université Paris-Saclay and Universidad Nacional de Cuyo
- [408] Lyuksyutov I F, Nattermann T and Pokrovsky V 1999 Theory of the hysteresis loop in ferromagnets *Phys. Rev. B* **59** 4260–72
- [409] Nattermann T, Pokrovsky V and Vinokur V M 2001 Hysteretic dynamics of domain walls at finite temperatures *Phys. Rev. Lett.* **87** 197005
- [410] Glatz A, Nattermann T and Pokrovsky V 2000 Domain wall depinning in random media by ac fields *Phys. Rev. Lett.* **90** 047201
- [411] Kleemann W, Rhensius J, Petravic O, Ferre J, Jamet J P and Bernas H 2007 Modes of periodic domain wall motion in ultrathin ferromagnetic layers *Phys. Rev. Lett.* **99** 097203
- [412] Dobrinevski A 2013 Field theory of disordered systems—avalanches of an elastic interface in a random medium *PhD Thesis* ENS Paris (arXiv:1312.7156)
- [413] Schwarz J M and Fisher D S 2001 Depinning with dynamic stress overshoots: mean field theory *Phys. Rev. Lett.* **87** 096107
- [414] Le Doussal P, Petković A and Wiese K J 2012 Distribution of velocities and acceleration for a particle in Brownian correlated disorder: inertial case *Phys. Rev. E* **85** 061116
- [415] Lebowitz J L and Spohn H 1999 A Gallavotti–Cohen-type symmetry in the large deviation functional for stochastic dynamics *J. Stat. Phys.* **95** 333–65
- [416] Majumdar S N and Schehr G 2014 Top eigenvalue of a random matrix: large deviations and third order phase transition *J. Stat. Mech.* P01012
- [417] Krapivsky P L, Mallick K and Sadhu T 2014 Large deviations in single-file diffusion *Phys. Rev. Lett.* **113** 078101
- [418] Sadhu T and Derrida B 2015 Large deviation function of a tracer position in single file diffusion *J. Stat. Mech.* P09008
- [419] Vinokur V M and Nattermann T 1997 Hysteretic depinning of anisotropic charge density waves *Phys. Rev. Lett.* **79** 3471–4
- [420] Marchetti M C, Middleton A A and Prellberg T 2000 Viscoelastic depinning of driven systems: mean-field plastic scallops *Phys. Rev. Lett.* **85** 1104–7
- [421] Marchetti M C and Saunders K 2002 Viscoelasticity from a microscopic model of dislocation dynamics *Phys. Rev. B* **66** 224113
- [422] Marchetti M C and Dahmen K A 2002 Hysteresis in driven disordered systems: from plastic depinning to magnets *Phys. Rev. B* **66** 214201
- [423] Saunders K, Schwarz J M, Marchetti M C and Middleton A A 2004 Mean-field theory of collective transport with phase slips *Phys. Rev. B* **70** 024205

- [424] Marchetti M C 2005 Models of plastic depinning of driven disordered systems *Pramana* **64** 1097–107
- [425] Marchetti M C 2006 Depinning and plasticity of driven disordered lattices *Jamming, Yielding, and Irreversible Deformations in Condensed Matter* (Berlin: Springer)
- [426] Le Doussal P, Marchetti M C and Wiese K J 2008 Depinning in a two-layer model of plastic flow *Phys. Rev. B* **78** 224201
- [427] Ferrero E E and Jagla E A 2019 Elastic interfaces on disordered substrates: from mean-field depinning to yielding *Phys. Rev. Lett.* **123** 218002
- [428] Nicolas A, Martens K, Bocquet L and Barrat J-L 2014 Universal and non-universal features in coarse-grained models of flow in disordered solids *Soft Matter* **10** 4648–61
- [429] Agoritsas E, Bertin E, Martens K and Barrat J-L 2015 On the relevance of disorder in athermal amorphous materials under shear *Eur. Phys. J. E* **38** 71
- [430] Vasisht V V, Le Goff M, Martens K and Barrat J-L 2018 Permanent shear localization in dense disordered materials due to microscopic inertia (arXiv:1812.03948)
- [431] Tyukodi B, Patinet S, Roux S and Vandembroucq D 2016 From depinning transition to plastic yielding of amorphous media: a soft-modes perspective *Phys. Rev. E* **93** 063005
- [432] Nicolas A, Ferrero E E, Martens K and Barrat J-L 2018 Deformation and flow of amorphous solids: insights from elastoplastic models *Rev. Mod. Phys.* **90** 045006
- [433] Balents L and Kardar M 1993 Delocalization of flux lines from extended defects by bulk randomness *Europhys. Lett.* **23** 503–9
- [434] Chauve P, Le Doussal P and Giamarchi T 2000 Dynamical transverse Meissner effect and transition in moving Bose glass *Phys. Rev. B* **61** 11906–9
- [435] Olive E, Soret J C, Doussal P L and Giamarchi T 2003 Numerical simulation evidence of dynamical transverse Meissner effect and moving Bose glass phase *Phys. Rev. Lett.* **91** 037005
- [436] Chen L-W, Balents L, Fisher M P A and Marchetti M C 1996 Dynamical transition in sliding charge-density waves with quenched disorder *Phys. Rev. B* **54** 12798–806
- [437] Le Doussal P, Cugliandolo L F and Peliti L 1997 Dynamics of particles and manifolds in random force fields *Europhys. Lett.* **39** 111
- [438] Le Doussal P and Wiese K J 1998 Glassy trapping of elastic manifolds in nonpotential static random flows *Phys. Rev. Lett.* **80** 2362
- [439] Wiese K J and Le Doussal P 1999 Polymers and manifolds in static random flows: a RG study *Nucl. Phys. B* **552** 529–98
- [440] Giamarchi T and Le Doussal P 1996 Moving glass phases of driven lattices *Phys. Rev. Lett.* **76** 3408
- [441] Le Doussal P and Giamarchi T 1998 Moving glass theory of driven lattices with disorder *Phys. Rev. B* **57** 11356–403
- [442] Balents L and Fisher M P A 1995 Temporal order in dirty driven periodic media *Phys. Rev. Lett.* **75** 4270
- [443] Balents L, Marchetti M C and Radzihovsky L 1997 Comment on ‘Moving glass phase of driven lattices’ *Phys. Rev. Lett.* **78** 751
- [444] Rosso A, Krauth W, Le Doussal P, Vannimenus J and Wiese K J 2003 Universal interface width distributions at the depinning threshold *Phys. Rev. E* **68** 036128
- [445] Moulinet S, Rosso A, Krauth W and Rolley E 2004 Width distribution of contact lines on a disordered substrate *Phys. Rev. E* **69** 035103
- [446] Fedorenko A and Stepanow S 2003 Universal energy distribution for interfaces in a random-field environment *Phys. Rev. E* **68** 056115
- [447] Kadanoff L P, Nagel S R, Wu L and Zhou S-m 1989 Scaling and universality in avalanches *Phys. Rev. A* **39** 6524–37
- [448] Aragón L E, Kolton A B, Le Doussal P, Wiese K J and Jagla E A 2016 Avalanches in tip-driven interfaces in random media *Europhys. Lett.* **113** 10002
- [449] Paczuski M and Boettcher S 1996 Universality in sandpiles, interface depinning, and earthquake models *Phys. Rev. Lett.* **77** 111
- [450] Nakanishi H and Sneppen K 1997 Universal versus drive-dependent exponents for sandpile models *Phys. Rev. E* **55** 4012–6
- [451] Delorme M, Le Doussal P and Wiese K J 2016 Distribution of joint local and total size and of extension for avalanches in the Brownian force model *Phys. Rev. E* **93** 052142
- [452] Colaioni F 2008 Exactly solvable model of avalanches dynamics for Barkhausen crackling noise *Adv. Phys.* **57** 287
- [453] Dobrinevski A, Le Doussal P and Wiese K J 2012 Non-stationary dynamics of the Alessandro–Beatrice–Bertotti–Montorsi model *Phys. Rev. E* **85** 031105
- [454] Muñoz M A 2004 Multiplicative noise in non-equilibrium phase transitions: a tutorial *Advances in Condensed Matter and Statistical Physics* ed E Korutcheva and R Cuerno (New York: Nova Science Publishers) pp 37–68
- [455] Dornic I, Chaté H and Muñoz M A 2005 Integration of Langevin equations with multiplicative noise and the viability of field theories for absorbing phase transitions *Phys. Rev. Lett.* **94** 100601
- [456] Watson H W and Galton F 1875 On the probability of the extinction of families *J. Anthropol. Inst. G. B. Ireland* **4** 138–44
- [457] Dobrinevski A, Le Doussal P and Wiese K J 2014 Avalanche shape and exponents beyond mean-field theory *Europhys. Lett.* **108** 66002
- [458] Thiery T, Le Doussal P and Wiese K J 2015 Spatial shape of avalanches in the Brownian force model *J. Stat. Mech.* **P08019**
- [459] Le Doussal P and Wiese K J 2009 Size distributions of shocks and static avalanches from the functional renormalization group *Phys. Rev. E* **79** 051106
- [460] Le Doussal P and Wiese K J 2011 First-principle derivation of static avalanche-size distribution *Phys. Rev. E* **85** 061102
- [461] Rosso A, Le Doussal P and Wiese K J 2009 Avalanche-size distribution at the depinning transition: a numerical test of the theory *Phys. Rev. B* **80** 144204
- [462] Laurson L private communication
- [463] Laurson L, Illa X, Santucci S, Tallakstad K T, Måløy K J and Alava M J 2013 Evolution of the average avalanche shape with the universality class *Nat. Commun.* **4** 2927
- [464] Dobrinevski A, Le Doussal P and Wiese K J 2013 Statistics of avalanches with relaxation and Barkhausen noise: a solvable model *Phys. Rev. E* **88** 032106
- [465] Thiery T and Le Doussal P 2016 Universality in the mean spatial shape of avalanches *Europhys. Lett.* **114** 36003
- [466] Kolton A B, Le Doussal P and Wiese K J 2019 Distribution of velocities in an avalanche, and related quantities: theory and numerical verification *Europhys. Lett.* **127** 46001
- [467] Le Doussal P and Wiese K J 2012 Distribution of velocities in an avalanche *Europhys. Lett.* **97** 46004
- [468] Thiery T, Le Doussal P and Wiese K J 2016 Universal correlations between shocks in the ground state of elastic interfaces in disordered media *Phys. Rev. E* **94** 012110
- [469] Le Doussal P and Thiery T 2020 Correlations between avalanches in the depinning dynamics of elastic interfaces *Phys. Rev. E* **101** 032108
- [470] Zapperi S, Castellano C, Colaioni F and Durin G 2005 Signature of effective mass in crackling-noise asymmetry *Nat. Phys.* **1** 46–9
- [471] Piterbarg V I 1995 *Asymptotic Methods in the Theory of Gaussian Processes and Fields (Translations of Mathematical Monographs vol 148)* (Providence, RI: American Mathematical Society)
- [472] Piterbarg V I 2015 *Twenty Lectures About Gaussian Processes* (London: Atlantic Financial Press)

- [473] Michna Z 2017 Remarks on Pickands' theorem *Probab. Math. Stat.* **37** 373–93
- [474] Delorme M and Wiese K J 2015 Maximum of a fractional Brownian motion: analytic results from perturbation theory *Phys. Rev. Lett.* **115** 210601
- [475] Wiese K J, Majumdar S N and Rosso A 2011 Perturbation theory for fractional Brownian motion in presence of absorbing boundaries *Phys. Rev. E* **83** 061141
- [476] Delorme M and Wiese K J 2016 Extreme-value statistics of fractional Brownian motion bridges *Phys. Rev. E* **94** 052105
- [477] Delorme M and Wiese K J 2016 Perturbative expansion for the maximum of fractional Brownian motion *Phys. Rev. E* **94** 012134
- [478] Delorme M, Rosso A and Wiese K J 2017 Pickands' constant at first order in an expansion around Brownian motion *J. Phys. A: Math. Theor.* **50** 16LT04
- [479] Wiese K J 2018 First passage in an interval for fractional Brownian motion *Phys. Rev. E* **99** 032106
- [480] Sadhu T, Delorme M and Wiese K J 2018 Generalized arcsine laws for fractional Brownian motion *Phys. Rev. Lett.* **120** 040603
- [481] Benigni L, Cosco C, Shapira A and Wiese K J 2018 Hausdorff dimension of the record set of a fractional Brownian motion *Electron. Commun. Probab.* **23** 1–8
- [482] Walter B and Wiese K J 2019 Monte Carlo sampler of first passage times for fractional Brownian motion using adaptive bisections Source code: <https://hal.archives-ouvertes.fr/hal-02270046>
- [483] Walter B and Wiese K J 2020 Sampling first-passage times of fractional Brownian motion using adaptive bisections *Phys. Rev. E* **101** 043312
- [484] Arutkin M, Walter B and Wiese K J 2020 Extreme events for fractional Brownian motion with drift: theory and numerical validation *Phys. Rev. E* **102** 022102
- [485] Rambeau J, Bustingorry S, Kolton A B and Schehr G 2011 Maximum relative height of elastic interfaces in random media *Phys. Rev. E* **84** 041131
- [486] Le Doussal P and Wiese K J unpublished.
- [487] Le Doussal P, Rosso A and Wiese K J 2011 Shock statistics in higher-dimensional Burgers turbulence *Europhys. Lett.* **96** 14005
- [488] Måløy K J, Santucci S, Schmittbuhl J and Toussaint R 2006 Local waiting time fluctuations along a randomly pinned crack front *Phys. Rev. Lett.* **96** 045501
- [489] Laurson L, Santucci S and Zapperi S 2010 Avalanches and clusters in planar crack front propagation *Phys. Rev. E* **81** 046116
- [490] Budrikis Z and Zapperi S 2013 Avalanche localization and crossover scaling in amorphous plasticity *Phys. Rev. E* **88** 062403
- [491] Le Priol C, Chopin J, Le Doussal P, Ponsou L and Rosso A 2020 Universal scaling of the velocity field in crack front propagation *Phys. Rev. Lett.* **124** 065501
- [492] Le Priol C, Le Doussal P and Rosso A 2021 Spatial clustering of depinning avalanches in presence of long-range interactions *Phys. Rev. Lett.* **126** 025702
- [493] Le Priol C Long-range interactions in the avalanches of elastic interfaces *PhD Thesis* PSL Research University (arXiv:2103.07701)
- [494] Terrot W 2021 Avalanches en présence d'interactions à longue portée *Internship Report* Université Paris-Saclay
- [495] Gutenberg B and Richter C F 1945 Frequency of earthquakes in California *Nature* **156** 371
- [496] Dieterich J H 1992 Earthquake nucleation on faults with rate- and state-dependent strength *Tectonophysics* **211** 115–34
- [497] Omori F 1894 On the aftershocks of earthquakes *J. Coll. Sci., Imp. Univ. Tokyo* **7** 111–200
- [498] Burridge R and Knopoff L 1967 Model and theoretical seismicity *Bull. Seismol. Soc. Am.* **57** 341–71
- [499] Ben-Zion Y and Rice J R 1993 Earthquake failure sequences along a cellular fault zone in a three-dimensional elastic solid containing asperity and nonasperity regions *J. Geophys. Res.: Solid Earth* **98** 14109–31
- [500] Ruina A 1983 Slip instability and state variable friction laws *J. Geophys. Res.: Solid Earth* **88** 10359–70
- [501] Carlson J M, Langer J S and Shaw B E 1994 Dynamics of earthquake faults *Rev. Mod. Phys.* **66** 657–70
- [502] Ben-Zion Y and Rice J R 1997 Dynamic simulations of slip on a smooth fault in an elastic solid *J. Geophys. Res.: Solid Earth* **102** 17771–84
- [503] Fisher D S, Dahmen K, Ramanathan S and Ben-Zion Y 1997 Statistics of earthquakes in simple models of heterogeneous faults *Phys. Rev. Lett.* **78** 4885–8
- [504] Scholz C H 1998 Earthquakes and friction laws *Nature* **391** 37–42
- [505] Shome N, Cornell C A, Bazzurro P and Carballo J E 1998 Earthquakes, records, and nonlinear responses *Earthq. Spectra* **14** 469–500
- [506] Monte-Moreno E and Hernández-Pajares M 2014 Occurrence of solar flares viewed with GPS: statistics and fractal nature *J. Geophys. Res.: Space Phys.* **119** 9216–27
- [507] Kagan Y Y 2002 Seismic moment distribution revisited: I. Statistical results *Geophys. J. Int.* **148** 520–41
- [508] Schwarz J M and Fisher D S 2003 Depinning with dynamic stress overshoots: a hybrid of critical and pseudohysteretic behavior *Phys. Rev. E* **67** 021603
- [509] Jagla E A and Kolton A B 2009 The mechanisms of spatial and temporal earthquake clustering *J. Geophys. Res.* **115** B05312
- [510] Le Doussal P, Müller M and Wiese K J 2010 Avalanches in mean-field models and the Barkhausen noise in spin-glasses *Europhys. Lett.* **91** 57004
- [511] Le Doussal P, Müller M and Wiese K J 2012 Equilibrium avalanches in spin glasses *Phys. Rev. B* **85** 214402
- [512] Pázmándi F, Záránd G and Zimányi G T 1999 Self-organized criticality in the hysteresis of the Sherrington–Kirkpatrick model *Phys. Rev. Lett.* **83** 1034–7
- [513] Bak P, Tang C and Wiesenfeld K 1987 Self-organized criticality—an explanation of  $1/f$  noise *Phys. Rev. Lett.* **59** 381–4
- [514] Majumdar S N and Dhar D 1992 Equivalence between the Abelian sandpile model and the  $q \rightarrow 0$  limit of the Potts-model *Physica A* **185** 129–45
- [515] Dhar D 1999 Studying self-organized criticality with exactly solved models (arXiv:cond-mat/9909009)
- [516] Dhar D 1999 The Abelian sandpile and related models *Physica A* **263** 4
- [517] Dhar D 2006 Theoretical studies of self-organized criticality *Physica A* **369** 29–70
- [518] Bonachela J A, Alava M and Muñoz M A 2009 Cusps in systems with (many) absorbing states *Phys. Rev. E* **79** 050106(R)
- [519] Bonachela J A 2008 Universality in self-organized criticality *PhD Thesis* University of Granada, Spain
- [520] Bonachela J A, Chaté H, Dornic I and Muñoz M A 2007 Absorbing states and elastic interfaces in random media: two equivalent descriptions of self-organized criticality *Phys. Rev. Lett.* **98** 155702
- [521] Uritsky V M, Paczuski M, Davila J M and Jones S I 2007 Coexistence of self-organized criticality and intermittent turbulence in the solar corona *Phys. Rev. Lett.* **99** 025001
- [522] Jeng M 2005 Conformal field theory correlations in the Abelian sandpile model *Phys. Rev. E* **71** 016140
- [523] Stapleton M and Christensen K 2005 Mean-field theory and sandpile models (arXiv:cond-mat/0510626)
- [524] Dhar D 2004 Steady state and relaxation spectrum of the Oslo rice-pile model *Physica A* **340** 535–43

- [525] Alava M 2003 *Self-organized Criticality as a Phase Transition* (New York: Nova Science Publishers) pp 69–102 arXiv:cond-mat/0307688
- [526] Alava M 2002 Scaling in self-organized criticality from interface depinning? *J. Phys.: Condens. Matter.* **14** 2353
- [527] Bassler K E, Paczuski M and Altshuler E 2001 Simple model for plastic dynamics of a disordered flux-line lattice *Phys. Rev. B* **64** 224517
- [528] Dickman R, Muñoz M A, Vespignani A and Zapperi S 2000 Paths to self-organized criticality *Braz. J. Phys.* **30** 27–41
- [529] Dickman R, Vespignani A and Zapperi S 1998 Self-organized criticality as an absorbing-state phase transition *Phys. Rev. E* **57** 5095–105
- [530] Bassler K E and Paczuski M 1998 Simple model of superconducting vortex avalanches *Phys. Rev. Lett.* **81** 3761–4
- [531] Jensen H J 1998 *Self-Organized Criticality* (Cambridge: Cambridge University Press)
- [532] Tanguy A, Gounelle M and Roux S 1998 From individual to collective pinning: effect of long-range elastic interactions *Phys. Rev. E* **58** 1577–90
- [533] Christensen K, Corral Á, Frette V, Feder J and Jøssang T 1996 Tracer dispersion in a self-organized critical system *Phys. Rev. Lett.* **77** 107–10
- [534] Frette V, Christensen K, Malthé-Sørensen A, Feder J, Jøssang T and Meakin P 1996 Avalanche dynamics in a pile of rice *Nature* **379** 49–52
- [535] Urbach J S, Madison R C and Markert J T 1995 Interface depinning, self-organized criticality, and the Barkhausen effect *Phys. Rev. Lett.* **75** 276–9
- [536] Sneppen K 1992 Self-organized pinning and interface growth in a random medium *Phys. Rev. Lett.* **69** 3539–42
- [537] Manna S S 1991 Two-state model of self-organized criticality *J. Phys. A: Math. Gen.* **24** L363–9
- [538] Dhar D and Majumdar S N 1990 Abelian sandpile model on the Bethe lattice *J. Phys. A: Math. Gen.* **23** 4333–50
- [539] Dhar D and Ramaswamy R 1989 Exactly solved model of self-organized critical phenomena *Phys. Rev. Lett.* **63** 1659–62
- [540] Tang C and Bak P 1988 Mean field theory of self-organized critical phenomena *J. Stat. Phys.* **51** 797–802
- [541] Frette V 1993 Sandpile models with dynamically varying critical slopes *Phys. Rev. Lett.* **70** 2762–5
- [542] Huynh H N, Pruessner G and Chew L Y 2011 The Abelian Manna model on various lattices in one and two dimensions *J. Stat. Mech.* P09024
- [543] Hinrichsen H 2000 Non-equilibrium critical phenomena and phase transitions into absorbing states *Adv. Phys.* **49** 815–958
- [544] Henkel M, Hinrichsen H and Lübeck S 2008 *Non-Equilibrium Phase Transitions* (Berlin: Springer)
- [545] Wei Q-H, Bechinger C and Leiderer P 2000 Single-file diffusion of colloids in one-dimensional channels *Science* **287** 625–7
- [546] Krapivsky P L, Mallick K and Sadhu T 2015 Dynamical properties of single-file diffusion *J. Stat. Mech.* P09007
- [547] Krapivsky P L, Mallick K and Sadhu T 2015 Tagged particle in single-file diffusion *J. Stat. Phys.* **160** 885–925
- [548] Shapira A and Wiese K J unpublished.
- [549] Basu M, Basu U, Bondyopadhyay S, Mohanty P and Hinrichsen H 2012 Fixed-energy sandpiles belong generically to directed percolation *Phys. Rev. Lett.* **109** 015702
- [550] Hexner D and Levine D 2015 Hyperuniformity of critical absorbing states *Phys. Rev. Lett.* **114** 110602
- [551] Lee S B 2014 Universality class of the conserved Manna model in one dimension *Phys. Rev. E* **89** 060101
- [552] Dickman R and da Cunha S D 2015 Particle-density fluctuations and universality in the conserved stochastic sandpile *Phys. Rev. E* **92** 020104
- [553] Garcia-Millan R, Pruessner G, Pickering L and Christensen K 2018 Correlations and hyperuniformity in the avalanche size of the Oslo model *Europhys. Lett.* **122** 50003
- [554] Berthier L, Chaudhuri P, Coulais C, Dauchot O and Sollich P 2011 Suppressed compressibility at large scale in jammed packings of size-disperse spheres *Phys. Rev. Lett.* **106** 120601
- [555] Tang L-H and Leschhorn H 1992 Pinning by directed percolation *Phys. Rev. A* **45** R8309–12
- [556] Buldyrev S V, Barabási A-L, Caserta F, Havlin S, Stanley H E and Vicsek T 1992 Anomalous interface roughening in porous media: experiment and model *Phys. Rev. A* **45** R8313–6
- [557] Glotzer S C, Gyure M F, Sciortino F, Coniglio A and Stanley H E 1994 Pinning in phase-separating systems *Phys. Rev. E* **49** 247–58
- [558] Barabási A-L, Grinstein G and Muñoz M A 1996 Directed surfaces in disordered media *Phys. Rev. Lett.* **76** 1481–4
- [559] Ertas D and Kardar M 1994 Critical dynamics of contact line depinning *Phys. Rev. Lett.* **49** R2532
- [560] Kardar M, Parisi G and Zhang Y-C 1986 Dynamic scaling of growing interfaces *Phys. Rev. Lett.* **56** 889–92
- [561] Lee C and Kim J M 2005 Depinning transition of the quenched Kardar–Parisi–Zhang equation *J. Korean Phys. Soc.* **47** 13–7
- [562] Tang L-H, Kardar M and Dhar D 1995 Driven depinning in anisotropic media *Phys. Rev. Lett.* **74** 920–3
- [563] Araújo N, Grassberger P, Kahng B, Schrenk K J and Ziff R M 2014 Recent advances and open challenges in percolation *Eur. Phys. J. Spec. Top.* **223** 2307–21
- [564] Dhar D 2017 Directed percolation and directed animals (arXiv:1703.07541)
- [565] Janssen H K 1981 On the nonequilibrium phase transition in reaction–diffusion systems with an absorbing stationary state *Z. Phys. B* **42** 151–4
- [566] Bronzan J B and Dash J W 1974 Higher order  $\epsilon$ -terms in the renormalization group approach to Reggeon field theory *Phys. Lett. B* **51** 496–8
- [567] Cardy J L and Sugar R L 1980 Directed percolation and Reggeon field theory *J. Phys. A: Math. Gen.* **13** L423
- [568] Janssen H-K and Täuber U C 2005 The field theory approach to percolation processes *Ann. Phys., NY* **315** 147–92
- [569] Abarbanel H D I, Bronzan J D, Sugar R L and White A R 1975 Reggeon field theory: formulation and use *Phys. Rep.* **21** 119–82
- [570] Adzhemyan L T, Hnatič M, Kompaniets M V, Lučivjanský T and Mižišin L 2019 Renormalization group Approach of directed percolation: three-loop approximation *11th Chaotic Modeling and Simulation International Conference* ed C H Skiadas and I Lubashevsky (Cham: Springer) pp 195–204
- [571] Havlin S, Amaral L A N, Buldyrev S V, Harrington S T and Stanley H E 1995 Dynamics of surface roughening with quenched disorder *Phys. Rev. Lett.* **74** 4205–8
- [572] Le Doussal P and Wiese K J 2003 Functional renormalization group for anisotropic depinning and relation to branching processes *Phys. Rev. E* **67** 016121
- [573] Atis S, Dubey A K, Salin D, Talon L, Le Doussal P and Wiese K J 2015 Experimental evidence for three universality classes for reaction fronts in disordered flows *Phys. Rev. Lett.* **114** 234502
- [574] Grassberger P 1982 On phase-transitions in Schlögl’s second model *Z. Phys. B* **47** 365
- [575] Jensen I 1993 Critical behavior of the pair contact process *Phys. Rev. Lett.* **70** 1465–8
- [576] Muñoz M A, Grinstein G, Dickman R and Livi R 1996 Critical behavior of systems with many absorbing states *Phys. Rev. Lett.* **76** 451–4

- [577] Muñoz M A, Grinstein G, Dickman R and Livi R 1997 Infinite numbers of absorbing states: critical behavior *Physica D* **103** 485–90
- [578] Muñoz M A, Grinstein G and Dickman R 1998 Phase structure of systems with infinite numbers of absorbing states *J. Stat. Phys.* **91** 541–69
- [579] Muñoz M A 1998 Nature of different types of absorbing states *Phys. Rev. E* **57** 1377–83
- [580] Vespignani A, Dickman R, Muñoz M A and Zapperi S 1998 Driving, conservation, and absorbing states in sandpiles *Phys. Rev. Lett.* **81** 5676–9
- [581] Vespignani A, Dickman R, Muñoz M A and Zapperi S 2000 Absorbing-state phase transitions in fixed-energy sandpiles *Phys. Rev. E* **62** 4564–82
- [582] Alava M and Muñoz M A 2002 Interface depinning versus absorbing-state phase transitions *Phys. Rev. E* **65** 026145
- [583] Jeong H, Kahng B and Kim D 1996 Anisotropic surface growth model in disordered media *Phys. Rev. Lett.* **77** 5094–7
- [584] Jeong H, Kahng B and Kim D 1999 Facet formation in the negative quenched Kardar–Parisi–Zhang equation *Phys. Rev. E* **59** 1570–3
- [585] Takeuchi K A, Kuroda M, Chaté H and Sano M 2007 Directed percolation criticality in turbulent liquid crystals *Phys. Rev. Lett.* **99** 234503
- [586] Takeuchi K A, Kuroda F, Chaté H and Sano M 2009 Experimental realization of directed percolation criticality in turbulent liquid crystals *Phys. Rev. E* **80** 051116
- [587] Wiese K J 2016 Coherent-state path integral versus coarse-grained effective stochastic equation of motion: from reaction diffusion to stochastic sandpiles *Phys. Rev. E* **93** 042117
- [588] Doi M 1976 Second quantization representation for classical many-particle system *J. Phys. A: Math. Gen.* **9** 1465–77
- [589] Doi M 1976 Stochastic theory of diffusion-controlled reaction *J. Phys. A: Math. Gen.* **9** 1479
- [590] Peliti L 1985 Path integral approach to birth–death processes on a lattice *J. Physique* **46** 1469–83
- [591] Cardy J 2006 Reaction–diffusion processes Lectures held at Warwick University unpublished
- [592] Andreev A, Biroli G, Bouchaud J P and Lefèvre A 2006 Field theories and exact stochastic equations for interacting particle systems *Phys. Rev. E* **74** 030101
- [593] Gredat D, Dornic I and Luck J M 2011 On an imaginary exponential functional of Brownian motion *J. Phys. A: Math. Theor.* **44** 175003
- [594] Täuber U C 2014 *Critical Dynamics: A Field Theory Approach to Equilibrium and Non-equilibrium Scaling Behavior* (Cambridge: Cambridge University Press)
- [595] Deloubrière O, Frachebourg L, Hilhorst H J and Kitahara K 2002 Imaginary noise and parity conservation in the reaction  $A + A \rightleftharpoons 0$  *Physica A* **308** 135–47
- [596] Gardiner C W, McNeil K J, Walls D F and Matheson I S 1976 Correlations in stochastic theories of chemical reactions *J. Stat. Phys.* **14** 307–31
- [597] Williams R M and Tuckey P A 1992 Regge calculus: a brief review and bibliography *Class. Quantum Grav.* **9** 1409–22
- [598] Rasetti M and Regge T 1975 Vortices in He II, current algebras and quantum knots *Physica A* **80** 217–33
- [599] Pastor-Satorras R and Vespignani A 2000 Field theory of absorbing phase transitions with a nondiffusive conserved field *Phys. Rev. E* **62** R5875–8
- [600] Bonachela J A and Muñoz M A 2008 Confirming and extending the hypothesis of universality in sandpiles *Phys. Rev. E* **78** 041102
- [601] Le Doussal P and Wiese K J 2014 An exact mapping of the stochastic field theory for Manna sandpiles to interfaces in random media *Phys. Rev. Lett.* **114** 110601
- [602] Janssen H-K and Stenull O 2016 Directed percolation with a conserved field and the depinning transition *Phys. Rev. E* **042138**
- [603] Uhlenbeck G E and Ornstein L S 1930 On the theory of the Brownian motion *Phys. Rev.* **36** 823–41
- [604] Krug J 1997 Origins of scale invariance in growth processes *Adv. Phys.* **46** 139–282
- [605] Halpin-Healy T and Takeuchi K A 2015 A KPZ cocktail—shaken, not stirred: toasting 30 years of kinetically roughened surfaces *J. Stat. Phys.* **160** 794–814
- [606] Takeuchi K A and Sano M 2012 Evidence for geometry-dependent universal fluctuations of the Kardar–Parisi–Zhang interfaces in liquid-crystal turbulence *J. Stat. Phys.* **147** 853–90
- [607] Burgers J M 1974 *The Non-linear Diffusion Equation* (Dordrecht: Reidel)
- [608] Gurbatov S N, Saichev A I and Shandarin S F 1989 The large-scale structure of the universe in the frame of the model equation of non-linear diffusion *Mon. Not. R. Astron. Soc.* **236** 385–402
- [609] Bertschinger E 1998 Simulations of structure formation in the universe *Annu. Rev. Astron. Astrophys.* **36** 599–654
- [610] Bernardreau F, Colombi S, Gaztañaga E and Scoccimarro R 2002 Large-scale structure of the universe and cosmological perturbation theory *Phys. Rep.* **367** 1–248
- [611] Hopf E 1950 The partial differential equation  $u_t + uu_x = \mu x x$  *Commun. Pure Appl. Math.* **3** 201–30
- [612] Cole J D 1951 On a quasi-linear parabolic equation occurring in aerodynamics *Quart. Appl. Math.* **9** 225–36
- [613] Feynman R P 1948 Space-time approach to non-relativistic quantum mechanics *Rev. Mod. Phys.* **20** 367–87
- [614] Kac M 1949 On distributions of certain Wiener functionals *Trans. Am. Math. Soc.* **65** 1–13
- [615] Brunet É and Derrida B 2000 Probability distribution of the free energy of a directed polymer in a random medium *Phys. Rev. E* **61** 6789–801
- [616] Forster D, Nelson D R and Stephen M J 1977 Large-distance and long-time properties of a randomly stirred fluid *Phys. Rev. A* **16** 732–49
- [617] Medina E, Hwa T, Kardar M and Zhang Y-C 1989 Burgers equation with correlated noise: renormalization-group analysis and applications to directed polymers and interface growth *Phys. Rev. A* **39** 3053
- [618] Meakin P, Ramanlal P, Sander L M and Ball R C 1986 Ballistic deposition on surfaces *Phys. Rev. A* **34** 5091–103
- [619] Krug J 1987 Scaling relation for a growing interface *Phys. Rev. A* **36** 5465–6
- [620] Frey E and Täuber U C 1994 Two-loop renormalization group analysis of the Burgers–Kardar–Parisi–Zhang equation *Phys. Rev. E* **50** 1024–45
- [621] Frey E and Täuber U C 1995 Reply to Comment on ‘Two-loop renormalization group analysis of the Burgers–Kardar–Parisi–Zhang equation’ *Phys. Rev. E* **51** 6319–22
- [622] Sun T and Plischke M 1994 Field-theory renormalization approach to the Kardar–Parisi–Zhang equation *Phys. Rev. E* **49** 5046–57
- [623] Sun T 1995 Comment on ‘Two-loop renormalization group analysis of the Burgers–Kardar–Parisi–Zhang equation’ *Phys. Rev. E* **51** 6316–8
- [624] Teodorovich E V 1996 Anomalous dimensions in the Burgers–Kardar–Parisi–Zhang equation *J. Exp. Theor. Phys.* **82** 268–77
- [625] Wiese K J 1997 Critical discussion of the two-loop calculations for the Kardar–Parisi–Zhang equation *Phys. Rev. E* **56** 5013–7
- [626] Lässig M 1995 On the renormalization of the Kardar–Parisi–Zhang equation *Nucl. Phys. B* **448** 559–74

- [627] Wiese K J 1998 On the perturbation expansion of the KPZ-equation *J. Stat. Phys.* **93** 143–54
- [628] David F, Duplantier B and Guitter E 1993 Renormalization theory for interacting crumpled manifolds *Nucl. Phys. B* **394** 555–664
- [629] David F, Duplantier B and Guitter E 1997 Renormalization theory for the self-avoiding polymerized membranes (arXiv:cond-mat/9702136)
- [630] Bundschuh R and Lässig M 1996 Directed polymers in high dimensions *Phys. Rev. E* **54** 304–20
- [631] Frey E, Täuber U C and Janssen H K 1999 Scaling regimes and critical dimensions in the Kardar–Parisi–Zhang problem *Europhys. Lett.* **47** 14–20
- [632] Kardar M 1987 Domain walls subject to quenched impurities (invited) *J. Appl. Phys.* **61** 3601–4
- [633] Nattermann T 1987 Interface roughening in systems with quenched random impurities *Europhys. Lett.* **4** 1241–6
- [634] Janssen H K, Täuber U C and Frey E 1999 Exact results for the Kardar–Parisi–Zhang equation with spatially correlated noise *Eur. Phys. J. B* **9** 491–511
- [635] Täuber U C and Frey E 2002 Universality classes in the anisotropic Kardar–Parisi–Zhang model *Europhys. Lett.* **59** 655–61
- [636] Lässig M and Kinzelbach H 1997 Upper critical dimension of the Kardar–Parisi–Zhang equation *Phys. Rev. Lett.* **78** 903–6
- [637] Fogedby H C 2005 Localized growth modes, dynamic textures, and upper critical dimension for the Kardar–Parisi–Zhang equation in the weak-noise limit *Phys. Rev. Lett.* **94** 195702
- [638] Newman T J and Kallabis H 1996 Strong coupling probe for the Kardar–Parisi–Zhang equation *J. Physique I* **6** 373–83
- [639] Bhattacharjee J K 1998 Upper critical dimension of the Kardar–Parisi–Zhang equation *J. Phys. A: Math. Gen.* **31** L93–6
- [640] Colaioni F and Moore M A 2001 Upper critical dimension, dynamic exponent, and scaling functions in the mode-coupling theory for the Kardar–Parisi–Zhang equation *Phys. Rev. Lett.* **86** 3946–9
- [641] Canet L and Moore M A 2007 Universality classes of the Kardar–Parisi–Zhang equation *Phys. Rev. Lett.* **98** 200602
- [642] Katzav E and Schwartz M 2002 Existence of the upper critical dimension of the Kardar–Parisi–Zhang equation *Physica A* **309** 69–78
- [643] Marinari E, Pagnani A and Parisi G 2000 Critical exponents of the KPZ equation via multi-surface coding numerical simulations *J. Phys. A: Math. Gen.* **33** 8181–92
- [644] Marinari E, Pagnani A, Parisi G and Racz Z 2002 Width distributions and the upper critical dimension of Kardar–Parisi–Zhang interfaces *Phys. Rev. E* **65** 026136
- [645] Alves S G, Oliveira T J and Ferreira S C 2014 Universality of fluctuations in the Kardar–Parisi–Zhang class in high dimensions and its upper critical dimension *Phys. Rev. E* **90** 020103
- [646] Gomes W P, Penna A L A and Oliveira F A 2019 From cellular automata to growth dynamics: the Kardar–Parisi–Zhang universality class *Phys. Rev. E* **100** 020101
- [647] Ala-Nissila T 1998 Comment on ‘Upper critical dimension of the Kardar–Parisi–Zhang equation’ *Phys. Rev. Lett.* **80** 887
- [648] Ala-Nissila T 1998 Comment on ‘Upper critical dimension of the Kardar–parisi–Zhang equation’ *Phys. Rev. Lett.* **80** 5459 (erratum)
- [649] Schwartz M and Perlsman E 2012 Upper critical dimension of the Kardar–Parisi–Zhang equation *Phys. Rev. E* **85** 050103
- [650] Tu Y 1994 Absence of finite upper critical dimension in the spherical Kardar–Parisi–Zhang model *Phys. Rev. Lett.* **73** 3109–12
- [651] Castellano C, Marsili M and Pietronero L 1998 Nonperturbative renormalization of the Kardar–Parisi–Zhang growth dynamics *Phys. Rev. Lett.* **80** 3527–30
- [652] Canet L, Chaté H, Delamotte B and Wschebor N 2010 Nonperturbative renormalization group for the Kardar–Parisi–Zhang equation *Phys. Rev. Lett.* **104** 150601
- [653] Bouchaud J P and Cates M E 1993 Self-consistent approach to the Kardar–Parisi–Zhang equation *Phys. Rev. E* **47** R1455–8
- [654] Lässig M 1998 Quantized scaling of growing surfaces *Phys. Rev. Lett.* **80** 2366–9
- [655] Lässig M 1998 On growth, disorder, and field theory *J. Phys.: Condens. Matter.* **10** 9905
- [656] Ódor G, Liedke B and Heinig K-H 2010 Directed  $d$ -mer diffusion describing the Kardar–Parisi–Zhang-type surface growth *Phys. Rev. E* **81** 031112
- [657] Pagnani A and Parisi G 2013 Multisurface coding simulations of the restricted solid-on-solid model in four dimensions *Phys. Rev. E* **87** 010102
- [658] L’vov V S, Lebedev V V, Paton M and Procaccia I 1993 Proof of scale invariant solutions in the Kardar–Parisi–Zhang and Kuramoto–Sivashinsky equations in  $1 + 1$  dimensions: analytical and numerical results *Nonlinearity* **6** 25–47
- [659] Prähofer M and Spohn H 2000 Statistical self-similarity of one-dimensional growth processes *Physica A* **279** 342–52
- [660] Prähofer M and Spohn H 2000 Universal distributions for growth processes in  $1 + 1$  dimensions and random matrices *Phys. Rev. Lett.* **84** 4882–5
- [661] Prähofer M and Spohn H 2002 Scale invariance of the PNG droplet and the Airy process *J. Stat. Phys.* **108** 1071–106
- [662] Johansson K J 2001 Universality of the local spacing distribution in certain ensembles of Hermitian Wigner matrices *Commun. Math. Phys.* **215** 683–705
- [663] Baik J, Deift P and Johansson K 1999 On the distribution of the length of the longest increasing subsequence of random permutations *Trans. Am. Math. Soc.* **12** 1119–78
- [664] Johansson K 2000 Shape fluctuations and random matrices *Commun. Math. Phys.* **209** 437–76
- [665] Baer R M and Brock P 1968 Natural sorting over permutation spaces *Math. Comput.* **22** 385
- [666] Dobrinevski A 2014 Simulating directed polymers and the Tracy–Widom distribution <https://inordinatum.wordpress.com>
- [667] Calabrese P, Le Doussal P and Rosso A 2010 Free-energy distribution of the directed polymer at high temperature *Europhys. Lett.* **90** 20002
- [668] Dotsenko V 2010 Bethe ansatz derivation of the Tracy–Widom distribution for one-dimensional directed polymers *Europhys. Lett.* **90** 20003
- [669] Dotsenko V 2010 Replica Bethe ansatz derivation of the Tracy–Widom distribution of the free energy fluctuations in one-dimensional directed polymers *J. Stat. Mech.* P07010
- [670] Calabrese P and Le Doussal P 2011 Exact solution for the Kardar–Parisi–Zhang equation with flat initial conditions *Phys. Rev. Lett.* **106** 250603
- [671] Le Doussal P and Calabrese P 2012 The KPZ equation with flat initial condition and the directed polymer with one free end *J. Stat. Mech.* P06001
- [672] Gueudré T and Le Doussal P 2012 Directed polymer near a hard wall and KPZ equation in the half-space *Europhys. Lett.* **100** 26006
- [673] Corwin I 2012 The Kardar–Parisi–Zhang equation and universality class *Random Matrices: Theory Appl.* **01** 1130001
- [674] Amir G, Corwin I and Quastel J 2011 Probability distribution of the free energy of the continuum directed random polymer in  $1 + 1$  dimensions *Commun. Pure Appl. Math.* **64** 466–537
- [675] Borodin A and Corwin I 2014 MacDonald processes *Probab. Theory Relat. Fields* **158** 225–400

- [676] Imamura T and Sasamoto T 2012 Exact solution for the stationary Kardar–Parisi–Zhang equation *Phys. Rev. Lett.* **108** 190603
- [677] Sasamoto T and Spohn H 2010 One-dimensional Kardar–Parisi–Zhang equation: an exact solution and its universality *Phys. Rev. Lett.* **104** 230602
- [678] Sasamoto T and Spohn H 2010 Exact height distributions for the KPZ equation with narrow wedge initial condition *Nucl. Phys. B* **834** 523–42
- [679] Takeuchi K A and Sano M 2010 Universal fluctuations of growing interfaces: evidence in turbulent liquid crystals *Phys. Rev. Lett.* **104** 230601
- [680] Kriecherbauer T and Krug J 2010 A pedestrian’s view on interacting particle systems, KPZ universality and random matrices *J. Phys. A: Math. Theor.* **43** 403001
- [681] Quastel J 2013 Introduction to KPZ *Curr. Dev. Math.* **2011** 125–94
- [682] Quastel J and Spohn H 2015 The one-dimensional KPZ equation and its universality class *J. Stat. Phys.* **160** 965–84
- [683] Halpin-Healy T 2012 (2 + 1)-dimensional directed polymer in a random medium: scaling phenomena and universal distributions *Phys. Rev. Lett.* **109** 170602
- [684] Halpin-Healy T 2013 Extremal paths, the stochastic heat equation, and the three-dimensional Kardar–Parisi–Zhang universality class *Phys. Rev. E* **88** 042118
- [685] Spitzer F 1970 Interaction of Markov processes *Adv. Math.* **5** 246–90
- [686] Krug J 1991 Boundary-induced phase transitions in driven diffusive systems *Phys. Rev. Lett.* **67** 1882–5
- [687] Derrida B 1998 An exactly soluble non-equilibrium system: the asymmetric simple exclusion process *Phys. Rep.* **301** 65–83
- [688] Myllys M, Maunukela J, Alava M, Ala-Nissila T, Merikoski J and Timonen J 2001 Kinetic roughening in slow combustion of paper *Phys. Rev. E* **64** 036101
- [689] Miettinen L, Myllys M, Merikoski J and Timonen J 2005 Experimental determination of KPZ height-fluctuation distributions *Eur. Phys. J. B* **46** 55–60
- [690] Dias C S, Yunker P J, Yodh A G, Araújo N A M and Telo da Gama M M 2018 Interaction anisotropy and the KPZ to KPZQ transition in particle deposition at the edges of drying drops *Soft Matter* **14** 1903–7
- [691] Hallatschek O, Hersen P, Ramanathan S and Nelson D R 2007 Genetic drift at expanding frontiers promotes gene segregation *Proc. Natl Acad. Sci. USA* **104** 19926–30
- [692] Kolmogorov A N 1941 On the energy distribution in the spectrum of a turbulent flow *C. R. Acad. Sci.* **30** 301–5
- [693] Fedorenko A A, Le Doussal P and Wiese K J 2013 Functional renormalization-group approach to decaying turbulence *J. Stat. Mech.* **P04014**
- [694] Berezin F 1965 *The Method of Second Quantization* (New York: Academic)
- [695] Wegner F 2016 *Supermathematics and its Applications in Statistical Physics* (Berlin: Springer)
- [696] Parisi G and Sourlas N 1982 Supersymmetric field theories and stochastic differential equations *Nucl. Phys. B* **206** 321–32
- [697] Cardy J L 1983 Nonperturbative effects in a scalar supersymmetric theory *Phys. Lett. B* **125** 470–2
- [698] Cardy J L 1985 Nonperturbative aspects of supersymmetry in statistical mechanics *Physica D* **15** 123–8
- [699] Cardy J L and McKane A J 1985 Field theoretic approach to the study of Yang–Lee and Griffiths singularities in the randomly diluted Ising model *Nucl. Phys. B* **257** 383–96
- [700] Kaviraj A, Rychkov S and Trevisani E 2019 Random field Ising model and Parisi–Sourlas supersymmetry part: I. Supersymmetric CFT *J. High Energy Phys.* **JHEP04(2020)090**
- [701] Kaviraj A, Rychkov S and Trevisani E 2020 Random field Ising model and Parisi–Sourlas supersymmetry: II. Renormalization group (arXiv:2009.10087)
- [702] Lawler G F 1980 A self-avoiding random walk *Duke Math. J.* **47** 655–93
- [703] Kozma G 2007 The scaling limit of loop-erased random walk in three dimensions *Acta Math.* **199** 29–152
- [704] Guttmann A J and Bursill R J 1990 Critical exponent for the loop erased self-avoiding walk by Monte Carlo methods *J. Stat. Phys.* **59** 1–9
- [705] Agrawal H and Dhar D 2001 Distribution of sizes of erased loops of loop-erased random walks in two and three dimensions *Phys. Rev. E* **63** 056115
- [706] Grassberger P 2009 Scaling of loop-erased walks in 2 to 4 dimensions *J. Stat. Phys.* **136** 399–404
- [707] Wilson D B 2010 Dimension of the loop-erased random walk in three dimensions *Phys. Rev. E* **82** 062102
- [708] Schramm O 2000 Scaling limits of loop-erased random walks and uniform spanning trees *Isr. J. Math.* **118** 221–88
- [709] Lawler G F, Schramm O and Werner W 2004 Conformal invariance of planar loop-erased random walks and uniform spanning trees *Ann. Probab.* **32** 939–95
- [710] Nienhuis B 1982 Exact critical point and critical exponents of  $O(n)$  models in two dimensions *Phys. Rev. Lett.* **49** 1062–5
- [711] Helmuth T and Shapira A 2020 Loop-erased random walk as a spin system observable *J. Stat. Phys.* **181** 1306–22
- [712] Viennot G X 1986 Heaps of pieces: I. Basic definitions and combinatorial lemmas *Combinatoire Énumérative* ed G Labelle and P Leroux (Berlin: Springer) pp 321–50
- [713] Viennot X 2017 *The Art of Bijective Combinatorics Online Lectures*
- [714] Kenyon R W and Wilson D B 2015 Spanning trees of graphs on surfaces and the intensity of loop-erased random walk on planar graphs *J. Am. Math. Soc.* **28** 985–1030
- [715] Lawler G F 2006 The Laplacian- $b$  random walk and the Schramm–Loewner evolution *Illinois J. Math.* **50** 701–46
- [716] Kasteleyn P W 1967 *Graph Theory and Theoretical Physics* ed F Harary (London: Academic)
- [717] Fedorenko A A, Le Doussal P and Wiese K J 2008 Field theory conjecture for loop-erased random walks *J. Stat. Phys.* **133** 805–12
- [718] Majumdar S N 1992 Exact fractal dimension of the loop-erased self-avoiding walk in two dimensions *Phys. Rev. Lett.* **68** 2329–31
- [719] Lyklema J W, Evertsz C and Pietronero L 1986 The Laplacian random walk *Europhys. Lett.* **2** 77
- [720] Niemeyer L, Pietronero L and Wiesmann H J 1984 Fractal dimension of dielectric breakdown *Phys. Rev. Lett.* **52** 1033–6
- [721] Witten T A and Sander L M 1981 Diffusion-limited aggregation, a kinetic critical phenomenon *Phys. Rev. Lett.* **47** 1400–3
- [722] Wiese K J and Kardar M 1998 Generalizing the  $O(N)$ -field theory to  $N$ -colored manifolds of arbitrary internal dimension *D Nucl. Phys. B* **528** 469–522
- [723] Wiese K J and Kardar M 1998 A geometric generalization of field theory to manifolds of arbitrary dimension *Eur. Phys. J. B* **7** 187–90
- [724] Belavin A A, Polyakov A M and Zamolodchikov A B 1984 Infinite conformal symmetry in two-dimensional quantum field theory *Nucl. Phys. B* **241** 333–80
- [725] Itzykson C and Drouffe J-M 1989 *Statistical Field Theory* vol 2 (Cambridge: Cambridge University Press)
- [726] Rushkin I, Bettelheim E, Gruzberg I A and Wiegmann P 2007 Critical curves in conformally invariant statistical systems *J. Phys. A: Math. Theor.* **40** 2165–95
- [727] Blöte H W J, Knops Y M M and Nienhuis B 1992 Geometrical aspects of critical Ising configurations in two dimensions *Phys. Rev. Lett.* **68** 3440–3

- [728] Janke W and Schakel A M J 2010 Holographic interpretation of two-dimensional  $O(N)$  models coupled to quantum gravity (arXiv:1003.2878)
- [729] Kirkham J E 1981 Calculation of crossover exponent from Heisenberg to Ising behaviour using the fourth-order  $\varepsilon$  expansion *J. Phys. A: Math. Gen.* **14** L437–42
- [730] Moghimi-Araghi S, Rajabpour M A and Rouhani S 2005 Abelian sandpile model: a conformal field theory point of view *Nucl. Phys. B* **718** 362–70
- [731] Kompaniets M V and Panzer E 2017 Minimally subtracted six-loop renormalization of  $O(n)$ -symmetric  $\phi^4$  theory and critical exponents *Phys. Rev. D* **96** 036016
- [732] Mera H, Pedersen T G and Nikolić B K 2018 Fast summation of divergent series and resurgent transseries from Meijer- $G$  approximants *Phys. Rev. D* **97** 105027
- [733] 't Hooft G 1974 A planar diagram theory for strong interactions *Nucl. Phys. B* **72** 461–73
- [734] Polchinski J 1984 Renormalization and effective Lagrangians *Nucl. Phys. B* **231** 269–95
- [735] Wetterich C 1993 Exact evolution equation for the effective potential *Phys. Lett. B* **301** 90–4
- [736] Hasenfratz A and Hasenfratz P 1986 Renormalization group study of scalar field theories *Nucl. Phys. B* **270** 687–701
- [737] Wegner F J and Houghton A 1973 Renormalization group equation for critical phenomena *Phys. Rev. A* **8** 401–12
- [738] Morris T R 1994 The exact renormalization group and approximate solutions *Int. J. Mod. Phys. A* **09** 2411
- [739] Berges J, Tetradis N and Wetterich C 2002 Non-perturbative renormalization flow in quantum field theory and statistical physics *Phys. Rep.* **363** 223–386
- [740] Dupuis N, Canet L, Eichhorn A, Metzner W, Pawłowski J M, Tissier M and Wschebor N 2021 The nonperturbative functional renormalization group and its applications *Phys. Rep.* **910** 1–114
- [741] Nattermann T 1997 Theory of the random field Ising model *Spin Glasses and Random Fields* ed A P Young (Singapore: World Scientific) cond-mat/9705295 cond-mat/9705295
- [742] Fisher D S 1985 Random fields, random anisotropies, nonlinear  $\sigma$  models, and dimensional reduction *Phys. Rev. B* **31** 7233–51
- [743] Feldman D E 2000 Quasi-long-range order in the random anisotropy Heisenberg model: functional renormalization group in  $4 - \varepsilon$  dimensions *Phys. Rev. B* **61** 382–90
- [744] Feldman D E 2001 Quasi-long range order in glass states of impure liquid crystals, magnets, and superconductors *Int. J. Mod. Phys. B* **15** 2945
- [745] Giamarchi T and Le Doussal P 1995 Elastic theory of flux lattices in the presence of weak disorder *Phys. Rev. B* **52** 1242–70
- [746] Tarjus G and Tissier M 2020 Random-field Ising and  $O(N)$  models: theoretical description through the functional renormalization group *Eur. Phys. J. B* **93** 50
- [747] Tissier M and Tarjus G 2012 Nonperturbative functional renormalization group for random field models and related disordered systems: III. Superfield formalism and ground-state dominance *Phys. Rev. B* **85** 104202
- [748] Tissier M and Tarjus G 2012 Nonperturbative functional renormalization group for random field models and related disordered systems: IV. Supersymmetry and its spontaneous breaking *Phys. Rev. B* **85** 104203
- [749] Baczyk M, Tarjus G, Tissier M and Balog I 2014 Fixed points and their stability in the functional renormalization group of random field models *J. Stat. Mech.* P06010
- [750] Le Doussal P and Wiese K J 2007 Stability of random-field and random-anisotropy fixed points at large  $N$  *Phys. Rev. Lett.* **98** 269704
- [751] Fedorenko A A and Kühnel F 2007 Long-range correlated random field and random anisotropy  $O(N)$  models: a functional renormalization group study *Phys. Rev. B* **75** 174206
- [752] Tarjus G, Baczyk M and Tissier M 2013 Avalanches and dimensional reduction breakdown in the critical behavior of disordered systems *Phys. Rev. Lett.* **110** 135703
- [753] Mouhanna D and Tarjus G 2016 Phase diagram and criticality of the random anisotropy model in the large- $N$  limit *Phys. Rev. B* **94** 214205
- [754] Fytas N G, Martín-Mayor V, Picco M and Sourlas N 2017 Restoration of dimensional reduction in the random-field Ising model at five dimensions *Phys. Rev. E* **95** 042117
- [755] Fytas N G, Martín-Mayor V, Picco M and Sourlas N 2018 Review of recent developments in the random-field Ising model *J. Stat. Phys.* **172** 665–72
- [756] Fytas N G, Martín-Mayor V, Parisi G, Picco M and Sourlas N 2019 Evidence for supersymmetry in the random-field Ising model at  $D = 5$  *Phys. Rev. Lett.* **122** 240603
- [757] Tarjus G and Tissier M 2016 Avalanches and perturbation theory in the random-field Ising model *J. Stat. Mech.* 023207
- [758] Wiese K J 2016 Dynamical selection of critical exponents *Phys. Rev. E* **93** 042105
- [759] Brézin E, Halperin B I and Leibler S 1983 Critical wetting: the domain of validity of mean field theory *J. Physique* **44** 775–83
- [760] Brézin E, Halperin B I and Leibler S 1983 Critical wetting in three dimensions *Phys. Rev. Lett.* **50** 1387
- [761] Fisher D S and Huse D A 1985 Wetting transitions: a functional renormalization-group approach *Phys. Rev. B* **32** 247–56
- [762] Brézin E and Halpin-Healy T 1987 Scaling functions for 3D critical wetting *J. Physique* **48** 757–61
- [763] Lipowsky R and Fisher M E 1987 Scaling regimes and functional renormalization for wetting transitions *Phys. Rev. B* **36** 2126–41
- [764] Forgas G, Lipowsky R and Nieuwenhuizen T M 1991 *The Behaviour of Interfaces in Ordered and Disordered Systems (Phase Transitions and Critical Phenomena vol 14)* (London: Academic) pp 136–376
- [765] Boltzmann L 1868 Studien über das Gleichgewicht der lebendigen Kraft zwischen bewegten materiellen Punkten *Wiener Berichte* **58** 517–60
- [766] Janssen H K 1992 On the renormalized field theory of nonlinear critical relaxation *From Phase Transitions to Chaos, Topics in Modern Statistical Physics* (Singapore: World Scientific) pp 68–91
- [767] Gumbel E J 1935 Les valeurs extrêmes des distributions statistiques *Ann. Inst. Henri Poincaré* **5** 115–8
- [768] Weibull W 1951 A statistical distribution function of wide applicability *J. Appl. Mech.* **18** 293–7
- [769] Fréchet M 1927 Sur la loi de probabilité de l'écart maximum *Ann. Soc. Math. Pol.* **6** 93
- [770] Levit S and Smilansky U 1977 A theorem on infinite products of eigenvalues of Sturm–Liouville type operators *Proc. Am. Math. Soc.* **65** 299–302
- [771] Coleman S 1985 *Aspects of Symmetry* (Cambridge: Cambridge University Press)



**Kay Wiese** studied physics in Heidelberg, followed by a PhD in Paris under the supervision of Francois David. He was a postdoctoral scholar in Essen, and visiting scientist at the KITP (Santa Barbara). Since 2004 he holds a permanent research position at Ecole Normale Supérieure in Paris, where he currently is Directeur de Recherche (DR1, full research professor). He works on basic questions in field theory, and is a world-leading expert on the functional RG approach to disordered systems. In this review he connects field theory, experiment, simulations and analytic solutions.